

# **BULETINUL INSTITUTULUI POLITEHNIC DIN IAȘI**

**Publicat de  
UNIVERSITATEA TEHNICĂ "GH.ASACHI", IAȘI**

**Tomul LI (LV)**

**Fasc. 4**

**Secția  
ȘTIINȚA ȘI INGINERIA MATERIALELOR**

**2005**

**President of the Editorial Board of Bulletin of the Polytechnic Institute**

**Prof. univ. dr. eng Nicolae Badea, Technical University “Gh. Asachi” Iași, Romania**  
Rector of Technical University “Gh. Asachi” of Iasi

**Editor-in-Chief of Bulletin of the Polytechnic Institute**

**Prof. univ. dr. eng Ion Giurma, Technical University “Gh. Asachi” Iași, Romania**  
Vice-Rector of Technical University “Gh. Asachi” of Iasi

**Managing Editor of Bulletin of the Polytechnic Institute**

**Prof. univ. dr. eng. Dan Gălușcă, Technical University “Gh. Asachi” Iași, Romania**  
Dean of the Faculty of Materials Science and Engineering

**Managing Editor of the *MATERIALS SCIENCE AND ENGINEERING***

**Assoc. prof. dr. eng. Iulian Ioniță, Technical University “Gh. Asachi” Iași, Romania**  
Scientific secretary of the Faculty of Materials Science and Engineering

**Editorial Board of the Section *MATERIALS SCIENCE AND ENGINEERING***

**Prof.univ.dr.eng. Yuri A. Burennikov, Vinnitsia State Technical University, Ukraine**

**Prof.univ.dr.eng. Borivoje Miškovič, Yugoslav Association of Metallurgical Engineers,  
Belgrad, Serbia-Montenegro**

**Prof.univ.dr.eng. Paolo Nanni, Universita degli Studi da Genova, Italy**

**Prof.univ.dr.eng. Strul Moisa, Ben-Gurion University of the Negev, Beer-Sheva, Israel**

**Prof.univ.dr.eng. Corneliu Munteanu, Technical University “Gh. Asachi” Iași,  
Romania**

**Prof.univ.dr.eng. Vasile Cojocaru-Filipiuc, Technical University “Gh. Asachi” Iași,  
Romania**

**Prof.univ.dr.eng. Constantin Baciu, Technical University “Gh. Asachi” Iași, Romania**

**Prof.univ.dr.eng. Luchian Zaharia, Technical University “Gh. Asachi” Iași, Romania**

**Prof.univ.dr.eng. Ioan Carcea, Technical University “Gh. Asachi” Iași, Romania**

**Prof.univ.dr.eng. Adrian Dima, Technical University “Gh. Asachi” Iași, Romania**

**Prof.univ.dr.eng. Ioan Alexandru, Technical University “Gh. Asachi” Iași, Romania**

**Assoc.prof.dr.eng. Leandru Gheorghe Bujoreanu, Technical University “Gh. Asachi”  
Iași, Romania**

**Assoc. prof.dr. eng. Ioan Rusu, Technical University “Gh. Asachi” Iași, Romania**

**Assoc. prof.dr. eng. Gheorghe Bădărău, Technical University “Gh. Asachi” Iași,  
Romania**

**Assoc. prof.dr. eng. Petrică Vizureanu, Technical University “Gh. Asachi” Iași,  
Romania**

**Editorial Secretary of the *MATERIALS SCIENCE AND ENGINEERING***

**Assoc.prof.dr.eng. Gheorghe Bădărău, Technical University “Gh. Asachi” Iași,  
Romania**

MATERIALS SCIENCE AND ENGINEERING

<b>CONTENTS</b>	
TAKAHIRO SAWAGUCHI, TAKEHIKO KIKUCHI, FUXING YIN, KAZUYUKI OGAWA, SETSUO KAJIWARA, ATSUMICHI KUSHIBE, MASAHIKO HIGASHINO and TAKATOSHI OGAWA - PSEUDOELASTICITY and DAMPING PROPERTIES ASSOCIATED WITH FCC/HCP MARTENSITIC TRANSFORMATION IN NbC CONTAINING Fe-Mn-Si-BASED ALLOYS	1
C. BEJINARIU, V. MOLDOVEANU, D. A. GHEORGHIU and St. L. TOMA - THE DETERMINATION OF THE FILLING DEGREE AT INDIRECT EXTRUSION FOR THE NUT-LIKE PRODUCTS MADE FROM CYLINDER SEMI-PRODUCTS	13
C. BEJINARIU, L. ZAHARIA, V. V. MOLDOVEANU and St. L. TOMA - THE ANALYTIC CALCULATION OF THE CYLINDER-TRUNCATED CONE SEMI-PRODUCT TO OBTAIN NUT-LIKE PRODUCTS BY INDIRECT EXTRUSION	17
IONEL BOSTAN - AUDITABLE INTRAORGANIZATIONAL ACTIVITIES	23
IONEL BOSTAN - THE UNIVERSALITY AND PERIODICITY OF THE FUNCTION OF INTERNAL AUDIT	29
MARIA BACIU, EMIL PASINKOVSKI, SILVIA GEORGESCU and CONSTANTIN BACIU - INFLUENCE OF THE ELECTROLYTIC PLASMA NITRIDING ON STEEL STRUCTURE	31
DRAGOȘ-VIOREL BREZOI and RODICA-MARIANA ION - PYRROLE POLYMERIZATION IN AQUEOUS FeCl <sub>3</sub> SOLUTIONS	35
LEANDRU-GHEORGHE BUJOREANU, CORNELIU MUNTEANU, IULIAN IONIȚĂ, MITICĂ TEMNEANU and VIOREL KOGĂNICEANU - ON THE SHAPE MEMORY BEHAVIOUR OF Cu-BASED ALLOYS AND POLYETHYLENE TEREPHTHALATE (PET)	43
OVIDIU CALANCIA, LEONACHE DRĂGOI, VASILE-VIOREL MOLDOVEANU and RADU DĂNILĂ - THE RESEARCH OF THE STRENGTH LEVEL OF THE WEAVING MACHINES' NOISE FOR THEIR RATIONAL DESIGN	51
GABRIELA CIOBANU, LAURENȚIU-DAN GHENGHEA, LĂCRĂMIOARA ISTRATI and GABRIELA CÂRJĂ - CORROSION OF ALUMINIUM ALLOYS IN ALKALINE MEDIA	55
GABRIELA CIOBANU, LAURENȚIU-DAN GHENGHEA, GABRIELA CÂRJĂ and LĂCRĂMIOARA ISTRATI - KINETIC AND THERMODYNAMIC ASPECTS CONCERNING CORROSION OF ALUMINIUM ALLOYS IN ALKALINE MEDIA	61
PETRU P. CONDREA - MANAGEMENT RISK DETERMINATION	67
PETRU P. CONDREA - ADVANTAGES OF USING THE MODERN MEANS IN ENTERPRISE COMMUNICATION	69
MIHAIL-LIVIU CRAUS and MIHAIL LOZOVAN - CORRELATION BETWEEN THE SEEBECK EFFECT, HIGH TEMPERATURE TRANSPORT AND STRUCTURE OF SOME La <sub>1-x</sub> Ca <sub>x</sub> Mn <sub>0.9</sub> Cu <sub>0.1</sub> O <sub>3</sub> COMPOUNDS	71
IULIAN CUCOȘ - COMPUTERIZED PROPERTIES PREDICTION IN THE HEAT TREATMENT OF STEELS	79

IULIAN CUCOȘ - THE CONTROL OF FURNACES FOR THERMAL TREATMENT	85
VASILE DIA, LEANDRU-GHEORGHE BUJOREANU, GABRIELA HRIȚULEAC and VIORICA DAVID - STUDY OF THE WORK GENERATING SHAPE MEMORY EFFECT	89
MIRCEA DOBRESCU, CONSTANTIN DUMITRESCU and RAMI SABAN - AEROSPATIAL MECHANICAL ENGINEERING OF TITANIUM ALLOYS	97
GABRIELLA FAUR-CSUKAT - FACTORS AFFECTING PERFORMANCE OF BULLETPROOF COMPOSITES	99
DIANA ANTONIA GHEORGHIU - MICROSTRUCTURAL CHANGES INTO THE HEAT AFFECTED ZONE OF CHROMIUM ALLOYED WHITE CAST IRON	105
CORNELIA IONESCU LUCA and ALINA DRAGOMIR - SAFETY, PROTECTIVE AND OCCUPATION FOOTWEAR CHARACTERISTICS USED IN METALLURGICAL INDUSTRY	109
CORNELIA IONESCU LUCA ET RODICA SILVIA VOLOCARIU - ALGORITHME DE PROJECTION DES MOULES POUR CONTREFORTS DE CHAUSSURE	117
MIHAI LOZOVAN and HORIA CHIRIAC - ON THE FUNCTIONAL STUDY OF A THERMOSTATIC DEVICE BASED ON INVAR ALLOYS	125
DORIN LUCA, ROXANA ARSENE and GEORGE ANDRIESCU - SOME PRELIMINARY EXPERIMENTS UPON THE WORKPIECE PARAMETERS PROCESSED BY ELECTROMAGNETIC FORMING	129
VALENTIN MIHAILOV, MARIA BACIU, SILVIA GEORGESCU and CONSTANTIN BACIU - ABOUT WEAR BEHAVIOUR OF STEELS NITRATED IN ELECTROLYTIC PLASMA	135
IOAN MILOȘAN - ON THE INFLUENCE OF THE HEAT TREATMENT PARAMETERS ON THE MICROHARDNESS VARIATION OF A BAINITIC S.G.CAST IRON	139
IOAN MILOȘAN - SOME ASPECTS ABOUT THE KINETICS AND THERMODYNAMICS OF THE TRANSFORMATIONS OF A BAINITIC S.G. CAST IRON BETWEEN 350 AND 400°C	145
VASILE-VIOREL MOLDOVEANU, LEONACHE DRĂGOI and OVIDIU CALANCIA - SOME ASPECTS OF THE DYNAMICS OF LAUNCHING DEVICE AT THE UNCONVENTIONAL WEAVING MACHINES	151
CORNELIU MUNTEANU and LEANDRU-GHEORGHE BUJOREANU - STUDY OF DIMENSIONAL UNIFORMITY AND ELECTRIC RESISTIVITY VARIATION IN AMORPHOUS RIBBONS FROM $Fe_{80-x}Sm_xB_{20}$ AND $Fe_{80-x}Gd_xB_{20}$ SYSTEMS	155
I.NAGY, DANIELA NAGY, A.NICOLAE and A.DIMON - MINIMIZING OF POLLUTION AT THE ROASTING ROTARY KILN USED FOR PYRITE CINDERS	159
CARMEN NEJNERU, NICANOR CIMPOESU, ION HOPULELE, ALEXANDRU MAXINIUC and DRAGOS ACHITEI - THE IMPROVEMENT OF THE WHITE BRASSES RECRYSTALLIZATION HEAT TREATING (TYPE Cu-Zn-Ni)	167
SILVIA PATACHIA and ADINA PAPANCEA - EFFECT OF THE MICROSTRUCTURE OF POLY(VINIL ALCOHOL) MEMBRANES ON THE DIFFUSION OF SOME IONIC SPECIES	177
S. PATACHIA and M. RINJA - EFFECT OF THE POLY (VINYL ALCOHOL) [PVA] HYDROGELS MICROSTRUCTURE ON THEIR WATER ABSORPTION	183
SILVIA PATACHIA and MARIA MICLAUS - PVA HYDROGELS AS INTELLIGENT MATERIALS	191
SILVIA PATACHIA and MIHAELA VOINEA - BIOLOGICAL MATERIALS AS SOLUTION FOR WATER DEPOLLUTION	199
SILVIA PATACHIA and ECATERINA SAMOILA - POLY(VINYL ALCOHOL) HYDROGELS AS CONTROLLED DRUG DELIVERY SYSTEMS	205
GHEORGHE T. POP, STEFAN LACATUSU, SIMONA STOLERIU and OCTAVIAN CIOBANU – GALLIUM-BASED RESTORATIVE DENTAL MATERIALS	211
OCTAVIAN POTECAȘU, FLORENTINA POTECAȘU, ELENA DRUGESCU, NELU CAZACU, and PETRICA ALEXANDRU - METALLIC COMPOSITES OBTAINED THROUGH EXTRUSION	219

OCTAVIAN POTECAȘU, FLORENTINA POTECAȘU, ELENA DRUGESCU and LAURA BUBURUZAN - HARDENED GRANITE COMPOSITES FROM THE DOBROGEA MOUNTAINS	227
MIHAELA RĂCUCIU, DORINA-EMILIA CREANGĂ, GHIORGHE CĂLUGĂRU and IRINA HORGA - FERROFLUIDS STABILITY-A COMPARATIVE STUDY	233
ADRIANA SAVIN, ROZINA STEIGMANN and RAIMOND GRIMBERG - DETERMINATION OF PHYSICAL-MECHANICAL PARAMETERS OF MULTILAYERED COMPOSITE MATERIALS THROUGH ULTRASONIC METHODS	239
ADRIANA SAVIN, ROZINA STEIGMANN, R.GRIMBERG, A.ANDREESCU, V.PALIOVICI and V.GOANTA - EVALUATION OF FATIGUE AT AISI 316L AUSTENITIC STEELS USING EDDY CURRENT MICROSENSORS ARRAY	247
ADRIANA SAVIN, ROZINA STEIGMANN and RAIMOND GRIMBERG - MICROSENSORS ARRAY FOR INTEGRITY EVALUATION OF FLEXIBLE MULTI-TRACES CIRCUITS	255
V. I. SAVULYAK and A. YU. OSSADCHUK - RECEPTION OF COMPOSITE COVERINGS ON WORKING SURFACES OF STEEL PRODUCTS	259
VICTOR SAVULYAK - INVESTIGATION OF THE CORRUGATED WORKPIECES MANUFACTURING PROCESS	267
D. V. ȘOLTUZ, D. CIOBANU and V. NECULĂIASA - ASPECTS REGARDING THE BEHAVIOR OF STAINLESS STEELS DURING THE WEAR PROCESSES	275
D. V. ȘOLTUZ, D. CIOBANU and V. NECULĂIASA - ASPECTS REGARDING THE VARIATIONS OF ELECTROLYTIC POTENTIAL IN TRIBOCORROSION WEAR PROCESS	279
ST. L. TOMA, I.ALEXANDRU, D.G. GĂLUȘCĂ and C. BEJINARIU - DEVICE FOR METALLIC COVERING BY ACTIVATED THERMAL SPRAYING	285
ST. L. TOMA, C. BACIU, C. BEJINARIU, A. ALEXANDRU, and D. GHEORGHIU - THE SHOT PENNING INFLUENCE ON THE ALUMINUM LAYERS POROSITY OBTAINED BY THERMAL SPRAYING USING ELECTRIC ARC	291
RODICA SILVIA VOLOCARIU and CORNELIA IONESCU LUCA - POSSIBILITIES OF PROGRAMMING MOULDS USED ON CAROUSEL INSTALLATIONS FOR THE INJECTION OF THE FOOTWEAR SOLES	297
ALINA ZAHARIUC, FLORIN MUNTEANU and VASILE MERTICARU - VIBRATION ANALYSES ON HIP PROSTHESIS	303

**ȘTIINȚA ȘI INGINERIA MATERIALELOR**

<b>CUPRINS</b>	
TAKAHIRO SAWAGUCHI, TAKEHIKO KIKUCHI, FUXING YIN, KAZUYUKI OGAWA, SETSUO KAJIWARA, ATSUMICHI KUSHIBE, MASAHIKO HIGASHINO și TAKATOSHI OGAWA - PSEUDOELASTICITATE ȘI PROPRIETĂȚI DE AMORTIZARE ASOCIATE CU TRANSFORMAREA MARTENSITICĂ CFC/HC ÎN ALIAJELE PE BAZĂ DE Fe-Mn-Si CARE CONȚIN NbC	1
C. BEJINARIU, V. MOLDOVEANU, D. A. GHEORGHIU și St. L. TOMA - DETERMINAREA GRADULUI DE UMLERE A MUCHIILOR PIESEI LA EXTRUDAREA INDIRECTĂ A PRODUSELOR DE TIP PIULIȚĂ DIN SEMIFABRICATE CILINDRICE	13
C. BEJINARIU, L. ZAHARIA, V. V. MOLDOVEANU și St. L. TOMA - CALCULUL ANALITIC AL DIMENSIUNILOR SEMIFABRICATULUI CILINDRO-TRONCONIC PENTRU OBTINEREA PRIN EXTRUDARE INDIRECTĂ A PRODUSELOR DE TIP PIULIȚĂ	17
IONEL BOSTAN - ACTIVITĂȚI INTRAORGANIZAȚIONALE CARE POT FI AUDITATE	23
IONEL BOSTAN - UNIVERSALITATEA ȘI PERIODICITATEA FUNCȚIEI DE AUDIT INTERN	29
MARIA BACIU, EMIL PASINKOVSKI, SILVIA GEORGESCU și CONSTANTIN BACIU - INFLUENȚA NITRURĂRII ÎN PLASMĂ ELECTROLITICĂ ASUPRA STRUCTURII OȚELULUI	31
DRAGOȘ-VIOREL BREZOI și RODICA-MARIANA ION - POLIMERIZAREA PIROLULUI ÎN SOLUȚII APOASE DE FeCl <sub>3</sub>	35
LEANDRU-GHEORGHE BUJOREANU, CORNELIU MUNTEANU, IULIAN IONIȚĂ, MITICĂ TEMNEANU și VIOREL KOGĂNICEANU - ASUPRA COMPORTAMENTULUI DE MEMORIA FORMEI LA ALIAJELE PE BAZĂ DE Cu ȘI POLIETILENTEREFTALAT (PET)	43
OVIDIU CALANCIA, LEONACHE DRĂGOI, VASILE-VIOREL MOLDOVEANU și RADU DĂNILĂ - CERCETAREA NIVELULUI DE TĂRIE A ZGOMOTULUI MAȘINILOR DE ȚESUT ÎN VEDEREA PROIECTĂRII RAȚIONALE A ACESTORA	51
GABRIELA CIOBANU, LAURENȚIU-DAN GHENGHEA, LĂCRĂMIOARA ISTRATI și GABRIELA CÂRJĂ - COROZIUNEA ALIAJELOR DE ALUMINIU ÎN MEDII ALCALINE	55
GABRIELA CIOBANU, LAURENȚIU-DAN GHENGHEA, GABRIELA CÂRJĂ și LĂCRĂMIOARA ISTRATI - ASPECTE CINETICE ȘI TERMODINAMICE PRIVIND COROZIUNEA ALIAJELOR DE ALUMINIU ÎN MEDII ALCALINE	61
PETRU P. CONDREA – DETERMINAREA MANAGEMENTULUI DE RISC	67
PETRU P. CONDREA – AVANTAJELE UTILIZĂRII MIJLOACELOR MODERNE ÎN COMUNICAREA DIN CADRUL ÎNTREPRINDERII	69
MIHAIL-LIVIU CRAUS și MIHAI LOZOVAN - CORELAȚIE ÎNTRE EFECTUL SEEBECK, TRANSPORTUL LA TEMPERATURA RIDICATĂ ȘI STRUCTURA UNOR COMPUȘI La <sub>1-x</sub> Ca <sub>x</sub> Mn <sub>0.9</sub> Cu <sub>0.1</sub> O <sub>3</sub>	71
IULIAN CUCOȘ - PREDICȚIA ASISTATĂ DE CALCULATOR A PROPRIETĂȚILOR LA TRATAMENTUL TERMIC AL OȚELURILOR	79

IULIAN CUCOȘ – CONDUCEREA CUPTOARELOR DE TRATAMENT TERMIC	85
VASILE DIA, LEANDRU-GHEORGHE BUJOREANU, GABRIELA HRIȚULEAC și VIORICA DAVID - STUDIUL EFECTULUI DE MEMORIA FORMEI GENERATOR DE LUCRU MECANIC	89
MIRCEA DOBRESCU, CONSTANTIN DUMITRESCU și RAMI SABAN - INGINERIA MECANICĂ AEROSPAȚIALĂ A ALIAJELOR DE TITAN	97
GABRIELLA FAUR-CSUKAT - FACTORI CARE INFLUENȚEAZĂ PERFORMANȚA MATERIALELOR COMPOZITE REZISTENTE LA PROIECTILE	99
DIANA ANTONIA GHEORGHIU - MODIFICĂRI MICROSTRUCTURALE INDUSE ÎN ZONA INFLUENȚATĂ TERMIC A FONTEI ALBE ALIATE CU CROM	105
CORNELIA IONESCU LUCA și ALINA DRAGOMIR - CARACTERISTICILE ÎNCĂLȚĂMINTEI DE SECURITATE, DE PROTECȚIE ȘI DE LUCRU UTILIZATĂ ÎN INDUSTRIA METALURGICĂ	109
CORNELIA IONESCU LUCA și RODICA SILVIA VOLOCARIU - ALGORITM DE PROIECTARE ASISTATĂ DE CALCULATOR A MATRIȚELOR DE FORMAT ȘTAIFURI PENTRU ÎNCĂLȚĂMINTE	117
MIHAI LOZOVAN și HORIA CHIRIAC - ASUPRA STUDIULUI FUNCȚIONAL AL UNUI DISPOZITIV DE TERMOSTATARE BAZAT PE ALIAJE INVAR	125
DORIN LUCA, ROXANA ARSENE și GEORGE ANDRIESCU - UNELE EXPERIMENTE PRELIMINARE ASUPRA PARAMETRILOR PIESEI DE LUCRU PROCESATE PRIN MAGNETOFORMARE	129
VALENTIN MIHAILOV, MARIA BACIU, SILVIA GEORGESCU și CONSTANTIN BACIU - ASUPRA COMPORTĂRII LA UZURĂ A OȚELURILOR NITRURATE ÎN PLASMĂ ELECTROLITICĂ	135
IOAN MILOȘAN - INFLUENȚA PARAMETRILOR TRATAMENTULUI TERMIC ASUPRA MICRODURITĂȚII UNEI Fgn BAINITICE	139
IOAN MILOȘAN - ASPECTE PRIVIND CINETICA ȘI TERMODINAMICA TRANSFORMĂRILOR ALE UNEI Fgn BAINITICE ÎNTRE 350 ȘI 400°C	145
VASILE-VIOREL MOLDOVEANU, LEONACHE DRĂGOI și OVIDIU CALANCIA - UNELE ASPECTE ALE DINAMICII MECANISMULUI DE LANSARE DE LA MAȘINILE NECONVENȚIONALE DE ȚESUT	151
CORNELIU MUNTEANU și LEANDRU-GHEORGHE BUJOREANU - STUDIUL VARIAȚIEI UNIFORMITĂȚII DIMENSIONALE ȘI A REZISTIVITĂȚII ELECTRICE LA BENZILE AMORFE DIN SISTEMELE $Fe_{80-x}Sm_xB_{20}$ ȘI $Fe_{80-x}Gd_xB_{20}$	155
I.NAGY, DANIELA NAGY, A.NICOLAE și A.DIMON - MINIMIZAREA POLUĂRII LA CUPTOARELE ROTATIVE DE PRĂJIRE UTILIZATE PENTRU CENUȘILE DE PIRITĂ	159
CARMEN NEJNERU, NICANOR CIMPOESU, ION HOPULELE, ALEXANDRU MAXINIUC și DRAGOS ACHITEI - OPTIMIZAREA TRATAMENTULUI TERMIC DE RECOACERE DE RECRISTALIZARE LA ALAME ALBE (tip Cu-Zn-Ni)	167
SILVIA PAȚACHIA și ADINA PAPANCEA - EFECTUL MICROSTRUCTURII MEMBRANELOR DE POLI(ALCOOL VINILIC) [PVA] ASUPRA DIFUZIEI UNOR SPECII IONICE.	177
S. PAȚACHIA și M. RINJA - EFECTUL MICROSTRUCTURII HIDROGELURILOR DE PVA ASUPRA ABSORBȚIILOR DE APĂ.	183
SILVIA PAȚACHIA și MARIA MICLAUS - HIDROGELURILE DE PVA CA MATERIALE INTELIGENTE	191
SILVIA PAȚACHIA și MIHAELA VOINEA - MATERIALELE BIOLOGICE CA O SOLUȚIE PENTRU DEPOLUAREA APEI	199
SILVIA PAȚACHIA și ECATERINA SAMOILA - POLI(ALCOOLUL VILILIC) CA SISTEM DE ELIBERARE CONTROLATĂ A MEDICAMENTELOR	205

GHEORGHE T. POP, STEFAN LACATUȘU, SIMONA STOLERIU și OCTAVIAN CIOBANU – AMALGAME CU GALIU UTILIZATE ÎN MEDICINA DENTARĂ	211
OCTAVIAN POTECAȘU, FLORENTINA POTECAȘU, ELENA DRUGESCU, NELU CAZACU, și PETRICĂ ALEXANDRU - COMPOZITE METALICE OBȚINUTE PRIN EXTRUZIUNE	219
OCTAVIAN POTECAȘU, FLORENTINA POTECAȘU, ELENA DRUGESCU și LAURA BUBURUZAN - COMPOZITE ARMATE CU GRANIT DIN MUNȚII DOBROGEI	227
MIHAELA RĂCUCIU, DORINA-EMILIA CREANGĂ, GHIORGHE CĂLUGĂRU și IRINA HORGA – SATABILITATEA FEROFUIDELOR-STUDIUL COMPARATIV	233
ADRIANA SAVIN, ROZINA STEIGMANN și RAIMOND GRIMBERG - DETERMINAREA PARAMETRILOR FIZICO-MECANICI A MATERIALELOR COMPOZITE MULTISTRAT PRIN METODE DE ULTRASUNETE	239
ADRIANA SAVIN, ROZINA STEIGMANN, R.GRIMBERG, A.ANDREESCU, V.PALHOVICI și V.GOANȚĂ - EVALUAREA OBOSELII LA OȚELURILE AUSTENITICE 316L UTILIZÂND ARII DE MICROSENZORI DE CURENȚI TURBIONARI	247
ADRIANA SAVIN, ROZINA STEIGMANN și RAIMOND GRIMBERG - ARIE DE MICROSEZORI PENTRU EVALUAREA INTEGRITĂȚII CIRCUITELOR FLEXIBILE MULTITRASE	255
V. I. SAVULYAK și A. YU. OSSADCHUK - RECEPȚIA ACOPERIRILOR DIN MATERIALE COMPOZITE PE SUPRAFEȚELE DE LUCRU ALE PRODUSELOR DIN OȚEL	259
VICTOR SAVULYAK – STUDIUL PROCESULUI DE PRELUCRARE A PIESELOR ONDULATE	267
D. V. ȘOLTUZ, D. CIOBANU și V. NECULĂIASA - ASPECTE PRIVIND COMPORTAREA OȚELURILOR INOXIDABILE ÎN TIMPUL PROCESELOR DE UZURĂ	275
D. V. ȘOLTUZ, D. CIOBANU și V. NECULĂIASA - ASPECTE PRIVIND VARIAȚIILE DE POTENȚIAL ELECTROLITIC ÎN PROCESE DE UZURĂ TRIBOCOROZIVĂ	279
ST. L. TOMA, I.ALEXANDRU, D.G. GĂLUȘCĂ și C. BEJINARIU - DISPOZITIV DE METALIZARE PRIN SPRAYERE TERMICĂ ACTIVATĂ	285
ST. L. TOMA, C. BACIU, C. BEJINARIU, A. ALEXANDRU și D. GHEORGHIU - INFLUENȚA ALICĂRII ASUPRA POROZITĂȚII STRATURILOR DE ALUMINIU OBȚINUTE PRIN PULVERIZARE TERMICĂ ÎN ARC ELECTRIC	291
RODICA SILVIA VOLOCARIU și CORNELIA IONESCU LUCA - POSSIBILITIES - POSIBILITĂȚI DE PROGRAMARE A MATRIȚELOR FOLOSITE PE INSTALAȚII DE TIP CARUSEL PENTRU INJECTAREA TĂLPILOR DIRECT PE FEȚELE ÎNCĂLȚĂMINTEI	297
ALINA ZAHARIUC, FLORIN MUNTEANU și VASILE MERTICARU - ANALIZA VIBRAȚIONALĂ PE PROTEZE DE ȘOLD	303

OVIDIU CALANCIA, VICTOR MULLER, MIHAI STEFAN, LEONACHE DRAGOI, MIRCEA BELOIU - DETERMINAREA CONTINUTULUI DE FERITA IN STRUCTURILE SUDATE ALE OTELURILOR AUSTENITICE 10TIMONICR175 CU ELECTROZI DIN OTEL INOXIDABIL 19.12.2.NB UTILIZAND DIAGRAME STRUCTURALE WRC 1992	191
RADU DANILA, VIOREL MOLDOVEANU, RALUCA DRAGOI, TUDOR RAILEANU, MIRCEA BELOIU - STABILIREA EFORTURILOR TERMICE A FORMELOR METALICE DIN FONTA CENSIE IN TIMPUL PROCESULUI DE TURNARE	197
PETRICĂ VIZUREANU, ADRIAN DIMA - UN MODEL MATEMATIC DE DETENSIONARE	203
R. COMANECI, D. G. GALUSCA, CONSTANTIN BACIU, L. ZAHARIA - DEFORMAREA IN REGIUNEA BIFAZICA ( $\gamma + \alpha$ ) LA LAMINAREA CONTROLATA	209



**PSEUDOELASTICITY AND DAMPING PROPERTIES  
ASSOCIATED WITH FCC/HCP MARTENSITIC TRANSFORMATION  
IN NbC CONTAINING Fe-Mn-Si-BASED ALLOYS**

BY

**TAKAHIRO SAWAGUCHI, TAKEHIKO KIKUCHI, FUXING YIN, KAZUYUKI OGAWA,  
SETSUO KAJIWARA, ATSUMICHI KUSHIBE\*, MASAHIKO HIGASHINO\* and  
TAKATOSHI OGAWA\***

**Abstract:** Fe-Mn-Si-based shape memory alloys containing NbC are a potential candidate for high damping materials. This paper reviews pseudoelasticity, internal friction, and tension-compression fatigue behavior, which were comprehensively investigated in a thermomechanically treated Fe<sub>28</sub>Mn-6Si-5Cr-0.53Nb-0.06C (mass %) alloy, especially focusing on the pseudoelasticity. The results are discussed in relation to the martensitic transformation behavior and microstructural characteristics of the alloy, and the effect of the thermomechanical treatment is also discussed. The results commonly indicate that the alloy exhibit a significant damping capacity against large strain amplitudes more than 0.1%, probably due to the reversible motion of fcc/hcp interfaces. From these results, the NbC containing Fe-Mn-Si-based alloys are considered to be applicable to the seismic dampers in civil constructions..

**Keywords:** pseudoelasticity, damping capacity, internal friction, iron-manganese-silicon-based shape memory alloy, niobium carbide, nano precipitate, martensitic transformation

## **1. Introduction**

Fe-Mn-Si-based alloys are well known as low cost shape memory alloys (SMAs) [1]. The SMAs exhibit one-way shape memory effect (SME) associated with the stress-induced martensitic transformation from an fcc structure ( $\gamma$  austenite) to an hcp structure ( $\epsilon$  martensite) by deformation and its reversion by heating. It is also known that the SME is improved by the special thermomechanical treatment called “training”, which consists of several cycles of the stress-induced transformation by deformation and its reversion by heating [2].

Kajiwara et al. reported that the SME in Fe-Mn-Si-based alloys containing nano-size NbC precipitates exhibit nearly perfect SME without being subjected to the training treatment [3-10]. The martensite plates formed by applied stress are extremely thin (nano-scale) and of a single variant, which are very similar to the microstructural characteristics observed in the “trained samples” of the conventional Fe-Mn-Si-based SMAs [11].

Recently, the present authors pay much attention on the feasibility of these newly modified SMAs as a high damping material [12]. In order to investigate their damping properties, three kinds of mechanical properties, i.e. pseudoelasticity, internal friction and tension-compression fatigue behavior are under investigation. All of these

phenomena are commonly ascribed to the reversible motion of  $\gamma/\epsilon$  interfaces. It is likely that the refinement of martensite plates in NbC containing Fe-Mn-Si-based SMAs improves the damping properties of the alloys because of increase in the total area of the  $\gamma/\epsilon$  interfaces. The preferred orientation of the martensites may also affect on the damping properties in the specific direction.

This paper introduces some important findings in our study on the damping properties of a thermomechanically treated Fe-Mn-Si-based SMA containing NbC. In the following sections, we firstly make a brief review on martensitic transformation behavior and microstructural characteristics of the alloy (section 2), and then describe the pseudoelasticity (section 3), internal friction (section 4) and tension-compression low cycle fatigue properties (section 5) of the alloy. A particular emphasis is placed on the section 3.

## 2. Martensitic transformation behavior and microstructural characteristics

The chemical composition of all the specimens shown in this paper is Fe28Mn-6Si-5Cr-0.53Nb-0.06C (mass %). After solution and homogenization treatment at 1470K for 10h, a thermomechanical treatment, consisting of 14% pre-rolling at 870K and subsequent aging at 1070K for 10min, was carried out to generate fine NbC precipitates. The combination of the alloy composition and the process was previously established as the best condition for obtaining a good SME [7, 8]. Hereinafter, the term “pre-rolled” will be used referring to this condition. In some parts of this paper, the result for as-“solution treated” specimen is also shown for comparison.

The forward martensitic transformation start temperature ( $M_s$ ) of this alloy is below room temperature, while the reverse martensitic transformation start temperature ( $A_s$ ) and so-called the  $M_d$  temperature, above which the martensitic transformation cannot be induced by applying stress, are above room temperature. Therefore, the sample is in the single  $\gamma$  phase state at room temperature, and the stress-induced martensitic transformation into the  $\epsilon$  phase is caused by deformation, and its reversion takes place by subsequent heating.

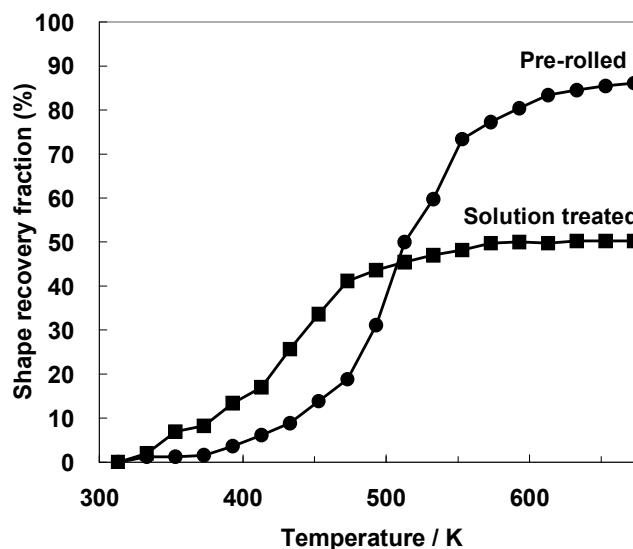


Fig. 1 The change in shape recovery fraction during heating. The initial strain of 3% was applied to the specimens prior to the measurements [12].

Here we mention the  $A_s$  and  $M_d$  temperatures of the alloy in detail, because the knowledge of these characteristic temperatures is very important for understanding the nature of pseudoelasticity that will be described in the next section. Figure 1 shows the change in shape recovery during heating, both for the pre-rolled and the solution treated specimens [12]. From the curves in this figure the  $A_s$  temperatures were obtained to be 320K for the solution treated specimen, and 370K for the pre-rolled specimen. The  $A_s$  is increased by the thermomechanical treatment. It is also found that the saturated value of shape recovery is higher for the pre-rolled specimen (90%) than that for the solution treated specimen (50%).

Figure 2 shows the 0.2% proof stresses measured at various temperatures [12]. The proof stress-temperature curves can be subdivided into two linear relationships with a positive and a negative slope for lower and higher temperature regions, respectively. It is considered that the deformation is dominated by stress-induced martensitic transformation in the lower temperature range, while by slip deformation in the higher temperature range. From this figure,  $M_d$  is determined as 370K for the solution treated specimen and 420K for the pre-rolled specimen, which indicates that the thermomechanical treatment to produce fine NbC carbides is effective to increase  $M_d$  temperature. It should be also noted that the stress level is much increased by the thermomechanical treatment for both the temperature regions.

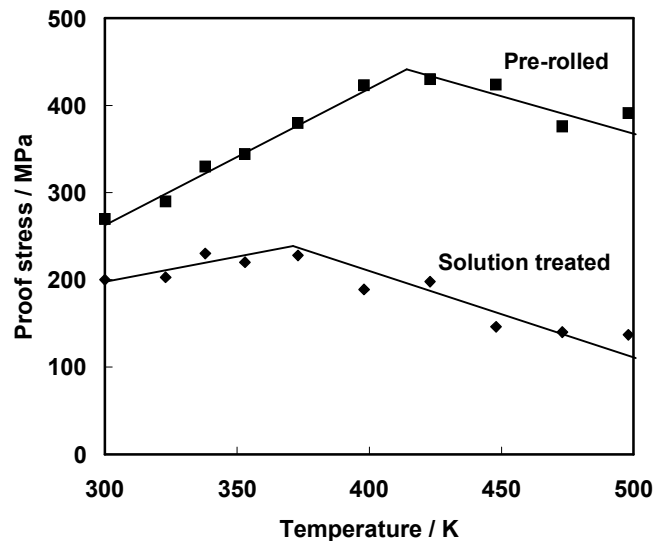


Fig. 2 The 0.2% proof stress as a function of temperature for pre-rolled specimens and solution treated specimens [12].

The microstructure of the pre-rolled specimen is characterized by nano-size NbC carbides dispersed inside grains (Fig. 3) and a considerable amount of stacking faults in the  $\gamma$  austenite [3, 9]. The  $\epsilon$  martensite plates formed by an external load are very thin because of the pretty fine NbC precipitates, which may act as nucleation sites of the  $\epsilon$  plates. The AFM observation revealed that the martensite is of a single variant, as shown in Fig. 4 [8], up to the deformation strain of about 4%. Most of the  $\epsilon$  plates reversely transform into the  $\gamma$  during heating, through the same crystallographic path with the forward transformation, and thus nearly perfect SME is achieved. When the deformation strain exceeds 4%, the other kinds of variants on different  $\{111\}$  habit

planes and in different  $\langle 112 \rangle$  shear directions start to generate, and SME starts to decrease.

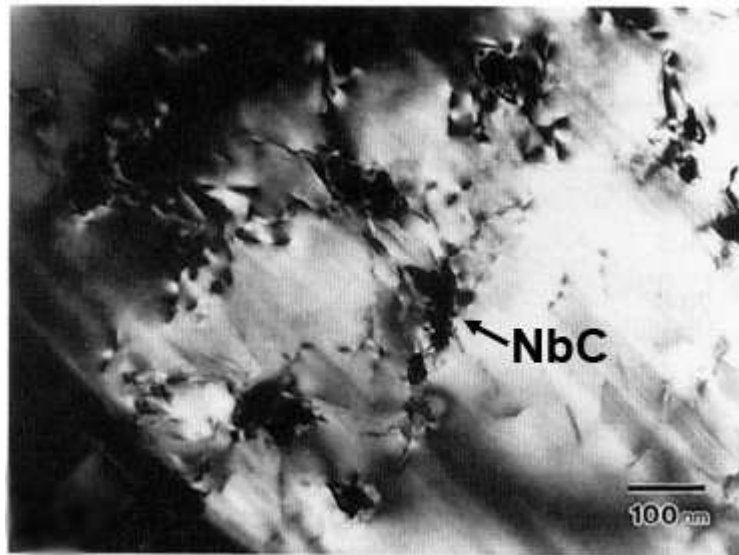


Fig. 3 Electron micrograph of NbC precipitates produced by aging at 1070K for 2h [9].

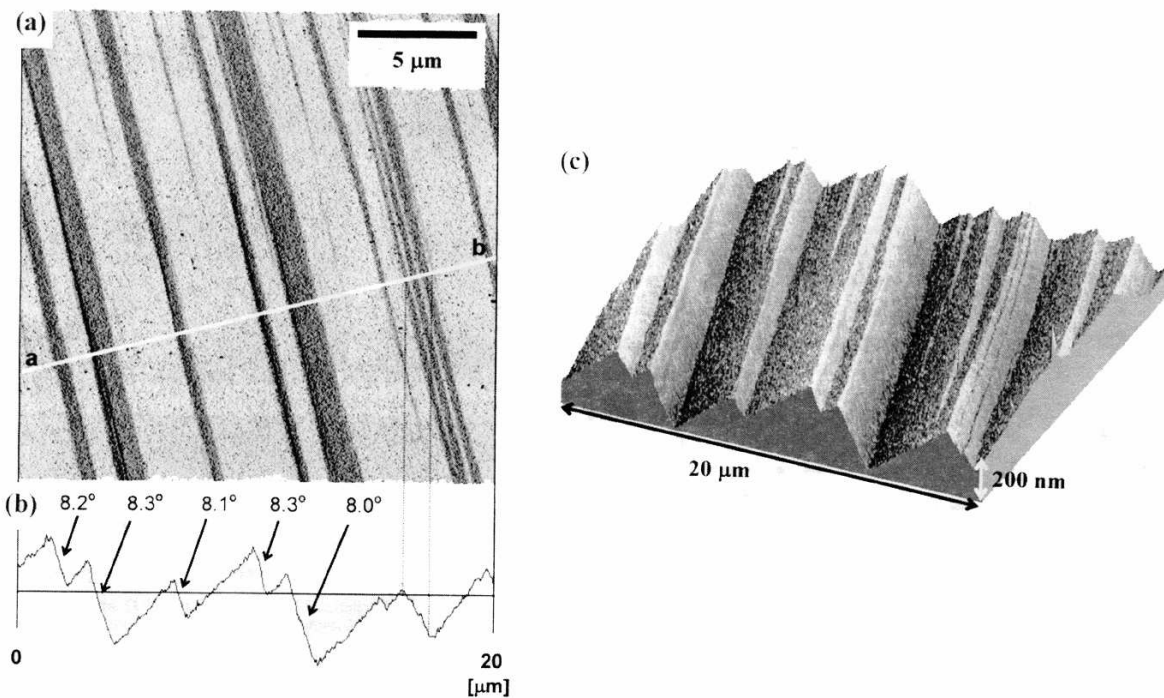


Fig. 4 (a) AFM micrograph of martensite plates formed in the thermomechanically treated sample. (b) Cross section curve along white line in (a). (c) Three dimensional picture of surface relief of martensite plates [8].

On the other hand, in the solution treated specimen, Nb and C are considered to exist as a substitutional atom and an interstitial atom, respectively. The  $\epsilon$  formed in the specimen is of multiple variants even for small deformation strains of about 2%, and the SME is incomplete.

### 3. Pseudoelasticity

It is widely accepted that the pseudoelasticity in thermoelastic SMAs such as Ti-Ni-based alloys and Cu-based alloys, which is also called as “superelasticity”, is caused by the stress-induced martensitic transformation on loading and the reverse martensitic transformation on unloading. In this paper, “transformation pseudoelasticity” is used referring to the pseudoelasticity based on the above mechanism, while solely the “pseudoelasticity” is used unless its physical nature becomes clear. It is traditionally believed that transformation pseudoelasticity cannot occur in “non-thermoelastic” Fe-Mn-Si-based SMAs. Recently, however, several researchers reported that the pseudoelasticity was observed when the test temperature was elevated above the reverse martensitic transformation temperature [13-15], which is similar to that of the thermoelastic SMAs. In these papers, however, the pseudoelasticity was described only as the one-time spring-back on unloading and, therefore, the reproducibility of the pseudoelasticity is still unclear.

The pseudoelasticity was also reported at and below room temperature, in spite of the fact that the testing temperatures are well below the  $A_s$  [16, 17]. The phenomenon was ascribed to the reversible motion of the  $\gamma/\varepsilon$  interfaces. However, it is impossible to explain the driving force of the reverse martensitic transformation at temperatures below  $A_s$  by the conventional theory of transformation pseudoelasticity. Because of these conflicting experimental results and the lack of the detailed mechanism, the existence of the pseudoelasticity in the Fe-Mn-Si-based SMAs is still questionable.

We investigated this issue by using our newly modified Fe-Mn-Si based SMAs containing NbC. The existence of pseudoelasticity was examined by measuring stress-strain curves during stepwise loading and unloading with increasing the maximum strain ( $\varepsilon_a$ ) up to 1.0% in the step of 0.2%. The measurements were done at RT, 350K, 400K, 450K and 500K for the solution treated and pre-rolled specimens. Figure 5 shows the results for the solution treated specimen at 350K as a representative.

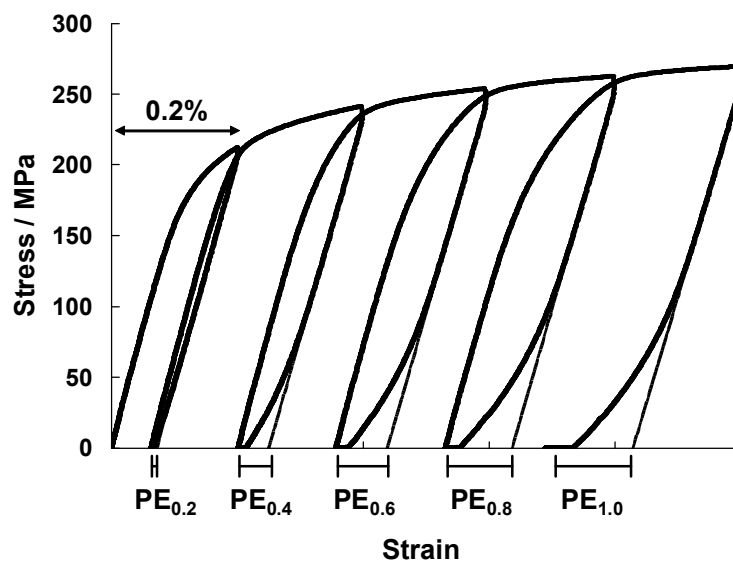


Fig. 5 Stress-strain curves during stepwise loading and unloading with increasing strain up to 1.0% in step of 0.2% at 350K for the solution treated specimens [12].

Non-linearity in the lower stress portion of unloading curves and strain hysteresis are clearly seen in these figures. The strain hysteresis increases with increasing  $\epsilon_a$ .

The pseudoelastic recovery strain (PE) was obtained from the stress-strain curves, by subtracting the elastic recovery (dotted lines) from the total recovery strain at each  $\epsilon_a$ , as illustrated in Fig. 5. The values of PEs are plotted as a function of deformation temperature in Fig. 6. The PE first increases with increasing deformation temperature, reaching the maximum value at 350K for the solution treated specimen and 400K for the pre-rolled specimen, respectively, and then decreases with increasing deformation temperature. The PEs of the pre-rolled specimen are smaller at room temperature than those of the solution treated specimen, while the maximum PEs of the pre-rolled specimen are larger than those of the solution treated specimen.

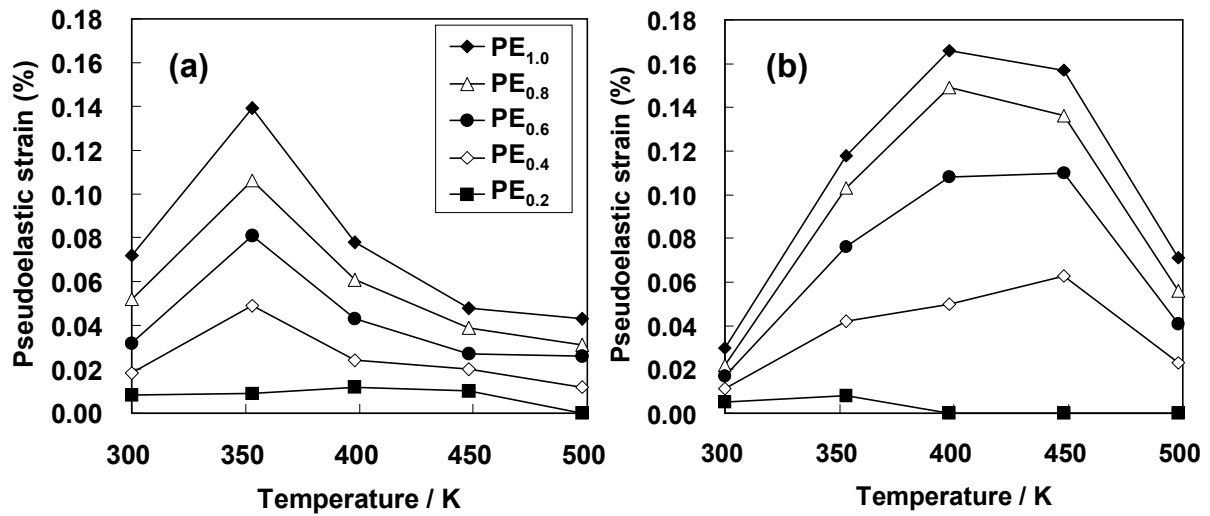


Fig. 6 Pseudoelastic strain as a function of deformation temperature for (a) the solution treated specimens and (b) the pre-rolled specimens [12].

Assuming that this partial shape recovery with non-linearity is due to transformation pseudoelasticity, the temperature dependence of pseudoelasticity can be successfully explained as follows.

- 1) The increase in pseudoelastic strain with increasing deformation temperature, shown in the lower temperature regime of Figs. 6, is expected to occur because the deformation temperature exceeds  $A_s$ .
- 2) The  $A_s$  of the solution treated specimen is lower than that of the pre-rolled specimen. The reverse martensitic transformation starts just above room temperature in the solution treated specimen, as shown in Fig. 1. That is the reason why the PE values at room temperature of the solution treated specimen are higher than those of the pre-rolled specimen.
- 3) It is found by comparing the curves in Figs. 2 and 6 that the temperature where the maximum PE value is obtained coincides with the  $M_d$  temperature for both the cases of the solution treated and pre-rolled specimens. This fact indicates that the decrease in PE value at higher temperature is due to that slip deformation becomes dominant than the deformation by the stress-induced martensitic transformation. It was also found that the thermomechanical treatment improves the pseudoelasticity of the alloy by increasing  $M_d$ .

As shown in Fig. 6, no obvious pseudoelasticity is observed in the stress-strain

curves for smaller  $\varepsilon_a$  at room temperature, while the pseudoelasticity can be seen for the case of larger  $\varepsilon_a$ . When the sample is in the two-phase state composed of the stress-induced  $\varepsilon$  and the remaining  $\gamma$ , the pseudoelasticity is more clearly recognized at room temperature. Figure 7 shows stress-strain curves during cyclic loading and unloading with  $\varepsilon_a=0.3\%$  measured in the pre-rolled specimen, in which a certain amount of the  $\varepsilon$  was initially induced by applying a strain of 2.0 %.

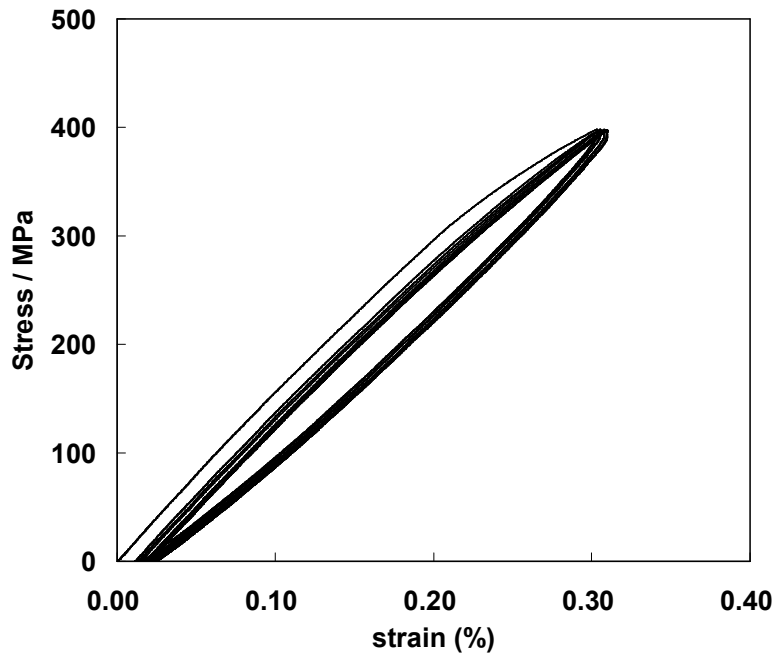


Fig. 7 Pseudoelasticity of the pre-rolled specimen during cyclic loading and unloading with  $\varepsilon_a = 0.3\%$  [12].

The strain rate was set at 0.1 mm/min from the first to the third cycles. Then the strain rate was increased to 0.2mm/min in the 4th cycle, 0.3mm/min in the 5th cycle, and decreased to 0.05mm/min in the 6th cycle and 0.025mm/min in the 7th cycle. The pseudoelasticity with non-linearity and strain hysteresis appears in the curves. The residual strain is about 0.01% in the first cycle, but it become negligible after the second cycle. Thus the perfect pseudoelasticity is reproducibly obtained in the further cycling. It should also be noted that the pseudoelasticity is almost independent of the strain rate.

These facts imply that the increase in the  $\gamma/\varepsilon$  interfaces contributes to enhancing the pseudoelasticity. This phenomenon cannot be explained only by the conventional idea of transformation pseudoelasticity, since the testing temperature is lower than  $A_s$ , where the stress-induced martensite is thermodynamically stable. It becomes possible to interpret the pseudoelasticity by the reversible motion of the  $\gamma/\varepsilon$  interfaces, if the back-stress produced around the tip of growing martensite plates is taken into account. In the case of the  $\gamma/\varepsilon$  martensitic transformation, there will be a large pile up of Shockley partial dislocations with the same sign [11, 18, 19]. The accumulation of dislocations with the same sign produces a large stress field around the tip of the martensite and acts as the back-stress on the growing martensite. The effect of the back-stress on the reversibility of the  $\gamma/\varepsilon$  transformation was also proposed by Bergeon et al. [18].

The pseudoelasticity below  $A_s$  was reported in some Fe-Mn-Si-based alloys [16, 17, 20]. In these papers, the pseudoelasticity was described as the large spring-back with non-linearity. In the present study, the reproducibility of the pseudoelasticity was also revealed, as shown in Fig. 7. It should be emphasized that the perfect pseudoelasticity was obtained reproducibly when the specimen was subjected to cyclic loading and unloading.

In summary, the existence of the pseudoelasticity in Fe-Mn-Si-based SMAs is proved by some indirect, but strong, evidences. The pseudoelasticity below  $A_s$  is probably due to the back-stress produced by Shockley partial dislocations residing at the tip of the martensite plates. The perfect pseudoelasticity was obtained reproducibly when the sample was subjected to cyclic loading and unloading. The pseudoelasticity is improved by pre-warm rolling and subsequent aging. Further studies are being carried out, especially on their microstructural evidence.

#### 4. Internal friction

The Fe-Mn-based alloys undergoing  $\gamma/\varepsilon$  martensitic transformation have been regarded as low cost high damping alloys [21-27]. The alloys exhibit strain-amplitude-dependent internal friction, which is ascribed to the reversible motion of  $\gamma/\varepsilon$  interfaces. Fe-Mn-Si-based SMAs were also found to show strain amplitude-dependent internal friction, but only a limited number of investigations have been performed on damping properties of the SMAs. We investigated the internal friction of the NbC containing alloys using a dynamic mechanical analyzer (DMA). Figure 8 shows the internal friction ( $\tan\Phi$ ) as a function of strain amplitude, for the pre-rolled specimen in the single  $\gamma$  phase state, the pre-rolled specimen in the two-phase state of the stress-induced  $\varepsilon$  and the remaining  $\gamma$ , and that solution treated in the single  $\gamma$  phase state.

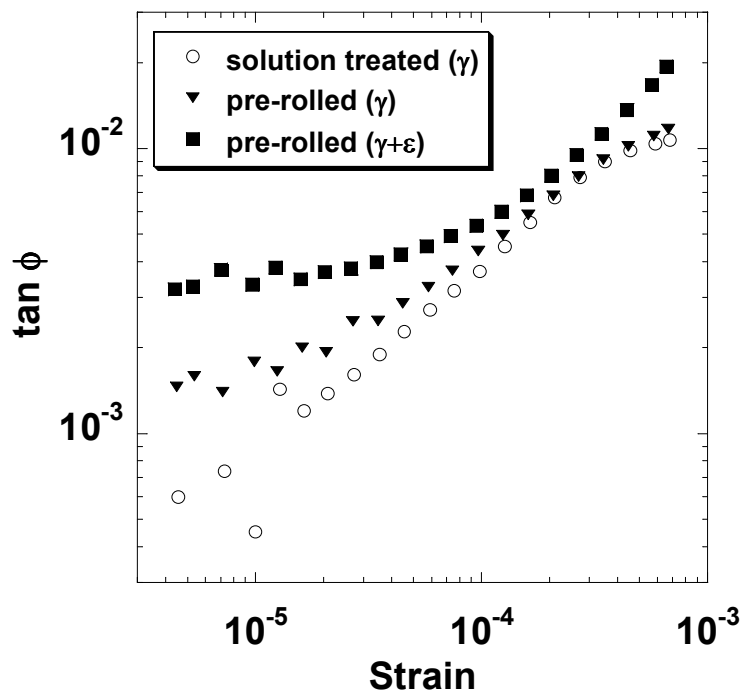


Fig. 8 Strain amplitude dependence of internal friction

Principal features shown in the figure are summarized as: 1)  $\tan\Phi$  increases with increasing strain amplitude. 2)  $\tan\Phi$  increases with increasing amount of the stress-induced  $\varepsilon$ . 3)  $\tan\Phi$  is enhanced by the thermomechanical treatment. We also measured the internal friction as a function of vibration frequency, and found that  $\tan\Phi$  is independent of vibration frequency. The above features are in a good accordance with the results of the pseudoelasticity.

### 5. Tension-compression fatigue behaviour

Nowadays, in the field of civil engineering of Japan, low yield point steels are paid much attention as a seismic damper in civil constructions [28]. As shown in Fig. 8, Fe-Mn-Si-based SMAs seem to show a significant damping capacity against vibrations with larger strain amplitudes above  $10^{-3}$ , indicating that they are also a prospective candidate as seismic damping material in civil constructions. Damping capacity in large strain amplitude region is usually evaluated by low cycle fatigue properties during cyclic tension and compression. However, no such effort has ever been done on Fe-Mn-Si-based SMAs.

The present authors investigated the damping capacity of the NbC containing Fe-Mn-Si-based SMAs in large strain amplitude region by tension-compression low cycle fatigue tests (LCF). The sinusoidal strain oscillation with the vibration frequency of 0.5Hz and with the  $\varepsilon_a$  of 0.2, 0.4, 0.8, 1.2, 1.6, and 2.0% was applied to the specimen and the resultant stress was measured. The measurements were repeated 10 cycles for each  $\varepsilon_a$ . The result is shown in Fig. 9.

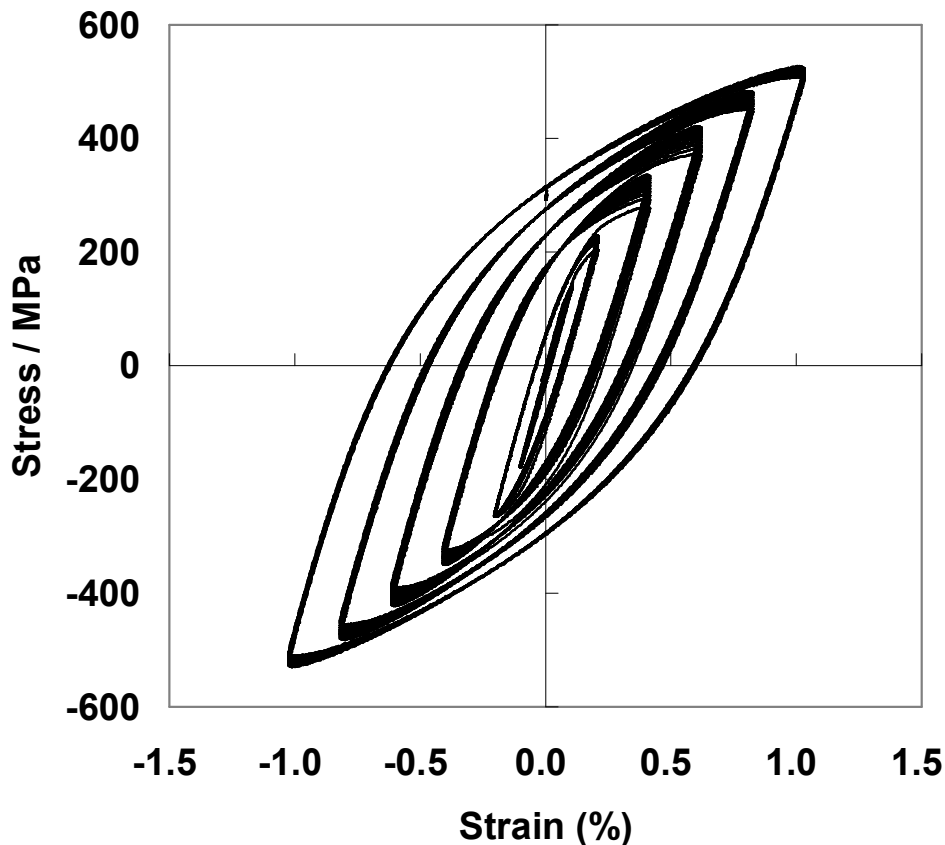


Fig. 9 Low cycle fatigue properties of the thermomechanically treated specimen

It is obvious in the stress-strain curves with a large strain hysteresis that the alloy exhibits a significant damping capacity. It is also noted that work hardening is very small and the damping property is stable during 10 cycles of loading.

The specific damping capacity (SDC) was calculated from the strain hysteresis for each  $\varepsilon_a$  in Fig. 9. The SDC values are plotted as a function of strain amplitude in Fig. 10. The values of  $\tan\Phi$  measured by DMA were also converted into the SDC, and plotted in Fig. 10. There is a good continuity between the SDC-strain amplitude relationship measured by DMA and that measured by LCF.

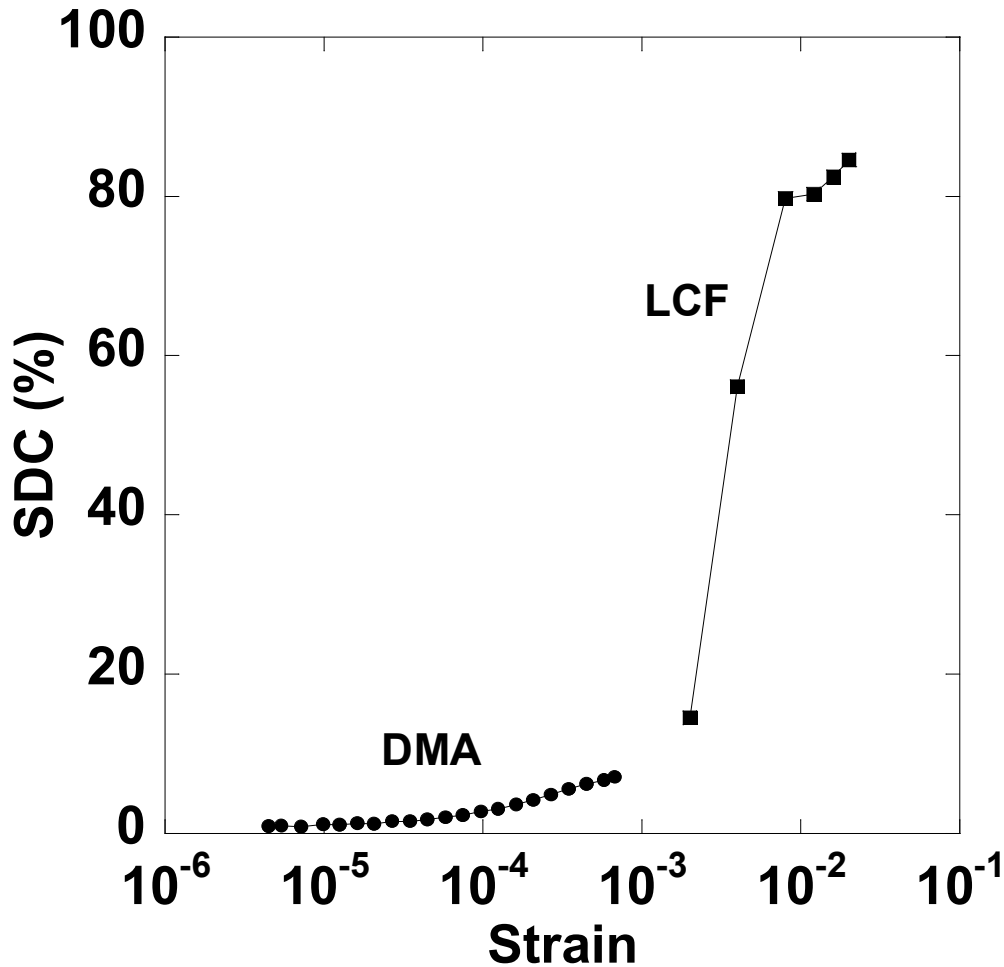


Fig. 10 Strain amplitude dependence of internal friction of the thermomechanically treated specimen measured by DMA and LCF.

## 6. Concluding remarks

Pseudoelasticity, internal friction, and tension-compression fatigue behavior were comprehensively investigated in a thermomechanically treated Fe-Mn-Si-based SMA containing NbC to clarify its damping capacity. The results commonly indicate that the alloy exhibit a significant damping capacity against large strain amplitudes more than 0.1%, probably due to the reversible motion of  $\gamma/\varepsilon$  interfaces. From these

results, it is concluded that the NbC containing Fe-Mn-Si-based alloys are considered to be applicable to the seismic dampers in civil constructions.

Received May 9, 2005

National Institute for Materials Science  
\*Takenaka Corporation  
Japan

## REFERENCES

- [1] A. Sato, E. Chishima, K. Soma, T. Mori, *Acta Metall.* 30 (1982) 1177-1183.
- [2] H. Otsuka, M. Murakami, S. Matsuda, *Proc. MRS Int'l. Mtg. on Adv. Mats.*, vol 9, Tokyo, 1989, pp. 451-456.
- [3] A. Baruj, T. Kikuchi, S. Kajiwara, *Mater. Sci. Eng. A* 378 (2004) 337-342.
- [4] A. Baruj, T. Kikuchi, S. Kajiwara, N. Shinya, *Mater. Sci. Forum* 394-3 (2002) 403-406.
- [5] A. Baruj, T. Kikuchi, S. Kajiwara, N. Shinya, *Mater. Trans.* 43 (2002) 585-588.
- [6] A. Baruj, T. Kikuchi, S. Kajiwara, N. Shinya, *J. Phys. IV* 112 (2003) 373-376.
- [7] A. Baruj, T. Kikuchi, S. Kajiwara, N. Shinya, *Mater. Sci. Eng. A* 378 (2004) 333-336.
- [8] S. Kajiwara, A. Baruj, T. Kikuchi, N. Shinya, *Proc. SPIE* 5053 (2003) 250-261.
- [9] S. Kajiwara, D. Liu, T. Kikuchi, N. Shinya, *Scripta Mater.* 44 (2001) 2809-2814.
- [10] S. Kajiwara, D. Z. Liu, T. Kikuchi, N. Shinya, *J. Phys. IV* 11 (2001) 199-204.
- [11] D. Z. Liu, S. Kajiwara, T. Kikuchi, N. Shinya, *Philos. Mag.* 83 (2003) 2875-2897.
- [12] T. Sawaguchi, T. Kikuchi, S. Kajiwara, *Smart Mat. Struct.* (2005) to be published.
- [13] C. L. Li, D. J. Cheng, Z. H. Jin, *Mater. Sci. Eng. A* 325 (2002) 375-379.
- [14] H. Otsuka, K. Nakajima, T. Maruyama, *Mater. Trans.*, JIM 41 (2000) 547-549.
- [15] O. Matsumura, T. Sumi, N. Tamura, K. Sakao, T. Furukawa, H. Otsuka, *Mater. Sci. Eng. A* 279 (2000) 201-206.
- [16] X. X. Wang, C. Y. Zhang, *Journal of Mater. Sci. Lett.* 17 (1998) 1795-1796.
- [17] J. H. Yang, H. Chen, C. M. Wayman, *Metall. Trans. A* 23 (1992) 1431-1437.
- [18] N. Bergeon, G. Guenin, C. Esnouf, *Mater. Sci. Eng. A* 242 (1998) 77-86.
- [19] S. Kajiwara, *Mater. Sci. Eng. A* 275 (1999) 67-88.
- [20] D. Wang, W. Liu, X. Xing, Z. Dong, J. Chen, *SMST-2000 Conf. Proc.* (2000) 141-146.
- [21] S. H. Baik, J. C. Kim, K. K. Jee, M. C. Shin, C. S. Choi, *ISIJ Int'l.* 37 (1997) 519-522.
- [22] N. Igata, H. Aoyama, Y. Kanja, Y. Habara, *J. Phys. IV* 6 (1996) 791-794.
- [23] K. K. Jee, J. H. Han, W. Y. Jang, *Mater. Sci. Eng. A* 378 (2004) 319-322.
- [24] K. K. Jee, K. Ito, M. C. Shin, *ISIJ Int'l.* 34 (1994) 912-916.
- [25] K. K. Jee, W. Y. Jang, S. H. Baik, M. C. Shin, *Mater. Sci. Eng. A* 275 (1999) 538-542.
- [26] K. K. Jee, W. Y. Jang, S. H. Baik, M. C. Shin, C. S. Choi, *Scripta Mater.* 37 (1997) 943-948.
- [27] H. Okada, H. Sahashi, I. S. Kim, C. Y. Kang, N. Igata, K. Miyahara, *Mater. Sci. Eng. A* 370 (2004) 519-523.
- [28] E. Saeki, M. Sugisawa, T. Yamaguchi, A. Wada, *J. Mater. Civil. Eng.* 10 (1998) 143-152.

## PSEUDOELASTICITATE ȘI PROPRIETĂȚI DE AMORTIZARE ASOCIATE CU TRANSFORMAREA MARTENSITICĂ CFC/HC IN ALIAJELE PE BAZĂ DE Fe-Mn-Si CARE CONȚIN NbC

### (Rezumat)

Aliajele cu memoria formei care conțin NbC sunt candidate potențiale pentru materialele cu înaltă capacitate de amortizare. Această lucrare recapitulează pseudoelasticitatea, frecarea internă și comportarea la oboseală prin torsiune-compresiune care au fost investigate în mod cuprinzător în cazul unui aliaj Fe<sub>28</sub>Mn-6Si-5Cr-0.53Nb-0.06C (%m.), tratat termomecanic, cu accent special asupra pseudoelasticității. Rezultatele sunt discutate în funcție de comportarea la transformarea martensitică și de caracteristicile microstructurale ale aliajului fiind de asemenea discutat și efectul tratamentului termomecanic. Rezultatele arată în mod obișnuit că aliajul prezintă o semnificativă capacitate de amortizare corespunzătoare unor amplitudini cu deformație mare de peste 0,1 %, datorată probabil deplasării reversibile a interfeței cfc/hc. Din aceste rezultate, aliajele pe bază de Fe-Mn-Si se consideră a fi aplicabile pentru amortizoare seismice în construcțiile civile.



## THE DETERMINATION OF THE FILLING DEGREE AT INDIRECT EXTRUSION FOR THE NUT-LIKE PRODUCTS MADE FROM CYLINDER SEMI-PRODUCTS

BY

C. BEJINARIU, V. MOLDOVEANU, D. A. GHEORGHIU and St. L. TOMA

**Abstract:** *The paper shows the analytic determination of the degree of the edges filling of the pieces and the conclusions which lead to the optimum shape determination of the semi-product to obtain a maximum degree of filling of the pieces edges.*

**Keywords:** *indirect extrusion; steel; cylinder semi-product; degree of filling.*

### 1. Introduction

On the indirect extrusion of the nut-like products, the analysis of the existing processes and of the experiments made, showed that complete filling of the edges on the entire high doesn't take place.

For these types of pieces between the margins of the mould and semi-product cylinder, during the initial moment, there is a movement, so the deforming process takes place in two stages – an open perforation in which contractions appear on the frontal side and the high is reduced until the semi-product contacts the edges of the mould and then comes the so-called extrusion phase when the metal come below the stamp it is distributed to the corners of the mould cavities lower from the frontal part of the stamp and the edges of the pieces start to complete during the deformation process.

### 2. The analytic determination of the filling degree of the pieces edges

Starting from cylinder-like semi-product showed in figure 1.a, through indirect extrusion a raw nut-like piece is obtained, figure 1.b, those edges are incompletely filled.

The value of the incompleteness edges on the vertical plane is noted with  $H_3$ .  $\alpha$  and  $\delta$  depend on the high deformation degree and on the surface and can be determined experimentally.





$$H_3 = D_2 B_2 = \frac{D}{2} \operatorname{tg} \alpha (1 + \cos \beta). \quad (10)$$

Then, particularizing for  $\beta = \frac{\pi}{6}$  (in this case the regular polygon becomes a hexagon) results:

$$H_3 = \frac{2 - \sqrt{3}}{4} \cdot D \cdot \operatorname{tg} \alpha. \quad (11)$$

Replacing (11) relation in relation (1) we have the degree of filling edges for nut-like products with a regular hexagonal exterior profile out of cylindrical semi-product.

$$G_u = \left( 1 - \frac{2 - \sqrt{3}}{4} \cdot \frac{D}{H_2} \cdot \operatorname{tg} \alpha \right) \cdot 100 \text{ [%]}. \quad (12)$$

### 3. Conclusions

Out of the relation (12) analysis results that the 100% of filling degree of the pieces edges is achieved when  $\operatorname{tg} \alpha \rightarrow 0$ , so the angle  $\alpha \rightarrow 0$ . Hence, we can draw the conclusion that for the achievement of a higher filling degree of the piece edges it is necessary that semi-product should be in the shape of a cylinder-truncated cone, the value of the chamfering angle being chosen so that after the extrusion the following formula results  $\alpha \approx 0$ .

*Received, May, 10, 2005*

*Technical University "Gh. Asachi" Iassy.*

#### DETERMINAREA GRADULUI DE UMLERE A MUCHIILOR PIESEI LA EXTRUDAREA INDIRECTA A PRODUSELOR DE TIP PIULITA DIN SEMIFABRICATE CILINDRICE

##### (Rezumat)

Lucrarea prezinta determinarea analitica a gradului de umplere a muchiiilor piesei si concluziile care conduc la determinarea formei optime a semifabricatului pentru obtinerea unui grad de umplere maxim a muchiiilor piesei.

## THE ANALYTIC CALCULATION OF THE CYLINDER-TRUNCATED CONE SEMI-PRODUCT TO OBTAIN NUT-LIKE PRODUCTS BY INDIRECT EXTRUSION

BY

C. BEJINARIU, L. ZAHARIA, V. V. MOLDOVEANU and St. L. TOMA

**Abstract:** *The paper shows the necessary knowledge for the analytic calculation of the cylinder-truncated cone semi-product to obtain nut-like products by indirect extrusion.*

*In the same time it determines the shape and size of a semi-product in the period of deformation by indirect extrusion.*

**Keywords:** *indirect extrusion; cylinder-truncated cone semi-product; union nut.*

### 1. Introduction

In general, nut-like products present in the front-side chamfering of the edges. At the indirect extrusion from the cylindrical semi-product a deformation of the front surface takes place because of the movement which takes place between the semi-product and the margins of the mould, having as effect the formation of a conical surface of  $\delta$  angle shown in figure 1.

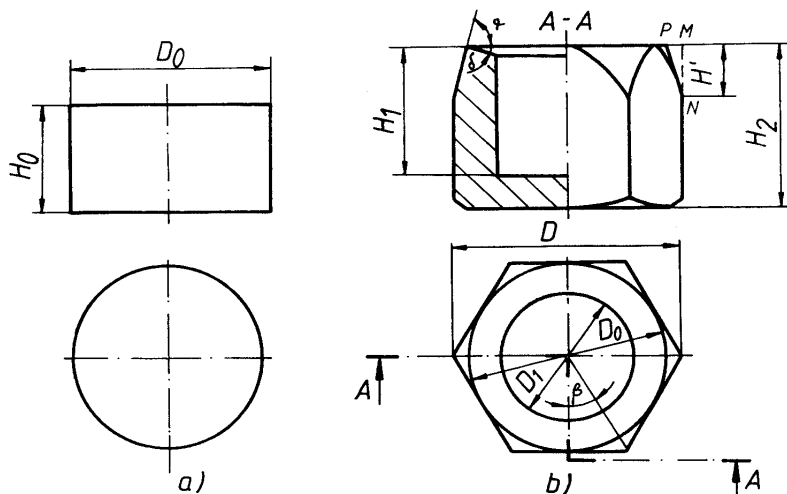


Figure 1. a) cylindrical semi-product ; b) raw nut-like piece.

This process leads to the conclusion that to obtain the chamfering prescribed angle of the edges of the pieces,  $\alpha_1$ , it is necessary to use a cylinder-truncated cone shape semi-product, figure 2.

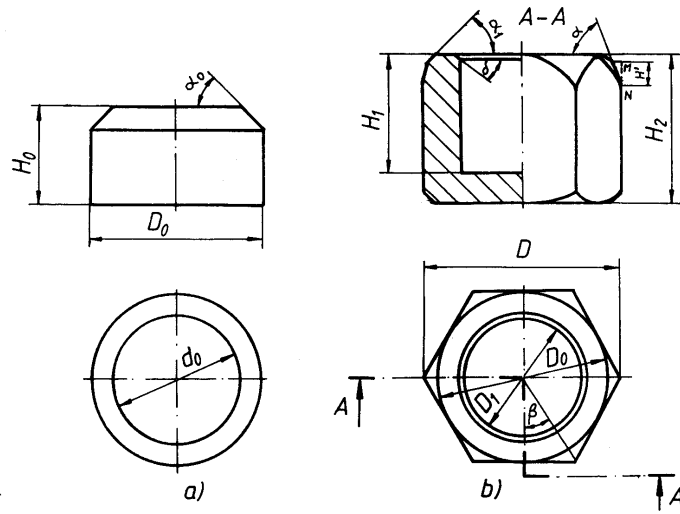


Figure 2. a) cylinder-truncated cone semi-product; b) raw nut-like piece.

On the other hand, this shape presents the advantage of creating a metal reserve within truncated-cone necessary for the filling the movement between the cylinder part of the semi-product and the margins of the mould, which leads to a maximum filling degree of edges of the pieces.

## 2. The analytic calculation of the size of the cylinder-truncated cone semi-product

### Initial data

For the semi-product:

- volume of the semi-product,  $V$ ;
- diameter of the cylinder semi-product side,  $D_0$ ;
- chamfering angle  $\alpha_0$ , which is determined by relation:

$$\alpha_0 = \alpha_1 + \delta. \quad (1)$$

For the stamp:

- diameter of the frontal side,  $D_1$ , according to figure 3;
- area of the frontal surface stamp,  $S_p$ , which is determined by relation:

$$S_p = \frac{\pi D_1^2}{4}. \quad (2)$$

For the mould:

- number of regular side of the polygon,  $n$ , according to figure 4;
- diameter of the regular polygon circumscribed the circle;
- transversal area between cylinder side of the semi-product and the margins of the mould,  $S_h$ , which is determined by relation:

$$S_h = \frac{n}{8} D^2 \cdot \sin \frac{2\pi}{n} - \frac{\pi}{4} D_0^2. \quad (3)$$

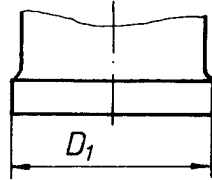


Figure 3. Active side of the stamp.

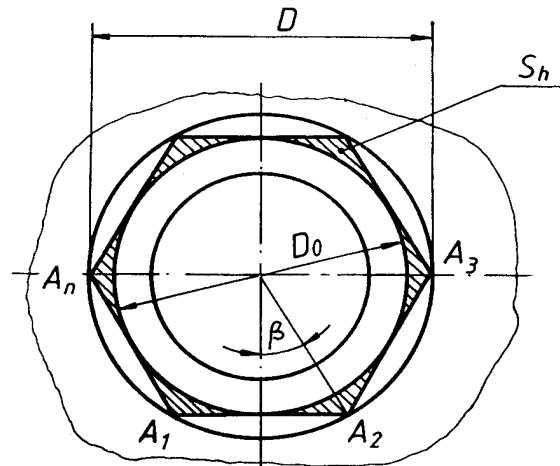


Figure 4. Generalized mould.

**Final data, figure 2.a)**

- semi-product high,  $H_0$ ;
- the chamfering value on axial direction,  $a$ ;
- diameter,  $d_0$ .

The value of the semi-product chamfering on the axial direction,  $a$ , is determined on condition that the volume of the metal moved out of place by the stamp,  $V_d$ , on the distance  $a$  should be bigger or equal with the metal volume,  $V_h$ , necessary for edges of the mould filling on the semi-product cylinder side, that is on the high  $H_0 - a$ . The analytic expression of the condition is:

$$V_d \geq V_h. \tag{4}$$

But:

$$V_d = S_p \cdot a, \tag{5}$$

$$V_h = S_h (H_0 - a). \tag{6}$$

By replacing relations (5) and (6) in relation (4), results:

$$S_p \cdot a \geq S_h (H_0 - a) \tag{7}$$

or:

$$a \geq \frac{S_h}{S_h + S_p} \cdot H_0. \tag{8}$$

Noting the surfaces report with  $R_s$ , so

$$R_s = \frac{S_h}{S_h + S_p}. \tag{9}$$

Results:

$$a \geq R_s \cdot H_0. \tag{10}$$

On the other hand, the volume of the semi-product,  $V$ , can be written as the sum between cylinder side volume,  $V_1$ , and truncated cone side,  $V_2$ , that is,

$$V = V_1 + V_2. \tag{11}$$

But,

$$V_1 = \frac{\pi}{4} \cdot D_0^2 (H_0 - a), \quad (12)$$

$$V_2 = \frac{\pi}{12} \cdot a \cdot \left( 3 D_0^2 - 6 \frac{a \cdot D_0}{\operatorname{tg} \alpha_0} + 4 \frac{a^2}{\operatorname{tg}^2 \alpha_0} \right). \quad (13)$$

By replacing relations (12) and (13) in relation (11), results:

$$V = \frac{\pi}{12} \left( 3 D_0^2 H_0 - 6 \frac{a^2 D_0}{\operatorname{tg} \alpha} + 4 \frac{a^3}{\operatorname{tg}^2 \alpha_0} \right). \quad (14)$$

By considering the equality case in relation (10), so

$$a = R_s \cdot H_0 \quad (15)$$

and replacing relation (15) in relation (14), results:

$$V = \frac{\pi}{12} \left( 3 D_0^2 H_0 - 6 \frac{R_s^2 D_0}{\operatorname{tg} \alpha_0} H_0 + 4 \frac{R_s^2}{\operatorname{tg}^2 \alpha_0} H_0^3 \right) \quad (16)$$

or

$$4 \frac{R_s^3}{\operatorname{tg}^2 \alpha_0} H_0^3 - 6 \frac{R_s^2 D_0}{\operatorname{tg} \alpha_0} H_0^2 + 3 D_0^2 H_0 - \frac{12}{\pi} V = 0. \quad (17)$$

Relation (17) represents a three degree polynomial equation in  $H_0$  unknown, equation which can have either two conjugated complex solutions and a real one or three real solutions. To establish this I appeal to the roots squares sum calculation. Thus:

$$\sum_{i=1}^{i=3} H_{0i}^2 = \frac{3}{2} \cdot \left( \frac{D_0}{R_s} \right)^2 \cdot \operatorname{tg}^2 \alpha_0 \cdot \left( \frac{3}{2} - \frac{1}{R_s} \right). \quad (18)$$

As for the indirect extrusion,

$$R_s < \frac{2}{3}, \quad (19)$$

results:

$$\sum_{i=1}^{i=3} H_{0i}^2 < 0. \quad (20)$$

From relation (20) it can be immediately deduced that equation (17) admits a real solution and two conjugated complex solutions.

Also, the sign and the minimum value of the real root can be established.

The associated function to equation (17) intersects the ordinate to the negative value  $-\frac{12}{\pi} \cdot V$ , so the sign of the real root is positive.

The minimum value of the real root is obtained when  $n \rightarrow \infty$ , and it leads to  $R_s \rightarrow 0$ . Replacing  $R_s = 0$  in equation (17), results:

$$H_{0\min} = \frac{4}{\pi} \frac{V}{D_0^2}. \quad (21)$$

so,

$$H_0 > \frac{4}{\pi} \cdot \frac{V}{D_0^2}. \quad (22)$$

By solving equation (17), the theoretical value of the semi-product high,  $H_{0t}$ , is obtained.

By replacing  $H_0$  with  $H_{0t}$  in relation (15), the theoretical value,  $a_t$ , of the semi-product chamfering on the axial direction is obtained:

$$a_t = R_s \cdot H_{0t}. \quad (23)$$

Considering relation (10):

$$a = [a_t] + 1, \quad (24)$$

where  $[a_t]$  is the entire part of the number  $a_t$ .

Knowing the practical value of the semi-product chamfering on the axial direction,  $a$ , the practical value of the semi-product high,  $H_0$ , from relation (14) can be determined. So:

$$H_0 = \frac{4V}{\pi D_0^2} + \frac{2a^2}{D_0 \cdot \operatorname{tg} \alpha_0} - \frac{4a^3}{3D_0^2 \cdot \operatorname{tg}^2 \alpha_0}. \quad (25)$$

Diameter,  $d_0$ , is determined by the relation:

$$d_0 = D_0 - \frac{2a}{\operatorname{tg} \alpha_0}. \quad (26)$$

### 3. Conclusions

To obtain nut-like products through indirect extrusion, the use of the cylinder shape semi-product is not reasonable.

The use of the cylindrical-truncated cone shape semi-product, in case  $d_0 \geq D_1$ , leads to the desired result, that is, the achievement of the raw nut piece through indirect extrusion, eliminating the supplementary operations of caulking and callipering.

If  $\alpha_0$  angle has low values, then  $d_0 < D_1$  and the condition given by relation (4) is not observed. In this case, the metal reserve below the stamp  $V_d$ , can not assure the mould edges filling on  $H_0 - a$  distance, so the piece will be incompletely filled.

To increase the metal reserve below the stamp, in case  $d_0 < D_1$ , the authors propose the cylindrical-ellipsoidal shape of the semi-product. The truncated cone side of the semi-product will be replaced by a semi-ellipsoid obtained through rotation around semi-product axis of a quarter of ellipse with semi-axes  $a$  and  $\frac{D_0}{2}$ .

Nut-like products are known to have chamfering to both frontal surfaces. Owing to this, both cylindrical-double truncated cone shape and cylindrical-double

ellipsoidal semi-products can be used. Depending on the metal volume necessary during the process, the high of the cylindrical side can be  $H_0 - 2a = 0$ , so the semi-product has an ellipsoidal shape. In the case in which the ellipsoidal semi-axes become equally,  $a = \frac{D_0}{2}$ , the semi-product has a spherical shape.

*Received, May, 10, 2005*

*Technical University "Gh. Asachi" Iassy.*

**CALCULUL ANALITIC A DIMENSIUNILOR SEMIFABRICATULUI CILINDRO-TRONCONIC  
PENTRU OBTINEREA PRIN EXTRUDARE INDIRECTA A PRODUSELOR DE TIP PIULITA**

**(Rezumat)**

Lucrarea pune la dispozitie cunostintele necesare privind calculul analitic al dimensiunilor semifabricatului cilindro-tronconic pentru obtinerea prin extrudare indirecta a produselor de tip piulita.

De asemenea, se urmareste determinarea teoretica a formei si dimensiunilor unui semifabricat in cursul deformarii prin extrudare indirecta.

## AUDITABLE INTRAORGANIZATIONAL ACTIVITIES

BY

**IONEL BOSTAN**

**Abstract:** Internal controls make this system coherent and may be grouped in the following six categories: objectives, means, information systems, organization, procedures and supervision.

**Key words:** audit missions, weaknesses, dysfunctions, errors, internal control, procedural chain

### 1. Introduction

The evolution of risks run by the functions/activities/sub-activities/operations and determination of their control activities is a major concern of management. Managers, like auditors, must know exactly the functions assigned to them in order to determine the control activities that need to be implemented in order to ensure an efficient operation.

Internal controls determined for implementation, which shall be identified by using Internal Control Inquiries, make the internal control system coherent and may be grouped into six categories: objectives, means, information systems, organization, procedures and supervision.

Within the internal control system, when weaknesses, dysfunctions or errors are ascertained, auditors will always find the primary cause in the non-existence or failure of an internal control, from the six presented above, of the procedural chain implemented by the function responsible person.

### 2. Objectives

The objectives are for the function/activity responsible person the first duty that he should fulfill, after the specification of the object of his mission, which means the determination of an action policy.

Folk lore says that "he who has no ends does not run the risk of reaching them". The determination of objectives must be a prime motivation for the function responsible person.

The determined objectives must fall into the category of the general objectives of the internal control that are unanimously known, such as:

- asset safety;
- information quality;

- observance of directives;
- resource optimization.

The function responsible person has to observe the general objectives of internal control and beside these ones, they will define the objectives specific to their missions, which afterwards will be appreciated by internal auditors, having in view the following criteria that they should meet:

- to participate in achieving the mission assigned to the responsible person;
- to be distributed within the function, having in view a pyramid-like design of objectives which all in all concur to achieve the general objective;
- to be measurable, expressed in real values, possible to achieve, quantitative and qualitative indicators of activity and so on;
- to be monitored by the management information system;
- to observe the schedule;
- to be concrete, clear, not to create confusions.

The deviations from these principles are weaknesses, dysfunctions or errors of the internal control system, instituted and approved by the function responsible person, and the absence of the activity objectives is a weakness for the entire entity.

### 3. Means

The means allow the responsible person to achieve the objectives. A problem that should permanently be in managers' attention is that of the adaptation of the means to the fixed objectives. In many cases, the analysis of these problems showed serious problems, unavoidable sources of failures and inefficiency.

Practice showed that checking the existence of means and making them compatible in order to reach objectives are very important control activities in the procedural chain determined by the responsible person.

With regard to means, we have to consider:

- *human means*, maybe the most important problem, but considered from the point of view of quality rather than of quantity. Many control activities are compromised if a competent personnel is missing and often this caused certain inefficiencies, serious anomalies and so on. The problem of human resources must be regarded from the perspective of recruitment, improvement of permanent training and professional ethics. All these are elements that involve sustained financial efforts, require time and often depend largely on the organizational culture.

- *financial means* materialized in exploitation or investment budgets corresponding to the fixed objectives that always raise the problem of observing these budgets for reaching the fixed targets, when we do not want to change the objectives. The internal auditors within the missions conducted have to examine the link that exists or existed between function objectives and approved budgets. They also have to take into account that there may be quality objectives, for instance, the fulfillment of which has no direct effect on budgets.

- *technical means* regard both the management systems and the information systems, the commercial or even the techniques without which the fixed objectives cannot be fulfilled;

#### 4. Information system

The information system that we may find in all businesses like an integrated system of the company made up both of informational system and of computer systems.

*Informational systems* aim should efficiently control any business and include the financial-accounting information systems. Computer systems are the computerized part of the informational system.

*Information systems* should meet a series of conditions to comply with the requirements of the internal audit, that is they should be:

- reliable;
- easy to check;
- exhaustive;
- available in due time;
- useful and pertinent.

Information systems are part of the communication system of the entity for the information of the whole personnel, depending on requirements, and contains:

- the management control system
- the budget control system;
- the statistical reporting system and so on.

The auditors are assigned the task of appreciating the information systems of the entity both from the perspective of costs and from the perspective of their usefulness and efficiency;

#### 5. Organization

Organization is a fundamental problem of management, and practice shows that there are no models that one can apply, due to the great variety of entities, of the business nature, of the legal structure etc. and last but not least, due to the organizational culture.

Auditors should supervise the observance of some generally-admitted organizational principles, such as:

- *Adaptation* that is a constant concern of the general manager for the achievement of an efficient organization, corresponding to the specificity of the entity in order to avoid a decentralization/excessive centralization or an organization reluctant to change;
- *Objectivity* in organization refers to the fact that organizational structures should not be build depending on people to prevent to disorganization of activity when an employee leaves or disappears;
- *Task separation/segregation* is a principle that, once respected, ensures greater security and means that certain tasks that are not compatible cannot be made by the same person;

In practice, manager generally admit that certain tasks need to be separated and due to lack of vigilance they can produce sometimes unwanted effects, such as:

- the decision-making function and the bookkeeping function are separated from the financial function of making payments;

- the asset-holding function is separated from the control function.

The actual separation of tasks may bring up some special problems, especially with companies that work with low number of employees.

To make an organization efficient, the following items are necessary:

- the tables of organization, to know who leads and who is led;
- the job description, so that every employee should know his assignments and tasks and the limits of his competency;
- the material framework for creating the adequate environment for operation and that also ensures the physical protection of assets and persons and the support of the institutional culture of the organization.

## **6. Work procedures and modalities**

The work procedures and modalities of the entity should be defined and formalized for all processes and activities run in such entity.

Currently, we should realize the fact that we are living in the 3rd Millennium, we cannot work any longer with managers who know everything just because they do their job for 10 or 20 years, or with employees who don't know what's next to do until the boss tells them so.

The lack of procedures or of their implementation in the work modalities means:

- to condemn oneself to a poor control over the activities performed;
- to deprive the organization of the indispensable memory without which it cannot operate;
- to deprive the auditor of the indispensable reference system on which it relies when procedures are formalized in order to evaluate differences, to evaluate and formulate recommendations and conclusions.

Management has the task of defining its own work modalities that should be formalized in simple and efficient procedures of assignment performance and they should be permanently updated. Furthermore, management has the duty to make available these work tools to all employees and to make them observe them. In this respect, a major concern of every responsible person is to draft and permanently update the procedures and the work instruments specific for the function they coordinate.

In modern organizations, these documents are computerized and anyone may see on the computer/INTERNET anything related to his activity. These facilities are important for the systematic update of procedures that are a useful tool in day-to-day operation.

Function responsible persons, when procedures are made, must not omit the controls that should be included in the procedure flow and depending on risk evolution, these should be diminished or extended to generate the fulfillment of function objectives.

## **7. Supervision**

The supervision represents an internal control, often omitted by the ones responsible person for performing it. Many managers evaluate their employees based

on the trust they have in them, not taking into account that supervision does not mean "lack of trust", often it contributes to the enhancement of trust.

Supervision does not mean:

- remaking employees' work;
- pursuance by all means to find errors;
- thorough and permanent examination.

Yet, supervision means:

- an act of assistance, in order to help the coworker to perform difficult, new tasks, to settle conflicts and to identify weaknesses and strengths;
- an act of verification to avoid the application or the interpretation of some procedures in the wrong way;
- an act of evaluation, from time to time, at random, of what is going on, in order to avoid temptations and to stimulate work improvement;
- an act of friendship, by which we show to the others that we are interested in what they do, that we want them to know that their difficulties and performances are not neglected and that we want to use any valuable initiative at all hierarchical levels.

In practice, it was proved that performing random supervision by managers and responsible persons has beneficial effects.

To be efficient, the supervision should meet certain requirements. Thus, it should leave a mark of its performance, that is a notice, an advice, a report regarding the appreciation of management quality and for the evaluation of the supervision frequency. Then, it needs to be universal, meaning that it should have in view any task, irrespective of its type and who has done it. The supervision act should not make any difference between essential tasks and less-essential tasks. Often, it is ascertained that they who do not observe the supervision activity are on the highest hierarchical levels. Last but not least, it should measure the achieved progresses in objective pursuance, ensuring via the information and communication system of the entity that real and precise targets have been reached.

*Received May 9, 2005*

*"Al.I.Cuza" University Iasi*

## REFERENCES

1. GHITA MARCEL, IONEL BOSTAN - *Theory and Practice of Internal Audit*, Universitas Publishing House, Iasi, 2004.
2. RENARD JACQUES - *Theory and Practice of Internal Audit*, 4th Edition, translation from French made by the Ministry of Public Finances within a PHARE Project, Bucharest, 2002.
- 3.\*\*\*THE INSTITUTE OF INTERNAL AUDITORS - *The Professional Practices Framework*.
- 4.\*\*\*THE FRENCH INSTITUTE OF CONSULTANT INTERNAL AUDITORS - IFACI - *Professional Standards of the Internal Audit*.
- 5.\*\*\**Law no. 672/2002* regarding the internal public audit, Official Gazette no. 953/2002.
- 6.\*\*\**Law no.133/2002* for the approval of the Governmental Urgency Ordinance no.75/1999-republished, regarding the financial audit, Official Gazette no. 598/2003.

**ACTIVITĂȚI INTRAORGANIZAȚIONALE CARE POT FI AUDITATE****(Rezumat)**

Controalele interne fac ca acest sistem să fie coerent și pot fi grupate în următoarele șase categorii: obiective, mijloace, sisteme de informație, organizare, proceduri și supervizare.

## THE UNIVERSALITY AND PERIODICITY OF THE FUNCTION OF INTERNAL AUDIT

BY

**IONEL BOSTAN**

**Abstract:** The internal audit is functioning in every organization, appearing from the practicing of international enterprises. Its organization as a part of entities imposes the taking into account of all characteristics of universality and periodicity.

**Keywords:** the audit function, internal audit, manager, processes, universality, periodicity.

### 1. Introduction

As it is well known, where there is an internal control there is also internal audit and that because "the raw material" of the internal audit it's the internal control. The internal audit helps the entities in the process of reaching its objectives, which it's being achieved through a methodical and systematic organization of the audit process, guided towards the control and leading processes improvement, at different periods of time. The internal audit must follow the general objectives, and also other elements such as: The existence of some dissensions between different levels of the organization, the existence of some things which disheartens people in working at their level, and so on.

The activity of internal audit is a programmed activity which is being achieved in concordance with all standards in order to lead to positive results and it develops according to a program, where all the audit's ideas will be cumulated into a constructive report, which will represent a benefit for the organization. Because the internal audit has the purpose of improving the internal control, and the internal control is universal, then we can assert that the internal audit is also universal. The internal audit is in fact a periodical function because it materializes according to a plan and also on the account of some activity programs, which where communicated and approved in advance. The frequency of the audits will be determined by the activity of evaluating the risks.

### 2. The universality of the function of internal audit

The universality of the function of internal audit must be perceived in report with the area of applicability, the purpose, the role and professionalism of the persons implicated in the act of materializing this function. The function of internal audit became a function of managerial assistance with the help of which the internal audits help managers, of any level, to master in a better way the other functions and all the activities. If we take into account the fact that managers exists every where the result is that the assistance extended in all the fields and refers now to all activities. That's why, the internal audit's standards specifies that into a internal audit's service we have to find all the possibilities in order to audit all the activities, and that's the reason why we must have specialists in all domains, not in all specialization.

The International Standard specifies that the internal audit does not have to know all the trades in the world. He can not be as good as the person who does the same thing every day. The specialty of the internal audit is being represented by the system of internal control. But, in order to exert its specialty he must have a well knowledge of the environment he audits he must understand and appropriate the culture of that organization. Into an internal audit compartment there are no people well trained in every field. Here we will find specialists who have appropriated: the managerial culture, the financial-book-keeping culture, the informational culture and also other cultures necessary into an entity. In this context of specialization an informatics audit will be accepted by the computer specialists from the department which is being the subject of the audit, only if he is also a specialist. The informatics audit is in fact a computer specialist who had learnt the internal audit and not conversely.

### 3. The periodicity of the internal audit

The periodicity of the internal audit is a permanent function inside an entity and also a periodic function for the ones who are being audited. The frequency of the audits will always be determined by the activity of evaluating the risks. Thus, the internal audits may audit an entity for eight to twelve weeks and then they might come back after a period of 2-3 years, depending on the risks that might appear. In this order of ideas, we must have a system of measuring the risks. This is in fact the audit plan, which is made for a strategically period of time, usually 5 years. This plan is yearly structured and comprises all the activities. The difference consists in the fact that some activities will be examined all at once and others for several times, depending on the risks. On the account of the audit plan there is chosen the number of auditors and depending on them there are chosen the risks that will be treated and the ones which will be ignored for the moment. The periodicity of the internal audit doesn't mean half of the entire norm, because we have to take into account the possibility of coming back at any time, if the internal audit considers it necessary. The process of the internal audit must be done periodical, step by step, and it also must take into account all the aspects not only the agreeable things. This process must be organized and planed in order to improve the internal control and the leading process. The audit is present there in order to help the line management in the process of improving the functional management and the activity of analyzing the risks. The discoveries and reviews of the internal audit are useful to the management line from the examined zones, especially in the potential improvements in the management process of the risks, and which the reviewer will reevaluate during his coming back, which will ensure and guarantee a plus of value to the organization.

Received May 9, 2005

“Al.I.Cuza” University Iasi

### REFERENCES

1. BOSTAN IONEL, PETRU RADU, *Controlul financiar si auditul intern la institutiile publice*, Editura Sedcom Libris, Iasi, 2003.
2. BOULESCU MIRCEA, GHITA MARCEL, MAREȘ VALERICA, *Fundamentele auditului*, Editura Didactică și Pedagogică, București, 2001.
3. BOULESCU MIRCEA, GHITA MARCEL, MAREȘ VALERICA, *Controlul fiscal si auditul financiar-fiscal*, Editura CECCAR, București, 2003.
4. GHITA MARCEL, MAREȘ VALERICA, *Auditul performanței finanțelor publice*, Editura CECCAR, București, 2002

### UNIVERSALITATEA ȘI PERIODICITATEA FUNCȚIEI DE AUDIT INTERN

#### (Rezumat)

Auditul intern funcționează în fiecare organizație, provenind din practica întreprinderilor internaționale. Organizarea sa, ca parte a entităților, impune luarea în considerare a tuturor caracteristicilor de universalitate și periodicitate.

## INFLUENCE OF THE ELECTROLYTIC PLASMA NITRIDING ON STEEL STRUCTURE

BY

MARIA BACIU\*, EMIL PASINKOVSKI\*\*, SILVIA GEORGESCU\* and  
CONSTANTIN BACIU\*

**Abstract.** OLC55 and 40Cr10 steels were nitrided and quenched in electrolytic plasma at three different diffusion temperatures,  $T_d = 650, 700$  and  $750^\circ\text{C}$  and two diffusion times,  $t_d = 3$  and  $6$  min. The X-ray diffraction investigations allowed the determination of  $d_{hkl}$  spacings and the identification of the phases within the superficial layer of each of the steel grades subjected to different variants of heating in electrolytic plasma.

The presence of both  $\alpha'$  martensite and  $\gamma$  retained austenite, super-alloyed with nitrogen were noticed as well as the  $\epsilon$ -type nitrides  $\text{Fe}_{2-3}\text{N}$ ,  $\text{Fe}_3\text{N}$  and  $\text{Fe}_4\text{N}$ . By means of the X-ray diffraction analyses substructure elements of the superficial layer of the two steels under study were also determined, namely: the dimension of the mosaic blocks and the elastic distortion of the crystalline lattice.

**Keywords:** electrolytic plasma, steels, nitrides, X-ray diffraction

### 1. Introduction

The application of a direct current between the two electrodes of an electrolytic cell causes electrolyte decomposition and high rate heating of the active electrode. In this way, favorable conditions are created for the occurrence of atomic diffusion, from the gaseous covering (designated as electrolytic plasma), that envelops the anode (specimen) to the specimen's superficial layer. This atomic migration causes the super-alloying of the metallic alloy within the diffusion depth.

If the electrolyte has a high nitrogen concentration, when direct current voltages higher than  $U_{DC} = 150$  V are applied it is possible to obtain nitrogen super-alloying of the superficial layer of steel parts. The intensity of the process is largely influenced by the duration of the diffusion process.

The determination of the structural changes caused within the super-alloyed superficial layer is required by the necessity to determine the optimum values of the technological parameters ( $T_d =$  diffusion temperature and  $t_d =$  diffusion time, chemical composition of electrolyte) for which maximum super-alloying effect would be obtained.

### 2. Experimental

Specimens made from tempering steels 40Cr10 and OLC55 were subjected to different variants of thermal and thermochemical processing performed into a nitrogen

based-electrolyte with the composition: 10 %  $\text{NH}_4\text{Cl}$  + 20 %  $\text{NH}_4\text{OH}$  +  $\text{H}_2\text{O}$ . The experimental values of the technological parameters for the diffusion process were:  $T_d = 650^\circ\text{C}$ ,  $t_d = 3$  and 6 min. For two of the variants, a heating stage at  $T_{\text{aust}} = 750^\circ\text{C}$  or  $800^\circ\text{C}$  was applied during 10 sec, after the holding at the diffusion temperature. In all cases the final quenching was performed in electrolyte (at voltage  $U = 0$  V).

The investigations of the structural changes caused within the superficial layer of the two steels were performed by X-ray diffraction, by means of a DRON 2,0 diffractometer. The accelerating voltage was  $U_{\text{acc}} = 30$  kV and the current intensity  $I = 10$  mA. The experiments were performed using  $\text{MoK}_\alpha$  and  $\text{FeK}_\alpha$  within the range  $2\theta = 15 \dots 40^\circ$ .

### 3. Results

The experimental research were focused on the following aspects:

- the identification of the phases present in the super-alloyed superficial layer and the calculation of their percental concentration;
- the determination of the nitrogen concentration of martensite and retained austenite.

Analyzing the recorded diffractograms allowed to determine interplanar distances  $d_{hkl}$  and to identify the phases present within the structure of each of the specimens. It has been noticed that, for all the imposed values of the parameters of thermal processing technology, in the structure of the super-alloyed superficial layer both nitrogen-based martensite (nitromartensite) and retained austenite have been observed. The former corresponds to the diffraction planes (110), (200) and (211) and the latter to (200), (220) and (311). Within the structure of both steels chemical compounds (nitrides) of the types  $\varepsilon\text{-Fe}_{2-3}\text{N}$  or  $\text{Fe}_3\text{N}$  were noticed.

An example of X-ray diffractogram is illustrated in Fig.1 for 40 Cr10 steel super alloyed with nitrogen.

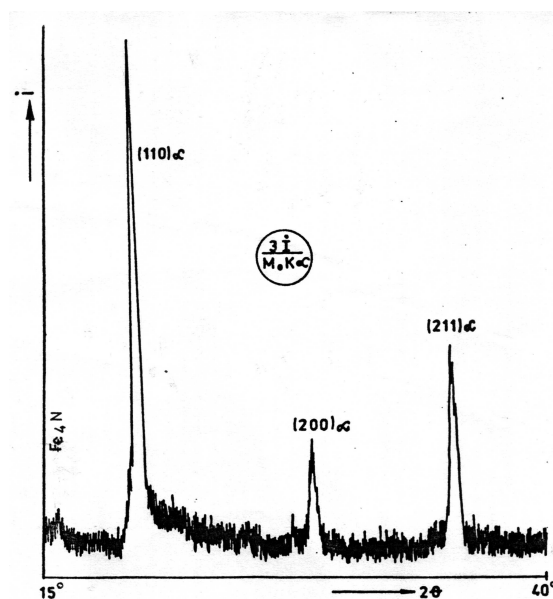


Figure 1. Diffractogram of 40Cr10 steel super-alloyed with nitrogen, by diffusion during heating in electrolytic in electrolytic plasma (specimen 3I)

The calculation of the concentration of phases present in the structure of the analysed specimens allowed obtaining the values of the percental volumes of nitromartensite ( $v_{\alpha'}$ ), retained austenite ( $v_{\gamma}$ ) and nitrides ( $v_{\text{nitrides}}$ ) listed in Table 1.

Table 1 Percental phase amounts

Steel grade	Marking	$v_{\alpha'}$ , [%]	$v_{\gamma}$ , [%]	$v_{\text{nitrides}}$ , [%]
40Cr10	3D	78.30	21.70	-
	3A	65.80	8.30	25.90
	3J	91.40	-	8.60
OLC55	4DD	70.30	12.40	17.40
	4Y	64.70	14.10	21.20
	4T	86.60	13.40	-

The results found at the determination of nitrogen concentration from the two solid solutions observed within the microstructure of the steels super-alloyed by diffusion during heating in electrolytic plasma are shown in Table 2.

Table 2 Nitrogen concentrations

Steel grade	Marking	Nitrogen concentration of martensite, [%]	Nitrogen concentration of retained austenite [%]
40Cr10	3A	0.66	1.35
	3B	-	0.20
	3I	-	0.20
OLC55	4DD	0.54	1.29
	4MM	-	0.50
	4Y	0.17	1.31

*Observation:*

After nitriding and quenching in electrolytic plasma the specimens were tempered in furnace ( $T_{\text{temp}} = 350^{\circ}\text{C}$ ,  $t_{\text{temp}} = 1 \text{ h}$ ).

#### 4. Conclusions

(i) Within the structure 40Cr10 and OLC55 steels, super-alloyed with nitrogen by diffusion during heating in electrolytic plasma, the presence of nitrogen-based martensite (nitromartensite) has been emphasized.

(ii) For the both steels under study rather close values have been determined for the percental concentration of nitrides.

(iii) Higher values of the nitrogen concentration were found in retained austenite as compared to the martensitic phase, no matter which was the applied technologic variant.

(iv) The application of a furnace tempering after thermal processing in electrolytic plasma causes total transformation of retained austenite to martensite.

Received, May, 10, 2005

\*Technical University "Gh. Asachi" Iassy.

\*\*Academy's Institute of Physics, Republic of Moldova

## REFERENCES

1. **Baciu, Maria**, *Contributions on the structural and property changes of thermally and thermochemically treated steels in electrolytic plasma* (in Romanian), PhD thesis, „Gh.Asachi” Technical University from Iași, 1999.
2. **Belkin, P.N., Ignat'kov, D.A., Pasinkovskÿ, E.A.**, *Azotirovanie v elektrolitnoj plazma*, *Kolloquium Eigen-sspannungen und Oberflächen-verfestigung*, p.265, 1982.
3. **Belkin, P.N., Pasinkovskÿ, E.A.** *Termičeskaâ i himiko - termičeskaâ obrabotka stalej pri nagreve v rastvorah elektrolitov*, *Metallovedenie i termičeskaâ obrabotka metallov*, nr.5, pag.12-17, 1989.
4. **Duradži, V.N.**, *Ob ustanovlenii stabil'nej stadii nagrena pri anodnom processe*, *Êlectronnaâ obrabotka materialov*, nr.5, pag.44-47, 1975.
5. **Duradži, V.N., Parsadonian, A.S.**, *Nagrev, metallov v elektrolitnoi plazme* (lb. rusă), Ed. Stiinca, Kișinev, 1988.

## INFLUENȚA NITRURĂRII ÎN PLASMĂ ELECTROLITICĂ ASUPRA STRUCTURII OȚELULUI

## (Rezumat)

Oțelurile OLC55 și 40Cr10 au fost nitrurate în plasma electrolică la trei temperaturi de difuzie, diferite,  $T_d = 650, 700$  și  $750^{\circ}\text{C}$  și la două durate de difuzie,  $t_d = 3$  și 6 min. Investigațiile prin difracție de raze X au permis să se determine distanțele interplanare  $d_{hkl}$  și să se identifice fazele din cadrul stratului superficial al fiecăreia dintre mărcile de oțel supuse la diferite variante de încălzire în plasmă electrolică.

Au fost remarcate prezențele martensitei  $\alpha'$  și a austenitei reținute  $\gamma$ , superaliate cu azot, precum și a nitrurilor  $\text{Fe}_{2-3}\text{N}$ ,  $\text{Fe}_3\text{N}$  și  $\text{Fe}_4\text{N}$ , de tip  $\epsilon$ . Prin intermediul analizelor prin difracție de raze X au fost determinate și elemente de substructură ale stratului superficial, al celor două oțeluri studiate și anume: dimensiunea blocurilor de mosaic și distorsiunea elastică a rețelei cristaline.

## PYRROLE POLYMERIZATION IN AQUEOUS FeCl<sub>3</sub> SOLUTIONS

BY

DRAGOȘ-VIOREL BREZOI<sup>1</sup> and RODICA-MARIANA ION<sup>1,2</sup>

**Abstract:** Conducting polypyrrole (PPy) films is prepared by chemical oxidation of pyrrole with FeCl<sub>3</sub> in aqueous methods by mixing a solution of pyrrole with an oxidizing solution of FeCl<sub>3</sub>. UV-VIS and IR spectroscopy is used for determining the reaction mechanisms. The rate of pyrrole polymerization is determined by the rate of the initial electron-transfer reaction. Py is the monomer and Py<sup>+</sup> is the radical cation which can dimerize with the expulsion of H<sup>+</sup>, such as given in the paper. The surface morphology is investigated with SEM.

**Keywords:** polypyrrole, oxidant, FeCl<sub>3</sub>, polymerization

### 1. Introduction

The  $\pi$ -conjugated polymer ultra thin films upon oxidation/reduction and doping/dedoping are of great interest to a number of applications. This includes electrochromic displays [1], battery electrodes [2], sensors [10] and others. Many papers discuss the electropolymerization of pyrrole and the properties of the resulting polypyrrole (PPy) film [1]. Less information exists concerning the chemical polymerization of pyrrole in homogeneous solution. Polymerization occurs readily in the presence of different oxidants, such as FeCl<sub>3</sub> [2,3] and K<sub>2</sub>S<sub>2</sub>O<sub>8</sub> [4]. Numerous studies have been reported about the formation of PPy films on solid surfaces by chemical polymerization of pyrrole (see a recent comprehensive review [5]). There are reports about the polymerization of pyrrole onto printed circuit boards [6,7] and various textile composites [8,9]. In the present work we synthesize conducting polypyrrole (PPy) films by chemical oxidation of pyrrole with FeCl<sub>3</sub> in aqueous methods by mixing a solution of pyrrole with an oxidizing solution of FeCl<sub>3</sub>.

### 2. Experimental part

#### 2.1. Chemicals used and polypyrrole synthesis

The following compounds are all of a reagent grade and used as purchased: ferric chloride, pyrrole (99%) (Acros). MilliQ water was used and all experiments were done at room temperature.

Polypyrrole (PPy) was chemically synthesized in water (50 ml) by mixing a solution pyrrole (Py) 0.043 M (2.881 g) with an oxidizing solution of FeCl<sub>3</sub> (0.1 M).

The synthesis was allowed to proceed at 5–7 °C [11,12]. The pyrrole solution was kept in the bath before adding FeCl<sub>3</sub> (16.25 g). Molar ratio of FeCl<sub>3</sub>/Py = 2.3.

Since this is a highly exothermic reaction, the addition was done slowly and at low temperature. The synthesis was performed for one hour without agitation and under nitrogen gas atmosphere. The polypyrrole precipitate was collected by filtration, rinsed with distilled water and dried in vacuum oven at 25–35 °C.

## 2.2. Apparatus

The absorption diffuse-reflectance spectra were recorded on a *SPECORD M400 Carl Zeiss Jena* spectrophotometer with double beam and microprocessor. The surface morphology was analyzed by a *JEOL (JSM 840)* scanning electron microscope. IR was recorded with a *SPECORD M80 Carl Zeiss Jena* spectrophotometer.

## 3. Results and discussion

The films formed in ferric chloride solution are blue-black in colour. We postulate that the colours of the ferric chloride PPy films differ from the black colour of the other PPy films because these films are not as fully oxidized as the others. We suggest that the mechanism for the formation of the PPy differs from the one that causes film formation on a nonconducting surface such as a textile, silica or other insulating surfaces. This mechanism is analogous to the one for deposition on metals or on insulating substrates treated to nucleate the initial deposition of the metal that one wishes to deposit (figure 1) [12].

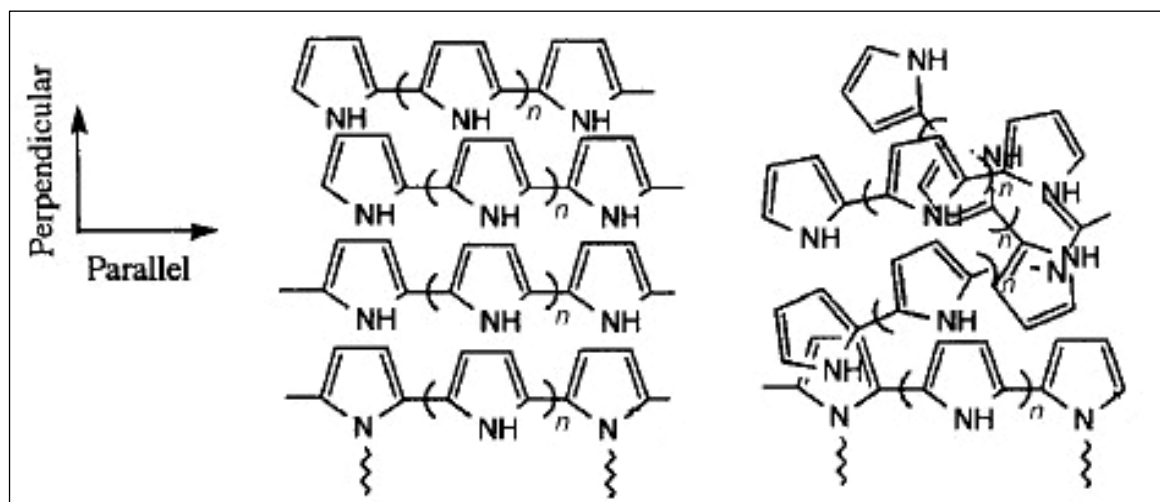


Figure 1. The possible orientations of polypyrrole chains in the polypyrrole film

### *Pyrrole polymerization in aqueous iron chloride solutions*

Polypyrrole is prepared in aqueous FeCl<sub>3</sub> solution and the mechanism reactions are given in figure 2 [12].

The rate of polypyrrole polymerization is determined by the rate of the initial electron-transfer reaction.

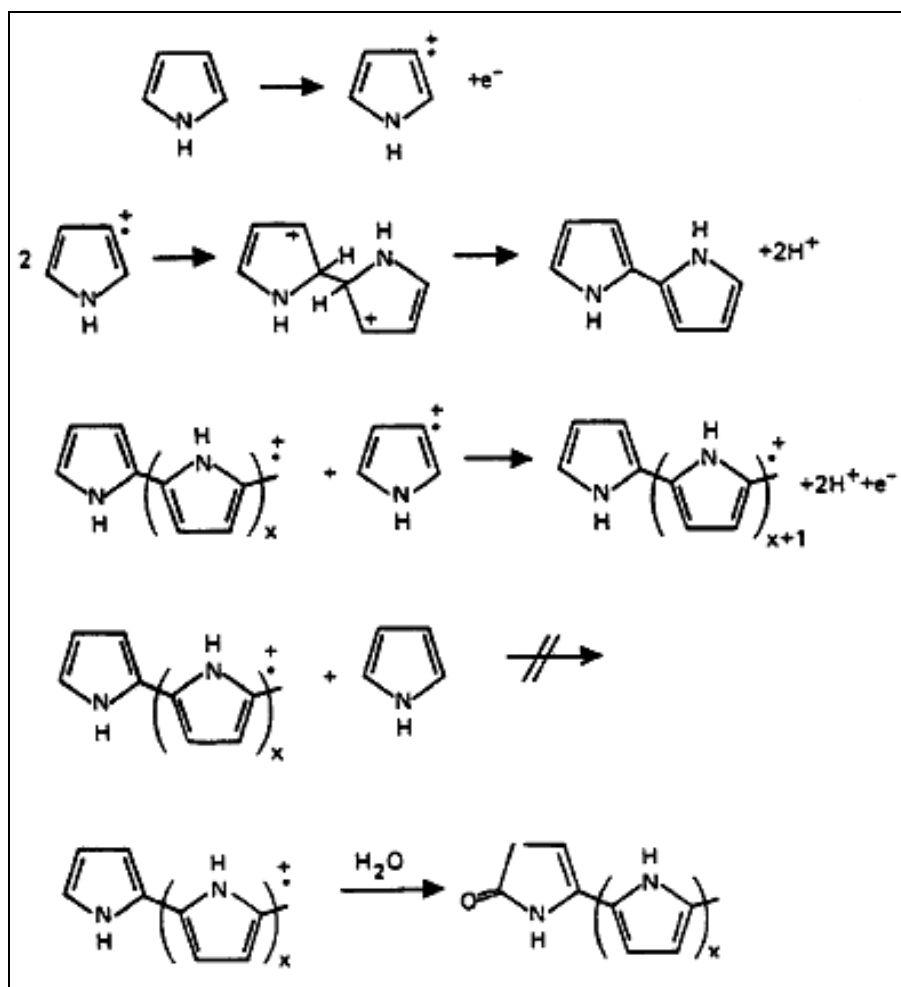
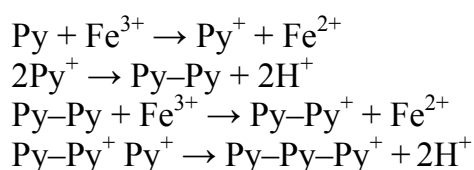


Figure 2. Chemical preparation of polypyrrole via radical cation formation

Py is the monomer and  $\text{Py}^+$  is the radical cation which can dimerize with the expulsion of  $\text{H}^+$ , such as given below [12]:



The mole ratio of monomer to oxidant affected the quality of the resulting polymer films. The reaction atmosphere and temperature did not have any obvious effects on the properties of the resulting films.

#### *UV-VIS spectroscopy*

The UV-VIS absorption diffuse-reflectance spectra (figure 3) are typical spectra for polypyrrole a constant and progressive increase of the pyrrole bands is observed due to the radical polymerization, associated with the character of the chemical bond between pyrrole rings in polymer chains and the chlorine anions from  $\text{FeCl}_3$ .

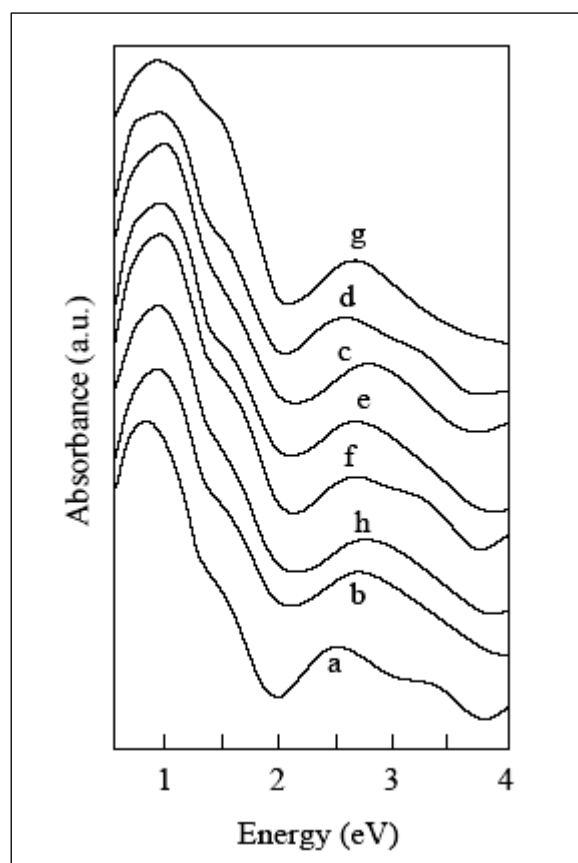


Figure 3. The UV-Vis spectra of PPy in the presence of  $\text{FeCl}_3$  in time ( $\Delta t = 10$  minutes)

### *IR spectroscopy*

The mechanism and kinetics of the formation of polypyrrole (PPy) films were studied by IR spectroscopy, too. IR spectroscopy made it possible to conclude that the anion is linked with the links of a polymer chain with a charge transfer, (figure 4).

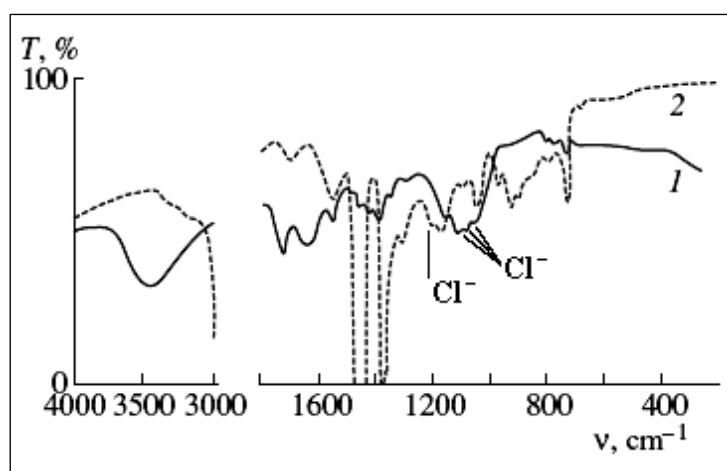


Figure 4. IR spectra of Py (1) and PPy (2) in the presence of chlorine ions

The IR spectra for pyrrole in water display intensive narrow bands of plane vibrations of deformation  $\delta_{pl}(\text{CH}^-)$  at 1015, 1045, and 1075  $\text{cm}^{-1}$ . Immediately, after adding  $\text{FeCl}_3$  to the pyrrole solution, new weak bands at 1100, 1125, and 1150  $\text{cm}^{-1}$  appear against the background of the pyrrole bands [13]. The intensity of the new bands increases with time, while that of the pyrrole vibrations simultaneously decreases [14]. The full width at half maximum and the mutual arrangement of these bands suggest that they refer to deformation vibrations of the pyrrole ring in a pyrrole complex.

An additional proof for the viability of the assumed mechanism involving a discharge of a complex which includes a protonated molecule of pyrrole with the anion is the fact that a strong quantum chemical interaction exists between anions and chains of pyrrole rings in the film, as will be shown below.

Thus, the discharge of pyrrole complexes with the anion and proton and their partial destruction yields radical-cation and radical species. When interacting with active ends of pyrrole links, these induce the growth and development of polymer chains. The formation of a polypyrrole film may probably be represented by the reactions shown in the figure 5.

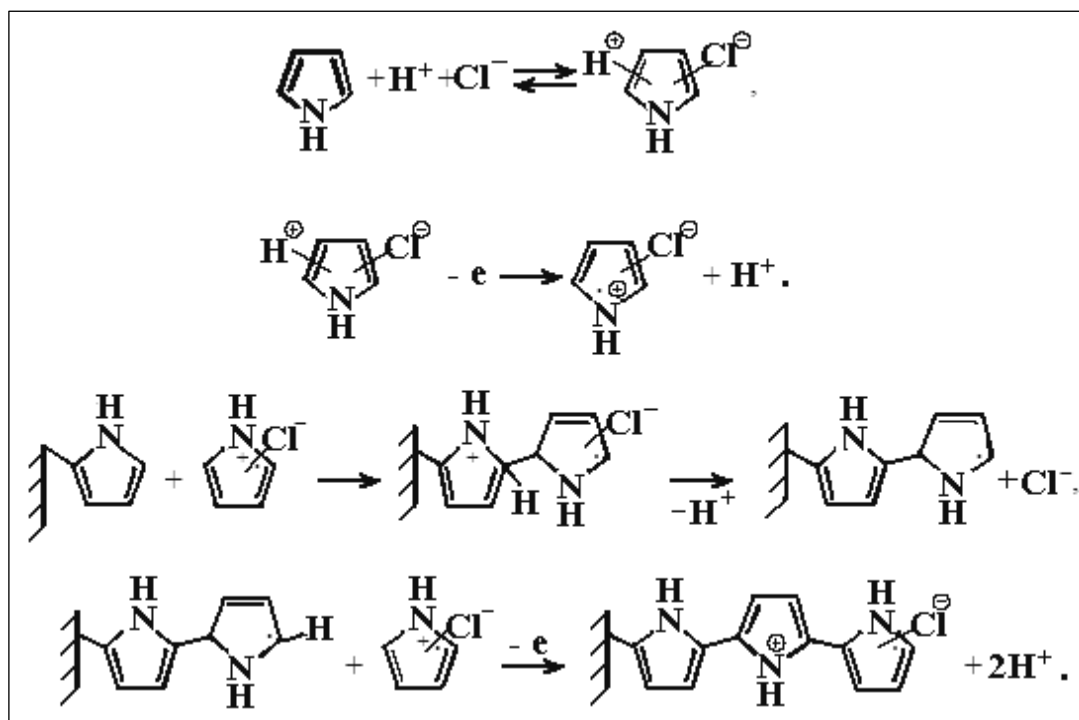


Figure 5. The development of PPy chains

In this scheme, the formation of a polypyrrole film involves very reactive intermediate species. Their interaction between themselves and the solution components may lead to deviation from ideal stoichiometry  $[(\text{C}_4\text{H}_5\text{N})_x\text{Cl}]_n$ , which is observed in reality, indeed. The proposed mechanism allows us to explain the dramatic deceleration of the synthesis of a polypyrrole film caused by the solution agitation as resulting from the polymer destruction.

### *SEM microscopy*

Figure 6 represents the SEM images of PPy film in contact with the substrate surface and shows the striations on the film surface and many pores and cavities. This result means the chemical synthesized deposition mechanism of the conducting polymer film is realized. The deposition mechanism mainly depends on the substrate material.

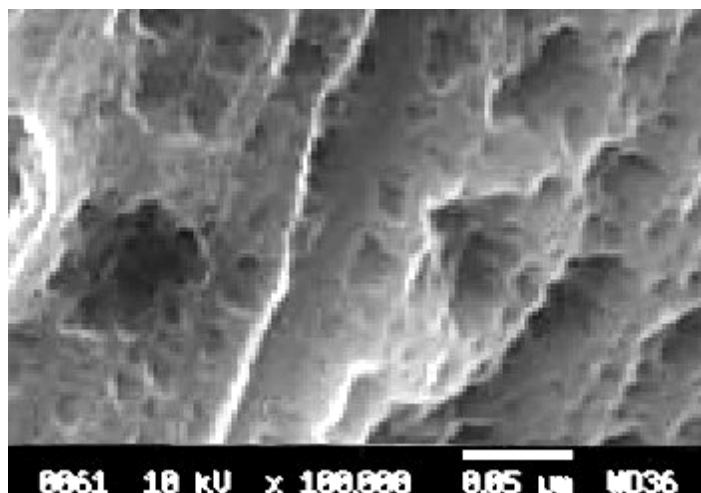


Figure 6. SEM image of the conducting PPy film surface in contacted with substrate

## 4. Conclusions

Conducting polypyrrole (PPy) films is prepared by chemical oxidation of pyrrole with  $\text{FeCl}_3$  in aqueous methods by mixing a solution of pyrrole with an oxidizing solution of  $\text{FeCl}_3$ . The rate of polypyrrole polymerization is determined by the rate of the initial electron-transfer reaction.

The mechanism and kinetics of the formation of polypyrrole (PPy) films were studied by UV-VIS and IR spectroscopy.

IR spectroscopy made it possible to conclude that the anion is linked with the links of a polymer chain with a charge transfer.

The UV-VIS absorption diffuse-reflectance spectra are typical spectra for polypyrrole a constant and progressive increase of the pyrrole bands is observed due to the radical polymerization, associated with the character of the chemical bond between pyrrole rings in polymer chains and the chlorine anions from  $\text{FeCl}_3$ .

Received May 4, 2005

<sup>1</sup>University Valahia, Târgoviște  
<sup>1, 2</sup>ICECHIM, București

## REFERENCES

1. Skotheim, T.A., **Handbook of Conducting Polymers**, Vols 1 and 2 Marcel Dekker, New York, 1986
2. Wolken, J.J., **Light Detectors, Photoreceptors, and Imaging Systems in Nature**, Oxford University Press, New York, 1995

3. Tourillon, G., in **Handbook of Conducting Polymers**, Vol.1, ed. T.A. Skotheim, Marcel Dekker, New York, 1986, **293-350**
4. Park, D.P., Sung, J. H., Lim, S. T., Choi, H. J., Jhon, M. S., *Synthesis and characterization of soluble polypyrrole and polypyrrole/organoclay nanocomposites*, **Journal Of Materials Science Letters** 22, 2003, **1299-1302**
5. Dongtao, G.E., Jixiao Wang, Shichang Wang, Jianbiao M.A., Binglin H.E, *Electrochemical synthesis of polypyrrole nanowires*, **Journal Of Materials Science Letters** 22, 2003, **839-840**
6. Li, X.H., Liu, W.M., Wang, C.W., Li, H.L., *Copolymerization of pyrrole and aniline nanofibrils and field emission property of the resulting copolymer*, **Journal Of Materials Science Letters** 22, 2003, **1519-1521**
7. Gandhi, M.R., Murray, P., Spinks, G.M., and Wallace, G.G., *Mechanism of electrochemical actuation in polypyrrole*, **Synthetic Met.** 73, 1995, **247-256**
8. Lee, S.K., Choi, Y., Sim, W.Y., Yang, S.S., An, H.J. and Pak, J.J., *Fabrication of electroactive polymer actuator composed of polypyrrole and solid-polymer electrolyte and its application to micropump*, **Proc. of SPIE's 7th International Symposium on Smart Structures and Materials**, 2000, **291-299**
9. Kim, D., Lee, D. and Paik, W.K., *Polypyrrole Film Studied by Three-Parameter*, **Ellipsometry Bull. Korean. Chem. Soc.** 27, 1996, **707-712**
10. Brezoi, D.V., Ion, R.M., *Phase Evolution Induced by Polypyrrole in Iron Oxide – Polypyrrole Nanocomposit*, **Proc. EMRS Fall Meeting Varsovia**, 2004, **39-40**
11. Madden, J.D., Cush, R.A., Kanigan, T.S., Brenan, C.J., Hunter, I.W., *Encapsulated polypyrrole actuators*, **Synthetic Metals** 105, 1999, **61-64**
12. Masuda, H., Asanov, D.K., *Preparation and properties of polypyrrole*, **Synthetic Metals** 135136, 2003, **43-44**
13. Milesa, M.J., Smith, W.T., Shapiro, J.S., *Morphological investigation by atomic force microscopy and light microscopy of electropolymerized polypyrrole films*, **Polymer** 41, 2000, **3349-3356**
14. Wu, C.G. and Chen, C.Y., *Chemical deposition of ordered conducting polypyrrole films on modified inorganic substrates* **J. Mater. Chem.** 7(8), 1997, **1409-1413**

### POLIMERIZAREA PIROLULUI ÎN SOLUȚII APOASE DE FeCl<sub>3</sub>

#### (Rezumat)

Filmele din polipirol conductor sunt preparate prin oxidarea chimică a pirolului cu FeCl<sub>3</sub> în medii apoase, prin amestecarea unei soluții de pirol cu o soluție oxidantă de FeCl<sub>3</sub>. Pentru determinarea mecanismelor de reacție se utilizează spectroscopia UV-VIS și IR. Viteza de polimerizare a pirolului este determinată de viteza reacției inițiale de transfer electronic. Py este monomerul și Py<sup>+</sup> este radicalul cationic care poate dimeriza cu expulzarea H<sup>+</sup>, așa cum este prezentat în lucrare. Morfologia suprafeței este investigată prin SEM.



## ON THE SHAPE MEMORY BEHAVIOUR OF Cu-BASED ALLOYS AND POLYETHYLENE TEREPHTHALATE (PET)

BY

LEANDRU-GHEORGHE BUJOREANU, CORNELIU MUNTEANU, IULIAN IONIȚĂ,  
MITICĂ TEMNEANU and VIOREL KOGĂNICEANU

**Abstract:** A comparative study is introduced concerning the shape memory behaviour of a Cu-Zn-Al Shape Memory Alloy (SMA) and polyethylene terephthalate (PET) fibres. In this purpose, their crystalline structures, with long period stacking orders, and SM mechanisms were reviewed. Mechanical memory has been described by means of tensile loading-unloading curves. Thermal memory was firstly analysed by means of thermal and calorimetric charts, emphasizing the transformations produced on heating and then ascertained under the form of work-generator Shape Memory Effect.

**Keywords:** long period stacking order, tensile curves, thermograms, work-generator shape memory effect

### 1. Introduction

Modern shape memory materials comprise ferrous and nonferrous alloys, ceramics, polymers and combinations of these categories, under the form of composite materials. All these materials present both mechanical and thermal memory, occurring at unloading and heating, respectively. These phenomena have different microstructural base in each material category. Thus, in Shape Memory Alloys (SMAs) there is a diffusionless (martensitic) phase transformation; in ceramics there is a paraelectric (anti-ferroelectric)  $\leftrightarrow$  ferroelectric transition and in polymers there is a glass transition. Although SMAs and polymers are driven by different types of transformations, since they are complementary in applications [1], the present paper aims to comparatively present the microscopic and macroscopic changes governing their shape memory behaviour.

The crystalline structures, with long period stacking order, of Cu-Zn-Al SMAs and polyethylene terephthalate (PET) are shown in Fig.1.

In Fig.1(a) the B2 cubic structure of  $\beta_2$  austenite from Cu-Zn-Al SMAs is shown, which transforms to 9R monoclinic structure of  $\beta_2'$  martensite, after Bain distortion, plane inhomogeneous shear on  $[100]_M$  direction and transformed lattice rotation around  $[010]_{M,A}$  direction [2, 3]. The crystalline structure of PET is formed under controlled cooling or heating conditions and has triclinic unit cell with the atomic arrangement depicted in Fig.1(b) [4]. The crystallographic parameters of 9R unit cell are:  $a = 0.441 \cdot 10^{-9}$  m,  $b = 0.268 \cdot 10^{-9}$  m,  $c = 1.92 \cdot 10^{-9}$  m and  $\beta = 88.4^\circ$  [5]. PET's unit cell has the parameters:  $a = 0.456 \cdot 10^{-9}$  m,  $b = 0.594 \cdot 10^{-9}$  m and  $c = 1.075 \cdot 10^{-9}$  m and the angles:  $\alpha = 98.5^\circ$ ,  $\beta = 118^\circ$  and  $\gamma = 112^\circ$  [6]. Obviously, both materials have long period stacking sequence along Oz axis.

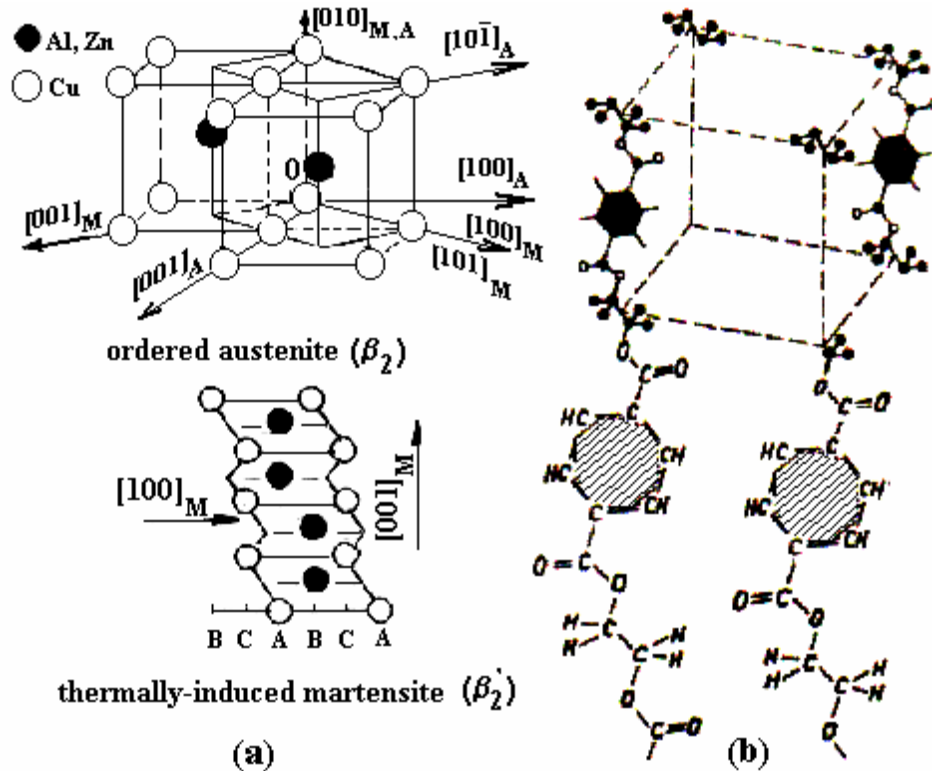


Fig.1 Hysteresis transformation loops in SMAs: with low frictional force (solid line); with high frictional force (dashed line) and with high elastic energy (dotted line) [1]

The properties of both Cu-Zn-Al SMAs and PET depend upon their actual condition. The former can be in austenitic or martensitic state while the latter can be amorphous or crystalline. In addition, PET's properties depend on both time and temperature. Table 1 gives an insight on the general properties of the two materials.

Table 1 Properties of Cu-Zn-Al SMAs and PET [1, 6, 7]

Property	Cu-Zn-Al SMAs	PET
Melting point, K	1223-1293	533
Density, $10^3 \text{kgm}^{-3}$	7.8-8*	1.33 (amorphous) 1.47 (crystalline)
Thermal conductivity, $\text{Wm}^{-1} \cdot \text{K}^{-1}$	84-120*	$16.8 \cdot 10^{-2}$
Coefficient off thermal expansion, $10^{-6} \text{K}^{-1}$	16-18*	4 (amorphous, 93 K) 7.8 (50 % crystalline, 423 K)
Electric resistivity, $\Omega\text{m}$	$0.12 \cdot 10^{-6}*$	$1.2 \cdot 10^{17}$ (293 K, 65%UR)
Tensile strength, MPa	700-800*	45-145
Elongation to failure, %	10-15*	11-35
Tensile modulus, GPa	70*	2.3-10.3

\*Properties corresponding to the martensitic condition

As compared to the rest of properties, it is noticeable that Cu-Zn-Al SMAs and PET have rather close mechanical characteristics therefore they behave similarly when subjected to tension, as it will be shown later. As a matter of fact, tension has been considered as the best way to emphasize the presence of Shape Memory Effect (SME), by heat-activated shrinkage of elongated SMA specimens [8] and is obviously the most accessible way to reveal SME in polymers.

In order to illustrate the mechanism of tensile SME in alloys and in polymers, Fig.2 schematically illustrates the microscopic changes accompanying a complete cycle within the space stress-strain-temperature.

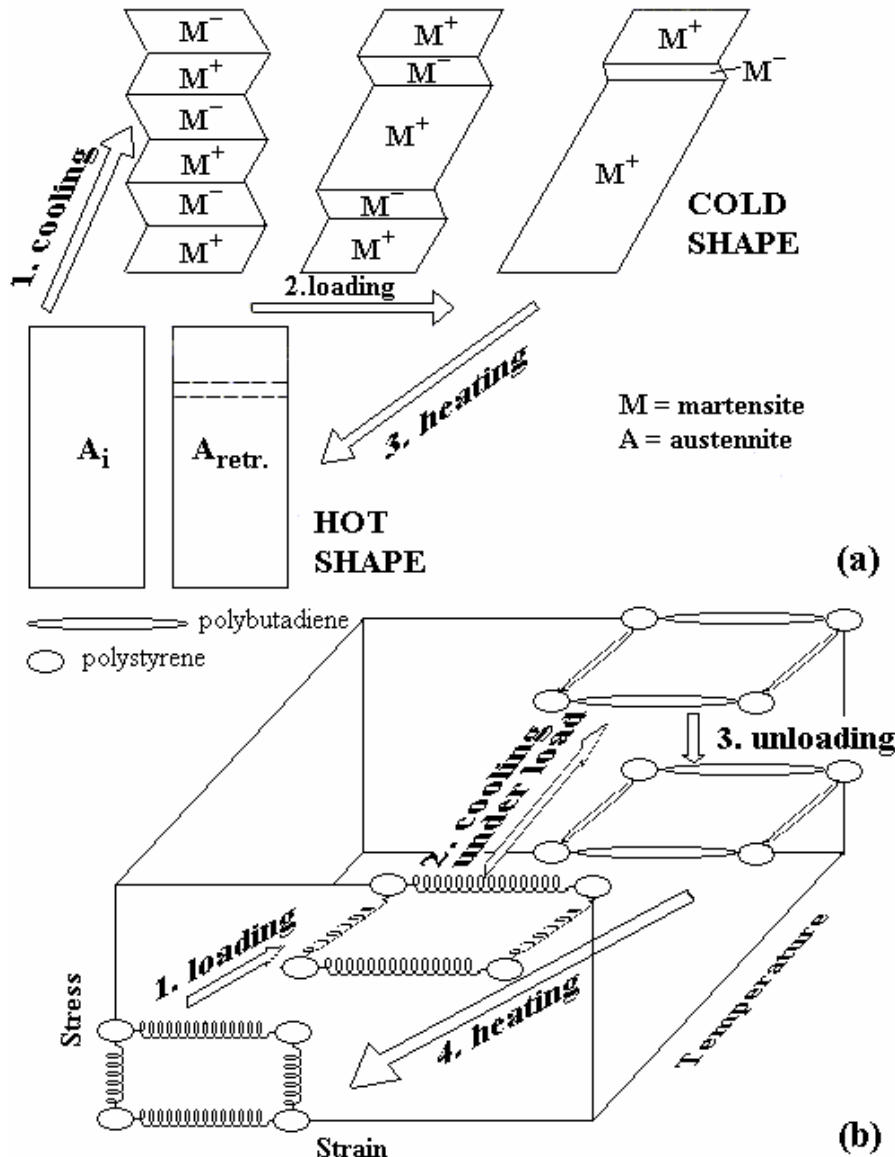


Fig.2 Schematization of SME mechanism during a complete cycle in stress-strain-temperature space: (a) in SMAs; (b) in styrene-butadiene copolymer [1, 9]

Fig.2(a) reveals the microscopic origin of SME in alloys, by means of the change of phase morphology during a cooling-loading-unloading-heating cycle. After cooling, initial austenite  $A_i$  transforms to thermally induced thermoelastic martensite organized into several domains, with different habit planes (but crystallographically equivalent), called variants. Twin-related martensite plate variants were designated as  $M^+$  and  $M^-$  since any applied mechanical stress causes the increase of  $M^+$  variants and the decrease of less favourably oriented  $M^-$  variants. After loading, the cold shape has been induced, being formed in majority by  $M^+$  variants. After heating, martensite reverts to retransformed austenite,  $A_{retr.}$  and the phase change is accompanied by shape recovery. The difference between  $A_{retr.}$  and  $A_i$  is that the former has kept the traces of the accommodation twin boundaries of martensite plate variants. The origin of SME in

alloys consists in the superior stiffness of austenite and the reversible character of martensitic transformation, enhanced by the elastic energy stored during cooling [9]. Fig.2(b) schematizes the SME produced in styrene-butadiene copolymer, during a loading-cooling-unloading-heating cycle. In initial state, the polystyrene parts are rigid but the polybutadiene parts are flexible. After loading, the polymer is cooled in elongated condition and the shape is frozen since polybutadiene parts become crystallized, therefore rigid. So, the elongated shape is kept after unloading. This is the actual state of usual PET bottles, obtained by blow-moulding and quenching [10]. In the final step, the micro-crystals from polybutadiene parts, that act as crosslink points of the polymer network, melt. The origin of SME in polymers consists in the superior stiffness of micro-crystal parts, which are formed during the cooling process and become flexible during heating [1].

In the following, the mechanical and thermal memory of a Cu-Zn-Al SMA and PET fibres will be compared and the transformation responsible for the latter will be analysed.

## 2. Experimental

Fully martensitic Cu-Zn-Al specimens, with the composition Cu-21.57 Zn-7 Al (wt. %), were hot-rolled and prepared according to a previously detailed procedure [11] for tensile tests, DSC analysis and bending work-generator SME experiments. The first used lamellar specimens ( $2 \times 20 \times 140 \cdot 10^{-3} \text{m}$ ), deformed at room temperature with a strain rate of  $8.33 \cdot 10^{-5} \text{sec}^{-1}$ , on a HECKERT FPZ 100/1 tensile testing machine. The precisions were  $\pm 0.01 \%$  and  $\pm 10 \text{MPa}$  for strain and stress, respectively. The second used  $25.5 \cdot 10^{-3} \text{kg}$  specimens, cut with a BUEHLER low speed saw and analysed by means of a 2920 Modulated DSC TA INSTRUMENTS unit, with measuring accuracies of  $\pm 0.1 \text{K}$  for temperature and  $\pm 1 \text{W/kg}$  for heat flow, equipped with professional software. The specimens were heated with  $0.16 \text{K/sec}$  up to  $873 \text{K}$ , in He + Ar protective atmosphere. Lamellar specimens were used, as well, for the third type of experiments, emphasizing bending work-generator SME according to the procedure detailed in [11]. In this purpose, the specimens were fixed in horizontal position and ten different loads were fastened at their free ends. The upwards displacement of their free ends, during heating to  $333 \text{K}$ , was measured with a precision of  $\pm 0.1 \cdot 10^{-3} \text{m}$ .

$0.5 \text{m}$ -long unstretched PET fibres, with  $0.32 \cdot 10^{-3} \text{m}$  diameter, were hung with four different loads into a steam chamber with controlled temperature, within work-generator SME. After being kept for 5 minutes in  $373 \text{K}$  steam, the fibres were slowly cooled and their contraction was measured with a precision of  $\pm 5 \cdot 10^{-3} \text{m}$ . For each applied load the specific contraction was determined as an average for five different fibres.

## 3. Results and discussion

The stress-strain curves, which were experimentally obtained for the martensitic Cu-Zn-Al SMA and taken from literature for PET [4] are shown in Fig.3

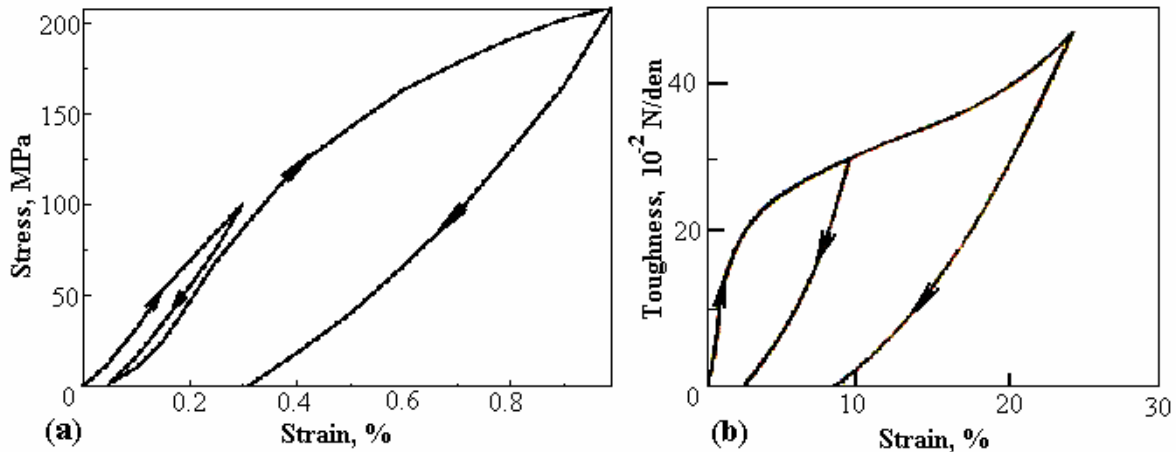


Fig.3 Characteristic tensile loading-unloading curves: (a) recorded for martensitic Cu-21.57 Zn-7 Al (wt.%) SMA; (b) given by literature [4] for PET fibres

In spite of the observed differences between stresses and strains, both curves have similar character, designated under the term of Pseudoelasticity, which represents by any non-linearity occurring at unloading and reflects mechanical memory at SMAs [8].

In order to reveal thermal memory, Fig.4 shows the transformations produced during heating, experimentally recorded for the SMA and given by literature for PET [6].

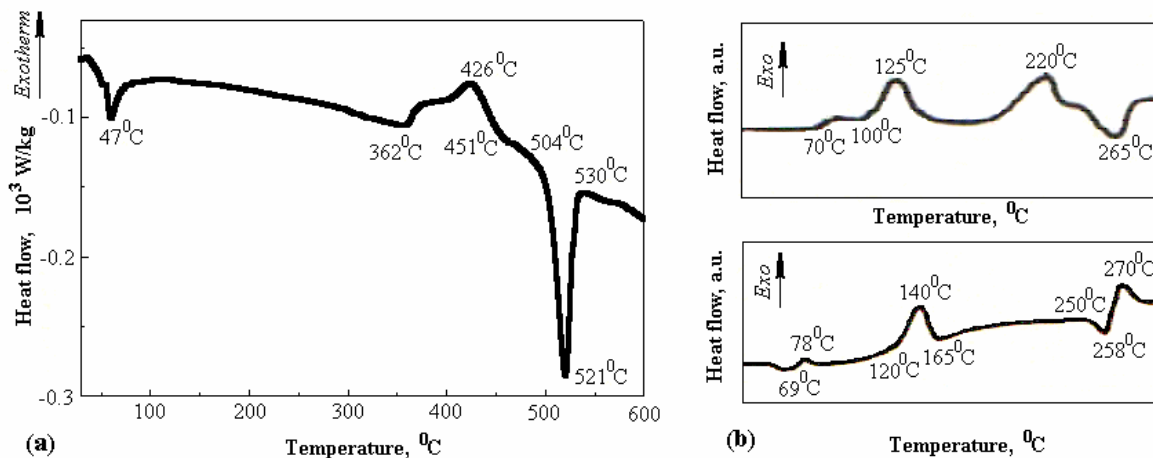


Fig.4 Evidence of the transformations produced during heating: (a) on recorded DSC curve for Cu-21.57 Zn-7 Al (wt.%) SMA; (b) on DTA curves given by literature [6] for PET fibres in extruded and quenched condition (up) or in unstretched condition (low)

The DSC thermogram from Fig.4(a) shows two endothermic and one exothermic peaks. In accordance with literature, the endothermic peak located at 320 K corresponds to reverse martensitic transformation that absorbs 5.974 kJ/kg and ends at 333 K. Martensite reversion is basically the single responsible for the presence of SME and thermal memory.

The exothermic peak located at 699 K represents the precipitation of  $\alpha$ -brass phase (fcc), which releases a specific heat of 10.7 kJ/kg, between 635 K and 724 K.

The third peak is located at 794 K and corresponds to austenite's order-disorder transition that absorbs 11.9 kJ/kg, between 777 and 803 K. For Cu-Zn-Al SMAs the specific heat has been determined as 390-400 J·kg<sup>-1</sup>·K<sup>-1</sup> [1]. From the above three

peaks only the first one corresponds to a diffusionless transformation. Since the other two are diffusion controlled, any Cu-21.57 Zn-7 Al (wt.%) martensitic alloy, when heated above 635 K would alter its shape memory characteristics. In order to recover its initial shape memory behaviour, such an alloy should be annealed for long periods in austenite region at temperatures above 1073 K and then quenched to room temperature.

The DTA thermograms illustrated in the upper and lower parts of Fig.4(b) correspond to PET fibres in extruded and quenched and in unstretched conditions, respectively. In the upper chart it is noticeable that at 343 K an exothermic inflexion occurs corresponding to glass transition, which is the only responsible for the occurrence of SME. The exothermic peak located at 398 K corresponds to “cold crystallization” that starts at 373 K. The second exothermic peak at 493 K corresponds to actual crystallization. Melting starts at 523 K and reaches the maxim at 538 K, the temperature of the endothermic peak. The thermal effects corresponding to the above four transformations were calculated between 33 and 60 kJ/kg. In the case of a 60 % crystalline “conditioned” (heated) PET specimen, with a density of  $1.41 \cdot 10^3 \text{ kg/m}^3$  melting heat was determined at a value of 120 kJ/kg. The average specific heat has been determined as  $1.26 \text{ kJ} \cdot \text{kg}^{-1} \cdot \text{K}^{-1}$ . In the lower chart, for unstretched PET fibres, it is noticeable that the first two transformations were maintained but their characteristic temperatures were slightly raised, from 343 to 353 K for glass transition and from 398 to 413 K for “cold crystallization”. It has been emphasized that the contraction of PET fibres is totally dependent on both the number and orientation degree of amorphous parts where molecular agitation occurs only above 353 K [6].

From the above data, it follows that reverse martensitic transformation and glass transition are the only responsible for the occurrence of work-generator SME in Cu-Zn-Al SMA and PET fibres, respectively. Therefore within the work-generator SME experiments, in order to ascertain the presence of thermal memory, the two materials must be heated at temperatures higher than the finish temperatures of the corresponding transformations. Thus, the Cu-21.57 Zn-7 Al (wt.%) martensitic SMA was heated at 333 K and the unstretched PET fibres at 373 K. The obtained experimental results are summarized in Fig.5

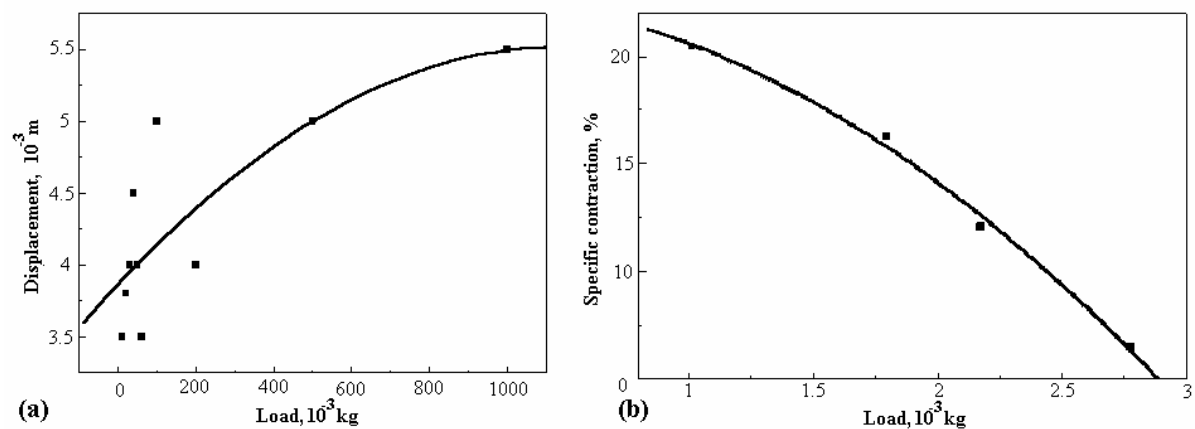


Fig.5 Results of the work-generator SME experiments: (a) variation of free-end displacement of lamellar Cu-21.57 Zn-7 Al (wt. %) martensitic SMA specimens subjected to bending, as a function of the applied load, during heating to 333 K; (b) variation of average contraction of unstretched PET fibres as a function of the applied load, after heating to 373 K

Obviously, in Fig.5(a) the displacement of the free-end of Cu-Zn-Al SMA lamellar specimens increased with the applied load that augmented the difference between hot (straight) and cold (bent) shapes. For loads higher than 1 kg the displacement decreased and SME was no longer noticeable. On the other hand, as expected, in Fig.5(b) average contraction (determined as the mean value for five fibres) decreased with the increase of applied load. For loads higher than  $2.8 \cdot 10^{-3}$  kg SME no longer occurred and the fibres were stretched instead of being contracted.

#### 4. Conclusions

In the case of two different shape memory materials, an alloy and a polymer, the shape memory behaviour was analysed, by comparing the data reviewed from literature with those experimentally determined.

From a microscopic point of view, it has been emphasized that: (i) both materials present crystalline structures with long period stacking order since the  $c$  parameter of unit cells is at least double as compared to the other two and (ii) the Shape Memory Effect-governing transformations are different but they have in common the release on heating of the deformation energy stored during cooling.

From a macroscopic point of view, both mechanical and thermal memories were discussed for the materials under study. Mechanical memory was revealed by the similar aspect of the stress-strain curves, even if the Shape Memory Alloy developed larger stresses and polyethylene terephthalate has been characterised by larger strains. By means of DSC and DTA charts the transformations produced on heating were examined and correlated with work-generator SME.

The maximum work developed in bending by the hot-rolled lamellar specimens ( $2 \times 20 \times 140 \cdot 10^{-3}$  m) of Cu-21.57 Zn-7 Al (wt.%) SMA, weighing  $43.7 \cdot 10^{-3}$  kg, was  $5.5 \cdot 10^{-3}$  J which gives a specific output of approximately  $0.126 \text{ J} \cdot \text{kg}^{-1}$ . The maximum work developed in tension by 0.5 m-long polyethylene terephthalate unstretched fibres, with  $0.32 \cdot 10^{-3}$  m diameter, weighing  $6 \cdot 10^{-5}$  kg, was  $0.1 \cdot 10^{-3}$  J, which gives an average specific work output of  $1.67 \text{ J} \cdot \text{kg}^{-1}$ .

#### ACKNOWLEDGEMENTS

The authors wish to thank Dr. S.Stanciu for his valuable help at the preparation of Cu-Zn-Al specimens and Mr. V.Dia for his kind support at tensile testing.

DSC analysis was performed during the visit of L.G.Bujoreanu at the Chair of Material Science, Institute for Materials, Faculty of Machine Building, Ruhr-University at Bochum, which was financially supported by the special research center **SFB 459 – Shape Memory Technology**

This paper was partially supported by the Romanian Ministry of Education and Research, under CNCSIS Grant No.476/ 2005.

## REFERENCES

1. Van Humbeeck, J., Stalmans, R. and Chandrasekaran, M. – *On the stability of shape memory alloys*, **Engineering Aspects of Shape Memory Alloys**, (Duerig, T.W., Melton, K.N., Stöckel, D. and Wayman, C.M., editors), Butterworth-Heinemann, London-Boston-Singapore-Sydney-Toronto-Wellington, 1990, ISBN 0-750-61009-3, **96-105**
2. Patoor, E. et Berveiller, M. (coordonateurs) – **Technologie des alliages à mémoire de forme. Comportement mécanique et mise en oeuvre**, Hermès, Paris, 1994, ISBN 2-86601-426-X
3. Funakubo, H. (editor), **Precision Machinery and Robotics, Vol.I, Shape Memory Alloys**, Gordon and Breach Science Publishers, ISSN 0889-860X
4. Harrison, J.D. – *Measurable changes concomitant with the shape memory effect transformation*, **Eng.Asp.Shape Mem.All.** (Duerig, T.W. *et al.* eds.) Butterworth-Heinemann, 1990, **106-111**
5. Duerig, T.W., Zadno, R. – *An engineer's perspective of pseudoelasticity*, **Eng.Asp.Shape Mem.All.** (Duerig, T.W. *et al.* eds.) Butterworth-Heinemann, 1990, **369-393**
6. Lieberman, D.S., Schmerling, M.A. and Karz, R.W. – *Ferroelastic "memory" and mechanical properties in gold-cadmium*, **Shape Memory Effects in Alloys**, (Perkins, J., editor), Plenum Press, New York-London, 1975, ISBN 0-306-30891-6, **203-244**
7. Van Humbeeck, J. and Stalmans, R. – *Characteristics of shape memory alloys*, **Shape Memory Materials**, (Otsuka, K. and Wayman, C.M., editors), Cambridge University Press, ISBN 0-521-44487-X, 1998, **149-183**
8. Bujoreanu, L.G., Ioniță, I. and Ailoei, E., *Devices based on work generating shape memory effect*, to be published
9. Bujoreanu, L.G., Craus, M.L., Rusu, I., Stanciu, S. and Sutiman, D. – *On the  $\beta_2$  to  $\alpha$  phase transformation in a Cu-Zn-Al-based shape memory alloy*, **Journal of Alloys and Compounds**, **278**, 1998, ISSN 0925-8388, **190-193**
10. Delaey, L. and Warlimont, H. – *Crystallography and thermodynamics of SME-martensites*, **Shape Mem. Eff. All.**, (Perkins, J., ed.), Plenum Press, 1975, **89-114**
11. Bujoreanu, L.G., *Variation of the critical point  $A_s$  during the thermomechanical training and subsequent cycling by two way shape memory effect of a Cu-Zn-Al-based shape memory alloy (in Romanian)*, **Metalurgia**, **52**, **Nr.3**, (2000), ISSN 0461-9579, **17-25**
12. Miyazaki, S. and Wayman, C.M. – *The R-phase transition and associated shape memory mechanism in Ti-Ni single crystals*, **Acta metall.**, **36**, 1988, **181-192**

**ASUPRA COMPORTAMENTULUI DE MEMORIA FORMEI  
LA ALIAJELE PE BAZĂ DE Cu ȘI POLIETILENTEREFTALAT (PET)**

**(Rezumat)**

S-a prezentat un studiu comparativ referitor la comportamentul de memoria formei la un aliaj cu memoria formei (AMF) Cu-Zn-Al și fibrele de polietilentereftalat (PET). În acest scop, au fost trecute în revistă structurile lor cristaline cu ordini de împachetare cu perioadă lungă și mecanismele de MF. Memoria mecanică a fost descrisă prin intermediul curbelor de încărcare-descărcare la tracțiune. Memoria termică a fost mai întâi analizată, prin intermediul termogramelor calorimetrice și termice care evidențiază transformările produse la încălzire și apoi a fost confirmată sub forma efectului de memoria formei generator de lucru mecanic.

## THE RESEARCH OF THE STRENGTH LEVEL OF THE WEAVING MACHINES' NOISE FOR THEIR RATIONAL DESIGN

BY

OVIDIU CALANCIA, LEONACHE DRĂGOI, VASILE-VIOREL MOLDOVEANU AND  
RADU DĂNILĂ

**Abstract:** The level of the acoustic pressure in the space where the machines are working is the highest one, most of the time exceeding the quote imposed by the ISO. In this paper, the level of the acoustic pressure in different weaving mills, is determined, as well as at the level of one machine, pointing out the influences and the needs to reduce the level of noise of the sound. The procedure which is used in this paper, or the results, can be used for other industrial machines.

**Keywords:** acoustic pressure, the noise from the weaving machines.

A very important matter concerning the noise produced by the textiles machines represents the global level of the noise from the weavings. The level of the acoustic pressure from the halls in which work classic weaving machines is higher (with 15÷20%) toward the level of the acoustic pressure from a weaving with unconventional machines.

ISO through the Committee TC-43 concerning the protection of the human hearing, the quality of the communication through speaking, and the annoying nature of the noise action, has settled standards for the noises. Actual standards from different countries don't differ in a major way of the ISO's recommendations. For example, the standards established the following maximal limits: for the intellectual work, the noise power T, is equal to 40 [sons] for paper work is 55 [sons], in hospitals, is 20 [sons], in industrials halls, is 85 [sons]. The measured values of the acoustic pressure level in different traditional weavings, table 1, show that, no matter what is the number and the type of the conventional weaving machines, the capacity or the halls type, the level of the acoustic pressure is considerably near and very high, over the ISO limit. For the noise measurement it is used many physics dimensions, some objectives, and other subjectives. The acoustic pressure of the sound, P, is an objective dimension and represents the local variation specific for the sound, which points out aided by a microphone.

Table 1. The level of the acoustic pressure in weavings

The type of hall	The type of machines	The number of machines	The level of the acoustic pressure dB			
			L	C	B	A
Multi-stage construction	Rutti and Diederich	72	102	100.5	100	100
Multi-stage construction	Rutti	98	101	100.5	99.5	98.5
Sheded construction	Unirea	192	102.5	101.5	101	101
Sheded construction	Unirea and Northrop	914	103.5	102.5	102	101.5
Armored construction	Rutti	500	101	100.5	99.5	99.5

In SI, the acoustic pressure has as units of measure  $N/m^2$  or the Pasqual. In the technical system are used another units of measure. The connection between the units of measure of the acoustic pressure is:

$$1 \text{ Pa} = 1 \text{ N/m}^2 = 10 \text{ dyn/cm}^2 = 10 \text{ } \mu\text{bar} = 1.02 \times 10^{-5} \text{ at}$$

where:  $1 \text{ bar} = 10^5 \text{ N/m}^2$ .

The level of the acoustics pressure,  $N_p$  is an objective unit and it is rendered by the formula (1):

$$N_p = 20 \log p/p_0 \quad (1)$$

where:  $p$  is the effectual acoustic pressure of the noise;

$p_0$  - the reference acoustic pressure;

$$p_0 = 2 \times 10^{-5} \text{ N/m}^2.$$

The level of the acoustic pressure is measured in [decibels] dB.

The power of the sound,  $N_t$  is a subjective unit and it is calculated with the formula (2):

$$N_t = 20 \log \left( \frac{p}{p_0} \right)_{f=1000\text{Hz}} \quad (2)$$

where:  $p$  is the effectual acoustic pressure of a pure sound (without double and harmonious frequencies) with the frequency of 1000 Hz estimated by a normal ottological listener, by having an intensity equal to the one of the reference sound.

$p_0$  - the acoustic pressure of reference

The level of the force of the sound is measured in [fons].

The force of the sound,  $T$ , is a subjective unit which shows out how many times is more powerful a sound appreciated by normal ottological listener than a sound of 1000Hz and a level of strength of 40 [fons]. The power of the sound is obtained with this formula (3):

$$T = 2^{\frac{N_t - 40}{10}} \quad (3)$$

The growth of the power level of the sound with 10 [fons] it is appreciated as a doubled strength of the sound. The power of the sound is measured in [fons].

### Experimental researches

To study the noise produced by a machine, we make the spectrum analyse of the level of the acoustic pressure produced by the parts from the noise comprised in different frequency bands.

The experiments are made with the precision soundmeter realized by the Bruel and Kjaer from Denmark .

The right measurement is made counting on a serial of initial conditions concerning the acoustic field in which are made the measurements, the microphone placement reported to the acoustic source, as well as some of the estimated criteria of the noise.

The disturbing noise (when the machine doesn't work) is maintained constantly and its acoustic level in the entire spectrum is maintained with at least 10 dB lower than the existent acoustic level at the machine functioning.

Because of the fact that the weaving machines produce a variable acoustic field, caused by the cyclical functioning of the component mechanisms, the measurement are realised in more points around them. The distance between the soundmeter microphone and machine depends on the halls dimensions where the measurements are made, the level of the fund noise, the shape and size of the machine, the degree of uniformity of the acoustic field made by a machine. The measurements are made in the free and diffuse acoustic field.

For a weaving machine, hypothetical surface of measurement is considered to be parallelipipedical, the placement points of the microphone are taken in the horizontal plane position, around the machine and in the vertical plane, at a distance of minimum one meter.

The experiments were made on a conventional weaving machine type A-100, finding out the values of the acoustic pressure level, table 2.

Table 2. Experimental and calculated values

Frequency band, Hz	31.5		63	125	250	500	1000	2000	4000	8000	16000	31500
Dimension												
$N_p$ , dB	I	62	68	74	77	83	85.5	86	85	81	71	51
	II	62	69	72	76	82	86	89	88	85	79	62
	III	62	69.5	73	75	81	84.5	87	85	81	72	50
	IV	64	69	75	76	83	86	86.5	84	78	69.5	48
$N_p$ , dB	62.5		68.8	73.5	76	82.2	85.5	87.1	85.5	81.2	72.8	52.75
$T_i$ , sons	1.3		2.5	5.2	8.0	14.7	23	30	35	34	-	-
$\sum T_i$ , sons	153.7											
$T_g$ , sons	70.61											
$N_t$ , fons	101.41											

Where: I- the mechanism zone of launching from the right;

II- the mechanism zone of launching from the left;

III- left –beck warp regulator zone;

IV- the electromotive zone.

It calculated the media values of the acoustic pressure level,  $N_p$ , for each frequency bands, according to the four measurement areas.

It was found the sound's intensity,  $T_j$ , in every frequency band, based on the media acoustic pressure level  $N_p$ , using Steven's nomogram [2]. Then, it was calculated the global strength of the sound,  $T_g$ , with the formula (4):

$$T_g = T_{\max} + k \left( \sum T_i - T_{\max} \right) \quad (4)$$

where:  $T_g$  is the global strength in [sons]

$T_{\max}$  - the highest value of the sound strength obtained in a frequency band;

k- coefficient which depends on the filter value ( $k=0.3$ );

$\sum T_i$  - the sum of the medium strength ness from all the frequency bands.

The strength level of the sound,  $N_t$ , in [fons], was obtained using the formula (3), which becomes:

$$N_t = \frac{10 \log T_g}{\log 2} + 40 \quad (5)$$

## Interpretations and conclusions

According to the experimental results processed in the second table, the level of the acoustic pressure, determined in different frequency bands, has an ascending evolution, with the frequency rise, till the level of the 2000 Hz band, and than lowers, reaching the minimal values, to the 31500 Hz frequency.

We observe differences of the acoustic pressure level, in the zone of the weaving machine and even same frequency bands.

It is not over fulfill the limit of the strength sound of 85 [sons], indicated by the ISO standards.

The global strength of the sound determined at only one machine is of 70.61 [sons]. But, considering the noise levels from the conventional weavings (Table 1), the strength of the sound over fulfill the ISO limit.

The level of the sound strength of only one weaving machine is already very high;  $N_t = 101.41$  [fons] (Table 2).

To reduce the sound level, it is imposed that the experts, in the design period of the equipment and the working halls, and in the exploitation period of the equipments, to adopt the following aspects:

- design of equipments with a higher weight of the pneumatic and hydraulic systems, reported to the mechanic- elastic systems, which are very important today;
- optimization of the maintenance strategies of the textiles equipments;
- casing and rigorous tighten of the mechanisms;
- redesign of silent mechanisms;
- optimal regulation of the functional parameters of the textiles equipments;
- elastically setting of the equipments on the exploitation place;
- the cover of the halls' walls and ceilings with phonoabsorbing panels;
- individual protection of the working against the noise using antiphonals.

The experiments can be extended to the other textiles machines to take some adequate decisions for the reduction of the noise level in the textiles domain.

*Received May 9, 2005*

*The "Gh.Asachi" Technical University from Iasi*

## REFERENCES

1. Drăgoi, L. – Elemente de proiectare a utilajelor din țesătorie, Editura BIT, 1997, Iași
2. \*\*\*Prospecte ale firmelor: Bruel și Kjaer, Hottinger- Baldwin, Messtechnik, Philips.

CERCETAREA NIVELULUI DE TARIE A ZGOMOTULUI MASINILOR DE TESUT IN VEDEREA PROIECTARII RATIONALE A ACESTORA

### (Rezumat)

Nivelul de presiune acustică din halele în care funcționează mașini de țesut clasice este mult mai ridicat față de nivelul de presiune acustică dintr-o țesătorie cu mașini neconvenționale și depășește normele ISO. Lucrarea prezintă modul de determinare a zgomotului la o mașină și măsuri de reducere.

## CORROSION OF ALUMINIUM ALLOYS IN ALKALINE MEDIA

BY

GABRIELA CIOBANU\*, LAURENȚIU-DAN GHENGHEA\*, LĂCRĂMIOARA ISTRATI\*\*  
and GABRIELA CÂRJĂ\*

**Abstract:** Aluminium, having attractive properties such as high energy density and high negative potential in alkaline media, combined with low density, high abundance in earth's crust and low cost, offers an attractive choice as galvanic anode in primary alkaline batteries. In the present investigation, the corrosion and inhibition of corrosion of aluminium and some of its alloys in sodium hydroxide solutions containing zinc oxide have been studied. The self-corrosion rate and hydrogen evolution rate were examined by weight loss measurements and by measuring the volume of the evolved hydrogen.

**Keywords:** aluminium, alloy, corrosion, alkaline solution, inhibition, zinc oxide

### 1. Introduction

In last period much interest has been focused on the development of aluminium alloys for use in metal - air batteries, respectively in primary alkaline batteries, as galvanic anode.

This because aluminium possesses attractive electrochemical properties like high energy density, high ampere and high negative open circuit potential in alkaline solutions combined with low density, high abundance in earth's crust and low cost [1,2].

But several problems have blocked the use of aluminium as galvanic anode in alkaline batteries, such as high self-corrosion with hydrogen evolution in alkaline solution at open circuit conditions and during cell discharge

In aqueous solution, corrosion of aluminium takes place with evolution of hydrogen. The self-corrosion of a metal to some extent is avoided in a neutral medium, through the intrinsic formation of a protective oxide film at the expense of the electrochemical characteristics.

The high protective oxide skin of aluminium is broken by the action of chloride ions in solutions and also by the action of alkaline solution.

In fact a close examination of the potential ÷ pH diagram of the Al ÷ H<sub>2</sub>O system, indicates clearly that highly negative potentials are attained by aluminium in the alkaline pH range and the corrosion of aluminium increases rapidly with pH. A protective film does not develop in alkaline solution, as the amphoteric aluminium hydroxide dissolves in it [3-6].

In alkaline media aluminium readily dissolves, it generates a useful voltage at a reasonable current provided its wasteful corrosion is suppressed.

This can be achieved in two ways. In the first method, inhibitors, addition agents or complexing agents are added to the electrolyte to make it less corrosive. In the second method, aluminium is mixed with other elements such as Zn, In, Ga, Pb etc. to render its less corrodible in alkaline media [7-12].

In the present paper, the corrosion and the inhibition of corrosion of aluminium and its some alloys in sodium hydroxide solution containing zinc oxide as inhibitor have been studied. The Al and their alloys were evaluated by determination of both the weight loss as well as the evolved hydrogen as function of time.

## 2. Experimental procedure

*Materials:* Measurements were made on Al (99.7 % Al) and some of its alloys, namely: Al – Mg (94.1 % Al, 5.4 % Mg) and Al – Mn (94.3 % Al, 5.2 % Mn). Rectangular pieces of size 5 cm x 2 cm x 1 cm were used for self-corrosion studies. Before immersion in the test electrolyte (i.e., NaOH solution with / without ZnO) the surface of the specimens were subjected to a sequence of surface treatment procedures. The pieces were abraded succesively with metallographic emery paper of increasing fineness, then degreased with trichloroethylene and washed with running distilled water.

Each experiment was carried out with a newly polished piece and with fresh electrolyte. The sodium hydroxide was of reagent quality and the zinc oxide was of 99 % purity. All the solutions were prepared using distilled water.

*Corrosion rate measurements:* Corrosion rate was measured by determining the weight loss of the weighed specimens after immersion in 500 ml of the test solution containing NaOH, with / without ZnO, for different durations of 5 until 30 minutes at room temperature. Also, corrosion rate was determined by measuring the volume of the evolved hydrogen.

At the end of each period, the specimens were removed, washed well with distilled water, dried, weighed and kept in a desiccator. During the course of these experiments the solution was not stirred, as in an actual battery the electrolyte is under stagnant conditions when the current is not drained.

The integral weight loss of the sample ( $\Delta m$ ) over the duration of the test was determined from the following relation:

$$\Delta m = m_1 - m_2 \quad (1)$$

where  $m_1$  and  $m_2$  represent the weight the specimen before and after weighing, respectively, reported at surface of the metallic piece.

## 3. Experimental results and discussion

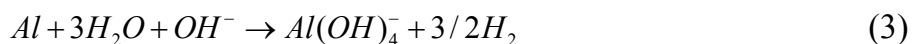
The self-corrosion rates of aluminium and its alloys obtained by weight loss and hydrogen evolution rate in 5m NaOH solution in absence and in presence of 0.3m ZnO were determined simultaneously.

Table 1 shows the variation of the integral weight loss and of the volume of the evolved hydrogen with time.

The results indicate that, for alloy samples, the hydrogen evolution rate increase with the time, which reveals the increased corrosion rate of alloys, can be attributed to

an increase in actual interfacial area resulting from progressive roughening of the surface due to the corrosion.

In the case of Al sample, the rate of hydrogen evolution increases slowly in the early moments of immersion then increases continuously after an exposure time of 5 min. The air-formed oxide layer initially dissolves in the early minutes of immersion at a low rate and then the dissolution reaction of the metal proceeds at a relatively fast rate. The process by which Al is chemically attacked in alkaline solution of high concentration is described by following equations:



The Eq.3 was obtained by following partial reactions:

- the partial anodic dissolution reaction of aluminium:



- the partial cathodic reaction, where the electrons produced by the partial anodic reaction (Eq.4) will be consumed immediately by the water reduction:



Therefore, hydrogen evolution takes place simultaneously with the dissolution of aluminium metal as a result of the overall corrosion reaction (Eq.3). The observation of gas bubbles on the corroding aluminium surface show that the corrosion of pure aluminium in alkaline solution proceeds mainly by water reduction.

Table 1 Corrosion behaviour of aluminium and its alloys in 5m NaOH with/without 0.3m ZnO, at room temperature

Sample	Al			Al – Mg			Al – Mn		
	5	10	20	5	10	20	5	10	20
Series 1: corrosion in 5m NaOH solution									
Integral weight loss; mg/cm <sup>2</sup>	5.2	12.1	26.1	7.8	16.8	34.5	10.7	22.9	47.8
Hydrogen evolved; ml/cm <sup>2</sup>	1.8	4.2	9.0	2.7	5.8	11.9	3.7	7.9	16.5
Corrosion rate; mg/cm <sup>2</sup> /min	1.04	1.21	1.30	1.56	1.68	1.72	2.14	2.29	2.39
Series 2: corrosion in 5m NaOH + 0.3m ZnO solution									
Integral weight loss; mg/cm <sup>2</sup>	3.4	10.1	24.9	6.3	14.7	31.0	8.7	21.1	46.1
Hydrogen evolved; ml/cm <sup>2</sup>	1.2	3.5	8.6	2.2	5.1	10.7	3.0	7.3	15.9
Corrosion rate; mg/cm <sup>2</sup> /min	0.69	1.01	1.24	1.27	1.47	1.55	1.74	2.11	2.30

The Fig. 1 shows the integral corrosion rate obtained by weight loss for tested samples in 5m NaOH solution with/without 0.3m ZnO at room temperature.

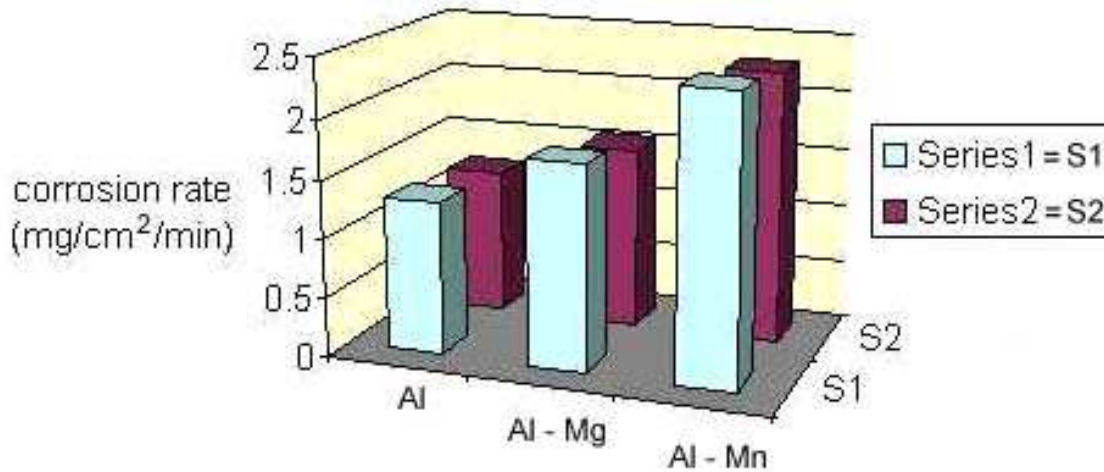
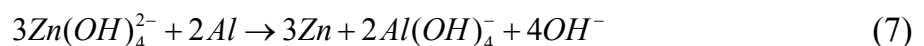


Fig.1 Corrosion rate of aluminium and its alloys: Al – Mg and Al – Mn in 5m NaOH solution (Series 1) and in 5m NaOH solution + 0.3m ZnO (Series 2), at room temperature

It can be seen that Al – Mn alloy shows higher corrosion rate and they cannot be considered for use as anodes in alkaline batteries.

The increased corrosion rate of Al – Mn alloy can be explained on the basis of the fact that Mn is cathodic to Al and this gives rise to anodic dissolution of the base metal Al. Also, Al – Mg alloy exhibits the lower corrosion rate compared Al – Mn alloy, but it is greater than the value of pure aluminium. This can be explained by the fact that the presence of Mg as an anodic impurity in alloy gives rise to cathodic polarization (cathodic protection) of the base metal aluminium.

Also, the experimental results presented in Table 1 and Fig. 1 show that the addition of zinc oxide to the NaOH solution inhibited the corrosion of Al and its alloys. This can be explained by the facts that in the zincate – containing alkaline solution occur following processes on aluminium piece surface: dissolution of aluminium, hydrogen evolution and deposition – dissolution of zinc:



The results reveal that ZnO produces an inhibition effect on the corrosion of aluminium by the formation of a zinc deposit on the surface of aluminium. Unfortunately, the adhesion between the zinc layer and the aluminium is poor and this possibly affects the safe use of aluminium as anode in batteries.

#### 4. Conclusions

The following main conclusions can be drawn:

(i) The self-corrosion of aluminium and some of its alloys in 5m NaOH solution alone follows the order: Al < Al – Mg < Al – Mn.

(ii) The self-corrosion of aluminium and some of its alloys in 5m NaOH containing 0.3m ZnO follows the order: Al < Al – Mg < Al – Mn.

(iii) The corrosion of aluminium and some of its alloys in 5m NaOH solution can be inhibited by the addition of ZnO. The results reveal that ZnO produces an inhibition effect on the corrosion of aluminium by the formation of a zinc deposit on the surface of aluminium. But poor adhesion between the zinc layer and the aluminium surface possibly affects the safe use of aluminium as anode in batteries.

Received April 26, 2005

\*The "Gh.Asachi" Technical University Iași

\*\*The University of Bacău

#### REFERENCES

1. Paramasivam, M., Jayachandran, M. and Venkatakrishna Iyer, S. – *Influence of alloying additives on the performance of commercial grade aluminium as galvanic anode in alkaline zincate solution for use in primary alkaline batteries*, **J. Appl. Electrochem.**, **33/3-4**, 2003, ISSN 0021-891X, **303-309**
2. Zein El Abedin, S. and Saleh, A.O. – *Characterization of some aluminium alloys for application as anodes in alkaline batteries*, **J. Appl. Electrochem.**, **34/3**, 2004, ISSN 0021-891X, **331-335**
3. Pyun, S.I. and Moon, S.M. – *Corrosion mechanism of pure aluminium in aqueous alkaline solution*, **J. Solid State Electr.**, **4/5**, 2000, ISSN 1432-8488, **267-272**
4. Van Gheem, E., Vereecken, J. and Le Pen, C. – *Influence of different anions on the behaviour of aluminium in aqueous solutions*, **J. Appl. Electrochem.**, **32/11**, 2002, ISSN 0021-891X, **1193-1200**
5. Paramasivam, M. and Venkatakrishna Iyer, S. – *Influence of alloying additives on corrosion and hydrogen permeation through commercial aluminium in alkaline solution*, **J. Appl. Electrochem.**, **31/1**, 2001, ISSN 0021-891X, **115-119**
6. Mazhar, A.A., Arab, S.T. and Noor, E.A. – *The role of chloride ions and pH in the corrosion and pitting of Al-Si alloys*, **J. Appl. Electrochem.**, **31/10**, 2001, ISSN 0021-891X, **1131-1140**
7. Fouda, A.S. and Elasmay, A.A. – *Efficiency of some phenylthiosemicarbazide derivatives in retarding the dissolution of Al in NaOH solution*, **Monatsh. Chem.**, **118/6-7**, 1987, ISSN 0026-9247, **709-716**
8. Salih, S.A., Gad-Allah, A.G., Mazhar, A.A. and Tammam, R.H. – *Effect of silicon alloying addition on the corrosion behaviour of aluminium in some aqueous media*, **J. Appl. Electrochem.**, **31/10**, 2001, ISSN 0021-891X, **1103-1108**
9. Lee, K.K. and Kum, K.B. – *Electrochemical impedance characteristics of pure Al and Al-Sn alloys in NaOH solution*, **Corros. Sci.**, **43/3**, 2001, ISSN 0010-938X, **561-575**
10. Kapali, V., Venkatakrishna Iyer, S., Balaramachandran, V., Sarangapani, K.B., Ganesan, M., Kulandainathan, M.A. and Mideen, A.S. – *Studies on the best alkaline electrolyte for aluminium / air batteries*, **J. Power Sources**, **39/2**, 1992, ISSN 1388-2481, **263-269**
11. Sarangapani, K.B., Balaramachandran, V. and Kapali, V. – *Aluminium as anode in primary alkaline batteries. Influence of additives on the corrosion and anodic behaviour of 2S aluminium in alkaline citrate solution*, **J. Appl. Electrochem.**, **14/4**, 1984, ISSN 0021-891X, **475-480**
12. Carbonini, P., Monetta, T. and Mitton, D.B. – *Degradation behaviour of 6013-T6, 2024-T3 alloys and pure aluminium in different aqueous media*, **J. Appl. Electrochem.**, **27/10**, 1997, ISSN 0021-891X, **1135-1142**

**COROZIUNEA ALIAJELOR DE ALUMINIU ÎN MEDII ALCALINE****(Rezumat)**

Aluminiul reprezintă o variantă atractivă de material din care se pot confecționa anozii pilelor alcaline primare. Aceasta se datorează în principal faptului că în medii alcaline aluminiul conferă pilei o mare densitate de energie și are un potențial negativ ridicat, dar și datorită abundenței în scoarța terestră și a costului său scăzut. În lucrarea de față se studiază procesul de coroziune a aluminiului și a unor aliaje proprii în medii alcaline, respectiv în soluții de hidroxid de sodiu de diverse concentrații în care s-a adăugat oxid de zinc drept inhibitor de coroziune. Viteza de autocoroziune a aluminiului și a aliajelor sale s-a determinat atât prin metoda gravimetrică, prin măsurarea pierderii de masă, cât și prin metoda volumetrică, prin măsurarea volumului de hidrogen degajat. Se constată că prezența ZnO în soluția de NaOH are efect de inhibare a coroziunii aluminiului și a aliajelor sale cu Mg și Mn, cu observația că stratul de oxid de zinc nu este perfect aderent la suprafața metalică.

## KINETIC AND THERMODYNAMIC ASPECTS CONCERNING CORROSION OF ALUMINIUM ALLOYS IN ALKALINE MEDIA

BY

GABRIELA CIOBANU\*, LAURENȚIU-DAN GHENGHEA\*, GABRIELA CÂRJĂ\* and  
LĂCRĂMIOARA ISTRATI\*\*

**Abstract:** In the present investigation, the influence of temperature on the corrosion and inhibition of corrosion of aluminium and some of its alloys in sodium hydroxide solutions containing zinc oxide have been studied. The self-corrosion rate was examined by weight loss measurements and by measuring the volume of the evolved hydrogen. A kinetic and a thermodynamic study have been developed. Thermodynamic functions obtained from this study indicate that the presence of the ZnO inhibitor increases the activation energy and the negative values of  $\Delta G$  indicated spontaneous adsorption of inhibitor on the metal surface.

**Keywords:** aluminium, alloy, corrosion, alkaline solution, inhibition, zinc oxide, temperature

### 1. Introduction

In last period much interest has been focused on the development of aluminium alloys for use in metal - air batteries, respectively in primary alkaline batteries, as galvanic anode.

This because aluminium possesses attractive electrochemical properties like high energy density, high ampere and high negative open circuit potential in alkaline solutions combined with low density, high abundance in earth's crust and low cost [1].

Several problems have blocked the use of aluminium as galvanic anode in alkaline batteries, such as high self-corrosion with hydrogen evolution in alkaline solution at open circuit conditions and during cell discharge.

A protective film does not develop in alkaline solution, as the amphoteric aluminium hydroxide dissolves in it [2,3]. In alkaline media aluminium readily dissolves, it generates a useful voltage at a reasonable current provided its wasteful corrosion is suppressed.

This can be achieved in two ways. In the first method, inhibitors, addition agents or complexing agents are added to the electrolyte to make it less corrosive. In the second method, aluminium is mixed with other elements such as Zn, In, Ga, Pb etc. to render its less corrodible in alkaline media [4-8].

In the present paper, the influence of temperature on the corrosion and the inhibition of corrosion of aluminium and its some alloys in sodium hydroxide solution containing zinc oxide as inhibitor have been studied.

The Al and its alloys were evaluated by determination of both the weight loss as well as the evolved hydrogen as function of temperature. Also, a kinetic and a

thermodynamic study of the processes of corrosion and inhibition of corrosion of aluminium and its some alloys in sodium hydroxide solution containing zinc oxide as inhibitor have been developed.

## 2. Experimental procedure

*Materials:* Measurements were made on Al (99.7 % Al) and some of its alloys, namely: Al – Mg (94.1 % Al, 5.4 % Mg) and Al – Mn (94.3 % Al, 5.2 % Mn). Rectangular pieces of size 5 cm x 2 cm x 1 cm were used for self-corrosion studies. Before immersion in the test electrolyte (i.e., NaOH solution with / without ZnO) the surface of the specimens were subjected to a sequence of surface treatment procedures. The pieces were abraded succesively with metallographic emery paper of increasing fineness, then degreased with trichloroethylene and washed with running distilled water. Each experiment was carried out with a newly polished piece and with fresh electrolyte. The sodium hydroxide was of reagent quality and the zinc oxide was of 99 % purity. All the solutions were prepared using distilled water.

*Corrosion rate measurements:* Corrosion rate was measured by determining the weight loss of the weighed specimens after immersion in 500 ml of the test solution containing NaOH, with / without ZnO, for different durations at various temperature. Also, corrosion rate was determined by measuring the volume of the evolved hydrogen. At the end of each period, the specimens were removed, washed well with distilled water, dried, weighed and kept in a desiccator. During the course of these experiments the solution was not stirred, as in an actual battery the electrolyte is under stagnant conditions when the current is not drained.

The integral weight loss of the sample ( $\Delta m$ ) over the duration of the test was determined from the following relation:

$$\Delta m = m_1 - m_2 \quad (1)$$

where  $m_1$  and  $m_2$  represent the weight the specimen before and after weighing, respectively, reported at surface of the metallic piece.

The percentage inhibition efficiency ( $\eta$ ) and the metal surface coverage ( $\theta$ ) were calculated using the following relations:

$$\eta = \left(1 - \frac{\Delta m_{pi}}{\Delta m_{ai}}\right) \cdot 100 \quad (2)$$

$$\theta = 1 - \frac{\Delta m_{pi}}{\Delta m_{ai}} \quad (3)$$

where  $\Delta m_{ai}$  and  $\Delta m_{pi}$  represent the integral weight losses in absence and in presence of inhibitor, respectively.

## 3. Experimental results and discussion

When temperature is raised, corrosive processes are usually accelerated, especially in media in which evolution of hydrogen accompanies corrosion, e.g. during corrosion of aluminium and its alloys in alkali.

The self-corrosion rates of aluminium and its alloys obtained by weight loss and hydrogen evolution rate in 5m NaOH solution in absence and in presence of 0.3m ZnO

were determined simultaneously at different temperatures. Table 1 shows the variation of the corrosion rate with temperature.

The results indicate that, for all samples, the weight loss and the hydrogen evolution rate increases with the temperature, which reveals the increased corrosion rate.

The results reveal that ZnO produces an inhibition effect on the corrosion of aluminium by the formation of a zinc deposit on the surface of aluminium. The results indicate that increase in temperature leads to an increase in the inhibition efficiency,  $\eta$ .

Table 1 Corrosion rates of aluminium and its alloys in 5m NaOH solution with/without 0.3m ZnO at various temperatures (test period: 10 min)

Sample	Al			Al – Mg			Al – Mn		
	293	313	323	293	313	323	293	313	323
Series 1: corrosion in 5m NaOH solution									
Integral weight loss; mg/cm <sup>2</sup>	12.1	23.7	41.5	16.8	29.3	51.2	22.9	37.1	65.3
Hydrogen evolved; ml/cm <sup>2</sup>	4.2	8.2	14.3	5.8	10.1	17.6	7.9	12.8	22.5
Corrosion rate, $V_{cor}$ ; mg/cm <sup>2</sup> /min	1.21	2.37	4.15	1.68	2.93	5.12	2.29	3.71	6.53
Series 2: corrosion in 5m NaOH + 0.3m ZnO solution									
Integral weight loss; mg/cm <sup>2</sup>	10.1	19.3	31.7	14.7	23.5	39.8	21.1	29.3	54.6
Hydrogen evolved; ml/cm <sup>2</sup>	3.5	6.6	10.9	5.1	8.1	13.7	7.3	10.1	18.8
Corrosion rate, $V_{cor}$ ; mg/cm <sup>2</sup> /min	1.01	1.93	3.17	1.47	2.35	3.98	2.11	2.93	5.46
Inhibition efficiency, $\eta$ ; %	16.5	18.5	23.6	11.1	19.7	22.2	7.8	21.0	16.3

The activation parameters such as apparent activation energy ( $E_a^*$ ), the enthalpy change ( $\Delta H^*$ ) and the entropy change ( $\Delta S^*$ ) for the corrosion / inhibition of aluminium and some of its alloys in 5m NaOH solution with / without ZnO are obtained from the Arrhenius-type equation:

$$\ln V_{cor} = -\frac{E_a^*}{R \cdot T} + A \quad (4)$$

and from the Eyring transition-state equation:

$$\ln \left( \frac{V_{cor}}{T} \right) = -\left( \frac{\Delta H^*}{R \cdot T} \right) + \ln \left( \frac{R}{N_A \cdot h} \right) + \left( \frac{\Delta S^*}{R} \right) \quad (5)$$

where  $V_{cor}$  is the corrosion rate,  $A$  is the pre-exponential factor,  $h$  is Planck's constant,  $N_A$  is Avogadro's number,  $R$  is the universal gas constant and  $T$  is the temperature.

Plots of  $\ln V_{cor}$  against  $1/T$  and  $\ln(V_{cor}/T)$  against  $1/T$  give straight lines with slopes of  $-E_a^*/R$  and  $-\Delta H^*/R$ , respectively. The intercepts are  $A$  and  $[\ln(R/N_A h) + \Delta S^*/R]$  for Arrhenius and Eyring transition-state equations, respectively.

The calculated values of  $E_a^*$ ,  $\Delta H^*$  and  $\Delta S^*$ , obtained from plots are tabulated in Table 2. Due to the presence of ZnO in the alkaline medium, the values of  $E_a^*$ ,  $\Delta H^*$  and  $\Delta S^*$  are lowest in the uninhibited solution.

Moreover, the existence of inhibitor in solution leads to an increase in the value of  $E_a^*$ , indicating an adsorption of the inhibitor molecules at the metal surface.

The results in Table 2 also show that the presence of the inhibitor produces higher values for  $\Delta H^*$  than those obtained for the uninhibited solution. This indicates higher protection efficiency.

This may be attributed to the presence of an energy barrier for the reaction, that is, the process of adsorption leads to a rise in the enthalpy of the corrosion process. In addition, the  $\Delta S^*$  in the presence and absence of the inhibitor is large and negative, indicating that a decrease in disorder takes place.

Table 2 Activation parameters for the corrosion of aluminium and its alloys in 5m NaOH solution with/without 0.3m ZnO at various temperatures (test period: 10 min)

Sample	Al			Al – Mg			Al – Mn		
T; K	293	313	323	293	313	323	293	313	323
Series 1: corrosion in 5m NaOH solution									
$E_a^*$ ; kJ/mol	28.834			24.004			22.689		
$\Delta H^*$ ; kJ/mol	26.348			21.999			20.145		
$\Delta S^*$ ; J/mol/K	- 248.49			- 239.96			- 235.97		
Series 2: corrosion in 5m NaOH + 0.3m ZnO solution									
$E_a^*$ ; kJ/mol	30.946			27.670			25.538		
$\Delta H^*$ ; kJ/mol	28.413			25.126			23.205		
$\Delta S^*$ ; J/mol/K	- 240.027			- 228.204			- 224.704		

The free energy of adsorption ( $\Delta G_{ads}^*$ ) for the adsorption of ZnO on surface of aluminium and its alloys in 5m NaOH solution at different temperatures (Table 3) was calculated from equation:

$$\Delta G_{ads}^* = -R \cdot T \cdot \ln(55.5 \cdot K) = -R \cdot T \cdot \ln\left(55.5 \cdot \frac{\theta}{(1-\theta) \cdot c}\right) \quad (6)$$

where  $\theta$  is the degree of coverage on the metal surface and  $c$  is the concentration of inhibitor in the bulk of solution.

Table 3 Thermodynamic parameters for the adsorption of ZnO on surface of aluminium and its alloys in 5m NaOH solution at various temperatures (test period: 10 min)

Sample	Al			Al – Mg			Al – Mn		
	T; K	293	313	323	293	313	323	293	313
$\theta$	0.16	0.18	0.23	0.11	0.19	0.22	0.07	0.21	0.16
$\Delta G_{ads}^*$ ; kJ/mol	- 8.65	- 9.63	-10.75	- 7.61	- 9.80	-10.62	- 6.40	- 9.90	-8.58

The negative values of  $\Delta G_{ads}^*$  suggest the strong interaction of the inhibitor molecules whereas low values of  $\Delta G_{ads}^*$  indicated spontaneous adsorption of inhibitor on the aluminium surface.

#### 4. Conclusions

The following main conclusions can be drawn:

(i) The self-corrosion of aluminium and some of its alloys in 5m NaOH solution alone, respectively in 5m NaOH solution containing 0.3m ZnO at various temperatures follows the same order: Al < Al – Mg < Al – Mn.

(ii) The corrosion of aluminium and some of its alloys in 5m NaOH solution can be inhibited by the addition of ZnO. The results reveal that ZnO produces an inhibition effect on the corrosion of aluminium by the formation of a zinc deposit on the surface of aluminium.

(iii) Thermodynamic functions obtained from this study, i.e.  $E_a^*$ ,  $\Delta H^*$ ,  $\Delta S^*$  and  $\Delta G_{ads}^*$ , indicate that the presence of the ZnO as inhibitor increase the activation energy. The negative values of  $\Delta G_{ads}^*$  indicated spontaneous adsorption on the metal surface.

Received April 26, 2005

\*The "Gh.Asachi" Technical University Iași

\*\*The University of Bacău

#### REFERENCES

1. Zein El Abedin, S. and Saleh, A.O. – *Characterization of some aluminium alloys for application as anodes in alkaline batteries*, **J. Appl. Electrochem.**, **34/3**, 2004, ISSN 0021-891X, **331-335**
2. Pyun, S.I. and Moon, S.M. – *Corrosion mechanism of pure aluminium in aqueous alkaline solution*, **J. Solid State Electr.**, **4/5**, 2000, ISSN 1432-8488, **267-272**
3. Paramasivam, M. and Venkatakrishna Iyer, S. – *Influence of alloying additives on corrosion and hydrogen permeation through commercial aluminium in alkaline solution*, **J. Appl. Electrochem.**, **31/1**, 2001, ISSN 0021-891X, **115-119**
4. Salih, S.A., Gad-Allah, A.G., Mazhar, A.A. and Tammam, R.H. – *Effect of silicon alloying addition on the corrosion behaviour of aluminium in some aqueous media*, **J. Appl. Electrochem.**, **31/10**, 2001, ISSN 0021-891X, **1103-1108**
5. Lee, K.K. and Kum, K.B. – *Electrochemical impedance characteristics of pure Al and Al-Sn alloys in NaOH solution*, **Corros. Sci.**, **43/3**, 2001, ISSN 0010-938X, **561-575**
6. Kapali, V., Venkatakrishna Iyer, S., Balaramachandran, V., Sarangapani, K.B., Ganesan, M., Kulandainathan, M.A. and Mideen, A.S. – *Studies on the best alkaline electrolyte for aluminium / air batteries*, **J. Power Sources**, **39/2**, 1992, ISSN 1388-2481, **263-269**

7. Sarangapani, K.B., Balaramachandran, V. and Kapali, V. – *Aluminium as anode in primary alkaline batteries. Influence of additives on the corrosion and anodic behaviour of 2S aluminium in alkaline citrate solution*, **J. Appl. Electrochem.**, **14/4**, 1984, ISSN 0021-891X, **475-480**
8. Carbonini, P., Monetta, T. and Mitton, D.B. – *Degradation behaviour of 6013-T6, 2024-T3 alloys and pure aluminium in different aqueous media*, **J. Appl. Electrochem.**, **27/10**, 1997, ISSN 0021-891X, **1135-1142**

#### ASPECTE CINETICE ȘI TERMODINAMICE PRIVIND COROZIUNEA ALIAJELOR DE ALUMINIU ÎN MEDII ALCALINE

##### (Rezumat)

În lucrarea de față se studiază influența temperaturii asupra procesului de coroziune a aluminiului și a unor aliaje proprii în medii alcaline, respectiv în soluții de hidroxid de sodiu de diverse concentrații în care s-a adăugat oxid de zinc drept inhibitor de coroziune. De asemenea, se urmărește o investigație a unor aspecte cinetice și termodinamice privind procesul de coroziune. Viteza de autocoroziune a aluminiului și a aliajelor sale s-a determinat atât prin metoda gravimetrică, prin măsurarea pierderii de masă, cât și prin metoda volumetrică, prin măsurarea volumului de hidrogen degajat. Funcțiile termodinamice obținute indică faptul că prezența ZnO în soluția alcalină conduce la o creștere a energiei de activare, ceea ce înseamnă o scădere a vitezei de coroziune. De asemenea, valorile vegative ale energiei libere de adsorbție indică o adsorbție spontană a inhibitorului pe suprafața metalică.

## MANAGEMENT RISK DETERMINATION

BY

PETRU P. CONDREA

**Abstract:** In order to determine and approach the risk, it should be identified and consistently defined, analyzed based on documents by the entity management. This approach enables the management to realize what is the nature of the risk interrelations. The more a risk grows, the more another risk grows or diminishes. When a risk is evaluated, the auditor and the entity management have to take into account the risk impact if it occurs and the probability for the risk to determine a proportional feedback.

**Key words:** management, audit, risk, procedures, control, evaluation.

A very important aspect of the development of some modern and efficient internal control systems is the risk management process. The risk management is the systematic application of management policies, procedures and practices with the purpose of analyzing, evaluating, controlling and communicating risk-related issues. Against this background, risk is understood as the probability that the entity's objective might not be achieved. Specifically, the internal control is the system by which the management of an audited structure will try to manage the risk. The process starts with a global strategy that specifies the approach and the attitude towards risk of an audited entity, and the policies it developed to manage the risk within acceptable limits. A framework of the risk management will never completely eliminate risks, wither financial or non-financial risks, but the framework applied will explain what risk level is acceptable for such entity and how it manages the operations of maintaining risk within these limits.

In risk determination, it is important that the definitions used for categorizing and evaluating the risk should be clear and adequate to the entity, and that the management specifies with precision how it is going to obtain the insurance that the risk is going to be adequately controlled.

Risk will be always defined in accordance with what is acceptable for the interested parties. This may include auditor members, from the management or politicians from Parliament. To successfully identify and manage risk, the management will have to become aware what risks are acceptable to all groups of interest.

To identify and approach the risk, it should be consistently identified and defined, analyzed based on documents by the entity management. This enables the management to realize what is the nature of the risk interrelations, for instance the more a risk grows, the more another risk grows or diminishes. When a risk is

evaluated, the auditor and the entity management have to take into account the risk impact if it occurs and the probability for the risk to determine a proportional feedback. When taking into account risks, it is important to evaluate the possible financial or money-value aspects and the risks for service provision, the ability to overcome the risk, the quality of the evidence held on the risk nature and scale, and the potential risk impact.

Any risk requires a feedback. This may vary from internal controls of risk occurrence prevention from the beginning, to a management decision that is ready to accept the risk level that an activity or a project carry.

The risk feedback will be communicated to everyone involved into the risk management process and the on-site controls will have to be revised regularly to make sure that they remain efficient, that they do not impair money value, that they are accurately documented so that both the management and the auditors may check them out.

The revision process will regularly analyze risk importance and any changed brought to the risk level will be explained with precision to enable accordingly the change of the feedback.

It is important to conduct an independent insurance process, maybe by using an internal audit in order to advise the management how adequate the selection, the evaluation and the feedback are with regards to the risk.

Consequently, risk management does not intend to prevent work assignment, but it ensures that an entity, when performing an activity plan, took into account the risks it may encounter and elaborated a corresponding system of internal controls that could manage and minimize potential risks.

*Received May 9, 2005*

*The "Gh.Asachi" Technical University from Iasi*

## REFERENCES

1. Allen, Richard and Tomassi D. (2002), *Management of Public Expenses; Reference Guide for Countries in Transition* (SIGMA)
2. Everard, Patrick and Diane Walker (1989), *Glossary: Selection of Terms and Expressions Used in Public Sector External Audit*. Luxembourg: ECA
3. M. Ghita, I. Bostan, *Introduction to Audit Theory and Practice*, Universitas Publishing House, Iasi, 2004
4. European Commission, *DG for Financial Control* (1999). *Management Handbook, Audit and Control Systems for Structural Funds - Financial Controls in Member States*. Bruxelles: European Commission

## DETERMINAREA MANAGEMENTULUI DE RISC

### (Rezumat)

Pentru a determina și a trata riscul, acesta trebuie identificat și definit în mod corespunzător, fiind analizat pe baza documentelor de către managementul entității respective. Această abordare permite managementului să determine care este natura interrelațiilor de risc. Cu cât riscul crește mai mult, cu atât mai mult crește sau se reduce alt risc. Atunci când un risc este evaluat, auditorul și managementul entității respective trebuie să țină cont de impactul riscului, dacă acesta apare și de probabilitatea ca riscul să determine un feedback proporțional.

## **ADVANTAGES OF USING THE MODERN MEANS IN ENTERPRISE COMMUNICATION**

**BY**

**PETRU P. CONDREA**

**Abstract:** I have chosen, as an object of my debate, from a lot of modern ways used in communication, those issues related to the introduction of advanced engineering techniques of computation. I refer exactly to Intranet, as a cross gating that gives the possibility to communicate, based on specific technology and communications standards.

**Keywords:** Intranet, internet, LAN, information, control, advantages.

### **1. Introduction**

From the beginning we should tell that the basic concept of Intranet means a computer group (network) as an equipment of a company, which has the possibility to communicate as a collective report, using the same technology and standards of communication, technology that is also at the base of the Internet. This network could be local (LAN - Local Area Network) - when computers are installed in a restricted area, or wide (WAN - Wide Area Network) - when computers are installed in dispersed geographic locations (cities or countries).

INTRANET is an easy to use informational structure, which allows all the employees, no matter of the level of computer use, to have full access to a large area of useful information in order to have the job well done. Intranet is a specialized informational program installed on the user's computer, offering him the possibility to access Intranet or Internet services.

The employees access is "exclusive intern access" which means that they are the only persons that can consult the information presented on the web pages. This policy is because the company Intranet is protected against unauthorized attempts from the members of Intranet world web.

Intranet could be more than a simple way to deliver information; Intranet is more precisely an implement of communication inside the company, taking the liberty of interchanging electronic documents between the staff.

Through Intranet we could access the following sorts of information: S General information: telephone agenda/E-mail, change of messages between departments, a calendar of events, seminars, workshops, company publications, decisions taken by The Board of Directors or the shortened report of plenary or board meetings.

Administrative information related to The Management of Human Resources, schedule of payments, inventories, financial-accountant management. V Information

about the control/audit activity: audit policy, procedures, audit reports, on-line bulletin boards of audit, laws bulletin boards, on-line libraries, full access to other entities bulletin boards.

All in all, talking about the system advantages, we can discuss the following points:

## **2. Reduction of time and costs.**

One of the most important arguments related to the use of the Intranet as part of a company is reducing the company expenses - is no use to make use of printed paper documents as the access to information is acquired through the computer. On the other hand, the entire activity is optimized by reducing the necessary time to deliver information to the employees, as the employees have a permanent access to the bulletin boards, without being bound to get out of the place or wait to receive the printed documents.

## **3. Providing for a better control of the information**

Intranet allows an actual state of information in one place, a property that gives the liberty of centralized control towards the presentation form.

- A better use of information in taking the final decision. As, in real time, is easier to access an information through Intranet, the employees could act and decide most favorable based on the needed information.
- A better use of complex information other then those offered by traditional ways as printing documents.

We need to point out, because of the high technology which is the base if Intranet, that information could be presented in a complex form and we talk about graphical, video images, sound, interactive applications, which represent efficient tools in the instruction and professional improvement development.

*Received May 9, 2005*

*The "Gh.Asachi" Technical University from Iasi*

### **REFERENCES**

1. D. Birchall, *The New Flexi-Managers*, IT Business press, 1996
2. V. Oprean, *Obiectivele intreprinderii privind managementul informatizat*, Tribuna economica, nr. 24/1998
3. E. A. Pateyron, *Les Nouvelles Technologies de l'Information et l'Entreprise*, Ed. Econo

### **AVANTAJELE UTILIZĂRII MIJLOACELOR MODERNE ÎN COMUNICAREA DIN CADRUL ÎNTRINDERII**

#### **(Rezumat)**

Am ales, ca obiect de al dezbaterii mele, dintre mai multe mijloace moderne utilizate în comunicații, acele soluții referitoare la introducerea tehnicilor ingineresti avansate de calcul. Mă refer, mai exact, la Intranet, ca portal de legătură care dă posibilitatea de comunicare, pe baza unei tehnologii și a standardelor de comunicare specifice.

## CORRELATION BETWEEN THE SEEBECK EFFECT, HIGH TEMPERATURE TRANSPORT AND STRUCTURE OF SOME $\text{La}_{1-x}\text{Ca}_x\text{Mn}_{0.9}\text{Cu}_{0.1}\text{O}_3$ COMPOUNDS

BY

MIHAIL-LIVIU CRAUS and MIHAI LOZOVAN

**Abstract:** The manganites with perovskites structure were obtained by means of standard ceramic technology. The obtained compounds structure is characterized by GS 62 Pbm, the unit cell volume increasing with the increase of the La concentration in the sample. For the first time was studied at high temperature the magnetoresistive effect of the  $\text{La}_{1-x}\text{Ca}_x\text{Mn}_{0.9}\text{Cu}_{0.1}\text{O}_3$  compounds. High values of the magnetoresistance were observed, at relatively low applied magnetic fields ( $\leq 20$  kOe). The Seebeck effect was studied at low temperatures, between 77 and 300 K. The nature and the charge carriers concentration modify near the Curie (transition) temperature.

**Keywords:** manganites, magnetoresistance, structure, Seebeck effect

### 1. Introduction

The magnetoresistance effect is associated with a large decrease in the resistance by application of an external magnetic field. Manganese perovskite oxides, with the general formula  $\text{A}_{1-x}\text{B}_x\text{MO}_{3\pm d}$  (where  $\text{A} = \text{La}$ ,  $\text{B} = \text{Ca}$  and  $\text{M} = \text{Mn}/\text{Cu}$ ) exhibit interesting magnetic and electric properties, such as a transition from insulator antiferromagnetic to metallic ferromagnetic behaviour, including colossal magnetoresistance [1-3]. The properties have been explained within the framework of Zener double exchange theory [4]. The Jahn-Teller effect, due  $\text{Mn}^{3+}$  cations, influences the metallic-insulator transition in manganites [5]. The superexchange interaction plays also an important role in the magnetic order of the manganites [6]. According to Goodenough-Kanamori rules, his mechanism gives rise to an antiferromagnetic interaction between cations with the same kind of d-shell and a ferromagnetic interaction between cations with more than half-filled d-shell and less than half-filled d-shell [7].

The aim of the present work is to establish the influence of the La with Ca on the transport properties at high temperature for the  $\text{La}_{1-x}\text{Ca}_x\text{Mn}_{0.9}\text{Cu}_{0.1}\text{O}_3$  compounds.

### 2. Experimental procedure

$\text{La}_{1-x}\text{Ca}_x\text{Mn}_{0.9}\text{Cu}_{0.1}\text{O}_3$  perovskites (where  $x = 0.5 \div 1.0$ ) were synthesized by standard ceramic technology, presintered 17 hours at  $700^\circ\text{C}$  and finally sintered at  $1190^\circ\text{C}$  2 hours. The presintered and sintered samples were investigated by X-ray diffraction using a DRON 2,0 diffractometer with  $\text{CoK}\alpha$  radiation and attached to a data acquisition system. The sintered samples were investigated also by means of a STOE diffractometer ( $\text{CuK}\alpha$  radiation), Guinier method. Zero shift and specimen

displacement corrections were introduced. Lattice constants and space group were determined and tested by using TREOR, DICVOL and, respectively, Ceckcell programs [8, 9, 10]. The position of the cations and oxygen in the perovskite lattice were determined by PowderCell and FullProf programs. These results were used to determine the distances Mn-O and the Mn-O-Mn bond angle.

The calculated and observed tolerance factor were determined with the formulas:

$$t_{calc} = \frac{r_A + r_O}{\sqrt{2}(r_B + r_O)} \quad (1)$$

$$t_{obs} = \frac{d_{A-O}}{\sqrt{2}d_{Mn-O}} \quad (2)$$

due to Jonker [14] and, respectively, Cherif et al. [15]. The average radii of A and B places,  $r_A$  and, respectively,  $r_B$  were calculated with the formulas:

$$r_A = (1-x)r_{La^{3+}} + xr_{Ca^{2+}} \quad (3)$$

$$r_B = y r_{Mn^{3+}} + (0.9-y) r_{Mn^{4+}} + 0.1r_{Cu^{2+}} \quad (4)$$

where  $r_{La^{3+}}$ ,  $r_{Ca^{2+}}$  etc represent the radii of  $La^{3+}$  and, respectively, those of  $Ca^{2+}$  on the A sites (12-fold coordination). As cationic radii we used the data of Huheey [16].

The magnetoresistance measurements were made on cylindrical samples of 10 mm diameter and about 2-3 mm height, with Ag covered basis, using an etalon resistance and a data acquisition system.

The Seebeck effect measurements were performed on a classical design, using the rectangular samples (3X3X20 mm) between 77 K and room temperature. The differences between the top and the bottom of the sample was maintained about 3 K during of the measurement. The potential between the bottom and the top of the sample and the sample temperature were measured with an XY – plotter. The plot was scanned and digitized.

### 3. Experimental results and discussion

The compounds have orthorhombic structure (Pbnm, SG 62). The Miller indices were established with the CeckCell program. The samples contain very small amount of the foreign phases (Fig. 1), the most important maxims have been indexed as being maxims of orthorhombic structure. The lattice constants and the unit cell volume increase with the increase of the La concentration in the sample (Tab.1), in agreement with the ratio between the ionic radii of La and Ca, respectively  $Mn^{3+}$  and  $Mn^{4+}$ .

The  $Mn^{4+}$  concentration decreases when the  $La^{3+}$  concentration increases in the samples. On the other hand, the calculated average radius of A and B places increase, while a small decrease of the calculated tolerance factor ( $t_{calc}$ ) take place with the decrease of Ca concentration (Tab.2).

$Mn^{4+}$  concentration decreases when the  $La^{3+}$  concentration increases in the samples. On the other hand, the calculated average radius of A and B places increase,

while a small decrease of the calculated tolerance factor ( $t_{\text{calc}}$ ) take place with the decrease of Ca concentration (Tab.2).

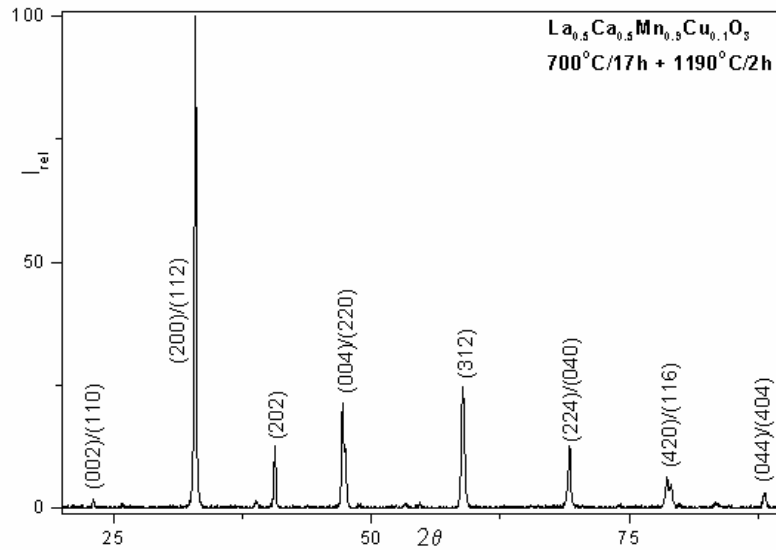


Figure 1 The diffractogram of sample  $\text{La}_{0.5}\text{Ca}_{0.5}\text{Mn}_{0.9}\text{Cu}_{0.1}\text{O}_3$

Table 1 The variation of the lattice constants (a,b, c) of the of  $\text{La}_{1-x}\text{Ca}_x\text{Mn}_{0.9}\text{Cu}_{0.1}\text{O}_3$  perovskites

x	a(Å)	b(Å)	c(Å)	V(Å <sup>3</sup> )
0.7	5.363 <sub>0</sub>	5.385 <sub>3</sub>	7.606 <sub>0</sub>	219.67
0.6	5.423 <sub>7</sub>	5.418 <sub>5</sub>	7.620 <sub>0</sub>	223.94
0.5	5.430 <sub>0</sub>	5.436 <sub>3</sub>	7.640 <sub>5</sub>	225.54

Table 2 The variation of the calculated average radii of A and B places ( $r_A$ ,  $r_B$ ) and of the tolerance factor with the Ca and  $\text{Mn}^{3+}$  concentrations (x, respectively,  $C_{\text{Mn}^{3+}}$ )

x	$C_{\text{Mn}^{3+}}$ <sup>*)</sup>	$r_A$ (Å)	$r_B$ (Å)	$d_{\text{La-O}}$ (Å)	$d_{\text{Mn-O}}$ (Å)	$t_{\text{calc}}$
0.7	0.1	1.43	0.7015	2.71	1.982	0.9671
0.6	0.2	1.44	0.7130	2.72	1.993	0.9650
0.5	0.3	1.45	0.7245	2.73	2.005	0.9630

<sup>\*)</sup>We consider the oxygen amount in the formula unit equal with 3.

Table 3 The cations and anion (O) positions in the unit cell of the  $\text{La}_{1-x}\text{Ca}_x\text{Mn}_{0.9}\text{Cu}_{0.1}\text{O}_3$  perovskites

Ca concentration →	x=0.7	x=0.6	x=0.5
<b>0</b>	<b>1</b>	<b>2</b>	<b>3</b>
Ion position ↓	Ca(La)		
x	0.5257	0.4910	0.4850
y	0.5018	0.5318	0.4900
z	0.2500	0.2500	0.2500
	Mn(Cu)		
x	0.5000	0.5000	0.5000
y	0.0000	0.0000	0.0000
z	0.0000	0.0000	0.0000

Table 3 (continued)

0	1	2	3
	O1		
x	0.4438	0.4431	0.3970
y	0.9490	0.9690	0.9500
z	0.2500	0.2500	0.2500
	O2		
x	0.6859	0.7059	0.7226
y	0.3304	0.3224	0.3254
z	0.0350	0.0520	0.0368

The refinement of the structure allows us to determine more exactly the dependence of the positions of the cations and anion (oxygen) on the La/Ca ratio (Tab.3). The Mn-O distances and the Mn-O-Mn angles, calculated on the positions of ions in the unit cell are presented in the Tab.4.

Table 4 The Mn(Cu)-O distances, La(Ca)-O and Mn-O-Mn angles of  $\text{La}_{1-x}\text{Ca}_x\text{Mn}_{0.9}\text{Cu}_{0.1}\text{O}_3$  compounds

	x=0.7	x=0.6	x=0.5
Mn-O <sub>1</sub> (Å)	1.9448	1.9779	1.9416
Mn-O <sub>2</sub> (Å)	2.0566, 1.9348	2.0830, 1.8734	2.1156, 1.9065
La-O <sub>1</sub> (Å)	2.5339, 2.4480	2.4527, 2.1379	2.3907, 2.3847
La-O <sub>2</sub> (Å)	2.8632, 2.6085	2.7598, 2.6041	2.7347, 2.6643
La-O <sub>2</sub> (Å)	2.0650	2.3359	2.2219
Mn-O <sub>1</sub> -Mn (°)	155.53, 155.78	148.79	159.33
Mn-O <sub>2</sub> -Mn (°)	144.36	151.30	145.29

Despite the monotonous increase of the volume and lattice constants, the Mn-O distances and Mn-O-Mn angles have nonmonotonous variation with the La/Ca concentration ratio (s.Tab.4). We concluded that:

1)The Mn(Cu)O<sub>6</sub> octahedra have a nonmonotonous variable distorsion with the La/Ca concentration ration, possible due to a nonmonotonous variation of the Mn<sup>4+</sup> or oxygen concentration;

2)The Mn-O<sub>1</sub> and Mn-O<sub>2</sub> distances, on [001] and, respectively, [110], have a minimum, while the Mn-O<sub>2</sub> distances on [-110] increase monotonously with the La concentration;

3)The Mn-O<sub>1</sub>-Mn (on [001]) and Mn-O<sub>2</sub>-Mn (on (110))angles have a minimum, respectively a maximum, for x=0.6;

4)The Mn(Cu)O<sub>6</sub> octahedron have a maximum distortion for x=0.6.

The dependence of the resistance with the temperature between 293 and 600 K was studied on the  $\text{La}_{1-x}\text{Ca}_x\text{Mn}_{0.9}\text{Cu}_{0.1}\text{O}_3$  perovskites (x=0.7, 0.6 and 0.5). The magnetoresistance depends on the temperature and the Ca/La concentration (Fig. 2).

The charge transport depends strongly on the composition and structure of the sample: a decrease of the resistance when the external magnetic field is applied can be observed for the samples corresponding to x=0.6, between 370 and 530 K, and x=0.5 between 300 and 530 K (Fig. 2). On other hand, for the  $\text{La}_{0.3}\text{Ca}_{0.7}\text{Mn}_{0.9}\text{Cu}_{0.1}\text{O}_3$  manganite we observed a large positive magnetoresistance (the resistance in applied field was higher as those measured in the absence of the magnetic field). The variation

of the magnetoresistance with the temperature indicates the change of the interaction between the charge carriers and the lattice. The observed magnetoresistance minimum moves toward the lower temperatures when the La concentration increases.

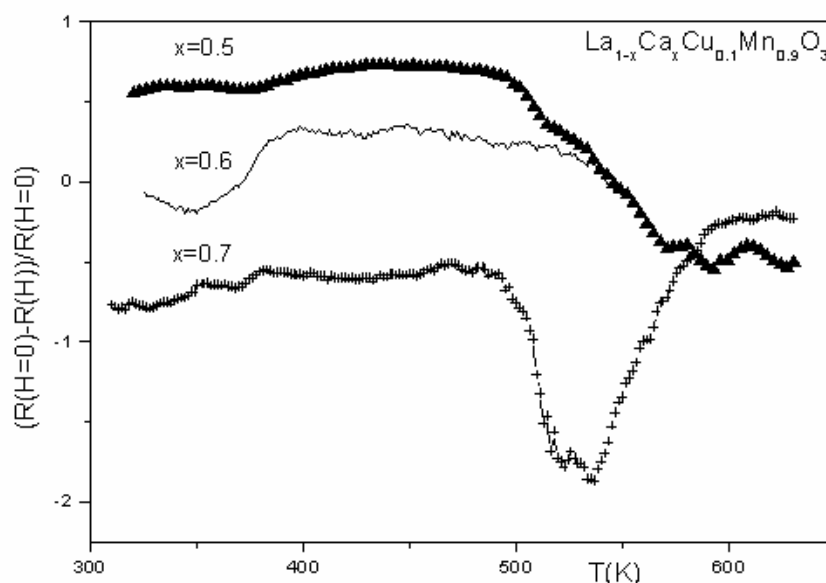


Fig. 2 The dependence of the magnetoresistance vs the temperature for some  $\text{La}_{1-x}\text{Ca}_x\text{Mn}_{0.9}\text{Cu}_{0.1}\text{O}_3$  perovskites

In the investigated range of temperature all the samples do not have the magnetic moment. The magnetic measurements performed between 77 and 293 K revealed that the Curie temperatures for the investigated compounds are generally lower than 250 K (the results were published elsewhere). Apparently the change of the resistance could be due to the thermal treatment, during the magnetoresistance measurements, but the X-ray measurements performed at room temperature before and after the thermal treatment did not revealed any change of the phase composition.

This behavior cannot explain directly the dependence of the magnetoresistance of the temperature in the range of high temperatures (Fig. 2) [14, 15]. The modification of the average radii of A sites in (ab) crystallographic plane leads to a change in the ferromagnetic interaction[15].

The substitution of the Ca with La enhances the chemical disorder and the local fluctuation in Mn-O distances and Mn-O-Mn bond angles. The increase of the chemical disorder and the decrease of the Mn-O-Mn bond angles is associated with a decrease of the DE interaction relatively to the SE interaction and destabilizes the ferromagnetic state. It is in agreement with the observed values of the observed Curie and transition temperatures (the result will be published elsewhere). It is well known that the DE interaction is insufficient to explain the phenomena found in the  $\text{La}_{1-x}\text{Ca}_x\text{MnO}_3$ . In a narrow temperature window the experiments performed by means of X-ray and electron diffraction confirm the existence of the ferromagnetic (FM) and charge ordered (CO) states for  $\text{La}_{0.5}\text{Ca}_{0.5}\text{MnO}_3$  perovskite. The substitution of the Mn with Cu leads to the interruption of the Mn-O-Mn-... bond and, implicitly, to a diminish of the magnetic moment of the samples, if supposes the Cu does not participate to the DE interaction. On other hand the Cu cation can be found in three state valence. The presence of  $\text{Cu}^{2+}$ , which is a Jahn-Teller ion, enhances in the

immediate neighborhood the density of  $\text{Mn}^{4+}$ .  $\text{Cu}^{2+}$  have also a small magnetic moment, which can contribute to the magnetic structure of the  $\text{La}_{1-x}\text{Ca}_x\text{Mn}_{0.9}\text{Cu}_{0.1}\text{O}_3$ . In agreement with the Goodenough-Kanamori rules and taking account that copper is present in perovskites as  $\text{Cu}^{2+}$  there are a few possible transfers for electrons:

- 1)  $\text{Mn}^{3+} + \text{Cu}^{2+} \leftrightarrow \text{Mn}^{4+} + \text{Cu}^{1+}$  (AFM intercation);
- 2)  $\text{Mn}^{3+} + \text{Cu}^{2+} \leftrightarrow \text{Mn}^{2+} + \text{Cu}^{3+}$  (FM or AFM interaction, depending on the state of the  $e_g\text{Cu}^{2+}$  orbital (half-filled, respectively, filled orbital));
- 3)  $\text{Mn}^{4+} + \text{Cu}^{2+} \leftrightarrow \text{Mn}^{3+} + \text{Cu}^{3+}$  (FM or AFM interaction, depending on the state of the  $e_g\text{Cu}^{2+}$  orbital (half-filled, respectively, filled orbital));
- 4)  $\text{Cu}^{2+} + \text{Cu}^{2+} \leftrightarrow \text{Cu}^{3+} + \text{Cu}^{1+}$  (AFM intercation) [15, 16].

We suppose that the  $\text{La}_{1-x}\text{Ca}_x\text{Mn}_{0.9}\text{Cu}_{0.1}\text{O}_3$  compounds are formed from an antiferromagnetic semiconductor (insulator) matrix, based on the  $\text{Mn}^{3+}\text{-O-Mn}^{3+}$ ,  $\text{Mn}^{4+}\text{-O-Mn}^{4+}$  and  $\text{Cu}^{2+}\text{-O-Cu}^{2+}$  bonds. The small (nano)regions, formed by  $\text{Mn}^{3+}\text{-O-Mn}^{4+}$  or  $\text{Mn}^{3+}(\text{Mn}^{4+})\text{-O-Cu}^{2+}$ , behave as ferromagnetic metal in a superparamagnetic state and are associated with the lattice distortions (small polarons). The volume of small FM clusters increase with the applied magnetic field.

In the high temperature region the conduction of the matrix is characterized by the relation:

$$\ln(R) = \ln(R_0) + \text{const}/T \quad (5)$$

With a good approximation, for small concentration of the ferromagnetic phase, the dependance of resistance on the temperature in the high temperature region follows the eq.(5) (Fig. 3).

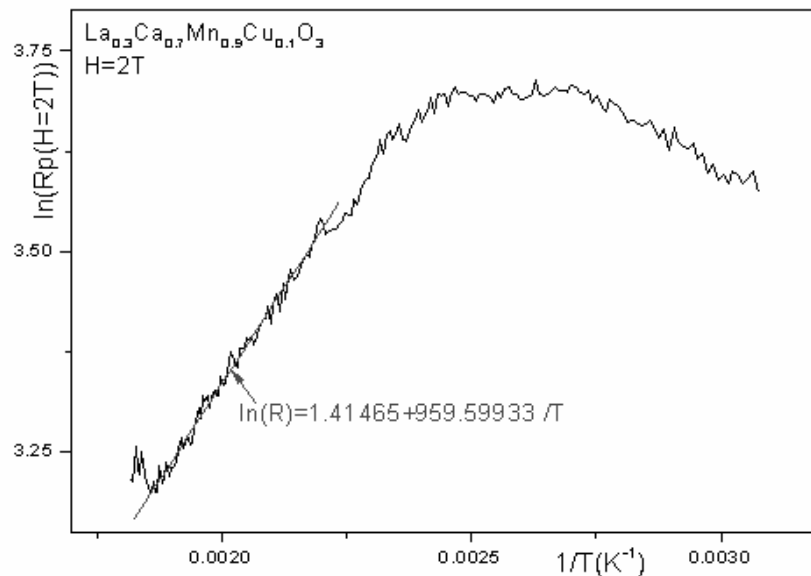


Fig. 3. The dependence of the resistance with the temperature for the  $\text{La}_{0.3}\text{Ca}_{0.7}\text{Mn}_{0.9}\text{Cu}_{0.1}\text{O}_3$  (semiconductor)

When the sample contains a large amount of the FM clusters, the resistance depends with the temperature in agreement with the variable range hopping (VRH) mechanism or the thermally activated small polaron hopping (SPH) model (Fig. 4). The parameters of these two mechanisms strongly depend on the chemical composition and the intensity of the applied field (the results will be published elsewhere).

The concentration of the charge carriers remains constant until near the Curie temperature, where abruptly increase about ten times (Fig. 5). For temperatures higher as the Curie temperature the charge carriers concentration decreases monotonously. Near the Curie temperature the concentration of the FM clusters increases, leading to an increase of the carriers concentration. On other hand, an important part of the charge carriers is due to the semiconductor matrix. At low temperature, the concentration of the charge carriers due to the matrix is relatively low, but increase near the Curie temperature.

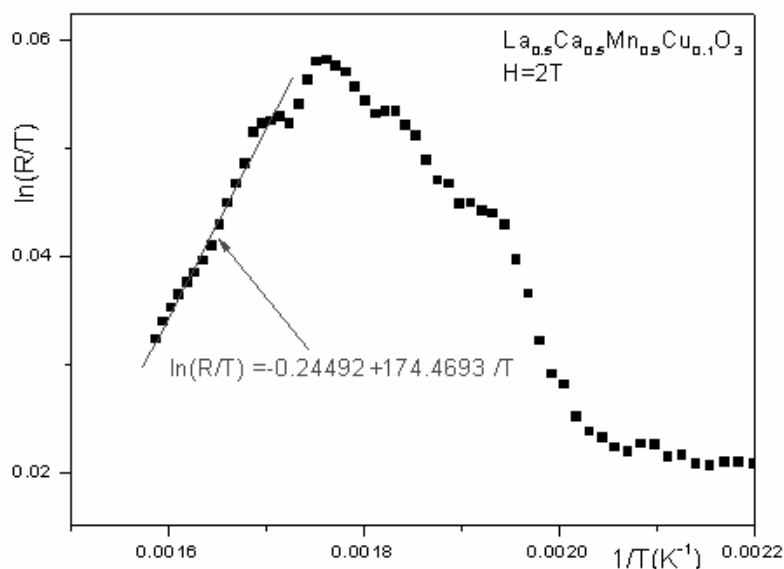


Fig. 4. The dependence of the resistance with the temperature for the  $\text{La}_{0.5}\text{Ca}_{0.5}\text{Mn}_{0.9}\text{Cu}_{0.1}\text{O}_3$  (SPH mechanism)

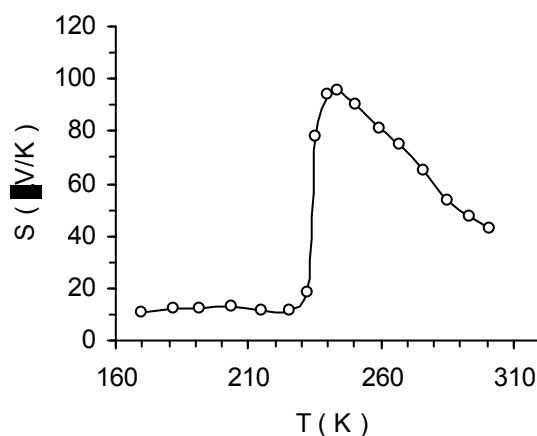


Fig. 5. The variation of Seebeck coefficient with the temperature for the  $\text{La}_{0.3}\text{Ca}_{0.7}\text{Mn}_{0.9}\text{Cu}_{0.1}\text{O}_3$  perovskite

For low doped La concentration at higher temperatures the carriers concentration due to the matrix becomes higher as those due the FM clusters, while for the compounds with a larger La concentration, prevails the charge carriers due to the FM clusters.

#### 4. Conclusions

The  $\text{La}_{1-x}\text{Ca}_x\text{Mn}_{0.9}\text{Cu}_{0.1}\text{O}_3$  perovskites, with large magnetoresistance at high temperatures were obtained by means of standard technology and it are designed for magnetic sensors applications. The increase of the distorsion on B places should be due to the increase of the  $\text{Mn}^{3+}$  or  $\text{Cu}^{2+}$  concentration (associated with John-Teller effect) in the sample. Because the radius of  $\text{Mn}^{3+}$  are higher as those of  $\text{Mn}^{4+}$ , the increase of the  $\text{Mn}^{3+}$  concentration should lead to an increase of the B radius. It is in agreement with the observed values of the  $\text{Mn}(\text{Cu})\text{O}_6$  octahedra distorsions. The increase of the relative value of the magnetoresistance with the increase of the La concentration is due to the increase of the ferromagnetic cluster concentration. The ferromagnetic clusters are in a superparamagnetic state.

Received May 9, 2005

National Institute for Research-Development  
in Technical Physics, Iasi

#### REFERENCES

1. C. N. R. Rao, A. K. Chettham, R. Mahesh, **Chem. Mater.** **8**, 2421(1996).
2. Y. Moritomo, A. Asamitu, Y. Tokura, **Phys. Rev. B** **51**, 16491(1995).
3. H. Tanaka, T. Kawai, **J. Appl. Phys.** **88**, 1559 (2000).
4. C. Zener, **Phys. Rev.** **82**, 403 (1951).
5. A. J. Millis, B. I. Shraiman and R. Mueller, **Phys. Rev.Lett.** **77**, 175 (1996).
6. P. W. Anderson, **Phys. Rev.** **79**, 350 (1950).
7. J. Kanamori, **J. Phys. Chem. Solids** **10**, 97 (1959).
8. A. Boulitif and A. Louer, **J. Appl.Cryst.** **24**, 987 (1991).
9. P.E.Werner, **J. Appl.Cryst.** **9**, 216 (1976).
10. J. Laugier and B. Bochu, **Checkcell**, programme développé dans Laboratoire des Matériaux et du Génie Physique, Ecole Nationale Supérieure de Physique de Grenoble (INPG)  
<http://www.inpg.fr/LMGP>.
11. G.H.Jonker, **Physica** **22**, 707 (1956).
12. K. Cherif, J.Dhahri, E.Dhahri, M.Oumezzine and H.Vincent, **J. Sol. State Chem.** **163**, 466 (2002).
13. J.E.Huheey, E.A.Keiter and R.I.Keiter, Chemistry. **Principils of Structure and Reactivity**, Ed. **Harpers Collins, College Publishers** (1993).
14. Y. Tokura and Y. Tomioka, **J. M. M. M.** **200**, 1 (1999); T.Okuda, T. Kimura and Y. Tokura, **Phys. Rev. B** **60**, 3370 (1999).
15. J.B.Goodenough, A.Wold, R.J.Arnott, N.Menyuk, **Phys.Rev.****124** (1961)373.
16. B.Vertruyen, A.Rulmont, R.Cloots,M.Ausloos,J.-F.Fagnard, S.Dorbolo and Ph.Vanderbemden, **J.M.M.M.** **268** (2004)364 –373

#### CORELATIE INTRE EFECTUL SEEBECK, TRANSPORTUL LA TEMPERATURA RIDICATA SI STRUCTURA UNOR COMPUSI $\text{La}_{1-x}\text{Ca}_x\text{Mn}_{0.9}\text{Cu}_{0.1}\text{O}_3$

##### (Rezumat)

Manganiti cu structura de perovskit simplu au fost obtinuti prin tehnologia ceramica standard. Structura compusilor este caracterizata de grupul spatial Pbnm, volumul celulei elementare crescand cu cresterea concentratiei de La in probe. Pentru prima data a fost studiat la temperatura ridicata efectul magnetorezistiv al compusilor cu compozitia  $\text{La}_{1-x}\text{Ca}_x\text{Mn}_{0.9}\text{Cu}_{0.1}\text{O}_3$ . Au fost observate valori mari ale magnetorezistentei, la campuri magnetice relativ joase ( $\leq 20$  kOe). Efectul Seebeck a fost studiat in zona de temperaturi joase, punandu-se in evidenta modificari ale naturii si concentratiei purtatorilor de sarcina in zona de temperaturi corespunzatoare temperaturii Curie.

## COMPUTERIZED PROPERTIES PREDICTION IN THE HEAT TREATMENT OF STEELS

BY

IULIAN CUCOȘ

**Abstract:** The establishment of prediction methods based on the phenomenological description and computer simulation of the transformation processes during heat treatment and the development of software for technological planning has been of major interest.

**Keywords:** properties prediction, heat treatment of steels, computer simulation

### 1. Introduction

The steady development of this topic is aimed at meeting the requirements of metallurgists producing basic materials, design engineers dealing with material selection and dimensioning, and technologists planning heat-treatment processes.

The development of computer simulation of heat treatments has been concentrated on two main areas of interest:

- modeling of transformation processes and the prediction of microstructures and/or properties ;
- developing program packages (designed in the majority of cases to be purchased on the market for direct industrial use) to help solve concrete tasks such as material selection, property prediction, and the design of heat-treating operations

Design engineers, metallurgists, and heat-treatment technologist need to assess the effects of material selection on heat treatment, dimensional control, and distortion. Consequently, one basic objective of computerized modeling is the use of algorithms for material selection.

This process may involve not only selection of the cheapest material or type of steel suitable for a particular application, but also the assessment of processing alternatives and their effect on manufacturing characteristics and properties.

By introducing computer methods, steel heat treatments can be analyzed and/or optimized in terms of product quality, property scatter, processing time, and energy consumption.

A proper computer algorithm makes it possible to select the heat-treatment parameters that result in minimum energy consumption and optimum mechanical

properties. Because of the many factors involved, reducing energy consumption is an optimization task that can be done only by applying a suitable simulation computer program.

Simulation software can be classified either as on-line programs for process control or as programs to assist decision making and process analysis. The classification of software programs can be subdivided into:

- property prediction programs
- process planning programs
- material selection programs and their data bases
- programs for special technical and economic problems in connection with heat treatment (programs estimating the energy consumption of a heat-treatment process or calculating the expenses of heat treatment, and so forth
- finite-element analysis for modelling the effects of quench severity on distortion and dimensional control of parts.

## 2. General Concept of a Property Prediction System

A property-prediction system used for simulating the metallurgical process occurring during heat treatment and predicting the microstructure and mechanical properties of quenched and tempered or case-hardened steel's is described in this section. The system consists of several subprograms, which form a logical chain for property prediction.

Before starting to design a property-prediction system, first those internal parameters (Ac3 temperature, transformation kinetic data, hardness values of the micro structural elements, and so on) that have the most determinative effects on the properties.

The programs are based on a phenomenological model of kinetics of transformation taking place in no isothermal conditions and permits the prediction of the progress of transformations, of the microstructure, and of the mechanical properties as a function of time and of position in the cross section of the heat-treated work piece. The equations forming the base of the model belong to three main groups as follows:

- the differential equation of heat conduction by a numerical method, the temperature field in the given work piece is solved
- the system of kinetic differential equations for describing the transformation processes occurring in the microstructure
- equations describing the relation between the microstructure and properties

Modelling of transformation kinetics can be done with differential equations such as:

$$\frac{\partial Y_j(r, t)}{\partial t} = g_j(Y_1, Y_2, \dots, Y_j, T, t) \quad (1)$$

where t denotes time;

r is the vector representing a given point of the work piece (the position vector);

T is the temperature, which is a function of time t and position r;

(j = 1, 2, . . . J) is a so-called micro structural parameter;

g = 1, 2, . . . J is an appropriately selected real value function.

The micro structural parameters  $Y$  in (1) are numerical quantities that may be interpreted within relatively wide limits.

The starting point for predicting mechanical properties such as hardness and yield point is that the properties are related to micro structural parameters. It was assumed that after transformation at a given location  $r$  in the work piece, a numerical property  $P(r)$  of the steel may be calculated with a precision satisfying practical demands as a function of a small number of elementary micro structural properties  $p$  ( $j=1,2,.. - . M$ ) according to the formula:

$$P(r) = f(p_1, p_2, \dots, P_M) \quad (2)$$

where  $f$ , is an appropriately selected function.

In most cases, the so-called generalized linear law of mixture represented by the following Stieltjes integral was used to calculate the elementary micro structural property ( $j=1,2,..M$ ):

$$p_j = \int \chi(T, Y_j) dY_j \quad (3)$$

where  $\chi [T(r, t), Y_j ]$  is a suitably defined weighting function containing and summarizing the numerical information on the given property of the micro structural parameter  $Y$ .

The input data are:

- chemical composition of the work piece to be hardened
- initial state of the work piece (annealed, normalized, quenched, and tempered)
- geometry: shape and size of the work piece (round bar or plate) characterized by its diameter or thickness, or Jominy specimen and the distance from the cooled surface to the point where the microstructure and properties are to be predicted
- heating conditions: heating medium, austenitizing temperature, and the total time spent by the work piece in the austenitizing furnace
- quenching conditions characterized by the HR value (relative heat transfer coefficient specifying the cooling severity) and the temperature of the quenching
- tempering conditions given by the tempering temperature and the duration of tempering

The chemical composition of the work piece is first verified against the specified composition range of the steel type for which the predictor program was developed. From the composition, we calculate  $A_1$ ,  $A_3$ ,  $B_s$ ,  $M_s$ , transformation temperatures by formulas based on dilatometrical measurements and regression analysis.

Computation of the heating curve takes into account the furnace features. Calculations are based on the application of an approximate method developed to solve heat conduction problems for simple geometries.

The accuracy of the following Newtonian approximation can also satisfy the requirements:

$$T = (T_0 - T_a) \exp\{-\alpha_h t\} + T_a \quad (4)$$

where:  $T$  the austenitization temperature;

$T_0$  is temperature at  $t = 0$ ;

$h$  is a constant depending on the furnace, mass of work piece, heating medium, quality of the face, and agitation of the medium.

The temperature to austenitization is determined by the initial microstructure and the heating rate. The experimental results may be described with the following equation:

$$Ac_3 = A_3 + a v^{1/3} \quad (5)$$

where  $v$  is heating rate at temperature  $A_3$  and  $a$  is a parameter depending on initial state of microstructure.

Computation of the austenite grain also requires consideration of non isothermal conditions. The extent grain growth taking place during austenitization is known to have a decisive effect is the characteristics of steel.

It was assumed that grain size  $D_a$  of steels at constant temperature  $T$  is described an isothermal kinetic function of the following type:

$$D_a = \left[ \int_0^t k_0 \exp\left(-\frac{Q_a}{RT}\right) dt + D_0^N \right]^{1/N} \quad (6)$$

The unknown parameters  $k_0$ ,  $N$ , and  $Q_a$  can be estimated by regression analysis using measured data.

The characteristics of the isothermal time- temperature transformation chart are calculated as a function of the chemical composition and austenite grain size, also taking into account the temperatures  $A_1$ ,  $A_3$ ,  $B_s$  and  $M_s$ .

One of the most frequently used equations for the isothermal transformation is Avrami's equation:

$$y = 1 - \exp\{-bt^n\} \quad (7)$$

where  $y$  is the volume fraction of the transformed austenite;  
 $t$  is the time spent on the isotherm;

$b$  and  $n$  are temperature, grain size, and composition-dependent constants, evaluated from the isothermal TTT diagram or from measurements with continuous cooling.

Computation of the cooling curve at the given point of the work piece can involve a simple method similar to the one described to use a Newtonian cooling:

$$T = (T_a - T_q) \exp\{-\alpha_c t\} + T_q \quad (8)$$

where  $T_a$  is the austenitization temperature;  
 $T_q$  is the temperature of the quenching;  
 $\alpha$  is the geometry and quenching-dependent parameter.

Calculating the progress of the transformation processing continuous cooling from the TTT characteristics is a crucial part in property prediction. Estimation of the ferritic, pearlitic and bainitic fractions during each step.

Information about transformation temperature defined for the initiation of the ferrite-pearlite faction and for the beginning temperature range,  $B$ , of the bainite reaction is first provided by this program.

When the hardness after quenching is calculated on the basis of microstructure and  $e$  carbon content, many investigations are necessary to ascertain the best rule of mixing.

In the calculation of the hardness after quenching, the transformed amounts of austenite on each isothermal step, and their individual isothermal hardness can be taken into account.

The amounts of the micro structural elements are calculated by the help of the stepwise method. The individual hardness's of the micro structural elements are taken from a hardness-temperature table or function valid for the actual steel, and the resultant as-quenched hardness  $H_q$  is composed from these components with the formula:

$$H_q = \sum_{i=1}^v y_i(T_i)H(T_i) + y_m \cdot H_m + y_a \cdot H_a \quad (9)$$

where  $T_i$  is the temperature of the this step;

$y_i(T_i)$  is the transformed amount at temperature  $T_i$ ;

$H(T_i)$  is the isothermal hardness;

$v$  is the number of isothermal steps, until temperature reaches  $M_s$ ;

$Y_m$  is the volume fraction of martensite;

$Y_a$  is the volume fraction of retained austenite;

$H_m$  is the hardness of martensite;

$H_a$  is the hardness of retained austenite.

The tempering of steels forms a significant part of practical heat treatment, and therefore its study and mathematical description are of greatest importance. Several generally applied methods are available for the isothermal case. From computational considerations, it is assumed that the kinetic equation describing the change in hardness under no isothermal conditions is of the form:

$$H_t = f_4(P_g) \quad (10)$$

where  $H_t$  stands for the instantaneous hardness after tempering;

$f_4$  is a suitably selected function;

$P_g$  is the so-called generalized time-temperature parameter, which is applicable to the description of tempering processes with changing temperature

The form of the parameter  $P_g$  can be selected in many ways.

The tempering chart is composed of two independent parts. The lower part of Fig 3 refers to isothermal heat treatment and shows the relationship of tempering parameter  $P_D$  temperature and time.

This chart can be applied to convert from one tempering time and temperature to any other, on the basis that combinations of tempering temperature and time having the same value of tempering parameter will produce the same hardness.

For tempering at varying temperatures, Eq the value of the parameter  $P$  required to achieve the specified hardness may be determined with the deferent figures. For isothermal tempering, the various time-temperature combinations for the given parameter value  $P_D$ , which may be used to achieve the specified hardness.

In the kinetic function employed for the phenomenological description of hardness decrease occurring during tempering, the value of the apparent activation energy ( $Q_D = 250$  kJ/mol) is essentially identical to the activation energy for the self-diffusion of ferrite in steel that is not alloyed with molybdenum.

It follows from this assumption that the lower chart in figures may be used generally for all hardenable steels free of molybdenum. However, the upper chart representing the so-called master curve must be deduced and plotted individually for the various steel types from measured data.

Mechanical Property Estimates not only the hardness, but also the other mechanical properties, namely the tensile strength, yield strength, elongation, reduction in area, and the Charpy value of the impact energy with the following formulas:

$$R_m = 3.412 HV - 64.3 \quad (11)$$

where  $R_m$  is the ultimate tensile strength in MPa, and HV is the Vickers hardness.

For the calculation of the yield point R (MPa), elongation  $A_{50}$  (%) in 50 mm, reduction in area Z (%), and Charpy value KU(Joules), the equations below have been suggested:

$$R = (1,17 - 0,0007Y_m) * R_m + 3,72Y_m - 484 \quad (12)$$

$$R_m = 3,412HV - 64,3$$

$$A_{50} = 40 - (0,03 - 0,0001Y_m)R_m$$

$$Z = 100 - (0,06 - 0,00024Y_m)R_m$$

$$KU = 296 - (0,285 - 0,00098Y_m)R_m$$

where  $Y_m$  is the volume fraction of martensite in %.

Received May 9, 2005

The "Gh.Asachi" Technical University Iași

## REFERENCES

1. Chiriac F., Leca A. - *Procese de transfer de căldură și masă în instalațiile industriale*, Ed. Tehnică, București, 1982
2. Cucuș I., Dănilă R., Catarschi V. - *Matematical modelling, optimisation and simulation assisted by personal computer of the heat transfer from the heat treatment furnaces* I Congres International de Știința și Ingineria Materialelor Iași, mai 1994.
3. Gheorghely M., Reti T. Somogyi S., Konkoly T. - *Aide au choix d'acier par calcul des caractéristiques mécanique*, Traitement thermique, Franța, sept. 1992
4. Ungureanu Șt., Cucuș I. Dima A - *Evaluated system computer assisted for designing and conducting the chamber type furnaces heat treatments*, I Congress International de Știința și Ingineria Materialelor, Iași, mai 1994

## PREDICȚIA ASISTATA DE CALCULATOR A PROPRIETĂȚILOR LA TRATAMENTUL TERMIC AL OTELURILOR

### (Rezumat)

Sistemul pentru predicția proprietăților este folosit pentru simularea proceselor metalurgice care apar în timpul tratamentelor termice și pentru prevederea microstructurii și proprietăților mecanice, sistemul are o structură modulară. Modelul matematic permite prevederea evoluției transformării și microstructurii, a proprietăților mecanice ca funcție de timp și de poziția în secțiunea pieselor tratate termic.

## THE CONTROL OF FURNACES FOR THERMAL TREATMENT

BY

IULIAN CUCOȘ

**Abstract:** The control of furnaces for thermal treatment is a consequence of permanent effort for relief of work through amplify of his capacity in solving problems of productions. The advanced system for conducting the furnaces of heat treatments has the main importance in different activities developed in hard conditions.

**Keywords:** designing and conducting system, computer simulation, electric furnaces, conduct, property prediction, PID and PID-predictive controller.

The process computer which conducts the electric furnaces takes the initial and current data through the system of acquisition of data from human operator and sensor in furnaces then the computer analyses on the base of mathematical model of transformation process and the prediction of microstructures and properties a optimum strategy for conduct the industrial strategy for conduct the industrial furnaces.

The program of the property prediction of microstructure and mechanical properties are based on a phenomagnetical model of kinetics of transformation taking plane in no isothermal conditions.

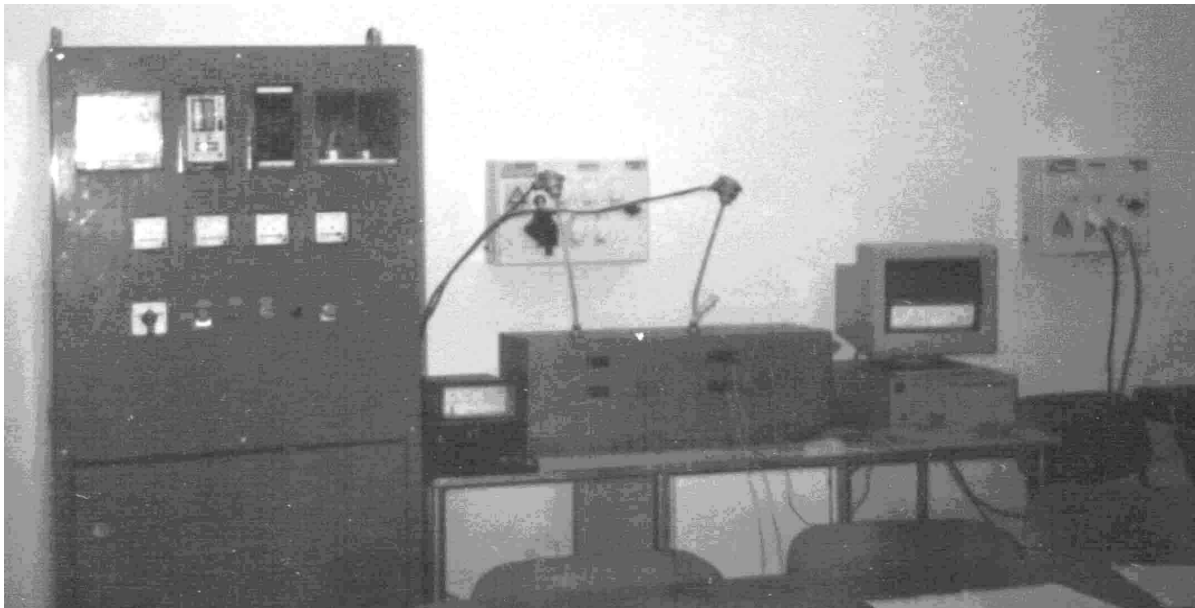


Fig.1 The system for conduct the electric furnace for heat treatments.

The functions offered through conduct system are:

- the modelling and simulation of heat transfer in electric furnace ;
- the sequential regulation of furnaces parameters ;
- the complete imagine above the process, checking of start / stop of furnaces, the function for alarm and safety stopping ;
- this system post parameters value from a certain part of process which is interesting at certain moment, on display are the references values, the sizes for actions and the signal of entrances in the limits ;
- the system offers possibility of work with a system of menus .

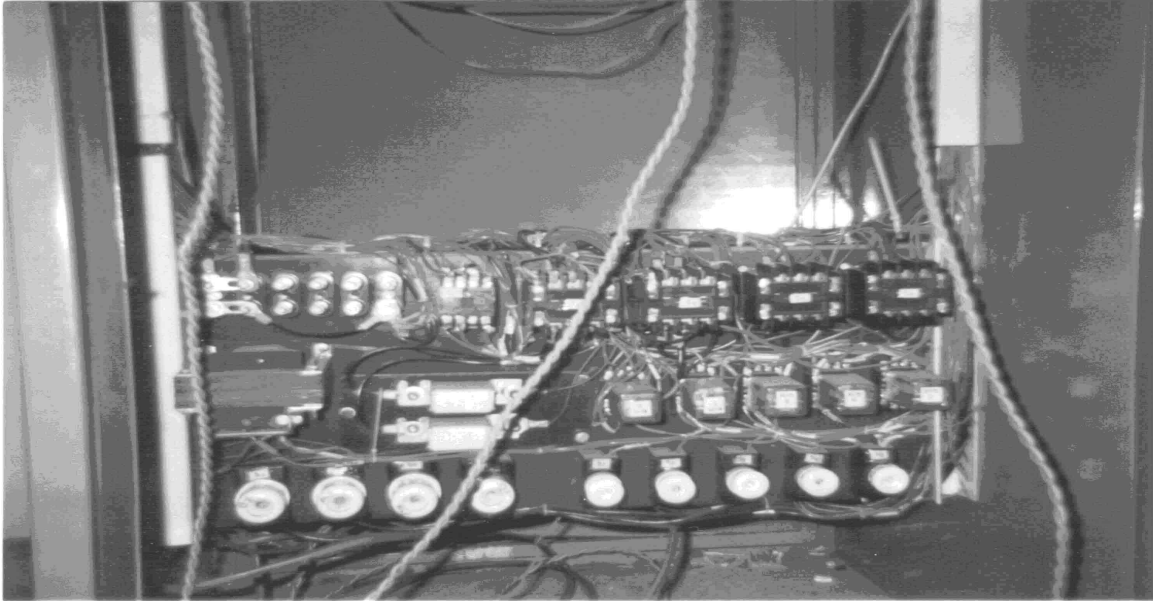


Fig.2 The electronic components of system for conduct the electric furnaces.

The computer which conduct the furnaces takes the initial and current data through the system of acquisition of data from sensors in the furnace then the computer analyses on the base of mathematical model a optimum strategy for conduct the electric furnaces .

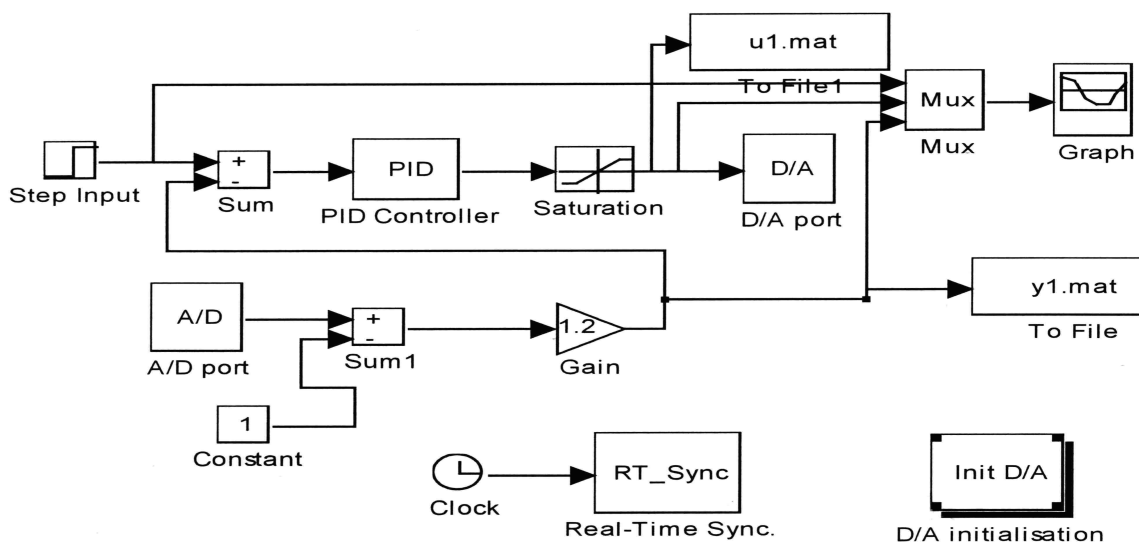


Fig.3 The system block scheme for conduct the electric furnace.

The structure of initial database is :

- the steel marks and the semi-products number and size ;
- the temperature of furnaces and semi-product .

In next figures we present the result of conduct the chamber type electric furnace for heat treatments with PID and PID – predictive algorithm.

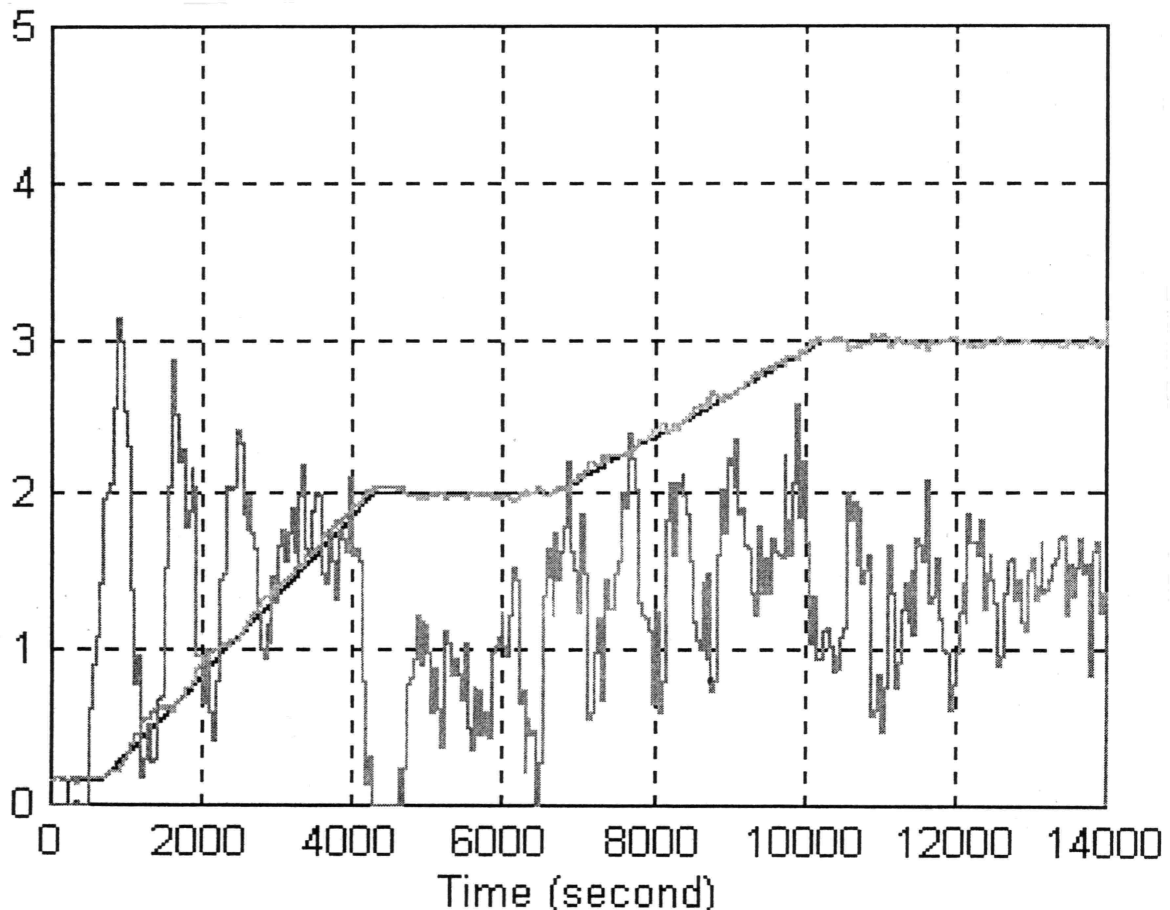


Fig.4 Results of conduct with PID algorithm.

The equations forming the base of model are:

- the system of kinetic differential equation for describing the transformation process ;
- the differential equations of heat transfer ;
- the relation between the properties and microstructure .

The tuning algorithm PID together with the supervision system was implemented on a PC with system of acquisition of data from conducted system.

The results show the improvement of the performances of controlled system with delay time as well as the increase of economical efficiency.

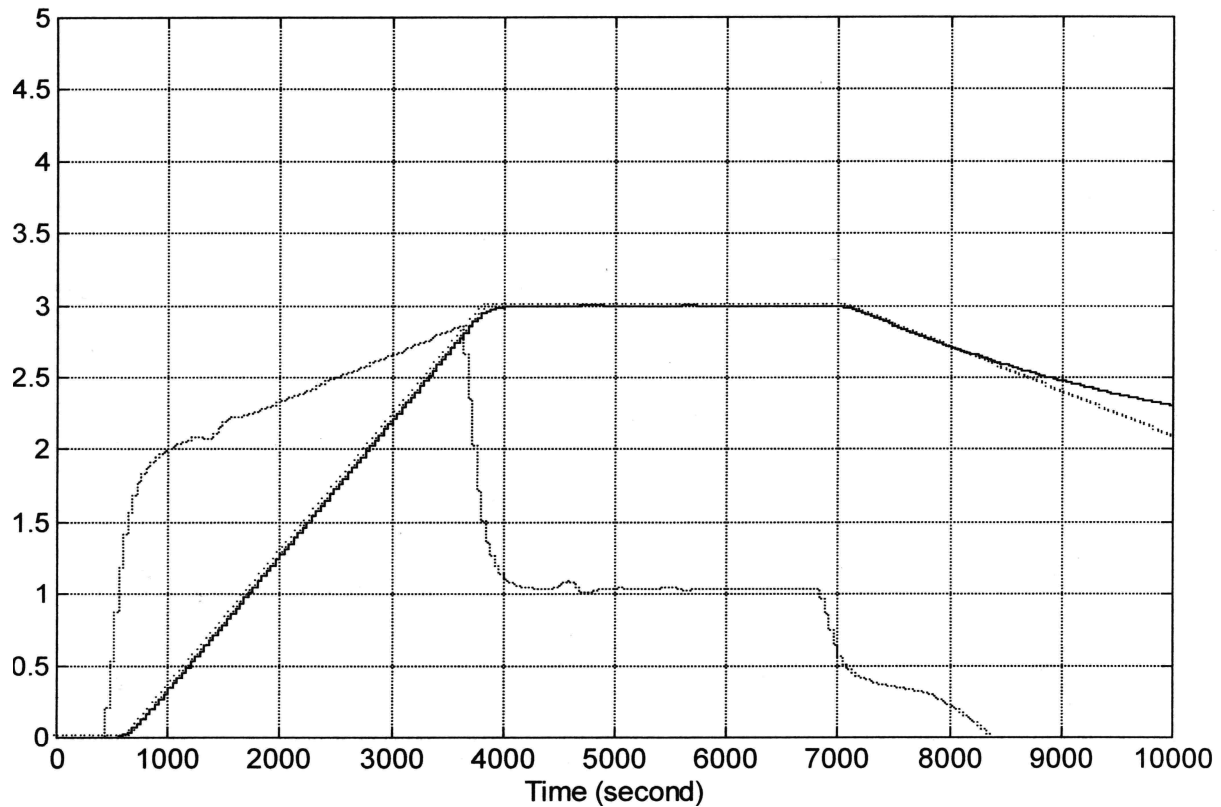


Fig.5 Results of conduct with PID - predictive algorithm.

Received May 9, 2005

The "Gh.Asachi" Technical University Iași

## REFERENCES

1. Lazăr, C., Păstrăvanu, O. – *Predictive auto-tuning Controller for variables time delay plants*, Electronica București 1992
2. Cucuș I., Dănilă R., Catarschi V. – *Matemathical modelling, optimisation and simulation assisted by personal computer of the heat transfer from the heat treatment furnaces* I Congres International de Știința și Ingineria Materialelor Iași, mai 1994.
3. Ungureanu Șt., Cucuș I. Dima A – *Evaluated system computer assisted for designing and conducting the chamber type furnaces heat treatments*, I Congress International de Știința și Ingineria Materialelor, Iași, mai 1994

## CONDUCEREA CUPTOARELOR DE TRATAMENT TERMIC

### (Rezumat)

Conducerea automată a cuptoarelor de tratament termic presupune variația temperaturii din incintă astfel încât aceasta să urmărească profilul impus de tehnolog.

Problema principală a conducerii cuptoarelor electrice de tratament termic o reprezintă controlul temperaturii din cuptor astfel încât aceasta să evolueze după profilul impus de tehnolog. Proiectarea sistemului de reglare automată presupune:

- caracterizarea matematică a comportării procesului condus din cuptor;
- stabilirea obiectivelor reglării și optimizarea valorilor parametrilor reglării;
- modelarea matematică a proprietăților fizico-mecanice a piesei după tratamentul termic;
- implementarea algoritmului de reglare PID-predictiv și validarea soluției propuse pe baza analizei performanțelor sistemului.

## STUDY OF THE WORK GENERATING SHAPE MEMORY EFFECT

BY

VASILE DIA\*, LEANDRU-GHEORGHE BUJOREANU\*\*, GABRIELA  
HRIȚULEAC\* and VIORICA DAVID\*

**Abstract:** The paper aims to determine the work generating capacity of a helical spring made from a Cu-Zn-Al-based Shape Memory Alloy (SMA). In this purpose experiments have been performed comprising electrical actuated lifting of different loads by the helical spring, during which the displacement variation with temperature has been accurately measured and recorded. By means of the displacement vs. temperature curves, which were perfectly reproducible, the critical transformation temperatures have been determined for different applied loads. In this way an accurately controllable electrical actuator has been developed, able to generate a 0,055 J/g specific work.

**Keywords:** shape memory effect, hysteresis, specific work,

### 1. Introduction

The aim of conventional helical springs is to produce a mechanical element that will store energy by generating the desired forces at given deflections. If the spring is made of steel, the load-deformation behaviour of a helical spring obeys Hooke's law, there is a linear relationship between load and deformation of the spring ( $F=K \cdot \Delta l$ , where K is a constant of proportionality known as the spring rate) [1].

Two-way shape memory materials create an opportunity for developing a wide variety of thermally sensitive actuators. With proper design, a shape memory element can be used as a thermo-mechanical actuator to lift loads, to proportionally control a thermal system, or to operate thermal switches [2].

Springs made for Cu-Zn-Al actuator applications are not used to store energy, but rather to perform useful work. They are suited for use as thermal actuators behaving as both a temperature sensor and work generating element. The load-deformation behaviour of Shape Memory Alloy (SMA) spring is best described in term of material rigidity. SMAs exhibit a large change in shear modulus over a relatively narrow temperature range, increasing from low to high temperature. The change in modulus with temperature is the result of a reversible martensite to austenite solid state phase [3].

Fig. 1 shows the load-deformation behaviour of a SMA spring at different temperatures. At 20°C and 30°C the spring is martensitic and does not return into its original length. Above 30°C the spring is austenitic but martensite is formed by load-

induced phase transition and returns to austenite upon decreasing load. The higher the temperature the less martensite is formed and therefore the spring gets stiffer.

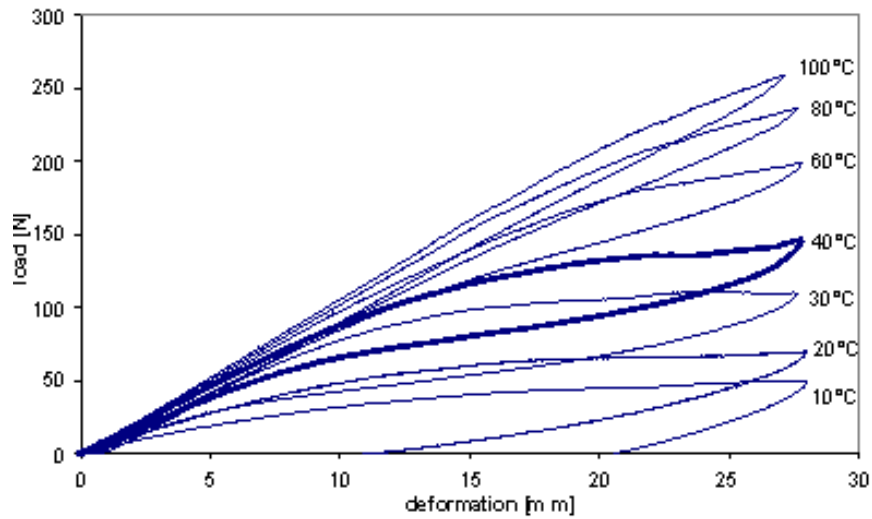


Fig.1 Load-deformation behaviour of a SMA spring at different temperatures [1]

Figure 2 demonstrates the behaviour of a SMA spring at two different temperatures (20°C and 100°C) and an ordinary steel spring. If the parameters of the springs are chosen like in this example, the steel spring is capable of compressing the SMA spring at low temperature. On the other hand, the SMA spring may compress the steel spring at high temperature.

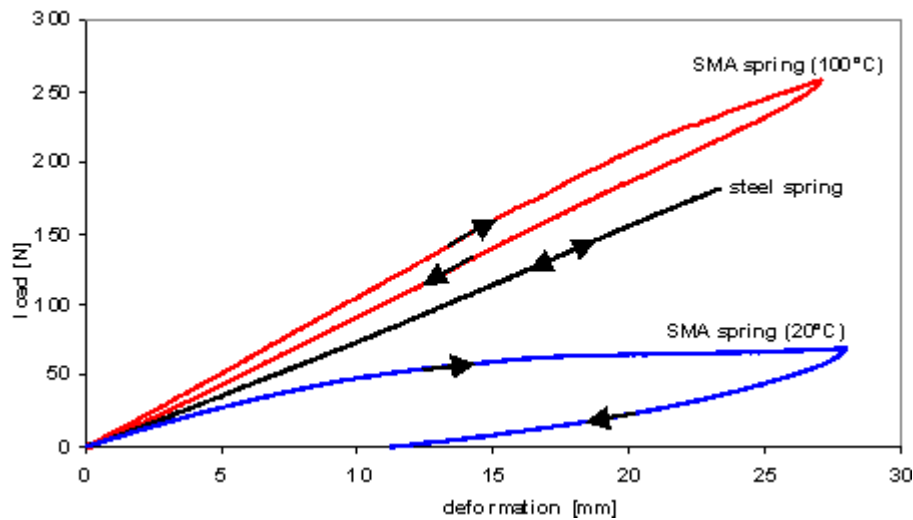


Fig.2 Load-deformation behaviour of a SMA spring at 20°C and 100°C and a steel spring [3]

The classic and most simply SMA actuator consists simply of a shape memory spring with a weight on the end (Fig. 3). As the spring is heated the weight is lifted and when the spring is cooled, the weight descends stretching the spring again. If the stress applied by the weight is less than the recovery stress of the alloy, the weight will be lifted and the amount of work done ( $L$ ) will be:

$$L = W(D-d) \quad (1)$$

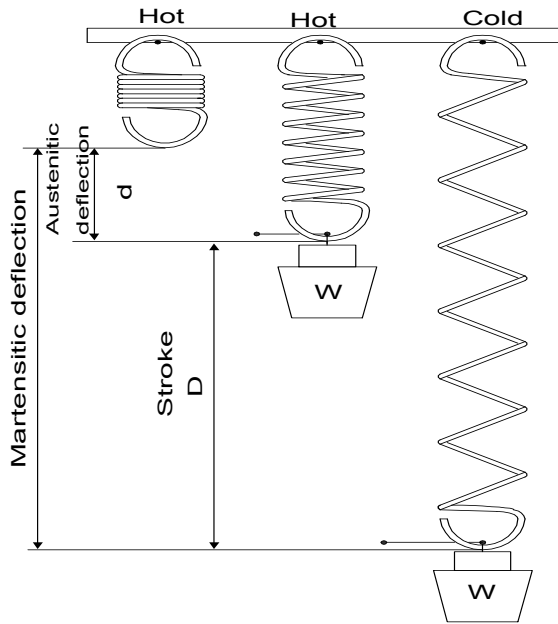


Fig.3 The classic SMA actuator consists of a shape memory extension spring with a weight on the end [4].

The extension spring provides a pulling force by contracting when transformed to the high austenitic state. The close coiled, zero load configuration of the extension spring is the shape which is “remember” at high temperature. This shape is set by constraining a close wound spring on a mandrel and giving it a special heat treatment. An important characteristic of the heating and cooling behaviour of shape memory springs is the hysteresis that occurs. As shown in Fig.4(a) at a temperature below  $M_f$  the spring is 100% martensite and fully extended. During heating it begins contracting at  $A_s$  and completes its motion at  $A_f$  when the spring is 100% austenite. During cooling the spring begins to extend (reset) until  $M_s$  is reached, and finishes its motion at  $M_f$

[4]. The transformation temperatures of the alloy and the hysteresis width depend on chemical composition, stress level, process heat treatment, etc. The hysteresis transformation loop offers information about both the macroscopic and the microscopic nature of the transformation. On one hand, the transformation temperatures can be graphically determined, by the so-called “tangent method” [2], as shown in Fig.4(b). We define this temperature as  $A_s$ , the temperature axis intersection of the tangent to the deflection-temperature curve on heating [5].

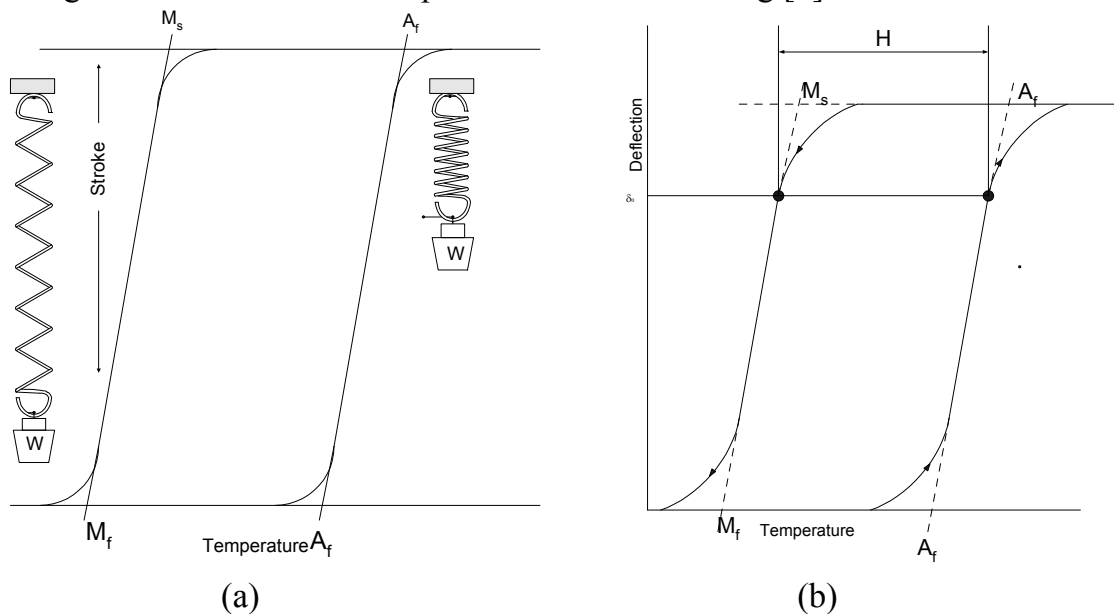


Fig.4 Illustration of the hysteretic behaviour of Shape Memory helical springs: (a) temperature hysteresis; (b) typical characteristic of the thermal hysteresis, demonstrating the graphical mode designated as “the tangent method” [5]

## 2. Experimental procedure

The alloy used in this study was a commercial polycrystalline material of chemical composition 70.88% Cu, 21.64% Zn, 7.14 Al, 0.23% Ni (wt.%) with a martensitic start transformation temperature ( $M_s$ ) of 55 °C. Extension springs were made from hot rolled SMA sheet with lamellar shape (0.38 x 10.7 x 410 mm) with seven coils. The heights of the spring were 87 mm, their diameter 18.2 mm and their weights 12.76 g (Fig 5).

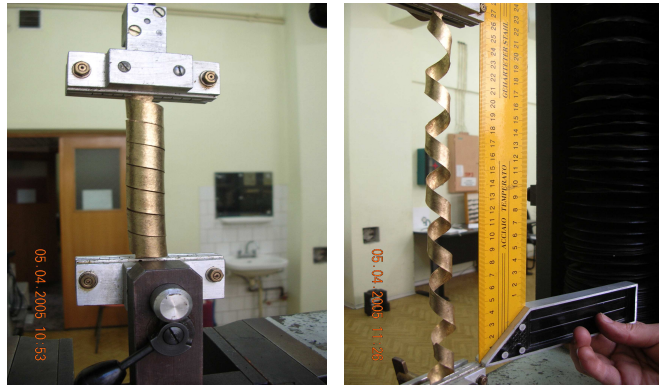


Fig.5 Initial shape and dimensions of the spring after forming and quenching heat treatment (850°C/ 15 min/ water) Fig.6 Training procedure of the spring, with controlled force application on Heckert FPZ100/1-type tensile testing machine: (a) initial shape of the spring; (b) deformed shape of the spring after about 15 cycles

Before training the spring was held in the  $\beta$  phase region at 850 °C for 15 minutes, followed by direct quenching into water at 20 °C. The training procedure, which began immediately after quenching, consisted in the application of a tensile force to the spring so as to achieve a fixed deflection, Fig 6(a) and (b). This will favour the growth of the variants which best accommodate the deformation sustained. The spring was aged at the training temperature for the training time, with the purpose to stabilise those martensite variants favoured by the applied deformation.

For the study of the work generated by the spring, during its loading under different forces, a special installation was designed, Fig. 7. It comprises a source for resistive heating able to provide a variable continuous electric current which can be very finely tuned, between 0 and 250 A, by means of an electronic block with thermal resistors and a multi turn potentiometer. For the accurate measuring of the electric current passing through the SMA spring a standard galvanometer with the precision class 1 was used.

For the measurement of the temperature of the SMA spring two multimeters were connected in parallel, one comprising a thermocouple and the other comprising a thermal diode. This setting allowed temperature measurement with an accuracy of  $\pm 0.1$  °C.

The recorded deflection-temperature curves were used for determining the specific work developed while lifting different loads (0.13 N, 1 N and 3 N, respectively). Aiming to design electrical actuators, the values of the electric current were also recorded as a function of the spring's deflection however a closed system could not be obtained, which would not be influenced by the environment.

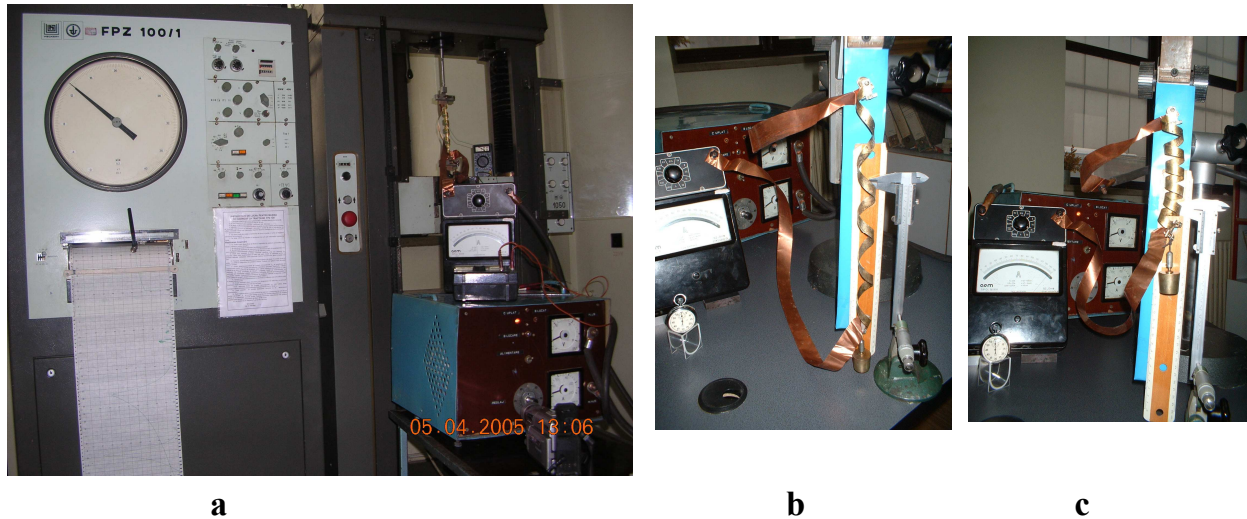


Fig.7 Functioning principle of the experimental installation for determining the specific work developed by the SMA spring: (a) adapting the installation on the Heckert FPZ 100/1 tensile testing machine; (b) the spring in martensitic state, stretched by a 100 g load; (c) the spring in austenitic state ( $\beta$  phase) lifts the 100 g load

### 3. Experimental results and discussion

The deflection (stroke)-temperature curves were recorded for the above mentioned three loads: 0.13 N – representing the proper weight of the spring; and for 1N and 3N, respectively. The results are shown in Fig.8. Based on these curves the critical transformation temperatures under mechanical stress,  $A'_s$  and  $M'_s$ , were also determined by means of the tangent method, as listed in Table 1.

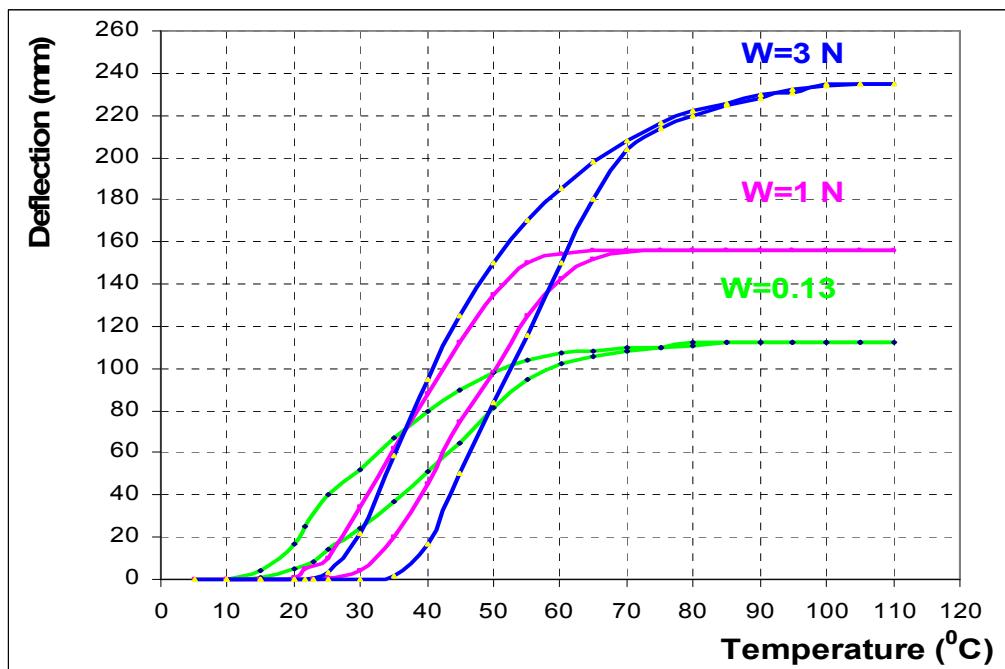


Fig 8. Thermal hysteresis curves representing the displacement of the load fastened at the end of the spring as a function of heating temperature

Table 1 Values of the critical transformation temperatures under stress, at different loads, determined by the graphical method

Load (N)	$A_s$ ( $^{\circ}\text{C}$ )	$A_f$ ( $^{\circ}\text{C}$ )	$M_s$ ( $^{\circ}\text{C}$ )	$M_f$ ( $^{\circ}\text{C}$ )
0.13	22.3	58.1	49.5	14.9
1	30.1	61	54	22.7
3	37.5	71	63	27

In Fig.9 the variation tendency of the critical transformation temperatures under stress is illustrated as a function of the applied load.

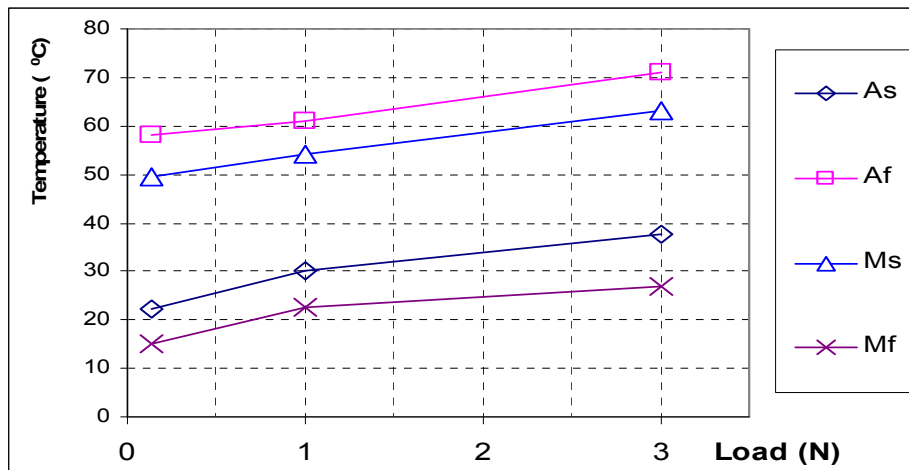


Fig 9. Variation tendency of the critical transformation temperatures under load, as a function of the loads applied at the end of the spring

The increase of the critical transformation temperatures with the increase of the load applied to the spring is obvious, which corresponds to the augmentation of the shear stress induced in spring. This dependency is in close correlation to the Clausius-Clapeyron relationship that considers as constant the ratio between stress variation and the variation of the transformation temperatures:

$$\Delta\sigma / \Delta M'_s = \Delta S / \varepsilon_0 = ct. \quad (2)$$

where  $\Delta S$  represents the transformation enthalpy and  $\varepsilon_0$  the deformation.

In Table 2 the stroke of the spring's end are illustrated as a function of the temperature variation, for the three applied loads. The values were graphically determined on the perfectly linear portions of the hysteresis curves.

Table 2 Stroke variation as a function of temperature variation

Parameter	Load =0.13 N		Load =1 N		Load =3 N	
	Increase	Decrease	Increase	Decrease	Increase	Decrease
$\Delta T$ ( $^{\circ}\text{C}$ )	28	25	18	24	29	30
$\Delta H$ (mm)	75	72	110	128	180	170
$\Delta H / \Delta T$ (mm/ $^{\circ}\text{C}$ )	2.68	2.88	6.11	5.33	6.21	5.67

In Fig.10 the variation curves of the specific work generated by the spring as a function of temperature are shown for the three applied loads.

It is noticeable that the generated specific work (J/g) markedly increases with the applied load.

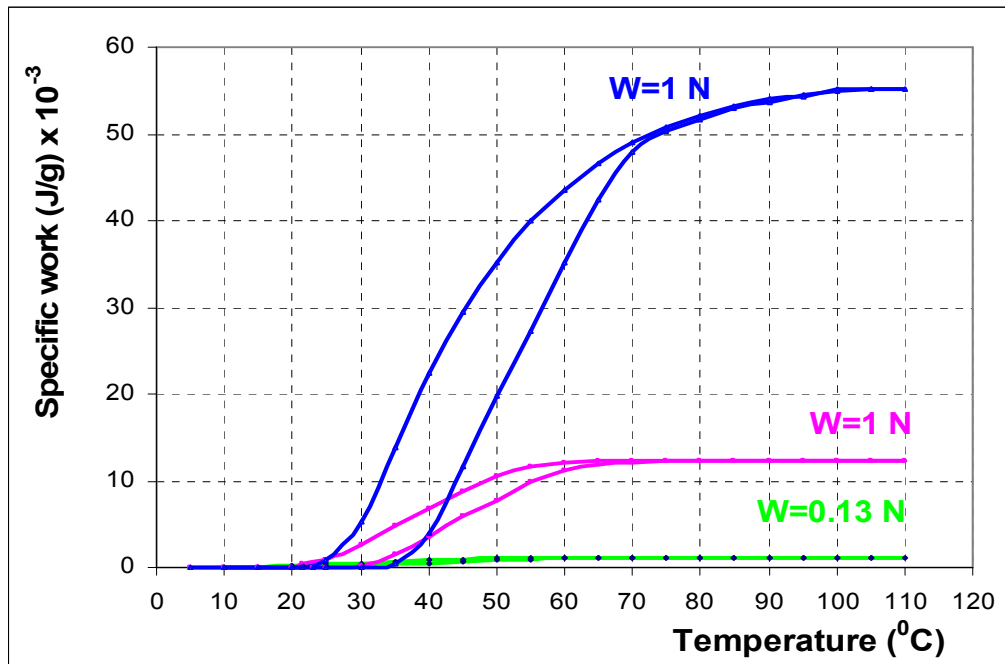


Fig 8. Variation curves of the specific work generated by the spring as a function of the applied load and the heating temperature

#### 4. Conclusions

By analysing the experimental results the following conclusions may be drawn:

- For an increase of 3 times of the applied load (from 1 to 3 N) the specific work increased 4.5 times (from 0.01223 J/g to 0.055 J/g, respectively) since the stroke (displacement of the load fastened at the end of the spring) increased 1.5 times (from 156 mm to 235 mm, respectively).
- With the increase of the applied load the slope of the deflection-temperature hysteresis curve was augmented, which markedly improves the tuning sensitivity of the SMA actuator stroke by means of temperature variation.
- Resuming the experiments, for different applied loads, similar results were obtained concerning deflection-temperature and the specific work-temperature variations. This involves a very good reproducibility of the work generating behaviour of the helical spring made from a Cu-Zn-Al-based SMA.

These results ascertain the idea that Cu-Zn-Al-type SMAs represent adequate candidates for active elements in a series of applications for work generation or for proportional control of temperature, owing to their special characteristics:

- the capacity to generate much higher specific work as compared both wax actuators and thermostatic bimetals;

- the ability to develop large nonlinear strokes for small thermal ranges, according to a proportional variation law, as a function of the constructive shape.

### Acknowledgment

This paper was partially supported by the Romanian Ministry of Education and Research, under CNCSIS Grant No.476/ 2005.

Received May 9, 2005

\*S.C.Mittal Steel Iasi S.A.

\*\*The "Gh.Asachi" Technical University of Iași

### REFERENCES

1. Richard F. Gordon. – *Design Principles for Cu\_Zn-Al Actuators*, **Engineering Aspects of Shape Memory Alloys**, (Duerig, T.W., Melton, K.N., Stöckel, D. and Wayman, C.M., editors), Butterworth-Heinemann, London-Boston-Singapore-Sydney-Toronto-Wellington, 1990, ISBN 0-750-61009-3, **245-255**
2. Bujoreanu, L.G., *Variation of the critical point  $A_s$  during the thermomechanical training and subsequent cycling by two way shape memory effect of a Cu-Zn-Al-based shape memory alloy (in Romanian)*, **Metalurgia**, **52, Nr.3**, (2000), ISSN 0461-9579, **17-25**
3. Van Humbeeck, J. and Stalmans, R. – *Characteristics of shape memory alloys*, , **Shape Memory Materials**, (Otsuka, K. and Wayman, C.M., editors), Cambridge University Press, ISBN 0-521-44487-X, 1998, **149-183**
4. Patoor, E. et Berveiller, M. (coordonateurs) – **Technologie des alliages à mémoire de forme. Comportement mécanique et mise en oeuvre**, Hermès, Paris, 1994, ISBN 2-86601-426-X
5. Ming ,H.W. *Cu- Based Shape Memory Alloys*, în "**Engineering Aspects of Shape Memory Alloys**", editată de Duerig, T.W., Melton, K.N., Stökel, D., Wayman, C.M., ButterworthHeinemann, London-Boston-Singapore-Toronto-Wellington, 1990, **pag. 69-95**

### STUDIUL EFECTULUI DE MEMORIA FORMEI GENERATOR DE LUCRU MECANIC

#### (Rezumat)

Lucrarea urmărește să determine capacitatea de generare de lucru mecanic a unui resort elicoidal confecționat dintr-un aliaj cu memoria formei (AMF) pe bază de Cu-Zn-Al. În acest scop au fost efectuate experimente constând din ridicarea activată electric a diferitor sarcini de către resortul elicoidal, în timpul căreia variația deplasării cu temperatura a fost precis măsurată și înregistrată. Cu ajutorul curbelor deplasare vs. temperatură, care au fost perfect reproductibile, au fost determinate temperaturile critice de transformare, pentru diferite sarcini aplicate. În felul acesta a fost dezvoltat un actuator electric care poate fi controlat cu precizie și care poate dezvolta un lucru mecanic specific de 0.055 J/g.

## **AEROSPATIAL MECHANICAL ENGINEERING OF TITANIUM ALLOYS**

**BY**

**MIRCEA DOBRESCU, CONSTANTIN DUMITRESCU and RAMI SABAN**

**Abstract:** Aerospace industry owes its development to the introduction of titanium alloys together with aluminium alloys and composite materials. In spite of titanium low castability or extremely expensive forged pieces used in aerospace, mechanical characteristics of titanium are not very inferior to hardened and tempered steel. Titanium's workability on machine tools is better than that of a stainless steel. The greatest effect on machining has the coefficient of thermal expansion and modulus Young (half the value in steel). In the paper is shown the influence of mechanical working on the properties of titanium and titanium alloys used in aerospace.

**Keywords:** titanium alloys, aerospace, mechanical working, mechanical surface preparation

### **1. Introduction**

Aircrafts are constantly subjected to a variety of alternating loads, ranging from ground movements, fuel distribution, pressure differentials, to the numerous structural cyclic loading [1] patterns occurring during flight conditions. These loadings may lead to the progressive degradation of the aircraft structure.

That is why mechanical working and mechanical surface preparation are very important for quality and mechanical characteristics of titanium alloys for aerospace.

### **2. Enhancing fatigue resistance by mechanical surface preparation**

Resistance to crack propagation is very important for improving fatigue life of titanium alloys that works under cycling loadings. A good preparation of titanium alloys products for aerospace must also compensate some disadvantages like medium hardness, chemical reactivity at high temperatures [2].

Surface treatments are recommended for parts that will see service at high temperatures.

Mechanical surface treatments as polishing, shot-penning, surface rolling, improved fatigue strength of titanium parts. By combining mechanical surface treatments with utilization of laser, ions, electron beams as well as CVD and PVD processes, energy field (magnetic, electric) we can improve surface properties and fatigue resistance.

### **3. Machining titanium**

Titanium workability on machine tools is better than that of stainless steel. The tooling of titanium is more similar to that of aluminium than of stainless steels [3].

The values which have the greatest effect on machining are the coefficient of thermal expansion and modulus of elasticity which gives an idea of the deformation of material in relation to a certain load applied to the piece. This value in titanium is about half value in steel (table 1).

Table 1 Mechanical properties of some common metallic materials

Material	Tensile strength (N/mm <sup>2</sup> )	Modulus of elasticity (N/mm <sup>2</sup> )	Coeff. of thermal expansion (W/m°C)
Steel	1200	200000	65
Aluminium	350	70000	180
Titanium	1000	100000	10

So titanium will be deformed in a more consistent way than steel and great care is required in assessing axially and radially, in both roughing and finishing operation.

The alloy grades of titanium are harder to machine than commercial pure grades of titanium. The different grades of titanium do not have identical machining characteristics, any more than all steels.

Like stainless steels, the low thermal conductivity of titanium inhibits dissipation of heat within the work piece itself.

#### 4. Conclusions

Good tool life and successful machining of titanium alloys for aerospace can be assured by:

- Maintain sharp tools to minimize heat build up and galling.
- Use rigid setups between tool and workpiece flexure
- Use a generous quantity of cutting fluids to maximize heat removal
- Utilize lower cutting speeds
- Avoid interruptions in feed
- Regularly remove turnings from machines

Received May 4 2005

University POLITEHNICA of Bucharest

#### REFERENCES

- [1] \*\*\* - Titanium Alloy Guide – 4/2000, p. 10-12  
 [2] T. Ronald – NASP Launches New Materials – Advanced Materials Processes – 9/1993, p. 24-29  
 [3] P. Carnevale – La lavorazioni meccaniche delle leghe di titanio, Titanium Industry , 6/2003, p. 40-46

#### INGINERIA MECANICĂ AEROSPAȚIALĂ A ALIAJELOR DE TITAN

##### (Rezumat)

Industria aeronautica isi datoreaza dezvoltareaintroducerii in exploatare a aliajelor de titan, alaturi de aliajele de aluminiu si materialele compozite. In ciuda turnabilitatii scazute a titanului si forjarii extrem de costisitoare a piselor utilizate in aeronautica, caracteristicile mecanice ale titanului nu sunt inferioare otelului recopt. Prelucrabilitatea titanului este superioara otelurilor inoxidabile. Cel mai mare efect asupra prelucrabilitatii o are coeficientul de dilatare termica si modulul lui Young (jumătate din cel al otelurilor). In lucrare este prezentata influenta prelucrării mecanice asupra proprietatilor titanului si aliajelor sale utilizate in aeronautica.

## FACTORS AFFECTING PERFORMANCE OF BULLETPROOF COMPOSITES

BY

GABRIELLA FAUR-CSUKAT

***Abstract:** As a consequence of political and economical changes in Eastern Europe, as well as the simplicity of border crossing violent crimes became more frequent, that gained need of using bullet- and splinterproof structures. The defences developed for military purposes could not or only partially could be applied in civil areas. A survey on theoretical background of development of bulletproof composites is given below.*

***Keywords:** fiber reinforcement, hybrid composites, ballistic performance, parameters affecting performance, ballistic test*

### 1. Forming effective ballistic protection

To develop effective bulletproof protection we have to know in which field of civil life to expect threatening. We have to know the possible locations, armours and other technical possibilities. The other functions of defence, necessary and affordable expenditure also must be known.

In Hungary –beside home burglary– bank, petrol station and shop robberies are more and more frequent. Among armours automatic pistols (i.e. 9 mm Parabellum) and AK47 rifles, also other guns and bullets from Eastern Europe and former Sovietunion are the most widespread.

In military applications the collective protection of mobile instruments is basically assured by steel armour, although the penetration ability of certain explosion projectile reaches 2000 mm [12].

Since the 1960s –due to the appearance of high modulus and high strength synthetic fibres– ratio of applied fibre reinforced composites increased dramatically.

The aim of our work is to develop light-weight composite structures that provide protection against high energy bullets and fragments. These structures could be used in civilian area as well.

### 2. Ballistic materials

The most important factor in selection of ballistic materials is the ballistic potential of the given material:

$$R^2 = w \times c \quad (1)$$

where  $w$  is the fracture energy of the material, and  $c$  is the sound propagation velocity in the material.

The sound propagation velocity in the material is given by

$$c = \sqrt{\frac{E}{\rho}} \quad (2)$$

where  $E$  is the elastic modulus, and  $\rho$  is the density.

The materials with high ballistic potential should have high impact strength, high modulus, and low density. Fibre reinforced composites could fulfil these requirements, which consist of at least two, in each other insoluble components, one of them –carrier or matrix– has lower modulus and strength, while the other has lower modulus and strength, while the other –reinforcement– has high modulus and strength. The composite, as a reinforced construction, is characterised by the interfacial adhesion, which is retained even under load or deformation. Among structures used for ballistic protection ballistic textiles (mainly for protective clothes and jacket), flexible and rigid composites can be differentiated.

Fibre types applied in ballistic textiles and reinforcement in composites are carbon fibre, glass fibre, high strength polyamide 6.6, aramide fibres (Kevlar® from DuPont, Twaron® from Akzo), high performance polyethylene (HPPE, Spectra® from Allied, Dyneema® from DSM), other organic fibres, such as polyphenylene-benzobisoxazole (PBO).

As matrix material almost exclusively thermosetting polymers, i. e. unsaturated polyesters, vinylesters, and epoxy resins are used in composites providing ballistic protection. Good mechanical properties, compatibility with the selected reinforcement, processability, and effect of reaction heat on reinforcing structure are the leading factors in selection of matrix resin.

Application of technical ceramics features hardness and rigidity of components against high energy projectiles. The ceramics applied on the loaded side of panels are the key of ballistic protection, damages the front of bullets, and absorbs majority of its kinetic energy. The fibre reinforced composite sheet supporting the rigid ceramics layer ensures high strength of ballisticproof structure. Mostly alumina based ceramics are used for ballistic purposes, due to their good technical properties and relatively low price. Their main disadvantage is high density, 3.4-3.9 g/cm<sup>3</sup>, depending on aluminium content. In special cases carbide or nitride type ceramics could be used.

### **3. Factors affecting ballistic performance of composite materials**

In the following sections factors affecting ballistic performance of fibre reinforced, rigid composites are reviewed: material properties of reinforcement; fabric structure; projectile geometry; projectile velocity; interaction of multiple plies; friction between yarns themselves and between the yarns and projectile.

#### **3.1 Material properties of fibres**

Interaction of yarns and projectile at impact are reported in studies. When a projectile impacts the fabric, it produces a transverse deflection in the yarns (defined

as principal yarns) that are in direct contact with the projectile and generates longitudinal strain waves that propagates at the sound speed of the material down the axis of the yarns [6]. The transverse wave causes misalignments of principal yarns toward the impact point, which movements occur with other yarns as well, due to the intersections of yarns. Numerical studies by Roylance [1] have shown that the majority of the kinetic energy of the projectile is transferred to the principal yarns as strain and kinetic energy, whereas, the contribution of the orthogonal yarns to energy absorption is small. While the profile of transverse wave of yarn-projectile impact is V-shaped, the orthogonal yarns of a fabric changes the profile to more of a parabolic profile [15].

Clearly, fibres possessing high tensile strengths and high failure strains can absorb considerable amounts of energy. In their study comparing the impact performance of dry Spectra fabrics and their corresponding armour-grade laminates, Lee et al. [13] have correlated the number of yarns broken to the levels of impact energy absorbed. Using a model developed to analyse the impact of fabric, Roylance and Wang [2] have shown that materials possessing high modulus,  $E$ , and low density,  $\rho$ , disperse the strain wave rapidly away from the impact point, which distributes the energy over a wider area and prevents large strains from developing at the impact point. Although tensile strength, modulus, and strain-to-failure of yarn play significant role in ballistic performance, each property individually does not control it. According to Laible [3] the relationship between the mechanical properties of a yarn and the ballistic resistance of a plies fabric from such yarn has never been established.

### 3.2 Fabric structure

It has been observed that loosely woven fabrics and fabrics with unbalanced weaves result an inferior ballistic performance [6]. Weave patterns typically used for ballistic applications are plain and basket weaves. The density of the weave, known as the “cover factor” is determined from the width and pitch of the warp and weft yarns and gives an indication of the percentage of gross area covered by the fabric. Chitrangad [7] notes that fabrics should possess cover factors from 0.6 to 0.95 to be effective when utilised in ballistic applications. When cover factors are greater than 0.95, the yarns are typically degraded by the weaving process and when the cover factors fall below 0.6 the fabric may be too “loose” that leads to “wedge through” of projectile. This “wedge through” phenomena has been observed by a number of researchers [17]. In the “wedge through” process when a projectile strikes a layer of fabric, the fabric deflects transversely and the mesh of yarns is distended, resulting enlargement of the spaces between the yarns. If the projectile is relatively small and/or impacts at any angle and/or the fabric is loose, the projectile can slip through the opening or “wedge through” by pushing yarns aside instead of breaking them. The hole formed this way is called “trap door” [11]. The hole is smaller than the projectile [11] and the number of broken yarns is less than the number of yarns that intersect the projectile [13]. Trap door formation depends not only on fabric structure, but also on the mobility of yarns and on the projectile geometry [5]. Yarn mobility can be influenced by the frictional behaviour of the yarns with themselves and with the projectile, and can be minimised by the actual physical restraint of the lateral motion of the yarns through the introduction of a matrix.

### 3.3 Projectile geometry

The geometry of a projectile influences its ability to perforate a fabric. Montgomery et al [4] investigated four different 0.22 projectile geometries on the ballistic performance of one, two and three layers of Kevlar 49. They have stated that pointed bullets had the ability to wedge through fabric and were not decelerated as quickly as blunt bullets.

Ulven et al. [16] investigated ballistic performance of carbon fibre/epoxy composites against hemispherical, conical, and flat projectiles, and FSP (fragment simulating projectile). The largest amount of energy was absorbed in the panel from the impact of the conical projectile (29 % greater), followed by the flat (17 % greater), hemispherical (15 % greater) projectile, compared to FSP (in case of 6.5 mm composite thickness). The significant difference in the amount of absorbed energy can be explained by the different failure mechanisms. The differences are limited in case of thinner composite panels –although the tendency remained the same– since the thinner sheets bend at impact (energy absorption) independently on the shape of projectile.

### 3.4 Impact velocity

In their work impacting Twaron fabric with steel spheres, Shim et al. [8] has described the differences observed between low- and high-velocity impact. With low-impact velocities, the yarns do not fail during the initial stress rise; therefore, the transverse deflection of the fabric has time to propagate to the edges of the panel, which allows the fabric to absorb more energy. Panels struck with a low-velocity projectile are characterised by extensive creasing and stretching, which may contribute to energy dissipation. With a high-velocity impact, the damage is localised and the yarns fail before significant transverse deflection can develop. Recent studies by Carr [9] on single yarn impact of Kevlar and ultra-high-molecular weight polyethylene (UHMWPE) has similarly found that at higher impact velocities, the yarns fail in shear; moreover, with UHMWPE yarns, melt damage of the filaments was also noted. Hiermaier et al. [10] in their investigation of bumper shields required for the protection of space vehicles from hypervelocity impact have stated that all the epoxy vaporised when Kevlar-epoxy composite plates were impacted at 788 m/s. At an impact velocity of 1015 m/s, the Kevlar-epoxy plate underwent a phase change, thermally decomposed and turned into a mass of fine Kevlar particles.

### 3.5 Multiple plies

Several studies report behaviour of multiple plies fabric and composite structures at high velocity impact, mainly from the aspect of failure mechanism. When multiple ply armour systems are impacted by sharp-edged projectiles, the first few layers are punched out in the shape of the impacting surface. The remaining layers behave as a membrane. In other words, the layers close to the impact surface behave inelastically, whereas the layers toward the back behave elastically. It was postulated that when the projectile initially impacts that panel, it produces a compressive wave that propagates

through the thickness of the laminate and reflects off the rear surface as a tensile wave, which may produce delamination. The damage mechanisms are dependent on the projectile geometry and velocity, the properties of the matrix and fibres and the fibre-matrix adhesion. It should be noted that for ballistic applications, weak fibre-matrix adhesion is wanted. This results in the ready delamination of the compliant laminate, which allows the fibres to extend to failure. However, depending on the application, a certain degree of structural stiffness may be warranted, thus increased fibre-matrix adhesion may be used [17].

### 3.6 Fibre-fibre, and fibre-projectile friction

The work of Lee et al. [13] has shown that by restricting the ability of the yarn to move laterally out of the path of the projectile during impact (by using small amounts of resin) increases the amount of energy the fabric can absorb. Or, more generally, increasing the friction between the projectile and the fabric and the yarns themselves will hinder the mobility of the yarn and require the projectile to engage and break more yarns, which would result in greater energy absorption.

## 4. Concluding remarks

From the above overview it is clear that the ballistic performance of composites is affected by several factors. The R&D works focus not only on new materials and technologies but also on modelling and simulation of impact. A promising direction of development is the preparation of hybrid composites, in which composite layers with different reinforcement and matrix of different hardness are combined.

## ACKNOWLEDGEMENT

Support of Ministry of Education Hungary (ALK-00150/2002) is gratefully acknowledged.

*Received May 4 2005-05-13*

*Bay Zoltán Institute for Materials Science and Technology, Budapest, Hungary*

## REFERENCES

- [1] Roylance, D., Stress wave propagation in fibers-effects of cross-overs, *Fiber Sci. Technol* **13**, 385-395, (1980).
- [2] Roylance, D., and Wang, S. S., Penetration mechanics of textile structures. In: *Ballistic Materials and Penetration Mechanics*, (Laible, R. C., ed), Elsevier Scientific Publishing Co, New York, 1980.
- [3] Laible, R. C., Fibrous armor. In: *Ballistic Materials and Penetration Mechanics*, (Laible, R. C., ed), Elsevier Scientific Publishing Co, New York, 1980.
- [4] Montgomery, T. G., Grady, P. L., Tomasino, C., The effects of projectile geometry on the performance of ballistics fabrics, *Text. Res. J.* **52**, 442-450 (1982).
- [5] Kirkland, K. M., Tam, T. Y., Weedon, G. C., New third-generation protective clothing from high-performance polyethylene fiber In *High-tech Fibrous Materials* (Vigo, T. L., Turbak, A. F. eds) American Chemical Society, Washington DC, 1991.

- [6] Cuniff, P. M., An analysis of the system effects of woven fabrics under ballistic impact, *Text. Res. J.*, **62**, 495-509 (1992).
- [7] Chitrangad, Hybrid ballistic fabric, United States Patent No. 5,187,003 (1993).
- [8] Shim, V. P. W., Tan, V. B. C., Tay, T. E., Modelling deformation and damage characteristics of woven fabric under small projectile impact, *Int. J. Impact Eng.* **16**, 585-605 (1995).
- [9] Carr, D. J., Failure mechanisms of yarns subjected to ballistic impact, *J. Mater. Sci. Lett.* **18**, 585-588 (1999).
- [10] Hiermaier, S. J., Riedel, W., Hayhurst, C. J., Clegg, R. A., Wentzel, C. M., Advanced material models for hypervelocity impact simulations AMMHIS, European Space Agency Contract Report, EMI-Report No. E43/99, 30 July 1999.
- [11] Prosser, R. A., Cohen, S. H., Segars, R. A., Heat as a factor in the penetration of cloth ballistic panels by 0.22 caliber projectiles, *Text. Res. J.*, **70**, 709-722 (2000).
- [12] 5<sup>th</sup> International Seminar on Ballistic Protection, Geneva, Switzerland, 21-22. September 2000.
- [13] Lee, B. L., Walsh, T. F., Won, S.T., Patts, H. M., Song, J. W., Mayer, A. H., Penetration failure mechanisms of armor-grade fiber composites under impact, *J. Compos. Mater.* **35**, 1605-1633, (2001).
- [14] Larsson, F., Svensson, L., Carbon, polyethylene and PBO hybrid fibre composites for structural lightweight armour, *Composites Part A* **33**, 221-231, (2002).
- [15] Duan, Y., Keefe, M., Bogetti, T. A., Cheeseman B. A., Modeling the impact behavior of high-strength fabric structures, Fiber Society Annual Technical Conference, Massachusetts, USA, 16-18 October 2002.
- [16] Ulven, C., Vaidya, U. K., Hosur, M. V., Effect of projectile shape during ballistic perforation of VARTM carbon/epoxy composite panels, *Composites Structures* **61**, 143-150 (2003).
- [17] Cheeseman, B. A., Bogetti, T. A., Ballistic impact into fabric and compliant composite laminates, *Composites Structures* **61**, 161-173 (2003).

**FACTORI CARE INFLUENȚEAZĂ PERFORMANȚA MATERIALELOR COMPOZITE  
REZISTENTE LA PROIECTILE**

**(Rezumat)**

Drept consecință a schimbărilor politice și economice din Europa de Est, precum și a ușurinței cu care se poate trece frontiera, crimele violente au devenit mai frecvente, ceea ce a dus la nevoia largită de a utiliza structuri rezistente la proiectile și așchii. Mijloacele de apărare dezvoltate pentru scopuri militare nu pot fi aplicate de loc sau doar parțial în domeniile civile. În lucrare se prezintă o sinteză a cunoștințelor teoretice legate de dezvoltarea materialelor compozite rezistenete la proiectile.

## MICROSTRUCTURAL CHANGES INTO THE HEAT AFFECTED ZONE OF CHROMIUM ALLOYED WHITE CAST IRON

BY

DIANA ANTONIA GHEORGHIU

**Abstract:** The paper focuses on the microstructure changes that occur into the heat affected zone, HAZ, of a chromium alloyed white cast iron. Even if the transformations that take place in HAZ are well known for most of the weldable materials as well as for some materials that offer less welding properties, it is the first time that intimate microstructure changes in white cast iron are enlightened.

**Keywords:** chromium nickel alloyed white cast iron, eutectic carbide, complex alloyed carbide, metallic matrix, heat affected zone – HAZ.

### 1. Introduction

Any low ductility material must be considered as having a poor response to welding process. It is generally accepted that during welding cast iron cracks. Cracking phenomenon is due to:

- changes into the carbon distribution along the weld and HAZ, these involving microstructural transformations that dramatically rise the possibilities for a brittle fracture;
- a local heat input, causing expansion and contraction stresses that can not be absorbed by the base material;
- a contracting weld bead, creating tensile strains on HAZ at cooling.

From these three arguments, only the last two are taken into consideration when attempts to weld white cast iron are being done.

For the hypoeutectic compositions, which are usually employed for unalloyed as well as for the alloyed white cast iron, the eutectic carbide network will not dissolve, as happens into the grey cast iron with the graphite. More precisely, the total effect of the thermal cycle will have a much poorer effect on the white cast iron structure. This statement is more legitimate for the alloyed grades, especially the chromium ones, where the alloyed carbide phase presents high hardness values and good high temperature properties – abrasion, erosion, corrosion resistance even for 750<sup>0</sup>C, all these involving a good temperature stability of the microstructure. Taking into account all this, the white cast iron, alloyed or unalloyed is firmly qualified unweldable, even if all foundry makers are very interested in the repairing of casting defects by welding. The repair of the cast parts would only be applied in case of a defect on a non critical area for the exploitation conditions.

## 2. Materials and experimental procedure

In the experimental work the base material, that is the weld metal is a chromium – nickel – molybdenum white cast iron grade, FaCrMo 1, STAS 11 246-79. This grade is known as having good abrasion and corrosion wear resistance properties; the parts to be cast are mud pumps body for salt water. Typical for this alloyed cast iron is that their mechanical properties are not standing out. The recommended values are not guaranteed, and are no design basis, Table 1. For their qualification hardness test, chemical composition and microstructure analysis are satisfactory.

Table 1

Mechanical characteristics for chromium – molybdenum alloyed cast irons

Grade / Symbol	Vickers Hardness HV 30	Brinell Hardness HB	Rockwell Hardness HRC	R <sub>m</sub> N/mm <sup>2</sup>	Modulus E KN/mm <sup>2</sup>	ρ Kg/dm <sup>3</sup>
GX 300 CrMo 15 3	380...750	380...680	39...62	450...1000	154...190	7.7
GX300 CrMoNi15.2 1	380...750	380...680	39...62	450...1000	154...190	7.7

The limits of the chemical composition for the FaCrMo1 as recommended and the real values for the specimens are in Table 2

Table 2

Chemical composition of the white cast iron

	Chemical composition, wt. %					
	C	Si	Mn	Cr	Ni	Mo
DIN 1695 GX300 CrMoNi 15/2/1	2.3...3.6	0.2...0.8	0.5...1	14...17	0.8...1.2	1...2.2
Specimens' composition	2.8	0.5	0.8	15.6	0.9	1.1

The properties of the cast iron are due to the chromium content as well as to the carbon content. First, the chromium addition replaces iron in the carbide phase, resulting eutectic ledeburite, with carbide (FeCr)<sub>3</sub>C that solidifies as network. At 8%Cr, the carbide structure changes. The network carbide is replaced by the filamentous Cr<sub>7</sub>C<sub>3</sub> or (CrFe)<sub>7</sub>C<sub>3</sub> which became the main compounds in the eutectic structure. These allied carbides are the support of the special properties of the cast iron. The cast iron structure will contain some of these carbides alone or carbide association as a function of the Cr, Fe and C content, significant being also the Cr/C ratio, [2]. On solidification, the leadership role is held by the carbide phase, no matter what its composition is. The carbide, especially the alloyed one, has a low diffusion rate – slow dissolve into austenite when heating and precipitates slow also from austenite on cooling.

On the other side, the metallic matrix, resulted from the pro-eutectic austenite will suffer changes too. The most possible structure for the metallic matrix at this chemical composition is some austenite, ferrite and martensite [1].

Specimens of white cast iron measuring 50 x 50 x 200 mm were green sand cast. The specimens were machined on two opposite sides. Weld beads of 40 mm length were accomplished on the prepared surface. Three electrode type were used, on the same welding conditions, that is electrode diameter 2.5 mm, welding current 70 A.

### 3. Experimental results

The visual control, eye and magnifying glass, of the as welded specimens do not make evident any surface crack. The specimens were cut off for metallographic and hardness tests.

Figure 1 presents some macroscopic images of the transverse sections. It worth emphasise that the sections are free of discontinuities – cracks, pores, nonmetallic inclusions. The different geometric shape is due only to the electrode chemistry.

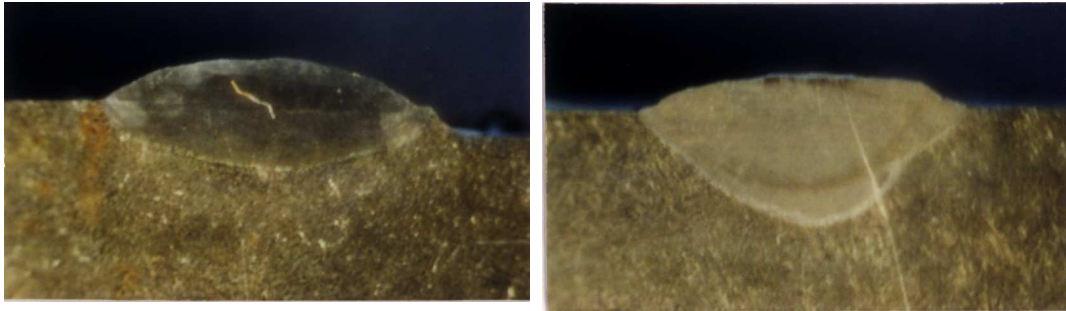


Fig.1 Macrographs showing the transverse section of some welds carried out on white cast iron.

The microstructure analysis enlightened a clear threshold between the added material and the cast iron. It can be seen that the base material structure did not change in a sensible mode, Figure 2.



Fig.2. Microstructure of the weld: a. the transition zone, b. base material structure, 200:1, Nital etched.

The microhardness tests were made at 500:1 magnification. At this scale it can be seen that the chromium alloyed white cast iron supports significant structural changes, Figure 3. First of all, just below the transition line the carbides are thin, and the metallic matrix has a clear martensitic structure, Fig. 3a. Here the measured hardness reach the maximum value. In the profoundness of the HAZ, the carbides manifest the tendency to dispose in the temperature gradient sense, Fig. 3b. and 3c. The metallic matrix suffers an important change: around the carbides the matrix is softer, and as can be seen, the chemical etched affects less this structure. Near the unaffected base metal carbides are thinner, fragmented as can be seen in Fig. 3d. The hardness has its minimum value, [3].

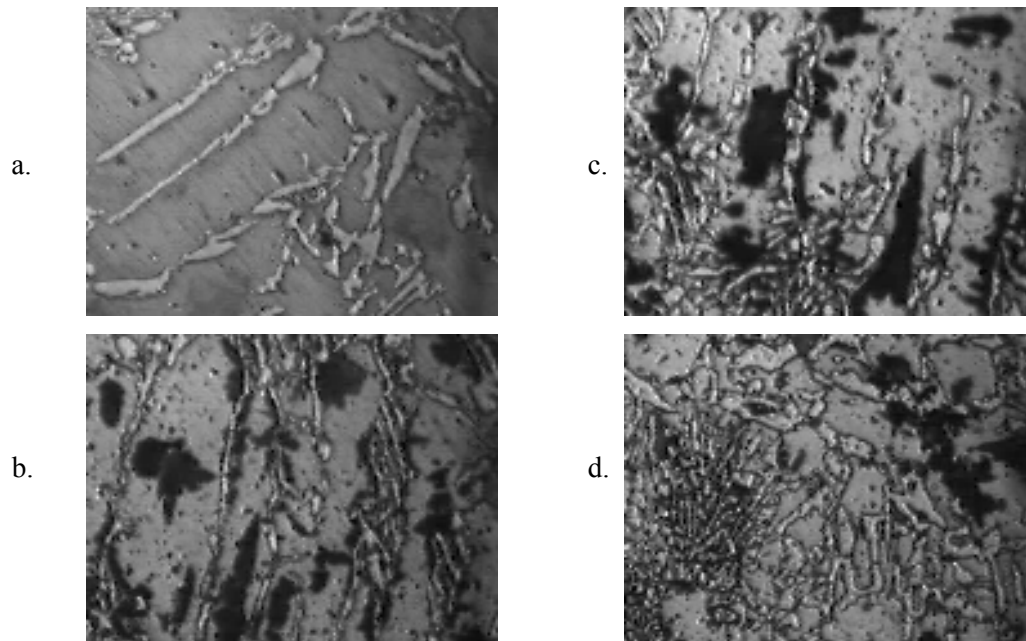


Fig.3 Microstructural changes in HAZ: a. base material structure in the close proximity of the transient zone; b, c.: carbides that have changed their disposal following the thermal gradient during welding; d. globular carbides located in the softer zone of the weld.

#### 4. Conclusions

The studied white cast iron has a good response at welding in the specified conditions; no external or internal cracks occur for the established welding parameters.

During the welding of white cast iron, the carbides in the HAZ partially dissolve into austenite. This phenomenon differs according to the peak temperature reached in the specific point of HAZ. At cooling, the carbides change their disposal and distribution into the metallic matrix. These changes slightly affect hardness.

Received May 9, 2005

The "Gh.Asachi" Technical University Iași

#### REFERENCES

1. Laplanche, H. – **Les fontes et leurs traitements thermiques, metallurgie structurale**, Edition Desforges, Paris, 1978.
2. Sofroni, L., Ripoșan, I., Chira, I. – **Fonte albe rezistente la uzare**, Editura tehnică, București, 1987
3. Gheorghiu, D., Nejneru, C., Hopulele, I. – *The influence of the electrode paste upon the relative durification of welds on cast iron*, **Bul Inst. Politehnic Iași**, T. XLIX(LIII), Fasc 1-4, 2003, **103-106**

#### MODIFICĂRI MICROSTRUCTURALE INDUSE ÎN ZONA INFLUENȚATĂ TERMIC A FONTEI ALBE ALIATE CU CROM

##### (Rezumat)

Articolul prezintă transformările microstructurale care au loc în zona influențată termic în cazul sudării unei fonte albe aliate cu crom. Transformările ce au loc în ZIT sunt bine cunoscute pentru marea majoritate a materialelor ce prezintă o sudabilitate bună și chiar pentru o bună parte din materialele greu sudabile, este prima oară când sunt urmărite transformările într-o fontă albă. Fontele albe, aliate sau nu sunt clasificate ca nesudabile, deși există interes din partea producătorilor de fonte, în special.

## **SAFETY, PROTECTIVE AND OCCUPATION FOOTWEAR CHARACTERISTICS USED IN METALLURGICAL INDUSTRY**

BY

**CORNELIA IONESCU LUCA and ALINA DRAGOMIR**

**Abstract:** This paper presents some characteristics requested by European Economical Community for safety, protective and occupation footwear and some principal sorts of footwear destined to metallurgical industry.

**Keywords:** metallurgy, foundry, safety, footwear, standard

### **1. Introduction**

In every industrial area are typical safety equipments depending on specific working conditions.

In this paper is presenting a study about safety, protective and occupation footwear used in metallurgical industry.

### **2. Safety, protective and occupation footwear defining**

The standards of European Economical Community for safety, protective and occupation footwear are: EN 344-2:1996, EN345:1992, EN 346:1992, EN 347: 1992. In according with this group of standards, the footwear is classified in three classes:

- safety footwear class includes any shoes or boots with safety metal toe and an impact resistance equivalent with 200 J level of energy used to protect the feet against the injure of work;
- protective footwear class includes any shoes or boots with safety metal toe and an impact resistance equivalent with 100 J level of energy used to protect the feet against the injure of work;
- occupation footwear which protects the feet against injures at work but the toe is not a metal one.

Those standards make reference to the European Economical Community request for different types of footwear [shoes(A), ankle – high boots (B), calf – high boots (C), knee – high boots (D) hip boots (E)] and methods to research the proprieties of materials, components and whole shoe.

### **3. Characteristics of safety protective and occupation footwear used in metallurgical industry**

In the work average of metallurgical industry, the feet of the workers are exposed to the chemical and physical noxious agents. In order, the footwear should present on the one hand, physiological – hygienically proprieties and on the other hand, safety and protection characteristics.

In the foundry works where the temperature is very high, the footwear must to protect the feet against the overheating caused by the thermal radiation, the burn which can be caused to the contact with over heat surfaces, sparks, drops of molten metal or metal dross etc.

Generally speaking, the design of this sort of footwear should provide lightness and fastness wearing and a good protection of the feet.

To be able to provide a good protection against the drops of molten metal or sparks, the top quarters of boot are fixed around of the ankle and in case of shoes or boots with not very high quarters; the legs are protected with thermal insulating legwarmers.

The shoes are recommended to be fixed on the feet by straps with buckles, not laced.

The upper materials should have a sleek grain, able to provide sliding of spark, drops of molten metal or metal dross, and a thermal irradiation resistance around of  $3500 \text{ J/m}^2\text{s}$  in 350 hours. Also, the materials for upper shoes should be resistant to 1,5 million flexes when the radius of curve flexing is 1,8 to 10 mm, except the toe area where the flexing endurance requested is around of 2,5 million flexes. In the same time, those materials should present a good resistance at different kind of liquids as are oil or coolan fluid, and a resistance of hydrocarbon actions as 4 hours at  $40^\circ\text{C}$  and 24 hours at  $20^\circ\text{C}$ .

In case of the work condition of air velocity of 1,5 m/s, the upper layers must be able to provide the thermal insulation of the feet against the  $65^\circ\text{C}$  working temperature, so that, the inside temperature of shoes to be up to  $30^\circ\text{C}$ .

The sole material is thermal resistant rubber, able to offer resistance to the contact with heated plates at more than  $150^\circ\text{C}$  and the sole together with the other layers of the bottom of shoe to be able to provide the thermal insulation of the feet, so that, the temperature of the insole to be no more than  $30^\circ\text{C}$ .

The footwear for metallurgical industry presents a metal toe and a rigid part for metatarsal protection with an impact resistance for protective shoes equivalent with 100 J level of energy and for safety shoes equivalent with 200 J level of energy.

In hot - metal working sections where heat and thermo-chemical treatments are made, the shoes are necessary to assure a thermal protection of feet and a protection against chemical substances also.

In other metal working sections as cold-working, surface finishing, engineering industry, the shoes are not necessary to posed thermal insulate proprieties but they must to present electrical insulate proprieties, a good impact resistance and resistance at different chemical agents: oils, solutions of alkali or acid, oxidizing agents, etc.

In order with European standards, the protective and safety footwear should answer at 2 groups of requirements: principal requirements (table no.1) and additional requirements (table no.2).

Table 1

Order number	Specific feature	Measure	Value
1.	Joint resistance of upper part with bottom part	N/mm	min. 4
2.	Impact resistance for 200 J and 100 J level of energy	Distance between toe and insole in order with length of shoes	12,5 – 15
3.	Compression resistance at 15 kN for safety shoes and at 10 kN for protective shoes	Distance between toe and insole in order with length of shoes	12,5 - 15
4.	Corrosion resistance of metal toe of rubber shoes	Number of corrosion points	max. 5
		Area of every point, mm <sup>2</sup>	2,5
5.	Rubber boot imperviousness	-	without air loss

Table 2

Order number	Specific feature	Measure	Value, symbol
1.	Penetration resistance	N	min. 1100, P
2.	Electrical resistance		
	- conductivity shoes	k $\Omega$	max. 100, C
	- antistatic shoes	k $\Omega$	10 <sup>2</sup> -10 <sup>6</sup> , A
3.	Insulation proprieties		
	- the heat insulation proprieties through the sole	°C	max. 22, HI
	- the cold insulation proprieties through the sole	°C	max. 10, CI
4.	Heel energy absorption	J	min. 20, E
5.	Water resistance	cm <sup>2</sup>	max. 3
6.	Cutting strength with chain saw		
	- the footwear of 1 <sup>st</sup> class	Speed of chain m/s	20
	- the footwear of 2 <sup>nd</sup> class		24
	- the footwear of 3 <sup>rd</sup> class		28
7.	Corrosion resistance of metal parts	Number of corrosion points	max. 5
		Area of every point, mm <sup>2</sup>	2,5
8.	Flexing proprieties of penetration – resistant inserts (midsoles)	Number of flexes	min. 1000000
9.	Heat resistance of bottom part of shoes in contact with a heat plate	Sole appearance: burning, melting, losing of shape, unsticking	Without damage of the sole after 40 minutes in sandbath at 250°C

Table 2 (continued)

10.	Heat resistance of upper shoes	Upper damages	Without damage after 40 minutes in sandbath at 250°C
11.	Burning resistance	The upper is exposed to the fair 15 seconds	- after-burning time, max. 2 sec. - after-glowing time, max. 5 sec.
12.	Impact resistance of the metatarsal safety features (impact force 100 J, 200 J)	Inside height of the shoes after impact, in mm	37 - 41
13.	Cutting strength with chain saw of the upper	Upper appearance	Without cut

The occupation footwear should respect the same requests as the safety and protective footwear without impact resistance, compression resistance, corrosion resistance of metal parts and hydrocarbons resistance.

In order with European Standards, the proprieties of the upper and bottom materials for safety, protective and occupation footwear are presented in table no.3 and no.4.

Table 3

Order number	Specific feature	Measure	Value
Upper materials			
1.	Thickness of the upper materials: - rubber - polymers	mm	- min. 1,5 - min. 1,0
2.	Minimal break resistance for: - leather - synthetic leather and textiles	N	120 60
3.	Tensile resistance of the grain split	N/mm <sup>2</sup>	min. 180
4.	Minimal break resistance of the rubber materials	N	min. 180
5.	Elongation at break of the polymeric materials	%	min. 250
6.	Flexing resistance for: - rubber - polymeric materials	number of flexes	125000 150000
7.	Water vapours permeability	mg/cm <sup>2</sup> h	min. 0,8

Table 3 (continued)

8.	Water vapours coefficient	mg/cm <sup>2</sup> h	min. 20
9.	pH number of leather	-	min 3,5 and if the pH number is smaller than 4, the number of difference to be smaller than 0,7
Lining materials			
10.	Thickness for: - leather - coated fabrics and textile materials	mm	0,8
11.	Tearing resistance of: - leather - coated fabrics and textile materials	N	min. 30 min. 15
12.	Abrasion resistance of the textile linings	- dry, cycle numbers - wet, cycle numbers	Without holes: - 25600 - 12800
13.	Water vapours permeability	mg/cm <sup>2</sup> h	min. 2
14.	Water vapours coefficient	mg/cm <sup>2</sup> h	min. 30
15.	pH number of leather lining	-	min 3,5 and if the pH number is smaller than 4, the number of difference to be smaller than 0,7
16.	Tearing resistance of the tongue for: - leather - coated fabrics and textile materials	N	min. 36 min. 18
Bottom materials			
Insole			
17.	Thickness	mm	min.2
18.	pH number	-	min 3,5 and if the pH number is smaller than 4, the number of difference to be smaller than 0,7
19.	Water absorption	%	min. 35
20.	Water desorption	%	min. 40
21.	Abrasion resistance	cycle numbers	400 without holes
Sole			

Table 3 (continued)

22.	Thickness and height of the crampon for: - direct injection process, direct vulcanized process and cementing process - rubber footwear and polymeric materials footwear - smooth soles	mm	- min.4 and min. 2,5  - min.3 and min.4  - min. 6
23.	Abrasion resistance of: - synthetic soles, density 0,9g/ml - synthetic soles, density bigger than 0,9g/ml - rubber soles	mm <sup>3</sup>	max. 250 max. 150  max.250
24.	Flexing resistance	flexes number	min. 30000
25.	Hydrolysis for PU soles	flexes number	min. 150000
26.	Adhesive strength between middle sole and out sole	N/mm	min. 4
27.	Hydrocarbon resistance	- decrease volume, %  - decrease of notch more than 6 mm after a number of flexing cycles	- min. 12 - 150000

Table 4

Order number	Specific feature	Measure	Value
Upper materials			
1.	Water resistance	- after 60 minutes, % - after 30 minutes, g	- max. 30 - max. 2
Out sole with crampons			
2.	Height of crampons for: - injected, vulcanized and cemented soles and multilayer soles - rubber and polymeric soles	mm	- min. 2,5  - min. 4
3.	Resistance of heat in contact with a plate heat at 300°C for - rubber and polymeric soles - leather soles	-	- without crack or melting around of the chuck  - without carbonizing around of the chuck

#### 4. Safety, protective and work footwear used in metallurgical industry

In Table no.5 are presented some assortment of footwear for metallurgical industry.

Table 5

Order number	Production area	Injurious factors	Recommended footwear assortment
1.	Foundry	- intensity of thermal radiations: 1400 – 1750 J/m <sup>2</sup> s; - metal sparks;	- calf – high, Russian leather boot with waterproof quarters, a metallic toe (impact resistance: 200 J) and a thermal resistant rubber sole;
		- intensity of thermal radiations: 1750 J/m <sup>2</sup> s - metal sparks; - drops of molten metal;	- knee – high boot with thermo resistant felt upper, a metallic toe (impact resistance: 200 J) and a thermal resistant rubber sole; - calf – high, Russian leather boot with a metal toe (impact resistance: 200 J) and a thermal resistant rubber sole; - legwarmers or safety and knee – high quarters;
		- intensity of thermal radiations: 1750 J/m <sup>2</sup> s - metal and silicates dust; - mechanical actions;	- ankle – high, Russian leather boot with a safety collar in the top of the quarters witch don't let the dust to get into the boot, a metal toe (impact resistance: 200 J) and a thermal resistant rubber sole;
2.	Founder's art	- intensity of thermal radiations: 1680 – 3500 J/m <sup>2</sup> s; - metal sparks; - drops of molten metal;	- knee – high boot with thermo resistant felt upper, a metal toe (impact resistance: 200 J), a heat insulating insole and a thermo resistant rubber sole; - calf – high, Russian leather boot with thermo resistant knee – high quarters or legwarmer, a metal toe (impact resistance: 200 J), a heat insulating insole and a thermal resistant rubber sole;
		- mechanical actions as nail penetration, strokes, etc.	- ankle – high, leather boot with a metal toe (impact resistance: 100 J or 200 J) and nail penetration resistant sole;

Table 5 (continued)

3.	Hot – metal workings	<ul style="list-style-type: none"> <li>- intensity of thermal radiations: 840 - 2800 J/m<sup>2</sup>s;</li> <li>- metal sparks;</li> <li>- drops of molten metal;</li> <li>- heat dross;</li> <li>- mechanical actions;</li> </ul>	<ul style="list-style-type: none"> <li>- knee – high boot with thermo resistant felt upper, a metal toe (impact resistance: 200 J), a heat insulating insole and a rubber sole witch provide protection against the high temperature and nail penetration;</li> <li>- calf – high, Russian leather boot with thermo resistant knee – high quarters or legwarmer, a metal toe (impact resistance: 200 J), a heat insulating insole and a rubber sole witch provide protection against the high temperature and nail penetration;</li> </ul>
4.	Thermal treatments	<ul style="list-style-type: none"> <li>- acid and alkali solution;</li> </ul>	<ul style="list-style-type: none"> <li>- vulcanized rubber boots resistant at acid and alkali actions;</li> <li>- thermoplastics boots resistant at acid and alkali actions;</li> </ul>

Received May 9, 2005

“Gh. Asachi” Technical University of Iasi

#### REFERENCE

1. EN 344-2: 1996 Safety, protective and occupation footwear for professional use – Part 2: Additional requirements and test methods

#### CARACTERISTICILE INCALTAMINTEI DE SECURITATE, DE PROTECTIE SI DE LUCRU UTILIZATA IN INDUSTRIA METALURGICA

##### (Rezumat)

In lucrare, se prezinta caracteristicile impuse conform normelor Comunitatii Economice Europene incaltamintei de securitate, de protectie si de lucru cu referire la sortimente destinate sectoarelor industriei metalurgice

## ALGORITHME DE PROJECTION DES MOULES POUR CONTREFORTS DE CHAUSSURE

PAR

CORNELIA IONESCU LUCA et RODICA SILVIA VOLOCARIU

**Abstract.** This paper presents a method and a programme for modification of last form in order to get a performing heel counter mould.

**Key words:** designing, moulds, soles

### 1. Introduction

Le formage des contreforts de chaussure est réalisé dans des moules composés d'un noyau, de deux pièces latérales de fermeture et d'un pièce qui ferme la zone active du noyau.

Le noyau du moule constitue la pièce de base qui détermine la forme spatiale du contrefort. Il comporte 2 zones, l'une active, sur laquelle se forme le contrefort et l'autre, inactive, qui contribue à fixer le contrefort sur la machine.

Les matières utilisées pour contreforts présentent, pendant le formage, un comportement élasto-plastique, caractérisé par un indice de formage dont la valeur est déterminée expérimentalement. [1].

À la base de la projection du noyau se trouve le conformateur sur lequel sera modelée la chaussure à contrefort spatialisé dans le moule.

Le passage du contour de la forme au contour de la zone active du noyau du moule repose sur une méthode géométrique de projection qui tient compte de l'indice de formage de la matière utilisée.

### 2. Projection géométrique du noyau de moule.

Dans ce processus on parcourt les étapes suivantes [2]:

- obtention des sections du conformateur dans les 3 plans;
- modification des sections du conformateur par application de l'indice de formage;
- corrélation des sections modifiées dans les 3 plans.

Les contours des sections copiés sur le conformateur se composent d'une succession d'arcs de cercle dont les rayons et les angles au centre sont différents comme dans la Fig.1.

En appliquant l'indice de formage on obtient les contours de la zone active du noyau du moule par relations [3]:

$$R_i' = R_i I_f \quad (1)$$

$$\alpha_i' = \alpha_i / I_f \quad (2)$$

ou:  $R_i'$  – longueur des rayons des arcs de cercle appartenant au cour du conformateur;  
 $R_i$  - longueur des rayons des arcs de cercle appartenant au noyau du moule;  $\alpha_i$  – angles  
 au centre des arcs de cercle sur le conformateur;  $\alpha_i'$  – angles au centre des arcs sur le  
 noyau de moule;  $I_f$  – indice de formage de la matière utilisée pour contreforts.

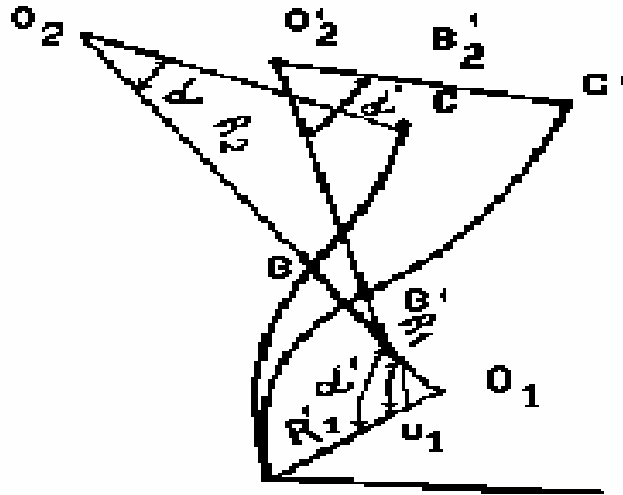


Fig. 1

La corrélation des contours modifiés du conformateur qui conduit au contour final du noyau du moule est illustrée dans la Fig.2

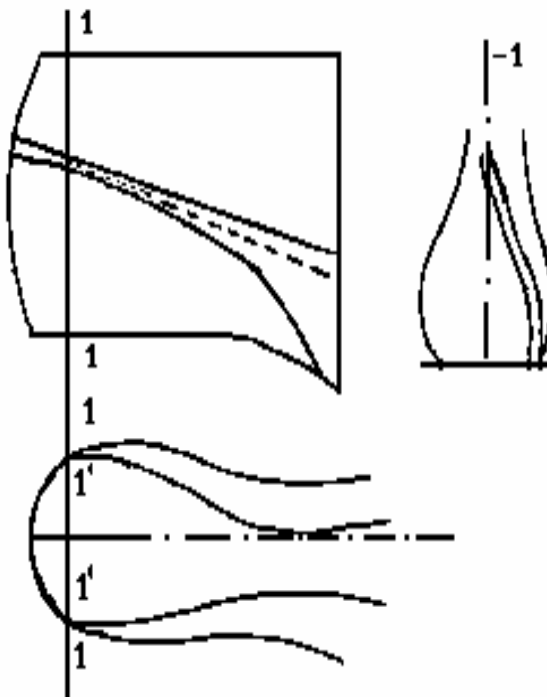


Fig.2

En considérant l'exemple général de la Fig.3, on identifie dans la structure de l'algorithme les indicateurs et les variables suivants:  $n$ - indicateur à 2 valeurs:  $ind = 1$  pour le contour réel;  $ind=2$  pour le contour modifié;  $j$  – indicateur à 2 valeurs:  $j=1$  pour le contour du côté gauche;  $j=2$  pour le contour du côté droit;  $i$  – nombre des arcs de cercle pour un contour;  $nc(j)$  – nombre des arcs de cercle pour chacun de nouveaux contours modifiés;  $m(n,j,i)$  – indicateur pour les zones concaves et convexes d'un contour:  $m(ind,j,i)$  – pour les zones concave;  $m(ind,j,i) = -1$  pour les zones convexes;  $r(n,j,i)$  – matrice tridimensionnelle qui mémorise les valeurs propres à chaque rayon tant pour le contour initial que pour le contour modifié;  $cx(n,j,i)$ ;  $cy(n,j,i)$ - matrice tridimensionnelle qui mémorise les valeurs propres aux centres des arcs de cercle tant pour le contour réel que pour le contour modifié;  $mi(n,j,i)$ ;  $ma(n,j,i)$  – matrice qui mémorise les valeurs de l'angle initial et de l'angle final des rayons polaires;  $fi(n,j,i)$  – angle du rayon polaire à l'axe  $ox$ ;  $u(a,j,i)$  –valeurs des angles de cercle résultés de la décomposition du contour réel.

La procédure CALCULS présentée aura comme valeurs de sortie les valeurs des centres des arcs de cercle du contour modifié,  $cx(n,j,i)$ ;  $cy(n,j,i)$  et les valeurs des coordonnées finals de chaque arcs de cercle du contour modifié,  $x(n,j,i)$ ,  $y(n,j,i)$ .

La schéma logique pour la procédure CALCULS est présenté dans la Schéma 1.

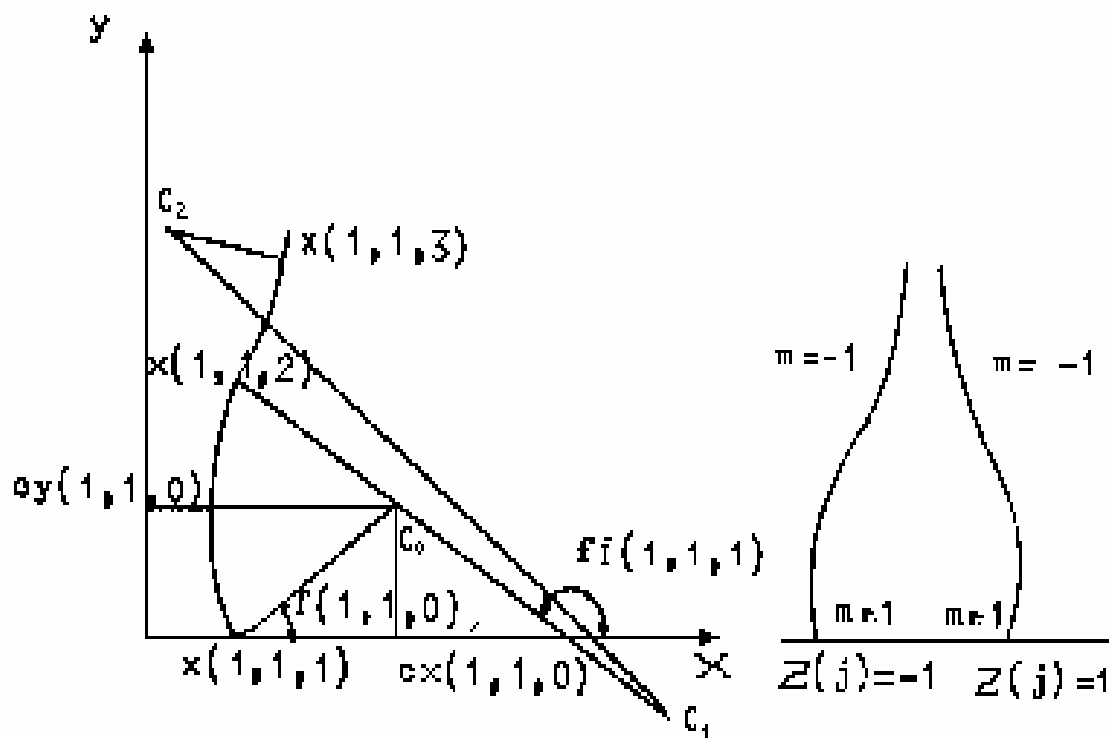


Fig.3

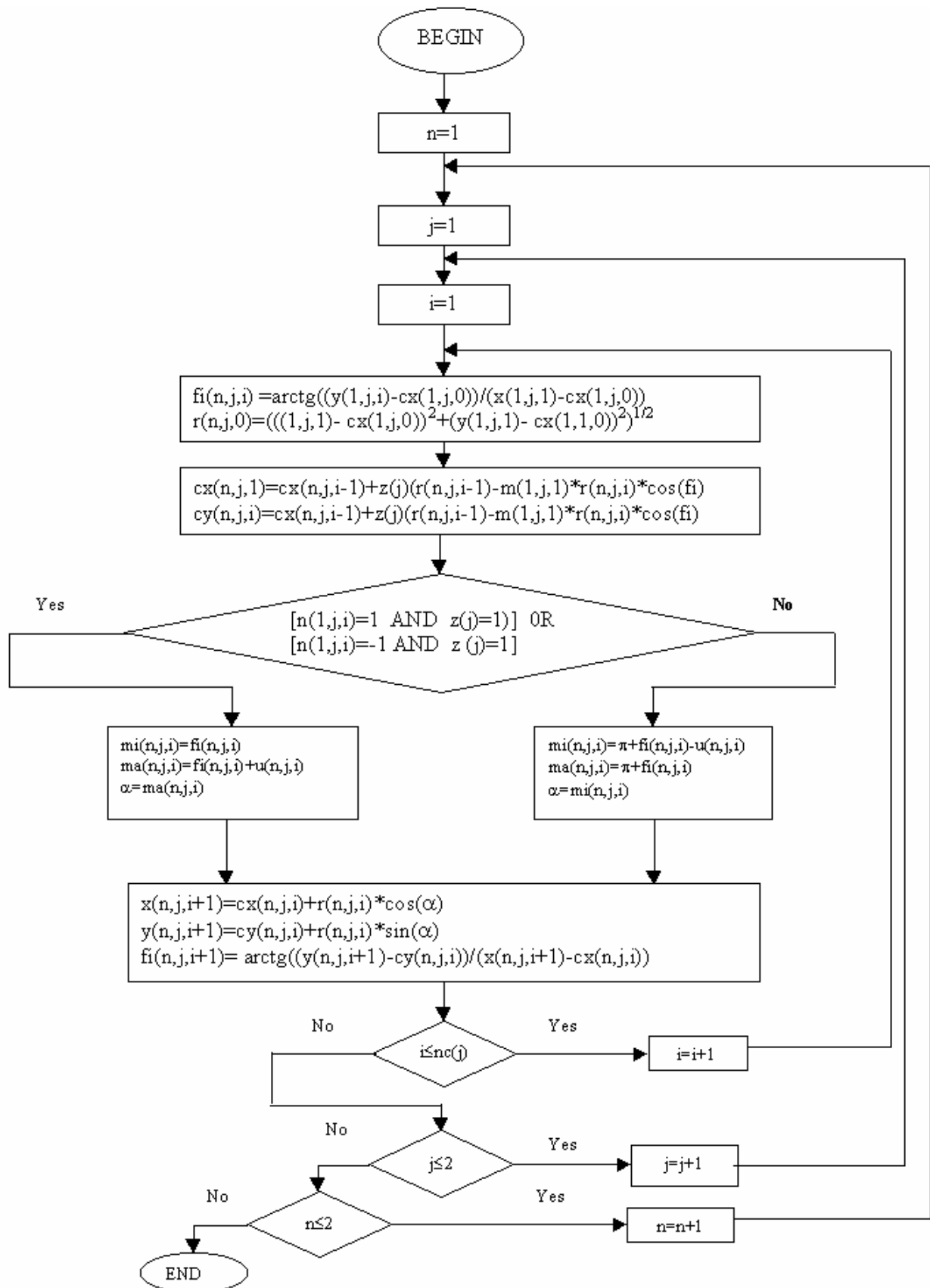


Schéma 1. Schéma logique pour la procédure CALCULS

### 3. Procédures CORECT 1 ET CORECT 2

Ces procédures fournissent à la procédure graphique les valeurs nécessaires à la translation du contour modifié du côté droit, correspondant à la section transversale, avec une valeur résultée de la modification de la section transversale par rapport à l'axe du contour de la surface plantaire.

Le rôle de la procédure CORECT 1 est de calculer la distance, mesurée sur le contour réel, entre le point d'origine et le point qui définit la position de la section transversale sur le contour de la surface plantaire de la forme comme la Fig.4.

Les valeurs d'entrée de la procédure CORECT 1 ont:  $ns$  – nombre des sections transversales;  $ln$  – variable qui mémorise les longueurs des arcs de cercle pour lesquelles on effectue le calcul;  $lg(1,j,k)$  – matrice qui mémorise les valeurs des longueurs définies dans la procédure CALCULS. Les valeurs  $d, h, \beta$  ont les significations de la Fig.4.

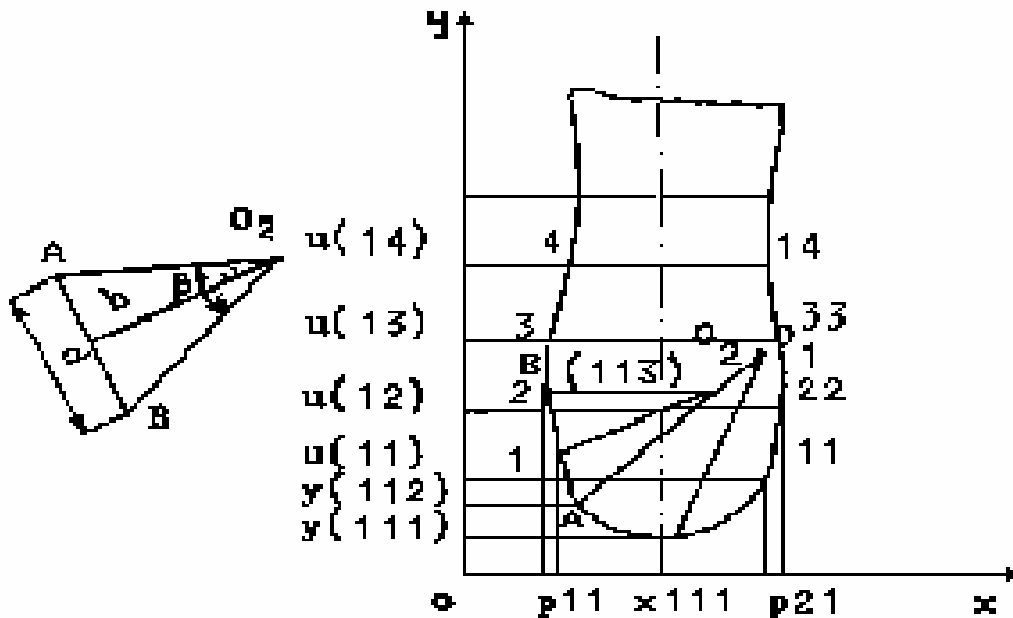


Fig. 4

La procédure CORECT 2 utilise comme valeurs d'entrée les valeurs de l'indice  $lg(1,j,i)$ , valeurs de sortie dans les procédures CORECT 1 et fournit comme valeurs de sortie les vecteurs  $xp(2,j,k)$  et  $yp(2,j,k)$  où sont mémorisées les coordonnées des points de base sections transversales modifiées.

Les valeurs d'entrée de la procédure CORECT 2 sont:  $r_1, r_2$  – longueurs entre lesquelles se situe la valeur de  $lg(1,j,i)$  dans une itération;  $lf$  – variable nécessaire à exprimer les longueurs des arcs de cercle additionnées, dont la valeur est inférieure à celle de  $lg(1,j,i)$ ;  $\gamma(2,j,k)$  – angle dont la valeur est inférieure à celle de  $u(2,j,i)$  correspondant à la position de la section transversale sur le contour modifié.

Les valeurs de sortie sont: les coordonnées  $xp(2,j,i)$  et  $yp(2,j,i)$  qui définissent l'intersection des sections transversales avec le contour de la surface plantaire.

Les schémas logiques pour les procédures CORECT 1 et CORECT 2 sont présentés dans les schémas 2 et 3.

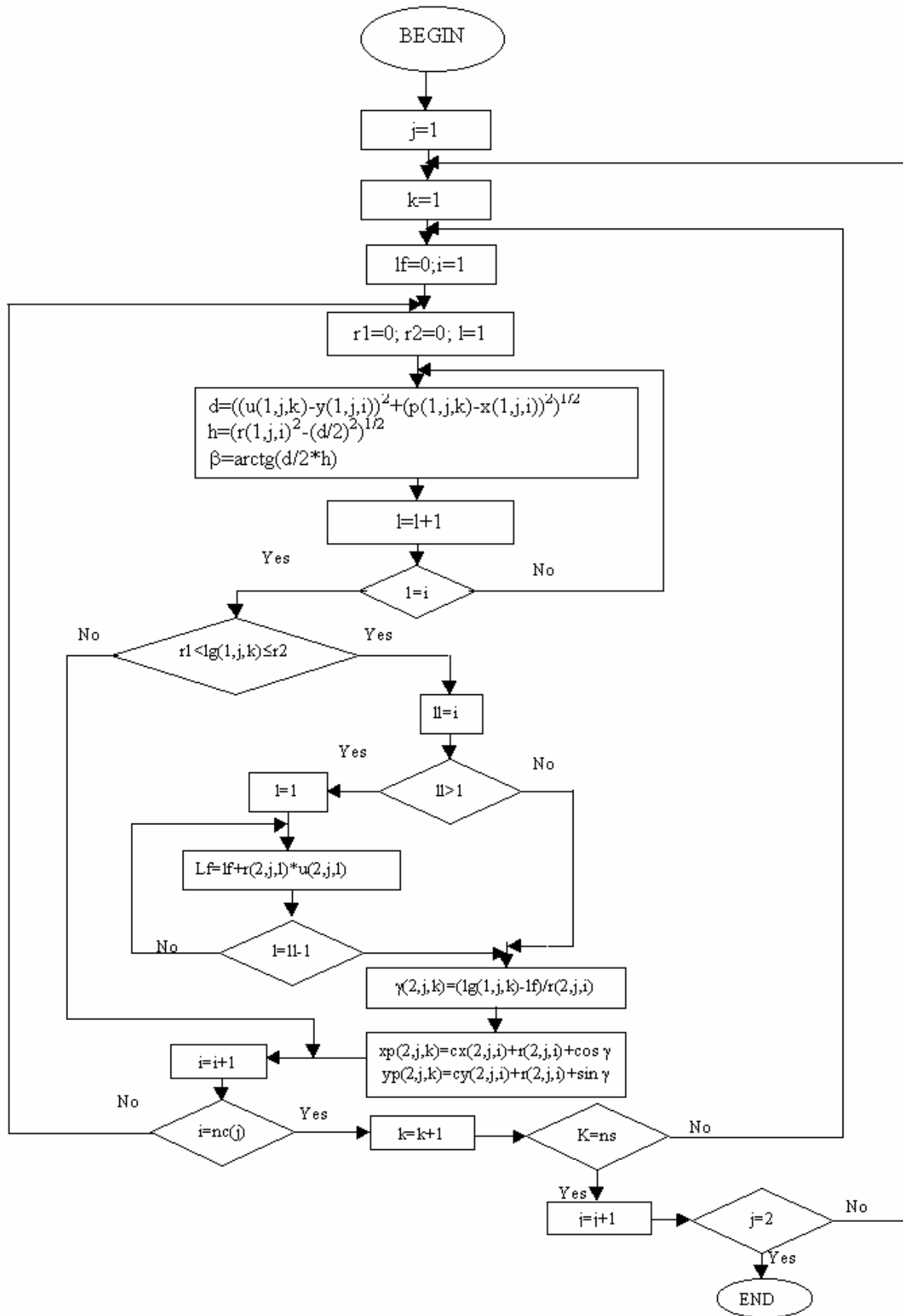


Schéma 2. Schéma logique pour la procédure CORECT 1

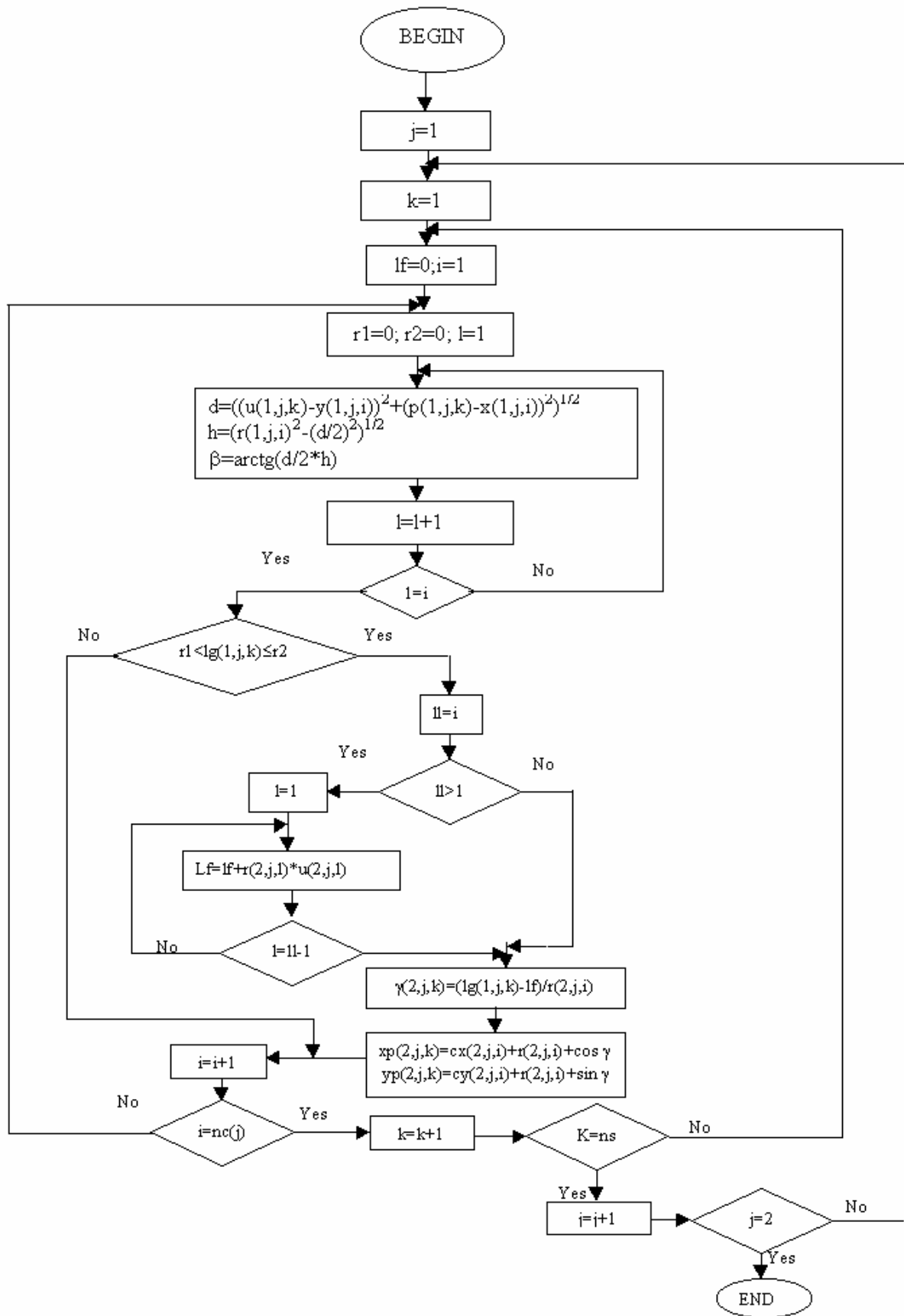


Schéma 3. Schéma logique pour la procédure CORECT 2

La schéma logique finale est présenté dans la Schéma 4.

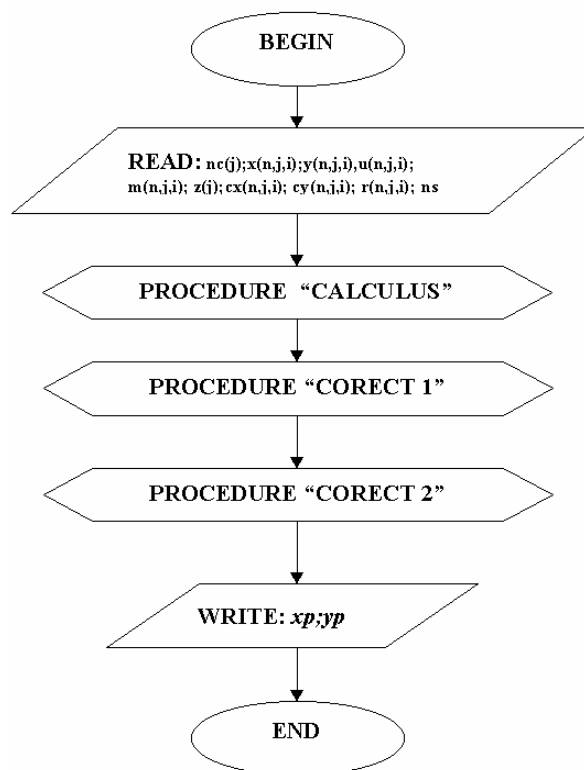


Schéma 4. Schéma logique finale

L'application sur ordinateur été réalisée en langage Turbo-Pascal.

Les algorithmes établis peuvent être appliqués pour la modification de n'importe quelle forme de la forme.

#### 4. Conclusions

L'utilisation de l'ordinateur réduit la durée de l'élaboration du projet de 80% et élimine complètement les erreurs de la méthode géométrique.

Reçu le 9 mai 2005

Université Tehique "Gh. Asachi" Iassy

#### BIBLIOGRAPHIE

1. Volocariu R.S., Cociu V., Croitoru D.F., Contribuții la proiectarea matrițelor pentru formarea branțului și ștaifului, vol. Simpozion Național Confecții din Piele Iași, 1986.
2. Cociu V., Volocariu R.S., Ionescu C., Matrițe și dispozitive de formare. Rotaprint, Univerisatea tehnică "Gh. Asachi" Iași, 1994, Ionescu C., Harnagea F., Projection assistée par ordinateur des moules pour contreforts de chaussure, Buletin I.P.Iași, tomul XLI (XLV), fasc. 1-2, 1995.

#### ALGORITHM DE PROIECTARE ASISTATĂ DE CALCULATOR A MATRIȚELOR DE FORMAT ȘTAIFURI PENTRU ÎNCĂLȚĂMINTE

(Rezumat)

În lucrare, se prezintă o metodă și un program de modificare a conturului calapodului în vederea obținerii matrițelor de preformat ștaifuri pentru încălțăminte.

## ON THE FUNCTIONAL STUDY OF A THERMOSTATIC DEVICE BASED ON INVAR ALLOYS

BY

MIHAI LOZOVAN and HORIA CHIRIAC

**Abstract:** In this paper we have studied some mechanical properties of alloys with technical applications in the thermostatic devices. The functioning data of a new thermostatic device are presented. The thermostat characteristics: temperature range 20-100°C, mechanical hysteresis  $\approx 250 \mu\text{m}$ , sensibility  $\pm 1^\circ\text{C}$ . The thermostat is available in electrical rating of 10 A, 240 V, AC/DC, with stem of 6-mm diameter.

**Keywords:** invar alloys, thermal expansion, thermostat

### 1. Introduction

The binary Fe-Ni alloys (30-50% wt. Ni) with small additions manifest unusual physical properties, such as: low expansion coefficient, very high forced volume magnetostriction, important pressure effects on the Curie temperature, a sudden decrease of the magnetization when the alloy composition changes etc [1-5].

As already mentioned, small Mn, Si, Co, Ti and Cu additions offer the basic invar alloy better machine working [6]. Accordingly, we have studied some mechanic properties of an invar alloy with technical applications. We have also analysed the influence of the heat treatments upon these properties and the functioning data of a new thermostatic device based invar alloy. The heat-sensing element of our thermostat is the rod and tube, most commonly used today in water heater controls. The tube is made of copper alloy (CuZn37) with a threaded plug in one end. Into this is screwed a rod of 36Ni-Fe invar alloy to give the combination of metals with high and low coefficients of expansion.

### 2. Experimental procedure

The chemical compositions of the studied alloys are presented in Table 1.

Table 1. The Chemical composition of alloys

Alloy	Chemical composition (wt %)						
	Ni	Mn	Si	Cu	Zn	Al	Fe
36Ni-Fe	36.21	0.35	0.12	-	-	-	rest
CuZn37	-	-	-	62.55	36.95	0.23	rest

The invar ingots were forged as 12x12 mm<sup>2</sup> bars which were annealed inside a furnace with hydrogen atmosphere for 10h at 1200°C and then cooled in water from

this temperature. This thermal treatment was meant to ensure the alloy homogenization, desulphuration and decarburation [7].

Prior to the measurements the invar studied alloys were subjected to the following thermal treatments inside a furnace with argon atmosphere:

a) heating at 830°C for 1 h + water quenching + 1h at 315°C + 50h ageing at 100°C + very slow cooling down to the room temperature.

The temperature dependence of the thermal expansion was measured for  $\varnothing 5 \times 35$  mm samples by means of the method and installation described in [8]. The sample heating rate during the measurements was 3°C/min.

### 3. Experimental results and discussion

Figure 1 illustrates the temperature dependence of the average coefficient of thermal expansion for the Cu Zn37 alloy and 36Ni-Fe invar alloy within the practically interesting temperature range 50-500°C. Up to 200°C the  $\Delta\alpha = \alpha_2 - \alpha_1$  is constant and important for technical applications.

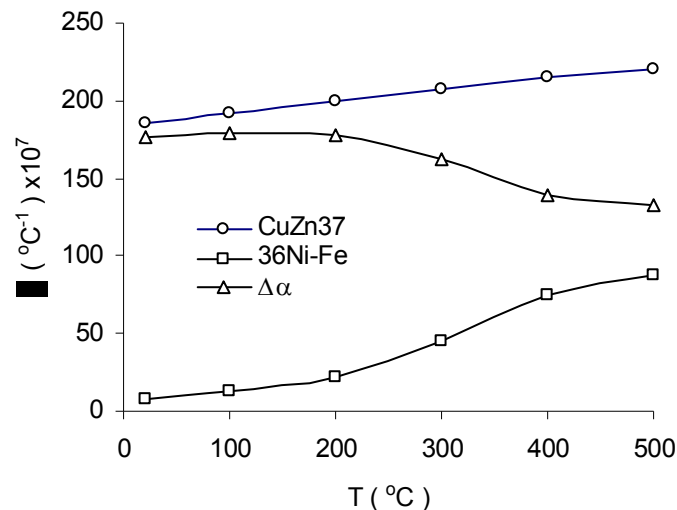


Fig.1. The temperature dependence of the average coefficient of thermal expansion for the CuZn37 and 36Ni-Fe alloys

A linear increase up to 500°C of the thermal expansion coefficient of CuZn37 alloy is observed.

Figure 2 presents a thermostat realised by invar studied alloys. Basically, all thermostats operate by means of expansion or contraction of a heat-sensing element-a gas valve is opened or closed, or an electrical contact is made or broken. The heat-sensing element is that part of the control that senses an increase or decrease in temperature and expands or contracts accordingly. The heat-sensing element of the thermostat is the rod and tube, most commonly used today in water heater controls. The tube is made of copper alloy (CuZn37) with a threaded plug in one end. Into this is screwed a rod of invar alloy to give the combination of metals with high and low coefficients of expansion.



Fig. 2. Invar thermostat for industrial applications

The thermostat characteristics: temperature range 20-100°C, mechanical hysteresis  $\approx 250 \mu\text{m}$ , sensibility  $\pm 1^\circ\text{C}$ . The thermostat is available in electrical rating of 10 A, 240 V, AC/DC, with stem of 6-mm diameter.

Figure 3 presents the sensing element of the thermostatic device. The mechanical hysteresis of the sensing element of the thermostat (about 250  $\mu\text{m}$ ) is present in figure 4.



Fig. 3. The sensing element of the Invar thermostat for industrial applications

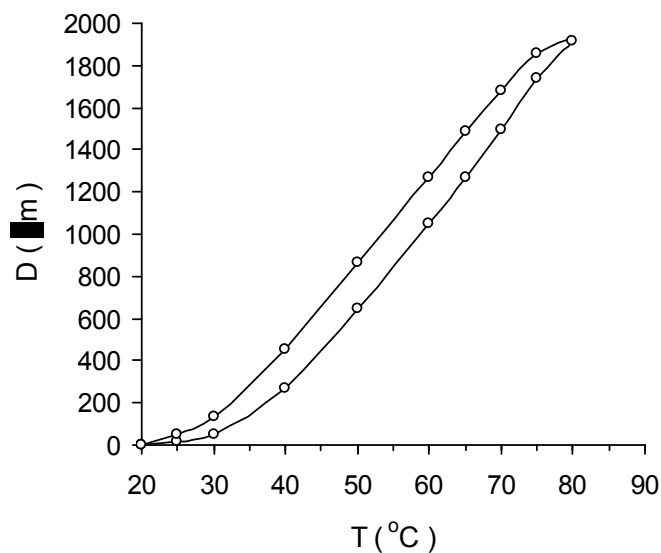


Fig. 4. The mechanical hysteresis of the sensing element (amplification x5) of the thermostat

#### 4. Conclusions

The temperature dependence of the average coefficient of thermal expansion for the Cu Zn37 alloy and 36Ni-Fe invar alloy within the practically interesting

temperature range 50-500°C are studied. Up to 200°C the  $\Delta\alpha = \alpha_2 - \alpha_1$  is constant and important for technical applications.

The functioning data of a new thermostatic device are presented. The thermostat characteristics: temperature range 20-100°C, mechanical hysteresis  $\approx 250 \mu\text{m}$ , sensibility  $\pm 1^\circ\text{C}$ . The thermostat is available in electrical rating of 10 A, 240 V, AC/DC, with stem of 6-mm diameter.

*Received: May 9 2005*

*National Institute for Research-Development  
in Technical Physics Iasi*

#### REFERENCES

1. H. Chiriac, M. Lozovan, M. Neagu, **Romanian Reports in Physics**, vol. 46, Nos. 2-3, 1994, 215-223
2. Y. Nakamura, **IEEE Trans.Magn.**, MAG 12, 4, 1976, 278
3. E. P. Wohlfarth, **IEEE Trans.Magn.**, MAG 11, 1976, 638
4. D. A. Cooling, J. Carr jr., **J. Appl. Phys.**, 41, 1970, 125
5. H. Chiriac, Gh. Pop, F. Borza, M. Sorohan, V. Tutovan, **Anall. Șt. Univ. Al. I. Cuza Iași, XXXIII, SIB, Fizica**, 1987, 12
6. Jon L. Everhart, **Engineering Properties of Nickel and Nickel Alloys**, Plenum Press, New York, 1971, 229
7. Y. Tanji, **J. Phys. Soc. Japan**, 31, 1971, 1366
8. H. Chiriac, M. Lozovan, **Primul Simpozion Național de Materiale Magnetice**, ICPE București, 1988, 488
9. H. Chiriac, M. Lozovan, **Conferința Națională de Fizică**, Constanța, 1993, 31
10. H. Chiriac, M. Lozovan, **Romanian Reports in Physics**, vol.47, Nos.7-10, 1995, 865-871
11. C. Chiriac, M. Lozovan, S. Mohorianu, H.Chiriac, V. M. Cosma, **Conferința Internațională TMCM'96, Iași**, vol.III, 1996, 279-282

#### ASUPRA STUDIULUI FUNCȚIONAL A UNUI DISPOZITIV DE TERMOSTATARE BAZAT PE ALIAJE INVAR

##### (Rezumat)

A fost studiată dependența de temperatura a coeficientului de dilatare termică liniară a aliajului CuZn37 și a aliajului 36Ni-Fe până la 500°C. Până la 200°C diferența coeficienților de dilatare termică liniară a celor două aliaje este constantă, lucru foarte important pentru aplicațiile practice. Este prezentat un dispozitiv de termostatare realizat pe baza acestor materiale. Caracteristicile tehnice ale termostatului sunt: histerezis mecanic  $\approx 250 \mu\text{m}$ , sensibilitate  $\pm 1^\circ\text{C}$ . Termostatul este proiectat să lucreze la o tensiune electrică de 240V și o intensitate a curentului electric de 10A.

## SOME PRELIMINARY EXPERIMENTS UPON THE WORKPIECE PARAMETERS PROCESSED BY ELECTROMAGNETIC FORMING

BY

DORIN LUCA, ROXANA ARSENE and GEORGE ANDRIESCU

**Abstract.** The paper describes a series of researches through preliminary experiments that observes the influence of some parameters (variables) that are specific to workpieces submitted to the processing through electromagnetic forming. The parameters chosen in this paper were: the nature of the material characterised by electric resistivity, structural state of the material, (with or without the recovery heat treatment) and the thickness of the workpiece. The workpieces disk-shaped prepared were independently deformed, than it was measured the maximum obtained deformation depth (flawless), considered to be the measure for the pieces deforming processed by flat electromagnetic forming. The data we obtained were statistically processed in order to select the significantly parameters that will be a part of the statistical-mathematical model that is to be studied in the next researches.

**Keywords:** flat workpiece, resistivity, structural state, thickness, formability, statistical-mathematical modelling, significant parameters, flat electromagnetic forming.

### 1. Introduction

The improvement of the production processes' performances requires to find the optimal combination value of the parameters that operates in those processes. The systemic approach of the electromagnetic forming processing, presented in paper [1], permitted the selection of the main parameters (factors) for experimental research of the plate pieces processing. The highlighted parameters in the eight research domains were set in three main groups: working piece parameters, working tool parameters and working installation parameters. In order to make the researches on the workpiece parameters suggested in this paper, have been established the preliminary experiment plans (*PrelExp*) as it follows:

- *PrelExp* 1: study of the influence of workpiece resistivity;
- *PrelExp* 2: study of the influence of workpiece structural state;
- *PrelExp* 3: study of the influence of workpiece thickness.

The data obtained by preliminary experiments are subdued to some statistic processing such as: *variance analysis* and *correlation analysis*. For this, the obtained data are organised in table form and we calculate the sum, the average, and the dispersion on the  $m$  columns. Next we calculate the Fischer *criterion*, to establish the significant factors that are couched by the rapport:

$$F_c = S^2 / S_a^2 \quad (1)$$

where  $S_a^2$  is the variance caused by random factors, and  $S^2$  is the variance given by the relationship,

$$S^2 = r S_x^2 + S_a^2 \quad (2)$$

with  $S_x^2$  the variance caused by the analysed factor  $X$  and  $r$  the number of repeated determinations.

Choosing the tabled values for Fischer criterion is made based on the level of significance  $\alpha$ , and of the freedom degrees  $\nu_1 = m - 1$  and  $\nu_2 = m(r - 1)$ . The signification level  $\alpha$  (also called trustful level) has been chosen according to the special literature recommendations [2], with the value  $\alpha = 0,05$  (5%), value that has been currently used for measurements in industry, laboratories, in control operations, in testing, expertise etc.

In order to eliminate the variances that radically differ from other variances, we calculate the Cochran *criterion*, in order not to repeat the experiment, with the expression:

$$G_c = \frac{\max S_j^2}{S_1^2 + S_2^2 + \dots + S_j^2 + \dots + S_m^2} \quad ; \quad j = 1 \dots m \quad (3)$$

where  $S_j^2$  are the variances on the  $m$  columns of the organised data table.

The tabled values of Cochran criterion are taken based on the level of signification  $\alpha$ , of the number of freedom degrees  $\nu_3 = m - 1$  and of the number of variances  $m$ .

Correlation analysis is used to estimate the connections between results and factors, and also for the selection of the significant connections that will be considered in the programmed experiment and will enter as variables in the mathematical model of the process. If it is to be found a certain connection, more or less tight, between the two variables  $Y$  and  $X$ , it is said that these are in *correlation* or that there is a *stochastic* relation between them.

In order to express the connection between the two variables  $Y$  and  $X$  it was introduced an indicator, called *coefficient of simple correlation*, whose estimation  $r_{yx}$  is determined with the relationship:

$$r_{yx} = \frac{\sum_{i=1}^n x_i y_i - n \bar{x} \bar{y}}{(n-1) S_x S_y} \quad (4)$$

where  $S_x$  and  $S_y$  are estimated squared medium variances and  $n$  is the number of determinations.

Simple correlation coefficient square is respectively called *simple determination coefficient* ( $R_{yx} = r_{yx}^2$ ) and it expresses that part from the variation of the result  $Y$  that can be attributed to factor  $X$ .

After calculating the correlation coefficients we check up their significance. This way, in the case of the simple correlation coefficient it is used the Student *criterion*, which is expressed by the relationship:

$$t_c = \frac{|r_{yx}| \sqrt{\nu_4}}{\sqrt{1-r_{yx}^2}} \quad (5)$$

where  $\nu_4 = n - 2$  is the number of freedom degrees and  $n$  is the number of determinations.

## 2. Experiment and results

For the *PreExp 1* experiment it was used metallic materials rolled sheet of different nature (aluminum, copper, brass, steel), from which it was prepared then, they were freely deformed on a die with the diameter of 80 mm and the connecting radius of 5 mm. Each specimen was deformed under the same conditions and with the same value of the applied energy, respectively 1,6 kJ (200  $\mu$ F/4 kV). After the plastic deforming the pieces we obtained were set on a control-table and with the help of a comparison measurer, was measured the deforming depth  $h$ , in the middle of the pieces. The specimens that were used, have been differentiated by the values of electrical resistivity  $\rho$  [3], the results of electromagnetic forming being presented in table 1 and figure 1.

Table 1. *PreExp 1* results: study of the influence of workpiece resistivity.

	Workpiece material			
	Cu-OF	EN AW-1200	CuZn 36	FeP04
Thickness $g$ [mm]	0,50	0,50	0,50+0,02	0,50-0,01
Resistivity $\rho$ [ $\mu\Omega$ m]	0,0177	0,0271	0,0640	0,1300
Depth $h$ [mm]	20,34	18,33	13,57	6,93

For this experiment it was necessary to use specimens made from materials of different nature who had the same thickness. Practically, it was not possible, the sheets from which it were made disk shaped specimens presenting positive and negative variations for about 0,50 mm. The exact thickness of the disks were measured with the help of a micrometer with a precision of  $\pm 0,01$  mm. Although the experiment has been made without repeating the tests, it was orientative established the regression equation that models the best experimental dates, this being confirmed by the maximal value that the determination coefficient  $R_{yx}$ , has in that researched case.

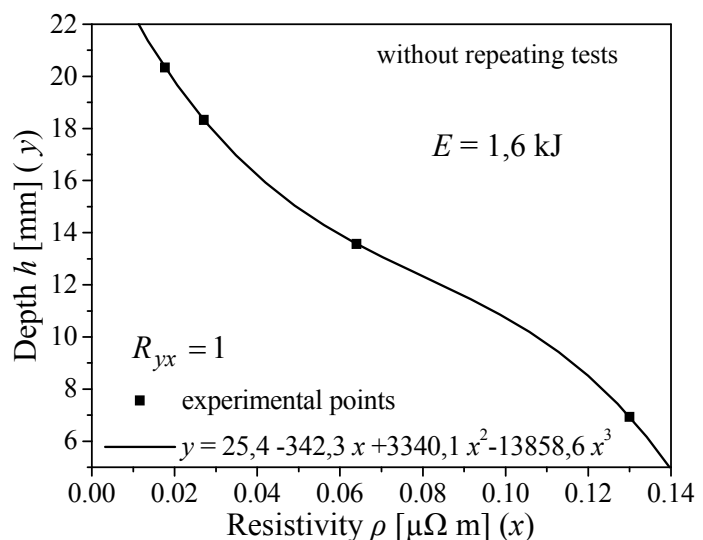


Figure 1. The effect of resistivity on deformation depth.

For *PreExp 2* experiment it was used specimens in two different structural states, which means specimens that were not thermally treated and also specimens that were thermally treated. The set of specimens non-thermally treated come

directly from the rolled sheet, and a second set of specimens was thermally treated before being processed by electromagnetic forming. The thermal treatment consisted in the heating of the pieces in package at a temperature of 400°C, the maintaining at this temperature for an hour, followed by the slow cooling in air. The specimens were aluminum with the thickness of 0,5 mm and the diameter of 110 mm, the material having the numerical symbol EN AW-1200 and the chemical symbol EN AW-Al 99,0. They were deformed with an electrotechnical copper flat coil having 3 windings, the inductance of 0,330  $\mu\text{H}$  and the resistance of 0,813  $\text{m}\Omega$ , on a die with the diameter of 80 mm and the connecting radius of 5 mm. The applied energy was different for each deformed specimen, and it was obtained by modifying the voltage of the energy stocker for a constant capacity of 200 $\mu\text{F}$ . The wanted result was also in this case, the deformation depth measured in the center of the pieces, the obtained values being mentioned in table 2.

Table 2. *PrelExp 2* results: study of the influence of workpiece structural state.

Workpiece structural state	Deformation depth $h$ [mm]				
	$E=0,4$ kJ	$E=0,9$ kJ	$E=1,6$ kJ	$E=2,5$ kJ	$E=3,6$ kJ
without heat treatment	0,11	1,82	4,00	6,46	9,83
with heat treatment	1,23	2,96	5,30	8,99	12,61

*Observation.* The factor *structural state* was not selected for the mathematical model, because it is a quality parameter, but it can be used in the case of stencil mode lings with the Taguchi *method* [4].

In order to verify the influence of thickness of the workpiece (*PrelExp 3*), [5], disk shaped specimens were prepared, with a diameter of 110 mm made by aluminum sheet, grade EN AW-Al 99,0 and thickness  $g$  differs: 0,15 mm, 0,45 mm, 0,80 mm and 1,20 mm. The specimens were free bulged on a die with the diameter of 80 mm and with the connecting radius of 5 mm, and then it was measured the deforming depth  $h$ , obtained in the middle of pieces with the help of a comparison measurer with a precision of  $\pm 0,01$  mm, resulting the values mentioned in table 3.

Table 3. *PrelExp 3* results: study of the influence of workpiece thickness.

Number of repeated determinations	Factor levels (thickness $g$ )			
	1 (0,15 mm)	2 (0,45 mm)	3 (0,80 mm)	4 (1,20 mm)
1	31,53	23,01	19,24	16,77
2	30,80	23,33	19,55	15,85
3	30,95	22,45	18,76	17,36
Sum	93,28	68,79	57,55	49,98
Average	31,093	22,930	19,183	16,660
Variance	0,149	0,198	0,158	0,579

The repeated tests in experiment were made at a value of applied energy of 2,5 kJ (200  $\mu\text{F}$ /5 kV). The flat spiral coil used for this experiment had 5 windings, the inductance of 0,920  $\mu\text{H}$ , the resistance of 0,712  $\text{m}\Omega$  and was made from electrotechnical copper. The data obtained from this experiment were subdued to variance analysis and to correlation analysis, and a series of conclusions are drawn from here, and these are presented in table 4.

Table 4. Results and conclusions of the variance and correlation analysis for *PrelExp 3*.

		Mod of decide	Value	$\alpha$	$m$	$r$	$\nu_1$	$\nu_2$	$\nu_3$	$\nu_4$	$r_{yx}$
				0,05	4	3	3	8	3	2	-0,9454
Fischer criterion	$F_c$	relationship (1)	1318,133	$F_c > F_t$ : thickness it is thought that is parameter and will be included in mathematical model							
	$F_t$	annex IV [6]	4,07								
Cochran criterion	$G_c$	relationship (3)	0,53413	$G_c < G_t$ : in conclusion the hypothesis regarding homogeneousness of the variances is verified							
	$G_t$	annex VIII [6]	0,6841								
Student criterion	$t_c$	relationship (6)	4,1021	$t_c < t_t$ : in conclusion don't exist correlation between variables or dependence is nonlinear							
	$t_t$	annex III [6]	4,303								

The condition imposed by the Student criterion is not verified, so they had to make a supplementary experiment with a different value of applied energy, the graphical representation of obtained data and establishing the regression equations. In figure 2 it is shown the variation of the deformation depth of the obtained pieces with different thickness for energy of 2,5 kJ, when it was considered the average of repeated determinations from table 3, and also for the energy of 0,4 kJ, when there were made determinations without repeating them. The established regression equation, in the form of some 3 degree polinoms, for which the determination coefficient  $R_{yx}$  has the value 1, it confirms the existence of a nonlinear dependence. Under these circumstances, also considering the conclusions of Fischer criterion, the thickness  $g$  could be selected for the mathematical model.

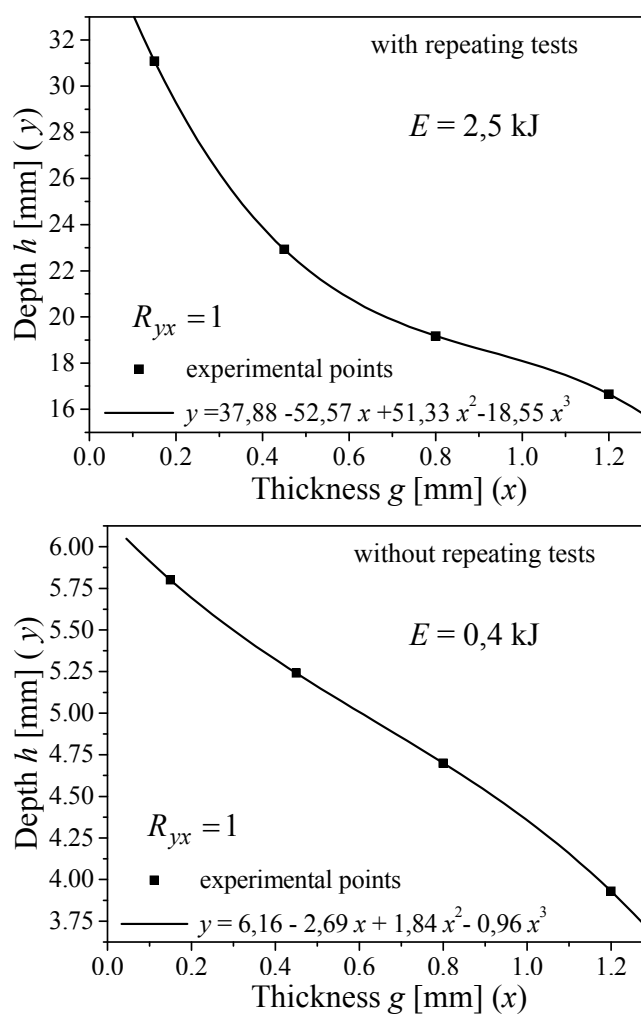


Figure 2. The effect of thickness workpiece on deformation depth.

### 3. Conclusions

As a result to the preliminary experiments regarding the parameters of the electromagnetic forming processed workpieces it results a series of conclusions that are presented next.

*The resistivity of the workpiece.* The experimental results, presented in table 1 and figure 1, show that while the workpiece resistivity grows, the obtained deforming

depth decreases. The pronounced decreasing of the deformation depth (deformation degree) is produced if the piece resistivity has higher values than  $0,030 \dots 0,040 \mu\Omega \text{ m}$ . The result is that the materials such as brass, steel etc. it will be harder to processing them by electromagnetic forming, increased energies being necessary.

*Structural state of the material of the piece.* The recrystallization recovery treatment applied to workpieces before electromagnetic forming contributes to the growing of the established deforming degree. In the case of pieces from aluminum EN AW-1200, the relative growth of the deforming degree was of about 28% on recovery pieces compared to the pieces that have been electromagnetic formed directly from the rolled state.

*Thickness of the workpiece.* Experimental results, presented in table 3 and figure 2, show that when the workpiece thickness grows the obtained deforming depth is minimised. In the case of the pieces from aluminum EN AW-1200, the relative decreasing of the deformation depth was of about 46% .

#### REMARK

This paper presents some results of the researches financed in Grant CNCISIS type A, cod 529/2005.

Received, May, 10, 2005

Technical University "Gh. Asachi" Jassy

#### REFERENCES

1. LUCA, D. - *Research and Contributions Regarding Plastic Processing by the Electromagnetic Forming Proceeding*, PhD Thesis (in Romanian). Iași: Technical University, 2000.
2. CICALĂ, E.F. - *Statistic Processing Methods of Experimental Data* (in Romanian). Timișoara: Publishing House Politehnica, 1999. 303 p. ISBN 973-9389-30-8.
3. GERU, N. et al. - *Metallic materials. Structure, Proprieties, Utilisations* (in Romanian). București: Publishing House Tehnică, 1985. 394 p.
4. MUSCĂ, G. et al. - *Experimentation, Modelling and Optimisation of the Products and Processes* (in Romanian). Chișinău: Publishing House Tehnica, 1998. 147 p. ISBN 9975-910-63-7.
5. LUCA, D.; GHEORGHIU, DIANA; PETRIȘOR, C.; GRIGORUȚĂ, G. - The Influence of the Workpiece Parameters at Electromagnetic Forming of Metal Sheets. *Bulletin of the Politechnic Institute of Jassy*, 1998, tom XLIV (XLVII), supliment II, p. 21-24. ISSN 1001-2855.
6. TALOI, D. et al. - *The Optimisation of the Metallurgical Processes* (in Romanian). București: Publishing House Didactică și Pedagogică, 1983. 340 p.

#### UNELE EXPERIMENTE PRELIMINARE ASUPRA PARAMETRIILOR PIESEI DE LUCRU PROCESATE PRIN MAGNETOFORMARE

##### (Rezumat)

Lucrarea descrie o serie de cercetări prin experimente preliminare care urmăresc influența unor parametri (variabile) specifici pieselor de lucru supuse procesării prin magnetoformare. Parametrii aleși în această lucrare au fost: natura materialului caracterizată prin rezistivitatea electrică, starea structurală a materialului (cu sau fără tratament termic de recoacere) și grosimea piesei de lucru. Piese de lucru pregătite sub formă de disc au fost deformate liber, după care s-a măsurat adâncimea de deformare maximă obținută (fără fisurare), considerată ca măsură a deformabilității pieselor procesate prin magnetoformare plană. Datele obținute au fost prelucrate statistic pentru a selecta parametri semnificativi ce vor face parte din modelul statistico-matematic, care se propune a fi elaborat în cadrul cercetărilor ulterioare.

## ABOUT WEAR BEHAVIOUR OF STEELS NITRATED IN ELECTROLYTIC PLASMA

BY

VALENTIN MIHAILOV\*, MARIA BACIU\*\*, SILVIA GEORGESCU\*\* and  
CONSTANTIN BACIU\*\*

**Abstract:** Considering OLC55 and 40Cr10 steels, nitrided and quenched in electrolytic plasma, their wear resistance was expressed by means of the intensity ( $I_m$ ) and rate ( $V_m$ ) of mass wear. The thermal processing variants applied to the two steels under study comprised: three different diffusion temperatures,  $T_d = 650, 700$  and  $750^\circ\text{C}$ ; two values of the diffusion time,  $t_d = 3$  and  $6$  min; the electrolyte with the composition:  $10\% \text{NH}_4\text{Cl} + 20\% \text{NH}_4\text{OH} + \text{H}_2\text{O}$ . Based on the experimental data recorded for the two steels under study, the variation curves were plotted, as a function of the diffusion temperature, for the average mass wear rate,  $\overline{V_m} = f(T_d)$  and for the average mass wear intensity,  $\overline{I_m} = f(T_d)$ .

**Keywords:** electrolytic plasma, steels, abrasive wear.

### 1. Introduction

Microstructural changes caused by the process of super-alloying by diffusion during steel heating in electrolytic plasma influence wear resistance. Mass wear of materials can be expressed by means of the mass wear rate,  $V_m$ :

$$V_m = \frac{\Delta m_c}{t}, [\text{g/h}] \quad (1)$$

and by the mass wear intensity,  $I_m$ :

$$I_m = \frac{\Delta m}{A_f \cdot L_f}, [\text{g/m}^3] \quad (2)$$

where;  $\Delta m_c$  represents cumulated mass loss,  $\Delta m$  - mass variation,  $t$  – time,  $A_f$  - friction surface and  $L_f$  – length of the friction path

### 2. Experimental

Wear behaviour of OLC55 and 40Cr10 steels, super-alloyed with nitrogen by heating in electrolyte solution has been studied under the conditions of a dry wear regime between the contact surfaces of the specimens and the diamond disk, Figure 1.

The technological variants of the nitriding treatments applied to OLC55 and 40Cr10 steels are shown in Figure 2.

The specimens, subjected to the wear tests, were super-alloyed with nitrogen in electrolytic plasma according to the conditions given in Table 1.

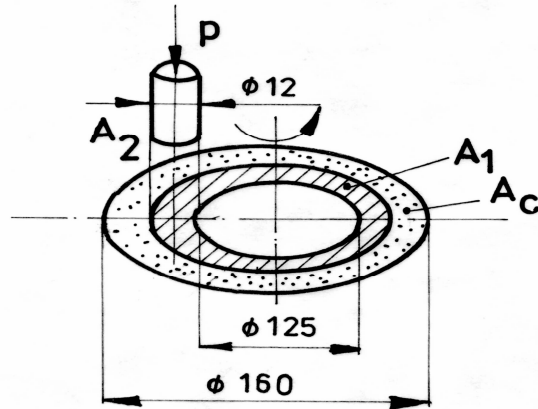


Figure 1 Conditions specific to the abrasive wear test ( $V_{\text{slip}} = 1.25$  m/min,  $p = 1.5$  MPa)

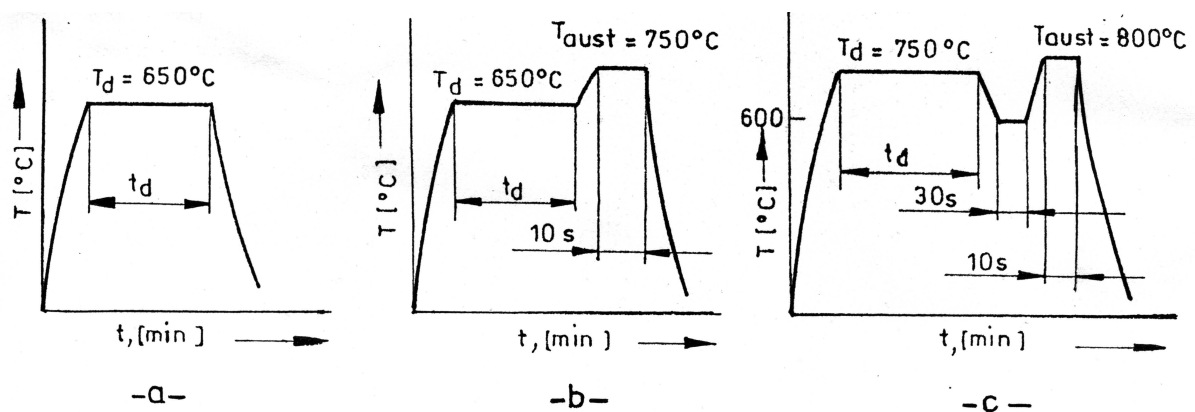


Figure 2. Technological parameters of the nitriding treatments by heating in electrolytic plasma:  
 variant a – nitriding ( $T_d = 650^\circ\text{C}$ ,  $t_d = 3; 6$  min) and quenching  
 variant b – nitriding ( $T_d = 650^\circ\text{C}$ ,  $t_d = 3; 6$  min) followed by heating for austenitization ( $T_{\text{aust}} = 750^\circ\text{C}$ ,  $t = 10$  sec) and quenching  
 variant c – nitriding ( $T_d = 750^\circ\text{C}$ ,  $t_d = 3; 6$  min) followed by a quenching step ( $600^\circ\text{C}$ ,  $t = 30$  sec) then heating for austenitization ( $T_{\text{aust}} = 750^\circ\text{C}$ ,  $t = 10$  sec) and quenching

Table 1 Conditions for nitrogen super-alloying in electrolytic plasma

No.	Steel grade	Marking	Technological parameters of diffusion		Initial mass, $m_i$ , [g]
			$T_d$ , [°C]	$t_d$ , [min]	
1	40Cr10	3R	650	3	40.3547
2		3I	700		40.4266
3		3M	750		40.5210
4	OLC55	4D	650		40.7285
5		4F	700		40.7407
6		4S	750		41.1910
7	40Cr10	3A	650	6	40.6015
8		3V	700		39.1349
9		3J	750		40.6167
10	OLC55	4Y	650		40.3947
11		4DD	700		40.9206
12		4T	750		40.4801

*Observations:*

- electrolyte: 10 %  $\text{NH}_4\text{Cl}$  + 20 %  $\text{NH}_4\text{OH}$  +  $\text{H}_2\text{O}$ ;
- after nitriding all specimens were quenched.

### 3. Results

Measurements of the mass losses,  $\Delta m$  and  $\Delta m_c$ , were performed by weighing the specimens on the analytical balance, at different time intervals (1; 2; 2.5; 3; 3.5; 4, 4.5 and 5 hours) of the test. Based on the relationships (1) and (2) the values of mass wear rate and mass wear intensity, respectively, were determined and subsequently the average values of these parameters were calculated (table 2).

Table 2

Average values	Specimen											
	3R	3I	3M	3A	3V	3J	4D	4F	4S	4Y	4DD	4T
$\bar{V}_m$	8.66	12.71	18.06	8.11	14.38	19.23	18.66	18.98	20.82	11.56	13.72	20.11
$\bar{I}_m$	6.503	10.802	13.568	6.094	9.544	14.445	14.014	14.252	15.633	8.683	10.301	15.105

The variation of the two mass wear parameters,  $\bar{V}_m$  and  $\bar{I}_m$ , as a function of the diffusion temperature, is shown in figure 3 and 4, respectively, for the two steels under study.

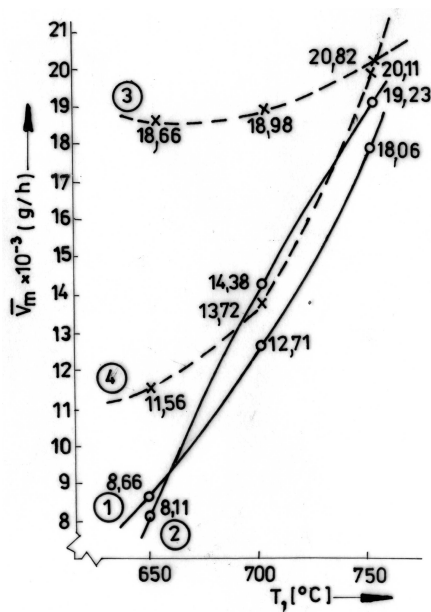


Figure 3. Variation of the average mass wear rate,  $\bar{v}_m = f(T_d)$ , as a function of diffusion temperature:

$$t = 3 \text{ min} \begin{cases} 1-40\text{Cr10} \\ 3-OLC55 \end{cases}$$

$$t = 6 \text{ min} \begin{cases} 2-40\text{Cr10} \\ 4-OLC55 \end{cases}$$

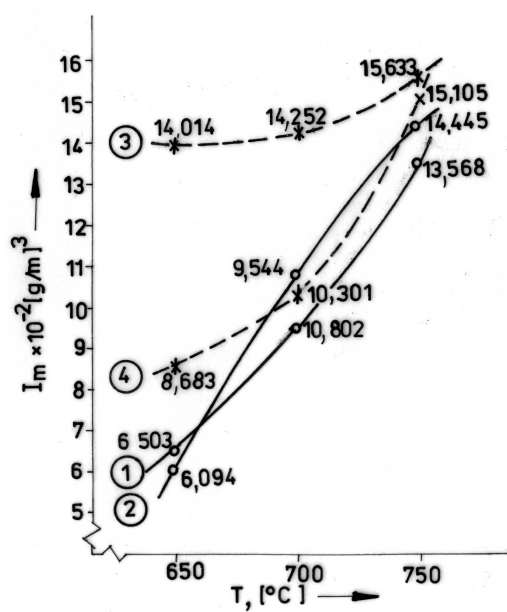


Figure 4. Variation of the average mass wear intensity,  $\bar{I}_m = f(T_d)$ , as a function of diffusion temperature:

$$t = 3 \text{ min} \begin{cases} 1-40\text{Cr10} \\ 3-OLC55 \end{cases}$$

$$t = 6 \text{ min} \begin{cases} 2-40\text{Cr10} \\ 4-OLC55 \end{cases}$$

#### 4. Conclusions

(i) Nitrogen super-alloying of steels, heated in electrolytic plasma provides considerable improvement of wear behaviour, in dry friction regime.

(ii) Under the condition of maintaining constant the diffusion time, the lowest values of the parameters of wear process correspond to  $T_d = 650^{\circ}\text{C}$ ; the increase of diffusion temperature causes the gradual increase of mass losses  $\Delta m$  and  $\Delta m_c$ .

(iii) By comparing the above two values of the diffusion time, better wear behaviour has been noticed for the specimens which were thermally processed for 6 minutes.

(iv) The analysis of the experimental data emphasizes the superior wear behaviour of 40Cr10 steel as compared to OLC55 steel under the conditions of the same values for the parameters of diffusion process.

Received, May, 10, 2005

\*Academy's Institute of Physics, Republic of Moldova

\*\*Technical University "Gh. Asachi" Iassy.

#### REFERENCES

1. Aleksandrov, V.N. Ignat'kov, D.A., Pasinkovskÿ, E.A., *Fizico-mehaničeskie svojstva stali 45, azotirovannoj v èlektrolitnoj plasme*, Elektronnaâ obrabotka materialov, nr. 2, p.17-18, 1982.
2. Baci, Maria, *Contributions on the structural and property changes of thermally and thermochemically treated steels in electrolytic plasma* (in Romanian), PhD thesis, „Gh.Asachi” Technical University from Iași, 1999.
3. Belkin, P.N, Ignat'kov, D.A., Pasinkovskÿ, E.A., *Azotirovanie v elektrolitnoj plazma, Kolloquium Eigensspannungen und Oberflächen-verfestigung*, p.265, 1982.

#### ASUPRA COMPORTĂRII LA UZURĂ A OȚELURILOR NITRURATE ÎN PLASMĂ ELECTROLITICĂ

##### (Rezumat)

Analizând oțelurile OLC 55 și 40 Cr10, nitrurate în plasmă electrolitică, s-a exprimat rezistența lor la uzură prin intermediul intensității ( $I_m$ ) și a vitezei de uzură masică ( $V_m$ ). Variantele de prelucrare termică aplicate celor două oțeluri analizate au presupus: trei temperaturi diferite de difuzie,  $T_d = 650, 700$  și  $750^{\circ}\text{C}$ ; două valori ale timpului de difuzie,  $t_d = 3$  and  $6$  min; electrolit cu compoziția: 10%  $\text{NH}_4\text{Cl}$  + 20%  $\text{NH}_4\text{OH}$  +  $\text{H}_2\text{O}$ . Pe baza datelor experimentale înregistrate pentru cele două oțeluri analizate, au fost trasate curbele de variație, în funcție de temperatura de difuzie, pentru viteza medie de uzură masică  $\overline{V_m} = f(T_d)$  și pentru intensitatea medie de uzură masică  $\overline{I_m} = f(T_d)$ .

## ON THE INFLUENCE OF THE HEAT TREATMENT PARAMETERS ON THE MICROHARDNESS VARIATION OF A BAINITIC S.G.CAST IRON

BY

IOAN MILOȘAN

**Abstract:** The paper presented here belongs to the researches about the influence of the heat treatment's parameters over the microhardness's variation of a Bainitic S.G. Cast Iron at the end of an wear process. It was determinate the variation of the rapport ( $\delta$ ) between the microhardness ( $\Delta H$ ) and the distance of the wear surface ( $\Delta l$ ).

**Keywords:** Materials Science, bainitic s.g. cast iron, heat treatment, wear

### 1. Introduction

At present, very limited information on the abrasive wear properties of austempered ductile iron is available. Wear is one of the major ways by which materials cease to be useful. Process plant and subsidiary processes contend with a much bigger wear problem than in the case of machine parts, although their life is often much shorter. Therefore, it is important to enhance the wear resistance of cast irons [1] - [6].

### 2. Materials

The studied cast iron had the following composition: 3,70 % C; 2,46 % Si; 0,564 % Mn; 0,038 % P; 0,009 % S; 0,21 % Mo; 0,12 % Ni; 0,17 % Cu; 0,072 % Mg.

This cast iron was elaborated in an induction furnace. Nodular changes were obtained with the "In mold" method, with the help of prealloy FeSiCuMg with 10-16% Mg, added into the reaction chamber in a proportion of 1,1% of the treated cast iron.

The structure in raw state is perlite-ferritic typical for a cast iron with geometrically regular nodular form. The casted raw iron had the following mechanical properties:  $R_m = 660$  [N/mm<sup>2</sup>];  $HB = 180$ ;  $KC = 12$  [J/cm<sup>2</sup>];  $A = 7$  [%].

### 3. Heat treating

The parameters of the heat treatment are:

- the austenitizing temperature,  $t_A = 900$  [°C]
- the maintained time at austenitizing temperature,  $\tau_A = 30$  [min].

- the temperature at isothermal level,  $t_{iz} = 300, 350$  and  $400$  [ $^{\circ}\text{C}$ ].
- the maintained time at the isothermal level,  $\tau_{iz} = 5, 30, 60, 120,$  and  $180$  [min].

All these 3 experiment groups: lot A ( $t_{iz} = 300$   $^{\circ}\text{C}$ ), lot B ( $t_{iz} = 350$   $^{\circ}\text{C}$ ) and lot C ( $t_{iz} = 400$   $^{\circ}\text{C}$ ), performed at isothermal maintenance in salt-bath (55%  $\text{KNO}_3$ + 45%  $\text{NaNO}_3$ ), being the cooling after the isothermal maintenance was done in air.

#### 4. Experimental procedure

From this material, 15 typical wear - test specimens ( $\phi 20 \times 3$  mm) was done.

The abrasive wear test were performed by a mechanism with ball-on-plane contact (manganese steel ball was actuated by an electric motor) under 40 N load at room temperature for 1 h.

It was determinate the microhardness ( $\text{HV}_{0,01}$ ) with an “Akashi MVK - E3” machine, in the  $50 \mu\text{m}$  of the section of the wear specimens.

An analysis of the transformation in the section of the wear specimens, it was made by calculating an study the variation of the rapport (relation 1) between the microhardness ( $\Delta H$ ) and the distance of the wear surface ( $\Delta l$ ):

$$\delta = \Delta H / \Delta l \quad (1)$$

where:  $\Delta H$  - the variation of the microhardness between the wear surface and some;

$\delta$  - distances [ $\text{HV}_{0,01}$ ];

$\Delta l$  - the variation of the distance between the wear surface and some;

$\delta$  - distances [ $\mu\text{m}$ ].

For exemplification:

$$\delta_1 = (\text{HV}_5 - \text{HV}_2) / (l_5 - l_2) \quad (2)$$

$$\delta_{10} = (\text{HV}_{50} - \text{HV}_2) / (l_{50} - l_2) \quad (3)$$

where :  $\text{HV}_{50}, \text{HV}_5$  - represent the microhardness for the distance  $d = 50 \mu\text{m}$ , and  $d = 5 \mu\text{m}$ , from the wear surface (considerate  $d = 2 \mu\text{m}$ ), [ $\text{HV}_{0,01}$ ]

$\text{HV}_2$  - represent the microhardness of the wear surface, [ $\text{HV}_{0,01}$ ];

$l_{50}, l_5$  - represent the distance “d” determinate (in section) from the wear surface of the specimen [ $\mu\text{m}$ ];

$l_2$  - represent the distance corresponding of the wear surface [ $\mu\text{m}$ ];

#### 5. Experimental results and discussion

The variation of the “ $\delta$ ” rapport function the isothermal temperature ( $t_{iz}$ ) and different isothermal times ( $\tau_{iz}$ ), is presented in the table 1.

Based on Fig.1, 2 and 3, the values presented in the table 1 were determined.

From the values presented in table 1 and figures 1 - 3, it can be certainly observed a normal evolution of the values of the  $\delta$  rapport.

For all the values of “ $\delta$ ”, the values decrease from  $\delta_1$  to  $\delta_{10}$  and that means a major different between the values of  $\delta$  for the specimen near to the wear and the specimen far away from the wear process.

Table 1. The variation of the “ $\delta$ ” values rapport

$t_{iz}$ [° C]	$\tau_{iz}$ [min]	$\delta = \Delta H / \Delta l$ , [HV <sub>0.01</sub> / $\mu\text{m}$ ];									
		$\delta_1$	$\delta_2$	$\delta_3$	$\delta_4$	$\delta_5$	$\delta_6$	$\delta_7$	$\delta_8$	$\delta_9$	$\delta_{10}$
300	5	11.33	8.37	11.38	12.05	10.34	8.5	9.45	7.8	7.26	7.46
	30	35.33	19.87	13.92	10.05	7.86	12.04	10.21	8.87	8.47	7.58
	60	17.66	27.12	22.46	16.94	12.69	10.43	8.85	8.03	6.79	6.35
	120	42	39.62	23.15	16	12.52	11.96	9.82	8.52	7.79	6.98
	180	96	39.12	25.92	18.72	14.65	11.96	10.12	8.82	7.79	6.98
350	5	38.66	23.75	18.53	13.94	10.91	8.96	7.61	6.24	5.84	5.23
	30	15.66	20.5	21.30	16.61	12.04	9.89	9.06	7.29	6.44	6.23
	60	22	23.37	15.46	12.66	12.43	10.21	8.96	7.53	6.88	6.16
	120	39	14.62	13.69	10.66	10	8.21	6.97	6.05	5.60	5.02
	180	7	19.5	19.3	15	12.13	11.74	8.18	7.11	6.48	5.63
400	5	30	16.12	12.61	14	10.95	10.28	9.06	7.66	7.20	6.46
	30	46.66	34.37	24.23	18	14.08	11.89	9.81	8.52	7.74	6.75
	60	1.66	5.12	14.07	10.88	10.47	8.96	7.90	6.60	6.07	5.43
	120	35.33	16.87	12.46	11.61	10.82	9.21	8.09	7.03	6.20	5.38
	180	24	11.5	16.15	11.66	9.47	7.5	6.61	5.73	4.88	4.48

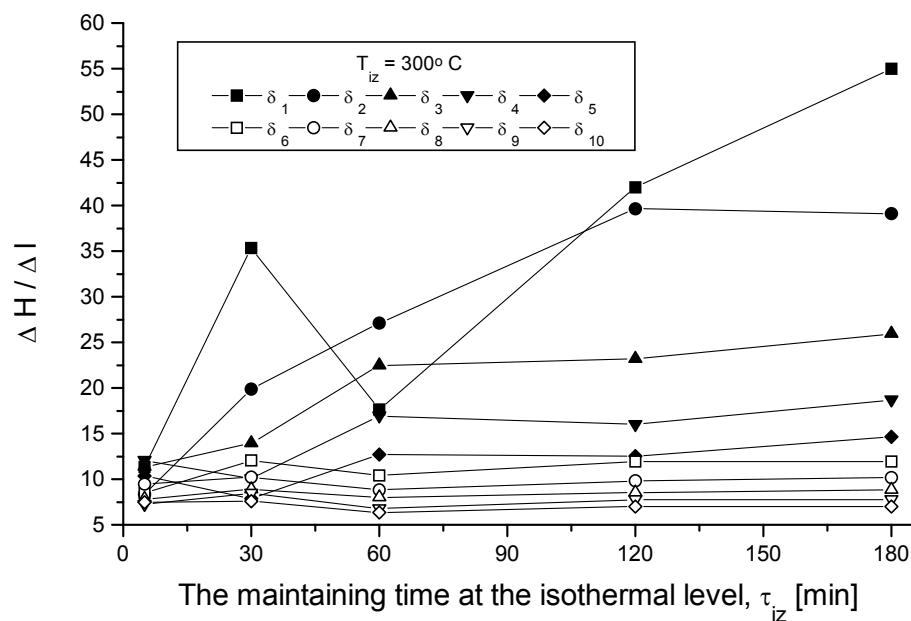


Fig.1 The variation of the  $\Delta H / \Delta l$  rapport, function the isothermal temperature  $t_{iz} = 300^\circ \text{C}$  and different isothermal maintaining times  $\tau_{iz}$ .

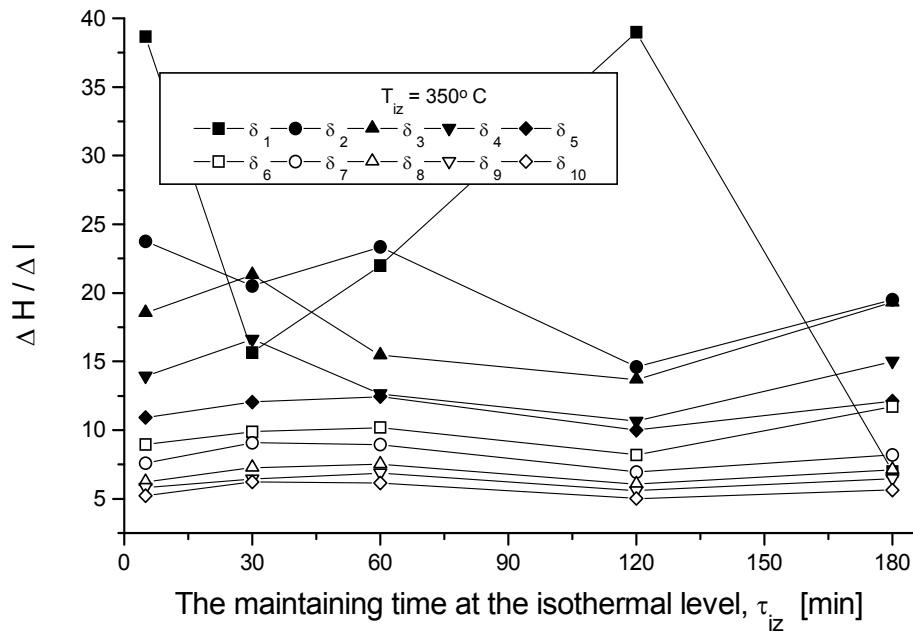


Fig. 2 The variation of the  $\Delta H / \Delta I$  rapport, function the isothermal temperature  $t_{iz} = 350^\circ \text{C}$  and different isothermal maintaining times  $\tau_{iz}$ .

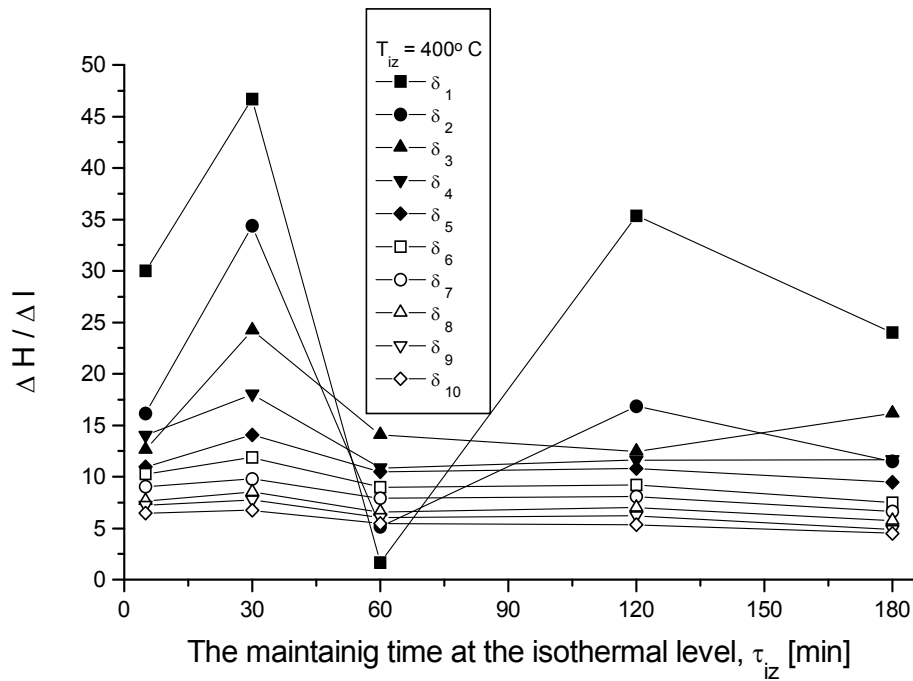


Fig. 3 The variation of the  $\Delta H / \Delta I$  rapport, function the isothermal temperature  $t_{iz} = 300^\circ \text{C}$  and different isothermal maintaining times  $\tau_{iz}$ .

For all the values of “ $\delta$ ”, corresponding to all the  $t_{iz}$  temperatures, it is observed the general remark that the values for the rapport  $\delta_1$  to  $\delta_6$  (corresponding for maximum

30  $\mu\text{m}$  from the wear surface), has a great variation of the values. That means that the wear process is more active near the wear surface.

The values for the  $\delta_6$  to  $\delta_{10}$  rapport's, has a small constant variation, and that means that the wear process influence in a small way the structural changes.

## 6. Conclusions

The wear process was influenced by the structural changes of the specimen's surface.

The microhardness of the nearest surface of specimens from the wear surface has a superior value and that values decrease with the increasing of the distance from the wear surface.

A general observation it is observed that the values of " $\delta$ ", decrease from  $\delta_1$  to  $\delta_{10}$  and that means a major different between the values of  $\delta$  for the specimen near to the wear and the specimen far away from the wear process.

Received: April 27 2005

"Transilvania" University, Braşov

## REFERENCES

1. Dorazil, E.: *High Strength Austempered Ductile Cast Iron*. Ed. Ellis Horwood Metals Associated Materials, 1991
2. Pearce, J.T.H.: *Abraisve wear behaviour of alloy cast irons*. The British Foundyman, n.78, 1985, **13-23**
3. Guang - Xi, L., Hong, Z.: *Sliding wear characteristics of Austempered Ductile Iron with and without laser hardening*. Wear, v. 138, 1990, **1-12**
4. Ping, L., Bahadur, S.,Verhoven, J.D.: *Friction and wear behavior of high silicon bainitic structures in Austempered Cast Iron and Steel*. Wear, vol. 138, n. 1-2, 1990, **269-284**
5. Fan, X.H., He, L., Zhou, Q.D.: *A study of high chromium cast iron on abrasion resistance and impact fatigue resistance*. Wear, Vol. 138, nr. 1-2, 1990, **47-60**
6. Miloşan, I. - *Cercetări privind variația ariei reale de contact la uzarea abrazivă a unei fgn trataă termic*, Metalurgia nr. 7, 1998, **63-65**

## INFLUENȚA PARAMETRILOR TRATAMENTULUI TERMIC ASUPRA MICRODURITĂȚII UNEI Fgn BAINITICĂ

### (Rezumat)

În acest studiu s-a utilizat o fontă cu grafit nodular aliată cu Mo-Ni-Cu, căreia i s-a aplicat un tratament termic de călire izotermă în domeniul de obținere a structurilor bainitice, iar apoi i s-a determinat comportarea la uzare ebrazivă a acesteia. S-a determinat variația raportului ( $\delta$ ) dintre microduratea ( $\Delta H$ ) și distanța de la suprafața uzată ( $\Delta l$ ), analizându-se rezultatele obținute.



## **SOME ASPECTS ABOUT THE KINETICS AND THERMODYNAMICS OF THE TRANSFORMATIONS OF A BAINITIC S.G. CAST IRON BETWEEN 350 AND 400°C**

BY

**IOAN MILOȘAN**

**Abstract:** The paper contains a study about the kinetics and thermodynamics of the bainitic transformation of a S.G. Cast Iron during the isothermal heat treatment. By the help of Johnson-Mehl and Arrhenius equations it was described the activation energy “Q”, rate coefficients dependent on temperature “k”, exponent of reaction “n” and a constant dependent on frequency “A”.

**Keywords:** Materials Science, bainitic s.g. cast iron, heat treatment, phase transformation

### **1. Introduction**

Austempered ductile iron (ADI) with a bainitic matrix, obtained by heat treatment and isothermal hardening is the material which combines a lot of superior attributes of the classical ductile iron or forged iron.

The paper presents an application for calculating the kinetics and thermodynamics parameters in the case of a phase transformation in solid state in A.D.I. S.G. grade. It is pointed out the influence of some factors (the temperature and the maintained time at the isothermal level) on the phase transformation and properties in the studied cast iron.

The kinetics of austenitization of S.G. Cast Iron, was described by the Johnson-Mehl-Avrami equation and for the determination of the activation energy “Q”, it was used the Arrhenius equation.

### **2. Materials**

The studied cast iron has the following chemical composition (% in weight): 3,63% C; 2,88% Si; 0,45 % Mn; 0,012%P; 0,006%S; 0,05%Mg; 0,40% Ni, 0,42%Cu. This cast iron was made in an induction furnace.

### **3. Heat treating**

The parameters of the heat treatment done were the following: the austenizing temperature,  $T_A = 900$  [°C]; the maintained time at austenizing temperature,  $\tau_A = 30$

[min]; the temperature at isothermal level,  $T_{iz} = 350$  and  $400$  [ $^{\circ}\text{C}$ ]; the maintained time at the isothermal level,  $\tau_{iz} = 1; 2; 5; 10; 15; 20; 25; 30; 35; 40; 45$  and  $50$  [min].

All these 2 experimental lots A ( $T_{iz} = 350^{\circ}\text{C}$ ) and B ( $T_{iz} = 400^{\circ}\text{C}$ ) were performed at isothermal maintenance in salt-bath, being the cooling after the isothermal maintenance was done in air.

#### 4. Experimental procedure

From this material, 19 typical HB test specimens was done ( $\phi 20 \times 50$  mm) and after the heat treating, it was determined the results of HB. The aim of the experiments is to determine the hardness (HB) at the isothermal temperature.

#### 5. Experimental results and discussion

The experimental values of the hardness are presented in table 1.

Table 1: The experimental values of hardness, for various  $t_{iz}$  and  $\tau_{iz}$

$t_{iz}, [^{\circ}\text{C}]$	$\tau_{iz}, [\text{min}]$	Hardness, [HB]		
		$H_0$	$H_f$	$H_{(t)}$
350	1	485	365	485
	2			471
	5			451
	10			438
	20			426
	30			415
	35			408
	40			393
	45			390
	50			379
	55			365
	400			1
2		398		
5		390		
10		375		
20		363		
30		344		
35		333		
40		325		

where:

$H_0$  – initial hardness, corresponding  $\tau_{iz} = 1$  min;

$H_t$  – hardness obtained after a maintaining time (t) at the isothermal level, [%];

$H_f$  – final hardness, corresponding at the maintaining time at the isothermal level, which are considered as a final time for the first stage of transformation of the bainitic reaction.

For the study of the phase transformation kinetics, it was used the first stage of the bainitic reaction [1 - 2]:



where:  $\gamma$  - metastable austenite;  
 $(\alpha)$  - bainitic ferrite;  
 $(\gamma)$  - austenite enriched in carbon

In this researches work it was used the methods of the variation's hardness analyse function of the time at the isothermal level ( $\tau_{iz}$ ), considering that this values are depended from the proportion of the transformed fraction " $X_{(t)}$ ". It was utilised the expression:

$$X_{(t)} = \frac{H_0 - H_{(t)}}{H_0 - H_f}, [\%] \quad (2)$$

where:  $X_{(t)}$  – the transformed fraction;

$H_0$  – initial hardness, corresponding  $\tau_{iz} = 1$  min;

$H_t$  – hardness obtained after a maintaining time (t) at the isothermal level, [%];

$H_f$  – final hardness, corresponding at the maintaining time at the isothermal level, which are considered as a final time for the first stage of transformation of the bainitic reaction.

In figure 1 is represented the sigmoidal solid curves of the austenitic transformation during the bainite reaction.

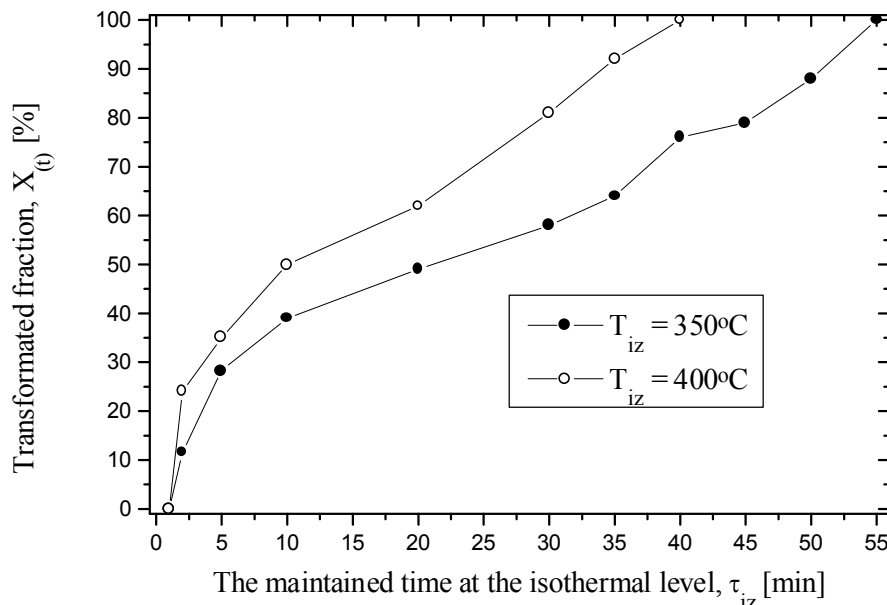


Fig. 1: Transformed fraction curves at  $T_{iz} = 350$  and  $400^\circ\text{C}$ , for different maintaining time,  $\tau_{iz}$ , at the isothermal level.

Like the transformation fraction curves have sigmoidal shape, it was used the “Johnson-Mehl-Avrami” equation:

$$X(t) = 1 - \exp(-k t^n) \quad (3)$$

where:

$X(t)$  - the transformed fraction;

$k$  - rate constant dependent on temperature;

$n$  - exponent of the reaction.

In order to determine “ $k$ ” and “ $n$ ”, the natural logarithmic expression was used:

$$\log[-\log(1-X)] = (n \log k + \log \log e) + n \log t \quad (4)$$

The plot of “ $\log[-\log(1-X)]$ ” against “ $\log t$ ” in the isothermal temperature range 350-400°C [1 – 2], for the isothermal maintaining time range 1 – 55 minutes, is shown in figure 2 and 3.

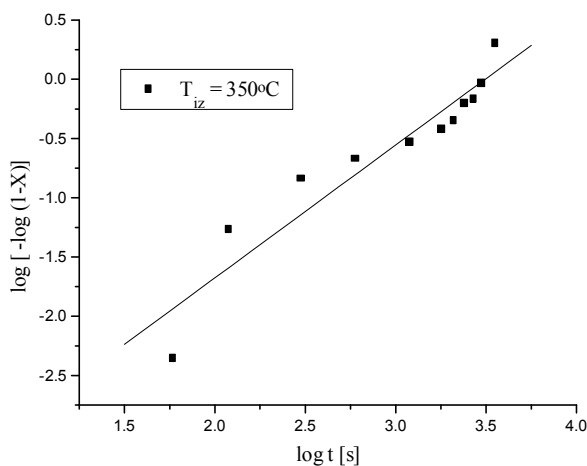


Fig. 2: The plot of “ $\log[-\log(1-X)]$ ” against “ $\log t$ ” in the isothermal temperature 380°C.

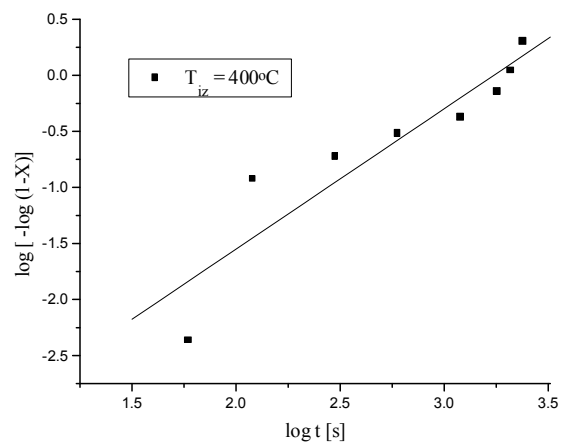


Fig. 3: The plot of “ $\log[-\log(1-X)]$ ” against “ $\log t$ ” in the isothermal temperature 400°C.

The obtained equations from the linear regression adjustment are:

$$Y_{350} = -3.92023 + 1.1218 * X, R^2 = 0.95; \quad (5)$$

$$Y_{400} = -4.05426 + 1.25209 * X, R^2 = 0.95; \quad (6)$$

Values of “ $n$ ” and “ $k$ ” determined from the slopes and intercepts of the linear regression lines are listed in table 2.

Table 2: Values of “n” and “k” for the formation of bainite

Lot	T <sub>iz</sub> [°C]	n	k [1 / s]
A	350	1.12	6.66 x 10 <sup>-4</sup>
B	400	1.25	11.26 x 10 <sup>-4</sup>

According to Liu [1], if the “n” exponent is between 1 and 2.3 the transformation is interfacial controlled.

At the same maintaining time in the isothermal level, the transformation process is different in the each maintaining isothermal temperatures. The bainitic reaction rate "k" increases when the isothermal temperature increases from 380 to 400° C.

For the determination of the activation energy “Q”, it was used the Arrhenius equation:

$$k = A e^{-Q/RT}; [1 / \text{min}] \quad (7)$$

where: k - constant rate dependent on temperature [1/s];

Q - activation energy [J /mol];

T - temperature [K]

R - gas constant 8.31 [J/mol.K]

A - constant dependent on frequency[1/s].

In order to determine “Q” and “A”, the natural logarithmic expression of eqn. (7) was used:

$$\log k = - \log e \frac{Q}{R} \frac{1}{T} + \log A \quad (8)$$

The plot of “log k” against “1/T” in the isothermal temperature range 350 - 400°C, for the isothermal maintaining time range 1 – 55 minutes, is shown in figure 4.

The equation of the linear regression is:

$$Y_{380-400} = -0.1245 - 1902.18772 * X, R^2 = -0.99; \quad (9)$$

Values of “Q” and “A” determined from the slope and intercept of the linear regression line are: Q = 37036 [J/mol] and A = 0,75 [1/s]

The activation energy of isothermal transformation are the same numerical order like the values obtained in the technical specialty literature [1-2].

From the linear regression, it was observed that the value of activation energy increases with the increasing of the maintaining temperature, from 350 to 400° C.

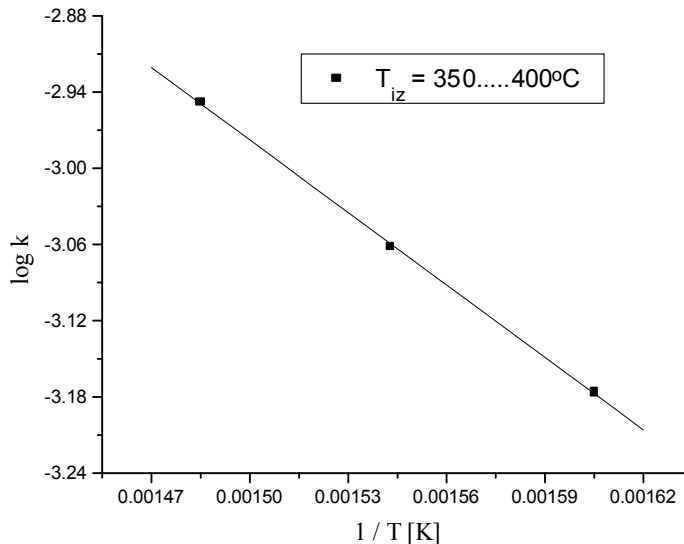


Fig. 4: Linear transform of the Arrhenius equation for the studied S.G. cast iron,  $T_{iz} = 350...400^{\circ}\text{C}$ .

## 6. Conclusions

The isothermal bainitic transformation in a Ni-Cu S.G. cast iron was studied in the temperature range of  $350\text{-}400^{\circ}\text{C}$  and with maintaining time between 1-55 minutes. The main results are summarized as follows:

- The kinetics of austenitization of S.G. cast iron, can be described by an Johnson-Mehl-Avrami equation .
- The reaction exponent “n”= 1.12 – 1.25 and the transformation is interface controlled.
- The bainitic reaction rate "k" increases with increasing isothermal temperature from  $350$  to  $400^{\circ}\text{C}$ .
- The activation energy of isothermal transformation was  $37036$  [J/mol]
- The constant dependent on frequency was:  $0,75$  [1/s]

Received: April 27 2005

“Transilvania” University, Braşov

## REFERENCES

- Liu, Y.C, Schissler, J.M, Chabout, J.P., Veters, H. - *Study of The Structural Evolution of Austempered Ductile Iron (ADI) during Tempering at  $360^{\circ}\text{C}$* , Metallurgical Science & Tech. 13, 1995, **12 - 20**
- Milosan, I., Munteanu, A. - *The study of the kinetics of the first stage of bainitic transformation of a nodular graphite cast iron using microhardness*, Metalurgia, 8, 1998, **74 - 79**

### ASPECTE PRIVIND CINETICA SI TERMODINAMICA TRANSFORMARILOR ALE UNEI Fgn BAINITICE INTRE $350$ SI $400^{\circ}\text{C}$

#### (Rezumat)

În lucrarea de față este prezentat un studiu asupra cineticii și termodinamicii transformării bainitice corespunzătoare unei fonte cu grafit nodulat tratate termic prin călire izotermă. Cu ajutorul ecuațiilor Johnson-Mehl și Arrhenius, sunt puse în evidență mărimi ca: energia empirică de activare “Q”, coeficientul vitezei de reacție “k”, coeficientul dependent de procesul de germinare și creștere “n” și factorul de frecvență “A”.

## **SOME ASPECTS OF THE DYNAMICS OF LAUNCHING DEVICE AT THE UNCONVENTIONAL WEAVING MACHINES**

**BY**

**VASILE-VIOREL MOLDOVEANU, LEONACHE DRĂGOI AND OVIDIU CALANCIA**

**Abstract:** This paper deals with the differential quadratic, which characterizes the dynamic of projectile launching device at the unconventional weaving machines, emphasize the importance of a correct functioning of the hydraulic shock absorber. Analyses and commentaries are being made regarding the real functioning conditions of the launching device, devices that equip the Sulzer and STB machines.

**Keywords:** tamp bearer, projectile, picker, hydraulic shock absorber, launching lever.

### **1. Introduction**

At the unconventional weaving machines like Sulzer and STB, the weft is axially uncoiled from the truncated cone spools displayed on the left part of the support; the weft is transported in the joint with the aid of the tamp bearer accepted in the textile field as a projectile. This is steel plate shaped, having 90x14x6,35 mm dimension and 40 grams weight. The lying of the weft in the joint is made with the aid of a series of devices:

- a) Transporter device, which moves the projectiles from the reception cassette to their launching point;
- b. Projectile rising device at a level where they are attached to the weft;
- c) The opening arch device of the projectile;
- d) The twisting device of the weft from the edge of the tissue to the charging point;
- e) The lying device of the projectile from the reception cassette to the transporter;
- f) The launching device itself. The launching device is the fact that the necessary energy for the speeding up of the projectile is obtained from the deformation of a shaft, subjected to the twisting which, once charged with the potential energy of working with the aid of the arm of the launching projectile.

### **2. The analysis of the dynamics**

The dynamics of the launching device is conditioned by the fact that the faraway extremity of the torsion bar is fixed on the support and the nearly extremity is initially rounded with 30 degrees.

The system formed by the torsion bar, the fixing tube, the launching arm, the rod, the picker and projectile is in every moment in equilibrium. The movement of the system components is described by the differential equation of movement, based upon the equilibrium of the moments:

$$M_1 + M_2 + M_3 = 0 \quad (1)$$

where:  $M_1$  is the torsion moment applied at a certain moment, to the torsion bar;  $M_2$ - the inert forces moment applied to the tube and to the launching arm;  $M_3$ - the inert forces moments applied to the rod, skate and projectile against the longitudinal axe of the torsion bar.

It is mentioned that plane- parallel movement of the push rod is very close to a movement of a rectilinear translation, this is the reason why it is considered the weight of the rod, skate and projectile in common in rectilinear movement.

From an analytical explanation of the shaft moments it results that:

$$M_1 = \frac{I_0 * G_0}{L} \varphi \quad (2)$$

where:  $I_0$  is the polar inert movement of the torsion bar section;

$G_0$  - the module of transversal elasticity of the material;

$L$  - the length of the portion from the torsion bar;

$\varphi$  - the angle at which the section from one side of the bar is rounded in relation to the opposite section, at a certain moment.

$$M_2 = - J_0 \times \ddot{\varphi} \quad (3)$$

where:  $J_0$  is the inert moment of the elements which performs the rotation movement- the tube and the launching lever;

$\varphi$  - the angled speeding of mobile elements movement.

$$M_3 = - m \times l^2 \times \ddot{\varphi} \quad (4)$$

where:  $m$  is the common weight of the rod, skate and projectile;

$l$  - the length of the launching lever.

Because of the fact that  $\varphi$  argument doesn't increase during the movement, on the contrary, it lowers from 30 degrees to 0 degrees, the sum  $M_2 + M_3$  must be taken with the changed sign, that is with plus:

Consequently, the differential equation of movement is rendered by (5) and (6):

$$(J_0 + m \times l^2) \times \ddot{\varphi} + \frac{I_0 * G_0}{L} \times \varphi = 0 \quad (5)$$

$$\ddot{\varphi} \times k^2 \times \varphi = 0 \quad (6)$$

Where:  $k^2 = \frac{I_0 * G_0}{L(J_0 + m * l^2)} * \varphi$

The general solving of the second power differential equation (6) is:

$$\varphi = A * \sin kt + B * \cos kt \quad (7)$$

where  $A$  and  $B$  are constants determined by the initial conditions of the movement.

Deriving successive the (7)'s equation results:

$$\dot{\varphi} = A * k * \cos kt - B * k * \sin kt \quad (8)$$

$$\ddot{\varphi} = - A * k^2 * \sin kt - B * k^2 * \cos kt \quad (9)$$

On the initial moment, the angled speed of the round moving elements is zero:

$t = 0, \dot{\varphi} = 0$ , it results

$Ak \cdot \cos kt = 0$ ,  $A = 0$ ; noting the twisting angle on the initial moment  $\varphi_0$ , is obtained  $\varphi = B \cdot \cos kt$ , so

$B = \varphi_0$ . The three equations become:

$$\varphi = \varphi_0 \cdot \cos kt \quad (10)$$

$$\dot{\varphi} = -\varphi_0 \cdot k \cdot \sin kt \quad (11)$$

$$\ddot{\varphi} = -\varphi_0 k^2 \cdot \cos kt \quad (12)$$

At the end of the movement, the torsion angle is  $\varphi = 0$ ; thus, noting the torsion duration  $t_1$  we obtain  $\varphi_0 \cos kt_1 = 0$ ; so  $kt_1 = \pi/2$ ; and  $t_1 = \pi/2k$

It considers the following specific elements determined:  $d = 0.015$  m;  $I_0 = \frac{d^4}{32} = 4.97 \cdot 10^{-9}$  m<sup>4</sup>;  $G = 8 \cdot 10^{10}$  N/m<sup>2</sup>;  $L = 0.71$  m;  $J_0 = 340 \cdot 10^{-5}$  kg·m<sup>2</sup>;  $m = 0.102$  kg;  $l = 0.185$  m. From this calculation it results that  $k = 285.1 \text{ s}^{-1}$ . If the initial torsion of the torsion bar has 30 degrees, then  $\varphi_0 = \pi/6$  rad, and the movement equation becomes:

$$\varphi = \frac{\pi}{6} \cdot \cos 285.1 \cdot t \quad (13)$$

The duration of the movement is:

$$t_1 = \pi/2 \cdot 285.1 \quad (14)$$

That is, the duration of the movement has the value 0.00551 s. The maximum speed of the projectile it's reached in the final moment of the movement:

$$v_{\max} = 1 \cdot \dot{\varphi}_{\text{final}} \quad (15)$$

So, the maximum speed of the projectile attains the minus value of 27.62 m/s. The meaning of the minus sign is the following: the movement of the launching lever is made in the opposite direction in relation to the initial rotation, performed to charge the torsion bar, charging with potential energy of deformation; the function  $\varphi$  decreasing from 30 degrees to 0 degrees, it results that its derivation is negative.

Then it is concluded that the maximum angled speeding of the launching lever is, on the initial moment of the launching process:

$|\dot{\varphi}| = |-\pi \cdot 285.1^2 / 6| \text{ s}^{-2} = |-42559| \text{ s}^{-2}$ , and the inert force applied only to the projectile, which has 40 g weight, is  $|I_{\max}| = 0.04 \cdot 42559 \cdot 0.185 = 314.9$  N

### 3. Comments and conclusions

The equation of the movement obtained in this paper doesn't take into account the influence of the oil shock absorber. Thanks to the performing of the shock absorber, the picker begins to obtain a speed decreasing earlier than the mathematical relation can render it, so the projectile is released from the picker earlier. Consequently, the launching process doesn't last 0,00551 s but only 0,0033s, and the maximum speed attained by the projectile is 22.5 m/s. The oil shock absorber is very important, as in the absence of it, the launching lever would have an increasing speed towards very high values, the projectile having maximum speed of 27.62 m/s, afterwards a tough shock appears as the result of the picker speed decreasing to zero, figure 1.

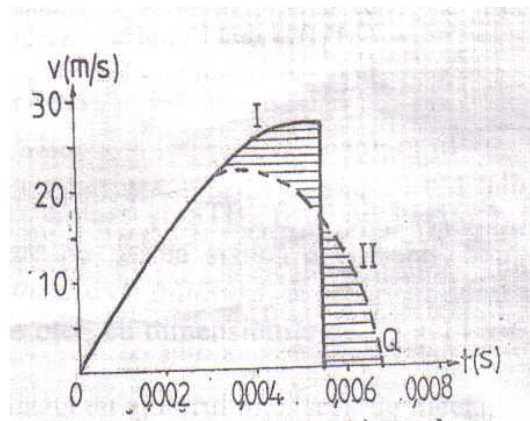


Fig. 1. The diagram of the picker's speed

The oil shock absorber influence renders the II allure to the speed diagram instead if I. When the picker reaches the maximum speed of only 22.5 m/s, the projectile falls apart from it, while the picker has a decreasing speed, marked by the dotted line. This is how a dangerous shock is avoided. It shows out the fact that the oil shock absorber works in two different phases: the first one when its influence is not very important, so that it can be neglected, and the movement of the launching lever is made according to the law of movement determined earlier; it is the phase of the acceleration of the launching lever and projectile. In the second phase the influence of the oil shock absorber is very strong and produced the breaking of the launching lever, which determines the separation of the projectile from the leading element and its movement with the maximum speed to the joint. The two phases of the oil shock absorber functioning are explained like this: the cylinder in which is moved the piston of the shock absorber is directly related with two channels of the oil repression.

In the first part of the piston race, the oil is repressed in the first channel, which has a big diameter and the opposite resistance is neglected; at a certain moment, the way out to this channel is stopped by the piston which moves on and the oil is repressed in the second channel, of much smaller section, which produces the intense breaking of the lever and the picker.

Received: May 9 2005

The "Gh.Asachi" Technical University from Iasi

#### REFERENCES

1. Drăgoi, L., Proiectarea utilajelor textile. Editura Dosoftei, Iași, 1995.
2. Drăgoi, L., Elemente de proiectare a utilajelor din țesătorie. Ed. BIT, 1997.

#### UNELE ASPECTE ALE DINAMICII MECANISMULUI DE LANSARE DE LA MASINILE NECONVENTIONALE DE TESUT

##### (Rezumat)

În lucrare se utilizează ecuația diferențială de ordinul doi, ce caracterizează dinamica mecanismului de lansare a proiectilului la mașinile neconvenționale de țesut, evidențiind importanța funcționării corecte a amortizorului hidraulic. Se fac analize și aprecieri privind condițiile reale de funcționare a mecanismului de lansare, mecanism ce echează mașinile Sulzer și STB.

**STUDY OF DIMENSIONAL UNIFORMITY AND ELECTRIC RESISTIVITY  
VARIATION IN AMORPHOUS RIBBONS FROM  
 $\text{Fe}_{80-x}\text{Sm}_x\text{B}_{20}$  AND  $\text{Fe}_{80-x}\text{Gd}_x\text{B}_{20}$  SYSTEMS**

BY

**CORNELIU MUNTEANU and LEANDRU-GHEORGHE BUJOREANU**

**Abstract:** The metallographic analysis of the surfaces and the dimensional uniformity of the metallic amorphous ribbons from the  $\text{Fe}_{80-x}\text{Sm}_x\text{B}_{20}$  and  $\text{Fe}_{80-x}\text{Gd}_x\text{B}_{20}$  systems are reported and discussed. Also, the variation of electric resistivity with temperature and chemical composition (degree of substitution  $x$  in atomic percentage) are studied.

**Keywords:** metallographic analysis, amorphous state, resistivity, ribbon surface, chemical composition

## 1. INTRODUCTION

The continuous metallic amorphous ribbons obtained by the melt quenching method have some specific properties different from materials with ordered structure, properties tight bound to the internal structure of alloys before and after amorphysation [1, 2, 3].

The aim of the present paper is to investigate the dimensional variation and the surface character of amorphous ribbons belonging to the  $\text{Fe}_{80-x}\text{Sm}_x\text{B}_{20}$  and  $\text{Fe}_{80-x}\text{Gd}_x\text{B}_{20}$  systems, by means of metallographic investigation. The variation of resistivity with temperature and degree of substitution  $x$  is analysed as well.

## 2. EXPERIMENTAL DETAILS

For preparing the amorphizable alloys pure powder shaped elements were used. They were mixed and homogenized and then isostatically compacted in a special die at 100 MPa pressure. Each portion (0.002 Kg) was melted under high vacuum ( $10^{-3}$  torr) in quartz crucibles. The resulted microingots were placed in the quartz crucible of an induction rapid-melting device. The melted alloy was ejected under the pressure created by an inert gas (Argon) through a nozzle, positioned at the bottom of the crucible. The liquid flow rapidly solidified on the external surface of a rotating metallic cylinder. Following this procedure metallic amorphous ribbons were obtained from the above systems, with  $x=0, 2, 5, 7$  for Sm and  $x=0, 5, 7, 10$  for Gd.

For the ribbon's dimensional variation study the external surface which freely solidified, the inner surface which was in contact with the quenching cylinder and final cross-section surface were metallographically analyzed. In this purpose a EPIVAL-

Interphako metallographic microscope was used, the images being taken by a video camera connected to a computer through an acquisition card.

In order to measure the variation of electrical resistivity a system was created which contained: a furnace with a heating rate of 1K/min (in which the ribbons samples were introduced); a thermoregulator (which controlled the inside furnace temperature); electric linking platinum wires and a thermocouple used to measure the samples temperature. This system was connected to a data acquisition system (a digital voltmeter, a digital ohmmeter, a data acquisition module consisting of an AT486DX2 computer with an electronic interface to the measurement devices).

### 3. EXPERIMENTAL RESULTS AND DISCUSSION

The analyze of the longitudinal section (Figure 1) revealed the presence of micro irregularities on the ribbon's surface with an amplitude ranging between  $\pm 2 \mu\text{m}$  for the inner surface and  $\pm 7 \mu\text{m}$  for the external one.

The study of external surface reveals a relatively clean face with small solidification irregularities (Figure 2). A variation of the ribbon's wideness was also observed due to the oscillations of the melt flow. Their wave length had an estimated value of 0,02 m (visually not detectable).

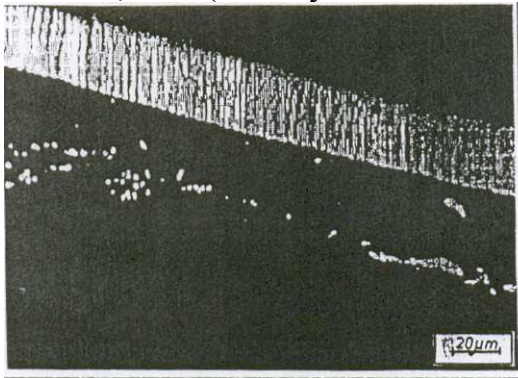


Fig. 1 Micrographic image of the longitudinal section for the  $\text{Fe}_{78}\text{Sm}_2\text{B}_{20}$  amorphous ribbon

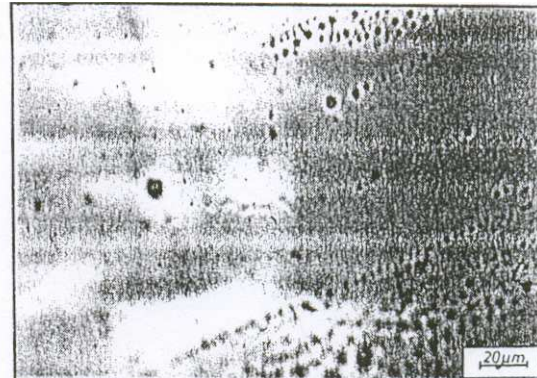


Fig. 2 Micrographic image of the external surface of the  $\text{Fe}_{75}\text{Gd}_5\text{B}_{20}$  ribbon, the width of  $0.9 \mu\text{m}$

Analyzing the inner surface (Figure 3) no marked irregularities were detected, although some defects were spotted due to the variation of the heat-transfer coefficient at the melt-support interface.

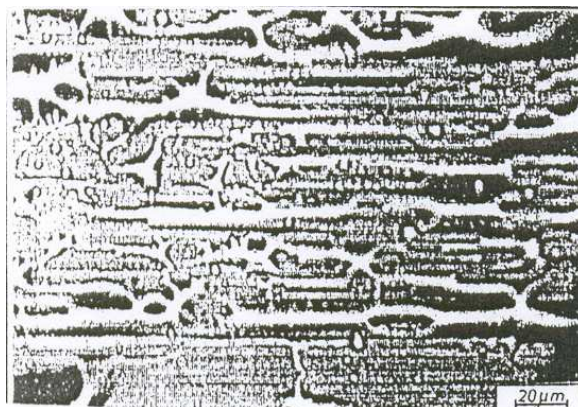


Fig.3 Micrographic image of the inner surface of the  $\text{Fe}_{75}\text{Gd}_5\text{B}_{20}$  ribbon's with a width of  $0.9 \mu\text{m}$

The substitution of Fe with Gd in the  $\text{Fe}_{80-x}\text{Gd}_x\text{B}_{20}$  system and with Sm in the  $\text{Fe}_{80-x}\text{Sm}_x\text{B}_{20}$  system progressively influenced the electrical and thermodynamic properties of the amorphous ribbon. It is seen from Figure 4 that the crystallization temperature increased with  $x$  from the  $\text{Fe}_{80}\text{B}_{20}$  alloy ( $T_{\text{cryst}} = 480^\circ\text{C}$ ,  $x = 0$ ) to the  $\text{Fe}_{80-x}\text{Sm}_x\text{B}_{20}$  ( $T_{\text{cryst}} = 580^\circ\text{C}$ ,  $x = 10$ ).

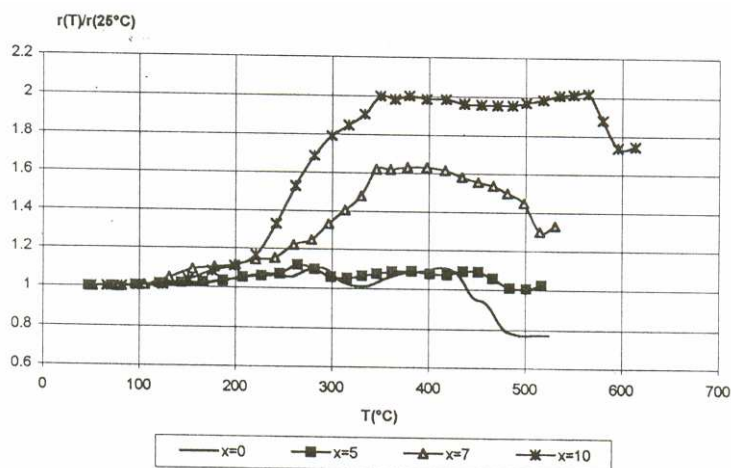


Fig.4 Relative resistivity versus temperature for amorphous ribbons from the  $\text{Fe}_{80-x}\text{Gd}_x\text{B}_{20}$  system.

It is noticeable that the resistivity increased with temperature up to about  $350^\circ\text{C}$ , which is a normal behaviour, beyond which it remained constant for the  $\text{Fe}_{70}\text{Gd}_{10}\text{B}_{20}$  alloy and decreased for the other ones. This effect could be the result of a structural (disorder) stability induced progressively by the Gd ions in the original amorphous system.

In order to increase  $T_c$  a higher degree of substitution had to be searched. However, in the Sm substituted system, the results presented in Figure 5 suggest a local optimum degree of substitution between  $x = 0$  and  $x = 2$ .

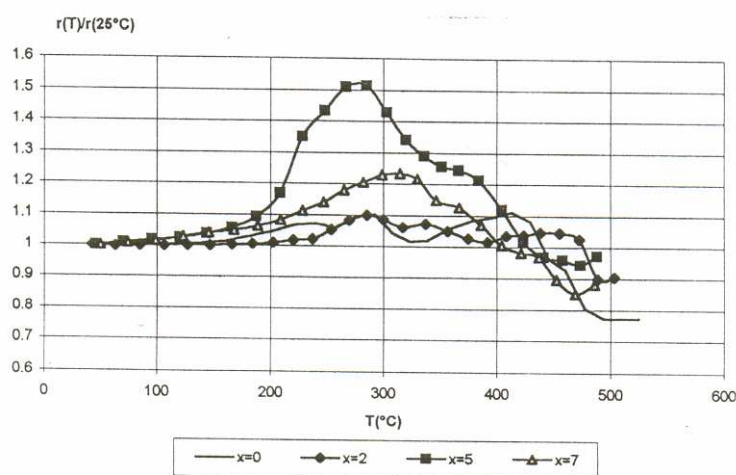


Fig.5. Relative resistivity versus temperature for amorphous ribbons from the  $\text{Fe}_{80-x}\text{Sm}_x\text{B}_{20}$  system

#### 4. CONCLUSIONS

The embrittlement temperature range was found to decrease with  $x$  in the Sm substitution system and to increase with  $x$  in the Gd-substitution system. A remarkable

stability in electrical properties was noticed up 250<sup>0</sup>C in the Fe<sub>78</sub>Sm<sub>2</sub>B<sub>20</sub> system and in the Fe<sub>75</sub>Gd<sub>5</sub>B<sub>20</sub> system, respectively.

It was observed that the latter amorphous alloy has been more stable as compared to the intermetallic compounds, which renders it interesting for electronic, electrotechnic and magnetic technological applications.

*Received: May 10 2005*

*The "Gh.Asachi" Technical University from Iasi*

#### REFERENCES

1. Suzuki, K., Fujimori, H., Hachimoto, K. – **Amorfnye Metally**, Metallurgia, Moskva, 1987, pp. 223 – 247;
2. Koster, V., Herald, V. – **Glassy Metals I**, Ed. By H.J.Gunththerodt & H. Beck, Topics in Applied Physics, Vol. 46, Springer Verlag, 1981;
3. Gilman, H., Leamy, H.J. – **Metallic Glasses**, A.S.M., 1979;
4. Munteanu, C. – Materiale Metalice Amorfe, Editura "Gh. Asachi" Iasi, 2001.

#### STUDIUL VARIAȚIEI UNIFORMITĂȚII DIMENSIONALE ȘI A REZISTIVITĂȚII ELECTRICE LA BENZILE AMORFE DIN SISTEMELE Fe<sub>80-x</sub>Sm<sub>x</sub>B<sub>20</sub> ȘI Fe<sub>80-x</sub>Gd<sub>x</sub>B<sub>20</sub>

##### (Rezumat)

Sunt prezentate și discutate analiza metalografică a suprafețelor și uniformitatea dimensională a benzilor metalice amorfe din sistemele Fe<sub>80-x</sub>Sm<sub>x</sub>B<sub>20</sub> and Fe<sub>80-x</sub>Gd<sub>x</sub>B<sub>20</sub>. De asemenea, este studiată variația rezistivității electrice cu temperature și cu compoziția chimică (grad de substituire x, în procente atomice).

## MINIMIZING OF POLLUTION AT THE ROASTING ROTARY KILN USED FOR PYRITE CINDERS

BY

I.NAGY\*, DANIELA NAGY\*, A.NICOLAE\* and A.DIMON\*\*

### *Abstract*

**Abstract:** At the rotary kiln for chloridizing roast of pyrite cinders following emissions of NO<sub>x</sub> and SO<sub>2</sub> exist, derived from the combustion of fuel for realizing some 700-1250 °C technological temperature. Combustion systems operating at high temperatures can produce many hundreds of parts per million by volume of nitrogen oxides. In exhaust gases from combustion processes nitric oxide is the predominant species, whereas nitrogen dioxide is normally present in much smaller concentrations. The pyrite cinders together with CaCl<sub>2</sub> go in against stream with waste gases. From reactions among the compounds of cinder to result volatile chlorides: CuCl, PbCl<sub>2</sub>, ZnCl<sub>2</sub>, AsCl<sub>3</sub>, SbCl<sub>3</sub>, HCl all are substance with a great toxicity. The cost of controlling the exiting gases, liquids and solids from a metallurgical plant is a substantial part of the capital and operating costs. With the increasing concern for our environment it is not unusual to find that these costs will exceed one quarter of the total capital requirements. Because there are usually a number of alternate processes than might be considered for a given situation, a rapid evaluation technique that permits the early identification of the more attractive alternates is useful. In the present paper a study of pollution control systems in metallurgical plants is achieved.

**Key words:** air pollution, particulate emissions, scrubber

### 1. INTRODUCTION

Air pollution, with its ever more apparent impacts on aquatic and terrestrial ecosystems, is a typical "environmental syndrome of the third generation". It is not reversible with relatively simple process approaches, economically measurable costs, and within a realistic scale of time and space. Despite clear successes in some regions, a significant worldwide reduction of air pollution will take decades.

Air pollution control may be achieved by simply hanging suitable dust collectors or scrubbers on the discharge end of every pipe venting off gases from the plant. Liquid and solid waste problems can be handled in a similar way but this approach is seldom the most economical method. With an existing facility, this approach is often viewed as the only practical one but it is an unusual situation where substantial improvements in pollution control costs cannot be obtained by carefully examining the process to minimize the quantity and the nature of the pollutants generated. On the other hand, a new metallurgical operation should always be engineered to minimize the output of emissions while optimizing the economics of the overall process including all of the elements (for example, power plant with flue gases, condenser, cooling water).

As a general rule, it is better to avoid the production and subsequent discharge of pollutants from the process rather than trying to capture them as they leave the process system.

## 2. EFFECTS OF AIR POLLUTION

With respect to SO<sub>2</sub> emissions, it must first be pointed out that the sulfur in fossil fuels exists in different forms of chemical bonding. In its inorganic form it is present as sulfate, e.g., CaSO<sub>4</sub>; in its sulfide form it exists primarily as pyrite (FeS<sub>2</sub>). In addition, sulfur occurs as gaseous hydrogen sulfide (H<sub>2</sub>S), as elemental sulfur in crude oil, and together with other forms of organic bonds in oil, brown coal, and hard coal (bituminous or anthracite). The organically fixed sulfur content in hard coal is on average 0.8%; this sulfur cannot be separated by mechanical processing. Only the inorganic sulfur bound in pyrite (~1%) can be removed prior to combustion with mechanical methods. With this method which is largely under control from a process-technology perspective, it is possible to reduce the sulfur content of power plant coal from 13 to 10 g/kg hard coal units (HCU)[1].

Most of the sources and mechanisms for creating air pollution in a metallurgical plant are rather obvious, others are more subtle and frequently overlooked. Particulate resulting from material handling and storage are found to occur at variety of locations. For example, conveyor belt transfer points and belt fed storage bins in the plants may have to be hooded. Ore decrepitating during processing steps such as roasting, calcining and reduction may result in larger than anticipated handling losses as fines are produced. Entrainment into a gas stream occurs when a material is being heated by direct contact with hot gases, such as in dryers, roasters, reverberatory furnaces etc. When ores are heated for processing, volatile components are vaporized. Gas phase oxidation of sulfur dioxide results in the formation of sulfuric acid vapor. These materials will pass through collection equipment such as electrostatic filters in the gas phase and upon exiting the stack condense to form particulates or mists.

Energy generation as a source of pollution has received considerable attention. If the metallurgical plant is to generate its own electricity, the cost of pollution abatement most likely will not be overlooked. Due to the impact of the more stringent pollution control requirements, a new dimension is added when taking the decision to make or to buy electricity for metallurgical plants. Another source frequently in metallurgical plants is the partial pressure of SO<sub>2</sub> over acid plant cleaning section bleed stream disposal areas and even possibly over lime/limestone SO<sub>2</sub> scrubber waste ponds for example.

Sulfur dioxide can be oxidized into sulfuric acid by "wet" or "dry" methods. A third possibility is the "catalytic" oxidation on soot and dust particles containing heavy metals. This reaction is facilitated by the presence of small droplets of water as fog and these droplets become strongly acidic. The resulting "acid smog" has a particularly deleterious effect on the respiratory system. In contrast to photosmog ("Los Angeles Smog"), which shows its strongest effects in the midday heat of the summer months, the "acid smog" ("London Smog") generally occurs in the mornings or evenings in the wet and cold season of winter.

## 2.1 Effects of NO<sub>x</sub> in the Atmosphere.

Today is known that in atmosphere, in the last 50<sup>th</sup> years the content in nitrogen oxides considerable increased. However, due to some prevention measures and control taken, beginning with 1980 it was observed that anthropogenic nitrogen oxides was stabilized.

The anthropogenic nitrogen oxides are special represented by NO, resulting after combustion (at temperature bigger of 1000 °C), but and some process as: nitrating, to make super phosphates, to wash out of metals with nitrogen oxide, to make explosive substances.

The formation of nitrogen oxides is not a simple reaction and is no definitive theory of their formation. "Thermal NO<sub>x</sub>" forms at high temperatures; "prompt NO<sub>x</sub>" forms during fuel conversion with an excess of oxygen atoms and is catalyzed through hydrocarbons. "Fuel NO<sub>x</sub>" is bound in fuel and is released at even moderate temperatures. Factors than influence the formation and quantity of NO<sub>x</sub> include: excess air, nitrogen content of the fuel, operating method (base load, start up, load sequence, the degree of contamination, the percentage of other fuels, and other emissions with possible catalytic effects.

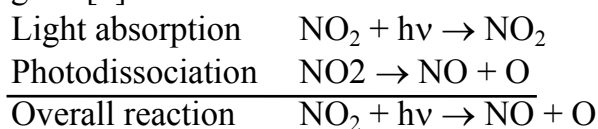
Many factors than determine the extent of NO<sub>2</sub> emissions during the combustion of coal include the firing method and the type of coal than is used. There are two major combustion mechanisms: dry firing and slag tap furnace [1]. The two methods are differentiated by the combustion temperature and by the ratio of generated slag to filter dust. In the former, only a small share of ash forms slag (~15%).

The majority of the dust is flyash and moves through the stack where it is captured very efficiently in electrostatic precipitators. The combustion temperatures in the dry furnace are between 1,100 and 1,350 °C. The temperatures in the slag tap furnace are between 1,400 and 1,550 °C, depending on the type of boiler and the type of coal used. This temperature exceeds the softening point of the ashes and 60 to 85% of the generated ash is pushed against the walls by the rotation of the flame and then flows into a water below the firing chamber.

The most important forms of air pollution from combustion processes are nitrogen oxide (NO) and nitrogen dioxide (NO<sub>2</sub>). Mixtures of both oxides are generally summarized as "NO<sub>x</sub>"; it is customary to report the mass concentrations for NO<sub>x</sub> as NO<sub>2</sub> in mg/m<sup>3</sup>. The formation can occur during the combustion process, on the way between the combustion chamber and its discharge from the facility (stack or exhaust vent), and in the atmosphere[2]:



Above a temperature of 120 °C to 200 °C, NO<sub>2</sub> breaks down into NO and oxygen. At normal temperatures, the breakdown of NO<sub>2</sub> is effected by light (photolysis). As a photo chemically very active compound, NO<sub>2</sub> absorbs the sunlight reaching the lower atmosphere at several magnitudes greater than all other trace gases[2]:



### 3. INDUSTRIAL AIR POLLUTION CONTROL METHODS

Air pollution emissions can be caused by technical reasons, but may also be caused by unsuitable, worn-out or defective facility components figure 1. gives an overview of the origin and causes of air pollution from industrial facilities, showing on the left side those processes where primarily gaseous emissions are generated by evaporation, valve discharges and chemical reactions.

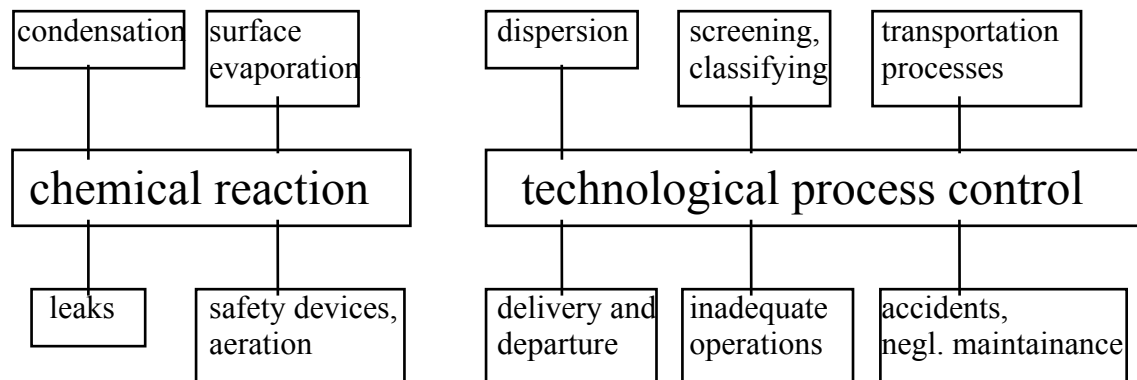


Fig.1 Causes for generation of industrial air pollutants

The most common origins from process technological methods of dispersing, sorting, and classifying and other specialized processes are listed at top right.

When developing new processes it is important to ensure that emissions are minimized. For existing facilities and processes, the causes for generating emissions must be analyzed carefully. In some cases it is possible to achieve an improvement in air quality by changing the input material for a specific process.

A typical example is energy production where, by using desulfurized heating oil or natural gas instead of high-sulfur coal, a significant reduction of SO<sub>2</sub> and nitrogen oxide emissions can be achieved. The use of natural gas eliminates flyash emissions, while the combustion of heating oil still produces considerable soot.

#### 3.1 Particulate Emissions.

Particulates are characterized by their mineralogy, their chemical composition, concentration, particle size distribution, and their morphological data. Other important physical characteristics, especially relevant for process engineers, are density, bulk and packing density, angle of slide and repose, abrasion factor, and specific surface.

Basis methods of particulate control are size reduction, screening and sifting, dispersing, granulating, sintering, drying, feeding, extracting, mixing, storing, hopper discharging, cleaning, packaging and transporting.

From the perspective of toxicity, substances like quartz, asbestos, soot, lead, cadmium, and vanadium compounds and radioactive particulates deserve special attention.

Particulate control-understood to mean phase separation solid/gaseous-takes place in several stages by utilizing different physical forces (Table 1.)

Table 1 Classification of dust collectors

	Type of Separator	Separation Efficiency
	gravity separator	0.4...0.6
	inertial separator	0.6...0.8
	electrostatic precipitator	0.9...0.999
Dry Separation	cyclone	0.7...0.95
	filtration separator	0.9...0.99
Wet Separation	water-spray separator	0.9...0.99

## 4. PRELIMINARY POLLUTION ESTIMATES

### 4.1 Air Pollution

A preliminary study estimate can be developed with a minimum of work if the following points are considered:

- First, we must decide whether the emission requires a particulate separation, such as for solids resulting from material handling, or whether a gas mass transfer system is required such as in the removal of SO<sub>2</sub> from a gas stream. In many instances both operations will be required.
- Second, we can calculate the actual gas volume which must be treated. Within rather broad ranges of pollutant concentrations and types the capital cost is dependent primarily upon the gas volume. It is necessary to correct the gas volume for the volume change on cooling when the gas is scrubbed in any wet scrubbing device since wet scrubbers are sized for the volume of saturated gas. A rule-of-thumb for metallurgical processes is that the actual saturated gas volume is 65% of the actual hot gas volume.
- Third, for particulate separations a semi-quantitative estimate of the difficulty of removal is required. For example, acid mists and particulates will be considerably more difficult to remove than particulates generated by solids handling.

It is known that the energy required to remove particulates from a gas stream increases as the particle size decreases.

We have assumed that a flow sheet of the process under evaluation has been developed in sufficient detail not only to determine sources of pollution but also to quantify the streams that must be treated.

The actual hot gas volume can be calculated using the rule-of-thumb that X watts will produce Y Atm of gas and then converting to an actual hot gas volume using the ratio of absolute temperatures of the actual off gases, if known. If a wet scrubber is employed, the 65% factor should be used as before. In general, the energy consumption will be the major factor in determining the volume of gas that must be treated from any process.

There will always be some air infiltration into metallurgical furnace off gases. However, there can be wide variations in the amount. In general, where there is no estimate of the actual infiltration, a rule-of-thumb than the actual gas volume will increase 50 to 150% as the result of air infiltration can be used for preliminary estimates.

## 4.2 Water Pollution

In general, water pollution comes from:

- Fouled process water. Examples would include filtrates or thickener overflows from which metal values have been removed, spent dirty reagents such as the black acid from an electro refining operation, solutions generated as a result of the abatement of gaseous pollutants such as those that might result from an operation sintering iron ore fines containing apatite and blowdown streams from boilers or cooling towers.
- Hot cooling water. Examples include the heated water from process heat exchanger and condensers, from power or steam plant condensers and compressor heat exchangers.

The characteristics that describe fouled process water include: flow rate, temperature, pH, soluble matter (composition, concentration), suspended solids (composition, concentration, size distribution).

The quantity of fouled water that must be treated is based upon the chemistry of the process and the amount of material which must be bled from the process to provide the operating conditions required to meet the purity requirements of the desired yields of metal from the ore or concentrate. The capital cost of such treatment systems is primarily a function of liquid flow rates so that minimum capital and operating costs result when volumes are at a minimum.

## 5. CONCLUSIONS

Minimization of gaseous emissions, consideration must be given to the relatively large concentration spectrum which influences the respective process technology (Fig.2).

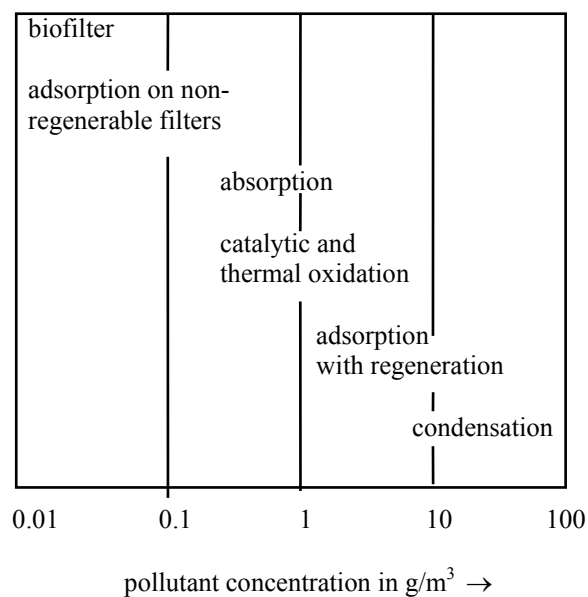


Fig.2 Use of various processes for minimizing gaseous emissions

The most common cleaning processes are absorption, adsorption and catalytic and thermal oxidation. The contaminants generated in these separation processes are either recovered or transformed through chemical reactions into relatively harmless substances.

The equipment used for flue gas scrubbing can be divided into absorbers with and without baffles. Absorbers without baffles are less susceptible to breakdowns and permit large gas throughput with minimal pressure loss.

Although the installation of baffles in the absorbers improves the contact between the gas and the liquid, it increases the pressure losses. Most commonly used are fixed bed adsorbers. These adsorbers are characterized by their low failure susceptibility and the long life expectancy of the adsorbing material.

The third group of gas scrubbing methods is comprised of thermal and catalytic after-burning processes. The facilities for thermal waste air incineration generally operate at higher temperatures, which is achieved by adding secondary air to the waste air stream.

Received: May 9 2005

\*The POLITEHNICA University of Bucharest

\*\* SC.INTEC SA Bucharest

## REFERENCES

1. Allhorn, H., Birnbauni, U., Huber, W.: *Kohleverwendung und Umweltschutz*. 215. Springer, Berlin-New York 1984
2. Winkler, F., Worch, E.: *Verfahrenschmic und Umweltschutz-eine Einföhrung*, Berlin 1986
3. Heintz, A., Reinhardt, G.: *Chemie und Umwelt*. 4<sup>th</sup>.ed., 366p. Verlag, Braunschweig 1990
4. Nriagu, J.O.: *Global Inventory of Natural and Anthropogenic Emissions of Trace Metals to the Atmosphere*. Nature 279, 1979
5. Moore, C. and Miller, A.: *Green Gold-Japan, Germany, the United States, and the Race for Environmental Technology*, 279p. Beacon Press, Boston 1994
6. Jugel, W., Busch, K.F., Hahn, M.: *Umweltschutztech* VEB Deutscher Verlag, Leipzig 1975
7. Nebers, N.: *Pollution Control Engineering*. 576p. Mc.Grow-Hill, New York-London 1995

## MINIMIZAREA POLUĂRII LA CUPTOARELE ROTATIVE DE PRĂJIRE UTILIZATE PENTRU CENUȘILE DE PIRITĂ

### (Rezumat)

La cuptoarele de prajire cloruranta a cenusilor de pirita exista urmatoarele noxe: NO<sub>x</sub>, SO<sub>2</sub> rezultate din arderea pacurii folosita pentru realizarea temperaturii tehnologice de lucru cuprinsa intre 700-1250 °C. Sistemele de combustie operand la temperaturi ridicate pot produce multe mii de parti per million de oxizi de azot. In gazele evacuate de la procesele de combustie oxidul de azot este predominant, in timp ce dioxidul de azot este prezent in mod normal inconcentratii mult mai reduce. Cenusă de pirita peletizata impreuna cu agentul de clorurare circula in contracurent cu gazele arse. In urma reactiilor dintre componentii cenusii rezulta cloruri volatile: CuCl, PbCl<sub>2</sub>, ZnCl<sub>2</sub>, AsCl<sub>3</sub>, SbCl<sub>3</sub>, FeCl<sub>3</sub>, HCl, substante cu toxicitate ridicata. Pretul pentru controlul noxelor sub forma de gaze, lichide si solide provenite din uzinele metalurgice reprezinta o parte substantiala din costurile de capital si de procesare. O data cu cresterea importantei pentru protectia mediului nu este normal sa constati ca aceste costuri vor depasi un sfert din totalul cheltuielilor de capital. Este folosita o evaluare tehnica ce permite cu usurinta identificarea noxelor provenite in sectorul metalurgic.



## THE IMPROVEMENT OF THE WHITE BRASSES RECRYSTALLIZATION HEAT TREATING (TYPE Cu-Zn-Ni)

BY

CARMEN NEJNERU, NICANOR CIMPOESU, ION HOPULELE,  
ALEXANDRU MAXINIUC and DRAGOS ACHITEI

**Abstract:** the paper contains an experimental study referring to the heat treatment of the recrystallisation reannealing of white brass. 27 bars were made with 3 degrees of deformation (25%; 50%; 75%). These bars after deformation were heat treated by maintaining at 3 temperatures (350<sup>0</sup>C; 450<sup>0</sup>C; 550<sup>0</sup>C) at 3 maintaining times (1h; 1,5h; 2h). After heat treatment the microhardness measurement were made, the results been sent in 3D graphics  $R_m=f(T,t)$  at  $\epsilon=25\%; 50\%; 75\%$ . Based on the graphic the treatment parameters can be determined for a desired specific medium grain size value at ( $t_{ment}, T_{ment}$ ) and any deformation degree between 25% and 75%.

**Keywords:** heat treating; anneal; white brass; phase; crystalline modification; forming property.

### 1. Introduction

The white brasses are Cu – Zn- Ni alloys with high strain resistance in brine and organic acid solutions, easily deformable and used as plates, straps bars, pipes, wires for non- salted water metal fittings mechanical components, art objects, medical instruments, telecommunications. Their composition (% Zn =20 ÷ 30; % Ni= 13 ÷ 19; % Cu = the rest) determines a monophasic structure ( $\alpha$  solid solution) coloured in yellow.

When cold – moulded, the brass cold – hardens strongly; to remove the tension and the anisotropy, the alloy is submitted to a recrystallization annealing heat treatment.

The brasses properties are decided by the size of the grains which depends on the annealing's temperature and on the precursory level of deformation. To obtain fine grains, a temperature of 340...450<sup>0</sup>C is required.

### 2. The recrystallization annealing

The heat treatment is used in order to eliminate the cold – hardening status resulted after the plastic deformation.

During the recrystallisation annealing that is the crystalline modification phase transformations take place. In this process the grains change only their shape, dimensions and distribution manner; the intrinsic tensions disappear and the hardness decreases.

The recrystallisation annealing resides in heating the metallic materials (items and parison) that were previously cold – hardened at temperatures greater (by 150-200<sup>0</sup>C) than the critical crystalline modification temperature; the purpose is to eliminate the work – hardening.

The chemical composition of the alloy under study is given in Table 1.

Table 1 Chemical composition of the analysed white brass

Cu	Zn	Ni	Sn	Pb	Fe	Mn	Co	Si	S	Ti	Mg	Cd	Al	P
61.474	23.83	13.4	0.19	0.25	0.37	0.04	0.04	0.01	0.244	0.004	0.002	0.03	0.07	0.01

The point corresponding to the above alloy can be approximatedly located in a vertical section corresponding to 13.4 %Ni of the ternary Cu-Zn-Ni phase diagram shown in Fig.1:

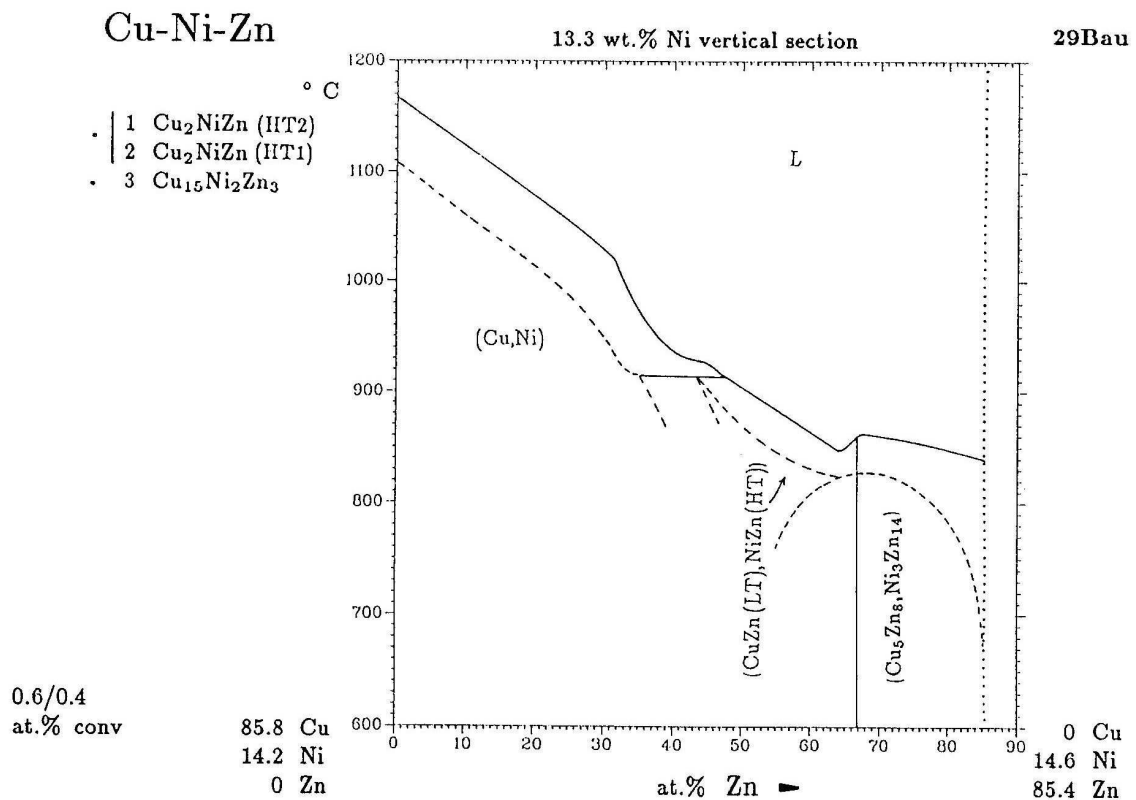


Fig. 1 Section through the Cu-Zn-Ni 3D diagram

For this experiment were used control cylinders with the following dimensions:  $\Phi=12\text{mm}$  and  $h=18\text{mm}$  and the structure composed of equally spaces grains having a fine granulation.

The control cylinders were cold-deformed at different deformation degrees: 25%, 50%, 75%. Their micrographs are shown in Figs.2, 3 and 4, respectively. Un upper view of the macroscopic shapes of the specimens is illustrated in Fig.5 while Fig.6 shows a lateral view.

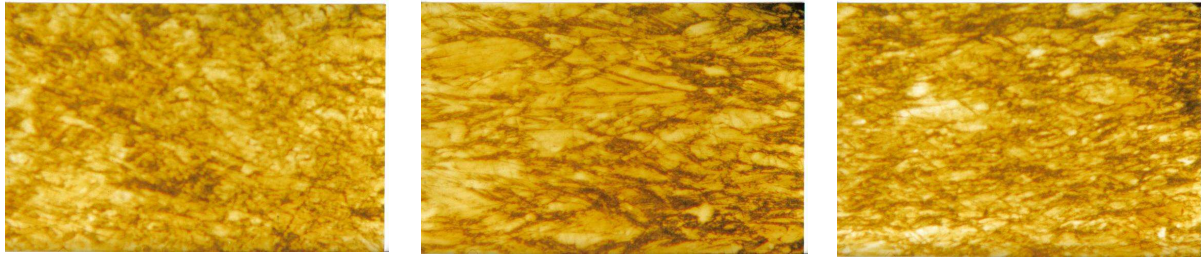


Fig 2  $\epsilon=25\%$  (size 400xphoto)  
Chemical attack  $\text{FeCl}_3$  30%

Fig 3  $\epsilon=50\%$  (size 400xphoto)  
Chemical attack  $\text{FeCl}_3$  30%

Fig 4  $\epsilon=75\%$  (size 400xphoto)  
Chemical attack  $\text{FeCl}_3$  30%



Fig.5 Deformed samples-up view  
a) Test bar, b)  $\epsilon=25\%$ , c)  $\epsilon=50\%$ , d)  $\epsilon=75\%$



Fig.6 Deformed samples-side view  
a) Test bar, b)  $\epsilon=25\%$ , c)  $\epsilon=50\%$ , d)  $\epsilon=75\%$

The cold-hardened samples structure has its grains elongated on the maximum tangential stress's direction.

### 3. Heat treatment

During the cold-forming, the metallic materials cold-strain, meaning that they elongate on the flow's direction forming fibres with a great hardness, but with an accentuated fragility also (because of the anisotropic structure).

The cold strained structure gives to the material properties like great hardness, mechanical resistance and low plasticity.

The treatment applied to the cold strained metallic material is the recrystallisation annealing.

During the recrystallisation annealing that is the crystalline modification phase transformations take place. In this process the grains change their shape, dimensions and distribution manner; the intrinsic tensions disappear and the hardness decreases.

The heat treatment temperature is :  $T_{\text{ther.trat.}} = T_{\text{rec}} + (150 \div 200)^\circ\text{C}$ ,

Where  $T_{\text{rec}}$  = crystalline modification  $^\circ\text{C}$ .

The crystal modification limit can be calculated with the following formula:

$$T_{\text{rec}} = (0.3 \div 0.4) T_{\text{melt}} \text{ --for monophasic solutions .}$$

$T_{\text{rec}}, T_{\text{melt}}$  are measured in K.

On the diagram can be easily observed that  $T_{\text{top}} \approx 980^\circ\text{C} = 980 + 273 = 1253 \text{ K}$

$$T_{\text{rec}} = (0.3 \div 0.4) 1253 = (102.9 \div 228.2)^\circ\text{C}$$

The crystalline modification limit depends on the deformation degree, Fig.7.

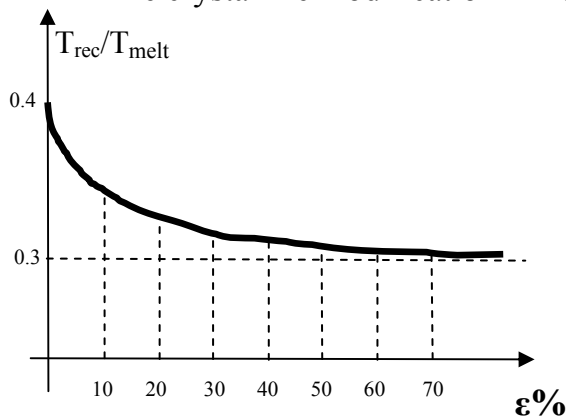


Fig. 7

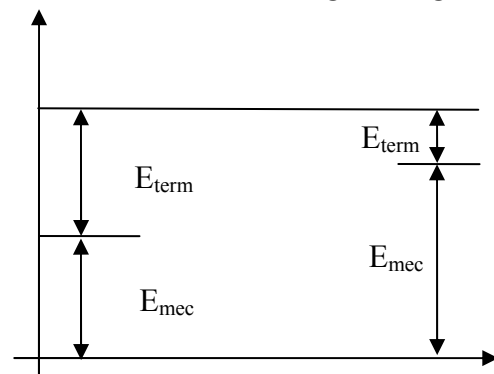


Fig. 8

This phenomenon occurs because the crystalline modification takes place when a specific energy level is overpassed inside the material .

The energetic contribution is brought to the process in two ways: the potential mechanical energy accumulated during the cold-forming and the thermal energy resulting from the material's heating preceding the treatment.

The graphic shows that as the cold-forming mechanical energy increases, a lower thermal energy is necessary to reach the crystallisation modification limits.

The heat treating for the recrystallisation annealing consists in placing the samples in an oven where the temperature reaches:  $T_{\text{trat}} = (120 \div 230)^\circ\text{C} + (150 \div 200)^\circ\text{C}$

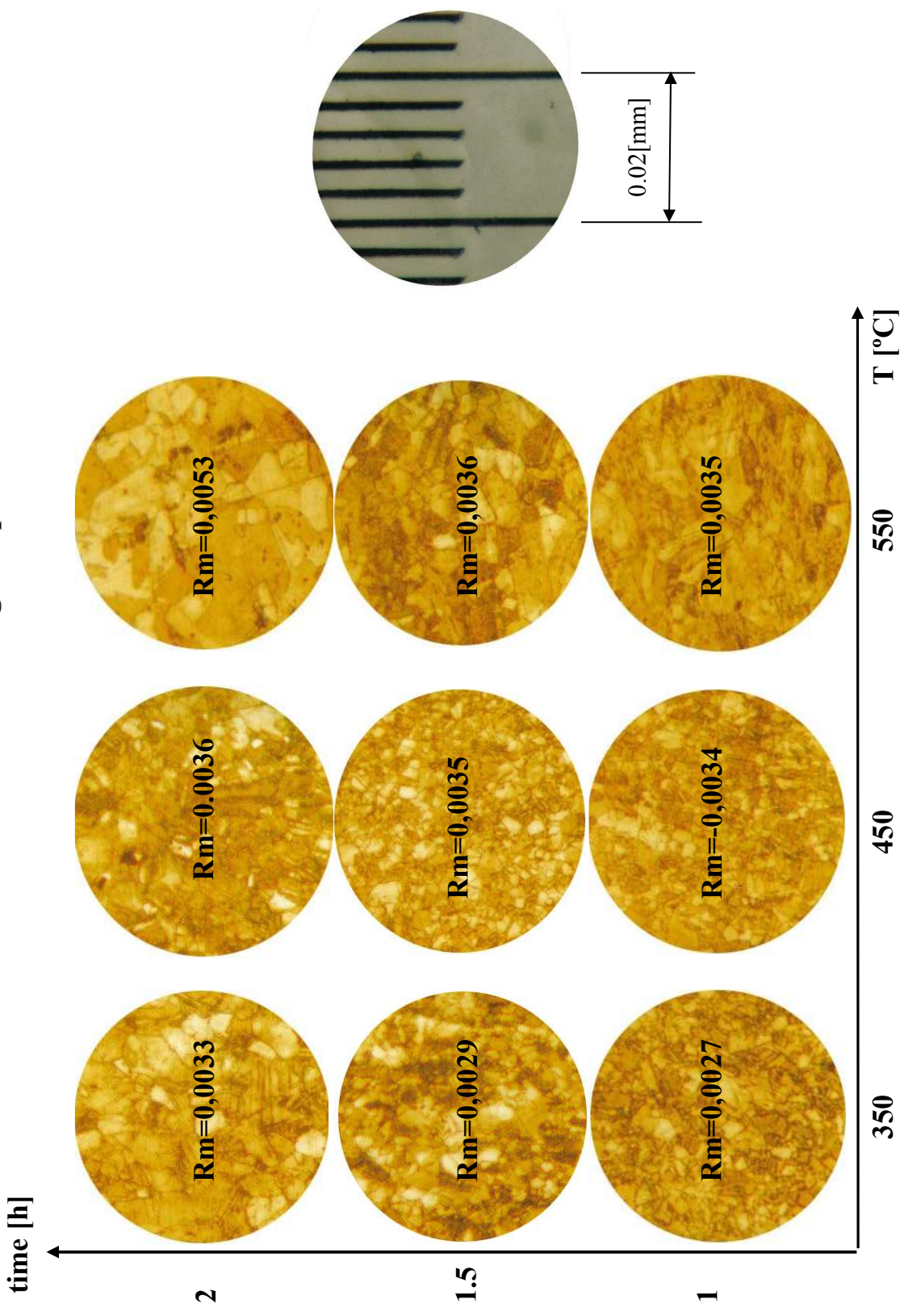
The tests were made at the following maintaining temperatures :  $T_1 = 350^\circ\text{C}$ ,  $T_2 = 450^\circ\text{C}$ ,  $T_3 = 550^\circ\text{C}$  with the specified maintaining intervals :  $t_1 = 1\text{h}$ ,  $t_2 = 1.5\text{h}$ ,  $t_3 = 2\text{h}$ .

The cooling took place in air at  $20^\circ\text{C}$ . The test matrix are displayed in graphic and the results in the table below.

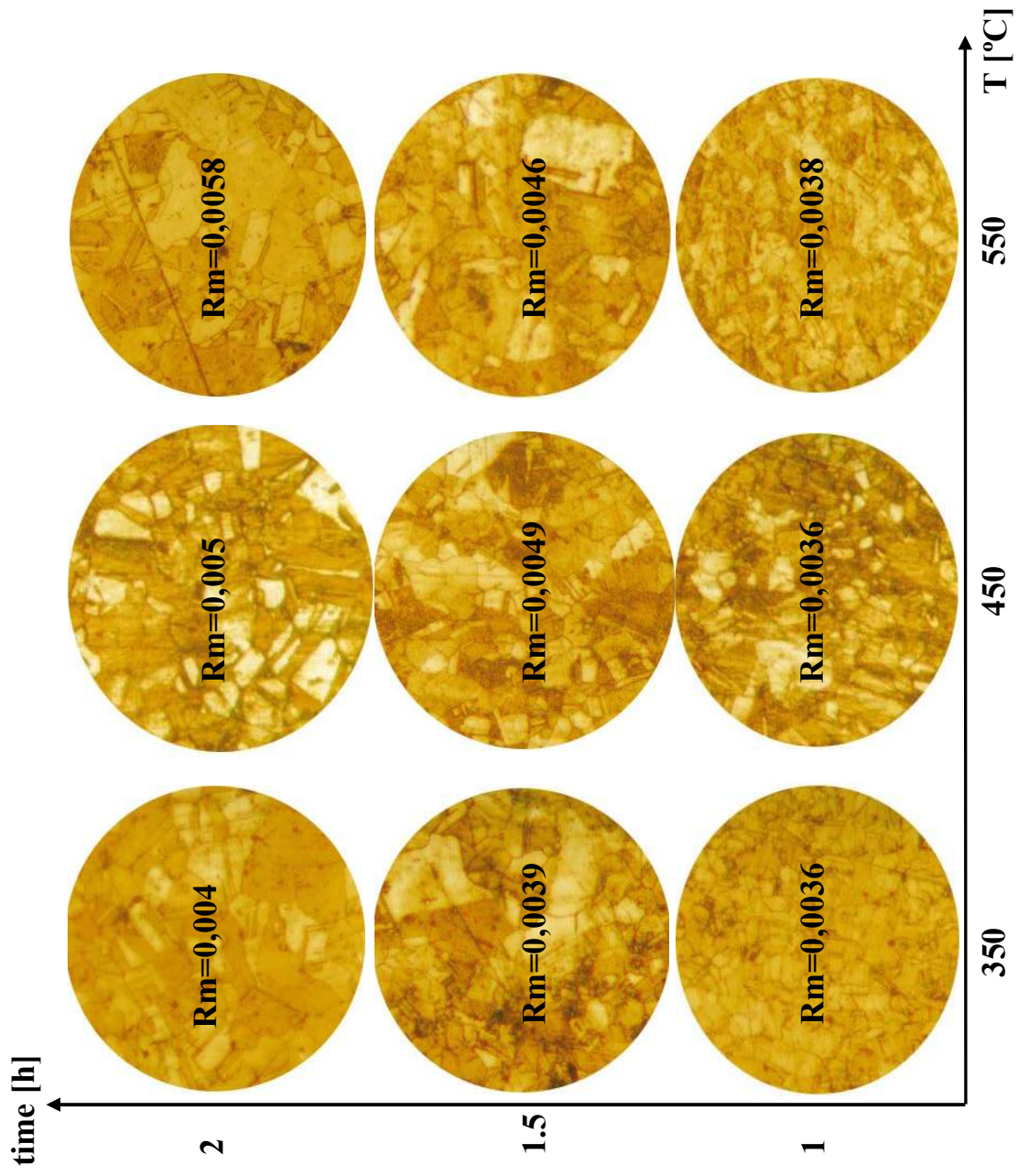
After the treatment, the specimens were planed and metallographic pictures were performed. Measurements were made of the medium grain size (using ten different fields). The data were centralised in the following three diagrams corresponding to the three deformation degrees: 25 %, 50 % and 75 %, respectively.

Finally, for each of the three deformation degrees, in Fig.9 space diagrams were plotted representing the variation of the average grain size as a function of both the heat treatment temperature and holding time.

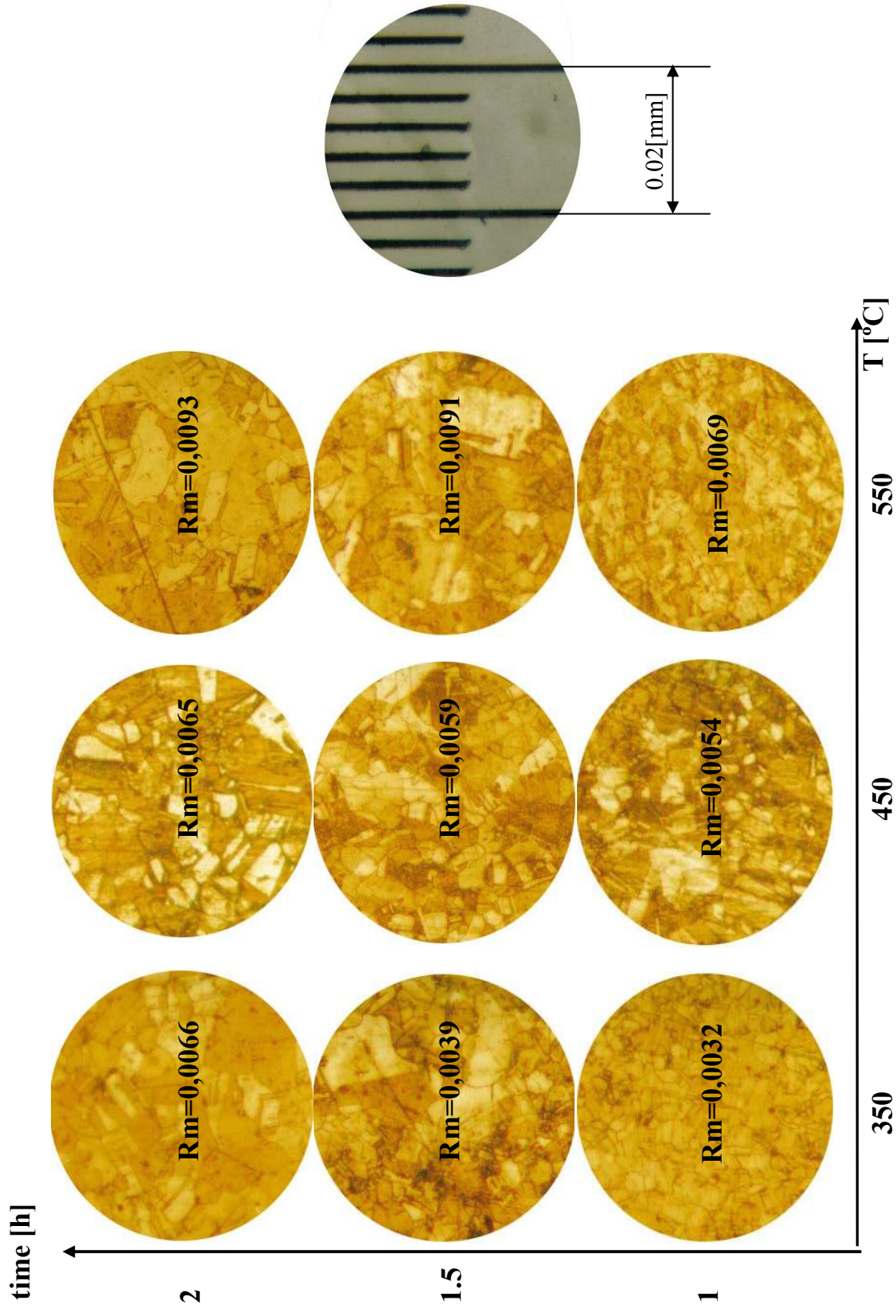
**The variation of medium grain size to constant deformation degree  $\epsilon_s=25\%$**

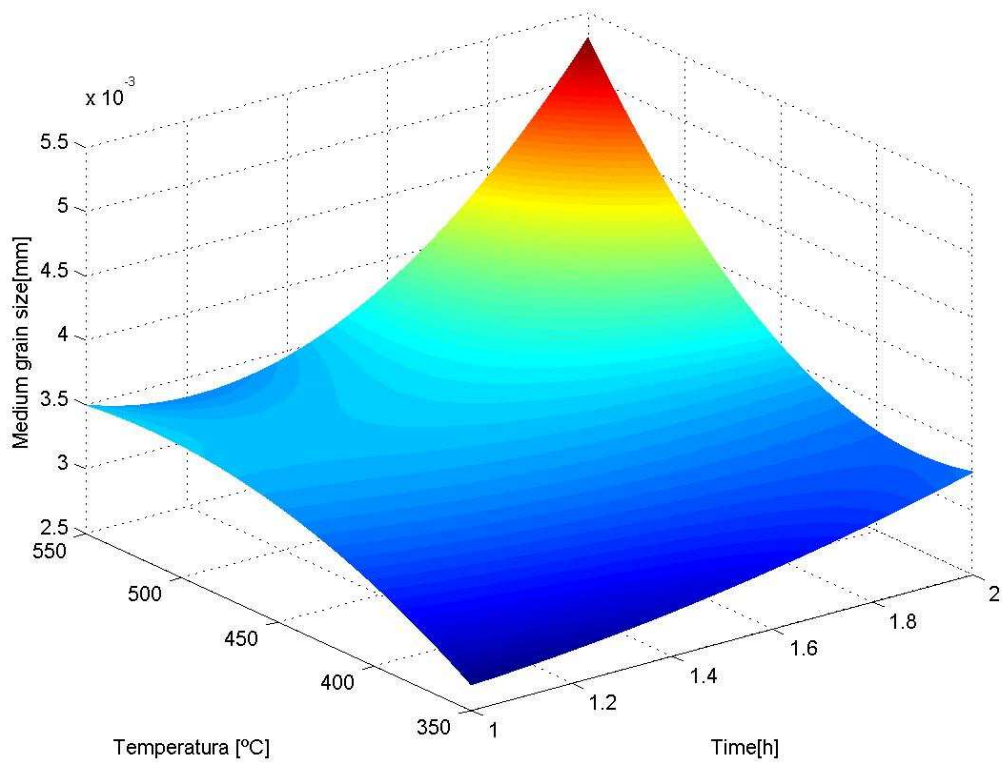
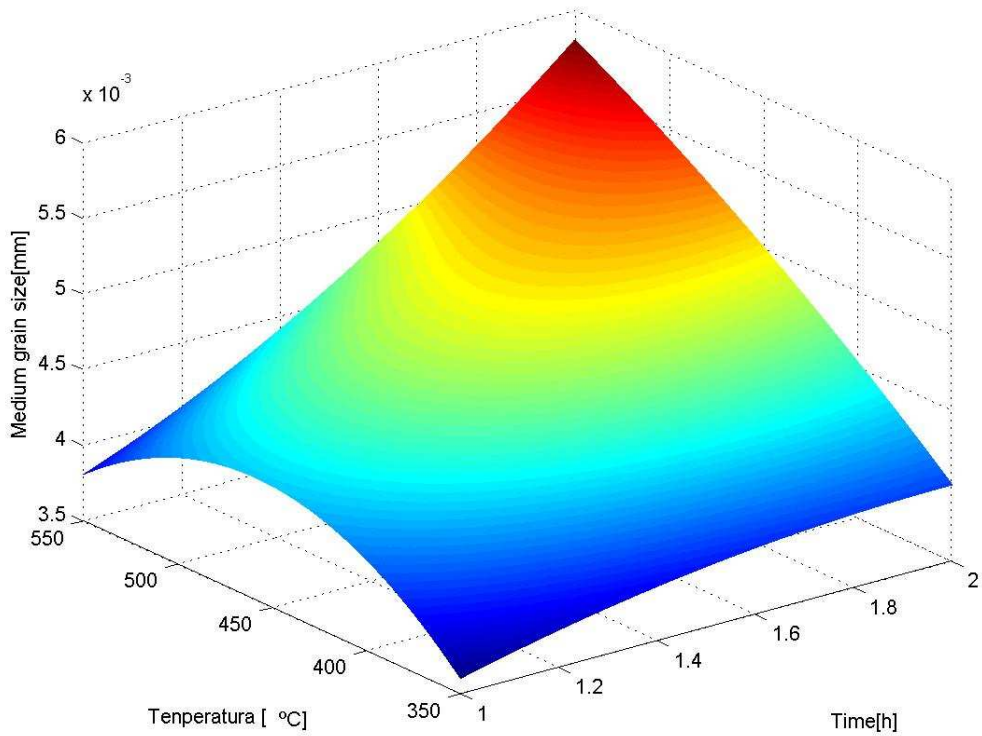


The variation of medium grain size to constant deformation degree  $\epsilon = 50\%$



The variation of medium grain size to constant deformation degree  $\epsilon_p=75\%$



The variation of medium grain size to constant deformation degree  $\epsilon_s=25\%$ The variation of medium grain size to constant deformation degree  $\epsilon_s=50\%$ 

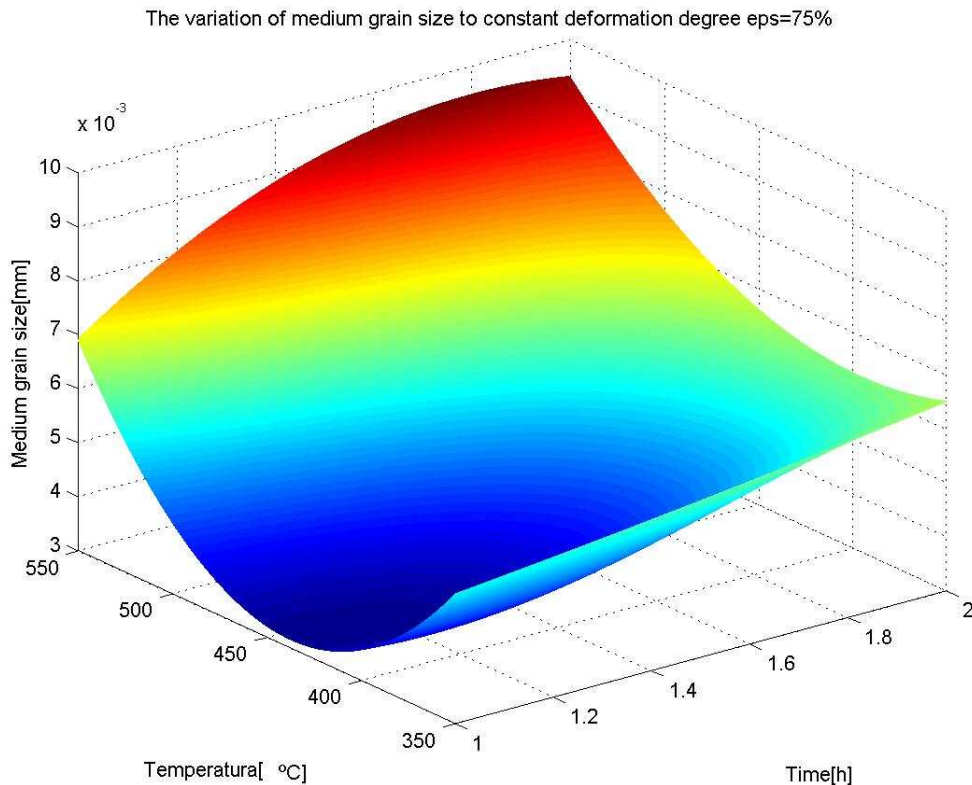


Fig.9 Space diagrams illustrating the variation of medium grain size as a function of recrystallization temperature and time, for the three deformation degrees

#### 4. Conclusion

The medium grain size is between  $0.0027 \dots 0.0093$  mm (  $R_m = 0.0027$  for  $\epsilon=25\%$ ,  $T = 350^\circ\text{C}$ ,  $t = 1$  h.;  $R_m = 0.0093$  at  $\epsilon=75\%$ ,  $T = 550$ ,  $t=2$ h).

From the analyse of the three space diagrams it is obvious that

- For all the three deformation degrees, the largest medium size of the twinned grains were obtained when both the heat treatment temperature and time were maximum.
- For the specimens deformed with 75 %, a minimum average grain size of about  $3.2 \cdot 10^{-6}$  m was obtained after heat treating at  $475^\circ\text{C}$  for 1 hour. For larger temperatures and holding times the grain size increased.

Based on the space diagrams, the treatment parameters can be determined for a specific hardness value ( $t_{\text{ment.}}$ ,  $T_{\text{ment.}}$ ) and any deformation degree between 25% and 75%.

In addition it is possible to calculate the medium size of the grains depending on the heat treatment's parameters.

**REFERENCES**

1. O. Hătărăscu, ș.a. – Îndreptar de metalurgie, Ed. Tehnică, 1998
2. I. Alexandru, ș.a. – Alegerea și utilizarea materialelor metalice, Ed. Tehnică și Pedagogică București, 1997
3. I. Hopulele, D. Gălușcă, I. Alexandru – Tratamente termice și termochimice vol. I, Ed. Rotaprint, Iași.

**OPTIMIZAREA TRATAMENTULUI TERMIC DE RECOACERE DE RECRISTALIZARE LA ALAME ALBE (tip Cu-Zn-Ni)****(Rezumat)**

Lucrarea cuprinde un studiu experimental al eficienței tratamentului termic de recoacere de recristalizare asupra alamelor albe. Au fost realizate 27 de epruvete având trei grade de deformare 25%; 50%; 75% acestea fiind tratate prin menținerea la trei temperaturi 350°C; 450°C; 550°C și trei timpi de menținere 1h; 1,5h; 2h. După tratament s-au făcut măsurători a razei medii a graunților folosind zece câmpuri de măsurare la fiecare probă, rezultatele fiind sintetizate în trei grafice spațiale  $R_m=f(T,t)$  la  $\epsilon=25\%$ ; 50%; 75%. Cu ajutorul graficelor se pot determina pentru materialul respectiv parametrii tratamentului termic ( $T$  și  $t$ ) necesari pentru obținerea unei anumite granulații cerute în exploatare.

## EFFECT OF THE MICROSTRUCTURE OF POLY(VINIL ALCOHOL) MEMBRANES ON THE DIFFUSION OF SOME IONIC SPECIES

BY

SILVIA PATACHIA and ADINA PAPANCEA

**Abstract:** The aim of this paper is to present the changes of the permittivity of some membranes based on poly(vinyl alcohol) [PVA] caused by their microstructure modifications. Porous PVA hydrogel membranes were obtained by repeated cycles of PVA solution's freezing and thawing. The modifications of the PVA structure were made by mixing the PVA solution with some natural products (beta-cyclodextrine or chitosan) or by complexing PVA hydrogel with  $\text{Cu}^{2+}$ . The influence of the presence of large cycles, of dispersed particles and of the supplementary crosslinking of the PVA hydrogel, due to complexation, on the membranes permittivity was studied. The diffusion of  $\text{Na}^+$  and  $\text{K}^+$  ions from the corresponding aqueous solutions to distilled water, through the above mentioned PVA non modified and modified membranes were studied by flamphotometric method. This study is important for separation processes of different ions from waste water and to tailor the membranes for controlled drugs delivery.

**Keywords:** poly(vinyl alcohol), membrane, permittivity, microstructure, crosslink.

### 1.Introduction

Hydrogels are three-dimensional and hydrophilic polymer networks capable of swelling in water or biological fluids and retaining a large amount of fluids in the swollen state. When in polymeric network the hydrophilic groups are hydrated a hydrogel structure is obtain. To prevent the disentanglement of hydrophilic polymeric chains the crosslinking is necessary. For the last few years the researches have focused on obtaining a family of chemical hydrogels with enhanced physical and chemical stability, without introducing toxic chemical crosslinkers [2].

PVA is known to form thermoreversible (physical) hydrogels upon freeze-thaw cycles [3,5]. These hydrogels have a good mechanical strength and a good elasticity [1,3].

The transport of electrolytes in polymeric materials has been studied to develop the knowledge of the transport mechanism of such specific solutes through PVA membranes. Moreover, the mechanism of electrolyte transport may involve a variety of interactions between the system constituents. So, these interactions of solute molecules with the molecular structure of the hydrogel are very important [6].

There are a number of models describing how diffusion coefficients of solutes in hydrogels vary with water concentration, polymer volume fraction, structure modifiers, etc.

In porous membranes the separation is induce by discriminating between particles size. High selectivity can be obtained when the solute size or particle size is large relative to the pore size in the membrane [4].

For this type of hydrogel membranes there are various parameters which will influence the membrane morphology and the pores size such as: the polymer concentration, the applied temperature for freeze and thawed, the cooling rate, the number of cycles, etc. [4].

In this work it has been studied the permittivity of some PVA hydrogel membranes obtained by freeze-thawed technique. A difference between the obtained permittivity values is due mainly to membrane microstructure modifications.

## 2. Experimental

### 2.1. Materials and apparatus

The following chemicals were used: poly(vinyl alcohol) [PVA 90-98] powder of industrial grade with 900 polymerization degree and 98% hydrolysis degree (SC CHIMICA Rasnov),  $\beta$ -cyclodextrine (Sigma), chitosan 652,  $\text{CuSO}_4$  ammonia solution with  $\text{pH} > 8$  and sodium and potassium chloride of pro-analysis quality. All chemicals were used without further purification.

The salt solutions were prepared by dissolving the corresponding quantity of salt – for 0,1 M solutions- in distilled water.

The following apparatus were used: diffusion cell, magnetic stirrer F 20 FALC and Sherwood Flam Photometer 410. The diffusion cell consists of two compartments filled with electrolyte solution (A) and water (B). The hydrogel membrane (M), previously swollen in water, was placed between the two cells (Fig.1).

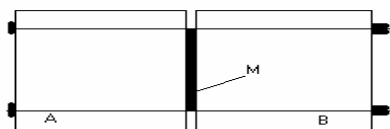


Figure 1. Diffusion cell

### 2.2. Membrane preparation

#### 2.2.1. PVA membrane

PVA solution 16-18% were prepared by dissolving a pre-weight dry PVA 90-98 in de-ionized water by stirring and by heating to  $70-80^{\circ}\text{C}$  for 3 hours. After cooling, PVA solution was cast in a PVC box (7 cm diameter) and freeze at  $-16^{\circ}\text{C}$  or at  $-19^{\circ}\text{C}$  for 12 hours. After that, the frozen cast solution was thawed at  $22^{\circ}\text{C}$  or at  $25^{\circ}\text{C}$  for 12 hours, too. These cycles were repeated for three times. It has been resulted a heterogeneous, porous, thermo-reversible hydrogel with a good mechanical strength. It has been kept in de-ionized water at room temperature for further use.

#### 2.2.2. $\beta$ -cyclodextrine, chitosan, $\text{Cu}^{2+}$ /PVA membrane

The PVA with  $\beta$ -cyclodextrine membranes were prepared as follows: to PVA 90-98 solution a  $\beta$ -cyclodextrine solution ( $\beta$ -cyclodextrine dissolved distilled water)

was added. The resulting solution was heated to aprox. 30<sup>0</sup>C stirring until homogenous solution was obtained. A certain volume of this solution was extracted with a syringe and cast in the PVC box with 7 cm diameter. The freeze-thaw cycles are similar with those described in the previous paragraph.

The PVA membrane complexed with Cu<sup>2+</sup> was prepared by immersing a PVA 90-98 membrane in a copper tetra-ammino complex solution having a pH>8, for 14 days. After that, the membrane was placed in water to eliminate the salt surplus.

### 2.3. Conductivity measurements

A Radelkis Conductometer OK-114, to determine the conductivity of the diffused solutions through PVA membrane has been used. These measurements were made for sodium and potassium chloride 0.1 M solutions.

The diffusion cell was placed on the magnetic stirrer. Between the two compartments the PVA membrane was set. The stirrer has been placed in B compartment. The diffusion process takes place due to the concentration gradient.

The conductivity was determined every two minutes for 80 minutes.

### 2.4. Flam photometric measurements

To determine the diffusion of Na<sup>+</sup> and K<sup>+</sup> ions from sodium and potassium chloride solutions, the flam photometric method has been used. The diffusion process took place like we described above. The process subsisted for 50 minutes. The concentration determinations were made by extracting a volume of solution from B compartment every 5 minutes. Then, the amount of the diffused ions has been determined by reading the ions concentrations on Sherwood Flam Photometer 410.

## 3. Result and discussions

The results obtained by conductivity measurements for PVA 90-98 membrane and PVA 90-98 complexed with Cu<sup>2+</sup> membrane were graphical represented in dependence with time in figure 1.

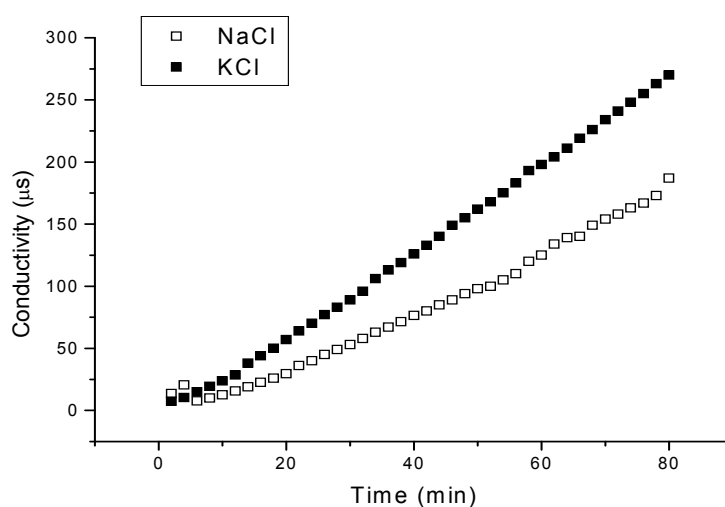


Fig. 1 The time-conductivity dependency of the diffused ions Na<sup>+</sup> and K<sup>+</sup> from the NaCl 0.1 M and KCl 0.1 M solutions through PVA90-98 membrane

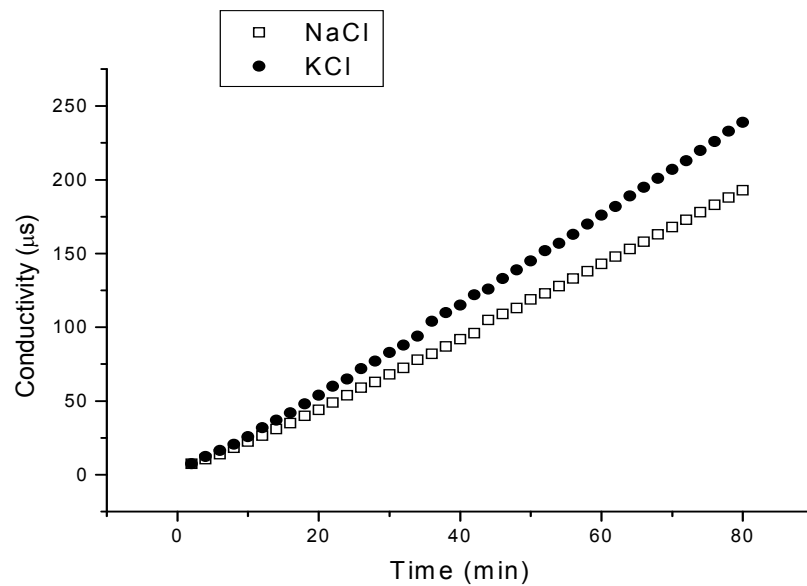


Fig. 2 The time-conductivity dependency of the diffused ions  $\text{Na}^+$  and  $\text{K}^+$  from the  $\text{NaCl}$  0.1 M and  $\text{KCl}$  0.1 M solutions through  $\text{PVA90-98}+\text{Cu}^{2+}$  membrane

The membrane thickness for  $\text{PVA90-98}$  hydrogel membrane was  $g_m=1.3\text{mm}$  and for  $\text{PVA 90-98} + \text{Cu}^{2+}$  membrane,  $g_m=1.5\text{mm}$ .

It can be observed that the solution conductivity for both diffused ions is increasing in time, but the potassium ions solution conductivity is higher than the sodium ions. That can be explained by the higher mobility of the potassium ion. The differences between the two types of membranes microstructure are not significant.

This can be explained by the fact that the microstructure- the total pores size- wasn't significantly modified. The complexed chains have been closed, due to the  $\text{Cu}^{2+}$  ions binding, but in the same time, its have been separated by the non-complexed chains and new pores have been formed.

We have tried to represent that, schematically, in the figure 3.

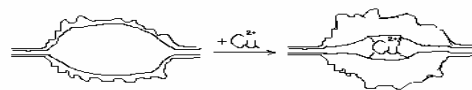


Fig.3 A pore representation: in the initial state and after copper complexation

In the swollen hydrogel the amorphous part, situated between the crystalline parts that act as crosslinking, are flexible, so even the large cycles of  $\beta$ -cyclodextrine can be included without a significant variation in membrane permittivity.

The permittivity was calculated with the following relations:

$$P=J \cdot g_m / c_{CA}$$

where:  $J=dc/dt \cdot V_A/S$ ;  $P$ =permittivity,  $m^2/s$ ;  $J$ =flow;  $g_m$ =membrane thickness;  $c_{CA}$ =initial concentration of the salt solution;  $dc/dt$ = concentration gradient ;  $V_A$ = volume of initial solution in the diffusion cell;  $S$ =the diffusion surface.

The membrane permittivity was determined for different types of PVA 90-98 membranes. Varying the polymer concentration and the temperature gradient different values for the PVA90-98 membrane permittivities have been obtained (see Table 1 and table 2).

Table 1. Membranes permittivity for different types of cation

Crt.Nr.	Diffused salt	Membrane material	Membrane thickness (mm)	Membrane permittivity for cations $\cdot 10^9 (m^2/s)$
1	NaCl	PVA 90-98	1.3	5.23
2		PVA 90-98+Cu <sup>2+</sup>	1.5	5.28
3		PVA 90-98+CD	1	4.54
4	KCl	PVA 90-98	1.3	1.3
5		PVA 90-98+Cu <sup>2+</sup>	1.5	1.5
6		PVA 90-98+CD	1	1

Table 2. Membranes permittivity for different types of cation

Crt. Nr.	Salt	Membrane material	Membrane thickness (mm)	Membrane permittivity for cations $\cdot 10^{10} (m^2/s)$
1	NaCl	PVA 90-98	1	4.46
2	KCl	PVA 90-98	1.05	3.5

One can observe that the calculated permittivity for sodium ions is higher than that for the potassium ions in PVA 90-98 membrane. Also the permittivity may vary with a magnitude order depending on the membranes preparation conditions.

#### 4. Conclusions

Hydrogel membranes based on PVA 90-98 have been obtained by freezing–thawing repeated cycle technique. These membranes have been modified by PVA blending with beta cyclodextrine, by loading with dispersed chitosan particles and by complexed with Cu<sup>2+</sup> ions. The obtained membranes were tested from permittivity point of view, for Na<sup>+</sup> and K<sup>+</sup> ions.

All the tested membranes showed a higher permittivity for Na<sup>+</sup> ions by comparing with K<sup>+</sup> ions, just like the cellular membranes.

This behavior could be explained by the known property of K<sup>+</sup> ions to be H-bonds broker. So, the H-bonds between the solvent (water) and the OH groups from

the polymer chains have been broken by  $K^+$  ions and higher interaction between  $K^+$  and polymer chains occurs. As consequence,  $K^+$  ions are strongly retained by PVA, comparing with  $Na^+$  ions. So the  $K^+$  ions diffuse slower than the  $Na^+$  ions.

The order of the permittivity magnitude for the obtained PVA hydrogel porous membranes is approximately the same with that reported in the literature for diffusion of alkaline cations through non-porous membranes made by polyacrylamide.

In porous membrane the number of the crosslinkings doesn't mainly influenced the membrane permittivity, unlike the nonporous membranes with a homogenous structure, where the permittivity is drastically affected by its. This means that the membrane permittivity in a porous membrane is mainly due to the pores size and not to the diffusion through the amorphous polymeric structure.

The made modifications of the PVA hydrogel membranes did not affect significantly the membranes permittivity, due to the flexibility of polymeric chains from the amorphous state.

In exchange the crosslinking agents can improve other membrane properties (i.e. the membrane copper complexed has a higher mechanical and thermal resistance and the membrane made by PVA-beta cyclodextrine is softer than that of unmodified PVA).

Received May 4 2005

The "Transilvania" University from Brasov

## REFERENCES

1. S. Pațachia, Cap.8. Blends based on poly(vinyl alcohol) and the products based on this polymer în "Handbook of Polymer blends and composites" Edited by C. Vasile and A.K. Kulshreshtha, RAPRA Technology LTD., England, p. 288-365, ISBN 1-85957-304-5, 2003
2. Poly(vinyl alcohol), Technical Book, Rasnov, 1979
3. S. Pațachia, C. Corboș, *Study on obtaining poly(vinyl alcohol) hydrogel*, Bulletin of the "Transilvania" University of Brașov, Vol. 9(44)- New Series, Series B, ISSN 1223-964X, , 2002
4. Marcel Mulder, Basic Principles of Membrane Technology, Kluster Academic Publishers, Netherlands, 1996
5. Christie M. Hassan, Nikolaos A. Peppas, Structure and Applications of Poly(vinyl alcohol) Hydrogels Produced by Conventional Crosslinking or by Freezing/Thawing Methods, Advances in Polymer Science, Vol.153, 2000
6. V.M.M.Lobo, A.J.M.Valente, A.Ya.Polishchuk and G. Geuskens, Transport of non-associated electrolytes in acrylamide hydrogels, Journal of Molecular Liquids 94, 179-192, 2001

## EFFECTUL MICROSTRUCTURII MEMBRANELOR DE POLI (ALCOOL VINILIC) [PVA] ASUPRA DIFUZIEI UNOR SPECII IONICE.

### (Rezumat)

Scopul acestei lucrari este de a prezenta modificarile de permitivitate ale unor membrane de PVA datorate modificarilor de microstructura. Au fost obtinute membrane poroase de PVA prin metoda ciclurilor repetate de inghet-dezghet. Modificarile materialului membranelor au fost realizate prin complexarea PVA-ului cu ioni de cupru ( $2^+$ ), prin amestecarea cu beta ciclodextrina sau prin dispersarea particulelor de chitoosan. S-au determinat coeficientii de permitivitate ai acestor membrane pentru ionii de sodium si potasiu proveniti din solutii de cloruri, utilizandu-se metoda conductometrica si flamfotometrica. S-a studiat influenta modificarilor de structura ale materialului membranelor asupra difuziei ionilor alcalini mentionati. Aceste studii sunt importante pentru procesele de separare a diferitilor ioni din apele reziduale ca si pentru realizarea unor noi materiale pentru sistemele cu difuzie controlata.

## EFFECT OF THE POLY (VINYL ALCOHOL) [PVA] HYDROGELS MICROSTRUCTURE ON THEIR WATER ABSORPTION

BY

S. PATACHIA and M. RINJA

**Abstract** The aim of this paper is to study the influence of microstructure of PVA hydrogels obtained by different techniques on their capacity of water absorption. Three PVA hydrogel types have been obtained by three physical methods: (i) repeated freezing and thawing cycles; (ii) freezing with liquid nitrogen and (iii) irradiation with beta radiation. The method of hydrogel obtaining determines its morphology. The kinetic of water absorption was determined by gravimetric method. A correlation between the hydrogel's microstructure and its capacity of water absorption has been made. This study is important in selection of hydrogels obtaining technique for obtaining new materials with a controlled water absorption capacity.

**Keywords:** hydrogel, irradiation, freeze-thawing, liquid nitrogen, swelling

### 1. Introduction

There has been increasing interest in the synthesis and various applications such as high water sorption of new hydrogels. Hydrogels are three-dimensional networks of hydrophilic polymers held together by cross links of covalent bonds or ionic bonds and secondary forces in the form of hydrogen bonds or hydrophobic interactions. These materials are of great interest due to their promising applications such as separators, separation membranes, adsorbents, and materials for medicine and pharmacy as drug delivery systems, in solving some ecological and biological problems as well as in modern technologies [1,3,7].

The physical gelation capability of the atactic and syndiotactic forms of PVA has been known for a long time. In aqueous solutions with a polymer concentration of more than 1% entangled aggregates of hydrogen bonded PVA molecules are formed. This is a consequence of time dependent formation of crystal nuclei and microcrystalline regions. Pioneering work proposed that spinodal liquid-liquid phase separation, followed by crystallization of parts of the PVA chains, is the origin of gel formation in PVA solutions in water.

Aqueous solution of PVA can also undergo gelation when submitted to a series of freezing-thawing cycles [1,3,4,5,7]. These physically cross linked PVA gels, present a high degree of swelling in water, a rubbery and elastic nature, a fibril network structure and high mechanical strength [4,5,6]. In the freezing-thawing process, water crystallization results in creating interstitial domains of high polymer concentration. Polymer chain belonging to these highly concentrated domains possibly will crystallize leading eventually to the gelation of the whole system. [4]

The properties of the gel depend on the PVA molecular weight, the PVA concentration in water, the temperature and time of freezing and the number of freezing cycles. Gel formation is ascribed to the formation of PVA crystallites which act as physical cross linking sites in the network. In the freezing-thawing-based techniques, fine crystallites are formed due to the slow cool treatment. [5]

In the literature [7] has been developed methods of preparation PVA hydrogels free of elutable impurities, such as emulsifiers, catalysts and uncreated cross linking agent-free. The preferred preparation method for medical or biological applications consists of a freezing-thawing process applied on aqueous solutions of PVA. When aqueous solutions of PVA are stored at room temperature they gradually form a gel with, however, a low mechanical strength. Interestingly, once aqueous solutions of this polymer undergo a freeze-thawing process, a strong and highly elastic gel is formed [1,3,4,5,6,7].

Radiation processing has many advantages over other conventional methods. In radiation processing, no catalysts or additives are needed to initiate the reaction. The advantages of the radiation methods are that they are relatively simple, and moreover, the degree of cross linking and grafting, which strongly determines the extent of swelling in hydrogels, can be controlled easily by varying the absorbed dose [7].

High energy radiation, in particular gamma and electron beam, can be used to polymerize unsaturated compounds. This means that water-soluble polymers derivative with vinyl groups can be converted into hydrogels using high energy irradiation.

During irradiation of aqueous solutions of polymers, radicals can be formed on the polymer chain by the homolytic scission of C-H bonds. Additionally, radiolysis of water molecules generates the formation of hydroxyl radicals which can attack polymer chains also resulting in the formation of macro radicals. Recombination of macro radicals on different chains results in the formation of covalent bonds and finally in a cross linked structure. Since the generated macro radicals can react with oxygen, radiation is normally performed in an inert (nitrogen, argon) atmosphere. Poly (vinyl alcohol), poly (ethylene glycol), poly (acrylic acid) are well know examples of polymer which can be cross linked with high energy irradiation. The properties of the formed hydrogels, in particular their swelling and permeability characteristic, depend on the concentration of the polymer and radiation dose: in general, the crosslink density increases with increasing polymer concentration and radiation dose.

The advanced of hydrogel formation by radiation-induced cross linking is that this process can be done in water under mild conditions (room temperature and physiological pH). Moreover, the use of (toxic) cross linking agents is avoided. However, the gels have to be loaded with biologically active materials after their preparation because the radicals formed during irradiation might potentially damage the biologically active substance. Further, since for example in irradiated PEG or PVA, the crosslink consists of C-C bonds, these gels will not be biodegradable. [6]

The aim of this paper is to compare the structure and water absorption capacity of the PVA hydrogels obtained by different techniques. The PVA hydrogels, using three physics cross linking techniques, were obtained. The swelling measurements have been made on these three dimensional networks.

## 2. Experimental data

### 2.1. Preparation of aqueous PVA solution

PVA 90-98 (900 polymerization degree and 98% hydrolysis degree), industrial grades, without further purification have been used. Aqueous 16-18 wt% PVA solutions were prepared by dissolving pre-weighed quantities of dry PVA in deionized water, by magnetic stirring and heating them at 70-80 °C for 3h. After cooling, this solution was used for hydrogels preparation.

### 2.2. Preparation of PVA hydrogels

By applying three cross-linking methods PVA hydrogels with different structures have been obtained.

a). Aqueous solution of PVA was introduced in PVC cylindrical tubs that were exposed to three freezing and thawing cycles (-15 : 24 °C). Decreasing temperature, determine forming ice crystals which lead to closure polymer chains in favor of their crosslinking through intermolecular H-bonds. The results are the nano-crystallites in which the PVA chains are united by hydrogen bonds. These act in the system as cross linking points. Their presence leads to the PVA hydrogel that is a three-dimensional network not soluble in water..

PVA hydrogel has the property to absorb large water quantities. After thawing aqueous solution the ice crystals melt, generating holes in hydrogel structure. That confers a porous structure. The size of pores is depending to the size of the ice crystals initial formed. The mechanical strength is determined by its cross linking degree that depends on the number of freezing-thawing cycles. The PVA hydrogel obtained by this method are white-opaque (demonstrating an obvious phase separation), heterogeneous, with a good mechanical strength.

b). The PVA hydrogels were obtained by applying of three cycles of freeze and thawing in liquid nitrogen. PVA aqueous solution has been introduced in PVC vials and then has been immersed in liquid nitrogen, for 1 h. Then, the frozen solution has been kept for 24 h at room temperature. As a result of very low temperature of the liquid nitrogen, the water within PVA aqueous solution has been instantaneously frozen.

The temperature gradient leads to a PVA hydrogels were the formed pores are much smaller than the case of slowly freezing process and they have a radial distribution. The layout of pores is a result of very fast freezing from the out side the inner of the gel.

Three freezing-thawing cycles were applied. Finally, at different freezing temperatures, PVA hydrogels with different structures have been obtained. The size of the pores is an important factor regarding later water absorption properties.

c). Another PVA hydrogel obtaining method that was studied in this paper was PVA aqueous solution  $\beta$  irradiation. The irradiation leads to a cross linking of the PVA by extracting some of the hydrogen atoms or hydroxyl groups from macromolecular chain and forming inter- or intramolecular bonds. The radicals had formed on the macromolecular chain.

The recombining of radicals leads to intercatenar covalent bonds forming and finally leads to a cross-linking structure. Recent studies showed that minimum  $\gamma$  irradiation dose for cross linking of PVA aqueous solution was 30 kGy. In this paper, the PVA hydrogel were obtained using an irradiation dose of 5.4 kGy. The conclusion is that, even at low dose radiation the PVA macromolecular chain can be cross linked. Increasing the irradiation dose the PVA hydrogels with a higher mechanical strength are obtained.

The PVA aqueous solution has been introduced in glass cylindrical vials and expose to  $\beta$ -irradiation, on different dose: 5.4; 10.8; 47.25 kGy. The PVA hydrogels were obtained. They have a different structure comparing with the previous gels. The PVA hydrogels obtained by using this method, are transparent, exhibiting a more homogeneous structure. The mechanical strength depends on the irradiation dose.

Figure 1 represents the three types of PVA hydrogel obtained by using different techniques.

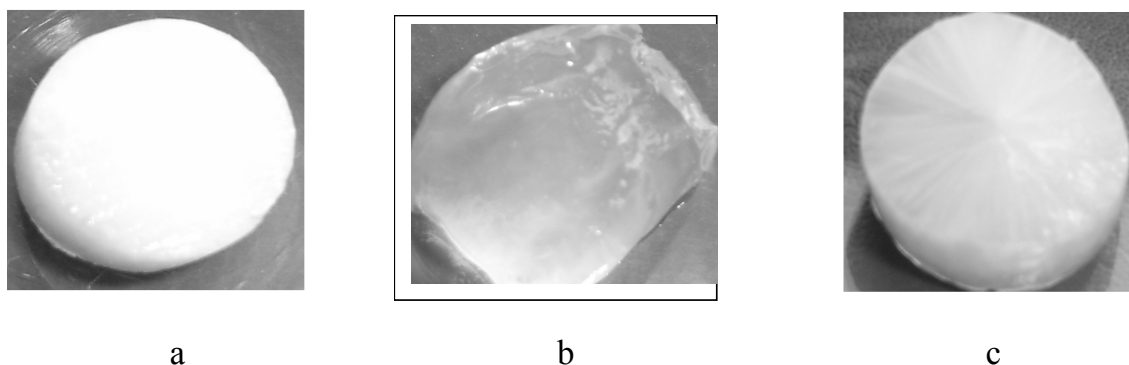


Figure 1. The PVA hydrogel obtained by different techniques: a) repeated freez-twaing (-15 : 24 °C) cycles, b)  $\beta$  irradiation, c) repeated freeze and thawing cycles in liquid nitrogen

### 2.3. Swelling properties

To determine the influence of the obtaining hydrogels techniques on the amount of water absorbed by the hydrogel, samples were weight and immersed in distilled water. The degree of water absorption was determined at several moments in time and was calculated using following formula:

$$S(\%) = \frac{m_f - m_i}{m_i} \cdot 100 \quad (1)$$

Where S (%) is the amount of absorbed water,  $m_f$ -is the mass of swollen gel at time t, and  $m_i$ - is the mass of the dry gel at the initial time.

## 3 Results and discussions

In Tables 1, 2 and 3, the obtained data for three types of PVA hydrogels level of water absorption are presented.

Table1. The equilibrium (%) swelling of PVA-HG obtained through different cycles of freezing (F-T) and thawing in liquid nitrogen technique

Time (min)	Freezing and thawing in liquid nitrogen techniques		
	1 cycle of F-T	2 cycles of F-T	3 cycles of F-T
	Water absorption (%)		
0	557.54	557.44	557.54
5	579.58	564.63	567.67
10	591.32	569.14	574.13
25	610.01	573.52	580.2
35	617.93	575.90	587.31
60	633.98	582.36	592.76
120	650.21	585.36	599.15
240	669.86	588.16	601.91
360	681.76	560.65	607.72
1440	699.95	557.64	587.86
2880	693.58	556.61	571.34
4320	678.92	555.65	566.407
5760	657.62	546.40	561.57
7200	642.54	544.98	558.81
8640	633.23	542.43	554.65

Table2. The equilibrium (%) swelling of PVA-HG obtained by freezing and thawing technique (F-T)

Time (min)	Freezing and thawing techniques
	Water absorption (%)
0	456.32
15	484.99
30	506.28
60	512.57
90	516.41
120	518.56
150	524.18
180	522.76
210	527.14
240	531.19
270	529.93
300	531.35
330	530.23
360	533.95
3720	544.19
5160	535.73

Table1. The equilibrium (%) swelling of PVA-HG obtained by  $\beta$ -irradiation technique

Time (min)	$\beta$ - irradiation techniques	
	10.7 kGy dose	47.25 kGy dose
	Water absorption (%)	
0	603.82	527.095
15	616.45	589.82
45	680.38	598.50
105	755.97	630.53
165	843.63	660.18
1440	1216.14	693.86
2880	1395.45	699.40
3720	1493.01	715.56
5160	1554.54	710.33
9480	1577.26	711.67

The amount of water absorbed by three types of hydrogels is shown in the Figure 2.

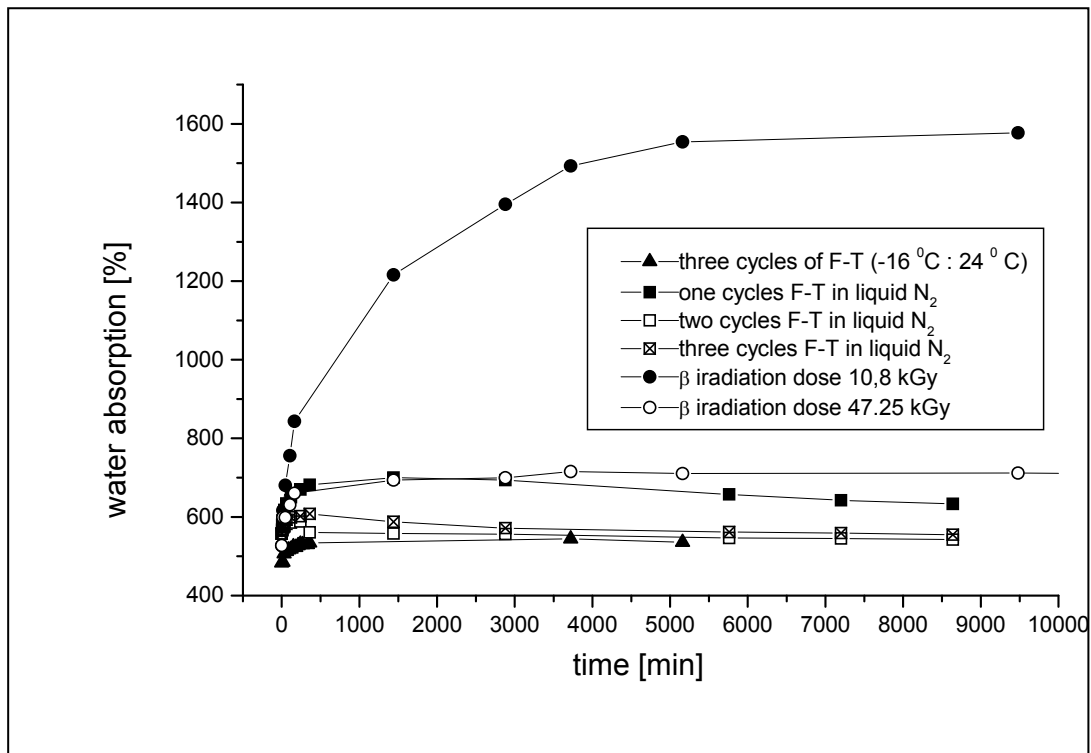


Figure 2. Water absorption in different types of PVA hydrogels

The figure 2 shows that the amount of water absorbed depends on the dose of irradiation that the hydrogels were exposed to. Increasing of the irradiation dose determines a lower absorption level. This is the results of a stronger crosslinking. The amount of water increases with the contact time increase. The swelling equilibrium was reached after approx. 1000 minutes for the higher crosslinked gels and after approx. 5000 minutes for weaker crosslinked ones. The PVA hydrogels obtained in liquid nitrogen have an absorption rate higher than these obtained by freeze and thawing methods. This is because of the size pores within the hydrogel.

The swelling equilibrium for the freeze and thawing techniques was obtained after 500 minutes. This fact pointing that these hydrogels have a higher permeability than those obtained by irradiation. The cause of this fact could be the porous structure of cryogels. The higher number of pores of the hydrogels obtained in liquid nitrogen determines a higher water absorption capacity than that of the hydrogel obtained by freeze and thawing method. The graphical representation shows that not only the crosslinking degree influences the hydrogels water absorption but also the pores dimensions.

#### 4.Conclusions

Different types of PVA hydrogels have been obtained by using three techniques. These hydrogels have different structures. The PVA hydrogels obtained by freezing and thawing techniques are white-opaque (demonstrating an obvious phase

separation), heterogeneous, with high dimension pores and with a good mechanical strength. The hydrogels obtained by  $\beta$ -irradiation technique are quite transparent, that means a more homogeneous structure. The mechanical strength depends on the irradiation dose. The hydrogels obtained by using the liquid nitrogen are white-opaque, that means a heterogeneous structure, but the pores are uniformly disposed in a radial structure and they have smaller size.

Structure differences of hydrogels influence the water absorption capacity. For the hydrogel obtained by irradiation techniques, the amount of water retained is influenced by the level of irradiation. In the case of the PVA hydrogels obtained by freeze and thawing method, water absorption is influenced by the size of the pores.

Comparing the water retaining capacity of the gels obtained by the three above mentioned techniques, it can be noticed that the highest retained amount of water has been evidenced by the irradiated gel. The draw backs of the irradiation technique are: the high price of the necessary equipment, the obtaining of intermolecular C-C bonds that make

PVA hydrogels less biodegradable and the possibilities of polymer degradation during the irradiation. That means, using freezing and thawing method, is more indicated in the hydrogels obtaining. This method eliminates the disadvantages of irradiation technique and makes it applicable in different activity areas.

Received May 5 2005

The "Transilvania" University from Brasov

#### REFERENCES

- 1.S. Pațachia, Cap.8. Blends based on poly(vinyl alcohol) and the products based on this polymer în "Handbook of Polymer blends and composites" Edited by C. Vasile and A.K. Kulshreshtha, RAPRA Technology LTD., England, p. 288-365, ISBN 1-85957-304-5, 2003
- 2.Poly(vinyl alcohol), Technical Book, Rasnov, 1979
- 3.S.Pațachia, C. Corboș, *Study on obtaining poly(vinyl alcohol) hydrogel*, Bulletin of the "Transilvania" University of Brașov, Vol. 9(44)- New Series, Series B, ISSN 1223-964X, , 2002
- 4.Christie M. Hassan, Nikolaos A. Peppas, Structure and Applications of Poly(vinyl alcohol) Hydrogels Produced by Conventional Crosslinking or by Freezing/Thawing Methods, Advances in Polymer Science, Vol.153, 2000
5. Rebecca Hernandez, Aurelie Sarafian, Daniel Lopez, Carmen Mijangos, Viscoelastic properties of poly(vinyl alcohol) hydrogels and ferrogels obtained through freezing-thawing cycles, Polymer 46, 5543-5549, 2004
6. Alla S. Hickey and Nikolaos A. Peppas, Solute diffusion in poly(vinyl alcohol)/poly(acrylic acid) composites membranes prepared by freezing/thawing techniques, Polymer Volume 38 Number 24 1997
7. W.E. Hennink, C.F. van Nostrum, Novel crosslinking methods to design hydrogels, Advanced Drug Delivery Reviews 54, 13-36, 2002

#### EFFECTUL MICROSTRUCTURII HIDROGELURILOR DE PVA ASUPRA ABSORBȚIILOR DE APA.

##### (Rezumat)

În această lucrare se prezintă studiul influenței microstructurii hidrogelurilor de PVA obținute prin diferite tehnici, asupra capacității lor de gonflare în apă. Hidrogelurile de PVA au fost obținute prin trei tehnici diferite de reticulare: cicluri repetate de îngheț (în azot lichid și la temperatura de  $-15\text{ }^{\circ}\text{C}$ )-dezgheț (la temperatura camerei:  $25\text{ }^{\circ}\text{C}$ ) și iradiere cu radiații  $\beta$ . Metoda de obținere a hidrogelurilor influențează morfologia acestora. Cinetica absorbțiilor de apă a fost determinată prin metoda gravimetrică. S-a studiat corelația dintre

microstructure hidrogelului si capacitatea sa de a absorbi apa. Acest studiu este important pentru selectarea metodei optime de obtinere a hidrogelurilor de PVA in vederea sintezei de noi materiale cu o capacitate controlata de absorbtie de apa.

## PVA HYDROGELS AS INTELLIGENT MATERIALS

BY

SILVIA PATACHIA and MARIA MICLAUS

**Abstract** Poly(vinyl alcohol) [PVA] hydrogels have the capacity to react to the environmental modification, that means intelligence. One of these environmental changes could be the electrolyte concentration. Immersed in salts aqueous solutions, PVA hydrogels shrank and an important modification of the sample's weight, volume, density and mechanical properties could be noticed. These changes could be reversible, when only a physical interaction between the hydrogel and the electrolyte takes place, or irreversible when a chemical reaction is produced. The aim of this paper is to study the behavior of the PVA hydrogel, obtained by repeated cycles of freezing and thawing, in sodium and potassium chloride aqueous solutions.. The influence of the salts concentration and nature on the hydrogel weight, volume and density changes has been determined. The results of this study could be used to obtain new sensors for electrolytes presence and nature, in aqueous solution.

**Keywords:** intelligent materials, poly(vinyl alcohol), hydrogel, electrolyte, sorption

### 1. Introduction

Intelligent materials have as a basic characteristic to react upon the environmental changes through modifying one or many of its own characteristics.

Hydrogels are intelligent materials, tri-dimensional polymeric network with huge absorbing water capacity, without solving themselves.

PVA is a polymer that can generate hydrogels through chemical or physical crosslinking [1, 2, 3,6].

From the ecological point of view physical crosslinking maintains the biodegrading of PVA and avoids the usage of the crosslinkers which are generally toxic and cancerous dialdehydes [1,2,6].

Hydrogels are intelligent materials because by immerging them with electrolytes solutions they change their mass, volume and density through eliminating a huge quantity of water which was initially absorbed in hydrogel [1]. Thus, PVA hydrogels can be used as electrolytes sensors.

The present work has as its main purpose to quantify the mass modifications of the hydrogel samples in the presence of NaCl and KCl aqueous solutions, due to the influence of the solution concentration upon the hydrogel contraction.

It was also been studied the reversibility grade of this phenomenon and the hydrogel capacity to keep in its structure a quantity of electrolyte. The distribution of the electrolyte between the hydrogel and the aqueous solution is important for studying the diffusing phenomenon of the electrolyte through hydrogel membranes, the constant of repartition that enters the calculation of the diffusing coefficient  $D_f = P / K$ , where  $D_f$

is the coefficient of diffusion; P is the coefficient of the membrane permeability; K is the repartition coefficient of the electrolyte between hydrogel and the aqueous phase [6].

## 2 The experimental part

### 2.1. Materials

A. The PVA hydrogel has been obtained from 90 – 98 PVA (the polymerization degree 900, hydrolyze degree 98%) got from The Chemical Plant Râșnov, industrial purity with no further purification.

The PVA powder was solved into magnetically stirred distilled water for 3 hours at 80°C getting a solution with the concentration in solid matter (CS = 11,14 %).

The solution obtained in this way was cooled and introduced in PVC cylindrical containers having a diameter of  $d = 1,80$  cm. Then the solution was three successive freezing cycled (at -15°C) and three successive defreezing cycled (at room temperature), each stage lasting 12 hours. So, we got a hydrogel mass with a good mechanical resistance, white, opaque which proves a heterogeneous structure.

B. Two electrolytes (KCl and NaCl) of p.a. purity have been used, to obtain solutions with 1M, 2M, 3M concentrations by solving the necessary quantities in distilled water.

### 2.2. Methods of study

#### 2.2.1 *The study of the desorption equilibrium*

It has been used two types of samples (some of small dimensions  $\sim 5 \cdot 6 \cdot 10^{-2}$  g; others of big dimensions  $\sim 9 - 11 \cdot 10^{-2}$  g) prevailed from the hydrogel mass and immersed in distilled water for 14 days, a period when the hydrogel reached the swollen equilibrium.

To study the water desorption phenomenon in electrolyte solutions presence, each sample was immersed into 100 ml of electrolyte solution with a concentration of 1M, 2M and 3M, respectively. The samples were taken from time to time and weighed with an analytical balance with a precision of  $10^{-4}$  g. The mass variation was graphically represented in relation with the time.

#### 2.2.2 *The study of the reversibility of the water absorption process in hydrogel*

After 48 hours of immersing into the solution of electrolyte the samples of hydrogel have been slightly wip and introduced into 100 ml of distilled water. At different intervals of time samples were taken out and weighed in order to determine the water re-absorption kinetics.

## 3. Experimental data. Discussions

The mass modifications of the immersed hydrogel samples into the NaCl and KCl electrolytic solutions with concentrations of 1M, 2M and 3M with regard of time are presented in figures 1, 2 and 3.

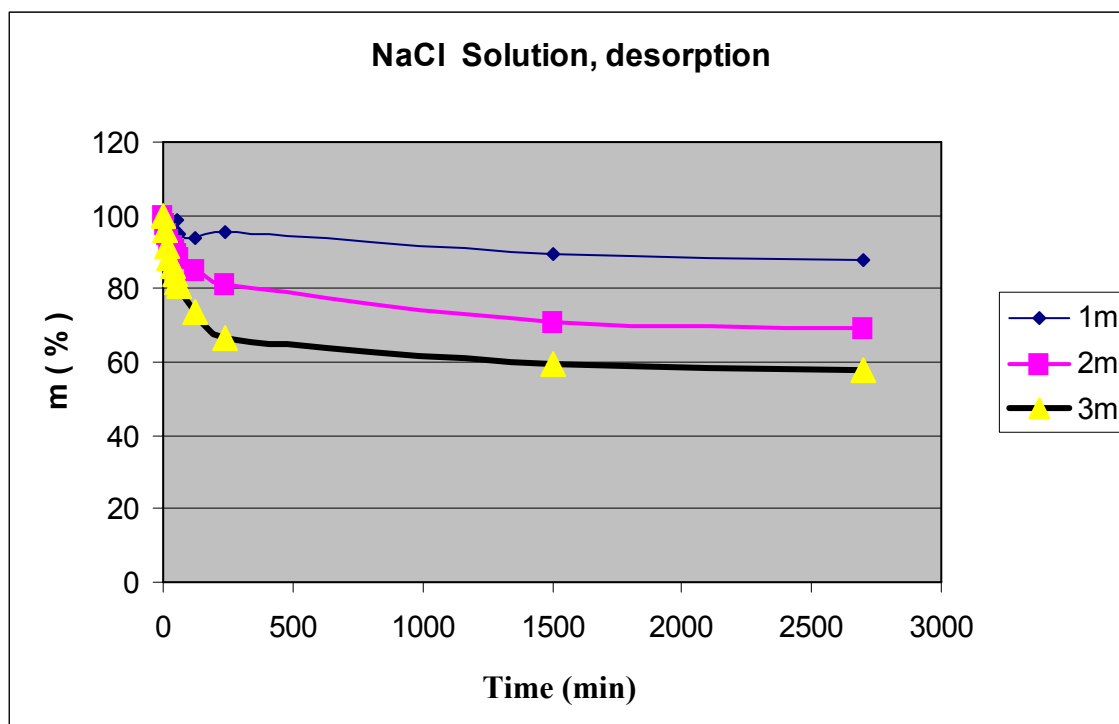


Fig.1. The influence of the NaCl solutions concentration on the hydrogel mass changes.

It can be easily observed that in the presence of the NaCl aqueous solution the hydrogel samples diminish their mass because of the elimination of a certain quantity of water. After 500 minutes the water mass eliminations become smaller, till approximately 1500 minutes at equilibrium state.

Once the NaCl concentration increases we can see an increasing loss of mass reaching to the following situation: when immersing into 3M solution the sample modifies its mass by 60%. This thing reveals the PVA hydrogel special sensitivity in the presence of NaCl.

In fig. 2 and 3 the mass modification of the PVA hydrogel samples in the presence of KCl is shown.

There have been used both big and small samples, for which the influence of the electrolyte concentration in the solution upon the hydrogel mass modifications were tested.

The conclusion is that in both cases the hydrogel sample mass variations regarding mass to time are similar; the diminishing of the hydrogel mass being bigger for more concentrated solutions.

The dimension of the samples has not an important influence upon the desorption phenomenon, it can vary with less that 6% between the mass diminishing for the hydrogel samples, regarding their dimensions.

From figure 4 it can be seen that a higher concentration of the initial immersion solution of electrolyte, determines higher hydrogel mass decreasing. The dependence of the hydrogel mass lost versus the initial immersion electrolyte solution concentration is quite linearly.

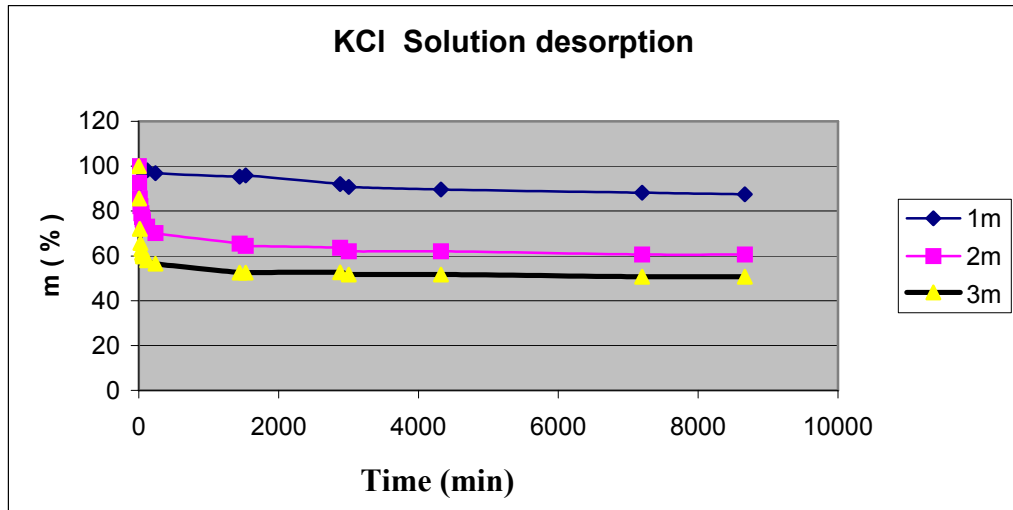


Fig.2. The influence of the KCl solutions concentration on the mass changes of the small hydrogel samples versus time

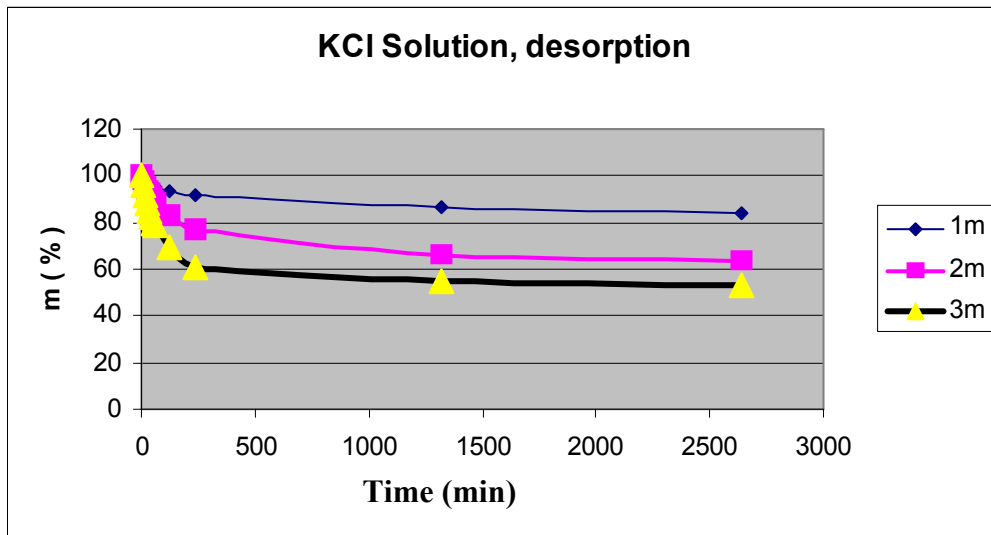


Fig. 3. The influence of the KCl solutions concentration on the mass changes of the big hydrogel samples versus time

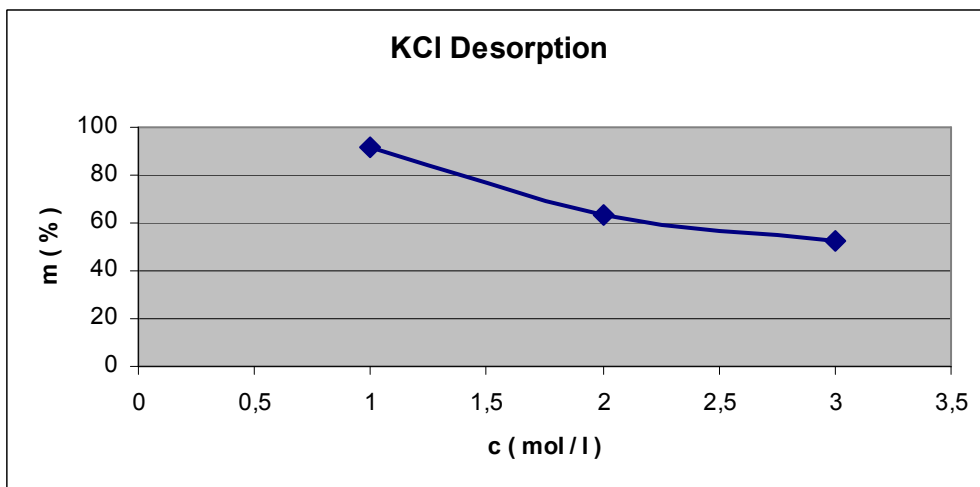


Fig. 4. The influence of the KCl solutions concentration on the hydrogel mass changing

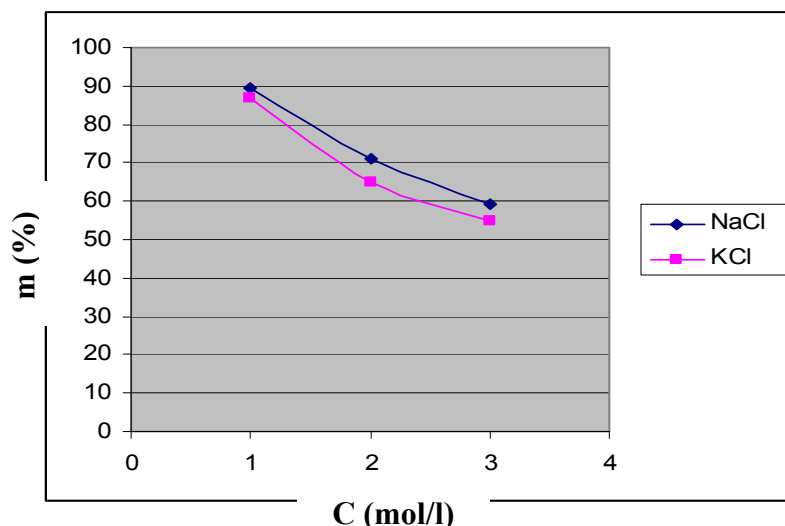


Fig. 5. Water desorption from the PVA hydrogels in function of the type and concentration of the electrolyte in aqueous solutions

In Fig. 5 there is represented the decreasing of hydrogel mass regarding the electrolyte concentration into the solution, in case of big samples, at a prestablished time (1440 min). There is no sign of essential difference concerning the desorption phenomenon regarding the nature of the cation and the addition of hydrogel mass variation regarding the concentration of the solution of the electrolyte can be considered steady (linearly) and decreasing.

In Figures 6 and 7 we illustrated the coming back of the initially swell balance, after the immersion into distilled water of the contracted samples under the influence of the electrolytes. It can be observed that the contracted samples reabsorb water that put into evidence the increasing of their mass until they reach the equilibrium, no matter what the nature of the electrolyte in which the samples were initially immersed for contracting. The observation is that the more the concentration of the electrolyte solution is, the slower the reaching of the equilibrium is. And the smaller the initial concentration of the electrolyte was, the higher the percentage of swelling is.

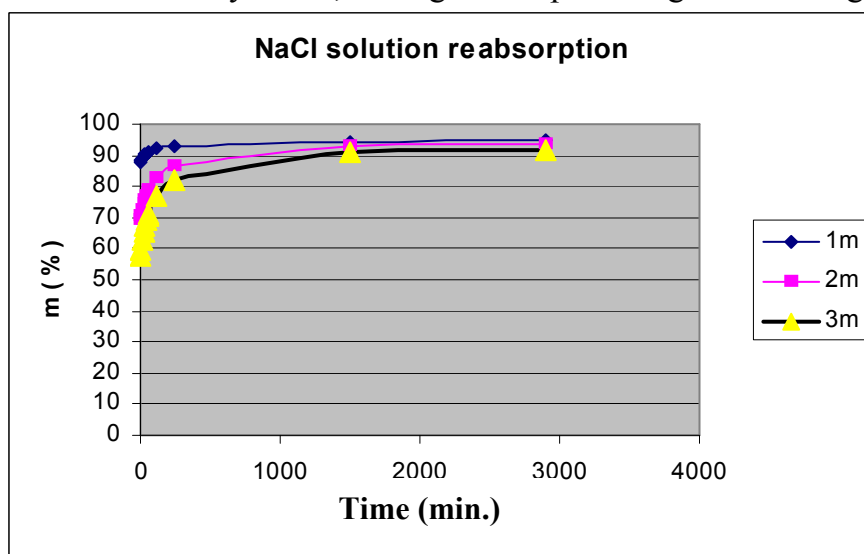


Fig. 6. Water reabsorption in contracted hydrogels, initial immersed in NaCl solutions, versus the electrolyte concentration

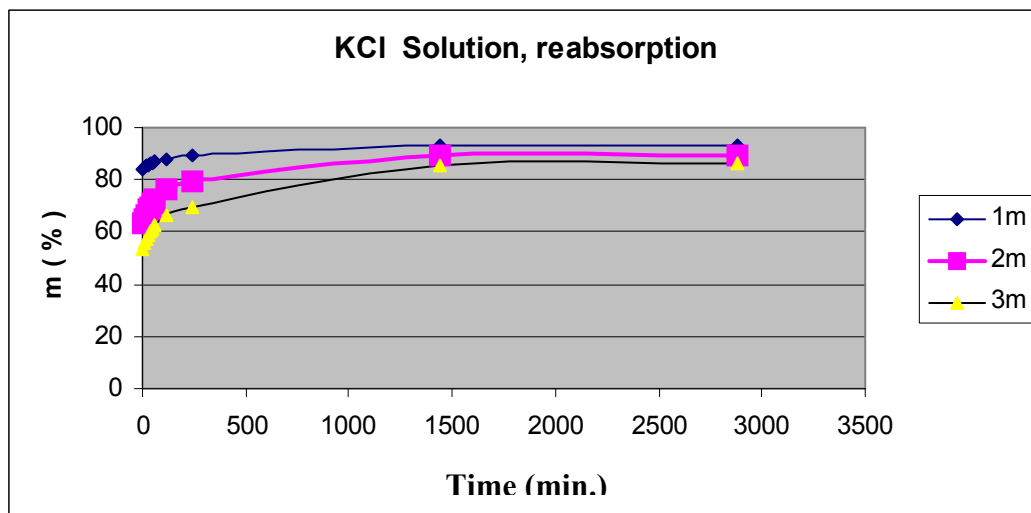


Fig.7. Water reabsorption in contracted hydrogels, initial immersed in KCl solutions, versus the electrolyte concentration

In conclusion, both in NaCl and in KCl case the coming back to the initial equilibrium of swelling is not total. Comparing the results obtained we draw to the conclusion that in the sample immersed into NaCl solution case, the coming back to the initial balance was at a smaller difference of 8% while in the samples immersed into KCl solutions the difference between the initial and the coming back stage was approximately 15%. This can be explained by the fact that KCl is well known for being able to break up the H bonds between the system components. So, that can break up the H bonds between the H<sub>2</sub>O molecules and the polymer molecules, producing a more powerful interaction between these ions (K<sup>+</sup>) and the PVA macromolecule. The Na<sup>+</sup> cations interact less with the polymer already involved in H bonds with H<sub>2</sub>O molecules, so it is less kept into the hydrogel structure. At re-immersing the samples into the water, the quantity of electrolyte kept into hydrogel structure will diffuse. The more concentrated the electrolyte solution will be obtained when diffusing them into the water, the more the quantity of kept in ions is bigger. This solution will determine the maintenance of the hydrogel into the contracted state, not permitting to it in the coming back to the initial equilibrium swelling state.

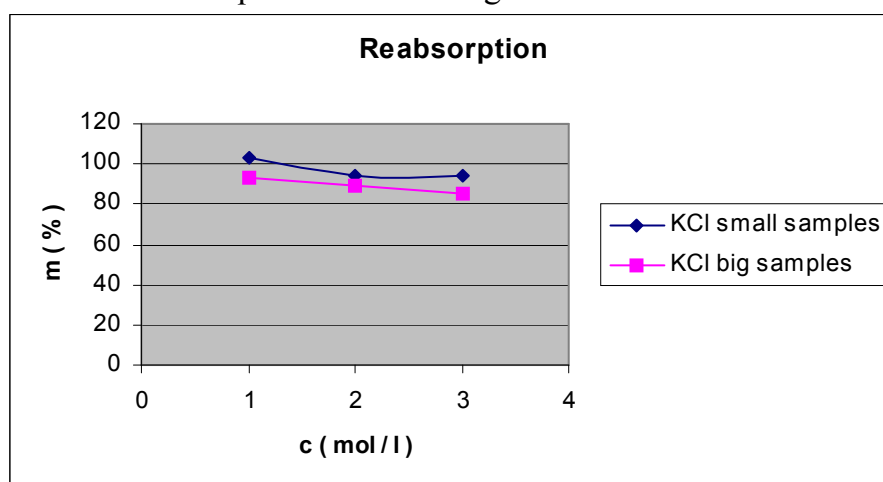


Fig. 8 The influence of the initial immersion solution concentration on the water re-absorption, for different hydrogel samples sizes.

From Fig. 8 it can be seen that big hydrogel samples, with a greater capacity of electrolyte absorption will determine, by electrolyte desorption, a more concentrated electrolyte solutions at their immersing in water. As consequence their dimensions will remain smaller compared to these of the small samples hydrogel.

From figure 9 it can be seen that the dimensions of hydrogel samples, initial immersed in KCl solution, can't attain the initial swelling equilibrium because of the higher amount of salt desorbed. That means a higher amount of KCl retained in the hydrogel structure, due to the higher interaction between  $K^+$  and PVA compared to this of  $Na^+$  ions.

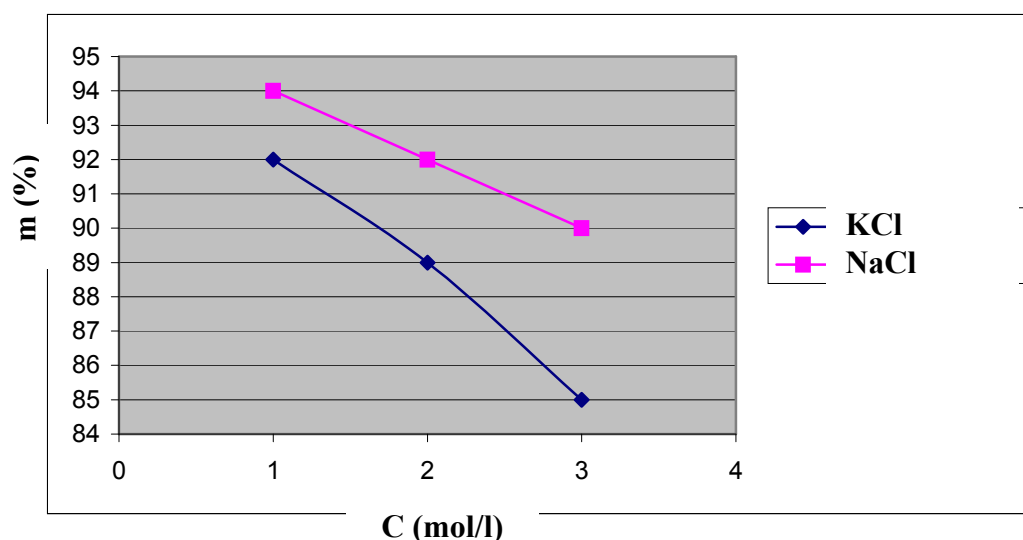


Fig.9. The influence of the initial immersion solution concentration on the water re-absorption in hydrogel, for different electrolyte types.

#### 4. Conclusions

Due to experimental determinations we can conclude the following:

- PVA hydrogels obtained by freezing-thawing method show a significant mechanical active behavior: its swell, at their immersion in water and shrink, at their immersion in NaCl or KCl solution.
- The hydrogels shrinkage is determined by water elimination from the hydrogel network;
- The loss in the mass of the hydrogel was higher when it was immersed in more concentrated solutions of NaCl or KCl.
- An approximate linear dependence between the hydrogel mass loss and the electrolyte concentration has been evidenced.
- The hydrogel changes in mass do not depend essentially on the hydrogel sample dimensions;
- The hydrogel changes in mass do not depend essentially on the cation nature;
- The equilibrium of water desorption has been reached after approximately 250 minutes;
- The water desorption is reversible;

- Considering the concentration of the solutions obtained by electrolyte desorption from the hydrogel, it could be concluded that  $K^+$  ions were strongly retained in the hydrogel network due to their higher interaction with PVA compared with  $Na^+$  ions.
- The higher concentration of the KCl solution obtained by salt desorption from the hydrogel led to the impossibility of the hydrogel to reach the initial swelling equilibrium.
- This behavior of the PVA hydrogels could be used for electrolyte sensors.

Received May 5 2005

The "Transilvania" University from Brasov

## REFERENCES

1. S. Pațachia, Cap.8. Blends based on poly(vinyl alcohol) and the products based on this polymer in "Handbook of Polymer blends and composites" Edited by C. Vasile and A.K. Kulshreshtha, RAPRA Technology LTD., England, p. 288-365, ISBN 1-85957-304-5, 2003
2. S. Pațachia, C. Corboș, *Study on obtaining poly(vinyl alcohol) hydrogel*, Bulletin of the "Transilvania" University of Brașov, Vol. 9(44)- New Series, Series B, ISSN 1223-964X, , 2002
3. Christie M. Hassan, Nikolaos A. Peppas, Structure and Applications of Poly(vinyl alcohol) Hydrogels Produced by Conventional Crosslinking or by Freezing/Thawing Methods, *Advances in Polymer Science*, Vol.153, 2000
4. Rebecca Hernandez, Aurelie Sarafian, Daniel Lopez, Carmen Mijangos, Viscoelastic properties of poly(vinyl alcohol) hydrogels and ferrogels obtained through freezing-thawing cycles, *Polymer* 46, 5543-5549, 2004
5. Alla S. Hickey and Nikolaos A. Peppas, Solute diffusion in poly(vinyl alcohol)/poly(acrylic acid) composites membranes prepared by freezing/thawing techniques, *Polymer* Volume 38 Number 24 1997
6. W.E. Hennink, C.F. van Nostrum, Novel crosslinking methods to design hydrogels, *Advanced Drug Delivery Reviews* 54, 13-36, 2002

## HIDROGELURILE DE PVA CA MATERIALE INTELIGENTE

### (Rezumat)

Hidrogelurile de poli(alcool vinilic) au capacitatea de a reacționa la modificările mediului înconjurător, ceea ce poate fi interpretat ca un comportament inteligent. Un tip de modificare a mediului poate fi schimbarea concentrației de electroliti. Hidrogelurile de PVA, la imersare în soluții de electroliti elimină apa din rețeaua tridimensională și se contractă evidențiind modificări importante ale masei, volumului și densității. Aceste modificări pot fi reversibile, când între hidrogel și electrolit nu se produc reacții chimice și ireversibile când acestea au loc. Scopul acestei lucrări este studierea comportamentului hidrogelurilor de PVA obținute prin metoda ciclurilor repetate de îngheț-dezghet, în prezența soluțiilor apoase de clorură de sodiu respectiv potasiu. S-a determinat influența naturii cationului și concentrației sării asupra modificărilor de masă ale hidrogelului, ca și reversibilitatea procesului de contractie. Rezultatele acestui studiu pot fi aplicate în obținerea unor noi senzori de electroliti.

## **BIOLOGICAL MATERIALS AS SOLUTION FOR WATER DEPOLLUTION**

**BY**

**SILVIA PATACHIA and MIHAELA VOINEA**

**Abstract** In this paper part of our recent analyses in the de-pollution of contaminated waste waters with chromium (III) ions is reported. In the last years, a special attention has been given to find more effective methods for de-pollution of contaminated waste waters loaded with a considerable amount of heavy metals. This report is focused in two main directions: testing of the bioaccumulation capacity of dried *Azolla Caroliniana* Wild fern and obtaining a new composite material by inserting the dry fern particles in a matrix of poly(vinyl alcohol) hydrogel [PVA-HG]. The capacity of this composite material to retain the chromium (III) ions from waste water was tested. The inserting of dry fern particles in a polymer matrix has been made in order to avoid the difficulties of very fine dispersed particles of fern separation by filtration from purified water and to regenerate the biological material that could be use in other purification processes.

**Keywords:** *Azolla Caroliniana*, poly(vinyl alcohol), hydrogel, PVA-HG, chromium (III).

### **1. Introduction**

There are very well known a series of biotechnologically environmental protection methods which taking advantage of the ability of plants to adapt to different life conditions in polluted environments.

The human impact on natural systems is becoming heavier and heavier in both technologically advanced and developing countries. Some of the resulting pollution problems are at global scale, giving rise to measure modifications in the air, water, soils, and living organisms, the long-term effects of which are un-known[1].

Biosorption, the process of passive cations binding by dead or living biomass, represents a potentially consecutive way of removing toxic metals from industrial wastewaters (Volesky, 1990). Biosorption could be employed most actively in a concentration range below  $100\text{mg L}^{-1}$ , where other techniques are inactive or costly (Schiewer and Volesky, 1995).

Metal ion binding during biosorption processes has been found to involve complex mechanism, such as ion-exchange, complexation, electrostatic attraction and microprecipitation (Volesky and Holan, 1995).

There have been some indications that ion-exchange plays an important role in metal sorption by algal biomass (Volesky et al., 2000). Although numerous papers on the metal–microorganism interactions are available in the literature, still large uncertainties exist. Biosorbents are complex and variable materials.

The composition of cell wall, to which metal ions are bound, depends not only on biosorbent species, but also on environmental conditions of its growth.

The heavy metals assure the normal course of many biological processes that have vital importance for human body. Some of them are:

a) heavy metals - copper, cobalt, iron, manganese, molybdenum, zinc and very small quantities of chromium, vanadium, nickel and lead;

b) light metals - calcium, magnesium, and sodium.

It is impossible to make a perfect separation between toxic, non-toxic, or neutral metals. This statistic separation could be inaccurate and it could provide many errors, because all metals are necessary for life but they become toxic at high concentration.

The differences between concentration ranges in which the metals are usefully or toxic for the life could be very small. Because of this reason, we have to know exactly the limit between the toxic and non-toxic concentration.

Chromium occurs mainly in three forms: metallic chromium Cr(0) is a steel-grey, trivalent chromium Cr(III) and hexavalent chromium Cr(VI) which are produced industrially. These forms of chromium have proven to have the most serious effects on environmental systems and health concerns. Of the various forms of chromium, Cr(VI) is the most toxic one.

There are a series of known tests which had been done in order to evaluate the toxicity of chromium substances to human, in this case a mammal was selected (e.g. rat, mouse, guinea pig, or non-human primate). For evaluating of effects in aquatic environment, fish, crustaceans, mollusks, and algae was selected [1,4].

The aim of this study is to present an alternative possibility for chromium (III) ions retention using the *Azolla Caroliniana* fern inserted in a matrix of poly(vinyl alcohol) hydrogel [PVA-HG]. The PVA hydrogel, is a non-toxic, non-carcinogenic biodegradable, biocompatible, and non-toxic material (Patachia 2003) [3].

The outstanding properties of PVA make it versatile for its following broad industrial uses: as a binder in adhesive formulations, in textile sizing, as an emulsion polymerization aid.

Other diverse applications are: as joint cement for building construction, water soluble film for hospital-laundry bags, emulsifiers in cosmetics, temporary protective film, soil binding to prevent erosion, intermediate in the production of polyvinyl butyral, adhesive interlayer in laminated safety glass, polyvinyl alcohol fibre [2], etc.

## 2. Materials and methods

*Poly(vinyl alcohol) [PVA 90-98]* with 900 polymerization degree and 98% hydrolysis degree, Risnov industrial grades without further purification has been used to obtain the PVA aqueous solution by 18% concentration. The solution has been obtained by stirring the pre-weighted PVA powder gradually introduced in distilled water at 80 °C, for 3 hours. The PVA solution will be used to obtain the matrix of composite material.

*Azolla Caroliniana Wild fern* has been dried and use in two forms: untreated and treated with nitric acid in order to eliminate the cations eventually retained in its structure.

*Composite material obtaining* involved preparing a mixture containing 2.5 ml hydrogel (PVA) and 0.0500 mg *Azolla Caroliniana* (either treated or untreated with nitric acid). It was inserted in tubes of 0.5 mm then immersed in liquid nitrogen in

order to rich the  $-198^{\circ}\text{C}$ . After one hour the content of the tube was removed and thawed at room temperature.

The retaining capacity of dry fern and composite material has been determined by its insertion into 25 ml chromium (III) aqueous solution  $C = 1.6 \text{ mg/L}$ . The contact period was one hour, and then chromium concentration was measured using a Unicam AAS Solaar 969 Atomic Absorption (AA) Spectrometer with air-acetylene flame at  $357.9 \text{ nm}$  and a measurement time of 4 seconds.

### 3. Experimental data and discussions

The experiments performed were intended to evaluate the ability of *Azolla Caroliniana* Wild. (Azollaceae) species to retain chromium (III) ions from aqueous solutions containing a well-defined concentration of the metal ion, while it is immersed in a matrix of poly(vinyl alcohol) (PVA).

The results presented in Table 1, shows the amount and the percent of chromium (III) ions absorbed by *Azolla Caroliniana* either treated and untreated with nitric acid ( $\text{HNO}_3$ ) solution after a measure contact period 10, 15 and 30 min, respectively at constant room temperature ( $20^{\circ}\text{C}$ ).

Table 1. Amount of  $\text{Cr}^{3+}$  absorbed by *Azolla Caroliniana* either treated or untreated with nitric acid ( $\text{HNO}_3$ ) solution.

No.	Time (min)	Biomass <i>Azolla</i> (mg)	Absorbed $\text{Cr}^{3+}$ (treated $\text{HNO}_3$ )		Absorbed $\text{Cr}^{3+}$ (untreated $\text{HNO}_3$ )	
			(mg $\text{Cr}^{3+}$ )	% $\text{Cr}^{3+}$	(mg $\text{Cr}^{3+}$ )	% $\text{Cr}^{3+}$
1	10	0.0501	0.0366	91.50	0.0379	94.89
2	15	0.0508	0.0367	91.75	0.0376	94.00
3	30	0.0505	0.038	95.00	0.0374	93.56

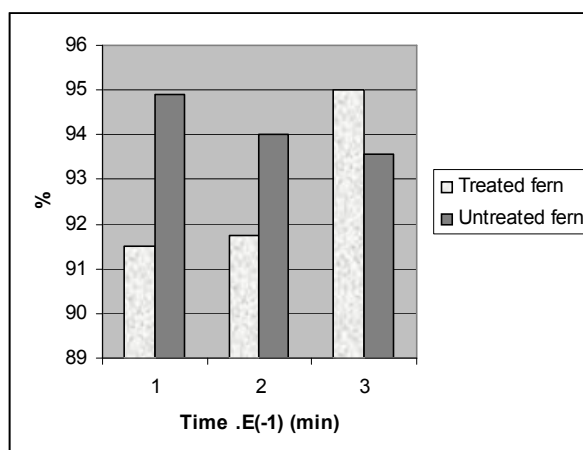


Figure 1. The amount of absorbed chromium ions versus the contact time of *Azolla Caroliniana* with aqueous solution

Figure 1 shows, that the dried-up *Azolla Caroliniana* is effective accumulator for chromium (III) ions. The percentage of chromium ions retained is higher than 91%. The retention time is very short with about 30 minutes.

The Table 2 shows that dried *Azolla Caroliniana* untreated with a nitric solution – inserted into a matrix of PVA hydrogel at  $-198\text{ }^{\circ}\text{C}$  (liquid nitrogen) is effective in chromium (III) bioaccumulation. The retained chromium ions are higher than 91%. The studied retention time within this experiment is 60 minutes.

Table 2. The amount of  $\text{Cr}^{3+}$  absorbed by *Azolla Caroliniana* untreated with nitric acid inserted into a PVA hydrogel matrix.

No.	Biomass Azolla (mg)	$C_{\text{fin}}$ (mg/l)	$C_{\text{abs}}=C_{\text{ini}}-C_{\text{fin}}$ (mg/l)	Absorbed $\text{Cr}^{3+}$	
				(mg)	% $\text{Cr}^{3+}$
1.	0.0500	0.1392	1.4608	0.0365	91.25

The Table 3 show that dried *Azolla Caroliniana* treated with a solution of nitric acid – inserted into a matrix of PVA hydrogel at  $-198\text{ }^{\circ}\text{C}$  (liquid nitrogen) is also very effective in chromium (III) bioaccumulation. The retained amount of chromium ions are higher than 91%. The studied retention time within this experiment is 60 minutes.

Table 3. The amount of  $\text{Cr}^{3+}$  absorbed by *Azolla Caroliniana* untreated with nitric acid immersed into a PVA hydrogel.

No.	Biomass Azolla (mg)	$C_{\text{fin}}$ (mg/l)	$C_{\text{abs}}=C_{\text{ini}}-C_{\text{fin}}$ (mg/l $\text{Cr}^{3+}$ )	Absorbed $\text{Cr}^{3+}$	
				(mg $\text{Cr}^{3+}$ )	% $\text{Cr}^{3+}$
1	0.050	0.1352	1.4648	0.0366	91.50

#### 4. Conclusions

This study confirmed that *Azolla Caroliniana* Wild fern, which is known as an effective bioaccumulator in living state, is effective also in dry state (higher than 91%).

The treatment with nitric acid determined the obtaining of higher mechanical resistant fern particles with higher size.

No important modification in bioaccumulation capacity of fern has been evidenced by its treatment with nitric acid.

The use of *Azolla Caroliniana* dry fern in water depollution avoid the problems of plant acclimatization in different climate conditions or polluted water characteristics and the water re-pollution by toxics delivery from died fern maintained in water.

The insertion of dried fern in a polymeric matrix avoids the fern particles mechanical degrading and permits the bioaccumulating material regeneration and it's reworking, determined the effectiveness of this advanced cleaning waste water.

Taking into account the non-toxicity and biodegradability of PVA, this depollution method is an ecological one.

**REFERENCES**

1. Eros Bacci, Ecotoxicology Katarzyna Chojnacka , Andrzej Chojnacki, Helena Go´recka, Biosorption of Cr<sup>3+</sup>, Cd<sup>2+</sup> and Cu<sup>2+</sup> ions by blue–green algae *Spirulina* sp.: kinetics, equilibrium and the mechanism of the process, *Chemosphere* 59, 75-84, 2005
2. Trieu, Hai Hong., The processing/structure/property relationships of polyvinyl alcohol hydrogels, Case Western Reserve University, Chemical Engineering, 1995, Syed Qutubuddin, pages 222p.
3. S. Paṭachia, Cap.8. Blends based on poly(vinyl alcohol) and the products based on this polymer in “Handbook of Polymer blends and composites” Edited by C. Vasile and A.K. Kulshreshtha, RAPRA Technology LTD., England, p. 288-365, ISBN 1-85957-304-5, 2003
4. K.Popa and all, Removal of 60Co<sup>2+</sup> and 137Cs<sup>+</sup> ions from low radioactive solutions using *Azolla Caroliniana* Willd. water fern, *CEJC2*(2), 434-445, 2004

**MATERIALELE BIOLOGICE CA O SOLUTIE PENTRU DEPOLUAREA APEI****(Rezumat)**

In aceasta lucrare au fost studiate patru variante de materiale biologice din punctul de vedere al capacitatii lor de bioacumulare a ionilor de crom (III) din apele reziduale. S-a studiat *Azolla Caroliniana* Wild, o feriga acvatica, a carei capacitate de bioacumulare, in stare vie a fost evidentiata in literatura, in stare uscata, tratata si respectiv netratata cu acid azotic. In ambele variante, feriga uscata evidentiaza o capacitate ridicata de bioacumulare (retinand mai mult de 91% din cromul din apa). In scopul conservarii materialului biologic, al regenerarii lui si reutilizarii in alte procese de separare, *Azolla Caroliniana* Wild uscata a fost incastrata intr-o matrice de poli(alcool vinilic) obtinuta prin metoda criogenica. Materialul rezultat este biodegradabil si are o capacitate ridicata de retentie a ionilor de crom din apa (mai mare de 91%). Utilizarea acestui nou material compozit in procesele de purificare avansata a apelor reziduale este o solutie eficienta si ecologica.



## **POLY(VINYL ALCOHOL) HYDROGELS AS CONTROLLED DRUG DELIVERY SYSTEMS**

**BY**

**SILVIA PATACHIA and ECATERINA SAMOILA**

**Abstract** Controlled drug delivery systems are modern ways for diseases treatment. They ensure a prolonged and constant concentration of the drug in the ill body and as consequence a more effective use of the drug. Poly(vinyl alcohol) is a non toxic, non carcinogenic, biocompatible and biodegradable polymer. It is water soluble but could generate hydrogels (water insoluble structures) by physical or chemical methods of curing. In this paper, we studied the diffusion of diltiazem from PVA hydrogel pills obtained by two different techniques: freezing by immersion in liquid nitrogen and repeated freezing and thawing cycles. The diffusion parameters of diltiazem from the two types of matrices were determined and correlated with the PVA hydrogel matrix morphology, modified by changing the method of synthesis.

**Keywords:** poly(vinyl alcohol), diltiazem, drug delivery system

### **1. Introduction**

The Poly(vinyl alcohol) [PVA] is a hydrosoluble, biocompatible, biodegradable, non-toxic and non-carcinogenic polymer. Due to its structure, it can generate hydrogels through physical or chemical reticulations.

The physical reticulation eliminates the use of toxic and carcinogenic organic reticulants, and this is the reason why the PVA hydrogels obtained through freezing – defreezing cycles were tested as matrices for controlled release medicine.

The most frequently employed physical methods of reticulation are the ones that make use of  $\gamma$  and UV radiations. There is a series of disadvantages regarding their use:

- They generate covalent carbon-carbon bonds between the macromolecular chains, thus diminishing the biodegradability of the polymer
- It can simultaneously produce its degrading and that of the active substance sealed in hydrogel
- The irradiation method is expensive and it requires special work conditions due to its negative effect on the human body

In this paper, we propose the use of the freezing – defreezing alternating cycles in order to obtain PVA matrices that assure the controlled diffusion of a medicine. The employment of this method on a PVA solution generates a non-toxic and non-carcinogenic hydrogel with good biocompatibility, biodegradability [1] and with a considerable mechanical resistance.

The properties of the PVA gel depend on the concentration of the watery PVA solution, on the freezing temperature, time and speed as well as on the number of the freezing – defreezing cycles it is subject to [2].

By increasing the number of the freezing cycles, the mechanical resistance, the elasticity and the insolubility in water of the obtained gel are higher due to the increase in the number of bonds formed between the molecules [2].

Due to the previously enumerated properties, the PVA hydrogel can be used in the medical and pharmaceutical fields.

The use of the hydrogels as matrices in the controlled release medicine systems reduces the amount of active substance that is lost in the classical therapy, and it preserves a constant concentration of the medicine in the body for a longer period of time, consequently, it produces an increase of the treatment efficiency.

In this paper, we propose obtaining PVA matrices for the controlled release of the diltiazem hydrochloride, through two techniques of physical reticulation: the cryogenic reticulation through immersion in liquid nitrogen, respectively by applying certain alternating freezing ( $-29^{\circ}\text{C}$ ) – thawing ( $25^{\circ}\text{C}$ ) cycles.

The diffusion of the diltiazem hydrochloride was studied comparatively, by pinpointing the correlation between the parameters for obtaining the matrix, the morphology of the obtained gel and the diffusion of the active substance.

## 2. Experimental section

### 2.1. Materials

The 90-98 Poly(vinyl alcohol) [PVA] (900 polymerization degree and 98% hydrolysis degree) used was taken from Rasnov, Romania, and it wasn't previously purified.

The diltiazem hydrochloride (with the molecular formula  $\text{C}_{22}\text{H}_{26}\text{N}_2\text{O}_4\text{S}\cdot\text{HCl}$ , its structure being illustrated in Figure 1) was made available by Europharm Romania.

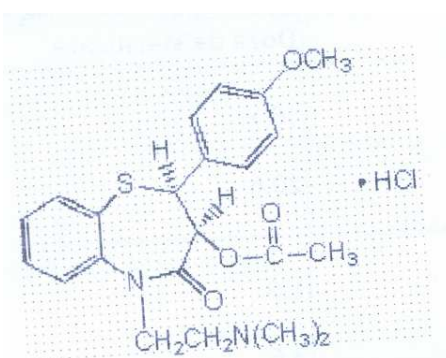


Fig.1 The structure of the diltiazem hydrochloride

### 2.2. Preparation of the pills

The PVA hydrogel pills that contain diltiazem hydrochloride were obtained by mixing the watery solution of diltiazem hydrochloride with a concentration of 10mg/ml with the watery solution of poly(vinyl alcohol) [PVA] with a concentration of approximately 14%.

The PVA solution was obtained by dissolving the 90-98 PVA powder in distilled water at 80°C for three hours through magnetic stirring.

The solids content of the PVA solution obtained is 13.32%.

The mixing ratio of the PVA solution with the diltiazem hydrochloride solution is 2:1.

Two series of samples were prepared and subject to freezing – defreezing cycles as follows:

- a sample was introduced in liquid nitrogen (-196°C) for an hour, and then it was stored at room temperature.
- a second sample was subject to three alternating freezing – defreezing cycles of 12 hours each.

The hydrogels were cut in the shape of cylindrical pills (Table 1).

Table 1. The characteristics of the hydrogel pills

Pill dimensions	Technique of PVA-HG obtaining	
	Freezing in liquid nitrogen	Repeated cycles of freezing-thawing
Diameter (cm)	1.89	1.55
Thickness (cm)	0.53	0.57

### 2.3. Study of the diffusion of the diltiazem from the PVA hydrogel matrix

In order to evaluate the quantity of diltiazem diffused from each pill, pills were introduced one by one in 200 ml of distilled water at 23°C and the solution was magnetically agitated.

Every 30 minutes, two ml of sample were extracted and analyzed with a UV-VIS spectrometer at 238 nm. The experimental results obtained are illustrated in Table 2.

The percentage and the quantity of diffused diltiazem were calculated with the following formula:

$$(\%)_{\text{dif}} = [c_t/c_o] * 100$$

$$Q = [c_t * V_{\text{sol}} / 1000] \text{ (mg)}$$

Table 2. Diffused Diltiazem amount from the two types of matrices after different periods of time

Matrix	PVA HG	
	Freezing in liquid nitrogen	Repeated cycles of freezing-thawing
Technique of PVA-HG obtaining	Q (mg)	Q' (mg)
Time (min)	Q (mg)	Q' (mg)
30	1.6476	2.0879
60	2.2641	2.7484
90	2.1319	3.1447
120	2.8805	3.4529
150	2.7924	3.8492
180	3.2328	4.0694
210	3.3208	4.2015
240	3.4089	4.2896
270	3.4970	4.5536
300		4.7618
330		4.7299

### 3. Results and discussions

The PVA hydrogel obtained by freezing in liquid nitrogen has a uniform heterogeneous structure with visible radial pores.

The pill obtained through alternating freezing – defreezing cycles has a more evidently heterogeneous structure, which is white and opaque. Moreover, its mechanical resistance is higher than that of the pill obtained through freezing in liquid nitrogen.

The percentage of diltiazem diffused after three hours from the pill obtained through alternating cycles (73.29%) is in accordance with the hypothesis that the lower cooling speed corresponding to this method leads to the formation of certain bigger pores in the hydrogel structure in comparison with the gel obtained through freezing in liquid nitrogen, where the very high cooling speed leads to obtaining certain small ice crystals, and implicitly certain small pores in the gel structure. Consequently, the percentage of diltiazem diffused from this hydrogel after three hours is lower, but it is 68.36%.

#### 3.1. Diffusion of diltiazem hydrochloride

The diffusion of diltiazem was estimated from the two series of samples of 270 minutes for the pill obtained through freezing in liquid nitrogen and respectively 390 minutes for the pill obtained through freezing – defreezing alternating cycles.

It was checked that the diffusion of the diltiazem hydrochloride from the two matrices complies with the Higuchi model in the following formula:

$Q = 2c_0\sqrt{(D*t)/\pi}$ , where:  $Q$  is the amount of diffused substance,  $c_0$  is the initial concentration of the solution,  $D$  is the diffusion coefficient, and  $t$  is the time.

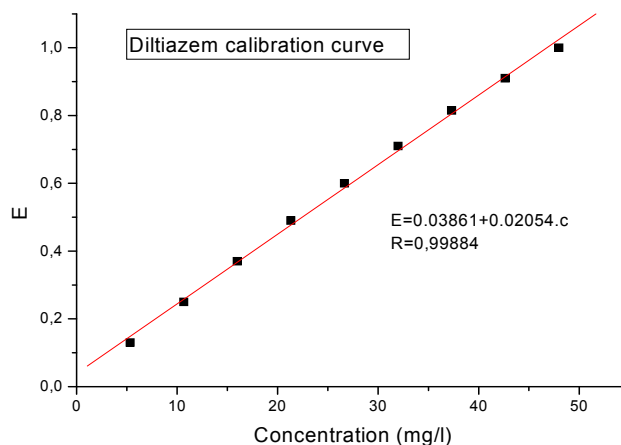


Fig.2. Calibration curve for diltiazem

In Figure 2, the linearity between the quantity of diffused substance and  $\sqrt{t}$  can be observed.

Tables 3 and 4 emphasize the amount of diltiazem hydrochloride diffused through the two types of matrices.

Table 3. Quantity of diltiazem hydrochloride diffused through the PVA matrix obtained by freezing in liquid nitrogen

t (min)	30	60	90	120	150	180	210	240	270
$\sqrt{t} \sqrt{\min}$	5.47	7.74	9.48	10.95	12.24	13.41	14.49	15.49	16.43
$E_{42}$	0.40	0.54	0.51	0.68	0.66	0.76	0.78	0.80	0.82
C (mg/ml)	8.23	11.32	10.65	14.40	13.96	16.16	16.60	17.04	17.48
Diffused (%)	34.98	48.07	45.26	61.15	59.28	68.63	59.28	68.63	70.50

Table 4. Quantity of diltiazem hydrochloride diffused through the PVA matrix obtained by freezing and thawing repeated cycles

t (min)	30	60	90	120	150	180	210	240	270	300	330
$\sqrt{t} \sqrt{\min}$	5.47	7.74	9.48	10.95	12.24	13.41	14.49	15.49	16.43	17.32	18.97
$E_{42}$	0.5	0.65	0.74	0.81	0.90	0.98	1.00	1.06	1.08	1.09	1.10
C (mg/ml)	10.13	13.74	15.72	17.26	19.24	20.34	21.01	21.44	22.76	23.20	23.42
Diffused (%)	37.60	49.50	56.64	62.19	69.33	73.29	75.67	75.67	93.12	84.40	84.44

It can be observed that the amount of substance diffused from the hydrogel pill obtained in liquid nitrogen is lower than the amount of substance diffused from the pill obtained through alternating freezing – defreezing cycles.

By using the Higuchi model, the Higuchi  $K_H$  constant can be calculated; it is used as speed constant for the diffusion of the diltiazem hydrochloride through the two types of matrices in accordance with the following formula:

$$Q = K_H * \sqrt{t} \quad (1)$$

The values obtained for this constant are  $0.2173 \text{ mg}/\sqrt{s}$  for the hydrogel obtained through alternating freezing – defreezing cycles, and respectively  $0.1786 \text{ mg}/\sqrt{s}$  for the hydrogel obtained through freezing in liquid nitrogen.

The  $K_H$  value depends on the type of macromolecular bonds of the hydrogel matrix.

For the hydrogel obtained by freezing in liquid nitrogen the Q and  $K_H$  values are lower when compared to the ones obtained for the hydrogel synthesized through alternating freezing – defreezing cycles.

#### 4. Conclusions

The diffusion of the diltiazem hydrochloride from the hydrogel pill is in compliance with the Higuchi model, with a linear elimination of the active substance depending on  $\sqrt{t}$  up to approximately 75% of the diffused substance, after which, a decrease of the diffusion speed is noticed due to the different porosities of the two types of pills.

In the case of the diltiazem hydrochloride, which has high water solubility, a slower elimination is observed if it is retained in a hydrophilic matrix immersed in water.

The diffusion of the diltiazem hydrochloride from the PVA hydrogel matrix obtained through alternating freezing – defreezing cycles is of the Fickian type (the Higuchi model).

Due to the different micro porosities of the two sets of samples, different values are obtained for  $Q$ ,  $K_H$  and the diffused substance percentage.

The possibilities of PVA-HG matrix permeability modification, by choosing the synthesis conditions of the hydrogel matrix ( $\Delta T$ , freezing duration, number of cycles, freezing rate), permit a better control of the drugs delivery.

Received May 9 2005

The “Transilvania” University from Brasov

## REFERENCES

1. A. Moretto, L. Tesolin, F. Marsilo, M. Schiavon, M. Berna, F.M. Veronese, Slow release of tow antibiotics of veterinary interest from PVA hydrogels, *J. Farmaco*, 2003
2. S.M. Shaheen, K. Yamaura, Preparation of theophylline hydrogels of atactic poly(vinil alcohol)/NaCl/H<sub>2</sub>O system for drug delivery system, *Journal of Controlled Release* 81 (2002) 367-377
3. N. A. Peppas, J.E. Scott, Controlled release from poly(vinyl alcohol) gels prepared by freezing-thawing processes, *Journal of Controlled Release*, 18 (1992) 95-100
4. A. Takamura, F. Ishii, H. Haidaka, Drug release from poly(vinyl alcohol), *Journal of Controlled Release*, 20 (1992) 21-28
5. T. Jana, B. C. Roy, S. Maiti, Modification of the film for control release of insecticides, *European Polymer Journal* 37 (2001) 861-864
6. J. M. Yang, W.Z.Su, T. L.Leu, M. C. Yang, Evaluation of chitosan/PVA bended hydrogel membranes, *Journal of Membrane Science* 236 (2004) 39-51
7. S. Pațachia, Cap.8. Blends based on poly(vinyl alcohol) and the products based on this polymer în “Handbook of Polymer blends and composites” Edited by C. Vasile and A.K. Kulshreshtha, RAPRA Technology LTD., England, p. 288-365, ISBN 1-85957-304-5, 2003
8. S.Pațachia, C. Corboș, *Study on obtaining poly(vinyl alcohol) hydrogel*, Bulletin of the “Transilvania” University of Brașov, Vol. 9(44)- New Series, Series B, ISSN 1223-964X, , 2002

## POLI(ALCOOLUL VILILIC) CA SISTEM DE ELIBERARE CONTROLATA A MEDICAMENTELOR

### (Rezumat)

Sistemele de eliberare controlata a medicamentelor sunt metode moderne de tratament a diverselor afectiuni. Ele asigura o concentratie constanta si de lunga durata a substantei active in corp si in consecinta, aceasta este mai efficient utilizata. PVA-ul este un polimer netoxic, necancerigen, biocompatibil si biodegradabil. Este solubil in apa dar poate genera hidrogeluri (structuri insolubile in apa) prin metode fizice si chimice de reticulare. In aceasta lucrare se studiaza difuzia diltiazemului din pastile de PVA hidrogel, obtinute prin doua tehnici de reticulare: inghetarea in azot lichid, respectiv aplicarea ciclurilor repetate de inghet-dezghet. Au fost determinati parametrii de difuzie al diltiazemului din cele doua tipuri de matrici polimerice si au fost corelati cu modificarile de morfologie ale matricii datorate tehnicilor diferite de sinteza.

## **GALLIUM – BASED RESTORATIVE DENTAL MATERIALS**

BY

**GHEORGHE T. POP, STEFAN LACATUSU, SIMONA STOLERIU  
and OCTAVIAN CIOBANU**

**Abstract:** Restorative metallic materials are widely used especially due to their superior mechanic features, as compared to ceramic and polymeric materials. Mercury-based amalgams, so far widely used in dental restoration, are prohibited nowadays due to the toxic effect of ions released into the body. New materials which can replace mercury on medical practice are being researched worldwide. This paper focuses on this direction, as it presents research on a new dental gallium-based material with features similar to mercury amalgams, but less toxic and easy to prepare in the dental office. Various lots of composite material were obtained and studied by triturating the two groups of metallic materials: liquid gallium alloys, melting temperature below 16 C, which stand for the liquid matrix, and a mixture of metallic powders frequently used in amalgams, which stands for the strengthening phase. These materials were examined in accordance with the international ANSI-ADA standards.

**Keywords :** amalgam, trituration, matrix, strengthening point

### **1. Introduction**

Rapid evolution in the research and use of new materials with improved specific characteristics has been known to take place in the medical field. One such material is the dental gallium-based amalgam, a composite material which replaces the classical mercury-based amalgam which was proved to be toxic to the organism.

Gallium as a metal has been known and used for a long time in medicine as it does not cause toxic phenomena in contact with the human body; gallium has been used lately as a restorative dental material.

International standard such as ANSI/ADA No.1 formulate the specific properties of dental metallic materials. Gallium-based amalgams were prepared and researched at the Academic Clinic of Dentistry in Iasi, in order to be used as dental restorative materials on human patients. The study and research of these metallic biomaterials were based on binary and ternary heat-balance diagrams of gallium with metals such as silver, antimony, copper, indium, etc., which show the interaction between and among these materials with forms of acid solutions, low-temperature eutectics and inter-metallic compounds. Low-temperature eutectics allow the preparation and maintenance of the metal alloy in a liquid state at room temperature, and inter-metallic compounds ensure the toughness of amalgams and wear resistance under the specific conditions of the chewing processes in the mouth cavity.

The present state of research boasts the achievement of the metallurgic processing of gallium amalgams and the physical and mechanic characteristic in accordance with international standards. The next stage in research has already started.

It includes pre-clinic tests on patients and the authorization procedures in accordance with the requirements of the Ministry of Health.

## 2. Materials and research method

### 2.1 Some considerations on processes of physical metallurgy

Processing of composite metallic amalgams is carried out on the basis of two groups of materials: a metal and a liquid metallic alloy at the temperature of the environment, which are the matrix, and a mixture of powders, which represent the reinforcement phase of the amalgam.

Our research studies two eutectic alloys of gallium as a liquid matrix: firstly, the binary gallium-indium alloy, an eutectic alloy, solidification temperature of 15.3°C, as shown in the phase diagram in Figure 1; secondly, ternary eutectic of gallium-indium-antimony, melting temperature 5 °C.

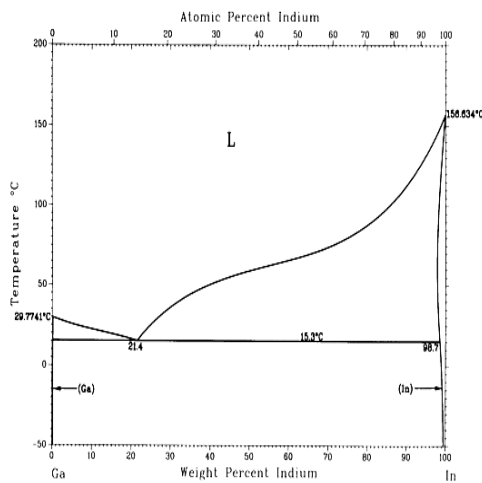


Fig.1. The Ga-In phase diagram

The reinforcement phase of the researched amalgams is a mixture of metallic powders made of elements which form different metallic phases with gallium at the temperature of the environment as solid and inter-metallic compounds. Mixtures of powders which commonly go as ingredients of mercury amalgams (with silver, antimony, copper as base metals) were used in this paper. As the heat-balance diagrams show (Figures 2 and 3), these elements and gallium make some metallographic constituents which give the amalgam its reinforcement and mechanic resistance to the temperature of the environment properties.

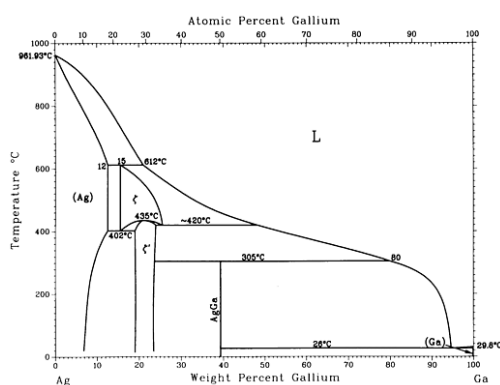


Fig.2. The Ga-Ag phase diagram

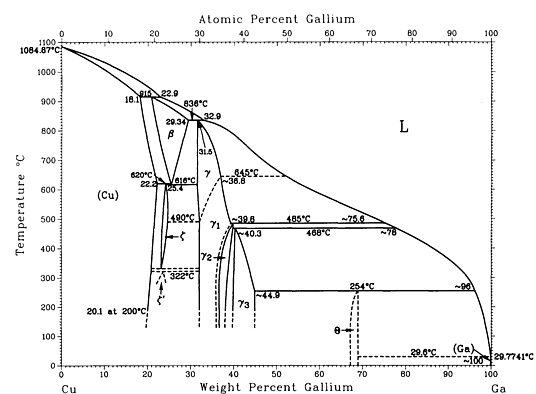
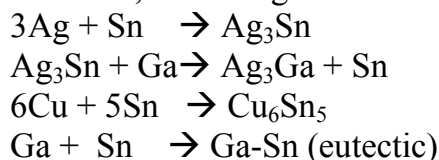


Fig.3. The Ga-Cu phase diagram

According to phase diagram in Figure 2, the GaAg compound is formed of gallium and silver for 39% Ga and phase  $\zeta$  for 15 - 25 % Ga content. Copper is present in all dental amalgams; it forms a range of solid phases with gallium, an aspect which ensures the reinforcement and tough solidification of the amalgam as well as improved

resistance to compression and abrasive wear specific to chewing processes in the mouth.

Other interaction takes place between materials present in the composition of dental amalgams at the temperature of the environment, by which inter-metallic and eutectic compounds are formed, according to the following reactions:



A gallium-based amalgam is obtained as a result of the interactions between the liquid alloy and the metallic powder mixture. This amalgam solidifies in the mouth in optimal time, (within 1-2 hours) and its physical properties are comparable to those of other natural and synthetic materials used in dentistry, as shown in the diagram in Figure 4.

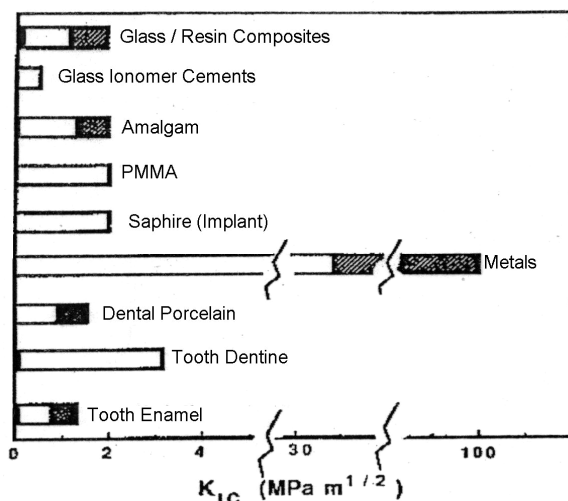


Fig.4. Comparison of typical fracture toughness values for a range of dental biomaterials

We would like to emphasize that all metallic materials used in making dental amalgams must meet the requirements of biocompatibility with the human organism and have highest chemical purity.

## 2.2. Experimental considerations

Several lots of dental amalgams were made on the basis of data in the special literature; the most significant of them are shown in Table 1. The chemical composition of the lots was based on low solidification temperature eutectic alloys were the basic ingredients and the available

expertise in dentistry as to the preparation, use and characteristics of dental mercury amalgams.

Table 1 Compositions of researched gallium-based amalgams

Amalgam lot.	Eutectic liquid alloy, %	Mixture of metallic powders, %				
		Ag	Cu	Sn	Zn	Cr
1	Ga-In 45	57	16.8	26	0.2	-
2	Ga-In 48	45	24	31	-	-
3	Ga-In 48	48.5	14	22	0.5	15
4	Ga-In-Sn 40	57	16.8	26	0.2	-
5	Ga-In-Sn 47	45	24	31	-	-

The amalgamation between the liquid alloy and powder mixture was made in the dental laboratory by the manual mixing of components in a ceramic jar according to the classical amalgamation procedure. 4 x 10 mm cylinder samples were prepared

out of each lot for physical, chemical and metallographic research and tests. The material in each lot was used for filling natural teeth previously extracted from different patients, in order to study specific aspects of dentistry such as time of amalgam strengthening, adherence to dentine surface, changes in size after strengthening.

Mechanic tests on authorized machines focused on the values of mechanical resistance at compression, yield and contraction on strengthening of tested amalgams, as compared to the procedure suggested by ANSI/ADA No.1 for classical mercury alloys.

### 3. Results and discussion

Laboratory tests carried out on dental amalgam samples led to some results which allow a physical and mechanic and metallographic characterization of these materials which meet the requirements in the field.

#### 3.1 Physical and metallographic properties of the gallium amalgams under study

Amalgams are known to be materials of a heterogeneous metallographic structure, made of inter-metallic compounds spread in a metallic mass of eutectic alloy, as shown in microstructure in Figure 5.

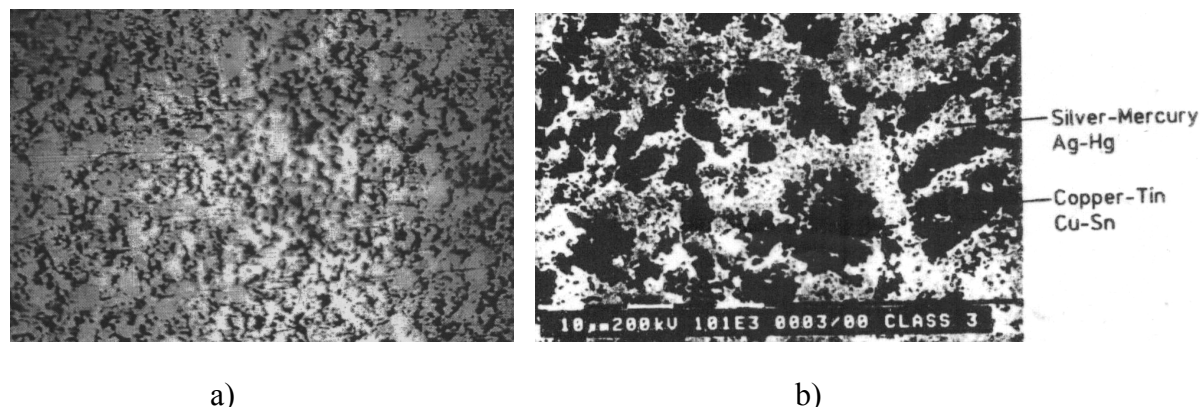


Fig. 5. The microstructure of dental composite: a. gallium dental composite; b. mercury dental composite

Two eutectic alloys were prepared and researched, with a view to improve the moistening properties between the liquid eutectic alloy and the metallic powders, on one hand, and of the adherence of amalgam to the surface of dentine cavity: the binary gallium-indium alloy, melting temperature 16 °C, and ternary gallium-indium-antimony alloy, melting temperature 5 °C.

Experimental results show a better moistening of the ternary alloy; this has been evidenced by the pull resistance on amalgam samples strengthened in the mouth, after 72 hours. The explanation of this behavior is the benefic influence of antimony in the ternary eutectic, a metal with good moistening properties which substantially lowers the alloy melting temperature, which in its turn improves the fluidity of the liquid and therefore the liquid alloy – metallic powder interaction. A higher percentage of antimony (from the ternary alloy) in the composition of the alloy intensifies

amalgamation reactions by forming inter-metallic copper bodies. The disadvantage of the ternary eutectic alloy is the delay in the set reaction with the metallic powders, an important aspect in dentistry.

An essential physical characteristic of dental amalgams is the size variation on strengthening in the dental cavity, an aspect expressed by the interstice which appears at the amalgam – dental cavity interface as a result of contraction. Dental practice suggests that this interstice should be as narrow as possible, ideally negative, that is the amalgam should expand after the strengthening set. Gallium amalgam show exactly this kind of physical behavior, as gallium expands by 3.25 % upon strengthening, which leads to a perfect tightening of the dental cavity. Table 2 shows experimentally determined values of size variation at setting for gallium amalgams, as compared to mercury amalgams; the chemical composition and sample lots are shown in Table 1. Micro-X-rays of the inter-phase zone interstice made on experimental dental cavities are shown in Figure 6. The microscopic aspect of the interface shows the adherence and corresponding tightening of the amalgam with the surface of the dental cavity.

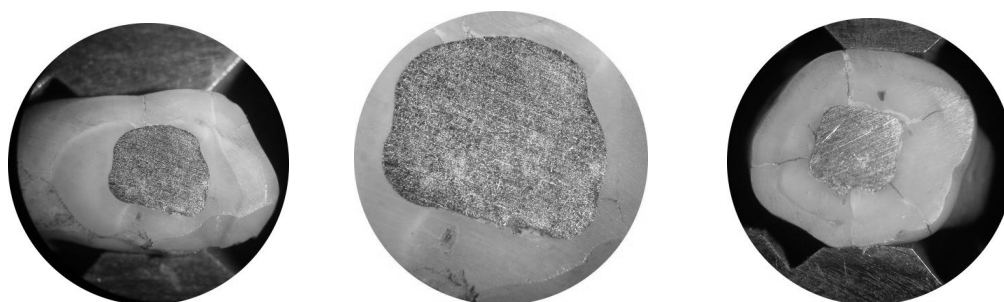


Fig. 6. Micro-X/rays of the amalgam-dental cavity inter-phase zone

Table 2. Experimentally obtained values of size modifications at strengthening of gallium amalgams

Amalgam lot	Contraction values allowed by ANSI/ADA, $\mu\text{m}/\text{cm}$	Experimentally obtained values, $\mu\text{m}/\text{cm}$
1.	max. 20	1-2
2.	max. 20	1-2
3.	max. 20	1-3
4.	max. 20	2-3
5.	max. 20	2-3

### 3.2 Experimental mechanical properties of gallium amalgams

These properties refer to two essential characteristics of amalgams, as specified by the international standards in the field: compression resistance and yield.

*The resistance to compression* expresses the behavior of amalgam fillings at crushing in the chewing process in the mouth. Compression resistance is given by the inter-metallic compounds which are formed by the amalgamation reactions between the liquid alloy and metallic powder. The experimentally obtained values of compression resistance experimentally obtained on sample lots show that gallium amalgam ensures good behavior as compared to the mercury amalgam and international norms, as shown in Table 3.

Table 3. Experimentally determined values of compression resistance and yield as compared to mercury amalgams

Amalgam lot	Values of compression resistance, MPa		Values of yield, %	
	According to ANSI/ADA	Determined	According to ANSI/ADA	Determined
1.	200-250	230	max.3	2.0-2.5
2.	idem	230	idem	2.0-2.5
3.	idem	250	idem	1.5-2.0
4.	idem	220	idem	1.5-2.0
5.	idem	220	idem	2.0-2.5

The best values at mechanic testing are found with amalgams with chrome powders; this behavior can be explained by the variety and properties of the inter-metallic compounds which are formed between gallium and chrome, as shown in the heat-balance diagram between the two metals. \

Special mention should be made of the fact that the remaining lots of amalgams showed corresponding values of compression strain, which shows a good amalgamation property between gallium and metallic powders at the temperature of the environment. The tests showed that amalgams show a tendency to fissure, so they are not ductile materials and have a reduced degree of plastic deformation. The explanation of such behavior may be in the inter-metallic compounds which are formed between the gallium and metals of the powder used as a reinforcement ingredient of the amalgam.

*Yield* is the property of dental amalgam to deform under constant static burden and expresses the viscosity-elasticity behavior of these materials. Dental amalgams constantly deform under strain and, unlike other metallic materials, do not show hardening. Yield test were carried out by means of a mechanic press by compression strain of some cylinder samples under the constant burden of 36 MPa by a main spring. The deformation in length of amalgam samples was measured with a comparing device, at an 1 – 4-hour interval since the beginning of strain. The results are shown in percents in Table 3.

Experimental results confirm a good behavior to yield of the amalgam lots, with values which do not exceed the international limit allowed by ANSI/ADA. Reduced values of yield (under 1 %) signify a breaking material with a risk of fissures under circumstances of real strain. As a rule there is a correlation between the yield behavior and compression behavior and both strains are of a similar mechanical nature, which can be seen in the information in the above-mentioned table.

The following aspects of research can be formulated according to experimental results obtained on researched amalgam lots and the comparative analysis with THE ANSI/ADA international standard:

- the mechanical characteristics obtained on amalgam lots have corresponding values of compression resistance, as specified in the special norm;
- gallium-based amalgams do not show contraction at strengthening, so the filling-dentine interstice characteristic of mercury-based amalgams is bypassed;
- improved adherence to the amalgam-dentine interface is ensued by the superficial properties of gallium and antimony and by the lack of contraction at

strengthening. This physical aspect was more prominent on the lots which used ternary Ga-In-Sn eutectic as a liquid alloy;

- the micro-hardness test carried on the experimental lots shows higher values (60 – 80 Hv), as compared to those specified in the standards (minimum 50 Hv).

#### 4. Conclusions

By summarizing the results of the theoretical and experimental research on the preparation and characteristics of gallium-based dental amalgams reported above, the following general conclusions can be formulated for the present state of study:

- Gallium-based amalgams are biocompatible materials, unlike mercury-based amalgams; the latter are toxic for the human organism and have been removed from active dental use.
- Experiments have shown that there exists a possibility of practical preparation in the dentistry office of gallium-based amalgams by the amalgamation of a binary or ternary eutectic alloy at the temperature of the environment and a mixture of metallic powders currently used in dental practice.
- Physical and chemical processes were studied and verified, which take place in the triturating process of composing metallic materials, so that optimal proportions, speed of amalgamation hardening, the technique of depositing in the mouth and the way of retention and adhesion to dentine surface.
- The physical and chemical properties were determined in specialized laboratories, in accordance with the ANSI/ADA international norms in the field; the experimental results obtained meet the requirements, some characteristics are superior as compared to mercury-based amalgams, such as, for instance, the absence of an interstice on hardening, the adherence to dentine surface and some mechanical characteristics.
- In the present state of research the technical aspects as to the procedure of preparation of amalgam, physical and mechanical characteristics and the technique of placing it into the dental cavity - in the dentistry office have been finalized.

The second stage of research has already started. It includes pre-clinical and clinical research on patients of the new dental material. Multiple functional aspects and possible corrections in gallium-based amalgam composition and preparation will be observed *in vivo*.

*Received May 4, 2005*

*“Grigore Traian Popa” University  
of Medicine and Pharmacy, Iasi*

#### REFERENCES

1. Craig G. Robert, *Materiale Dentare Restaurative*, Ed. ALL Educational, Bucuresti, 2001.
2. Helsen A, Bremo H. Jorgen, *Metal as Biomaterials*, Ed. John Wiley-Sons, 1999.
3. Pop T. Gh., *Biomateriale si Componente Protetice Metalice*, Ed. Tehnica-Info, Iasi 2004.
4. Williams F. David, *Medical and Dental Materials*, Ed. VCH, 1992.

---

**AMALGAME CU GALIU UTILIZATE IN MEDICINA DENTARA****(Rezumat)**

Materialele restaurative metalice sunt larg utilizate în special datorită proprietăților mecanice superioare în comparație cu materialele ceramice și polimerice. Amalgamele pe bază de mercur care au fost până acum larg utilizate în restaurarea dentară, astăzi sunt considerate materiale prohibite datorită efectului toxic asupra organismului viu. În consecință, în toată lumea sunt cercetate noi materiale care să înlocuiască mercurul în practica medicală. În prezenta lucrare sunt prezentate cercetări recente privind utilizarea unui nou material dentar și anume amalgamul dentar pe bază de galiu, asemănător din punct de vedere al proprietăților cu amalgamele pe bază de mercur, dar mai puțin toxic și la fel ușor de preparat în cabinetul dentar. Amalgamul dentar cu galiu se obține din două grupe de materiale metalice: un aliaj lichid cu temperatura de topire sub 16°C – care constituie matricea și un amestec de pulberi metalice frecvent utilizate în amalgame – care constituie faza de ramfort. Au fost obținute și cercetate mai multe loturi de amalgame cu galiu ale căror tehnici de preparare și proprietăți sunt prezentate în lucrarea de față.

## METALLIC COMPOSITES OBTAINED THROUGH EXTRUSION

BY

OCTAVIAN POTECAȘU, FLORENTINA POTECAȘU, ELENA DRUGESCU,  
NELU CAZACU, and PETRICA ALEXANDRU

**Abstract:** The paper describes the experiments carried out on electrical conductors made from lamellar-oriented Al-Cu composites with Cu percentage up to 20%. The mechanical resistance and electrical resistivity have been measured on conductors of three different deformation degrees with final diameters of 4, 5, 6 and 8 mm. The higher copper content results in a higher mechanical resistance of the conductor both in the post deformation state and after the thermal treatment for all the degrees of deformation applied. The higher copper content leads to an acute decrease of the plastic characteristics (elongation, striction) both in the deformed conductors and in those thermally treated for all the degrees of deformation applied. The range of the mechanical resistance values for the thermally treated conductors is lower than that of the material in hardened stage; the elongation range takes higher values for the thermally treated material. For all the degrees of plastic deformation, the electrical conductivity of the thermally treated material increases with the copper content which is lamellar oriented in the aluminium matrix.

**Keywords:** electroconducting composites, components arranged in coils, electrical resistivity

### 1. Introduction

The extrusion devices were containers of various sizes, punches for direct and reverse extrusion (having the diameters equal to the containers inner diameter), matrices, (upper and lower) covers. These were all made of steel Cr120 to stand the high pressures specific to extrusion processes and were thermally treated by tempering and annealing.

### 2. Experimental conditions

The container bores have 0.4-roughness while their diameters vary depending on the extrusion samples diameters.

The moulds were made of two parts. For the purpose of reverse extrusion, one-piece blind mould with diameter adjusted to the container bores was manufactured. The upper cover was so constructed as to suitably guide the punch while the lower cover is designed to prevent the mould from coming out of the container during extrusion.

The foundry ladle was made of inner lined steel with refractory concrete to prevent the metal bath from iron contamination.

The final samples which were prepared for the plastic deformation test resulted as a two-component assembly in which a glass of aluminium and an Al-Cu strip coil were introduced.

The aluminium glasses were made by reverse extrusion of the Al samples cast in cylinder shapes of 30mm diameters and 60mm height. In order to fit them to the containers, the aluminium samples were machined on a lathe and brought to proper sizes. For coils Al and Cu strips rolled to the desired thickness were used.

To avoid hardening, the strips were annealed by recrystallization, the Al samples to 450 degrees and the Cu ones to 650 degrees. After being polished to remove the oxide films and impurities, the strips were coiled over a Cu conductor which had been previously treated in the same way, namely annealed and polished.

The coiling operation was made manually keeping the aluminium strip externally to obtain a tighter coil. All the coils thus obtained, having different compositions of Al and Cu, had the same diameter  $\phi=20\text{mm}$ .

Aluminium from Slatina ingots and electrolyte Cu strips were employed. The researches resorted to the Al glass variant as other solutions proved invalid.

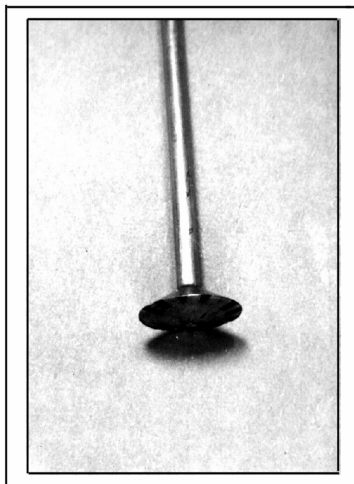


Fig 1. The aspect of Al-Cu composite materials through reverse extrusion

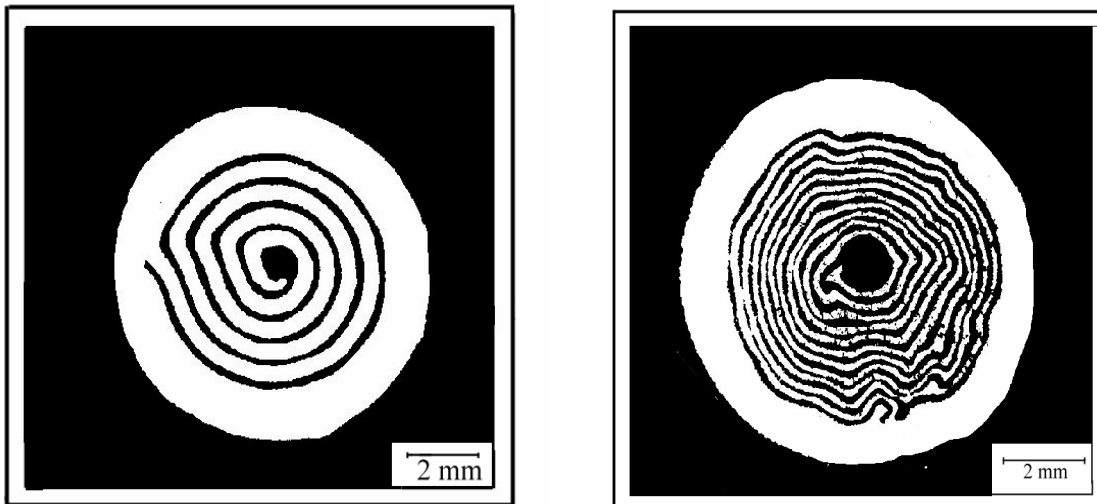
Al specimens deformed (fig.1) under the same conditions as the Al-Cu composites were used with final diameters of 4,5, 6 and 8mm. Extrusion of the initial semi products was made in two stages. The first extrusion stage is aimed at consolidating the semi products and consists in reducing the diameter from 25 mm to 20mm. For this a force of 110 daN/mm is necessary. After extrusion, the semi-products were cut on the lathe so that they can be introduced into a container of  $\phi=20\text{mm}$ , and removing the end of free lamellar-oriented copper. The second stage of extrusion focused on making the Al Cu conductors in three variants reducing the diameter from 20mm to 8, 6 and 4.5 mm, respectively.

### 3. Experimental Results

Fig 2 illustrates the macrostructure of the conductors having different copper percentages and lamellar orientation.

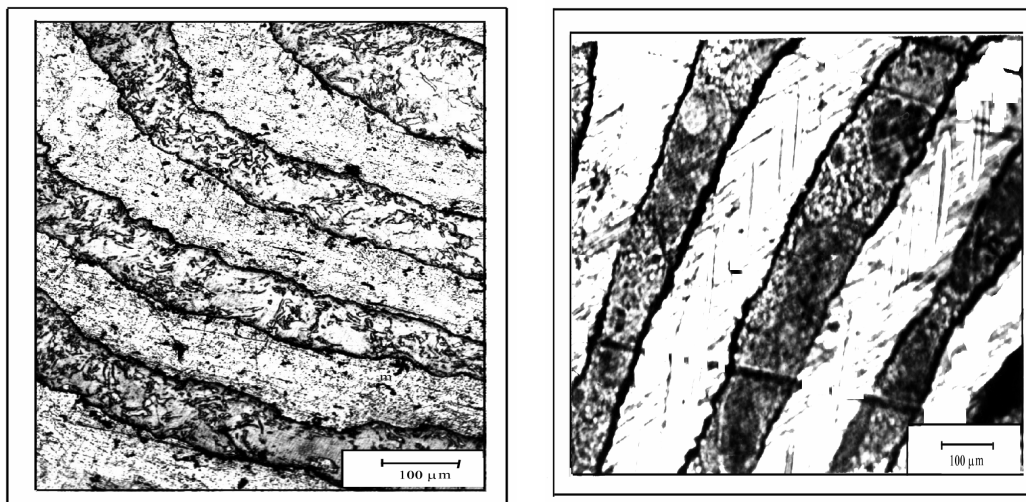
The influence of the extent of deformation and copper percentage as reinforcement phase of the aluminium matrix was investigated for the three composite variants. For this purpose the mechanical (resistance, elongation, throttle) and electrical characteristics (electrical resistivity) were measured on series of ten samples each for each percentage of copper (4, 8, 12, 16, 20%).

The microstructural analysis of the composite materials carried out through the conductor cross sections is presented in fig 3.



a) b)  
Fig.2 Copper distribution as reinforcement phase and lamellar orientation of Al-Cu composite material.

On the conductors thus obtained the mechanical resistance and breaking elongation as well as the electrical resistivity were measured. In fig. 4 and 5 are presented bar charts with the average values of mechanical characteristics of resistance, elongation and striction obtained at stretching breaking test for extruded semi-products of composite materials with diameters of  $\phi_1=8\text{mm}$ ,  $\phi_2=6\text{mm}$ ,  $\phi_3=4,5\text{mm}$  for hardening condition (fig.4) and for heat treated condition (fig.5).



a) b)  
Fig.3 Microstructure of the Al-Cu composite material in cross section: a) hardened state; b) thermally treated state

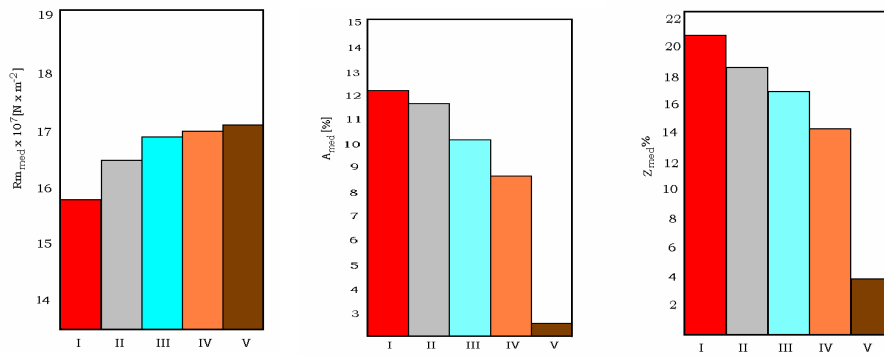


Fig.4.1. Variation of average characteristics of resistance, elongation, striction, depending on copper content, for extruded Al-Cu conductors of composite material at  $\phi_1 = 8$  mm, hardened condition: I – 4% Cu; II – 8% Cu; III – 12% Cu; IV – 16% Cu; V – 20% Cu

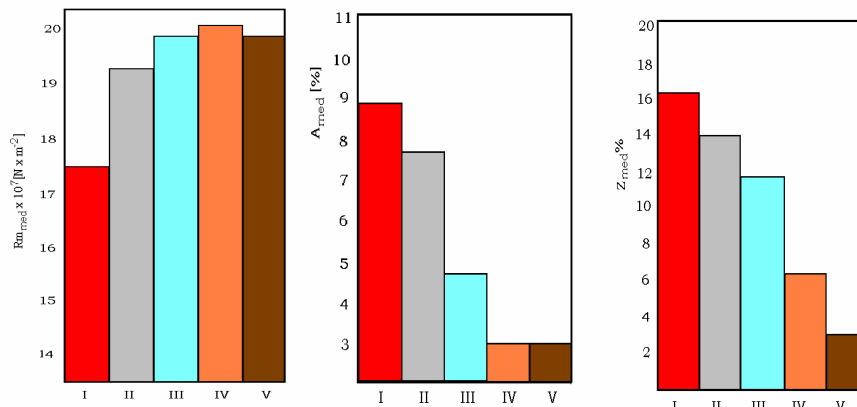


Fig.4.2 Variation of average characteristics of resistance, elongation, striction, depending on copper content, for extruded Al-Cu conductors of composite material at  $\phi_2 = 6$  mm, hardened condition: I – 4% Cu; II – 8% Cu; III – 12% Cu; IV – 16% Cu; V – 20% Cu

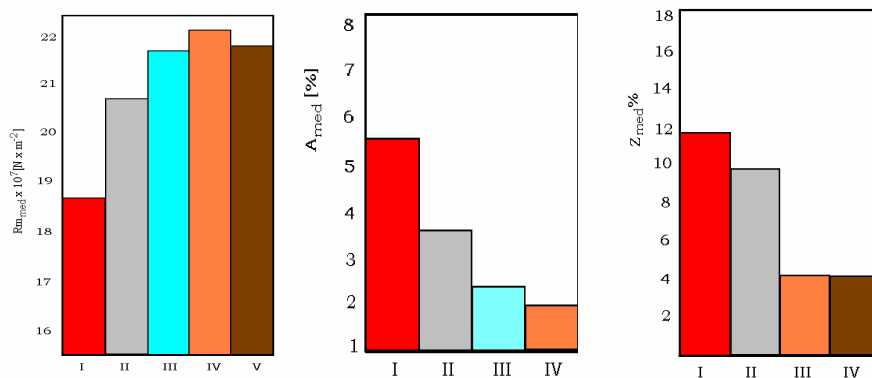


Fig.4.3. Variation of average characteristics of resistance, elongation, striction, depending on copper content, for extruded Al-Cu conductors of composite material at  $\phi_3 = 4.5$  mm, hardened condition: I – 4% Cu; II – 8% Cu; III – 12% Cu; IV – 16% Cu; V – 20% Cu

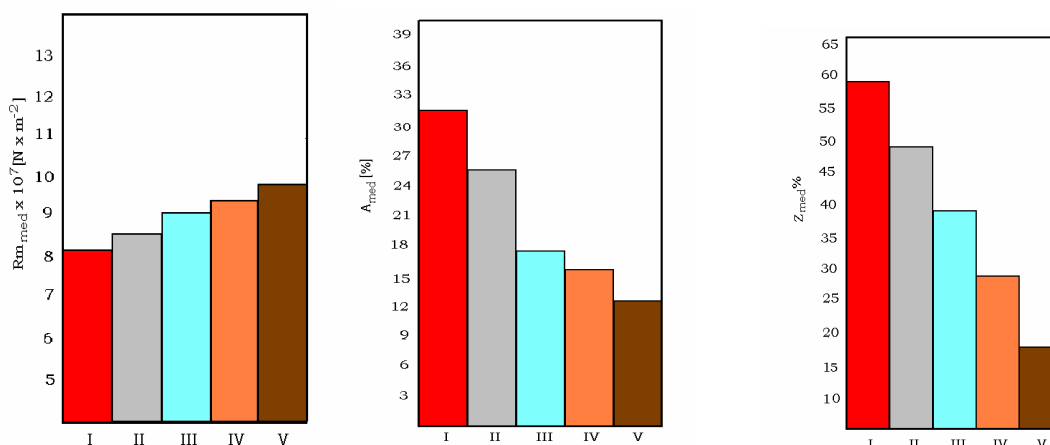


Fig.5.1. Variation of average characteristics of resistance, elongation, striction, depending on copper content, for extruded Al-Cu conductors of composite material at  $\phi_1 = 8$  mm, thermic treated condition: I – 4% Cu; II – 8% Cu; III - 12% Cu; IV – 16% Cu; V – 20% Cu

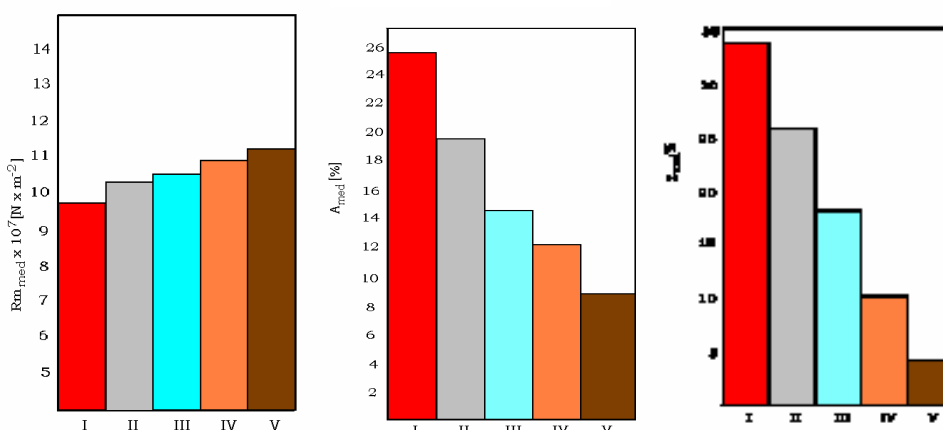


Fig.5.2. Variation of average characteristics of resistance, elongation, striction, depending on copper content, for extruded Al-Cu conductors of composite material at  $\phi_2 = 6$  mm, thermic treated condition: I – 4% Cu; II – 8% Cu; III - 12% Cu; IV – 16% Cu; V – 20% Cu

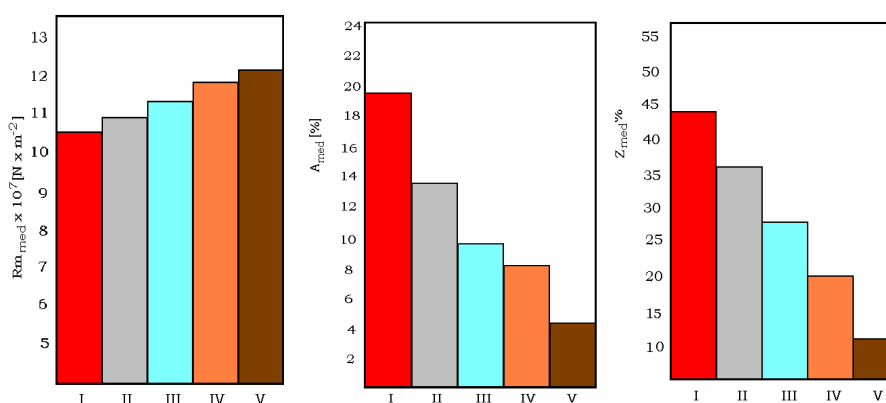


Fig.5.3. Variation of average characteristics of resistance, elongation, striction, depending on copper content, for extruded Al-Cu conductors of composite material at  $\phi_3 = 4,5$  mm, thermic treated condition: I – 4% Cu; II – 8% Cu; III - 12% Cu; IV – 16% Cu; V – 20% Cu

Fig. 6 and 7 show in brief show the dependence the mechanical and the electrical resistance characteristics on the copper content and structural state of the electroconductive composite material.

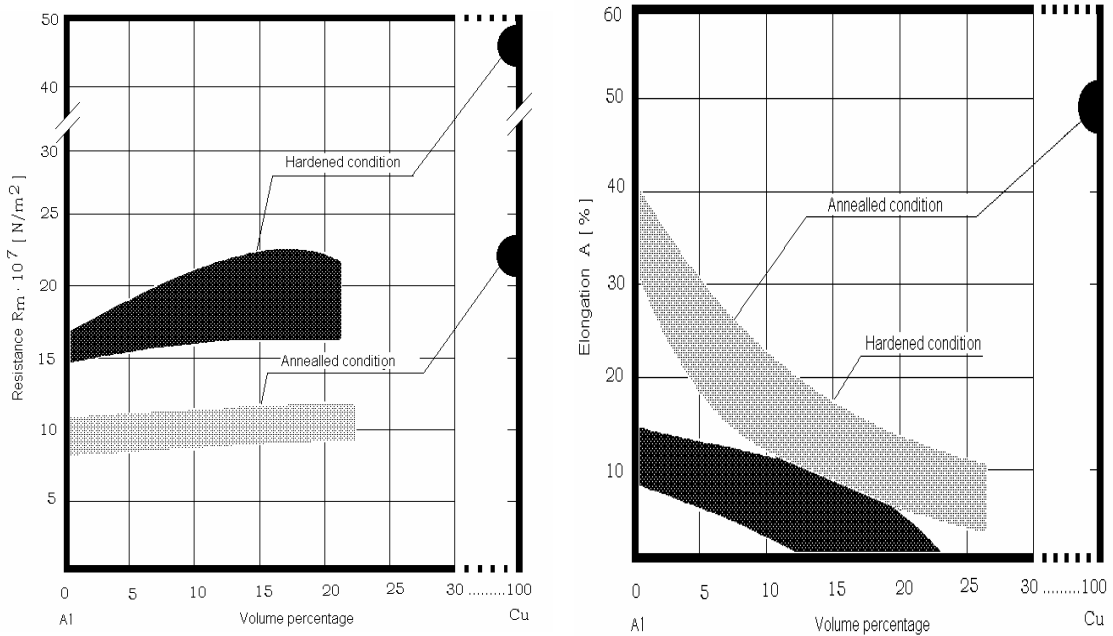


Fig.6 The variation of the mechanical resistance and elongation depending on the copper content for the Al-Cu composite with lamellar orientation of the component elements

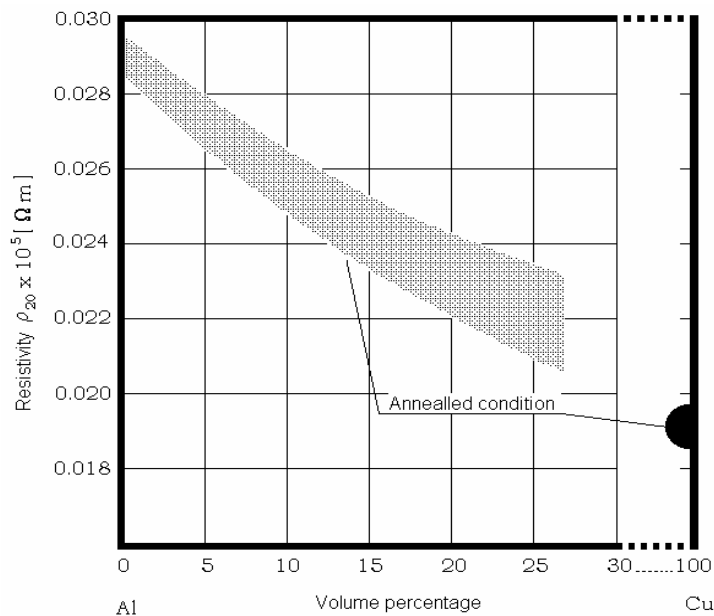


Fig.7 Variation of the electrical resistivity depending on the copper content for the Al Cu composite having copper lamellar orientation

#### 4. Conclusions

The method employed facilitated the use of copper as reinforcement phase up to percentage of 20%.

The products obtained after deformation are electrical conductors of 8, 6, 4.5 mm.

The higher copper content results in a higher mechanical resistance of the conductor both in the post deformation state and after the thermal treatment for all the degrees of deformation applied.

The higher copper content leads to an acute decrease of the plastic characteristics (elongation, striction) both in the deformed conductors and in those thermally treated for all the degrees of deformation applied.

The range of the mechanical resistance values for the thermally treated conductors is lower than that of the material in hardened stage; the elongation range takes higher values for the thermally treated material.

For all the degrees of plastic deformation, the electrical conductivity of the thermally treated material increase with the copper content which is lamellar oriented in the aluminium matrix.

Received May 6, 2005

“Dunarea de Jos” University, Galati

#### REFERENCES

- [1]. **O.Potecasu, F. Oprea, F. Potecasu, E. Drugescu** - Research on Obtaining and Characterizing Al-Cu Composite Materials -Bulletin of the Polytechnic Institute of Jassy - Fasc. 3 -4, Tomul XLVI (L), Materials and Engineering, 2000, p. 177.
- [2]. **O.Potecasu, F.Potecasu, N.Cazacu, P.Alexandru-** *Electroconducting composites with components arranged in coils* - The 41th International Seminar on modelling and optimization of composites MOC`41, „Prediction in Materials Science” Odessa, 2002, p.147.
- [3]. **Florentina Potecașu, Octavian Potecașu, Elena Drugescu** - Aspects concerning the diffusion in metallic composites - *Metalurgia International nr. 3* , 2005, p.

#### COMPOZITE METALICE OBȚINUTE PRIN EXTRUZIUNE

##### (Rezumat)

Lucrarea prezintă cercetările efectuate de autori privind obținerea și caracterizarea materialelor compozite Al-Cu, destinate fabricării conductorilor electrici, cu scopul reducerii consumului de cupru, element scump și deficitar. Procedeele de obținere a materialului compozit Al-Cu electroconductor, cuprind ca etapă principală extruziunea la rece, care realizează îmbinarea componentelor și constituirea ca atare a compozitului cu proprietăți diferite față de elementele componente și de cele ale aliajelor Al-Cu convenționale. În lucrare sunt prezentate rezultatele cercetărilor privind variația proprietăților mecanice și electrice în funcție de starea structurală și de cantitatea de cupru dispus sub formă de rulou în matricea de aluminiu.



## **HARDENED GRANITE COMPOSITES FROM THE DOBROGEA MOUNTAINS**

**BY**

**OCTAVIAN POTECAȘU, FLORENTINA POTECAȘU, ELENA DRUGESCU  
and LAURA BUBURUZAN**

**Abstract:** The paper presents the results of the authors' scientific research on a composite material with polymeric matrix, hardened with rock particles. It was studied the influence of the quantity of the hardening phase on the compression resistance of the product. These weather resistant materials have a long period of ageing, a permanent finishing and require almost no maintenance. For the research was used granite from the Măcin Mountains, Dobrogea Romania with greenish shade, which was crushed and then granulometric sorted. Granite is an acid volcanic rock, with over 65% SiO<sub>2</sub>; it has granular structure and massive texture. Polyesteric thermoset resin was used for the matrix. These resins can be characterized by: easy obtaining and accessibility of the raw materials, quick strengthening without side-off products, good chemical resistance at acids and alcohols. Composite samples were made through shaping in steel mould. After shaping and maturation, the samples were tried at compression.

**Keywords:** polymeric matrix, composite material, rock particles

### **1. Introduction**

Dynamic development of the consumer's goods manufacture has imposed new materials to be setting up.

From the advanced materials with great usage expectation are the Composites, named in reference material as Future's Materials. Composites answer to every industrial demands and almost all human needs. Composites can be obtained by suitable staples association and they can have simultaneous new combinations: rigidity, resilience, toughness, refractoriness, corrosion resistance, dimensional steadiness, absorption of vibration, electrical and thermal conductivity, and, unlike other building traditional materials, composites' price is lower. Today, Composite Materials applications cover very different fields, such as: aeronautics, naval-building industry, electronics, radio- location, machine-building industry, industrial equipments, light industry, industrial and civil –building industries.

In buildings field, composites prefab are either even elements or technical ingots. These bad weather resistant materials have long life seasoning, facing continuous and they require almost no maintenance. Mechanical properties concerning building industry are: compression strength, abrasive resistance, impact, bending strength, traction resistance, dimensional steadiness, modulus of elasticity and yield impact resistance.

Composite materials are generally made from a hardening phase and a binding compatible matrix. In building industry the most used matrix is polymeric and reinforcement phases could be mineral rocks, like granite, basalt, marble, pumice, and a wide range of products can be made from the outcome materials.

The hardened rocks composites offer buildings personality and style being in the same time very practical due of their easier maintenance, being used in various purposes, such as exterior plating and floors for public institutions or areas with intensely traffic, either in ornamentally purposes, for fitting out the indoor of private houses.

The raw materials used for obtaining the composites were granite and polyester thermo rigid resin.

The granite is a volcanic rock made up from over 65%  $\text{SiO}_2$ ,  $\text{CaO}$ ,  $\text{MgO}$ ,  $\text{R}_2\text{O}_2$ ,  $\text{Mn}_2\text{O}_3$ ,  $\text{TiO}_2$ ,  $\text{Fe}_2\text{O}_3$ , etc., in different percentage; it has granular structure and massive texture. Due these integrant elements, the granite can be white, grey, yellowish, pink, auburn –brown, greenish, or bluish. Sometimes, presence of feldspath crystals wide grown dents the rock a freckless structure.

The granular structure can be characterized by mineral grains crystallized which are visible with naked eye. This structure is formed in earth depth, where the cooling magma is made very slowly, and mineral crystals have enough time for growing. The granular structure is found out in all depth magmatic rocks. Our country has mountainous massive all built from granite. Such mountains can be found in Măcin Mountains, Apuseni, Meridional Carpathians and running granite quarry are in Săvârșin, Cladova, Radna, Măcin, Turcoaia, Greci.

## 2. Experimental procedure

For the research was used granite from the Măcin Mountains, with greenish shade, which was crushed and then granulometric sorted.

Polyesteric thermoset resin was used for the matrix. These resins can be

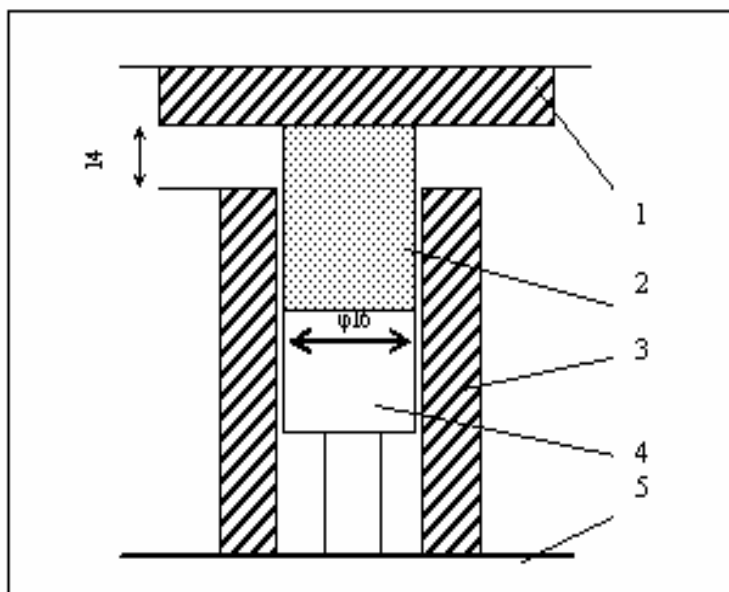


Fig.1. The diagram of the compression test  
 1 - anvil;  
 2 - cylindrical die;  
 3 - controlled support,  
 4 - blank assay;  
 5 - the press table

characterized by easy obtaining and accessibility of the raw materials, quick strengthening without side-off products, good dimensional steadiness, coloring properties, transparency, good chemical resistance at acids and alcohols.

Table 1 Recipes of experimental composite manufacturing

No. recipe	Composition	Pressure (daN/cm <sup>2</sup> )	Force (daN)	Section (cm <sup>2</sup> )	Compression resistance (MPa)
0	Natural Granite	11	2200	3.5	62.8
1	<ul style="list-style-type: none"> <li>• 11 g granitee grain size 0,73-1,27mm;</li> <li>• resin 9%</li> </ul>	12.5	2500	2.7	92.5
2	<ul style="list-style-type: none"> <li>• 11 g granitee grain size 0,73-1,27mm;</li> <li>• resin 18%</li> </ul>	12	2400	2.7	88.8
3	<ul style="list-style-type: none"> <li>• 11 g granite grain size 0,73-1,27mm</li> <li>• resin 27%</li> </ul>	11	2200	2.7	81.4
4	<ul style="list-style-type: none"> <li>• 11 g granite grain size 1,85-2,17mm;</li> <li>• resin 13%</li> </ul>	9	1800	2.7	66.6
5	<ul style="list-style-type: none"> <li>▪ 10 g granite grain size 1,85-2,17mm</li> <li>▪ 1 g granite grain size &lt; 0,040 mm;</li> <li>▪ resin 22%</li> </ul>	12	2400	2.7	88.8
6	<ul style="list-style-type: none"> <li>• 5 g granite grain size 1,85-2,17mm;</li> <li>• 5 g granite grain size 0,73-1,27mm;</li> <li>• resin 22%</li> </ul>	10	2000	2.7	74.0

Polyesteric usage should be aware from following restriction: increased shrinkage through shaping, decreased resistance at alkali and hot water.

### 3. Experimental results and discussion

Composite samples were manufactured in accordance with the recipes from Table 1, through shaping in 18,6 mm steel mould diameter. After shaping and maturation, the samples were compression tested in hydraulic press, according to diagram 1.

The results are shown in Table 1 and hystogram Figure 2.

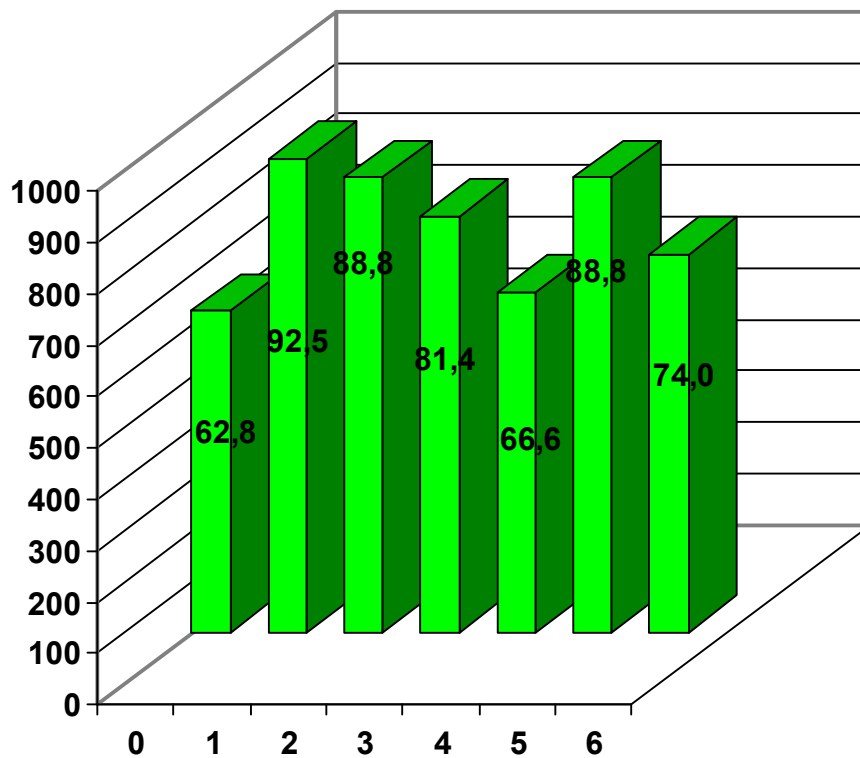


*Figure 2. The variation of the compression resistance varying with the granite granulation and the resin percent, compared to the granite*

Macrostructure of the composites obtained concordant with recipes 2, 4 and 6 are shown in figures 3, 4, 5.



Figure 3. The macrostructure of the composite, recipe 2

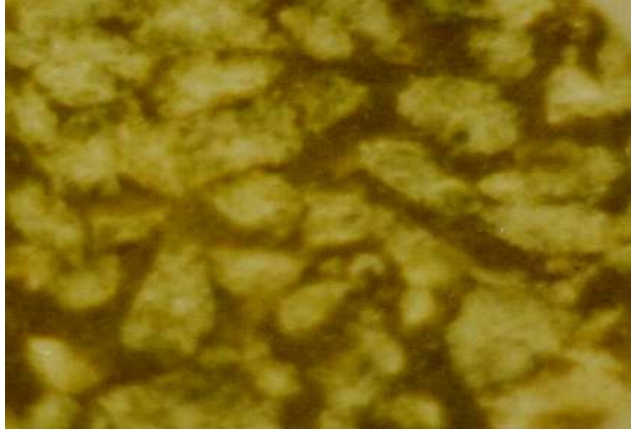


Figure 4. The macrostructure of the composite, recipe 4

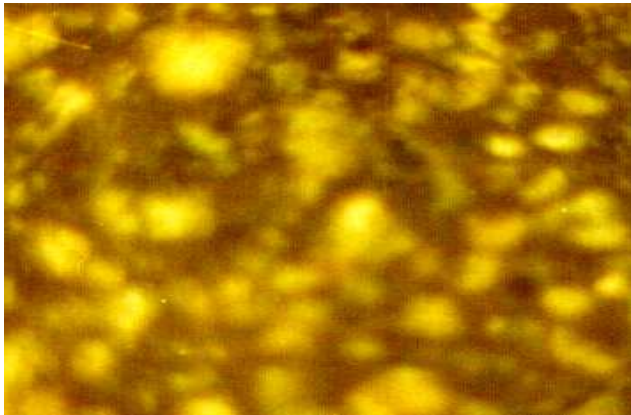


Figure 5. The macrostructure of the composite, recipe 6

#### 4. Conclusions

- During the experiments, especially effect in composite has the granite grain size. It's obvious that the composite samples 1 and 2 (with the finest grain size) have a higher compression resistance than composite 4 (with a bigger grain size).
- If a smaller quantity from the finest granite grain size (below 0.040 mm) is added in composite by a bigger grain size (1,85-2.17 mm) for filling the space between the particles, the compression resistance will be increased with 25% compare to the composite sample made only of the finest granulation particles.
- Set beside samples 1, 2 and 3 from histogram 2, the compression resistance has been decreased with 12% by increasing the amount of resin.
- Compression resistance of the composite obtained is higher than the compression resistance of natural rocks used for research.

**REFERENCES**

- [1]. **Mihalcu M.** - *Materiale plastice armate*- Editura Tehnică, București. 1973.
- [2]. **Dumitraș C., Oprau C.**- *Prelucrarea materialelor compozite ceramice și minerale*- Editura Tehnică, București, 1994.
- [3]. **Tentulescu D., Tentulescu L.** – *Fibre de sticlă*, Editura Tehnică, București, 1994
- [4]. **Nica A.**- *Ceramica Tehnică*- Editura Tehnică, București, 1988.
- [5]. **O.Potecasu, L.Buburuzan, E.Drugescu** - *Compozite durificate cu roci* - Conferinta cu participare internationala Tehnologiei si Materiale Avansate, 20-22 noiembrie 2003, Galati, Romania, ISBN 966-549-916-5, p.105

**COMPOZITE ARMATE CU GRANIT DIN MUNȚII DOBROGEI****(Rezumat)**

Evoluția dinamică a producției de bunuri de consum a impus crearea de noi materiale. Printre materialele avansate cu mari perspective de utilizare sunt și cele compozite, numite în literatura de specialitate materialele viitorului. Materialele compozite răspund nevoilor tuturor industriilor și aproape tuturor activităților omenești. Prin asociații corespunzătoare ale materiilor prime de bază se pot realiza compozite care să prezinte simultan noi combinații: rigiditate, rezistență mecanică, duritate, refractaritate, rezistență la coroziune, stabilitate dimensională, posibilitatea de amortizare a vibrațiilor, conductibilitate termică și electrică și, spre deosebire de alte materiale de construcție tradiționale, costă din ce în ce mai puțin. Aplicațiile materialelor compozite acoperă în prezent domenii foarte diverse cum sunt: aeronautică, construcții navale, electronică, radiolocație, construcția de autovehicule, echipamente industriale, industria ușoară, construcții industriale și civile, etc. În domeniul construcțiilor, prefabricatele din materiale compozite sunt fie elemente plane, fie blocuri tehnice. Aceste materiale rezistente la intemperii, au durată mare de îmbătrânire, au o finisare permanentă și nu pretind aproape nici un fel de întreținere. Caracteristicile mecanice care interesează industria construcțiilor sunt: rezistența la compresiune, forfecare și abraziune, șoc, încovoiere, tracțiune, variațiile dimensionale, modulul de elasticitate și fluajul sub sarcină. Materialele compozite sunt alcătuite, în general, din materialul de rigidizare și din matricea de legătură compatibilă. În industria construcțiilor cele mai utilizate matrici sunt de natură polimerică iar dintre elementele de armare amintim rocile minerale, cum ar fi granitul, bazaltul, marmura, piatra ponce, rezultând materiale din care pot fi executate o gamă largă de produse.

## FERROFLUIDS STABILITY – A COMPARATIVE STUDY

BY

MIHAELA RĂCUCIU, DORINA-EMILIA CREANGĂ, GHIORGHE CĂLUGĂRU  
and IRINA HORGA

**Abstract:** The complex structure of the magnetic colloids, i.e. ferrofluids, involves the assurance of their stability as required by both technical and biomedical applications. In order to prevent ferrophase particles agglomerations, good quality coating of small size particles need to be carried out. Small size ferrophase is essential not only for the homogeneity of the magnetic colloid but also for the efficient penetration of biological structures. In this respect, we carried out a comparative study regarding a ferrofluid prepared in our laboratories (based on petroleum) as well as other similar products presented in the literature reports. In all cases, the physical diameter of the ferrophase particles was measured using electron microscopy data. The average values were first considered but the whole distribution histogram was also analyzed. The percentage of relatively small particles (under 5 nm) was compared with the percentage of relatively large particles (over 10 nm). The presence of exceptionally large aggregates was also discussed in order to assess the quality of the magnetic colloids prepared by us in comparison with the products from several other countries.

**Keywords:** ferrofluids, box-plot, size distribution

### 1. Introduction

Ferrofluids are colloidal solutions of magnetic particles suspended within a carrier fluid. The magnetic particles, are usually ferrites, having the general composition  $MFe_2O_4$  (M being a bivalent metal cation such as Ni, Co, Mg or Zn, the magnetite,  $Fe_3O_4$  being frequently present in combination with the maghemite  $\gamma$ - $Fe_2O_3$ ).

Initially produced by grinding large particles in suitable organic solvents and sieving [1], ionic ferrofluids are now prepared chemically, mostly by following the Massart method [2].

To prevent ferrophase particles agglomerations, good quality coating of small size particles need to be carried out. The small size of ferrophase particles in ferrofluids intended for biological applications is needed for the good penetration of biological tissue but larger particle aggregates are not necessary dangerous if their biodegradability is considered.

Many efforts of the physicists from Iassy (Romania) University (1978 – 2004) were dedicated to the production of stable magnetic colloids and successful projects have opened new promising ways for both technical and biological applications. Significant results in ferrofluid preparation, ferrofluid characterization and biological applications (experiments with plants and microorganisms) have been obtained.

In the future the applications of the magnetic fluids will be focused more toward the biological uses where the ultra fine ferrophase is particularly important the size distribution of the magnetic colloids remaining a major problem.

## 2. Experimental procedure

We carried out a comparative study regarding one ferrofluid prepared in our laboratories (based on petroleum [3] and some other ferrofluids used in biological applications accordingly to in the literature reports mentioned below.

The ferrophase (about 5% volume) was obtained by chemical precipitation from autocatalytic reactions of  $\text{FeSO}_4 \cdot 7\text{H}_2\text{O}$  and  $\text{FeCl}_3 \cdot 6\text{H}_2\text{O}$  in the presence of the NaOH aqueous solution, according to Massart's project. Oleic acid (10% volume) has been used to stabilize the ferrophase particles while petroleum (85% volume) was the carrier liquid.

Particle size distribution was studied using transmission electron microscopy (Tesla TEM device with a resolution of 1.0 nm) on collodion sheet, the ferrofluid being diluted  $10^{-4}$  in toluene.

The box-plot technique, proposed by Koopmans [4], was applied to get comparative picture of this ferrofluid size distribution and some other similar products.

The box-plot representation is able to represent a distribution curve by means of a draw box, being recommended for both large and small data series, since practically all the values are shown. This representation method is consistent with the transformation of any distribution curve into a "box" provided with two "tails" and certain "outliers". The range of experimental data is divided into three subintervals defined as follow:

- 1) The box length, limited by  $Q_1$  and  $Q_3$ , i.e., the data corresponding to cumulative percentile frequencies between 25% and 75%. This subinterval contains about 50% of the total data points of the studied series.
- 2) the subinterval contained within the box tails,  $A_1$  and  $A_3$ , given by relations (1) and (2)

$$Q_1 - 1.5(Q_3 - Q_1) < A_1 < Q_1 \quad (1)$$

$$1.5(Q_3 + Q_1)_1 > A_3 > Q_3 \quad (2)$$

(About 80% of the total data points in the studied series can be found within this larger subinterval, which includes the box length);

- 3) exceptionally large or small values (which are represented as white circles placed near the box), according to relations (3) and (4):

$$Q_1 - 3(Q_3 - Q_1) < \circ < A_1 \quad (3)$$

$$Q_3 + 3(Q_3 - Q_1)_1 > \circ > A_3 \quad (4)$$

A "median"  $M$ , corresponding to the cumulative percentile frequency of 50%, is plotted as a vertical line within the box (Fig.1). For symmetrical curves, this line overlaps the average value. In other cases,  $M$  is able to indicate curve asymmetry, as do the box tails.

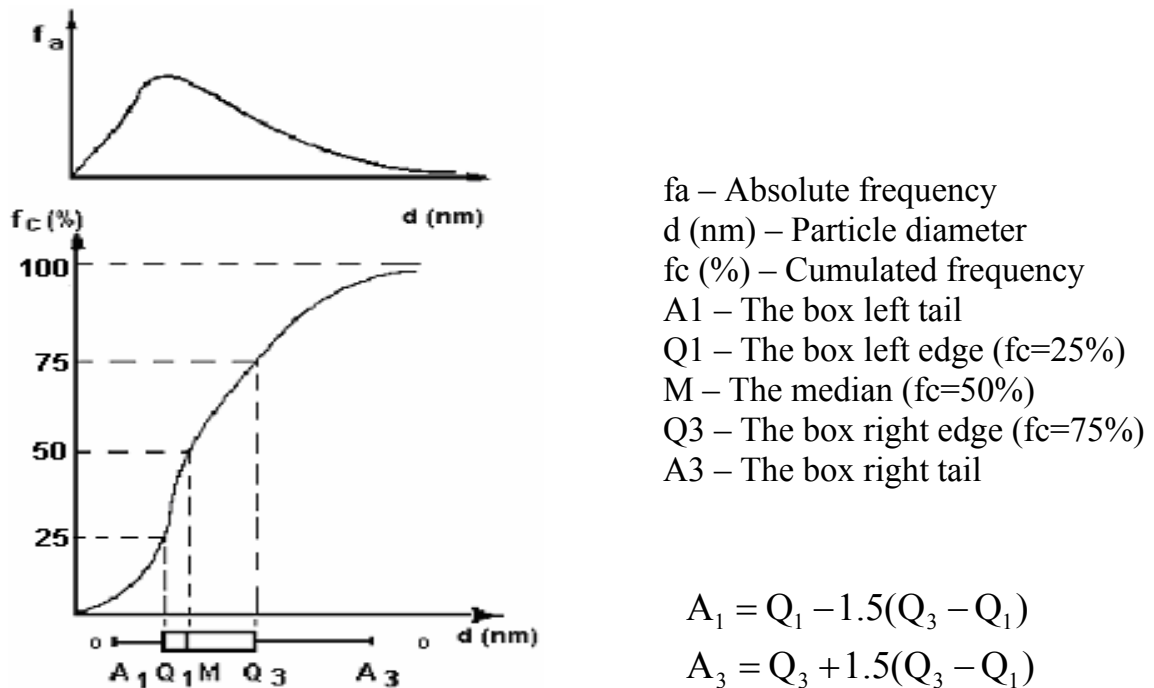


Fig.1. The transformation of the absolute frequency curve of the analyzed data series into the cumulated frequency curve and further into the box plot. Exceptional values are plotted by white circles.

Comparisons between related or similar data point set can be successfully carried out in a very convenient manner using the box-plot representation, no matter if symmetrical or nonsymmetrical, monomodal or multimodal, ranging from large to small size intervals.

### 3. Experimental results and discussion

The visual inspection of the box-plot representation corresponding to the particle size distribution for sample S (petroleum based ferrofluid synthesized in our laboratory), led to the next issues:

- About 50% of the data points are smaller than  $Q_3=5.5$  nm but not smaller than  $Q_1=3.0$  nm; box length are 2.5 nm.
- At least 80% of the data points are not smaller than  $A_1=2.0$  nm but not larger than  $A_3=11.0$  nm. The exceptionally large size aggregates “outliers”, were found at 17.0 nm and 25.5 nm. The asymmetry is accentuated: the median position is closer to the left edge where the most values are concentrated.
- The right tail ( $A_3-Q_3$ ) is longer than the left one ( $Q_1-A_1$ ), consequently the small particles are dominated (no smaller than 2.0 nm) in comparison to the large ones (not larger than 11.0 nm).

The comparison (Fig.2) of the analyzed sample “S” with other six ferrofluids used in biological applications:  $S_1$  – water based ferrofluid (stabilized with carboxidextran)

[5, 6],  $S_2$  - water based ferrofluid (stabilized with dimercaptosuccinic acid) [7],  $S_3$  - water based ferrofluid (stabilized with dodecanoic acid) [8],  $S_4$  - iron oxides in aqueous suspension (stabilized with polyvinyl alcohol) [9],  $S_5$  - iron oxides in petroleum (stabilized with oleic acid) [10],  $S_6$  - hydrocarbon based ferrofluid (stabilized with oleic acid) [11], led to the following results.

After the application of box-plot technique to these six samples the characteristic parameters presented in the Table 1 are obtained.

Table 1 Statistical analysis by means of box-plot technique

Sample	$A_1$ (nm)	$Q_1$ (nm)	$M$ (nm)	$Q_3$ (nm)	$A_3$ (nm)	Exceptional values (nm)	
S	2.00	3.00	4.00	5.50	11.00	17.00	25.50
$S_1$	4.00	6.64	9.45	12.27	20.71	24.93	
$S_2$	3.82	5.68	6.80	8.18	11.88	0.1	13.76
$S_3$	3.36	7.00	8.96	11.88	19.18	20.19	
$S_4$	3.98	6.71	8.50	10.36	15.83	18.57	
$S_5$	7.00	9.00	10.75	12.50	14.00	16.00	17.00
$S_6$	4.30	6.23	8.57	10.93	17.98	21.50	

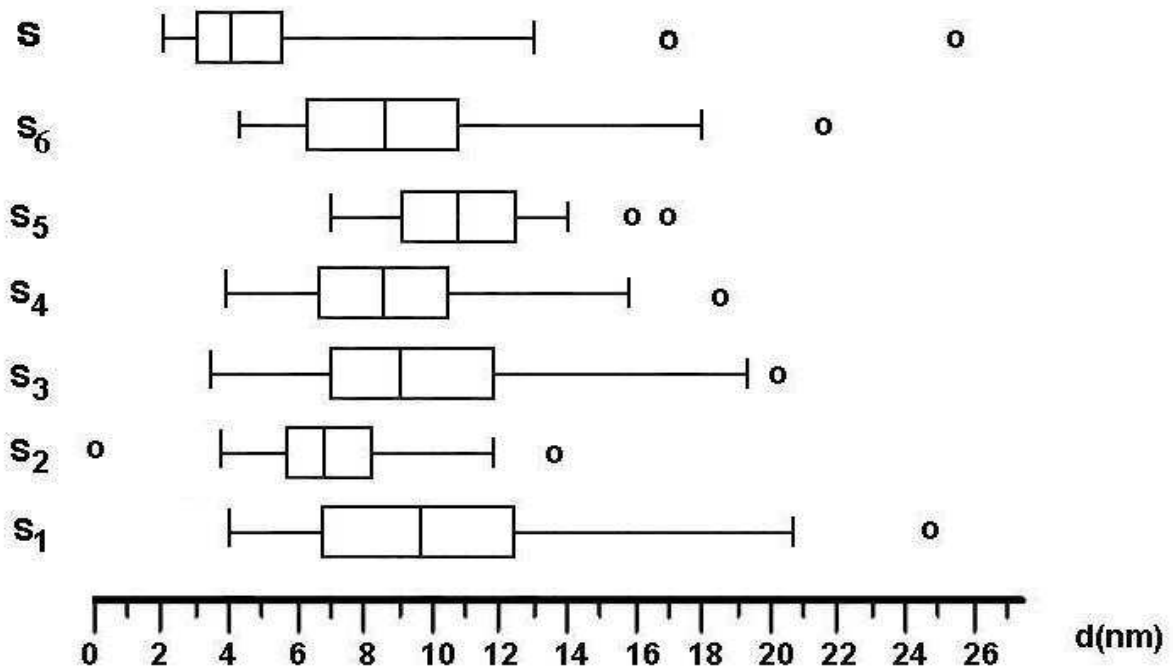


Fig.2 Comparison analysis between samples S and  $S_i$  ( $i = 1..6$ ).

Regarding the comparison picture (Fig.2) and Table 1, we may see that the sample S has the smallest  $A_1$  value from all data.

All the  $Q_1$  values for samples  $S_i$  ( $i=1..6$ ) are the larger than  $Q_3$  value for sample S. In the Table 2 are presented the box length ( $Q_3-Q_1$ ) values, left tail ( $Q_1-A_1$ ) values and right tail ( $A_3-Q_3$ ) values for sample S and samples  $S_i$ .

Table II Experimental values of the box length, left tail and right tail

Sample	$(Q_3-Q_1)$ (nm)	$(Q_1-A_1)$ (nm)	$(A_3-Q_3)$ (nm)
S	2.50	1.00	5.50
S <sub>1</sub>	5.63	2.64	8.44
S <sub>2</sub>	2.50	1.86	3.72
S <sub>3</sub>	4.88	3.64	7.30
S <sub>4</sub>	3.65	2.73	5.47
S <sub>5</sub>	3.50	2.00	1.50
S <sub>6</sub>	4.70	1.93	7.05

Sample S has the smallest box length. One may see that the ferrofluid S<sub>2</sub> has the same box length value as the sample S, analyzed inhere, but its A<sub>1</sub>, Q<sub>1</sub>, Q<sub>3</sub> and A<sub>3</sub> values are the smallest.

So, we might say that the sample S is representing a more stable ferrofluid than the samples S<sub>i</sub>. Also, the ferrophase size distribution of the sample S is characterized by preponderantly small particles, with small number of large aggregates, which is making it suitable for both technical and biological applications.

#### 4. Conclusion

The box-plot representation method seems to be a convenient analytical method for the comparative study of ferrophase dimension regarding the special importance of this ferrofluid feature in the assurance of stability and biocompatibility.

Received: April 27 2005

The "Gh.Asachi" Technical University from Iasi

#### REFERENCES

1. Kaiser R, Rosensweig R.E (1969), Study of ferromagnetic fluid. NASA CR, 1407
2. Massart R. (1982) Magnetic fluids and process for obtaining them. US Patent 4. 329 - 241.
3. Creanga, D., Calugaru, Gh., Journal of Magnetism and Magnetic Materials, vol. 289, 2005(81-83)
4. Koopmans, L.H., Introduction to contemporary statistical methods, Duxbury, Boston, 1987, 683.
5. C. Groß, K.Büscher, E. Romanus, C, A, Helm, W.Weitschies, European cells and Materials vol.3, suppl.2, 2002 (163-166)
6. C. Groß, E. Romanus, K.Büscher, C,A, Helm, W.Weitschies, 3<sup>rd</sup> Colloquium DFG SPP 1104, Benediktbeuern, Germany, Sep.30-Oct.2, 2002
7. A. Halbreich, J. Roger, JN Pons, D, Geldwerth, MF Da Silva, M. Rodier, JC Bacri, Biochimie (1998), 80, 379-390
8. L.M.Lacava, B.M. Lacava, R.B. Azevedo and all, JMMM 225(2001) 79-83
9. M. Chastellain, A Petri, M. Hofmann and H. Hofmann, European cells and Materials vol.3, suppl.1, 2002 (11-12)
10. Trusculescu, M., Lita, M., Rev. Roum. Sci. Tech. 30, 317, 1985
11. Massart, R., Zins, D., Gendron, F., Mehta, R.V., Upadhyay, R.V., Goyal, P.S., Aswal, V.K., Electron spin resonance investigation of Mn-Zn ionic ferrofluid, 8<sup>th</sup> ICMF, Abstract book, 47-48.

**STABILITATEA FEROFUIDELOR – STUDIU COMPARATIV****(Rezumat)**

Structura complexă a suspensiilor coloidale magnetice, numite ferrofluide, implică asigurarea stabilității lor ca cerință pentru ambele aplicații; tehnice și biomedicale. Pentru prevenirea aglomerării particulelor de ferofază este necesară obținerea unei bune stabilizări. Particulele de ferofază de dimensiuni mici sunt esențiale nu doar pentru omogenitatea ferrofluidului cât și pentru o penetrare eficientă a structurilor biologice. În această direcție, am pornit un studiu comparativ privind un ferrofluid preparat în laboratoarele noastre (cu petrol ca lichid de bază) cât și alte produse similare prezentate în literatura științifică relatată. În toate cazurile, diametrul fizic al particulelor de ferofază a fost măsurat utilizând microscopia electronică. În primul rând au fost considerate valorile medii, dar au fost de asemenea analizate și curbele de distribuție. Procentul particulelor relativ mici (sub 5nm) a fost comparat cu cel al particulelor relativ mari (peste 10nm). Prezența agregatelor excepțional de mari a fost discutată în legătură cu aprecierea calității ferrofluidelor preparate de noi în comparație cu produsele din alte câteva țări.

## DETERMINATION OF PHYSICAL-MECHANICAL PARAMETERS OF MULTILAYERED COMPOSITE MATERIALS THROUGH ULTRASONIC METHODS

BY

ADRIANA SAVIN, ROZINA STEIGMANN and RAIMOND GRIMBERG

**Abstract:** In solid materials, so electrical longitudinal as well as transversal waves can propagate. If the material has small thickness, the possibility of producing of guided waves, Lamb wave, exist. The propagation speed of these waves, depend by physical and mechanical parameters as density, elasticity modulus, shearing modulus, Poisson coefficient. In this paper, we present two determination methods: using hertzian contact for the materials with high elasticity modulus (carbon-epoxy, glass-epoxy composite materials) and using transducers without contacts for the materials of which surface can't be impress (wood-based composites, veneered and varnished).

**Keywords:** ultrasonic nondestructive evaluation, mechanical parameters, multilayered composite materials, noncontact transducers, transducers with hertzian contact, wavelets

### 1. Introduction

In acoustic – ultrasonic nondestructive evaluation (NDE), an ultrasonic stress or shear wave is introduced into, or generated within, the interrogated structure and detected after it has propagated through the structure. Stress or shear wave propagation is affected by the micromechanical and morphological materials states of the medium of propagation [1], [2]. Thus, ultrasonic NDE involves the characterization of the tested structure on the basis of information containing in the transmitted wave signal.

The state of the structure, which governs wave propagation and detection, can be described by a broad range of properties and conditions, some of which are:

Material properties: elastic and shear modulus, density, attenuation coefficients, etc.  
Geometrical properties: structural dimensions, discontinuities, micro and macro structural defect states, etc.  
Environmental conditions: mechanical loading, residual stresses, temperature, etc.  
Measurement conditions: location and size of transducers, sensitivity and frequency response of transducers, characteristics of electronic equipment, etc.

Even from this incomplete list, it is clear that the quantitative ultrasonic determination of a specific material property state, independent of all other states, is difficult [3]. To complicate matters further, many NDE parameters can be measured from an ultrasonic interrogation of material and a large amount of data can be generated from a single ultrasonic measurement via Fourier transform, wavelet

transform, etc. Large multivariate data sets are difficult to decipher thus, methods of summarizing and extraction are accomplished in an ad hoc qualitative manner. One approach for quantitative acquisition of discriminatory information that can often isolate a single structural state is pattern recognition.

Determining the state of a sample via ultrasonic NDE using pattern recognition techniques consists of three basic steps:

- (i) Generating and processing ultrasonic NDE data
- (ii) Selecting significant features of the data
- (iii) Determining the sample state from the selected features.

In this paper, ultrasonic NDE data are obtained by two methods: hertzian contact [4] and without contact ultrasound transducers [5]. First method is utilized for the control of the materials with high elasticity modulus (carbon-epoxy, glass-epoxy composite materials), and the second for the control of the materials of which surface can't be impress (wood-based composites, veneered and varnished). Data generation consists of measurements of transmitted ultrasound signals that are expected to contain information about mechanical properties of samples and signal conditioning. The processed data are arranged in an order set called a pattern vector. A subset of the pattern vector is selected and is called the feature vector which lies in a vector space called feature space. Geometrically speaking, the feature vectors form distinct and no overlapping clusters in feature space. A suitable feature vector produces the maximum separation between clusters, measured by means Mahalanobis distance. The last step of our algorithm is the classification using discriminant functions.

## 2. Theoretical background

It exist quantitative substantiation correlations between ultrasound velocities and mechanical properties of samples provided by

$$v_L^2 = \frac{E}{\rho} \frac{(1+\nu)}{(1+2\nu)(1-\nu)} \quad (1)$$

$$v_T^2 = \frac{G}{\rho} \quad (2)$$

Where  $v_L$  is longitudinal velocity,  $v_T$  is transversal velocity, E elastic modulus, G shear modulus,  $\rho$  sample density,  $\nu$  Poisson ratio.

Supplementary, we can utilized and the normal velocity of Lamb wave provided by [6]

$$c_y = -ik\alpha cA \cosh(\alpha y) + k^2 cB \cosh(\beta y) \quad (3)$$

where c is given by

$$c = \left( \frac{D_1}{2\rho_2 h} \right)^{1/4} \omega^{1/2} \quad (4)$$

with

$$D = \frac{3}{4} \left( \frac{1-\nu_1^2}{E_1} + \frac{1-\nu_2^2}{E_2} \right) \quad (5)$$

h is the plate thickness, and  $r_2$ ,  $l_2$ ,  $m_2$  are the density and the Lamé constants respectively, for the wood plate.

In the case of without contact ultrasound transducers, we can measure longitudinal and transversal velocities and we must determine 4 mechanical parameters. In the case of Hertzian contact ultrasound transducers we can measure only the normal velocity of Lamb wave and we must determine the same number of mechanical characteristics of samples [7].

In these conditions we must multiply the number of ultrasound data, using, for example, the wavelet transform of transmission signals.

### 3. Experimental set-up

The principle of experimental set-up for the evaluation with non contact transducers is presented below.

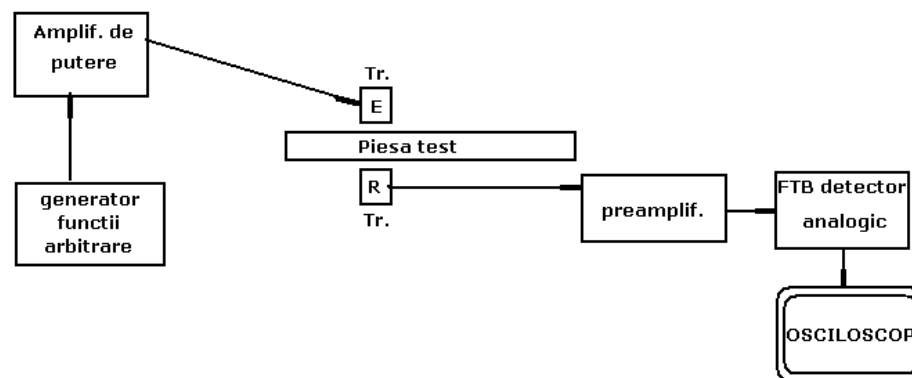


Fig.1 Experimental set-up for US control with noncontact transducers

The electronic part of equipment is a SFT4001G board that allows the functioning in send-receive way, assuring the amplitude of impulse between 100V and 400V; the wave type – negative impulse with increasing time lower than 10ns, the impulse duration, measured at 50% from amplitude on a standard charge for the characteristic impedance of cable  $50\Omega$ , being at least 30ns; the wave shape of emission impulse - rectangular or spike with different energies, the frequency of emission impulse being between 150Hz and 16KHz, the gain of 70dB, in 1dB steps covering any situation. The filtering of received signals are made by high pass filter with at least 50dB attenuation on decade, starting from 800kHz frequency (the 10<sup>th</sup> harmonic of work frequency), low-pass filter with at least 50dB attenuation on decade, starting from 500kHz frequency.

For the coupling of the US board with the PC, the system shall have an internal clock at 100MHz.

The analog-digital convertor used to digitize the received signals has 500MHz sampling rate.

The level of noise imposed being 400mV, shows that a rapid convertor, flash type, with 500MHz sampling rate shall be enough, the precision of quantification being enough in the case of 8 bits quantizer. If it is starting from 2V, reference tension, one LSB (Least Significant Bit) represents 7,843 mV.

To transfer the data to computer, the acquisition system should contain a memory buffer of minimum 32Ko, thus meaning 1000 samples memorated and, from

this reason, using a flash convertor, the complete examination in  $\sim 3\text{m}$ , enough for the US propagation in multilayered material, can be assured.

Figure 2 presents a sketch of the measuring equipment. The frequency of the ultrasound beam was 60kHz.

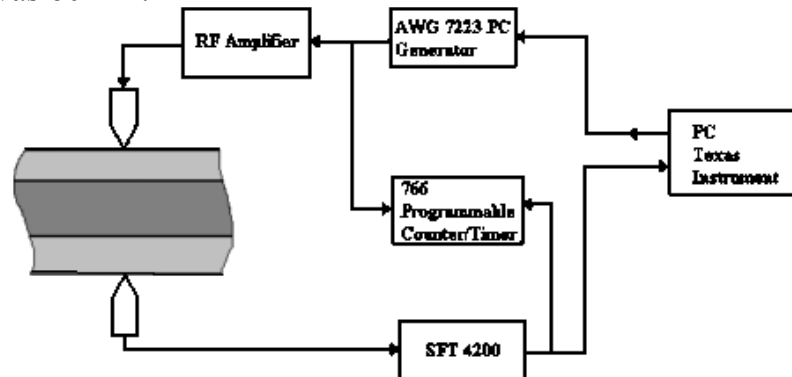


Fig 2: The basic diagram of the equipment

The two buffer rods used at the emission and reception are both identical, being made of the 7075-T6 aluminum-magnesium alloy, with the density  $2.7 \times 10^3 \text{ kg/m}^3$ , the Young modulus  $7 \times 10^{10} \text{ N/m}^2$ , the Poisson coefficient 0.34 and a point curvature radius of 3mm.

Figure 3 schematically presents a ultrasonic transducer with Hertzian contact at the buffer rod-plate interface, which converts the P waves from the buffer rod to Lamb's wave from the plate.

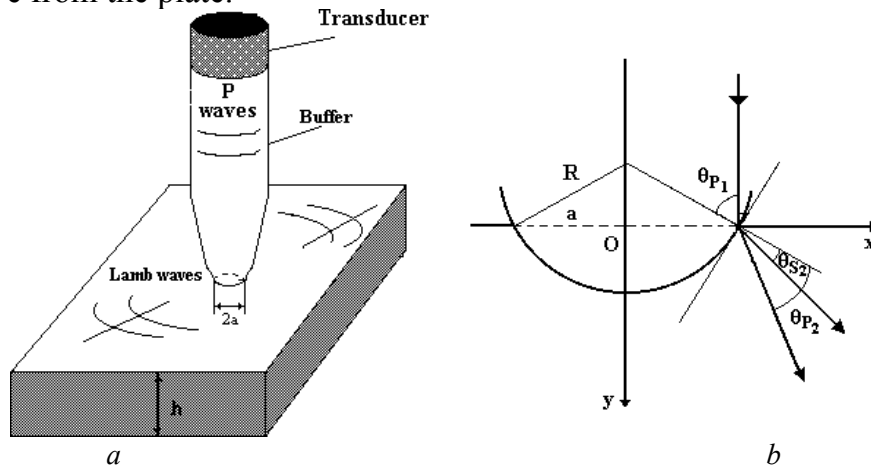


Fig. 3: a. Transducer with Hertzian contact b. The detail of the control

#### 4. Samples

The samples from carbon epoxy composite materials were:

1. T300/5208 with carbon fibres Hercules AS4 type, average diameter  $18\mu\text{m}$ , the matrix from thermosetting epoxy resin 5208 made by Boeing have Young longitudinal modulus 116GPa, Young transversal modulus 12.1GPa, the shear modulus  $G=5.5\text{MPa}$ , the density  $1.54 \times 10^3 \text{ Kg/m}^3$  and Poisson coefficient 0.329.
2. IM7/8551 Hercules with carbon fibres Hercules IM7 type, average diameter  $17\mu\text{m}$ , the matrix from thermosetting epoxy resin 8551 made by Boeing have Young longitudinal modulus 107GPa, Young transversal modulus 11.3GPa, the

shear modulus  $G=4.3\text{MPa}$ , the density  $1.58 \cdot 10^3 \text{Kg/m}^3$  and Poisson coefficient 0.30.

3. IM12/7652 Hercules with carbon fibres Hercules IM12 type, average diameter  $17\mu\text{m}$ , the matrix from thermosetting epoxy resin 7652 made by Boeing have Young longitudinal modulus  $112\text{GPa}$ , Young transversal modulus  $9.2\text{GPa}$ , the shear modulus  $G=5.1\text{MPa}$ , the density  $1.53 \cdot 10^3 \text{Kg/m}^3$  and Poisson coefficient 0.38.

For wood based products the samples are panel type. The most important quality criteria, respective the bonding strength is the shearing bonding strength. The samples have a simple construction. The measurement equipment used for destructive testing is one of National Institute of Wood, Bucharest. For shearing and bending testing, the universal machine for wood strength testing type VEB WERKSTOFF-PROFMASCHINEN-Leipzig was used. For determination of elastic modulus was used testing machine type 2D90/100 with mechanical system for the recording of deformation function of tension.

The panel samples with  $250 \times 250\text{mm}$  and  $450 \times 450\text{mm}$  from 3, 5, 7, and 9 layers of veneer are preponderant from beech (*Fagus Silvatica L*), the most used in our country. The results obtained from US nondestructive testing were compared with the destructive. The results are presented in the Table 1.

Table 1 Wood based panel samples

No.	Species	No.of layers	Thickness [mm]	Dimensions [mm]	Glue	Density $\text{Kg/m}^3$	Elastic modulus [MPa]	Shearing modulus [MPa]
1	beech	3	3.55	450x450	Urelith C	756	11795	2.042±32%
2	Beech	5	6.58	450x450	UrelithC	740	10683	1.9044±29%
3	Beech	5	6.46	250x250	Urelith C	715	10721	1.9514±29%
4	Beech	3	3.20	250x250	polyurethane	697	11545	2.042±32%

The glue used for experiments was Urelith C for the panels, but for comparing other glues were used: FENOPLAC and Polyurethane. The pressing-on was made in laboratory press Siempell Kamp. The samples tested have allow to correlate mechanical parameters (density, elastic modulus, shearing modulus) and the time of US flight for all the types of multilayered panel considered. These methods allow the nondestructive evaluation of mechanical properties and the existence of discontinuities in multilayered composite materials based on wood, taking into account by the especially applications of these products.

## 5. Experimental results

For nondestructive determination of mechanical parameters of the samples from carbon-epoxy composite materials, Lamb waves generated in material with transducers with hertzian contact were used. In this case, only the normal component of Lamb wave speed and the shape of signal transmitted through composite plate were measured [8], to multiply the information, the transmitted signal was decomposed using wavelets transform with Daubechies wavelet type.

Thus, a feature vector with 7 components (Lamb wave normal speed, the amplitude of transmitted signal, the coefficients of the first 5 wavelets) was obtained, as well as a super-determined linear algebraic system

$$X_i = a_{1i}E + a_{2i}G + a_{3i}(1/\rho) + a_{4i}\nu; \quad i=1, \dots, 7 \quad (6)$$

where  $E$  is Young's modulus,  $G$  – shear modulus,  $\rho$  – density,  $\nu$  Poisson's ratio,  $X_i$  –  $i^{\text{th}}$  component of feature vector.

The maximisation of Mahalanobis distance was experimentally made by modification of the signal frequency applied to emission transducer, the optimal frequency being 80kHz.

The system (6) as matrix is write as

$$\{X\} = [a]\{M\} \quad (7)$$

where  $\{X\}$  is feature vector,  $[a]$  model matrix and  $\{M\}$  mechanical characteristics vector. Using a board from carbon-epoxy composite material with known properties, the model matrix  $[a]$  is determined using the inverse method in More-Penrose sense. Then, obtaining the feature vector from measurements and knowing model matrix, for the same materials, the principally mechanical characteristics can be determined. The relative error for determination of transversal Young modulus is 9.3%, for shear modulus is 5.3%, for density is 6.2% and for Poisson's ratio is 6.3%.

The using of ultrasound transducers without contact is a premiere in Romania, and thus we will insist on this [9].

The shape of electric signal applied to the emission transducers is presented in Figure 4.

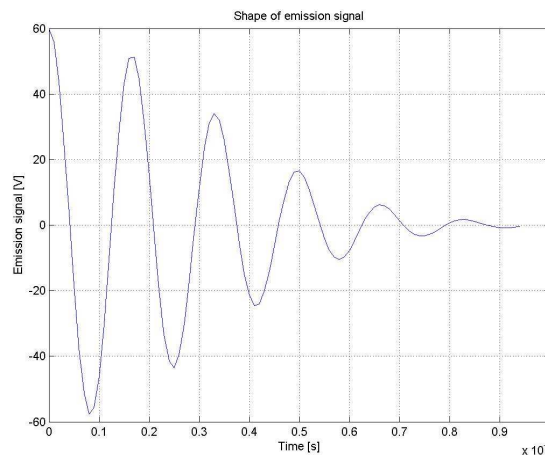


Fig.4 The shape of emission signal

Measuring the time between the emission of the ultrasound signal and his reception, taking into account the material thickness and the air zone thickness, knowing the ultrasound propagation speed through air at the temperature at what experiment is done, immediately is determined the longitudinal waves speed. For the generation of transversal waves into material, the emission transducer without contact is tilted reported to the normal at sample surface with an angel of  $44^{\circ}$ . According to Snell law, a changing of propagation mode will have place, the incident longitudinal wave being transformed in transversal wave at the boundary air material surface. The second changing will take place at the interface material air. The tilting angle of the

transducer is experimentally determined thus the amplitude of received signal shall be maximum.

In Figure 5 is presented the shape of the signal received by the reception transducer without contact, after the ultrasound fascicle has traveled through a wood panel with 6.58 mm thickness.

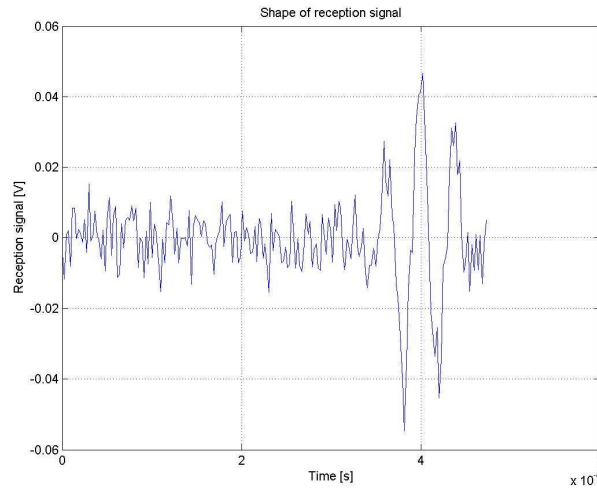


Fig. 5 The shape of received signal

To multiply the information, the Daubechies [10] wavelets transforms are used, the results being presented in Figure 6.

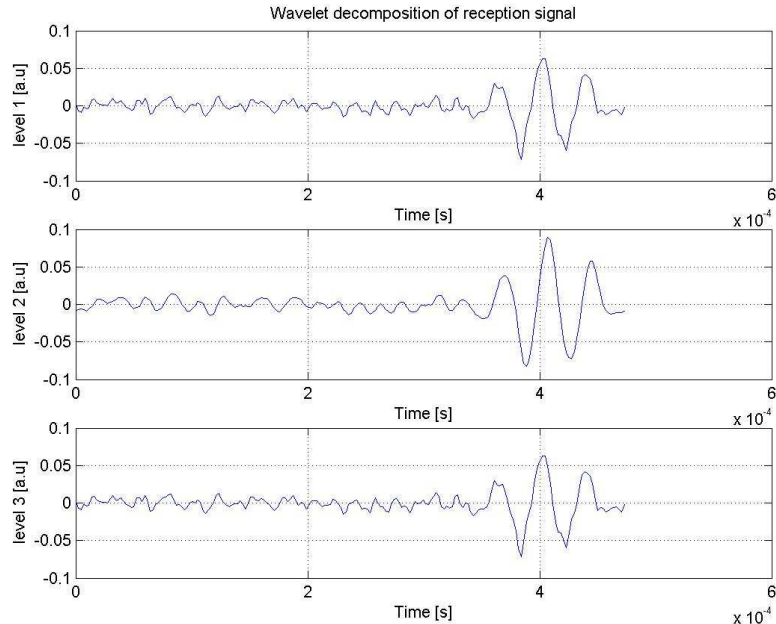


Fig.6 The wavelet decomposition of received signal

The Mahalanobis distance is maximized for the frequency of emission pulse by 60kHz.

The error in determination of Young modulus is 4.8%, for density is 5.6%, for shear modulus is 6.5% and for Poisson's ratio is 5.7%.

## 6. Conclusions

The ultrasonic NDE data are obtained by two methods: hertzian contact and without contact ultrasound transducers. First method is used for the control of the materials with high elasticity modulus (carbon-epoxy, glass-epoxy composite materials), and the second for the control of the materials of which surface can't be impress (wood-based composites, veneered and varnished). The experimental results contain information about mechanical properties of samples and signal conditioning.

## Acknowledgements

This paper was partially support by Romanian Ministry of Education and Research, under CERES Contract No. 3-4/2003.

*Received April 28 2005*

*National Institute of Research and Development  
for Technical Physics Iasi*

## REFERENCES

1. C.S.Wang, F.K.Chang, Built in diagnostic for impact damage identification of composite structures, Structural Health Monitoring 2000, ed. F.K.Chang Technomic Publishing Co, Lancaster, 1999, p.612-621
2. V.Bucur, MP Ausell, C.Y.Barlow, J.Pritchard, S.Gaross, X.Deglise, Physical methods for characterizing wood composites, Holzforshung (52), 1998, p.553-561
3. J.C.Krapez, D.Balageas, A.Deom, F.Lepoutre, Comparison of established and emerging NDE techniques applied to delamination in composite materials, 6<sup>th</sup> European Conference on NDT, Nice, 1994, p.257-261
4. R. Grimberg, Savin A, Lupu A, Rotundu C. (2000), A Method to Determine the Debonding Zones in Multilayers Wood Materials, Proceedings of 15th World Conference on Nondestructive Testing, Roma , Italy, IDN522.
5. M.C.Bhardwaj, High efficiency noncontact transducer and a very high coupling piezoelectric composite, 16<sup>th</sup> World Conference on Nondestructive Testing, Montreal, Canada, IDN716
6. L.W.Schmerr Jr., Fundamentals of Ultrasonic Nondestructive Evaluation, A modeling approach, Plenum Press, NY, 1998
7. F.Levent Degertekin, T. Butrus Kuriyakub, Single mode Lamb wave excitation in thin plates by hertzian contact, J.Appl.Phys.Letter, 69, 2, 1996, p.146-148
8. R. Grimberg, Adriana Savin, A.Andreescu, Lelioara Iancu, Rozina Steigmann, Nondestructive evaluation of timber, panels and batten board, The 1<sup>st</sup> INTERNATIONAL CONFERENCE ADVANCED CONCEPTS IN MECHANICAL ENGINEERING, Bul.Inst.Polit.Iasi, t. L(LIV), Fasc.6B, 2004, pg.147-152
9. NDT Solutions Ltd – User manual for US noncontact transducers NCG100D25
10. B. Dubuisson, Diagnostic et reconnaissance des formes, Hermes, Paris, 1990

## DETERMINAREA PARAMETRIILOR FIZICO-MECANICI A MATERIALELOR COMPOZITE MULTISTRAT PRIN METODE DE ULTRASUNETE

### (Rezumat)

In materialele solide se pot propaga atat unde electrice longitudinale cat si transversale. Daca materialul are grosime mica exista posibilitatea producerii de unde ghidata, unde Lamb. Viteza de propagare a acestor unde depinde de parametrii mecanici si fizici ca densitate, modul de elasticitate, modul de forfecare, coeficient Poisson. In acesta lucrare prezentam doua metode de determinare a acestora: utilizand contactul hertzian pentru materiale cu modul de elasticitat eridicat (carbon epoxy) si utilizand traductori fara contact pentru materiale a caror suprafata nu poate fi amprentata (compozite pe baza de lemn, furniruite sau lacuite).

## EVALUATION OF FATIGUE AT AISI 316L AUSTENITIC STEELS USING EDDY CURRENT MICROSENSORS ARRAY

BY

ADRIANA SAVIN\*, ROZINA STEIGMANN\*, R.GRIMBERG\*, A.ANDREESCU\*,  
V.PALIOVICI\*\* and V.GOANTA\*\*

**Abstract.** This paper presents the realization of 2D eddy current sensors array and the improved response of the array using a super-resolution algorithm. This application was realized to emphasize fatigue cracks, appeared on AISI 316L samples subdued to cyclical loading.

**Keywords:** austenitic steel, fatigue, eddy current, 2D sensors array

### 1. Introduction

The very first nondestructive examination was recorded in Holy Bible, Genesis. After God created the Universe, He stopped and “saw that it was good “.

Since that time, in nondestructive testing examination domain, the perfection in the sense of detection of probability increasing for a highest reliability coefficient, control speed growing and decrease of afferent cost, it is searched. Furthermore, the nondestructive testing is applied to various materials and in different experimental conditions. For electrical conductive materials, structures, pieces and subassemblies, the eddy current control is imposed by specific quality standards, product norms or by direct contracts between producer and beneficiary.

The eddy current control allows the emphasizing of surface-breaking as well as subsurface discontinuities, but not too deep, due to skin effect [1], [2]. The relationship between eddy current frequency and flaw’s detection possibility is rather subtle. It seems evident that for subsurface discontinuities, the work frequency shall be lower, but then, the sensitivity is reduced. This thing is clearly arising from existents analytical modeling.[3-6]. In the moment when from the modeling is passed to real situations, in which the noise inevitably appears, the probability of detection is reduced so for surface-breaking as well as for subsurface discontinuities, too [7,8, 9]. Using inversion methods, the determination of position as well as the shape and geometrical dimensions of discontinuities are allowed. The programs for testing the capability of eddy current method to detect various discontinuities, which are made in robin round system with blind control, shown that still are stage to run-up until the reach of perfection [9].

The development of advanced diagnostic systems that are able to identify and detect material degradation in the microstructures of steels is a new challenge for non-destructive evaluation. The detection of material degradation due to mechanical and/or thermal fatigue can contribute to the increase of exploitation reliability of pieces and

metallic structures as well as to life-time management of certain components [10], [11]. Lifetime extension of nuclear power plants has become an important topic and resulted in the requirement for advanced safety management tools [12]. The appearance and development of martensite phase, ferromagnetic phase that crystallizes in cubic body centered lattice, are specifically to fatigue phenomenon. In the case of austenitic steels (the austenite is a paramagnetic phase that crystallize in cubic face centered lattice) the appearance and development of martensite leads to modification of magnetic permeability of zones that present fatigue phenomenon due to cyclical loading exceeding a specified threshold [13].

## 2. Eddy current linear sensors array functioning

Being for example, a coil of arbitrary shape, placed in vicinity of a plate conductor. An alternative electric current, with temporary dependence  $e^{j\omega t}$  will circulate through coil. Eddy currents will be induced in material. The field created by the coil will be scattered by the eventual discontinuities or material inhomogeneities. With another coil, a Hall element, or an element based on GMR phenomenon [14], a SQUID sensor [15], etc the field scattered by discontinuity can be marked out, so the discontinuity will be detected.

We simulate, in these conditions, the operation of detecting one slot with  $4 \times 0.2 \times 1$  mm dimensions, practiced in AlMg alloy block having  $1.556 \cdot 10^7$  S/m electric conductivity. The emission coil has squared shape with 20mm side, 2mm high and 2 mm width, 100turns and is fed with 0.1A amplitude electrical current and 10kHz frequency. The center of coil is placed over center of slot and it is oriented so the length of slot shall be parallel with a side of coil. To receive the scattered field, a little reception coil, squared too, with 2mm side and 30 turns, is used. The simulations are made with a numerical code, based on dyadic Green's functions and volume integral's method. In the conditions in which the reception coil is displaced over a direction perpendicularly on slot orientation direction, the results are presented in Figures 1a, b.

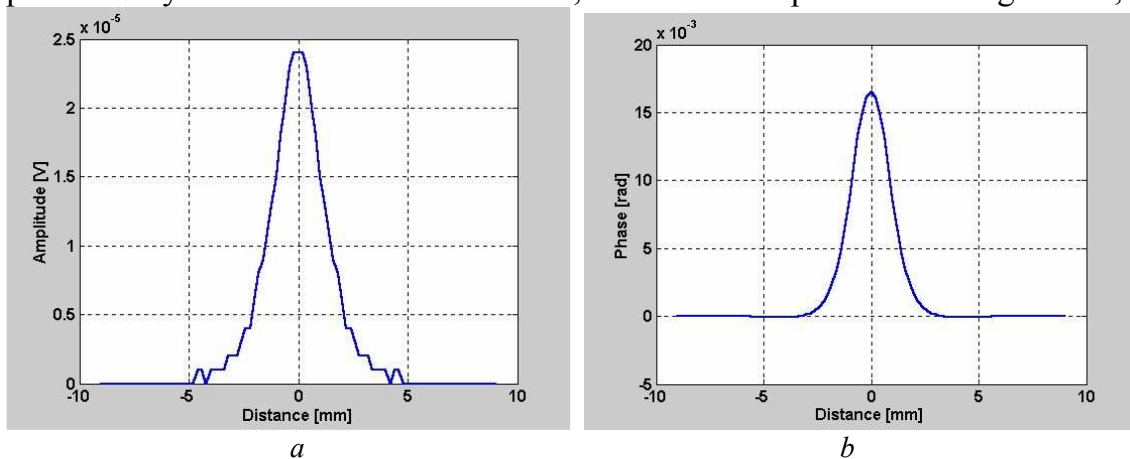


Fig.1. The response of eddy current transducer for the slot positioned in the origins:  
 (a) Amplitude of induced e.m.f. balanced to unflawed region; (b) Phase of induced e.m.f. balanced to unflawed region

In the conditions of noise existence, the discontinuity is perfectly detected, being able to make predictions about its location, solving the inverse problem.

We consider now, the case of two identical slots, parallels, one in the origins and another placed at 2mm from the first (exactly the dimension of a reception coil). The results of simulation are presented in Figures 2 a and b.

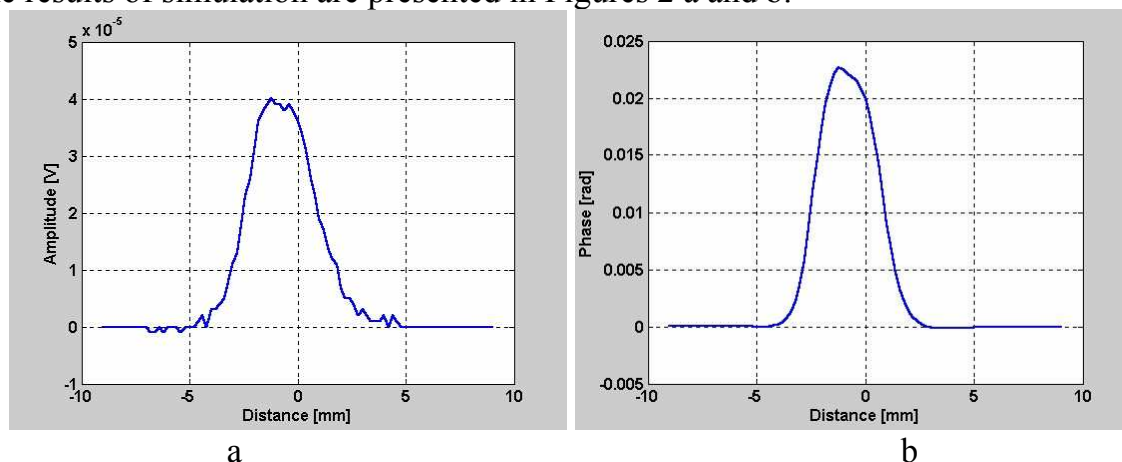


Fig.2. The response of eddy current transducer for two parallel slots positioned one in the origins and another at -2mm: (a) Amplitude; (b) Phase

The analysis of the data from Figure 2 has shown that the problem of determination of discontinuities numbers and their location became much complicate.

If we replace the displacing of reception coil by a number of fix identical reception coils, placed tangential one to each other along to scan direction. For facility, we consider 5 identical squared coils, 2mm sides. The coordinates of reception coils will be  $C_i(-6+2*i,0)$  with  $i=1,2, \dots,5$ .

For the situation described above, the values of induced fem, in the 5 coils having  $C_i$  coordinate centers are presented in Figure 3 a. Due to the distribution of the field in the interior of examined piece, as well as intended disposition of the slots, the amplitudes of signals delivered by the reception coils placed exactly over the center of slots (coils #2 and #3) aren't the same. To equalize, in a certain manner, the sensitivity characteristic of this linear array of which goal is double, will be constructed.

The goals are to make that the response of reception coil should be approximately equal as amplitude and phase for the same material discontinuity, indifferent where it is positioned under the length of array; to prevent the situation in which one discontinuity shall be under exactly 2 coils, which will lead to the fact that the coils from their vicinity shall be influenced and the determination of discontinuity location aren't possible. This situation represents a rank I ambiguity [12] and must be avoided.

The simplest way is to choose a sinusoidal characteristic, having 0 on coil's sides and maximum in center. This value is established, function of linear array response to various discontinuities, diverse situated, making a weight vector.

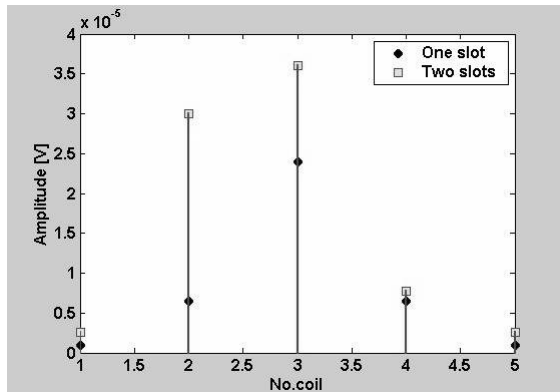
In Figure 3 b we show such characteristic for the case of 2 slots positioned under coils #2 and #3, and in Figure 3 c the results of convolution between the amplitude of signal delivered by array's coils (fig 3a)(constant considered for a coil) and sensitivity characteristic presented in Figure 3b.

For the phase of e.m.f, it is proceed similarly.

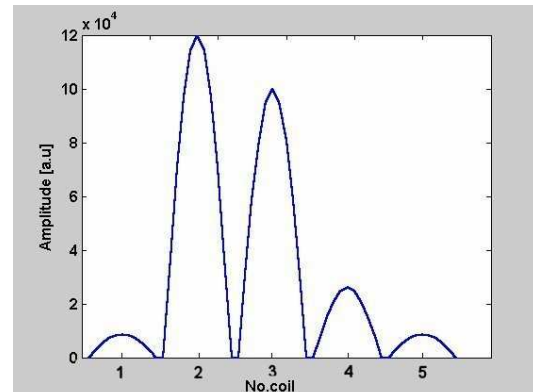
If the vector of reception coils responses is noted  $\bar{x}$  and the weight vector is noted  $\bar{w}$ , the response of array is write as

$$\bar{y} = \bar{x}\bar{w}^H \quad (1)$$

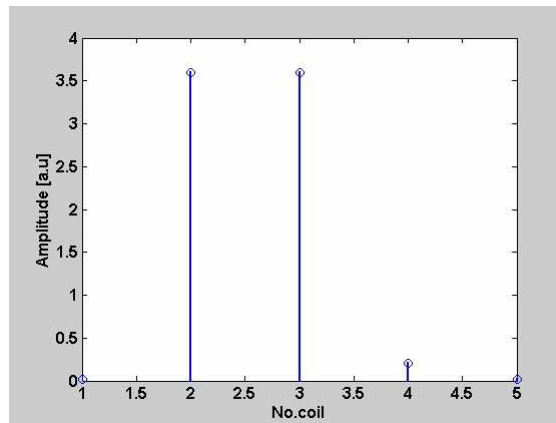
where superscript H denotes the Hermitic operation (i.e. conjugate-transpose). The maximum of response corresponds to discontinuity position.



a) the amplitude delivered by array's coils for one slot under coil 3 and two slots under coils 2 and 3



b) sensitivity characteristic of linear array for 2 slots.



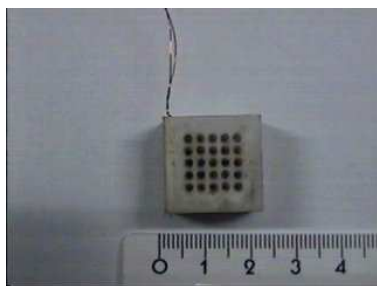
c) the equalization of the responses using sensitivity characteristic.

Fig.3.

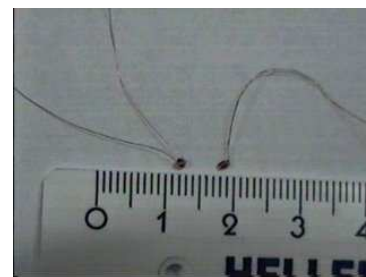
### 3. 2D Eddy current sensor array

Now, we consider a 2D sensor array, made from one emission coils and a 2D reception coils arrangement. The realization of this array is presented in Figure 4 a, b.

The emission part is made from one coil with 20x20mm dimensions, having 100 turns. The reception part is made from 5x5 identical coils having each outer diameter 2mm, the distance between the centers of coils being 2.4mm



a) general view



b) reception coils

Fig.4. Eddy current sensor array

The connection of array to the measurement equipment is presented in Figure 5. The function generator is AWG 7223PC type. The lock-in amplifier is 500MC, connected to a PC through IEEE 488 interface.

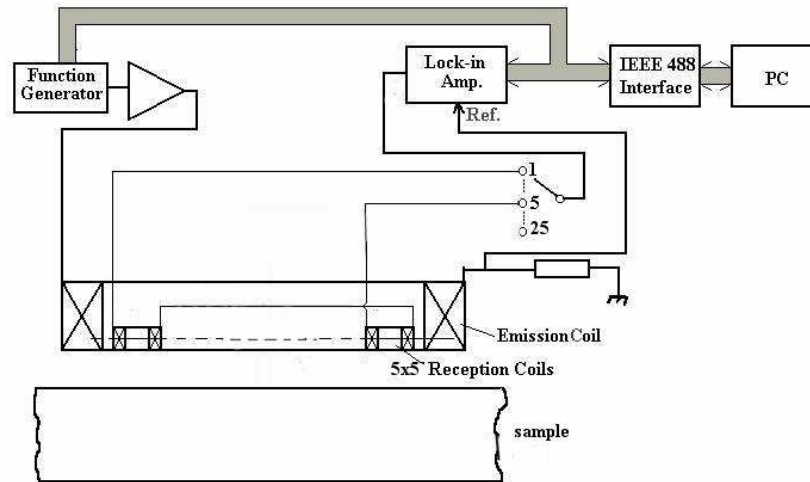


Fig.5 Experimental set-up

Placing the array over the surface of a homogeneous, isotropic plate conductive material, the array response will be obtained. If the material is AISI 316L, 5 mm thickness, the frequency of current in emission coil is 10kHz and amplitude is 0.1A. The results are presented in Figures 6 a and b.

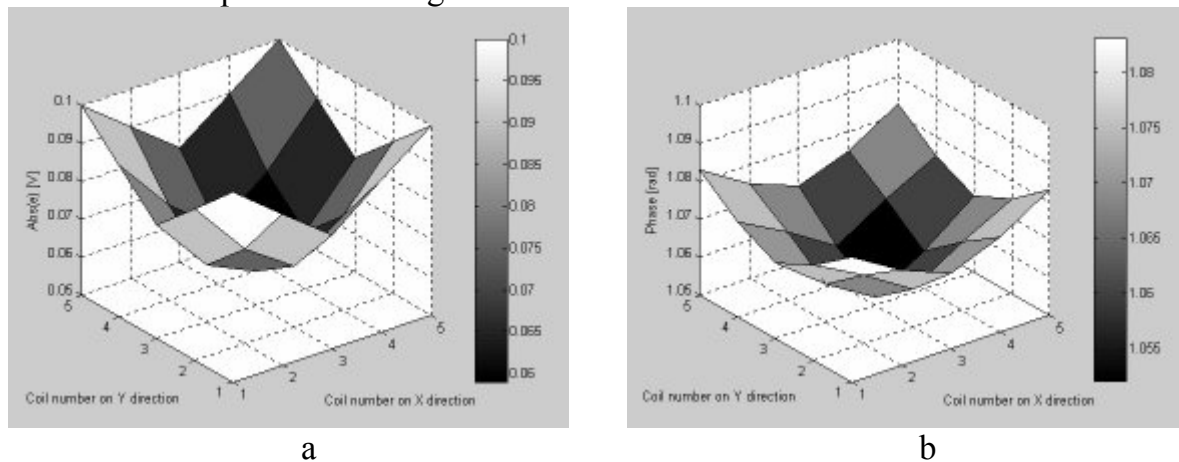


Fig.6. Amplitude (a) and phase (b) of induced electromotive force recorded by each of receiving coils; the sensors array is placed on AISI 316L sample

Placing the array on a plate from the same material, that present 2 hole with flat bottom, having 1mm diameter and 1mm depth, disposed so that they are placed under the center of the reception coils (5,2) and (4,4) (the number from brackets represent the position of sensor in array), the response signal presented in Figure 7 is obtained.

The resolution of eddy current sensors array can be substantial improved using super-resolution procedures, similarly with those developed for radar and sonar [16]

The sensitivity matrix of sensors array will be defined as

$$\bar{A} = \bar{w} * \bar{w}^H \quad (2)$$

with annotations from (1)

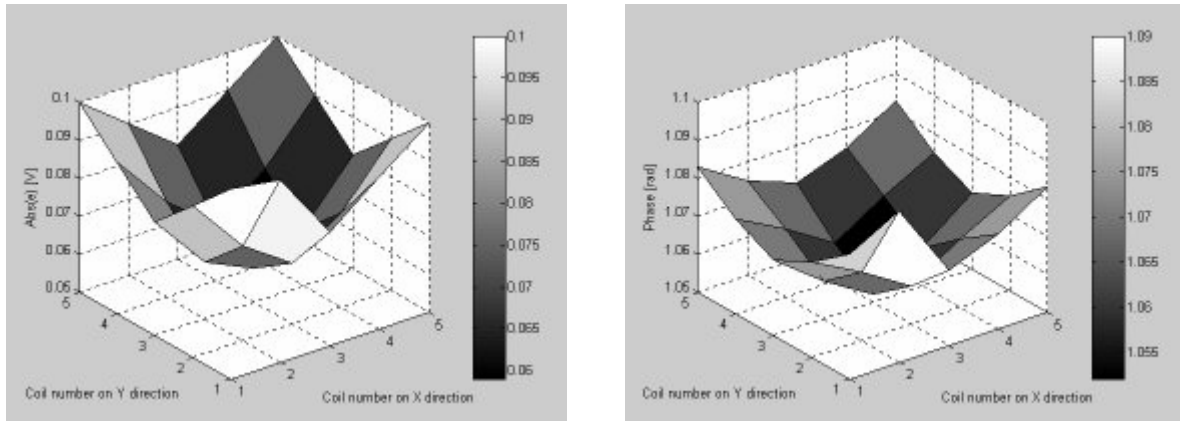


Figure 7. Amplitude (a) and phase (b) of induced electromotive force recorded by each of receiving coils. 2 holes with flat bottom are placed under coils (5,2) and (4,4)

We note

$$\bar{S} = \bar{A}(\bar{A}^H \bar{A})^{-1} \bar{A}^H \quad (3)$$

The autocorrelation matrix of signal delivered by array being

$$\bar{R}_{xx} = \bar{x} * \bar{x}^H \quad (4)$$

The maximum likelihood procedure [17] used as super-resolution method, in the case of coherent sources location, applied to sensors array presented above, shown that the maximum of probability to localize the source is in the region where

$$\max(\bar{S} * \bar{R}_{xx}) \quad (5)$$

is obtained.

#### 4. Application to detection of fatigue in austenitic steel

The appearance and development of martensite phase, ferromagnetic phase that crystallizes in cubic body centered lattice, are specifically to fatigue phenomenon. In the case of austenitic steels (the austenite is a paramagnetic phase that crystallize in cubic face centered lattice) the appearance and development of martensite leads to modification of magnetic permeability of zones that present fatigue phenomenon due to cyclical loading exceeding a specified threshold [13].

The investigations were performed on austenitic stainless steel AISI 316L specimens according to ASTM E606, (Figure 8).



Fig.8 The specimen

The fatigue tests were performed with alternating loading with a test frequency of 2 Hz at room temperature. The amplitude of loading was 150MPa. The samples were electrochemically skived to wear off the eventually oxide track. Metallography

analyses by standard procedure [18] were effect, as well as X ray diffraction using  $\text{MoK}_\alpha$  radiation.

The fatigue cracks were emphasized using penetrant liquid technique [19]. After  $7.5 \times 10^5$  cycles, for samples made from AISI 316L, damage factor had 0.8 value.

In Figure 9 is presented the response of array in this situation and the variation of martensite content in the length of sample determined by X ray diffraction for damage factor de 0.8.

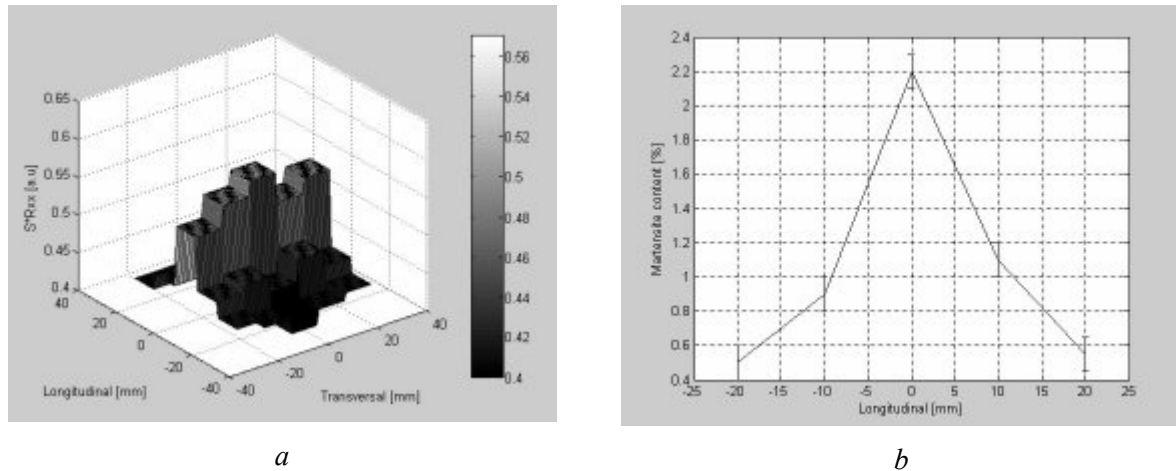


Figure 9. a) Sensor array response; b) Distribution of martensite content along sample's length

After  $8 \times 10^5$  cycles, on samples, fatigue cracks begin to appear.

In Figure 10 is presented the fatigue cracks lattice as well the response of eddy current sensors array after the application of super-resolution algorithm described above.

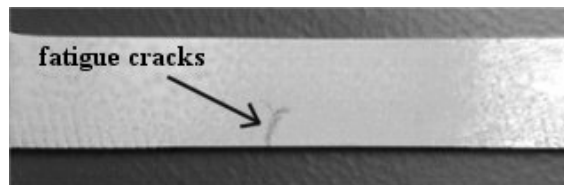


Figure 10. a) Fatigue cracks on AISI 304 sample; b) sources location with super-resolution algorithm, starting from array response.

## 5. Conclusions

Austenitic steels subdued to cyclical loading, suffers fatigue phenomenon that leads to martensite phase appearance. The localization of cracks is made using a eddy current sensor array. For a good resolution, for the using of  $5 \times 5$  2D array, a super-resolution algorithm was realized, the response of sensors array allowing the localization of fatigue cracks.

## Acknowledgments

This paper was partially support by Romanian Ministry of Education and Research, under CNCSIS Grant No.982/2004.

Received April 28 2005

\*National Institute of Research and  
Development for Technical Physics Iasi  
\*\*Technical University Gh.Asachi, Iasi

## REFERENCES

1. V.S.Cecco, G.Van Drunen, Eddy Current Manual, Chalk River, 1981
2. W.J.McConnagle, Nondestructive Testing, 2<sup>nd</sup> Edition, Gordon and Breach, NY, 1961
3. C. V. Dodd and W. E. Deeds, "Analytical solutions to eddy-current probe-coil problems," *J. Appl. Phys.*, vol. 39, pp. 2829–2838, 1968.
4. J. R. Bowler and N. Harfield, "Evaluation of probe impedance due to thin-skin eddy-current interaction with surface cracks," *IEEE Trans. Magn.*, vol. 34, pp. 515–523, Mar. 1998.
5. H.A.Sabbagh, L.D. Sabbagh, Development of a system to invert eddy current data and reconstruct flaws, International Advances in Nondestructive Testing, 1984, vol.10, p.267-305
6. R. Grimberg, L. Udpa, S. Udpa, A. Savin, A Novel Rotating Magnetic Field Eddy Current Transducer for the Examination of Fuel Channels in PHWR Nuclear Power Plants, 31<sup>st</sup> Annual Review of Progress in QNDE, Colorado, July 25-30, 2004.
7. R.Grimberg, A.Savin, O.Mihalache, N.Rezlescu, E.Bradu, S.Chifan, V.Iftimi, A.Andreescu, *Reliability of Automatic Eddy Current Equipment with a Rotating Magnetic Field*, NDT&E International, 28, 5, (1995), 297-301
8. Baldev Raj and T.Jayakumar, Keynote Nuclear: A Perspective on Development in NDE to Enable a Safe & Reliable Nuclear Power Industry , proceedings of 10<sup>th</sup> APCNDT, Brisbane, 2001, IDN 801.
9. M.Bieth, C.Birac, R.Comby, G.Magica, W.Neumann, Final Results of the PISC III Round Robin Test on Steam Generator Tube Inspection, First International Conference on NDE in Relation to Structural Integrity for Nuclear and Pressurized Components, 20 - 22 October 1998, Amsterdam, Netherlands
10. Rontola R., "Thermal Fatigue Experiences Countermeasures in Finland", Report IAEA TC 485.27 (1991)
11. Grimberg R., Savin A., Leitoiu S. and Craus M.L., *INSIGHT*, 38, 9, (1996),p. 650-655
12. Ebine N., Suzuki M. and Ara K., "Nondestructive measurement to evaluate changes of material properties of ferromagnetic structural steels with planar coils", Studies in Applied Electromagnetics and Mechanics, 21, Electromagnetic Nondestructive evaluation (V), eds. J.Pavo, G.Vertesy, T.Takagi and S.S. Udpa, IOS Press (2001), p. 283-290
13. Lemaitre J.and Choboche J.L., *Mechanics of Solid Materials*, Cambridge Univ. Press, NY, (1994)
14. Teodor Dogaru, Stuart T. Smith, Integrated giant magnetoresistive transducer for eddy current testing, proceedings of 15<sup>th</sup> World Conference in Nondestructive Testing, Roma, 2000, IDN 565
15. Ludwig Bär, Gabriel M. Daalmans, Lars Ferchland, Erich Becker, Hans-Peter Lohmann, Annette Sperling, Michael Mück, Rainer Meier, SQUID Eddy Current Technique Applying Conformable Eddy Current Probes, proceedings of 7<sup>th</sup> ECNDT, Copenhagen, 1998, IDN 391.
16. Shell S.V.and Gardner W.A., "High Resolution Direction Finding", Handbook of Statistics, vol.10, eds. N.K.Bose, C.R.Rao, Elsevier, Amsterdam, 1993,p.755-817
17. Zhao L. Krishnaiah P. and Boi Z., *J.Mutivariate Anal*, 20, (1986), p.1-25
18. Honeycombe R.W.K., *Steels, Microstructures and Properties*, Ed. Arnold Publishers Ltd. (1981)
19. Lovejoy D., *Penetrant Testing*, Chapman & Hall, London, (1991)

## EVALUAREA OBOSELII LA OȚELURILE AUSTENITICE 316L UTILIZÂND ARII DE MICROSENZORI DE CURENȚI TURBIONARI

### (Rezumat)

Aceasta lucrare prezinta realizarea unei arii de senzori de curenti turbionari si imbunatatirea raspunsului ariei utilizand algoritmul de superrezolutie. Aplicatia a fost realizata pentru a evidentia fisurile datorate obozelii , ce pot apare in otelurile austenitice AISI 316L supus incercarilor ciclice.

## MICROSENSORS ARRAY FOR INTEGRITY EVALUATION OF FLEXIBLE MULTI-TRACES CIRCUITS

BY

ADRIANA SAVIN, ROZINA STEIGMANN and RAIMOND GRIMBERG

**Abstract.** The micro and nanostructured materials used in IT technology, telecommunication, medicine, require a high level of safety in usage. The small dimensions and encapsulation made the technique of nondestructive testing to evolve in the same direction. The necessity of blistering tracking down (for the case of coating on photo-resist material) or the no uniformities of traces as well as possible manufacturing cracks lead to miniaturization of transducers and to appearance of corresponding data acquisition software. This paper presents a microsensors array concept for the inspection of materials with finite thickness. The response in amplitude of the microsensors array was obtained using a holography program.

**Keywords:** nanomaterials, microsensors array, multitraces circuits,

### 1. Introduction

The using of microsensors in NDE supposes the knowledge of the field generated by microsensors and the simulation of their functioning. The simulation of functioning is required to determine the geometrical and electrical parameters and to develop adequate methods for acquisition, processing and post processing of the signal [1]. For these, is required a high technique for calculation and modeling to evaluate materials and MEMS elements, being necessary microelements that can allows a good focusing of the field and that shall not have losses in low radio frequencies.

To modeling the focused microsensors developed at NIRDTP Iasi, it has started from the using of the existence of some microsensors [2], the using of a ferrite cylinder inside of the coil traversed by an alternative current. The presence of the ferrite focusing the magnetic field lines, but the focal distance of this microsensor remain in the range 10-15 mm. A microsensors developed at INCDFT (magnetic circuit cup-core type), made from ferrite with 10 initial magnetic permeability and electrical conductivity at high frequency 5S/m, the dimensions were choused thus the sintering die can be constructed to obtain the cores [3].

The modeling of microsensors was made taking into account the technical aspects lied to using of MSF, realization of sintering die, choice the materials, (the behavior taking into account the existence of remnant stresses, electromagnetic and distention forces that can appear). Due to possibilities of focusing optimization by modification of the magnetic circuit geometry, to obtain the distribution of magnetic flux and induction, the modeling were made by finite element method. The calculation

was made in FEMLAB3, using a graphical station Silicon Graphix with 32 microprocessor, working in Unix and using parallel calculus.

For the studies preformed to simulate MSF functioning, other types of geometries were used [4]. The examination of simulation's results has shown that for the focused microsensor that presents the best focusing, the focal distance is 7.9 mm [5], [6]. In this way, a substantial decreasing of focal distance was obtained, with direct implication in the testing of flexible multitraces circuits with this sensor. The simulations were performed at Michigan State University (MSU), College of Engineering, Department of Electrical and Computer Science. The obtaining of magnetic microcircuit is difficult thus the problem of sintering die design was made at the Center for Micro and Nano Technology from MSU, in the frame of work stage in 2004.

## 2. Tested samples and experimental set-up

The studied samples are presented in figure 1.

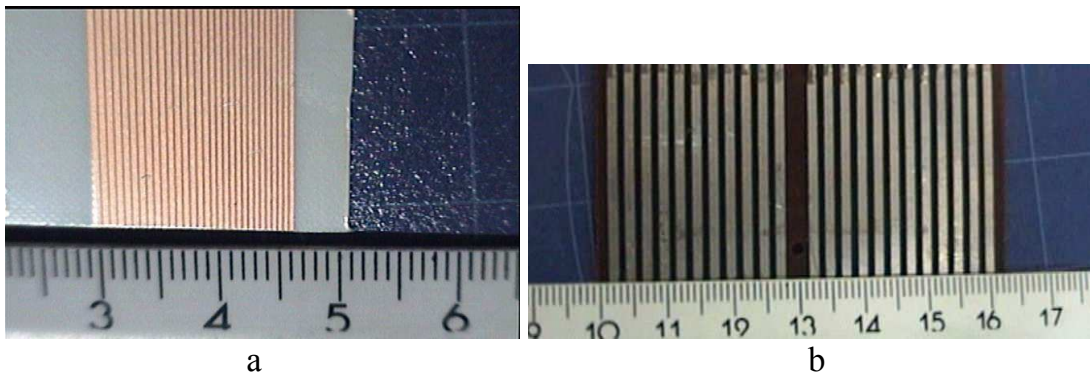


Fig.1. Tested samples: a) flexible traces with 0.3 mm; b) flexible traces with 0.5 mm width

The transducer used for the integrity evaluation of multitraces circuits is an array made-up from orthogonal coils type [6] made in collaboration with MSU. One of the sensors from array is presented in Figure 2.



Fig.2. One element from microsensor array

The measurement conditions are:

Control equipment: SFT 6000N – SOFRATEST – France  
 Control conditions: Frequency - 6MHz  
 Injection – 10Vpp  
 Gain – 65  
 Phase - 169°  
 Low pass filter with cut-off: 20Hz

The experimental results obtained at the perpendicularly scanning of the traces surface are presented in Figures 3 and 4.

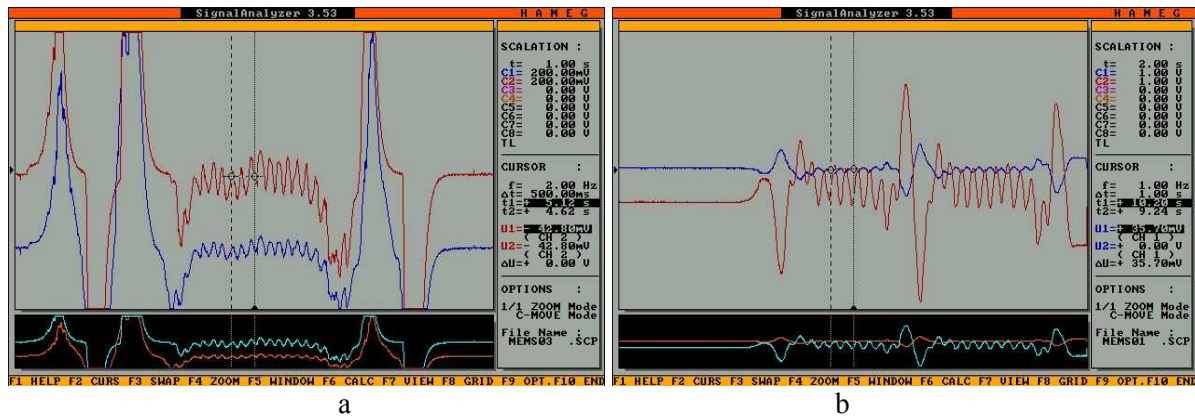


Fig.3. Signal recorded by equipment: a) flexible traces with 0.3 mm; b) flexible traces with 0.5 mm width

At the scanning of a controlled surface, a C-scan image is obtained. In the case of investigation of a 5x5 mm surface of the central zone of flexible multitraces circuit, the obtained results are presented in Figure 4a.

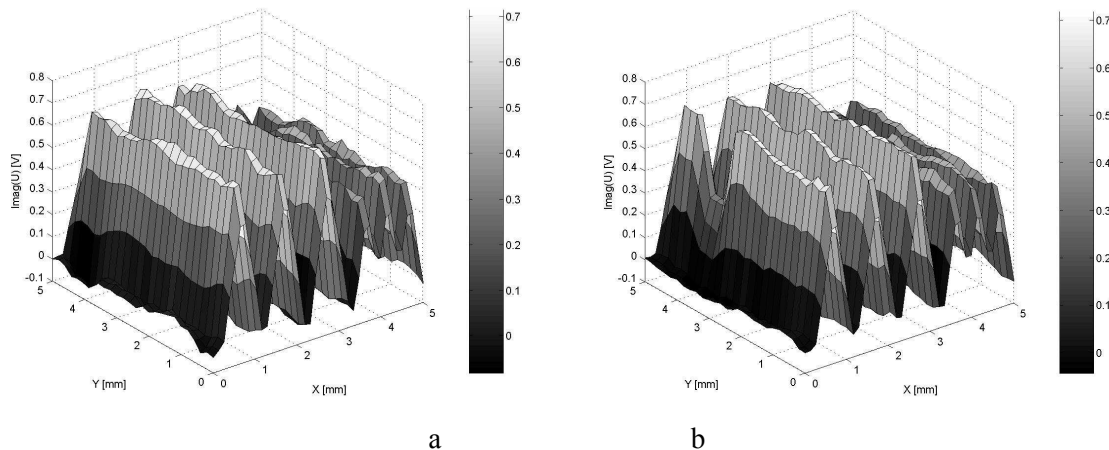


Fig.4. C-Scan image of the multi traces circuits

In the case in which the traces is discontinue, the interruption zone being 0.25 mm (Fig.4b) the aspect of C-Scan representation is changed. The presence of the interruption zone is easy to identify due to the decrease of the value of the imaginary component of the signal delivered by the equipment, case presented in figure 4b.

### 3. Conclusions

This paper has presented the microsensors used for the making of microsensors array for the eddy current nondestructive evaluation of multi-traces flexible circuits, as well as the signal processing and post processing algorithms that allow the emphasizing of the interruption of traces.

## Acknowledgments

This paper was partially support by Romanian Ministry of Education and Research, under Nucleus Program PN 03-310105.

## REFERENCES

1. R. Grimberg, S.C.Wooh, A.Savin, R.Steigmann, D. Prémel, Linear Eddy-Current Array Transducer, INSIGHT, vol.42, 5, 2002
2. X.E.Gros, Some aspects of electromagnetic testing of composites, INSIGHT, (38), 7, 1996
3. R. Grimberg, D.Premel, A.Savin, R.Steigmann, D.Placko, Super-Resolution in eddy current imaging, Proceedings of the 2001 International Conference on Quality Control by Artificial Vision, Le Creusot, France, 21-23 May, (2001), 60-64
4. J. Keller, A. Gollhardt, D. Vogel, B. Michel, Characterization of microcracks by application of digital image correlation to SPM images, Journal of Micromech and Microeng, 7, 2, (2003), pp.265-281
5. W.C.Chew, Waves and fields in inhomogeneous media, Van Nostrand Reinhold, NY, 1990
6. R. Grimberg, A.Savin, C. Rotundu, Eddy Current Microscopy Applied to Graphite - Epoxy Composite , Sensors and Actuators A 3035, (2001), 73-75

## ARIE DE MICROSEZORI PENTRU EVALUAREA INTEGRITATII CIRCUITELOR FLEXIBILE MULTITRASE

### (Rezumat)

Micro materialele si materialele nanostructurate utilizate in tehnologia IT, telecomunicatii, medicina necesita un nivel ridicat de siguranta in exploatare. Dimensiunile mici si incapsularea fac tehnica de control nedistructiv sa evolueze in aceeasi directie. Necesitatea depistarii blisteringurilor (in cazul utilizarii depunerilor pe material fotorezistor) sau a neuniformitatilor traselor ca si posibilelor fisuri de fabricatie au condus la miniturizarea sensorilor si aparitia programelor de date corespunzatoare. Lucrarea prezinta un tip de arie de microsensori conceput pentru inspectia materialelor cu grosime finita. Raspunsul in amplitudine a ariei de sensori s-a obtinut utilizand un program de holografie.

## RECEPTION OF COMPOSITE COVERINGS ON WORKING SURFACES OF STEEL PRODUCTS

BY

V. I. SAVULYAK, and A. YU. OSSADCHUK

**Abstract:** Carbon fibres and textiles made from them, are more and more used to reinforce composite materials. In this study they are applied to the surface of steel, heated to temperatures higher than the eutectic range. Molten metal produced by the inverse eutectic reaction readily impregnates the carbon fibres, thus liberating the carbon-metal interface for further «contact melting» and at the same time facilitating the final phase, when the fibres completely disappear. After cooling, a surface of steel is obtained clad with ledeburite. By charging carbon fabric or felt with powders (or a foil) of metals or ferroalloys it was thus possible to obtain alloyed ledeburite or other metal + carbide ( $\text{Fe}_3\text{AlC}_x$ , VC, TiC, WC, etc) structures. Pulse electric heating and rapid cooling makes the new processes very productive. The layer of carburised (or alloyed and carburised) metal may be up to 6 mm deep.

**Keywords:** carbides, exothermal mixtures, local carburising.

### 1. Introduction

The fundamentals of new methods of superficial or local carburising and alloying of steel using carbon fibres and carbon textiles were published in References 1-5. In this work, the authors have reproduced some of the results of metallographic investigations of the surface layers produced by electric current pulse heating of steel with carbonaceous materials applied to its surface. The circuit of such treatment is shown in Fig. 1. The electric regime is: 13 - 20 kA; 2.3 V; duration of pulse 0.5 - 3.0 s. Circuit of stacking carbonaceous materials are shown on Fig. 2.

When fibrous carbon materials is used and the electric regime is optimum, the carburised layer is composed of ledeburite together with dendrites of austenite (transformed into products of its decomposition — from sorbite to martensite — depending on the cooling rate). No residual carbon fibres are then visible — they are completely dissolved in the liquid phase produced by «contact melting» (inverse eutectic reaction).

The fibrous constitution of woven or knitted carbon fabric or felt enables the liquid phase to be rapidly extracted from the reaction front because of the capillarity of the fibres and their good wetting characteristics. This strongly enhances the reaction speed of the whole process until the stage is reached that all the fibres disappear.

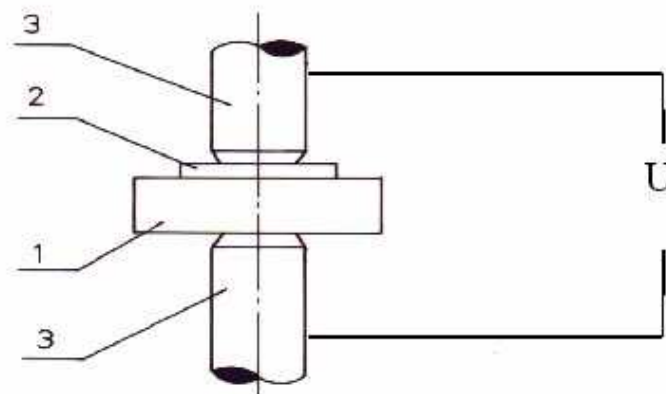


Fig. 1. Circuit of heating by means of an electric current, metallic parts in the form of a plate and a cylinder using equipment designed for spot welding. Key: (1) part to be locally treated; (2) layer of fibrous carbon material; (3) copper electrodes

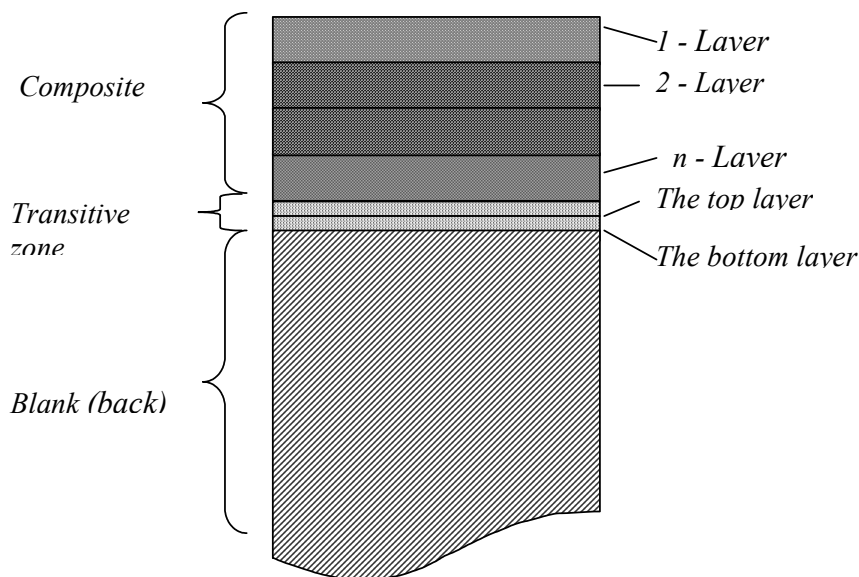


Fig. 2. Circuit of stacking carbonaceous materials

Under the ledeburitic layer «B», it is usual to find a small transition layer «C» composed of residual austenite and martensite needles of low etchability (Fig 2). The depth of the ledeburitic layer depends on the amount of carbon material applied to the surface to be treated. In Fig 3 are shown layers of large «A», medium «B» and small thicknesses «C». Layer «A» seen produced by a very thin strip of mild steel, placed between the surface of the carbon cloth and the upper watercooled copper electrode in order to preserve the latter from fast erosion.

Layer «A» becomes also carburised, although it consists mainly of retained austenite, martensite needles and more or less separate pools of fine ledeburite. As a result, the maximum pool depth in the region of axis can reach 6 mm. The maximum diameter of the bead is 25 - 30 mm.

The «growth» of the treated metallic surface towards the exterior is also a function of the input of carbon fibres per unity of area surface, but if these fibres are not charged with metallic powders this «growth» is quite small, usually 0.1-0.3 mm. Similar processes of

surface carburising of steel are being developed using other means of heating, such as in ovens; by high frequency induction; by direct electric current transmission through the metal, and by use of laser and electron beam heating. Fig 4 shows the surface of a ledeburitic layer formed at 1200°C on a plate of an 0.2% C steel by applying to it a strip of UUT-2 grade cloth. It can be seen that, although these fibres have disappeared completely, the «fabric» of the cloth still remains very visible in the form of rows of ledeburitic beads, produced by the «sucking» of the eutectic (more exactly hypoeutectic) liquid into the intersecting knots between the threads. This technology is attractive large surfaces are to be coated. The use of carbon felt instead of fabric makes the outer surface of the coating more even.

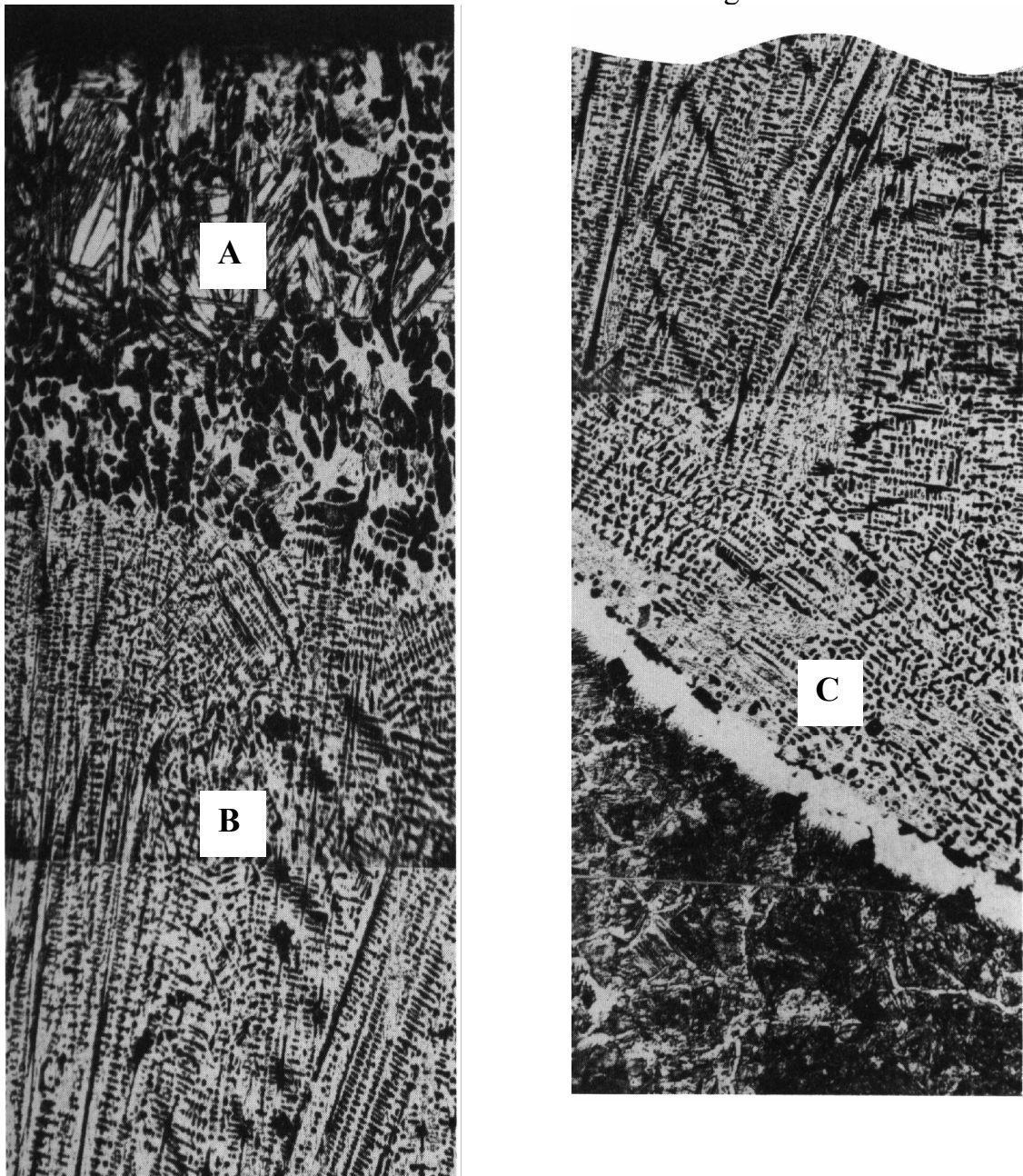


Fig. 3. Microstructure of a thick, superficial ledeburitic layer on the surface of steel, treated with woven carbon cloth of TGN-2M type: (A) a thin surface layer formed by a sheet of mild steel placed under the upper electrode (to preserve it from excessive wear) and strongly carburised during the heating pulse; (B) the ledeburitic zone with a hypoeutectic structure; and (C) the retained austenite + martensite transition zone between the bead and the parent metal. Optical micrographs after Nital etching; Original magnification x200 (reduced to approx x120)

Further investigations were aimed at the charging or impregnation of carbon felt with powders of carbide-forming metals and ferroalloys in order to produce superficial layers of high-hardness wear-resistant tool steels and alloys.

Fig 5 shows the microstructure of a valve steel with the composition 0.45% C, 14% Cr, 14% Ni, 2% W, 0.5% Mo coated using carbon felt together with a mixture of aluminium and mild steel powders. The superficial layers obtained contain a large amount of the hard and wear-resistant  $\gamma^1$  phase ( $\text{Fe}_3\text{AlC}_x$ ) in the form of dendrites.

Fig 6 reproduces the microstructure of a deep superficial layer obtained on a 0.2% C carbon steel with the aid of a felt filled with a mixture of powdered mild steel and ferrovandium. In this case, the possibility of producing very thick layers is enhanced by the evolution of heat inside the layer as a result of the strong exothermic reaction of vanadium carbide synthesis. Carbides of the  $\text{VC}_{1-x}$  type are formed as small equiaxed separate inclusions cemented by vanadium-alloyed highcarbon steel. Such a composite material (called «Carbidostal» in Ukraine) is in accord with the Charpy principle, which requires the matrix material to be formed by those structures which have maximum plasticity and toughness.

In Fig 6 the layer with the coarsest structure (although still very fine) can be seen just under the intermediate zone of the alloyed layer. This is because the highest cooling rate is to be found in the upper zone where heat is rapidly transmitted to the upper copper water cooled electrode after the ending of the heating pulse. In the lower zone, adjacent to the HAZ, the cooling rate is also sufficient, because of heat transfer into the colder parent metal.

Fig 7 and 8 shows, respectively, a «Carbidostal» and a high-hardness carbide tool alloy which were deposited on the surface of steel. In the first case, a spot-welding machine MTPU-300 (300 kW) was used and in the second instance, high frequency induction heating.

These technological processes involving deposition of carbonaceous materials (as well as boron compounds) on steel (and other metals) are certain to find a number of new applications.

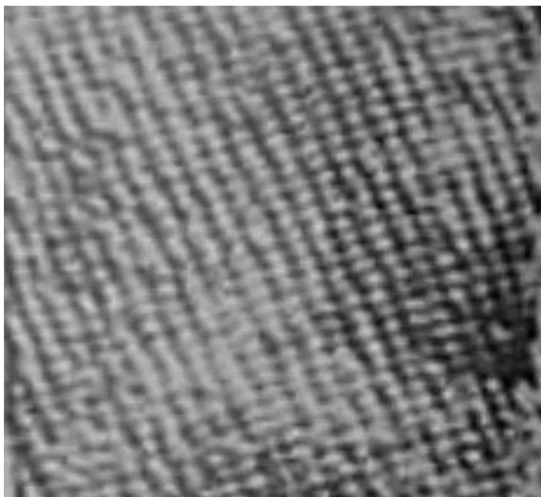


Fig. 4. Outer aspect of a steel plate coated with a ledeburitic layer that has inherited the «fabric ghost» of the carbon cloth applied to the surface at 1200°C; Original magnification x3 (reduced to approx x2.1)

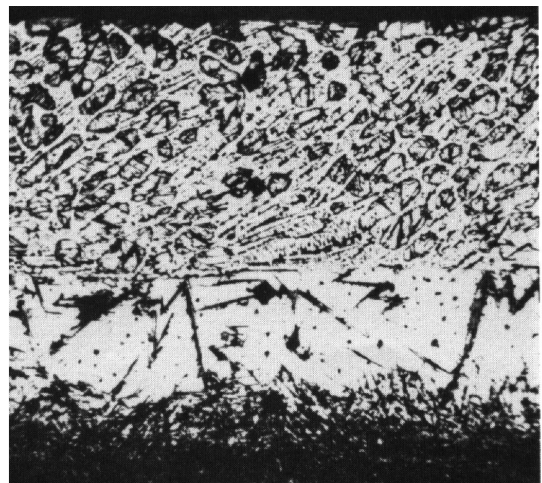


Fig. 5. Microstructure of valve steel with deposited metal containing dendrites of  $\gamma^1$  phase. Optical micrograph after Nital etching; Original magnification x300 (reduced approx x150)

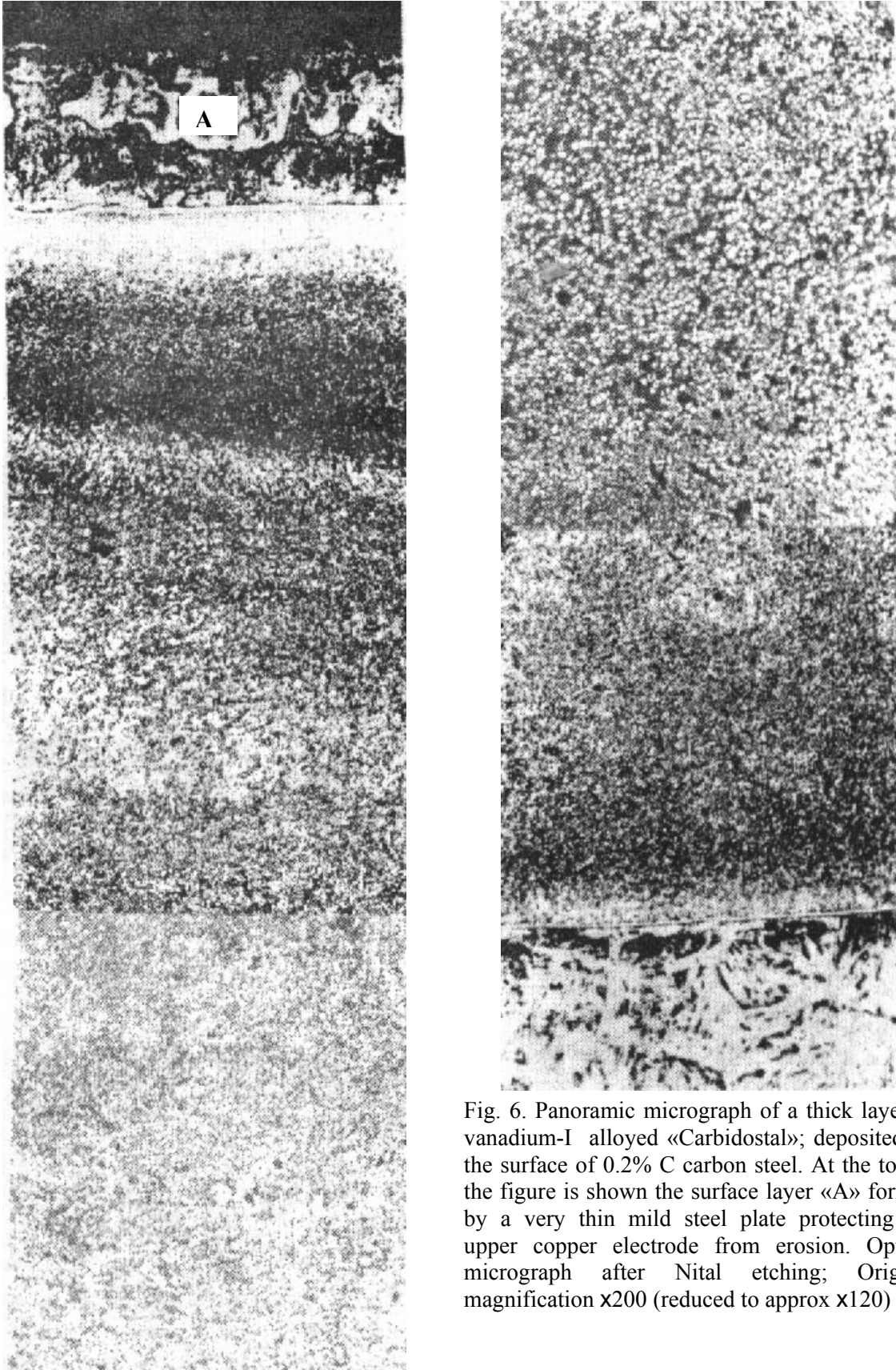


Fig. 6. Panoramic micrograph of a thick layer of vanadium-I alloyed «Carbidostal»; deposited on the surface of 0.2% C carbon steel. At the top of the figure is shown the surface layer «A» formed by a very thin mild steel plate protecting the upper copper electrode from erosion. Optical micrograph after Nital etching; Original magnification x200 (reduced to approx x120)

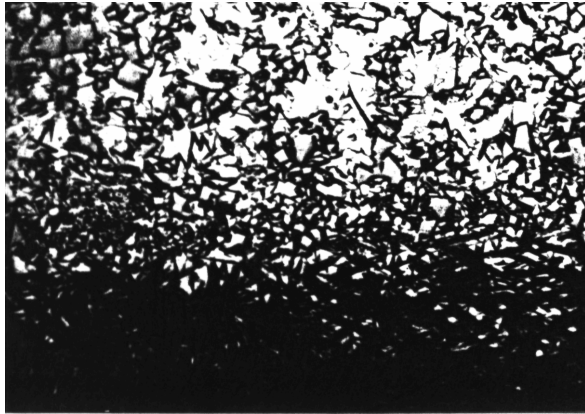


Fig. 7. "Carbidostal" deposited on the surface of a 0.45% carbon steel using charged carbon felt in conjunction with a MTPU-300 spot-welding machine. Optical micrograph after Nital etching; Original magnification x400 (reduced to approx x200)

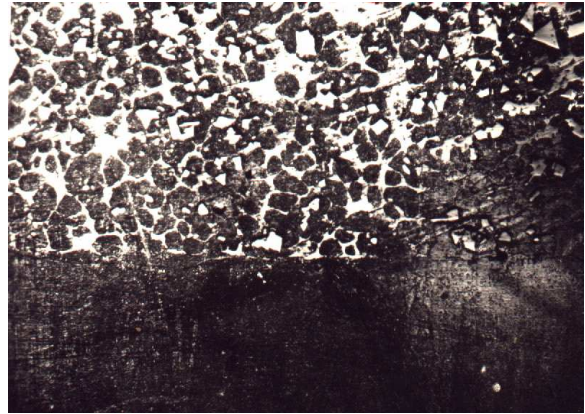


Fig. 8. A layer of carbidic tool alloy deposited on low-alloyed 0.45% C - 1% Cr steel using charged carbon felt and high-frequency induction heating. Optical micrograph after Nital etching; Original magnification x400 (reduced to approx x200)

## 2. Conclusions

1. New technological processes involving the use of carbon fibres (and textiles made from them) have been proposed to deposit carbides on the surface of the steel.
2. Pulse heating processes, including those types which are used in welding equipment, are more than adequate because they prevent excessive oxidation by air and are, as a result, highly productive.
3. Ledeburitic structures of deposited metal are obtained when only carbon fibres are used; special structures can be obtained when these fibres are charged or impregnated with alloying powders.
4. Exothermic reactions between the fibres and the powder are very helpful in producing thick carbidic (or boridic) coatings. The synthesis of highly refractory compounds (carbides and borides) surrounded by a low melting point eutectic liquid is very useful in forming a «slurry» rather than fully liquid pools which are more difficult to handle and require more exacting technological regimes.

*Received: March 23 2005*

Vinnitsa National Technical University, Ukraine

## REFERENCES

1. Савуляк В. І. Синтез зносостійких композиційних матеріалів та поверхневих шарів з екзотермічних компонентів. Універсум. Вінниця. 2002. – 160с.
2. Жуков А. А., Бондаренко А. В. и Семенов А. Н. Упрочнение стальных деталей с использованием волокнистых углеродных материалов // *Металловедение и термическая обработка металлов*. 1989, № 4.
3. Savulyak V. I., Zhukov A.A. Formation of Carbin (Cyanopolyne) and of Diamond in Fe-C Alloys. // *Modelling and Optimization in the Machines Bulding. Field*. Romanian Academy. - V.5, 1999. – P.1-4.
4. Жуков А. А., Савуляк В. І., Черная Г. А., Осадчук А. Ю. Цементация и поверхностное легирование литой стали // *Литейное производство*, 1998, № 1.

5. Савуляк В. И., Осадчук А. Ю. Нанесение композиционных покрытий на рабочие поверхности инструмента из углеродистых сталей // Оборудование и инструмент для профессионалов. –2003. –№5. – С.21-25.

#### **RECEPȚIA ACOPERIRILOR DIN MATERIALE COMPOZITE PE SUPRAFEȚELE DE LUCRU ALE PRODUSELOR DIN OȚEL**

##### **(Rezumat)**

Fibrele de carbon și materialele textile obținute din ele sunt utilizate din ce în ce mai mult pentru ranforsarea materialelor compozite. În acest studiu, ele sunt aplicate pe o suprafață din oțel care este încălzită până la o temperatură mai ridicată decât domeniul eutectic. Materialul topit, produs prin reacția eutectică inversă, este ușor impregnat cu fibrele de carbon, eliberând astfel interfața carbon-metal pentru „topirea de contact” ulterioară care ușurează în același timp obținerea fazei finale, atunci când fibrele dispar complet. După răcire, se obține o suprafață de oțel acoperită cu ledeburită. Prin încărcarea țesăturii sau a păslei de carbon cu pulberi (sau cu o folie) de metale sau de feroaliaje, s-au putut astfel obține structuri de ledeburită aliată sau de alte structuri metal + carbură ( $\text{Fe}_3\text{AlC}_x$ , VC, TiC, WC, etc). Încălzirea în impulsuri electrice și răcirea rapidă fac ca noul proces să fie foarte productiv. Stratul de metal carburat (sau aliat și carburat) poate avea o adâncime de până la 6 mm.



## INVESTIGATION OF THE CORRUGATED WORKPIECES MANUFACTURING PROCESS

BY

VICTOR SAVULYAK

**Abstract:** This paper is devoted to the formation of goffer sheet materials using highly productive equipment. Mathematical model for determining sheet strained condition in the process of stamping is presented.

**Keywords:** goffer, corrugated surface, plasticity, plastic forming.

Development of the low-waste technologies for product manufacturing as well as reducing the material consumption is one of the vital problems of modern production. In order to increase the manufacturability it would be logical to replace the construction of fig.1 for the one presented in fig.2 [1]. However such change was limited by the production capabilities and absence of the available technologies and facilities for obtaining products using the method of plastic forming as one of the practically zero-waste processes.

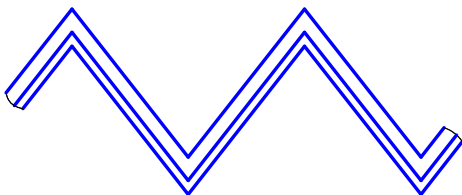


Fig.1 – Profile of corrugated surface

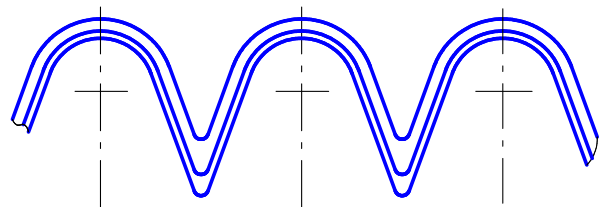


Fig.2 - Profile of corrugated surface

The attempts to organize corrugated parts manufacture (fig.2) using the methods of rolling did not give the satisfactory results as in this case metal thickness, withstanding the treatment without damage, was 2.5 times as large as the nominal one and reached 3 mm. As a result of these attempts it was found, that stresses reach critical value during goffer formation due to the considerable tensile deformation and flexural strain, with their localization in the areas of most curvature. Such a scheme practically dips out the plasticity resource as compared to a simple bend and compression. So to reduce plasticity resource utilization it is necessary to decrease rigidity index  $\eta$  of the strained condition and to increase Lode strained parameter  $\mu_{\sigma}$ . In order to avoid the above-mentioned problems we proposed deformation scheme with hydrostatic lift [2],

which makes it possible to eliminate considerable tensile stress and even if necessary to shift the whole sheet (along its width) in the compression zone. This reduces index  $\eta$ . Disadvantages of this forming scheme are high pressures of hydrostatic lift, which should comply with the workpiece strength, and also complicated structure.

For analyzing strained condition scheme and evaluating its influence on the deformed metal plasticity, strained condition in plastic region was determined in the following way [3].

According to the balance equations and Tresk-Saint-Venant plasticity condition for flat strained state (assuming that stress in axial direction  $z$  is absent) we write

$$\rho \frac{d\sigma_\rho}{d\rho} + \sigma_\rho - \sigma_\theta = 0. \quad (1)$$

$$\sigma_\rho - \sigma_\theta = \pm \sigma_u, \quad (2)$$

where minus sign is related to the zone of tension in the tangential direction, and sign plus - to the compression zone.

To solve the problem taking into account strain hardening, hardening curve is approximated by the power function

$$\sigma_u = Ae_u^n, \quad (3)$$

where  $e_u = \ln \frac{\rho}{\rho_H}$ ,  $\rho_H = \sqrt{R \cdot r}$  - radius of the neutral surface curvature;  $R$  and  $r$  - external and internal radii of the sheet.

Joint solution of balance equation (1) and plasticity equation (2) has the form [3]:

for tension zone

$$\sigma_\rho = -\frac{A}{n+1} \left[ \left( \ln \frac{R}{\rho_H} \right)^{n+1} - \left( \ln \frac{\rho}{\rho_H} \right)^{n+1} \right], \quad (4)$$

$$\sigma_\theta = A \left( \ln \frac{\rho}{\rho_H} \right)^n - \frac{A}{n+1} \left[ \left( \ln \frac{R}{\rho_H} \right)^{n+1} - \left( \ln \frac{\rho}{\rho_H} \right)^{n+1} \right],$$

for compression zone

$$\sigma_\rho = -\frac{A}{n+1} \left[ \left( \ln \frac{\rho_H}{r} \right)^{n+1} - \left( \ln \frac{\rho_H}{\rho} \right)^{n+1} \right], \quad (5)$$

$$\sigma_\theta = -A \left( \ln \frac{\rho_H}{\rho} \right)^n - \frac{A}{n+1} \left[ \left( \ln \frac{\rho_H}{r} \right)^{n+1} - \left( \ln \frac{\rho_H}{\rho} \right)^{n+1} \right],$$

where  $A$ ,  $n$  are constants of the material.

In case of compressing stress  $\sigma_\kappa$  acting on a free surface, radius of the neutral surface curvature can be calculated from the formula [3]:

$$\rho_H = \sqrt{Rr \exp \frac{\sigma_\kappa}{\sigma_u}}. \quad (6)$$

Analysis of the equation (6) shows that when  $\sigma_k$  increases, the radius of the neutral surface curvature increases as well and therefore the compression zone will expand.

From the above-mentioned it can be concluded that for the optimization of the corrugated surfaces manufacturing process it is necessary: 1) to avoid tensile stress of the material in order to reduce its plasticity resource utilization and 2) to create such value of compression stress on free surface of the material, that plasticity resource utilization will be limited to the required magnitude. In order to satisfy the first condition it is possible to use the process of the initial goffer rolling as described in [4]; the goffer length after rolling and of the finished one should coincide. At the second stage the final workpiece forming should be performed and its calibration in the closed stamp according to the chart shown in fig.3. Such method of the final forming consists in the following. During stamping process working fluid in the stamp will be forced out through the throttling orifice creating compression strain of the definite value on the free surface of a workpiece (fluid pressure value can be regulated by throttles). As a result it will be possible to regulate the plasticity resource utilization and also to provide small radii of curvature in the goffer peaks.

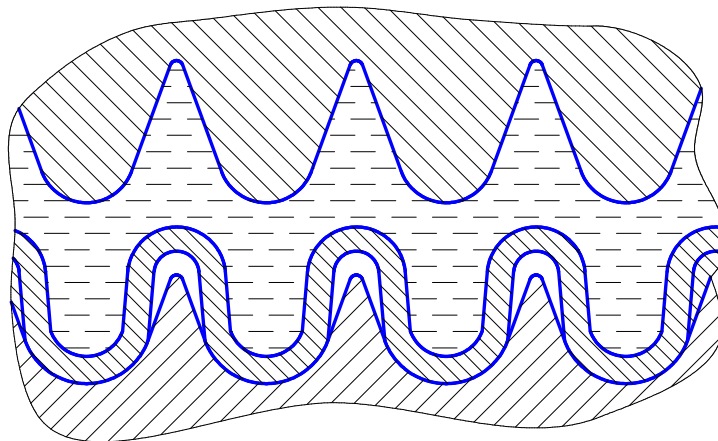


Fig.3. Scheme of hydrostatic punching

From the point of view of manufacturability and structural simplicity, a stamp for making corrugated ribbon presented in [5] is a more perfect variant. This facility realizes the scheme of sheet material bending almost without extension in radial and tangential directions. In this paper the model of such forming is presented with the analysis of the strained condition.

The model is based on the balance equations for that strained condition [3]

$$\begin{cases} \frac{\partial \sigma_\rho}{\partial \rho} + \frac{1}{\rho} \frac{\partial \tau_{\rho\theta}}{\partial \theta} + \frac{\sigma_\rho - \sigma_\theta}{\rho} = 0, \\ \frac{\partial \sigma_\theta}{\rho \partial \theta} + \frac{\partial \tau_{\rho\theta}}{\partial \rho} + 2 \frac{\tau_{\rho\theta}}{\rho} = 0, \end{cases} \quad (7)$$

coupling equations

$$\left\{ \begin{array}{l} \sigma_{\rho} - \sigma = \frac{2}{3} \sigma_u \frac{\dot{\epsilon}_{\rho}}{\dot{\epsilon}_u}, \\ \sigma_{\theta} - \sigma = \frac{2}{3} \sigma_u \frac{\dot{\epsilon}_{\theta}}{\dot{\epsilon}_u}, \\ \sigma_z - \sigma = \frac{2}{3} \sigma_u \frac{\dot{\epsilon}_z}{\dot{\epsilon}_u}, \\ \tau_{\rho\theta} = \frac{1}{3} \sigma_u \frac{\dot{\gamma}_{\rho\theta}}{\dot{\epsilon}_u}, \end{array} \right. \quad (8)$$

and condition of incompressibility

$$\dot{\epsilon}_{\rho} + \dot{\epsilon}_{\theta} + \dot{\epsilon}_z = 0, \quad (9)$$

where  $\sigma_{\rho}, \sigma_{\theta}, \sigma_z, \tau_{\rho\theta}$  are normal and tangent stresses;

$\dot{\epsilon}_{\rho}, \dot{\epsilon}_{\theta}, \dot{\epsilon}_z$  - deformation rates in corresponding directions;

$\dot{\gamma}_{\rho\theta}$  - rate of shear deformation;

$\sigma = \frac{1}{3} \sigma_{ij} \delta_{ij}$  - average strain (hydrostatic pressure).

Deformation rates are described by

$$\left\{ \begin{array}{l} \dot{\epsilon}_{\rho} = \frac{\partial \vartheta_{\rho}}{\partial \rho}, \\ \dot{\epsilon}_{\theta} = \frac{\partial \vartheta_{\theta}}{\rho \partial \theta} + \frac{\vartheta_{\rho}}{\rho}, \\ \dot{\epsilon}_z = \frac{\partial \vartheta_z}{\partial z}, \\ \dot{\gamma}_{\rho\theta} = \frac{\partial \vartheta_{\theta}}{\partial \rho} + \frac{\partial \vartheta_{\rho}}{\rho \partial \theta} - \frac{\vartheta_{\theta}}{\rho}. \end{array} \right. \quad (10)$$

In order to solve the model it was assumed that strain intensity is constant and the speeds  $v_{\theta}$  and  $v_z$  of material points movement are described by the equations

$$\left\{ \begin{array}{l} v_{\theta} = a(\theta)(\rho - \rho_H) = a(\rho - \rho_H), \\ v_z = b \cdot z + c. \end{array} \right. \quad (11)$$

After substituting (11) in (9) and taking into account the boundary conditions we obtain

$$\rho \cdot v_{\rho} + a' \rho (0.5\rho - \rho_H) + \frac{b\rho^2}{2} + c_1 = 0, \quad (12)$$

where  $a' = \frac{\partial a(\theta)}{\partial \theta} = \frac{\partial a}{\partial \theta}$ ,  $c_1 = a' \rho_H r - \frac{r^2}{2} (a' + b)$ ,  $r$  - radius of the sheet internal surface.

From (12) it follows, that

$$\vartheta_{\rho} = a' \left( \rho_H - \frac{\rho}{2} \right) - \frac{b\rho}{2} - \frac{c_1}{\rho}. \quad (13)$$

After substituting (11) and (13) in (10) and simplification we obtain

$$\begin{cases} \dot{\varepsilon}_\rho = -\frac{a'}{2} - \frac{b}{2} + \frac{c_1}{\rho^2}; \\ \dot{\varepsilon}_\theta = \frac{a'}{2} - \frac{b}{2} - \frac{c_1}{\rho^2}; \\ \dot{\varepsilon}_z = b; \\ \dot{\gamma}_{\rho\theta} = a \frac{\rho_H}{\rho} + \frac{a''(2\rho_H - \rho)}{2\rho}, \quad a'' = \frac{\partial^2 a}{\partial \theta^2}. \end{cases} \quad (14)$$

That is

$$\begin{cases} \dot{\varepsilon}_\rho - \dot{\varepsilon}_\theta = -a' + \frac{2c_1}{\rho^2}; \\ \dot{\varepsilon}_\theta - \dot{\varepsilon}_z = \frac{a'}{2} - \frac{3b}{2} - \frac{c_1}{\rho^2}; \\ \dot{\varepsilon}_z - \dot{\varepsilon}_\rho = \frac{a'}{2} + \frac{3b}{2} - \frac{c_1}{\rho^2}. \end{cases} \quad (15)$$

We assume that  $v_\theta = a(\rho - \rho_H)$  in tangential direction changes according the linear law, i.e.  $a' = \text{const}$  and  $a'' = 0$ . Hence, deformation rate intensity will be defined by

$$\dot{\varepsilon}_u = \frac{1}{\sqrt{2}\rho} \sqrt{(a'\rho - 2c_1/\rho)^2 + 3b^2 + (a'\rho_H)^2}. \quad (16)$$

From the coupling equation (8) and balance equation (7)

$$\begin{cases} \frac{\partial \sigma_\rho}{\partial \theta} = -\rho \frac{\partial \tau_{\rho\theta}}{\partial \rho} - 2\tau_{\rho\theta} + \frac{2}{3}\sigma_u \cdot f(\rho, \theta), \\ \frac{\partial \sigma_\rho}{\partial \rho} = \frac{\partial \tau_{\rho\theta}}{\rho \partial \theta} - \frac{\sigma_\rho - \sigma_\theta}{\rho}, \end{cases} \quad (17)$$

where  $f(\rho, \theta) = \frac{\partial}{\partial \theta} \left( \frac{\dot{\varepsilon}_\rho - \dot{\varepsilon}_\theta}{\dot{\varepsilon}_u} \right)$ .

According to the formula of complete stress differential

$$d\sigma_\rho = -\frac{1}{3}\sigma_u \left( \left( \rho \frac{\partial}{\partial \rho} \left( \frac{\dot{\gamma}_{\rho\theta}}{\dot{\varepsilon}_u} \right) + 2 \frac{\dot{\gamma}_{\rho\theta}}{\dot{\varepsilon}_u} \right) d\theta + \left( \frac{1}{\rho} \cdot \frac{\partial}{\partial \theta} \left( \frac{\dot{\gamma}_{\rho\theta}}{\dot{\varepsilon}_u} \right) + \frac{\dot{\varepsilon}_\rho - \dot{\varepsilon}_\theta}{\dot{\varepsilon}_u} \right) d\rho \right)$$

or in an expended form

$$d\sigma_\rho = -\frac{1}{3}\sigma_u \left( \left( a \cdot \frac{f_1(\rho)}{f_2(\rho)} \right) d\theta + \left( \frac{a'\rho_H - a'\rho + \frac{2c_1}{\rho^2}}{\rho^2 \dot{\epsilon}_u} \right) d\rho \right), \tag{18}$$

where  $f_1(\rho) = 4\rho^4 \rho_H \dot{\epsilon}_u^2 + \rho_H \left( (a'\rho^2)^2 + 4c_1^2 \right)$ ,  $f_2(\rho) = 2\rho^6 \dot{\epsilon}_u^3$ , and  $\dot{\epsilon}_u$  function depends only on the curvature radius  $\rho$ .

If we assume that deformation rate in the direction of axis  $z$  is small and can be neglected ( $b=0$ ) (18), taking into account boundary conditions of integration we re-write

$$\sigma_\rho = \frac{\sqrt{2}}{3}\sigma_u \left( \frac{\rho_H (\rho^4 - c_2^2) \theta}{\rho^2 \left( \sqrt{\left( \rho - \frac{c_2}{\rho} \right)^2 + \rho_H^2} \right)^3} - \int_\rho^R \frac{(\rho_H \rho - 2\rho^2 + c_2) d\rho}{\rho^2 \sqrt{\left( \rho - \frac{c_2}{\rho} \right)^2 + \rho_H^2}} - \frac{\rho_H (R^4 - c_2^2) \theta}{R^2 \left( \sqrt{\left( R - \frac{c_2}{R} \right)^2 + \rho_H^2} \right)^3} \right), \tag{19}$$

where  $c_2 = 2r\rho_H - r^2$ .

After numerical integration of (19) taking into account (8) we obtain graphic representation of normal stress depending on the point coordinates (radius  $\rho$  and angle  $\theta$ ) for steel 10 with the following parameters:  $A=720$  MPa,  $n=0,21$ ,  $r=2$  mm,  $s=0,8$  mm – sheet thickness (fig.4, fig.5).

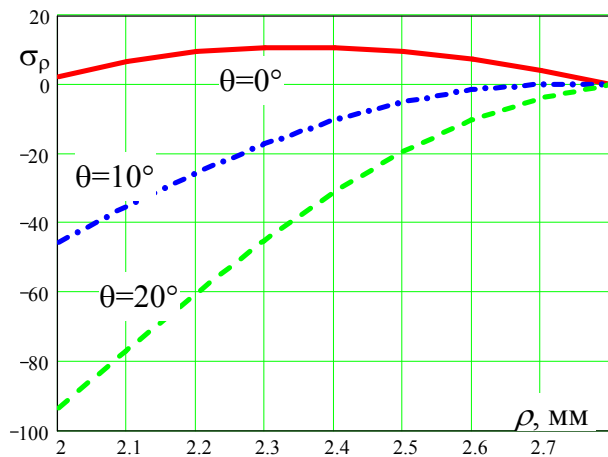


Fig.4. – Dependence of normal tension  $\sigma_\rho$  on radius  $\rho$ , MPa

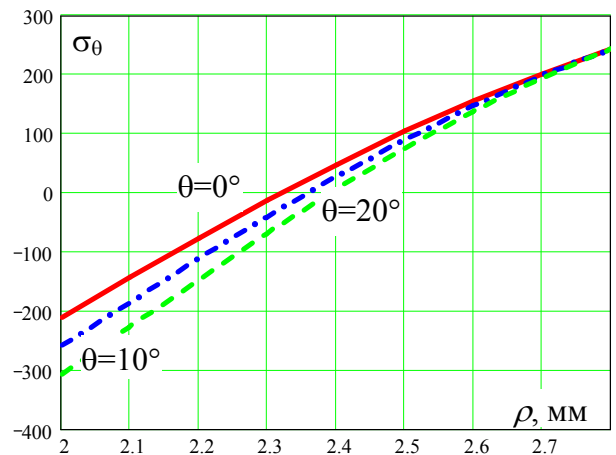


Fig.5. - Dependence of normal tension  $\sigma_\theta$  on radius  $\rho$ , MPa

### Conclusions

Computer analysis by numeral methods of the model of the corrugated surface forming using the developed equipment [5] has made it possible to determine the

strained condition of the workpiece material depending on the process parameters. This allows to calculate power characteristics of the corrugation-forming equipment.

*Received: April 15 2005*

Vinnitsa National Technical University, Ukraine

#### REFERENCES

1. Патент України №2496. МКл С13С1/08. Ніж бурякорізальний, Близнюк А.С., Законов О.П., Піддубецький П.І., Савуляк В.В., Савуляк В.І. №2003087726. Заявка від 14.08.2003// Бюл.№5. - 2004.
2. Савуляк В.В. Штампування гофрованих заготовок малих радіусів кривизни з використанням гідростатичного підпору. Вісник ВПІ. №6. -2004. с.74-76.
3. Попов Е.А. Основы теории листовой штамповки. – М.: Машиностроение, 1977. –278 с.
4. Сивак І.О., Савуляк В.В. Получение гофрированных заготовок методами локальной пластической деформации //Удосконалення процесів та обладнання обробки тиском в металургії і машинобудуванні. –Краматорськ: ДДМА. – 2003. –С.392-394.
5. Патент України №3883. МКл В21D13/00 . Штмп для виготовлення гофрованої стрічки. Савуляк В.В., Савуляк В.І., Сивак І.О. №2004020945. Заявка від 10.02.2004// Бюл.№12.2004.

#### STUDIUL PROCESULUI DE PRELUCRARE A PIESELOR ONDULATE

##### (Rezumat)

Această lucrare este dedicată formării materialelor din tablă gofrată utilizând un echipament de înaltă productivitate. Este prezentat un model matematic pentru determinarea stării de deformare a tablei în cadrul procesului de ștanțare.



## ASPECTS REGARDING THE BEHAVIOR OF STAINLESS STEELS DURING THE WEAR PROCESSES

BY

D. V. ȘOLTUZ, D. CIOBANU and V. NECULĂIASA

**Abstract:** Active parts of the machines or installations from food industry, which come in direct contact with processing food products, are realized in general from different types of stainless steels. The friction couples realized from these steels work in conditions by inadequate lubrication imposed by hygienic – healthy prescriptions, which prohibit the lubricant penetrations in processing food products. In these conditions is necessary to make an analysis of the stainless steels behaviors during the wear processes.

**Key words:** stainless steel, martensitic transformation, wear

### 1. Theoretical considerations

During the wear processes are produced structural modifications in superficial layers due to plastic deformations. Kirk and Swanson [4] show that for small load and low sliding speed conditions are formed a thin zone with great microhardness closed to superficial layers. The microhardness measured at 10  $\mu\text{m}$  and 80  $\mu\text{m}$  are 125% and 160% face to the hardness measured at 250  $\mu\text{m}$ , which show a continuous reduction of the hardness at the superficial layer level.

Garbar and Skorinin [1] consider that the hardness reduction is a result of the dislocations from surface and the material depth. Thus, the cells from the surface present a pronounced elongation on the sliding direction, and the dislocation density are much great in the cell wall than in the inner of this. At 5  $\mu\text{m}$  depth the dislocations concentrate in specific regions from the inner of cells, formed the dislocation wells in the initial steady. At the 15  $\mu\text{m}$  depth are present a great dislocation density, which are not uniform distributed in the entire volume of the material.

The modified zone from material surface is the result of relative reduced dislocations density, while the interior hard zone is a consequence of the material cold-hardness. As a result, the elongated form of the cells from the surface show a growth of the stress state in superficial layer, respective the formation of an obstacle for deformation continuously in the depth of material.

The friction and wear behavior of austenitic stainless steels depend by their stability in ratio of martensitic transformation to  $\varepsilon$  (hcp) and  $\alpha'$  (bcc) phases. The appearance of martensitic phases, either  $\varepsilon$  phase or  $\alpha'$  or both, will influence the mechanical properties of steels, determining the tendency to cold-hardening, while through the increasing of the deformation state of superficial layers the occurrence of  $\alpha'$  phase is advantaged. Furthermore the  $\varepsilon$  phase helps at the forming of  $\alpha'$  phase,

which also can form directly from  $\gamma$  phase. The forming of  $\varepsilon$  phase is advantaged by a low energy level.

Hsu, Ahn and Rigney [3] determine that on the wear path of an 18% Cr - 8% Ni stainless steel appear  $\alpha'$  martensite, and at a 10  $\mu\text{m}$  depth is forming a very fine cellular structure with cell smaller than 0.1  $\mu\text{m}$  in diameter, in which are present  $\alpha'$  and  $\gamma$  phases. As a result, are produced a hard superficial layer, but fragile by  $\alpha'$  martensite on the soft base material, determining a negative hardness gradient and a reduction of the shear resistance. By another hand, the forming of the martensite can inhibited the crack propagation through the dwindling of local flow and through the dispersion of deformation over a bigger material volume. Nevertheless this structure influence negatively the tribological properties of austenitic stainless steel, because the shearing must localized in superficial layers and not in material structure, through what are continued the propagation of plastic deformation in depth. The avoidance of this aspect can be realized through the addition of the chemical element that can create a superficial layer with low shear resistance, respective through the alloying with nitrogen or with elements that formed fine precipitates (carbides, nitrates, silicates, boron and so on).

The carbides influence the wear resistance, both quality and quantity of the carbides phases formed, and the properties of metallic structure. Thus, through the high alloying with different elements become possible the matrix saturation with atoms of those elements, which prohibit the dislocation activity and implicit the growth of wear resistance [2]. Also, the high content of chromium, 20...25%, in an austenitic structure can cancelled the alphasen effect of the chromium.

By the other hand, the carbon associate with divers components with great affinity for this migrate in the material microstructure toward cell wall, which can contain a great quantity of carbon or interstitial atoms, through that the martensite and carbides disappear. The martensite disappears through direct diffusion and the carbides through deformation induced by dissociation and migration processes [8]. These processes have produced, in special, in the cells of  $\alpha$  ferrite with a low content of carbon disposed in solution and the wall of cell with a high content of carbon under the form of carbon disposed in the dislocation field delimited by the walls of cells.

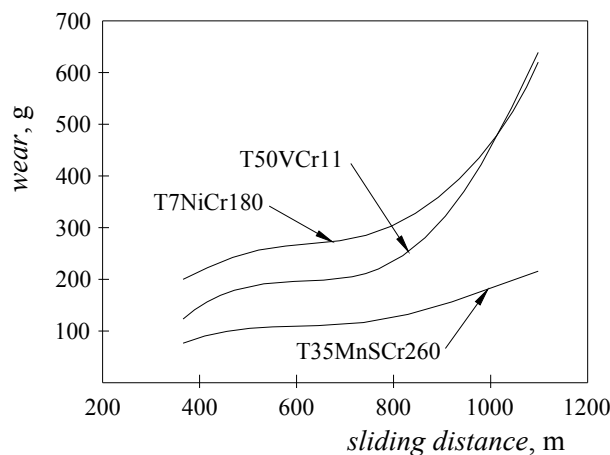


Fig.1. The wear resistance relative to chromium content [2].

Gramaticu and Băncescu [2] analyze the wear behavior of some steels with different content of chromium: T50VCr11 (0.51%C, 0.8%Mn, 0.05%V, 1.06%Cr –

with perlitic structure), T7NiCr180 (0.22%Cr, 0.9%Mn, 18.6%Cr, 9.3%Ni – with austenitic structure) and T35MoSCr260 (0.35%C, 1.4%Mn, 25.74%Cr, 14.2%Ni – with austenitic structure). From Figure 1 it results that T35MnSCr260 due the high content of carbon and chromium carbides determine a superior behavior relative to another two elements, although its structure is austenitic. By another hand, the austenitic stainless steel 7NiCr180 have the inferior wear resistance, which is justified through the reduced content of carbon. The influence of chromium is disputable [5].

Prodaniuc [6], [7] explain the tendency of stainless steels toward adhesion wear through the nature of alloying elements, chemical and metallurgical affinity of these. Thus the 40Cr130 martensitic stainless steels present wear particles under the form of chips (flakes) produced through abrasion, 8TiCr170 ferritic stainless steel present particles under the form of irregular spheres resulted through dislocation and the 12NiCr180 austenitic stainless steel through the cold-hardness of superficial layer form particles under the forms of flakes.

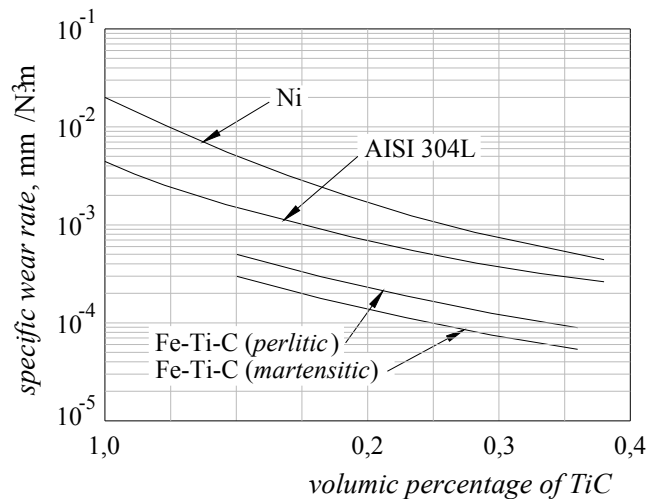


Fig.2. The influence of TiC content incorporated in structure over the specific wear rate of steel [9].

Vardavoulis [10] show that through plastic deformation of the surface of AISI 304L and AISI 316 L austenitic stainless steels, during the friction process, are produced the transformation of austenite to martensite. The carbides with maxim dimension by 2  $\mu\text{m}$  from structure of superficial layer diminish the thickness of plastic deformed zone till to a depth by 10...15  $\mu\text{m}$ . Furthermore, the carbides can be easily removed together with wear particles. As a result, in the structure not-influenced by plastic deformation remain hard carbides with dimensions by 50...100  $\mu\text{m}$ . In these conditions the wear behavior of stainless steels depends by the resistance of the interface wear particle/steel matrix and by the mechanical properties of carbides.

Skolianos and Kattamis [9] have studied the influence of titan carbides over the nickel structure and in the structure of AISI 304L austenitic stainless steel. They establish that wear behavior improve through the increase of volume percentage of TiC carbide incorporated, fig. 2. Furthermore, can observe that the wear diminish with the increase of the microhardness of material structure. Thus, the wear for a martensitic structure of Fe-17%Ti-4.22%C steel is much reduced than in the case of nickel. The carbides have the dimensions by 5...12  $\mu\text{m}$ .

## 2. Conclusions and subsequent research directions

The modifications from the superficial layers depend by stress state of the contact zone and by the properties of steels. Presence of zones with different microhardness determines the wear behavior of steels through the formation of barriers for continuous deformation in the depth of material. In the case of stainless steels, through martensitic transformations, are formed a structure with a hard and fragile superficial layer by  $\alpha'$  phase and a soft substrate by  $\alpha'$  and  $\gamma$ , through that continue the propagation of plastic deformations in the depth of material. Improving the wear behaviors of the stainless steels are obtained through alloying with nitrogen or with elements that formed fine precipitates. As a result, it is necessary to continue the research for establishing the wear behavior of stainless steels used at the construction of machines and installations from food industry.

Received April 26 2005

The "Gh.Asachi" Technical University from Iasi

### REFERENCES

1. Garbar I. I. and Skorinin J. V., 1978, *Metal surface layer structure formation under sliding friction*. Wear, 51, 327-336.
2. Gramaticu M. și Băncescu N., 1980, *Influența compoziției chimice și microstructurii asupra rezistenței la uzură a unor oțeluri aliate cu crom*. Tribotehnica'80 Hunedoara, 773-778.
3. Hsu K. L., Ahn T. M. and Rigney D. A., 1980, *Friction, wear and microstructure of unlubricated austenitic stainless steels*. Wear, 60, 13-37.
4. Kirk J. A. and Swanson T. D., 1975, *Subsurface effects during sliding wear*. Wear, 35, 63-67.
5. Pavelescu D. și Dumitrescu C., 1984, *Dependența rezistenței la uzura de abraziune a materialelor metalice de duritate, conținut de carbon și structură*. Tribotehnica'84, Iași, vol. III, 5-12.
6. Prodaniuc N., 1985, *Aspecte privind comportarea la uzură a oțelurilor inoxidabile*. Construcția de Mașini, 37 (1), 13-16.
7. Prodaniuc N., 1984, *Unele considerații privind comportarea la uzură a oțelurilor inoxidabile*. Tribotehnica'84, Iași, vol. III, 95-101.
8. Rigney D. A. and Hirth J. P., 1979, *Plastic deformation and sliding friction of metals*. Wear, 53, 345-370.
9. Skoliadis S. and Kattamis Z. T., 1996, *Solidification processing and tribological properties of particulate TiC-reinforced Ni-Base and steel matrix composites*. Balkantrib'96 Thessaloniki – Greece, 291-298.
10. Vardavoulias M., 1996, *A model on the unlubricated sliding wear of particulate composite materials*. Balkantrib'96 Thessaloniki – Greece, 281-290.

### ASPECTE PRIVIND COMPORTAREA OȚELURILOR INOXIDABILE ÎN TIMPUL PROCESELOR DE UZURĂ

#### (Rezumat)

Părțile active ale unui utilaj sau instalații din industria alimentară, care intră în contact direct cu produsele alimentare prelucrate, se execută în general din oțeluri inoxidabile de diferite mărci. Cuplele de frecare realizate din aceste oțeluri funcționează, în general, în condiții de lubrifiere necorespunzătoare, impuse de prescripțiile igienico-sanitare, care interzic pătrunderea lubrifianților în produsele alimentare prelucrate. În aceste condiții este necesară o analiză a comportării oțelurilor inoxidabile în timpul proceselor de uzură.

## ASPECTS REGARDING THE VARIATIONS OF ELECTROLYTIC POTENTIAL IN TRIBOCORROSION WEAR PROCESS

BY

D. V. ȘOLTUZ, D. CIOBANU and V. NECULĂIASA

**Abstract:** The wear processes, in presence of aggressive medium, determine the exposure of contact surfaces both the action of tribological phenomenon and the chemical action, respective the apparition of the specific phenomenon by tribochemistry. Mechanical stresses don't initiate chemical reaction, but through the modification which it produce in superficial state or in the material structure advantage or accelerate chemical reaction between the materials of the friction pair and aggressive medium. The apparition of the cracks depends by correlation between the characteristics of friction pair with those of aggressive medium. In these conditions is necessary to study the variations of electrolytic potential and the speeds of chemical reactions during the wear processes.

**Key words:** tribocorrosion wear, electrolytic potential, chemical reactivity, cracks

### 1. Theoretical considerations

The tribocorrosion wear process distinguishes by another kind of the mechanical wear processes through the existence of tribochemical reactions [7], [8]. These are defined as the formation of reaction produces due to superposition the effect of tribological loading between the two surfaces and the chemical reactions of the friction surfaces materials with environmental medium, DIN 50 320.

The tribocorrosion wear processes can produced both in dry atmosphere (non-electrolytic media) and in presence of electrolytic media, which in food industry are aqueous media (diluted solutions of divers organic or/and inorganic chemical compounds) [6], [7].

The activation of chemical reaction between the metallic surfaces and electrolytic media in presence of mechanical friction is realized by *chemostress effect*. This effect produce the modification of chemical potential of an when an adsorbed the solid substrate (adsorbent) is subjected to a high stress state, induced either by exterior stress, or residual intern stress from the nearness of the surface, or through simultaneous action of those two stresses.

The modification of electric potential determines the variation of friction coefficient. Broszeit, Hess and Wagner [1] have obtain for electrolytic solutions by  $\text{Na}_2\text{SO}_4$  of such modification of friction coefficient relative to sliding distance for divers values of electric potential. Furthermore, Zhu, Kelsall and Spikes [10] ascertain the increasing of friction coefficient of iron, in solution by 0.02 M  $\text{Na}_2\text{SO}_4$ , till to a maxim value by 0.39 for a potential by -850 mV of saturated calomel reference electrode. The reduction of friction coefficient through the increasing of chemical potential involve a modification of the charge of electrolytic double layer [2], in other

words a maxim value for electrostatic repulse forces [10]. However this effect is important only for small contact stress, fig. 1.

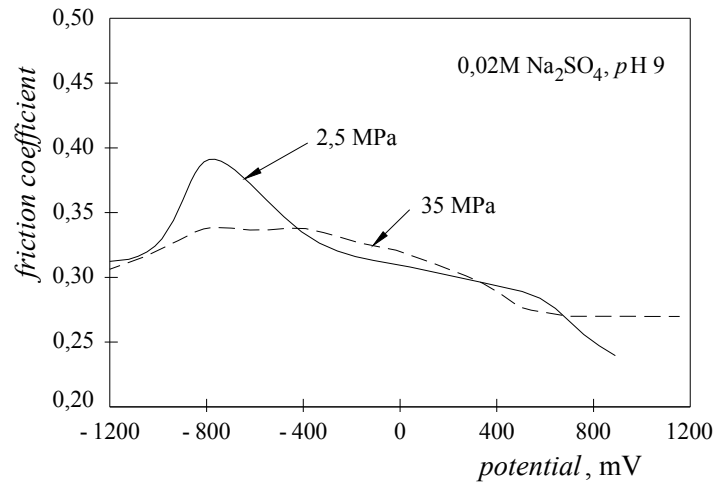


Fig.1 The variation of friction coefficient for different chemical potential of the electrolytic medium (0,02M Na<sub>2</sub>SO<sub>4</sub>, pH 9) related to contact stress [10].

Palagian and Gheorghieş [5] have determined the existence of an initial leap of the electrode potential toward electronegative domains both for the destruction of oxide films from friction surfaces through wear processes in absence of corrosive media, and for cyclic fatigue loading of the material in 3% NaCl solution, fig. 2. As a result, the potential variations indicate the presence of the modifications in superficial layer. The potential leap increase with the growth of the contact stress magnitude.

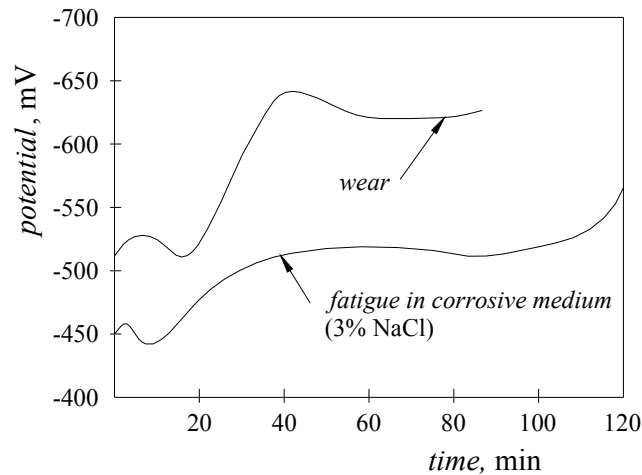


Fig.2. Variations of electrode potential in wear processes and fatigue processes in 3% NaCl solutions [5].

Tudor [9] presents a comparison between behavior at corrosion and at wear of 13.8% Cr – 0.16% C martensitic stainless steel in sulfuric acid solution. Through the local removal of passivity layer during the friction, the exposed zone becomes anodic. As a result, between adjacent (cathodic) zones of the surface and anodic zone establishes a great potential difference, fig. 3. Furthermore, can be observed that through friction is generated a potential passage in anodic zone with great values of current density, in contrast with corrosion that registers small current density. Development of anodic reaction is advantaged by the generation of structural defects.

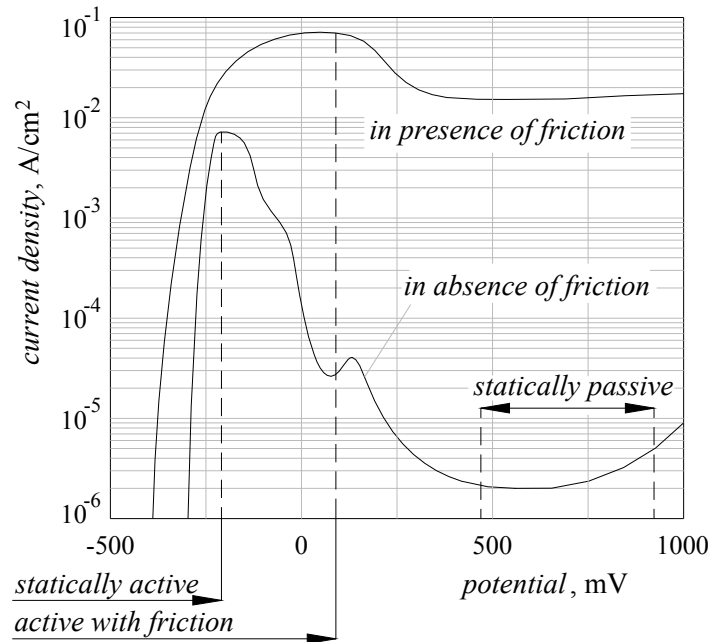


Fig.3. Variations of electrical potential in absence and in presence of friction [9].

Iwabuchi et al. [4] have examined the surface of steel (0.35%C, 4.5%Cr, 1.1%V and 1.2%Mo) subjected to the wear process in a 0.1 mol/l  $\text{Na}_2\text{SO}_4$  (pH 6.5) electrolytic medium and a load by 10 N. From fig. 4 can observe that the surface is smooth at negative potential, fig. 4 *a*, but at positive values appear cracks on the surface, fig. 4 *b* and *c*. Interesting is the crack apparition just in passivity domain of steel.

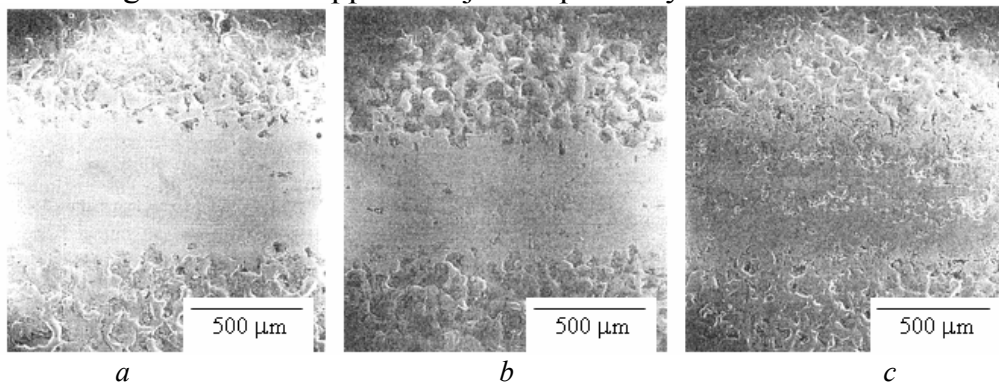


Fig.4. Surface modification related with potential variation applied [4]: (a)  $-600$  mV potential de; (b)  $0$  mV potential; (c)  $600$  mV potential.

Ciftan and Saibel [2] consider that the mechanism of crack formation is induced by chemostress effect and Gouy effect. These two effect act over the increasing of migration and concentration rate of the ions or of the colloidal particles on the crack peaks found nearly to metal surface, which involve a chemical composition difference and a concentration gradient. Reactions are development at the abnormal higher speed in the vicinity of material defects from superficial layer. Because the increasing of stress determine a growth of chemical potential of the impurity ions, the process are transformed in a chain reactions, which in final conduce to the increasing of structural defects, dividing the liaisons and material detachments.

Heidemeyer [3] shows that chemical reactivity of material increase through the heat development during the friction process, named thermochemical effect. This

effect represents an important factor for the cracks development anterior formed. Furthermore, when an ion or a colloidal particle is nearly sufficiently on metallic surface, the magnitude order of some atomic rays, respective is enough near to the crack peak, the thermochemical effect become very strong [2], due to the great stress concentration factors by the order of  $10^3$ . By another hand, the chemostress effect produces the adsorbent migration toward the crack peak and consequently determines the apparition of some strong reaction with electron exchange (chemosorption).

Palaghian and Gheorghieş [5] consider that the substances adsorption with superficial activity influence the interaction between dislocations and material surface. The dislocations propagation to metallic surface is realized after the overtaking the energy barrier of surface. After of this phenomenon on the friction surface appear the sliding steps. By another hand, displacement through diffusion of electrolytic medium components, in atomic or ionic state, lead to concentration of these on the crack peak, which of that propagation determine the damage of crystalline system. The output places of dislocations on the metal surface form active centers by adsorption and hydrogenation of metal.

## 2. Conclusions and subsequent research directions

The material transfer from wear processes in electrolytic media is led by dissociation processes and mechanical deteriorations of the superficial layers of those two bodies in contact. The protector film formed on the metallic surface, in general, inhibit the dissociation, and the activation effect resulted through friction advantage their partial destruction, which induce the polarization between protected (cathodic) zones or exposed (anodic) zones. This polarization increase the dissociation from anodic zone, and the changes produced in the surface potential modify the kinetics of the adsorption – desorption process. Furthermore, elastic and plastic deformations of the superficial layers lead at the growth of surface temperature. In the same time, the polarization induced through friction influence only the speed of electrochemical dissociation and, by this, the formation rate of the oxides superficial films and the wear of these.

The variations of electrolytic potential and the chemical reaction speeds from the tribocorrosion wear processes are determined by stress state from contact zone, by the presence of modifications from superficial layers and by chemical reactivity of the material. An electronegative potential determine the increase of wear intensity, and an electropositive potential lead to the apparition of crack in superficial layers. As a result, is necessary to continue the research for establish of parameters regarding the oxidation and chemical reactivity of superficial layers in the conditions of the tribocorrosion wear, respective to establish the relation between the contact stress and the polarization state of the superficial layers.

**REFERENCES**

1. Broszeit E., Hess F. J. and Wagner E., 1974, *An electrochemical investigation of corrosive wear of electroplated nickel*. Wear, 30, 311-319.
2. Ciftan M. and Saibel E., 1979, *The effect of the zeta potential on pitting*. Wear, 53, 201-209.
3. Heidemeyer J., 1981, *Influence of the plastic deformation of metals during mixed friction on their chemical reaction rate*. Wear, 66, 379-387.
4. Iwabuchi A. și alții, 1992, *Electrochemical approach to corrosive wear of SKD61 die steel in Na<sub>2</sub>SO<sub>4</sub> solution*. Wear, 156, 301-313.
5. Palaghian L. și Gheorghieș C., 1987, *Considerații privind o corelație între distrugerile prin oboseală de coroziune și uzură*. Tribotehnica'87 București, 221-225.
6. Șoltuz D. V. and Neculăiasa V., 2005, *Aspects regarding the influences of some substances from agriculture and food industry on the durability of the machines and installations from this domain*.
7. Șoltuz D. V., Neculăiasa V. and Țenu I., 2004, *Aspects regarding aggressive medium from food industry*. Buletinul Institutului Politehnic Iași, Tomul L (LIV), Fascicola VI B2, Secția Construcția de Mașini, 132-141.
8. Șoltuz D. V., Neculăiasa V. and Țenu I., 2004, *Appearance forms of mechano-chemical wear at machines and installations from food industry*. Buletinul Institutului Politehnic Iași, Tomul L(LIV), Fascicola Vc, Secția Construcția de Mașini, 951-957.
9. Tudor I., 2001, *Tribologie*. Ploiești, Editura Universității din Ploiești.
10. Zhu Y. Y., Kelsall G. H. and Spikes H. A., 1994, *The influence of electrochemical potentials on the friction and wear of iron oxides in aqueous systems*. Tribology Transactions, 37 (4), 811-819.

**ASPECTE PRIVIND VARIAȚIILE DE POTENȚIAL ELECTROLITIC ÎN PROCESE DE UZURĂ TRIBOCOROZIVĂ****(Rezumat)**

Procesele de uzură, în prezența mediilor agresive, determină expunerea suprafețelor de contact atât acțiunii fenomenelor tribologice, cât și acțiunii chimice, respectiv apariția fenomenelor specifice de tribochimie. Tensiunile mecanice nu declanșează reacții chimice, dar prin modificările pe care le produc în starea suprafeței sau în structura materialului favorizează sau accelerează reacțiile chimice dintre materialele cuplei de frecare și mediul agresiv. Apariția fisurilor este dependentă de corelația dintre caracteristicile cuplei de frecare cu cele ale mediilor agresive. În aceste condiții este necesar să se studieze variațiile de potențial electrolitic și a vitezelor reacțiilor chimice din timpul proceselor de uzură.



## DEVICE FOR METALLIC COVERING BY ACTIVATED THERMAL SPRAYING

BY

ST. L.TOMA, I.ALEXANDRU, D.G. GĂLUȘCĂ and C. BEJINARIU

**Abstract:** This paper has as main purpose the presentation of a metallization device by using the thermal spray activated and works under high pressure conditions (over 6 ph. atmosphere), it uses as energy source the heat developed by electric arc formed between two electrodes coupled to source of continuous current having as kinetic agent the compressed air, and as thermal activating agent acetylene, using its combustion we create an thermal field outside the spraying cone. The obtaining of the continuous melted situation at the contact between the tow electrodes during the spraying is ensured by the permanent modification of the advancement speed of wires. This facility is obtained by the drive mechanism of wires which is electronic controlled with and electronic circuits special make to create the pull-push effect. The electronic control of the electric arc allows the growth of the kinetic agent work pressure. The situation determines the growth of the particles scattering degree and of course the obtaining of some fine drops from the supplement material. The temperature maintaining during the particles trajectory is ensured by the outside thermal field, which covered the spraying cone, obtained by the acetylene burn or using another gaseous fuel.

**Keywords:** Thermal-spraying activated, metallic layer deposition.

### 1. Introduction

The modification, of the chemical composition of the structure and proprieties of superficial layers of parts can be achieved by various techniques of treating at the surfaces with as without added material.

These methods aims to obtain a layer that will give to the part the needs of the operational environment.

### 2. Content

Metallic deposition by thermal spraying gives the possibility of a new alloy, with an arbitrary chemical composition (layer, on a surface of a substrate)

Sometimes, the obtaining of the same alloy by classic technology of casting is expensive or even impossible because at the various proprieties of the components

Metallization procedures by thermal spraying are various and a classification can be made by:

- source of energy used for the meting of the deposited material;
- physical aspect of added material before deposition

These procedure aim is to obtain layers with high mechanical (hardness, wear resistance, corrosion), electrical and thermal proprieties.

Because these proprieties are determined by the chemical composition, porosity degree and oxides contraries of the layer, by the adherence layer-substrate as well as by the size of the zone layer interface-substrate we have considered the direction at the resources in new modifying these parameters.

The influence factors of these parameters are:

- the preparation of the substrate surfaces;
- the nature of the added material;
- the size, the temperature and speed of particles during impact;
- distribution of particles inside the spraying jet;
- the external reaction medium.

In such conditions we designed a device for metallic deposition with electric arc in controlled atmosphere, the operation of which take account at the previous considerations.

The metallization with electric arc in a controlled atmosphere is being designed to:

- the allay fusion;
- spraying and acceleration at the melted drop;
- maintaining particles in melted state;
- maintaining at a controlled atmosphere around the spraying cave;
- high shock and impact of particles.

We considered that the initial particle speed modification, their temperature and insulating the spraying cave from the environment determines the modification of the zone – layer interface substrate, the modification of the adherence, porosity degree and oxides contraries. Figure 1 shows a design of the device.

The metallization pistol with electric arc in controlled atmosphere is endowed with two separate circuits of compressed air (over  $p=6$  ph. atmosphere) each of them having its own role: - drop spraying;  
- kinetic agent;

The electric arc develops at the contact of the two electrodes and determines their melting. Under pressure generated by compressed air that exits the main nozzle (14). The melted drop is being scattered and accelerated on the substrate.

Compressed air that exists chamber 10 is being conducted so to ensure a cave for the protection of the spraying jet. Its part in this case is to enhance the speed of particles in the peripheral zone of the jet, modify their trace toward the cave core and protect the electric arc from the oxygen in the environment.

The ends of the wire guides (7) are exchangeable parts made from 12TNC18 quenched and tempered. They have high rigidity high electric resistance and high thermal resistance. Their positioning under an angle of  $15^\circ$  by rapport with longitudinal axis of the pistol enables the obtaining of a high stability of the electric arc and a good concentration of the spraying jet.

The main spraying nozzle 4 – made by duralumin has a shape that enables the obtaining of a gas flow rate necessary for the fragmentation of the drops of melted metal and induce on the gas a laminar flowing regime.

The frontal cap directs the inert gas toward the cave exterior for obtaining a protection by means at the 6 secondary nozzles.

Between the pistol body and the frontal cap is a mixing chamber that equalizes pressure of the kinetic agent used.

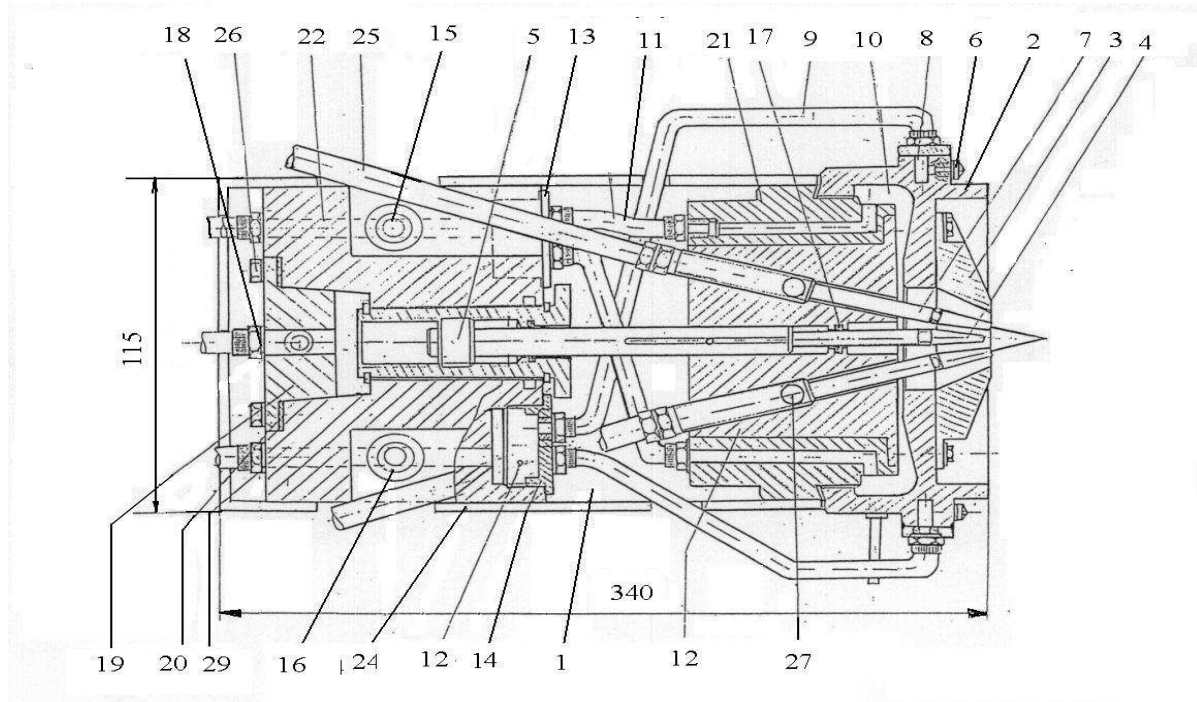


**Figure 1.** Device for metallization by thermal spraying deposition with electric arc activated  
**1** – base plate; **2** – frontal case; **3** – frontal nozzle; **4** – main spraying nozzle; **5** – advance mechanism at the main nozzle; **6** – secondary nozzle; **7** – guides for wire; **8** – chamber; **9** – pipes for mixture acetylene and air; **10, 12** – chamber, **11** – pipes for compressed air supplying; **13, 14** – cap; **15, 16** – valve; **17** – simmering; **18** – gap; **19** – inferior conic cap; **20** – insulation gap; **21** – body I; **22** – body II; **23** – teflon part; **24** – exterior case; **25** – flexible tube with metallic insertion; **26** – screw; **27** – insurance; **28** – electrical contact.

The optimum regime of operation of the apparatus is being characterized by:

- the arc stability;
- fine sizes of sprayed particles;
- concentrated jet;
- high speeds of sprayed particles.

For determining this regime the pistol is being endowed with a displacement mechanism on the direction of the main nozzle for compressed air (14) – fact that enables the modification of the distance between nozzle and the electric arc formation zone; gas valves that regulate the compressed air pressure on the three circuits, regulation systems for the electric parameters, regulation system for advance adjusting.

The pistol is being designed to work in direct current supplied by means of a welding type source – RCS-400 with the following characteristics:

Crt. No.	Technical characteristics	Values
1.	Nominal current	400 (A)
2	Minimum current	500 (A)
3	Voltage	51; 44; 37; 30; 23(V)
4	Supply voltage	380 (V)
5	Current adjustment	In 5 steps and continuous
6	External characteristic	Rigid

The added material used is wire type with maximum 2mm diameter.

The use of an electronic adjustment device for the wire speed gives the possibility of stability insurance for the electric arc by correlating the speed with the current characteristics and pressure characteristics of the kinetic agent.

Figure 2 shows the metallization equipment necessary. This installation is endowed with independent gas sources as well as a dose-establisher to introduce in the compressed air jet of fluxes (like graphite, wolfram carbide, B – carbide). Compressed air used is being filtered to eliminate oil dust and grease.

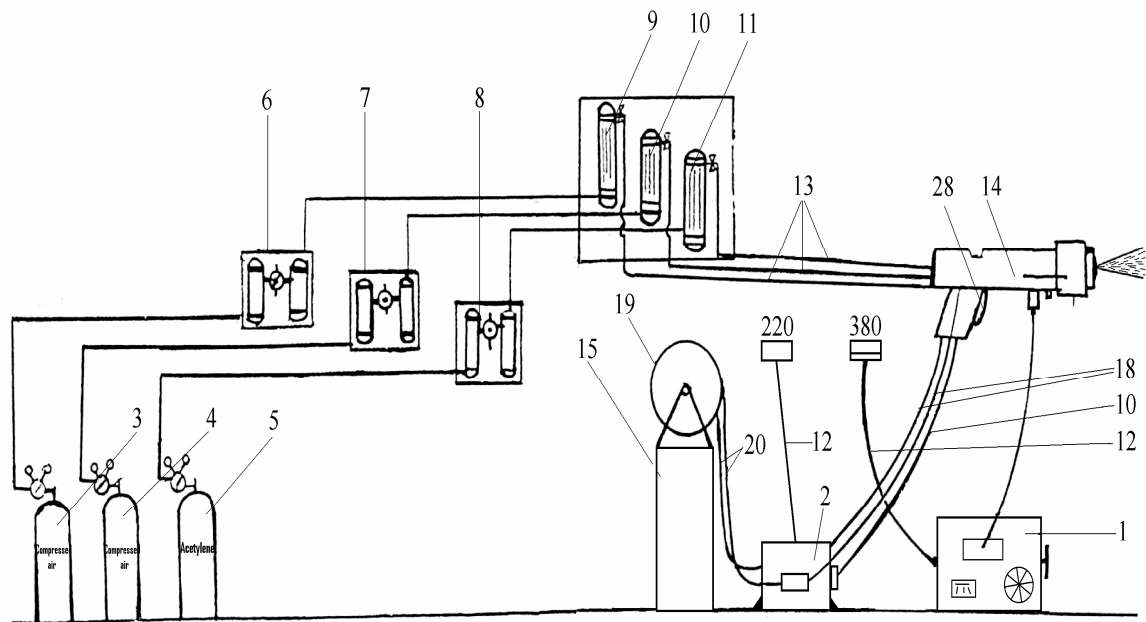


**Figure 2.** Installation for metallization by thermal spraying with electric arc in controlled atmosphere

1 – welding source RSC-400 type; 2 – wire advance mechanism; 3, 4 – Compressed air bottle; 5 – vacetylene bottle 6, 7, 8 – cleaning system; 9, 10, 11 – gas flow rate meter; 12, 17 – electric supply cable; 13 – inert gas supply duct; 14 – metalisation device; 15 – wire developer; 16 – flexible pipes for wire guidance; 18 – flexible pipes made from rubber with sheet iron for wire guidance; 19 – wire coil; 20 – wire; 21 – switch for the wire advance mechanism.

### 3. Conclusions

The utilization of the metal coating device with thermal spraying activated offers:

- the possibility to enhance the initial speed of sprayed particles; the possibility of use of a controlled atmosphere; maintaining a constant temperature of particles inside the spraying cave;
- possibility of distance regulation between the main nozzle of compressed air and the zone of arc formation that enables the modification of the spraying angle;
- obtaining of layers with a low degree of impurity;
- introduction of supplementary fluxes in the kinetic agent.

## REFERENCES

- /1/. Alexandru I., Popovici R. ș.a. - Alegerea și utilizarea materialelor metalice. Editura Didactică și Pedagogică - R.A. București 1997
- /2/. \*\*\* - The thermal spray technology leader - Tafa, 1999
- /3/. \*\*\* - Thermal Spray Buys Guide - National Thermal Spray Conferens - In Advansed Materials & Processes ASM - International Nr. 5, Vol. 145, mai 1994.

## DISPOZITIV DE METALIZARE PRIN SPRAYERE TERMICĂ ACTIVATĂ

### (Rezumat)

Lucrarea are ca scop prezentarea unui dispozitiv de metalizare prin sprayere termică activată ce funcționează în condiții de presiune ridicată (peste 6 at) și care utilizează: (i) ca sursa de energie, căldura dezvoltată de arcul electric - ce se formează între doi electrozi cuplați la o sursă de curent continuu; (ii) ca agent kinetic, aerul comprimat; (iii) ca agent activator, acetilena – a cărei ardere generează un câmp termic situat în exteriorul conului de pulverizare. Obținerea continuă a stării topite la contactul dintre cei doi electrozi în timpul pulverizării este asigurată prin adaptarea permanentă a vitezei de înaintare a sârmelor la parametrii de lucru (I, P). Această facilitate este realizată de mecanismul de antrenare a sârmelor care este prevăzut cu un circuit electronic suplimentar, special conceput pentru a crea efectul de pull-push sârmei. Controlul electronic al arcului electric permite creșterea presiunii de lucru a agentului cinetic, fapt ce determină creșterea gradului de dispersie a particulelor și implicit obținerea unor picături de material de adaos. Câmpul termic exterior - obținut prin arderea acetilenei - învește conul de pulverizare și determină menținerea temperaturii de topire a particulelor aflate în con.



## **THE SHOT PENNING INFLUENCE ON THE ALUMINUM LAYERS POROSITY OBTAINED BY THERMAL SPRAYING USING ELECTRIC ARC**

BY

**ST. L.TOMA, C. BACIU, C. BEJINARIU, A. ALEXANDRU and D. GHEORGHIU**

**Abstract:** This paper propose it self to present the effect of the mechanical hardening by shot penning on the aluminum layers porosity, obtained by thermal spraying in electric arc. The surface treatment applied to metallized layers by thermal spraying determinates: the increase of the deposition corrosion resistance as a result of permeability decrease of wear resistance by increasing deposition hardness, the increase of fatigue resistance by introducing compression tensions in deposition.

**Keywords:** Thermal-spraying, the porosity aluminium layer deposition.

### **1. Introduction**

The hardening mechanic treatment by shot penning of metallic deposition obtained by thermal spraying has as main effect the modification of some physical and mechanical proprieties as higher density, higher hardness, reduction of residual tensions, by introduction compression tensions.

These modifications have as main results the increase of the depositions corrosion resistance, as a result of permeability decrease, the increase of wear resistance by introducing compression tensions in depositions.

Logically the mechanical hardening treatment by shot penning must influence porosity of the coatings obtained with thermal spraying.

### **2. Content**

The porosity of the metallic deposition can be express with the porosity degree of the layer. For this reason we realized aluminum depositions by thermal spraying in electric arc on plane or cylindrical steel (OLC15) samples – figure1. The work conditions of the metallization by thermal spraying in electric arc are given in Table 1.

Because the electric arc is moving away the wires while spraying process, the material is ejected on the main piece. That is way we realized a mechanical mixture uniform distribution. With the metallic particles in depositions we find oxides (which cover the melted particles during their moving on the piece) and opened or closed pores in a net shape - figure 2.

The tested material was aluminum wire (ST 99.5 cu 99%AL-0.5%CU) with the next chemical composition and the hardening technology regime fixed:

- grits: Ø0,8 mm;
- the distance between the nozzle and the piece 100mm;
- compressed air pressure 2.5barr.

The samples have been made by OLC with these dimensions:

- plane samples-band-OLC15-20x30x200
- cylindrical samples Ø36 x 170 mm.

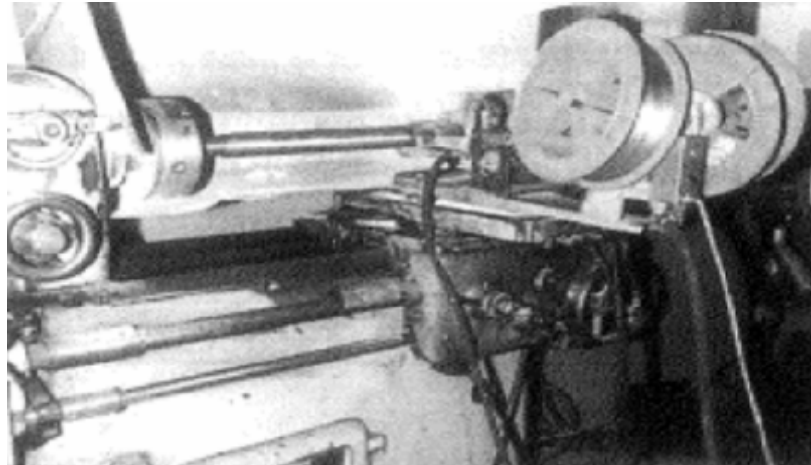


Figure 1 The metallization process in electric arc

Table 1 Work conditions of the metallization by thermal spraying in electric arc

Parameters	Layer 1	Layer 2, 3, 4
The distance layer – substratum [mm]	80	120
The rotation speed of the universal [rot./min]	105	63
The mooring speed of the pistol [m/min]	1,9	1,6
The diameter of the wire of Al [mm]	1,2	1,2
The pressure of the compressed air [at]	5,5	6,5
The force of the meting current [A]	180	190
The preheating temperature of the substratum [°C]	120	120
Inclination angle of the spraying jet given the perpendicular line on the surfaces [grad]	15	0
The advancement speed of the wires [m/min]	2	2,5

After a sand blasting on the samples we depose aluminum by thermal spraying with electric arc. From these we have obtained by cutting with a disc some samples which were necessary for the determination of the first porosity, and the other samples were cold hardening by shot penning and then they were cluster sampling for the determination of the porosity.

The structure of the aluminum layers by thermal spraying and shot penning is in the figure 2. For obtain the porosity degree we chose the gravimetric method.

This method consists in weighting the samples and their immersion in H46A (STAS 9691-87) oil heated at 130 °C during two hours. After these two hours the samples have been taken out and they have been weighted.

The porosity degree has been calculated with this relation:

$$P_g = \frac{G_i - G_u}{G_u} \cdot 100 [\%] \quad (1.1)$$

$G_i$  - is the sample weight after bucking, [g];

$G_u$  - is the sample weight before bucking [g]

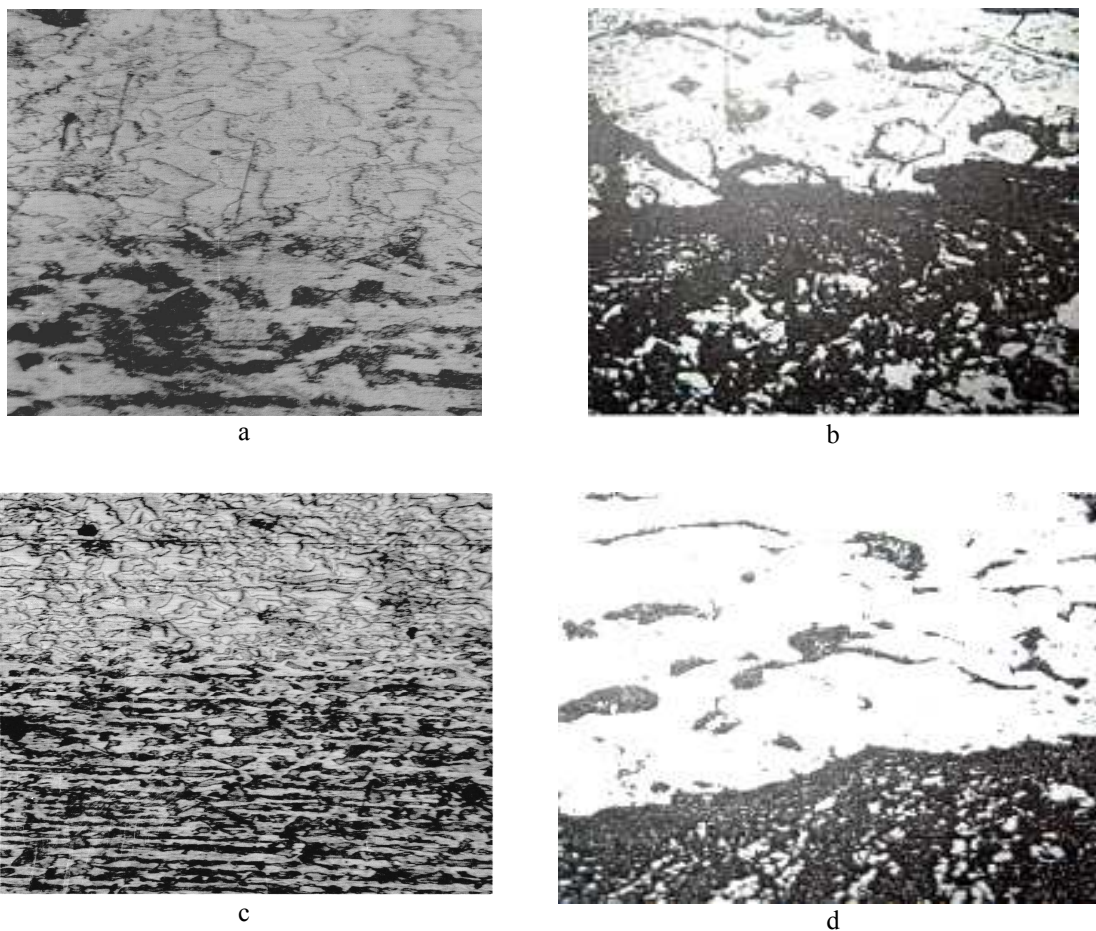


Figure.2 Microstructure, metal sprayed –: base OLC15, deposited layer –Al (ST 99,5); multiplication 100x (a) and 400x (b); 5% attack nital: a,b) before shot penning treatment; c,d) after shot penning treatment

After we used the cold hardening mechanic treatment the aluminum layers obtained by thermal spraying it was established that the thickness of the deposited layer was and on other little parts this was decreased. The measurements results are in the tables 2 and figure 3, 4.

After we applied the thermo mechanic treatment, the dimension of the sprayed aluminum layer clearly decreased because of the pore disposition bas well as because of the particles deformation.

Table 2 Experimental results

No layer	Sample type	Layer thickness [mm]	The sample weight metallized and not shot panned	The sample weight wet and not shot panned	The sample weight dry and shot panned	The sample weight metallized wet and shot panned	Porosity of the non treaty layer, $P_{g1}$	Porosity of the treaty layer, $P_{g2}$	$\Delta P = P_{g1} - P_{g2}$
			[g]	[g]	[g]	[g]	[%]	[%]	[%]
I	Cylindrical	0,25	1376	1522	1371	1514	10.61	10.43	0.18
	Plane	0,25	484	546	479	532	12.81	11.06	1.75
II	Cylindrical	1,01	1432	1712	1428	1612	19.55	12.88	6.67
	Plane	1,10	526	652	521	598	23.95	14.75	9.20
III	Cylindrical	2,26	1514	1831	1506	1656	20.93	9.96	10.97
	Plane	2,03	573	712	556	631	24.26	13.49	10.77
IV	Cylindrical	3,96	1596	1916	1566	1785	20.05	13.98	6.07
	Plane	3,01	0621	753	607	668	21.25	10.05	11.20

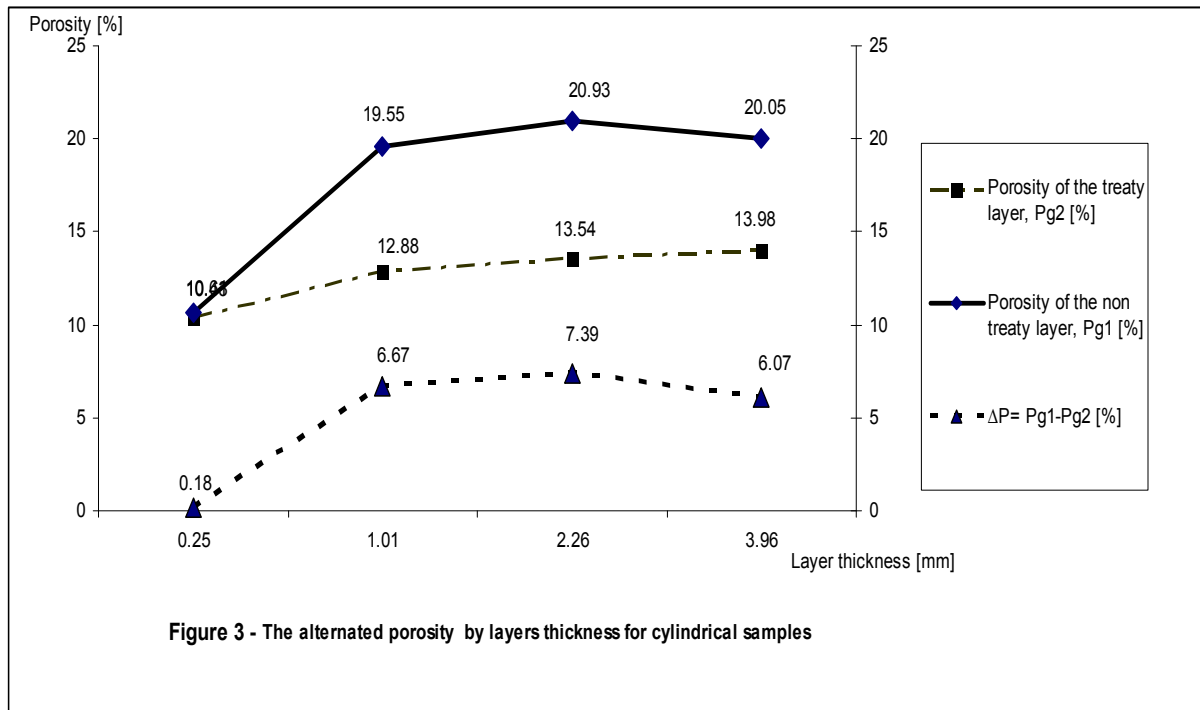
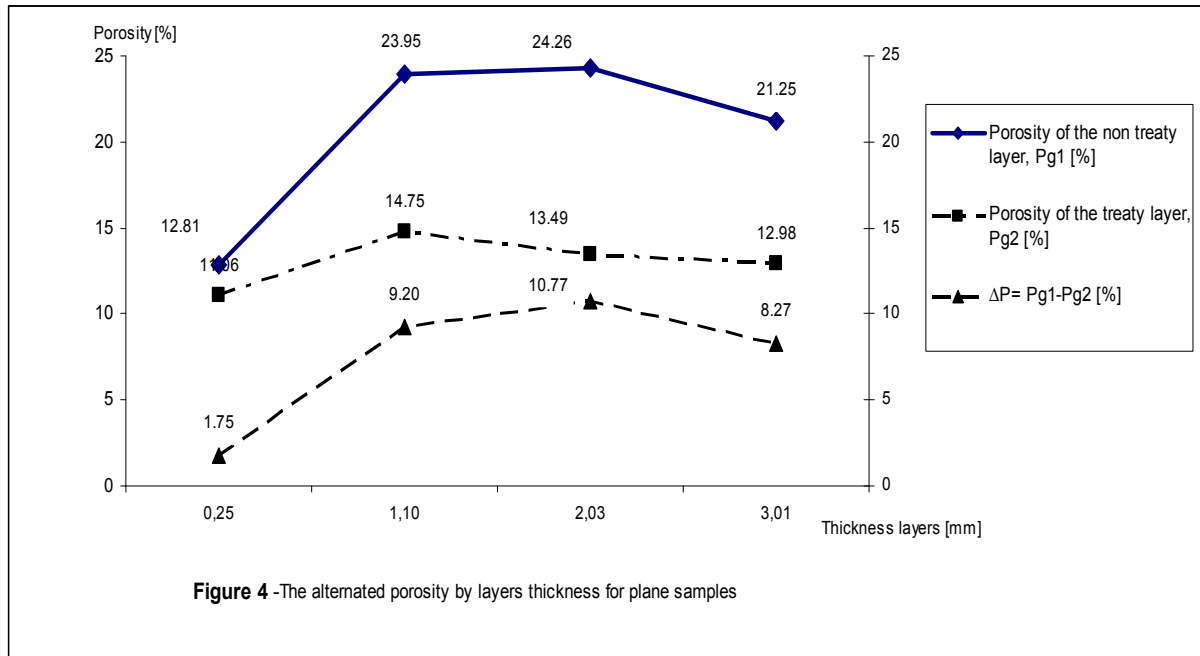


Figure 3 - The alternated porosity by layers thickness for cylindrical samples



### 3. Conclusions

From what presented in the table before we registered the next aspect:

- the porosity of the metalised layers by thermal spraying and by shot penning it less than the porosity of the sprayed layer and not treaty. That is why the alloys wear resistance shot penning treatment is much higher than that of alloys that were not subjected to shot penning;

- for thickness very small of basis metal, the porosity degree is reduce .That is because the spraying process has been made at a little distance to the sample (80mm),the particles temperature was higher , the particles velocity was higher too ,so it was allowed to attach the particles in the roughness of the surface;

- For higher thickness the shot penning effect on the porosity process is reduced because a part of the pores transform themselves from opened pores in closed pores and they don't permitted the oil penetration;

- for quite equal thickness of the deposited layer the porosity degree is higher on plane surfaces than cylindrical surfaces .That's happens because of the shrinking-ring effect, which appear at cylindrical samples and tend to compress the deposited layer.

After the dates from tables no 2 the porosity degree of the aluminum layer with a thickness more than 0.25mm, has a various between 11.62-24,25%. These values are accepted in the specialty literature.

**REFERENCES**

- /1/. \*\*\* - Catalog materiale – Sultzer Meteo
- /2/. Good fellow – Mettalle und Materialle für Forschung und Industrie, Katalog 1990.
- /3/. Levy A., McAdam S – The Behavior of ceramic Thermal Barrier Coatings on Diesel
- /4/. \*\*\* - Engine Combustion Zone Components Surface Coating Technologies, No 30,1987, pg. 51 – 61
- /5/. \*\*\* - Plasma Sprayed Thermal Barrier Coating – Process specification – P16B – AG3, General Electric 1994

**INFLUENȚA ALICĂRII ASUPRA POROZITĂȚII STRATURILOR DE ALUMINIU  
OBȚINUTE PRIN PULVERIZARE TERMICĂ ÎN ARC ELECTRIC****(Rezumat)**

Lucrarea de față își propune să prezinte efectul tratamentului mecanic de alicare porozității straturilor de aluminiu obținute prin pulverizare termică în arc electric. Acest tratament de suprafață aplicat straturilor metalizate prin pulverizare termică determină creșterea rezistenței la uzare prin creșterea durității depunerii, creșterea rezistenței la oboseală prin introducerea de tensiuni de compresie în depunere, precum și creșterea rezistenței la coroziune.

## **POSSIBILITIES OF PROGRAMMING MOULDS USED ON CAROUSEL INSTALLATIONS FOR THE INJECTION OF THE FOOTWEAR SOLES**

**BY**

**RODICA SILVIA VOLOCARIU and CORNELIA IONESCU LUCA**

**Abstract:** This paper presents different aspects referring to the injection of PVC soles directly on the upper parts at an Carousel injection installation with a set of moulds in a certain structure, in programmed condition to the obey the percentage of the sizing numbers of a certain number of sets. The use of programmed moulds is supposed to ensure the economic efficiency by reducing the timing for the production period of different sizes in the production series.

**Keywords:** injection footwear soles, mould, rotating table, moulds programming, balance, time

### **1. Introduction**

The injection shaping of thermoplastic polymers used to making shoe soles asks for a fluid process at high temperatures (180 – 200<sup>0</sup> C) and moulding them under pressure. In the mould cavity, through a cooling process, there is an icing process followed by a hardening of the polymer in the desired shape.

The injection of the material in the mould is done in special installations, with the help of a special equipment, of different shapes, among which those of the carousel type which renders important economic advantages. These advantages are due to the fact that the same group of injection offers a great number of work posts (moulds) that are successively brought just on the injection top giving identical conditions for all semi-manufactured products.

The moulds are set on a rotating table of the installation and the preparation of the polymer and its injection is made with the help of plasticizer device. The chart of the carousel installation/equipment is supplied by the DESMA firm represented in Fig.1

According to Fig.1, next to the rotating table with moulds (1) of circular shape there is the injection carriage (2) which has the role of heating, plasticization, dosing and injecting the material, the control panel (3)-with measuring and control devices of time and temperature, hydraulics station (4), cooling installation of pump (6) which ensures the pneumatic energy/power necessary to turn off and on the moulds.

The installation has 12 work posts equipped with moulds on which 6 pairs of shoes are made with injected soles directly on the front part of the shoe, at a complete rotation of the rotating table (a cycle).

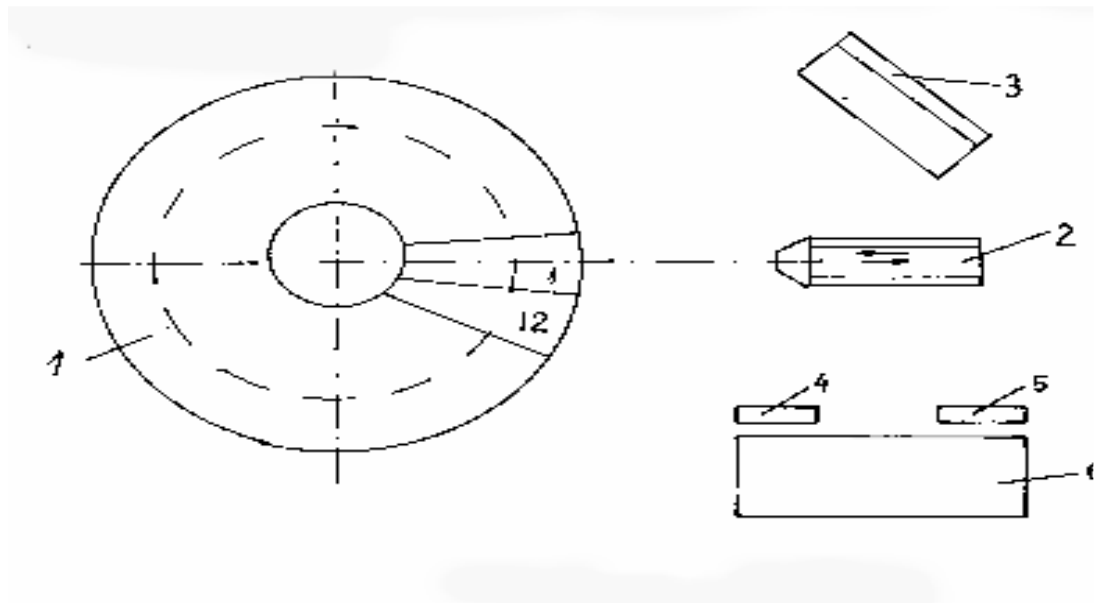


Fig.1

Due to the fact that shoes with different purposes are made for distinct size series, the moulds set on the rotating table of the installation will not be identical in size. The quantity of the shoes isn't delivered equally on size numbers but according to a normal law of distribution seen in the checking system on the series of sizes. This leads to a non-conforming loading of the work posts of the installation or even to run empty/ idle for some of them. Hence, the necessity to program the assembling of the moulds of the work posts of the installation and to find out their loading, for each concrete case.

Next we present the way we have found out the degree of balance of the injection installation. The paper refers to a concrete case taken from a production unity which produces footwear with injected soles.

## **2. The programming of the assembly of the moulds and the workpost balance of the work posts in the proposed case**

The lot of products taken into consideration has the size  $P=7500$  pairs of footwear of the perforated type, for the teenagers, with injected sole directly on the upper part, in the VAMOS model. To make the lot of footwear/shoes which covers sizes from 22 cm to 28.5 cm. there will be used a set of moulds which have a cavity corresponding to the model of the sole.

The delivery of the footwear according to sizes and of the moulds in the VAMOS set is presented in the Table no.1 below.

From Table no.1 we draw the conclusion that the set contains 20 pairs of moulds which will have to be set on the 12 work posts of the installation to get

different quantities of footwear according to size numbers; this will lead to the coupling of the moulds of different sizes on the same post in order to ensure a balanced loading of the work posts.

*Table 1*

Footwear size (cm)	Quantity (pairs)	Number of moulds (pairs)
22	40	1
22,5	80	1
23	130	1
1	420	
24	780	2
24,5	690	2
25	1270	2
25,5	1010	2
26	1010	2
26,5	680	2
27	650	1
2,5	410	1
28	230	1
28,5	10	1
Total	7500	20

It is considered that the balance of the work posts of the installation can be appreciated by the degree of balance of the loading, symbolized by E, expressed in % and which can be determined using the equation :

$$E = \left[ 1 - \frac{M(n - n_{\min})}{(M - 1)n_{\max}} \right] \cdot 100 \quad (1)$$

in which:

M= the number of work posts of the installation;

$n$  = the number of cycles of the rotating table necessary to make the lot of products  $P$ , for a certain assembly program and rolling of the moulds ;

$n_{\min}$  = minimum number of cycles of the rotating table necessary to make the same lot of products  $P$ , in the condition of an ideal balance of 100%, of  $M$  posts;

$n_{\max}$  = possible maximum number of cycles necessary to make the lot of products in the condition of null balance, 0%, respectively when all moulds of the set would be set successively only on one workpost.

In short, the degree of balance  $E$  can be calculated using the equation:

$$E = \frac{M(P-n)}{P(M-1)} \cdot 100 \quad (2)$$

In the equation (2) the terms have the same meaning as in the equation (1). For the concrete case under discussion:

$$M=12; \quad n_{\min} = \frac{P}{m} = \frac{7500}{12} = 625; \quad n_{\max}=P=7500;$$

$$n = \frac{P}{\text{number of pair / cycle}} = \frac{7500}{6} = 1250$$

The degree of balance  $E$ , calculated using both equations, has the value of 90.9% in the case under discussion.

To make the lot  $P=7500$  pair of shoes with the set formed of 20 pairs of moulds, which surpass the number of work posts ( 12 ) of the installation , there appears the problem of establishing the type of coupling of the moulds of different sizes on certain work posts. This time, symbolized  $T$ , is expressed in hours and can be determined using the equation:

$$T = \frac{PAS(M.L + I - M) + \sum Ts_i}{3600} \quad (3)$$

in which:

$PAS$  = the rhythm of the installation, in seconds, that is the time between 2 successive injections;

$M$  = number of posts of the installation;

$L$  = the loading of the respective mould expressed through the quantity of products which are made on it, expressed in pairs;

$I$  = number of the order of the respective work post on the rotating table of the installation;

$\sum Ts_i$  = the sum of the changing time of the moulds from other posts on which the moulds where replaced, in seconds, if the replacement demanded to stop the

installation. At the injection installation of carousel type, the DESMA make,  $PAS = 6s$  and  $\Sigma T_{s_i} = 400 s$ .

### 3. The obtained results and their interpretation

Taking into consideration the concrete values of the above sizes, through the automatic processing of the data there were obtained the results presented in Table 2.

The results in Table no.2 show that out of the set of 20 moulds only 19 will be used, when the installation starts to function and they will be assembled on the 12 posts of the installation in the following order 28/1, 25/2, 25/3, 22.5/4, 28.5/5, 22/6, 25.5/7, 27/8, 23/9, 26.5/10, 26.5/11, 24.5/12. After producing the quantity of shoes, the moulds that correspond to the extreme numbers of the series will be replaced with others as follows: 28 ----27.5 ( post 1 ), 22.5 ---26 ( post 4 ), 28.5----26 (post 5), 22----25.5(post 6), 23---- 23.5(post 9), 26.5---24(post 10), 26.5----24(post 11).

Table no. 2

Order number of work post	Size number of the mould set on the post(cm)	Quantity of shoes made on the post and mould(pairs)
1	initial 28	230
	27.5	410
2	25	640
3	25	635
4	initial 22.5	80
	26	550
5	initial 28.5	10
	26	550
6	initial 22	40
	25.5	505
7	25.5	545
8	27	505
9	27	650
9	initial 23	130
	23.5	420
10	initial 26.5	340
	24	390
11	initial 26.5	340
	24	390
12	24	730
12	24.5	690
Total	19 moulds	7500 pairs

Through coupling the moulds of different sizes on the work posts shown, the variable loading is between the limits of ( 505 – 730 ) pairs/posts; and after a number

of 15.3 h of continuous functioning of the injection installation there can be achieved the entire lot of shoes of 7500 pairs.

For the variant of distribution and use of moulds on the work posts of the presented installation in Table no. 2, the concrete degree of balance of the installation (E), calculated with the equation (2) has the value:

$$E = \frac{12(7500 - 730)}{7500(12 - 1)} \cdot 100 = 98,47\%$$

#### 4. Conclusions

1. To balance the loading of work posts of the injection installation of carousel type presented in the paper, can be achieved only when the number of moulds of the set is bigger than the number of the work posts of the installation.
2. The balance degree ( E ) is influenced by the type of rotation of the set of moulds on the work posts of the installation, the total size of the lot of shoes, the series of sizes in the lot, the quantity of shoes, on each size number of the series.
3. The automatic processing program of data used in the concrete case presented in the paper has a general character and it is used in all cases which obey the specified restriction in the first formulated conclusion.

Received May, 9 2005

The "Gh.Asachi" Technical University Iași

#### REFERENCES

1. Cociu V., Volocariu R., Ionescu C., *Moulds and Shaping Devices*, Rotaprint IP Iași 1983.
2. Croitoru D., *Tools and Automation for Leather Products*, Rotaprint IP Iași 1987.

#### POSSIBILITĂȚI DE PROGRAMARE A MATRIȚELOR FOLOSITE PE INSTALAȚII DE TIP CARUSEL PENTRU INJECTAREA TĂLPILOR DIRECT PE FEȚELE ÎNCĂLȚĂMINTEI

##### (Rezumat)

Lucrarea prezintă aspecte referitoare la injectarea tălpilor din PVC direct pe fețele încălțăminții la o instalație de tip Carusel, dotată cu un parc de matrițe de o anumită structură, în condiții programate, astfel încât să se respecte repartiția procentuală a numerelor de mărime în cadrul scriei de mărime în care se confecționează produsul. Utilizarea programată a matrițelor vizează asigurarea eficienței economice prin reducerea duratei ciclului de fabricație a loturilor de producție de mărime diferite.

## VIBRATION ANALYSES ON HIP PROSTHESIS

BY

ALINA ZAHARIUC\*, FLORIN MUNTEANU\*\* and VASILE MERTICARU\*

**Abstract:** Mechanical vibration analyses, a traditional nondestructive testing tool, have been widely used by mechanical engineer to inspect for structural integrity. So, the purpose of the present paper is to present some vibration analyses for three types of hip prosthesis, from different materials. The three types of prosthesis are: “Exeter”, made from steel, ABG II (Anatomical Bernoist – Girard), made from cobalt – chrome alloy, both from Stryker – Howmedica – Osteonics, and IMP ( a custom made prosthesis - courtesy of Advanced Custom Made Implants, Leuven, Belgium), made from titanium. As the results showed, the material properties are very important in vibrational analyses. The experiments were backed up with some very encouraging modal analyses by finite elements modeling. The importance of these experiments and simulations is revealing for diagnosing the phenomena of early loosening, one of the problems of the total hip replacement.

**Keywords:** vibration analyses, modal analyses, hip implants, loosening.

### 1. Introduction

As well established from all over the entire scientific community, there is no perfect hip prosthesis. In spite of the advanced techniques of designing and technologies of manufacturing hip prosthesis, the average age of an implanted prosthesis is somewhere between 10 and 15 years. The most common cause of failure in time of these implants is the phenomena known as loosening, when the prostheses is no longer fixed in the bone and it is starting to move, causing additional loading in the local area and furthermore, pains or other septic complications. So, the specialists were trying to asset a tool for diagnosing the loosening in its early stages, so the surgeon could be able of performing an operation of revision before the appearance of bone destructions.

For several years, conventional imaging based techniques have been used (plain film radiography, digital subtracted arthrography, Roentgen stereophotogrammetric analysis, scintigraphy), but the diagnostic sensitivity and specificity are not entirely satisfactory [1]. A non-destructive testing tool, widely used by mechanical engineers to inspect for structural integrity, is mechanical vibration analysis. This technique has been successfully used to determine bone mechanical properties [2, 3]. Clinical applications of this research were monitoring of fracture healing [3] and in vivo assessment of bone mechanical properties [4]. Mechanical vibration analyses, a traditional non-destructive testing tool, have been widely used by mechanical engineer to inspect for structural integrity. The potential application of this technique in the orthopaedic area has been demonstrated to augment information from clinical

radiography, scintigraphy and arthrography [4, 6]. The conclusion of these studies [2] was that vibration testing method was more sensitive than traditional X-ray.

Loosening in hip implants has two consequences. The first one is the change of the system parameters, the shifts of frequencies (in Frequency Response Function) and the changes in amplitude. The stiffness decreases, so the resonance frequencies decrease. Several references measurement is necessary in these cases. The second consequence is the development of non – linearities, measuring the distortions, the harmonic excitation, higher harmonics in output signal, the distorted signal. An important problem to consider in this case is the “background” distortion.

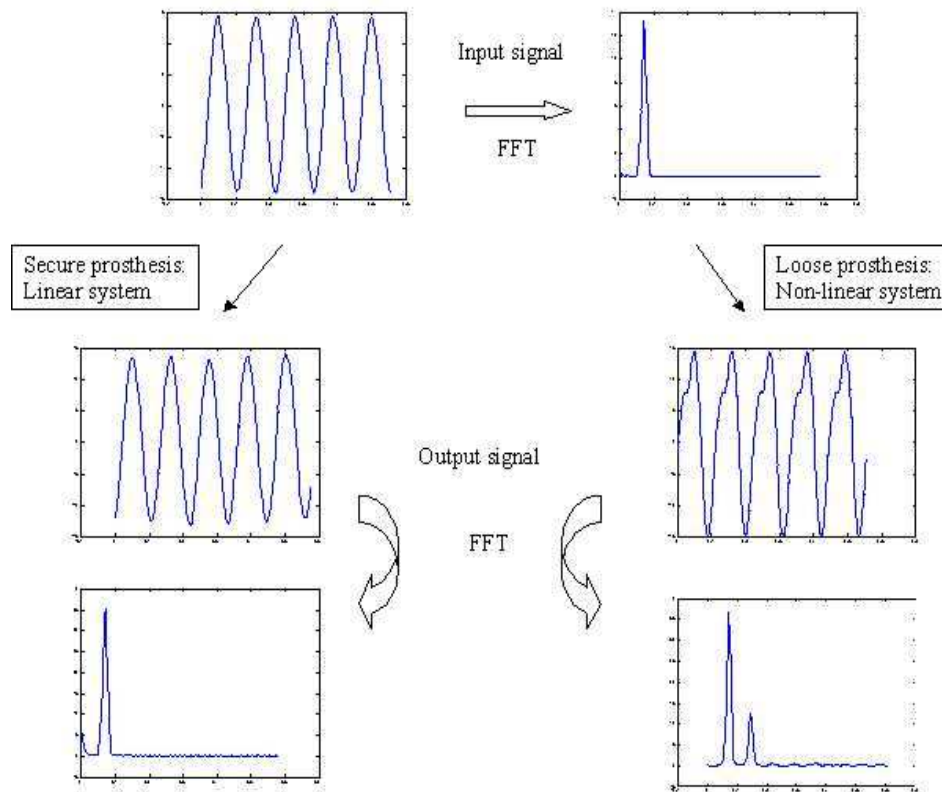


Fig. 1 Analogical scheme of the principle of the vibration analyses

For total harmonic distortion:

$$\text{thd} = \frac{\delta}{a_0 + \delta} \cdot 100\% \quad (1)$$

where  $\delta$  = sum of amplitudes of higher harmonics;  
 $a_0$  = sum of amplitudes of all harmonics.

$$\Delta RF = f_0 = \alpha \sqrt{\frac{EI}{ml^3}} = \alpha \sqrt{\frac{EI}{\mu l^4}} \quad (2)$$

$\Delta RF$  = the average of the resonance frequencies; [5]

$f_0$  = the natural frequency; [Hz]

$\alpha$  = material coefficient;

$EI$  = flexural rigidity;

$m$  = mass;

$l$  = total length;

$\mu$  = mass density per unit length.

It is clear from the formula (2) the relationship between the material properties and the free vibration.

## 2. Methods and procedures

Three types of prosthesis were analyzed. The three types of prosthesis are: “Exeter”, made from steel, ABG II (Anatomical Bernoist – Girard), made from cobalt – chrome alloy, both from Stryker – Howmedica – Osteonics, and IMP ( a custom made prosthesis - courtesy of Advanced Custom Made Implants, Leuven, Belgium), made from titanium.



Fig. 2 The three types of hip prosthesis described above (from left to right, ABG II, Exeter and IMP)

Modal analyses mean some very sensitive analyses, so the virtual model in finite element must be as closer as possible to reality. The modeling started from the scanned images with computer – tomography technique. The number of images was equal to the slice number. The images have been loaded in *Mimics 8.0*, from *Materialise Software* package, respecting the slice distance = 0.4210 and the pixel size = 0.1305. Then, after building the two dimensional model of each prosthesis and enhancing the model, the file has been imported in *MSC\_Patran\_2001*, the preprocessing component of *MSC Marc*, a commercial finite element software package, so the three dimensional models were built. These ones have, after enhancing the quality of the meshes, have been imported in *MSC\_Mentat\_2001*, one of the postprocessing component of *MSC Marc* package.

Modal analyses mean the calculation of the modes of free vibration for a body, which are the microdeformations of the body. A very important characteristic of modal analyses is applying the material properties.

Table 1. Material properties for the prosthesis

Prosthesis (material)	Young modulus (GPa)	Density (kg/mm <sup>3</sup> )
Exeter (steel)	200000	7.85e-009
IMP (titanium)	110000	7.51e-009
ABG (cobalt – chrome)	250000	8.50e-009

The Poisson coefficient was set to 0.3 in all three cases.

After establishing the material properties and checking the concordance between the units (the unit in finite element is millimeter), the mechanical boundary condition, like “fixed displacement” must be applied in all three directions, because the prosthesis is not floating in the air, but it is fixed in the bone.

The next step was to apply a load case, a dynamical modal one type, in the range 200 – 25000 Hz. It is very important to verify if the model is a solid one, by activating the three dimensional button of the analyses dimension. Then, the method “Lanczos” is activated and all the setting from “job results” menu must be cleared, because for the modal analyses is no need to apply another type of loading.

### 3. Results and discussions

The modal analyses were performed using three different sizes of the finite elements of the model, 1, 1.2 and 2. The results were almost the same, with some insignificant differences. The number of the increments was in the same range for the three types of prosthesis, 16 for Exeter (Fig. 3), 11 increments for the IMP prosthesis (Fig. 4) and 8 for the ABG prosthesis (Fig. 5). Different kind of vibrations ways have been noticed, like torsional and longitudinal ones and it is clear that the largest deformations occur in the distal part of the prostheses.

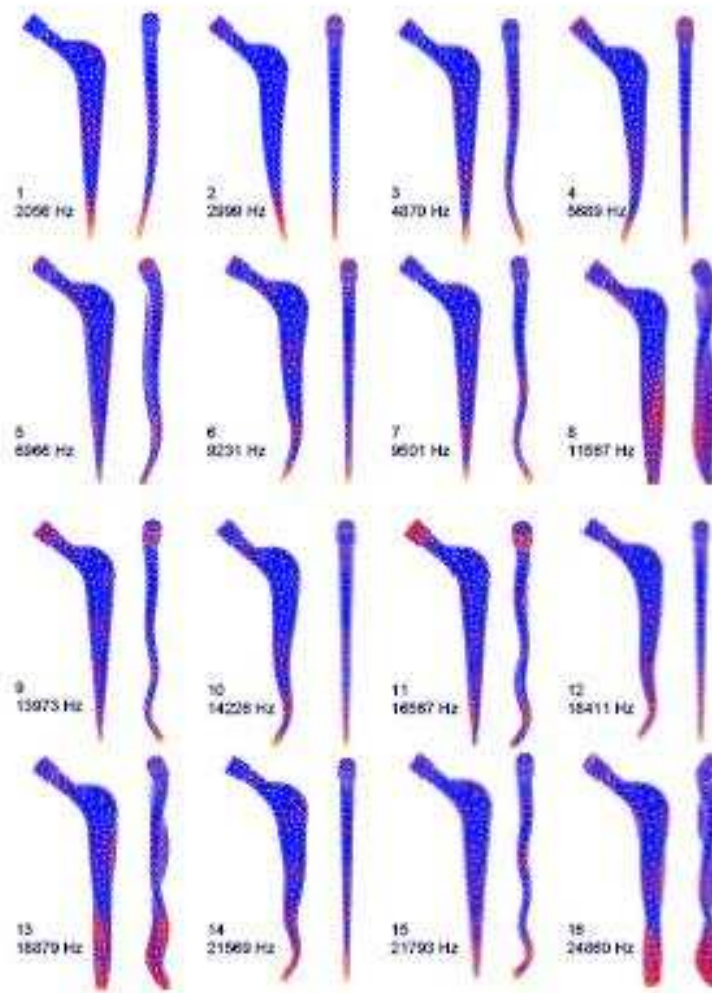


Fig. 3 Resonance frequencies and mode shapes of the first 16 natural vibration mode of an Exeter prosthetic stem, as calculated by FE modelling.

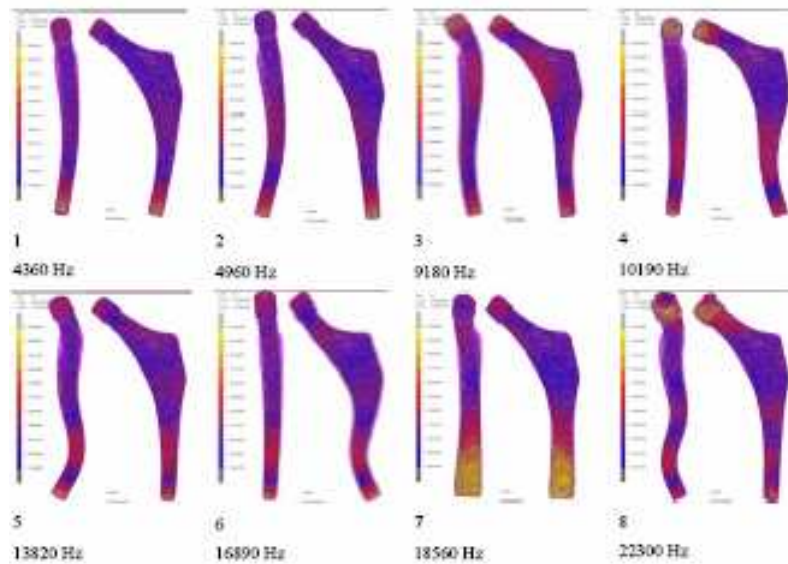


Fig. 4 Resonance frequencies and mode shapes of the first 8 modes of an ABG prosthesis.

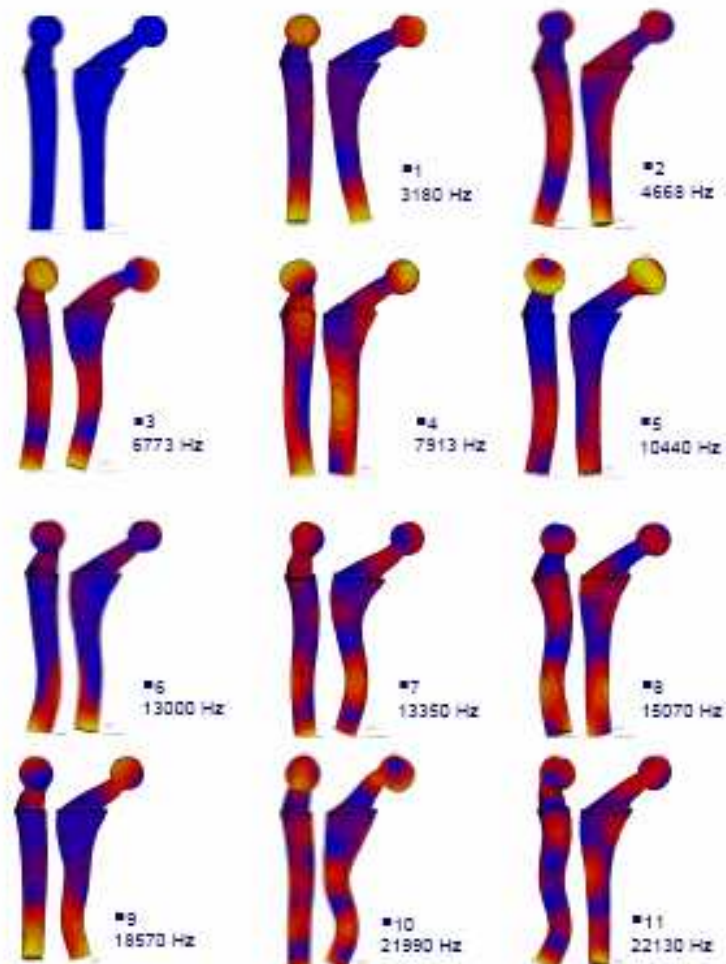


Fig. 5 Resonance frequencies and mode shapes of the first 11 modes of a custom made prosthesis (IMP)

The formula showing the dependence between the material properties and the natural frequencies is respected, so the first way of vibration, the first way of vibration of Exeter prosthesis being at 2056 Hz, of IMP at 3180 Hz and of ABG II at 4378 Hz, with the respect of the material properties of each prosthesis (Fig. 6).

$$f_0 = \alpha \sqrt{\frac{EI}{ml^3}} = \alpha \sqrt{\frac{EI}{\mu l^4}}$$

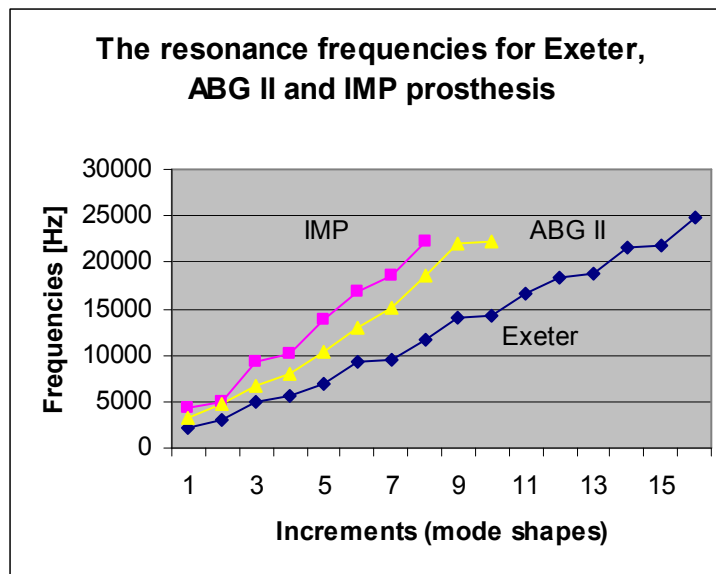


Fig. 6 The resonance frequencies (increments) for the three types of prosthesis

The increase in resonance frequency shift with increasing complexity of the mode shape of the prosthesis system was also observed. This observation is in accordance with the work of Qi *et al* [3] who state that the most sensitive frequency band for observing defects in the femur/prosthesis connection is above 2500 Hz. The results of the simulations are very encouraging, because they are in the same range as the results of the experiments performed in reality. An experimental set-up was used for measuring the resonance frequencies in the range 0 – 20000 Hz the Exeter prosthesis. The set – up components were (from the left side in Fig. 7) a power amplifier, a spectrum analyzer, a signal amplifier, a shaker and an accelerometer, put on the neck of the prosthesis, an area which is accessible during the operation. So, the measurements could be performed in the same time with the implantation and any mistake of placing the prosthesis in the femur would be avoided. The Exeter prosthesis was suspended horizontally in approximately free-free conditions by means of compliant elastic bands. The noise excitation from the shaker was used, and the FRF (frequency response function) was recorded with the spectrum analyzer. These experiments are the some preliminary results. In the future, there is to predict that some prosthesis with an accelerometers mounted inside would be implanted successfully and early loosening would be easy to measure at that level. Figure 8 presents on the same graphic two series of five measurements, compared with the resonance frequencies calculated with finite elements analyses.

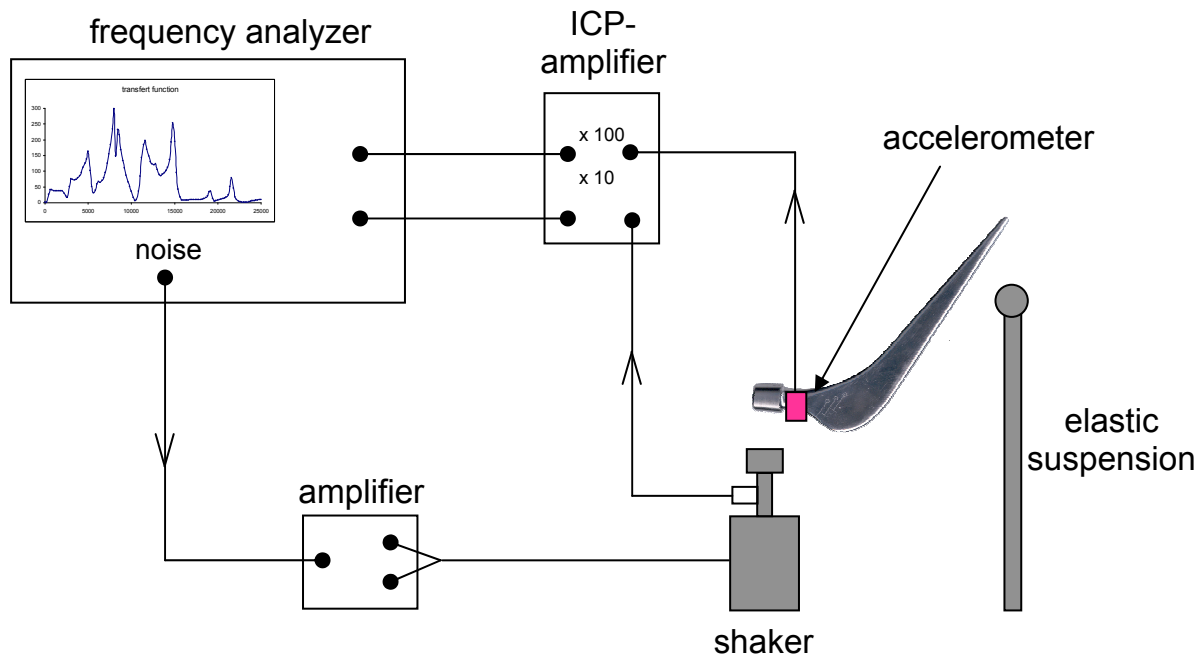


Fig. 7 Experimental set-up for measuring the frequency response function for an Exeter prosthesis

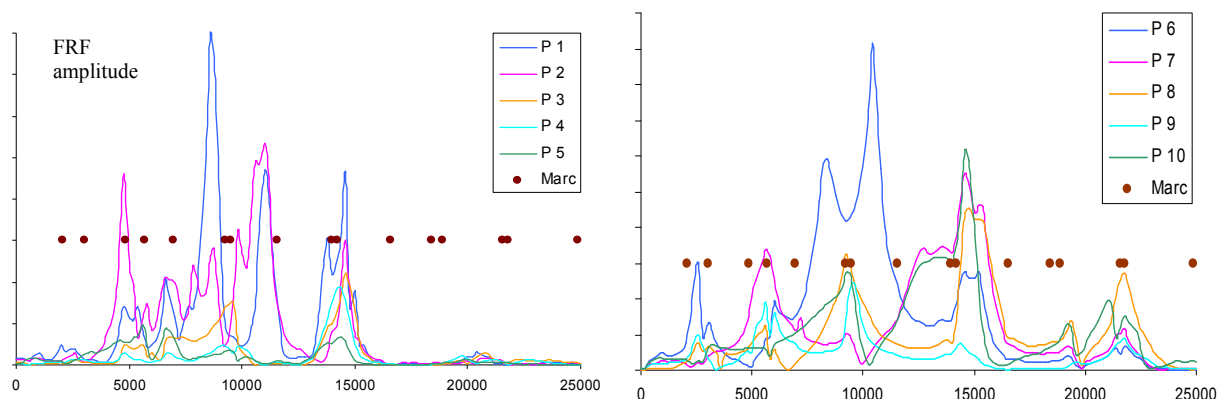


Fig. 8 The graphic representation of the frequency response function (on the ordinate axis) with the respect of the resonance frequencies, captured from the screen of the frequency analyzer – the brown point are the resonance frequencies calculated with MSC Marc – Mentat

#### 4. Conclusion and future work

The results of the finite elements analyses of all three prosthesis are very revealing and the experimental measurements confirm them. Vibrational analyses represent a very sensitive tool for measuring non-invasively the degree of loosening, so the imperfections of the material integrity, which could not be detected using usual techniques. After the operation, to measure non-invasively, an instrumented prosthesis with telemetry is necessary. A prototype version with built-in accelerometer is available [7]. To avoid excitation through the skin, an actuator should also be included in a future version. Also, a complete model of the bone – cement – prosthesis system should be analyzed and discussed.

Received May, 10 2005

\*The "Gh.Asachi" Technical University, Iași

\*\*The "Gr. T. Popa" University of Medicine and Pharmacy, Iași

## REFERENCES

1. Jaecques S.V.N., Păstrăv C., Zahariuc A., Van der Perre G. - *Analysis of the Fixation Quality of Cementless Hip Prostheses Using a Vibrational Technique*, **International Conference of Noise and Vibration Engineering**, Leuven – Belgium, 2004, **443-456**
2. A.P. Georgiou, J.L. Cunningham - *Accurate Diagnosis of Hip Prosthesis Loosening Using a Vibrational Technique*, **Clinical Biomechanics**, 16, 4 , 2001, **315-323**
3. G. Qi, W.P. Mouchon, T.E. Tan - *How Much Can a Vibrational Diagnostic Tool Reveal in Total Hip Arthroplasty Loosening*, **Clinical Biomechanics**, 2001, 18, 5, **444-458**
4. D. Rosenstein, G.F. McCoy, C.J. Bulstrode, P.D. McLardy-Smith, J.L. Cunningham, A.R. Turner-Smith A.R. - *The differentiation of loose and secure femoral implants in total hip replacement using a vibrational technique: an anatomical and pilot clinical study*, Proc. Inst. Mech. Eng. Part H: **J. Eng. Med.**, 203, 2, Professional Engineering Publishing, 1989, **77-81**
5. Thomson W. - *Theory of vibration with applications*, Fourth Edition, Stanley Thomes Publishers Ltd., 1998, **18-28**
6. R.J. Collier, R.J. Donarski, A.J. Worley, A. Lay, A. - *The use of externally applied mechanical vibrations to assess both fractures and hip prosthesis*, in A.R. Turner-Smith, Editor, **Micromovement in Orthopaedics**, University Press, Oxford , **151**
7. A.D. Heiner, T.D. Brown - *Structural Properties of a New Design of Composite Replicate Femurs and Tibias*, **J. Biomechanics**, 34, 6, 2001, **773-781**
8. R. Puers, M. Catrysse, G. Vandevoorde, R.J. Collier, E. Louridas, F. Burny, M. Donkerwolcke, F; Moulart - *A telemetry system for the detection of hip prosthesis loosening by vibration analysis*, **Sensors and Actuators A-Physical**, Vol. 85, No. 1-3, Elsevier, 2000, **42-47**

## ANALIZA VIBRAȚIONALĂ PE PROTEZE DE ȘOLD

### (Rezumat)

Analiza mecanică vibrațională, un procedeu de testare nedistructivă tradițional, a fost utilizată pe larg de inginerii mecanici pentru a verifica integritatea structurală. Deci, scopul lucrării de față este de a prezenta câteva analize vibraționale, pentru trei tipuri de proteze de șold, din materiale diferite. Cele trei tipuri de proteze sunt: „Exeter”, fabricată din oțel de tip Orthinox, ABG II („Anatomical Bernoist – Girard”), din aliaj de cobalt – crom, ambele fabricate de „Stryker – Howmedica – Osteonics și IMP (o proteză pe măsură fabricată la Advanced Custom Made Implants, Leuven, Belgia), din titan. După cum o demonstrează și rezultatele, proprietățile de material sunt foarte importante în analizele vibraționale. Experimentele au fost susținute de câteva foarte încurajatoare analize modale în element finit. Importanța acestor analize este relevantă pentru diagnosticul fenomenului de slăbire precoce a fixării implanturilor de șold, una din problemele operației de înlocuire totală a șoldului.

**Tipar Digital** realizat la **Tipografia pim**

Șoseaua Ștefan cel Mare nr. 11

Iași - 700498

Tel. / fax: **0232-212740**

e-mail: [editurapim@pimcopy.ro](mailto:editurapim@pimcopy.ro)

[www.pimcopy.ro](http://www.pimcopy.ro)